A Characterisation and Understanding of the Germinal Centre B Cell Response to Atherosclerosis in Mice using Lineage Tracing

Anna Meryl Francis

Pembroke College

University of Cambridge

This thesis is submitted for the degree of

Doctor of Philosophy

June 2022

Declaration

This thesis is the result of my own work and includes nothing which is the outcome of work done in collaboration except as declared in the preface and specified in the text.

It is not substantially the same as any work that has already submitted, or is being concurrently submitted, before for any degree or other qualification at the University of Cambridge or any other university or similar institution except as declared in the preface and specified in the text. No substantial part of this thesis has already been submitted or is being concurrently submitted for any such degree or other qualification at the University of Cambridge or any other university or similar institution except as declared in the Preface and specified in the text.

This thesis does not exceed the prescribed word limit of 60,000 words as specified by the Degree Committee for the Faculty of Clinical Medicine and Veterinary Medicine.

Abstract

A Characterisation and Understanding of the Germinal Centre B Cell Response to Atherosclerosis in Mice using Lineage Tracing

Anna Meryl Francis

Atherosclerosis is the most common cause of ischaemic heart disease and stroke which represent a global health concern responsible for significant levels of morbidity and mortality worldwide. It is a chronic inflammatory disease characterised by plaque build-up within arterial walls initiated by low density lipoprotein cholesterol. Elevated plasma LDL is a major risk factor for atherosclerosis and its immunogenic oxidation creates neo-epitopes that drive inflammatory immune responses underlying the pathogenesis of atherosclerosis.

The germinal centre is found within secondary lymphoid organs and is responsible for the production of high affinity antibody-producing plasma cells and long-lived memory B cells against antigens such as epitopes of oxidised LDL. Class-switched plasma cells and anti-oxLDL IgG antibodies have been detected within atherosclerotic plaques and sera of human and mice suggesting that the germinal centre response is pathogenically dysregulated in atherosclerosis.

The tamoxifen-inducible AID-CreERT2-Rosa-EYFP lineage tracing mouse model was used and crossed with the atherosclerosis-prone LDLr-deficient mouse model. This model inducibly and specifically labels germinal centre B cells and their progeny using tamoxifen allowing for tracking of atherosclerosis-specific B cell clones comprising germinal centre, memory, and plasma cells. $LDLr^{-/-}$ and $LDLr^{+/-}$ ('WT') mice were fed chow or high fat diet for up to 8 weeks and upon tamoxifen dosing (timing varied throughout studies) via intra-peritoneal injection or oral gavage, AID-expressing cells (germinal centre B cells) were fluorescently labelled with EYFP. Cells were analysed using flow cytometry and FlowJo software. All graphs and statistics were created using the GraphPad Prism 7.0.

In this thesis, I sought to characterise and understand the germinal centre B cell response in atherosclerosis using a lineage tracing mouse model. Firstly, the model was validated as EYFP cells were only detected after tamoxifen administration and were only present in germinal centre-derived cell populations. Furthermore, labelling efficiency was independent of time, diet, or genotype.

The germinal centre response was characterised in both WT and $LDLr^{-/-}$ mice demonstrating an time-dependent increase in germinal centre responses. Germinal centre reactions were exacerbated, greater in magnitude and degree of class-switching, by increased plasma cholesterol levels consequent of both HFD and knock out of the LDL receptor. The combination of HFD and $LDLr^{-/-}$ genotype, replicating atherosclerotic conditions, synergistically exacerbated germinal centre responses biased towards pathogenic cellular output due to elevated levels of class switching.

Due to the permanence of EYFP labelling, it was possible to track EYFP labelled cells over time and throughout the course of atherosclerosis. Tracking studies revealed that hyperlipidaemic conditions induced by HFD resulted in longer-lived EYFP clones which had increased propensity to undergo class-switching. Furthermore, there was a greater output of EYFP labelled memory and plasma cells.

To investigate the mechanism by which HFD induced greater germinal centre responses, interventions were conducted to block the impact of cholesterol and inflammation separately. Use of a cholesterol inhibitor drug and cholesterol free diet revealed that dietary cholesterol is key in driving the exacerbated germinal centre responses observed at early stages i.e., 4 weeks of atherosclerosis. Use of a cytokine inhibitor to dampen inflammation limited germinal centre responses at later stages of atherosclerosis i.e., 8 weeks, suggesting that inflammation plays an important role in germinal centre responses at this later timepoint. Thus, the model proposed is that dietary cholesterol is critical early on in atherosclerosis as disrupted lipid homeostasis results in autoimmune B cell responses with germinal centres primarily reacting to accumulated oxidised LDL while at later stages, the inflammation associated with atherosclerosis fuels exacerbated and pathogenic germinal centre responses.

To examine the role of IgG2c and its receptor FcγRIV in atherosclerosis, the impact of IgG2c antibody complexes was tested *in vitro*. IgG2c significantly enhanced TNF secretion, a marker of inflammation, in FcγRIV-expressing myeloid-derived monocytes. Thus, IgG2c has the potential to exacerbate inflammatory responses from plaque macrophages and dendritic cells.

In conclusion, the AID lineage tracing mouse model has been validated for use in the atherosclerosis setting. It has been characterised showing that germinal centre responses are exacerbated during the course of atherosclerosis and are skewed towards production of class-switched longer-lived B cell clones. Dietary cholesterol is the main driver of this pathogenic response in tandem with the inflammatory conditions caused by atherosclerosis. Germinal centre-derived IgG2c antibodies could play an important role in exacerbating inflammation within the plaque through plaque macrophages and dendritic cells. This thesis presents a model whereby atherogenic dyslipidaemia, as a result of elevated serum LDL levels, breaks down B cell tolerance. This results in autoimmune pathology characterised by exacerbated germinal centre responses skewed towards pathogenic antibody isotype clone production in response to LDL-induced inflammation. This provides an opportunity to target B cell-related atherosclerosis-specific responses therapeutically.

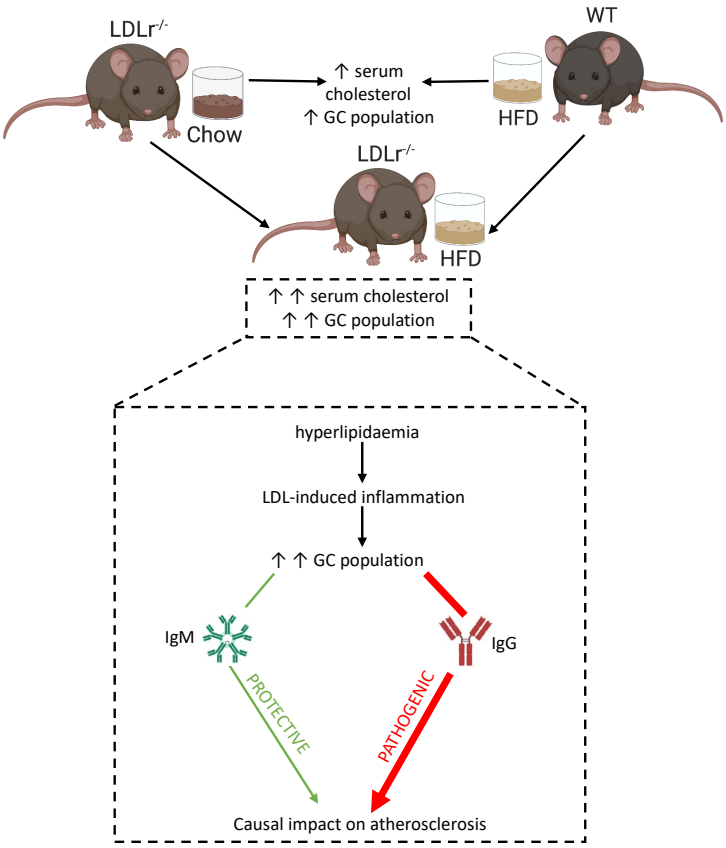

Figure 1. ***Model proposed in this thesis.*** *Both LDLr$^{-/-}$ mice fed chow diet and WT mice fed HFD have elevated serum cholesterol levels and increased population of germinal centre B cells. The combination of LDLr-/- genotype and HFD results in augmented serum cholesterol levels and exacerbated germinal centre responses with greater production of IgM- germinal centre-derived clones demonstrating increased levels of class switching. Thus, hyperlipidaemia produces LDL-induced inflammation which drives pathogenic germinal centre responses during atherosclerosis skewed towards IgM- isotype clones.*

Acknowledgements

Firstly, I would like to thank my supervisor Dr Andrew Sage for his constant guidance, advice, and intellect throughout the course of my PhD. We have worked as a team to develop new hypotheses and conduct in vivo experiments and have developed a friendship through many hours together in AMB and Forvie. From first discovering his research to his kind, reassuring demeanour in my interview and teaching me the "Andy tips and tricks" of the trade, he has always been a pillar of support enabling me to develop into an independent scientist.

I would like to thank all members of Professor Ziad Mallat's lab for always being helpful and providing words of encouragement. In particular, I would like to thank Leanne for keeping the lab running and functional at all times and to Toni, Magda, James and Charlotte for managing the *in vivo* aspect. I would like to thank every single person who enables smooth running of Level 5, AMB and the flow cytometry hub – underappreciated unsung heroes of the research world. It has been a stimulating environment to work in given the diverse range of research conducted and I have thoroughly enjoyed the plentiful opportunities to learn more about biomedical research through the range of seminars hosted on the Cambridge Biomedical Campus. I would not have survived my PhD without the enduring friendship from Toni who kept me sane and entertained and distracted me when required – thank you so very much. To my fellow PhD companions Christian and Marta, thank you for teaching me the ropes and your reassurance that everything would be okay. I would like to thank my fellow BHF PhD pals Matt, Robyn and Jennie for their friendship and support throughout the PhD.

I would like to thank everyone who has ever piqued my interest in biology from my parents for bringing me up with an appreciation of nature and an endless source of curiosity to my Grandad who taught me all about trees from a young age to my Granny who would always take me to the zoo. Furthermore, to all my biology teachers and lecturers over the years, in particular Dr Toffolo, Dr Turnbull, Dr Hole, and Dr Benham, who have helped pave the way to this degree. Thank you to Professor Neil Henderson who gave me the chance to experience research in his lab for an internship, you were the inspiration that began my journey to a PhD.

Thank you to Stewart Jones for your supervision and mentorship during my year at AstraZeneca, building up my confidence as a researcher and a valued team member.

I am so very glad I chose Pembroke College has my home for the last 4.5 years. I will forever treasure my time spent in the college and all the friends it has brought me including Tobias, Cameron, Dom, Coco, Verner, Helen, Ben, Joana, Tom, Helena, Emma, Alice, and numerous others. It has been such a fun social environment to escape from the PhD pressures and has enabled me to develop my interpersonal skills through various roles on the committee and I'm sure all those formals I attended must contribute somehow. Cambridge introduced me to the world of Effective Altruism for which I will be forever grateful as it has provided me a source of like-minded inspirational people and a framework by which to live my life.

I would like to thank the British Heart Foundation for generously funding this work and providing the COVID19 6-month extension. I would like to thank every single person who has ever raised money for BHF from those who participate in sporting events, to hosting charity bake sales to those such as my Granny who keep the charity shops afloat. Thanks to them I have had the most amazing experience conducting research at a world-class university to further the knowledge on heart disease and I will be forever grateful. Without them, none of this would have been possible and they should know that every single penny counts!

I would not have got to where I have today without the unwavering support and love from my boyfriend Tobias. He has been there for me from Day 1, always kind, caring and selfless, willing to do whatever I needed and more to help me out including endless massages to ease tension migraines and always providing a hot meal after intense lab days. He has helped me keep my head above water and provide endless reassurance when things got tough. He has always been up for trying out yet another restaurant and making sure we did every daytrip possible from Cambridge by foot, bike, or car.

My final thank you must go to my family for their enduring love and support and encouragement over all the years. Thank you to Mum and Dad for comforting me every time I had a wobble, believing in me when I didn't and encouraging me to always be the best I can be. To Maya, thank you for being an amazing sister and not holding your grudge against

Cambridge and not being bitter – I know that cannot have been easy. I feel so very lucky to have the most incredible, supportive family, grandparents, aunts, and uncles, and I appreciate every phone call had over the PhD years and every moment spent with them.

This PhD is in honour of Hazel. I'm sure my love of biology has to be genetic, and I wish you could see where I have got to today. You are my guardian angel always watching over me and helping me to achieve what I have. I strive to make you proud every day and live life to the fullest for you.

Contents

Glossary

ABCA – ATP-binding cassette transporter 1
AFC – antibody-forming cell
AID – activation induced cytidine deaminase
AP – apurinic/apyrimidinic
APCs – antibody presenting cell
APRIL – a proliferation-inducing ligand
AScl2 – achaete-scute complex homolog 2
AT1R – angiotensin II receptor type 1
ATF6 – activating transcription factor 6
ATLO – arterial tertiary lymphoid organ
ATP – adenosine triphosphate
ATR – ataxia and telangictasia and Rad3-related protein
BAFF – B cell activating factor
BAFFR – B cell activating factor receptor
BATF – basic leucine zipper ATF-like transcription factor
BCL – B cell lymphoma
BCR – B cell receptor
BER – base excision repair
BLIMP1 – B lymphocyte-induced maturation protein-1
BM – bone marrow
BMDC – bone marrow derived dendritic cell
BMDM – bone marrow derived macrophage
BMT – bone marrow transfer
BREG – B regulatory cell
BSA – bovine serum albumin
BTK – Bruton's tyrosine kinase
BTLA – B and T-lymphocyte attenuator
C – cytosine
CAD – coronary artery disease
CANTOS – canakinumab anti-inflammatory thrombosis outcome study
Cbl – casitase B-lineage lymphoma
CCL – chemokine ligand 2
CCR – C-C chemokine receptor
CD – cluster of differentiation
cDC – conventional dendritic cell
CDR – complementarity determining region
CFH – complement factor H
cFLIP – cellular flice-inhibitory protein
CHD – coronary heart disease
CoA – coenzyme A
CRC – CXCL12-producing reticular cell
CRP – C reactive protein
CS – class switch
CSR – class switch recombination
CSTF64 – cleavage stimulation factor
CT – PCR cycle number
CVD – cardiovascular disease
CXCR – C-X-C chemokine receptor
Da - dalton
DAMP – damage-associated molecular pattern
Dapk2 – death associated protein kinase 2
DC – dendritic cell
DMSO – dimethylsulfoxide
DNA – deoxyribonucleic acid
DOCK8 – dedicator of cytokinesis
DS – double stranded
DSB – double stranded break
DZ – dark zone
EAF2 – Ell-associated factor 2
EAS – European Atherosclerosis Society
EBI – Epstein-barr virus-induced GPCR
ECM – extracellular matrix
EDTA – ethylenediaminetetraacetic acid
EF – extrafollicular
ELISA – enzyme-linked immunosorbent assay
ELL2 – elongation factor for RNA polymerase II
ER – endoplasm reticulum
ERK – extracellular signal-regulated kinases
EYFP – enhanced yellow fluorescent protein
EZH2 – enhancer of zeste homolog 2
FA – fatty acid
FAO – fatty acid oxidation
FBS – foetal bovine serum
FCRL3 – Fc receptor-like protein 3
FDC – follicular dendritic cell
FFA – free fatty acid
FO - follicular

Foxo1 – forkhead box protein O1
FRC – fibroblastic reticular cell
FSC – forward side scatter
G – guanine
GC – germinal centre
GI - gastrointestinal
GLUT1 – glucose transporter 1
GM-SCF – granulocyte macrophage colony-stimulating factor
GPCR – G-protein coupled receptor
GSK3 – glycogen synthase kinase 3
GWAS – genome wide association study
GZ – grey zone
H&E – haematoxylin and eosin
HDL – high density lipoprotein
HEV – high endothelial venule
HF – high fat
HFD – high fat diet
HFHC – high fat high cholesterol
HIF – hypoxia induced factor
HMG - β-hydroxy β-methylglutaryl
HPRT – hypoxanthine-guanine phosphoribosyltransferase
HRP – horse radish peroxidase
IC – immune complex
ICAM – intracellular adhesion molecule
IDOL – inducible degrader of LDL
IFITM3 – interferon-induced transmembrane protein 3
IFN – interferon
Ig – immunoglobulin
IL – interleukin
iNOS – inducible nitrogen oxide synthase
IP - intraperitoneal
IRE1 – inositol-requiring enzyme 1
IRF – interferon regulatory factor
ITAM – immunoreceptor tyrosine based activation motif
ITIM – immunoreceptor tyrosine based inhibitory motif
JNK – c-Jun N-terminal kinases
KO – knock out
LDL – low density lipoprotein
LDLr – low density lipoprotein receptor
LEC – lymphatic endothelial cell
LFA – leukocyte function associated antigen
LLPC – long-lived plasma cell
LN – lymph node
LPS - lipopolysaccharide
LTB – lymphotoxin β
LV – lymphatic vessel
LXR – liver x receptor
LYVE – lymphatic vessel endothelial hyaluronan receptor 1
LZ – light zone
M-CSF – macrophage colony stimulating factor
MAML1 – mastermind-like protein 1
MAPK – mitogen-activated protein kinase
MBC – memory B cell
MBD4 – methyl-CpG binding domain protein 4
MDA – malondialdehyde-modified
MDM2 – mouse double minute 2
MEF2C – myocyte-specific enhancer factor 2C
Mfge – milk fat globule EGF and factor V/VII domain containing
MHC – major histocompatibility class
MI – myocardial infarction
MLN – mesenteric lymph node
MMP – matrix metalloproteinase
MMR – mismatch repair
MRC – marginal reticular cell
mRNA – messenger RNA
MSRN – macrophage sterol-responsive network
Mst1 – macrophage-stimulating protein
mTORC1 – mammalian target of rapamycin complex 1
MTP – microsomal triglyceride protein
MYD88 – myeloid differentiation primary response 88
MZ – marginal zone
MZM – marginal zone macrophage
NCP1L1 – Niemann-Pick C1-like 1
NFκB – nuclear factor κ-light chain-enhancer of activated B cell
NHEJ – non-homologous end joining
NOTCH2 – neurogenic locus notch homolog protein 2
NR4A1 – nerve growth factor subfamily 4 group A member 1

OCT – optimal cutting temperature compound
OG – oral gavage
OHC - dihydroxycholesterol
ORO – oil red O
OSE – oxidation specific epitope
oxLDL – oxidised LDL
OXPHOS – oxidative phosphorylation
PALN – para-aortic lymph node
PB – plasmablast
PBS – phosphate buffered saline
PC – plasma cell
PC – PHOSPHORYLCHOLINE
PCR – polymerase chain reaction
PDGF – platelet-derived growth factor
PDL2 – programmed death ligand 2
PFA – paraformaldehyde
PhD – Doctor of Philosophy
PI3K – phosphatidylinositol 3-kinase
PIP3 – phosphatidylinositol (3,4,5)-trisphosphate
PIR-B – paired immunoglobulin-like receptor B
PKB – protein kinase B
PKCβ - protein kinase C β
PLC – phospholipase C
PNA – peanut agglutinate
POLB – DNA polymerase beta
POLH – DNA polymerase eta
PP – Peyer's patches
PRR – pattern recognition receptor
RA – rheumatoid arthritis
RAG – recombination-activating gene
Rap1 – Ras-related protein 1
RBC – red blood cell
RCT – reverse cholesterol transport
RNA – ribonucleic acid
RNAPII – RNA polymerase II
ROS – reactive oxygen species
RP – red pulp
RT – reverse transcriptase
S – switch
S1P – sphingosine-1-phosphate
SAA – serum amyloid alpha
SAP97 – synapse associated protein 97
SCS – subcapsular sinus
SH2 – Src homology 2 domain
SHM – somatic hypermutation
SHP1 – Src homology 2 domain-containing protein tyrosine phosphatase 1
SLAM – signalling lymphocytic activation molecule
SLAN – 6-sulfo LacNAc
SLE – systemic lupus erythematous
SLO – secondary lymphoid organ
SLPC – short-lived plasma cell
SMC – smooth muscle cell
SMUG1 – single strand selective monofunctional uracil DNA glycosylase 1
SNP – single nucleotide polymorphism
SR-A – scavenger receptor A
SR-BI – scavenger receptor class B type I
SREBP – sterol regulatory element-binding protein
Ss – single stranded
SSC – side-scatter
STAT – signal transducer and activator of transcription
TCR – T cell receptor
TDG – thymine DNA glycosylase
Tfh – T follicular helper help
TGF – transforming growth factor
TG – triglyceride
Th1 – T helper 1
Th2 – T helper 2
TLO – tertiary lymphoid organ
TLR – Toll-like receptor
TMAO – trimethylamine N-oxide
TNF – tumour necrosis factor
TRAF2 – TNF receptor-associated factor 2
TREG – T regulatory cell
TSS – transcriptional start site
U – uracil
UNG2 – uracil DNA glycosylase 2
UPR – unfolded protein response
VCAM – vascular cell adhesion protein 1
VLA – very late antigen
VLDL – very low density lipoprotein
VSMC – vascular smooth muscle cell
WASP – Wiskott-Aldrich syndrome protein
WD – western diet
WP – white pulp
WT – wildtype
XBP – X-box binding protein

1 Introduction

This thesis focuses on the role of the germinal centre response within the context of atherosclerosis in the mouse. Atherosclerosis is a major cause of mortality globally and is driven by lipid-induced inflammation resulting in atherosclerotic plaque formation. The most prominent risk factor for atherosclerosis is elevated plasma low density lipoprotein (LDL) levels; once LDL enters vessel wall it undergoes immunogenic modifications triggering an inflammatory cascade. B cells play an important role in the response to LDL through production of antibodies against oxidised LDL and the germinal centre response by which antibodies are made, has been shown to be pathogenically involved in the process of atherosclerosis. However, the mechanisms of the germinal centre (GC) response involvement in the disease are not fully understood and must be elucidated in order to identify potential new avenues for clinical demand.

1.1 Secondary lymphoid organs

Secondary lymphoid organs are key to the production of an effective adaptive immune response as they provide an enclosed environment for the interaction of antigen-specific lymphocytes with antigen presented on antigen-presenting cells (APCs)[1]. Secondary lymphoid organs include the spleen, lymph nodes and Peyer's patches, all of which are discussed in detail below. Additionally, the bone marrow is also described due to its important role as niche for antibody-secreting plasma cells.

1.1.1 Spleen

The spleen is the biggest secondary lymphoid organ in the body and facilitates a multitude of immune functions[2]. It is unique in its separation of 2 distinct zones – the red pulp (RP) and the white pulp (WP)[1]. The RP filters the blood to recycle iron from aged red blood cells, facilitated by red pulp macrophages, and captures and clears pathogens[1], facilitated by marginal zone macrophages[3]. The WP contains B cells, T cells and APCs[1] and is encircled by innate immune cells keeping it separate from the red pulp[2]. Within the WP, B and T cell entry

is facilitated by αLβ2 and α4β1 integrins and are compartmentalised into distinct zones[2]. The movement and placement of lymphocytes within splenic microenvironments is guided by networks of stromal cells, integrins and chemokines, and allows for APC scanning[3]. Antigens larger than 60k Dalton (Da) cannot enter alone but must be transported in by marginal zone cells[2]. Splenic cell types are responsible not only for the removal of blood-borne pathogens but also for the generation of innate and adaptive immune responses against antigens[3].

1.1.2 Bone marrow

The bone marrow is encapsulated by the bone and contains extensive vasculature which forms a concentrated network of fenestrated sinusoids[4]. Associated closely with this network is the perivascular reticular cell population which ranges across the bone marrow (BM)[4]. The bone marrow is the site where B cell development occurs as well as the location that plasma cells home to where they secrete antibodies into circulation for long periods – months to years[4]. C-X-C chemokine receptor (CXCR)4-deficient B cells had reduced motility demonstrating the CXCR4 is required for B cell movement within the BM[5]. α4β1 integrin is activated by CXCR4 and plasma cell (PC) VCAM1 binding[6] facilitates rolling, adhesion, and arrest of PCs on fenestrated endothelium lining BM sinusoids[7]. Very late antigen (VLA)4, cluster of differentiation (CD)44, CD28 and CD93 are involved in the maintenance of ASCs in the BM[8]. Antibodies against VLA4 and leukocyte function associated antigen (LFA) 1 prevent PC presence within the BM demonstrating the necessity of stromal cell contact for long term PC survival[9].

1.1.3 Lymph nodes

The lymph nodes (LNs) function as part of the lymphatic circulation to filter pathogens and associated pathogenic molecules and prevent their dissemination beyond inflicted tissue[10]. Circulation of lymph plays a key role in regulating fluid homeostasis, lipid transport and immunity[11]. The lymphatic system transports lymph through lymphatic vessels from interstitial spaces to the thoracic duct and back into blood circulation[11]. Lymph travels through afferent lymphatic vessels (LVs) into LNs via high endothelial venules (HEVs)[12] and

encounters the subcapsular sinus (SCS) before draining via cortical sinuses into the cortex and medullary sinuses into the medulla and leaves by the efferent LVs[12]. Lipid, antigen, protein and immune cells are all transported in this manner[12]. Molecules that are less than 70kD gain entry to the LNs via conduits[13] that span from the SCS to HEVs located where B cells enter into LNs[14]. Molecules larger than 70kD undergo proteolysis upon arrival at LN to enable movement to the follicle[13].

The SCS is a specialised region in which SCS macrophages and marginal reticular cells (MRCs) sample antigen from the lymph and transport them to B cells in a complement-dependent manner[15]. The medulla contains MRCs which provide support to plasma cells (PCs) to maintain their population[15]. SCS macrophages capture antigen by extending their cytoplasmic protrusions into the sinus to sample lymph[16] and present to follicular B cells which routinely migrate to the subcapsular region and lower their velocity enabling macrophage interaction[17]. SCS macrophages have limited endocytosis capacity thus leaving antigen intact on the cell surface[16] and aid in the antibody affinity maturation process by continuously delivering antigen[18]. Depletion of SCS macrophages impairs B cell activation highlighting the crucial role of these macrophages[16].

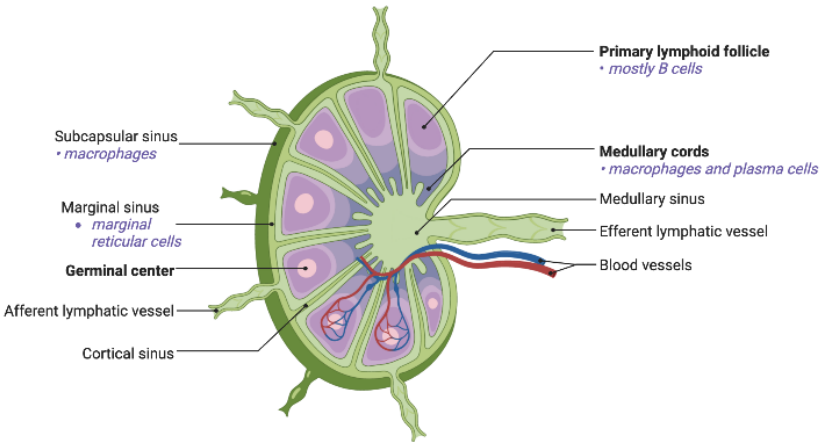

Figure 2. ***Structure of the lymph node.*** *Lymph travels in via the afferent lymphatic vessels into the subcapsular sinus where subcapsular sinus macrophages sample lymph for antigen to present to B cells. Marginal reticular cells within the medulla provide support to plasma cells. Lymph drains via cortical sinuses into the cortex and medullary sinuses into the medulla before exiting via the efferent lymphatic vessels. Created using BioRender.com template made by Akiko Iwasaki, PhD and Ruslan Medzhitov, PhD.*

The Ras-related protein 1 (Rap1)-RAPL-macrophage-stimulating protein (Mst)1 axis is key to LFA1-dependent B cell arrest on endothelial cells which is essential to B cell homing into peripheral LNs[19]. CXCR4 and the C-C chemokine receptor 7 (CCR7)-chemokine ligand 21

(CCL21) interaction[20] promote lymphocyte entry into LNs[21]. CYP7B1 is essential in the generation of Epstein-barr virus-induced GPCR (EBI)2 ligand within LNs which is needed for EBI2-mediated B cell migration to inter- and outer follicular regions[22]. CD8 dendritic cell (DC) HSD3B7 activity inhibits 7α25-dihydroxycholesterol (OHC) and sustains EBI2 ligand gradients critical to B cell transport within LNs[23]. Cortical sinuses protruding into the B cell follicles express lymphatic vessel endothelial hyaluronan receptor 1 (LYVE-1) which aids in lymphocyte egress[21]. Lymphocytes exit the LNs in a sphingosine-1-phosphate (S1P) signal dependent manner which is produced by LECs[12].

Within LNs, memory B cells are located in the outer B cell follicle, mainly restricted to the subcapsular region[24]. In this location, memory B cells can interact frequently with SCS macrophages to hunt for antigen[25].

The creation of new lymph vessels, lymphangiogenesis, has been linked with atherosclerosis as the adventitial lymphatic density is increased and is positively associated with intimal thickness[11]. Transport of aortic lymph is compromised during atherosclerosis and contributes to the progression of the disease[11].

1.1.4 Peyer's patches

As Peyer's patches (PPs) are in direct proximity to commensal microbiota from the gut, they have a greater population of B cells, around 80% of all cells, than LNs with around 30% B cells[21]. HEVs of PPs mediate entry of lymphocytes from circulation through expression of CXCL13 which encourages attachment of B cells[13]. To enter the PPs, B cells require α4β7 integrin and mucosal addressin cell adhesion molecule-1[21] as well as CXCR4-CXCL12[20]. Additionally, CXCR4 encourages B cell transit through PPs as demonstrated by the accumulation and overrepresentation of CXCR4 knock out (KO) B cells compared with wildtype (WT) B cells in PPs[21]. Meanwhile, CXCR5 promotes B cell retention in PPs as deficiency in CXCR5 results in reduction in B cell population in the PPs after 18h[21]. Furthermore, B cells spend less time in PPs, around 10hrs, than in LNs, around 16hrs[13]. To emigrate from the PPs, B cells require S1PR1 and endothelial cell-produced S1P[21].

1.1.5 ATLOs

Arterial tissue lymphoid organs (ATLOs) are lymphoid structures which coordinate local B cell immunity during atherosclerosis[26] and are formed in the lamina adventitia of the abdominal aorta[27]. Tertiary lymphoid organs (TLOs) augment B cell activation and differentiation and enable local memory B cell (MBC) or PC differentiation[10]. B cells within the aorta can be found in ATLOs and the proximal draining LNs[26]. Local formation of a lymphoid structure enables communication between atherosclerotic lesions and cells within the ATLO, including GC B cells as well as memory B cells and PCs[26], via the medial vascular smooth muscle cell (VSMC) layer[27]. ATLOs enhance B1 and B2 cell recruitment into the arterial wall[26] enabling local B cell differentiation and maturation[28]. B1 cells within ATLOs locally secrete immunoglobulin (Ig) M[28] demonstrating that these structures are sites of functional B cell responses[29].

1.2 B cells

B cells fortify immune barriers for pathogen evasion, remove pathogens which have breached said barriers and supply immunological memory[10]. B cells continuously produce antibodies, secrete cytokines and can carry antigens within lymphoid tissues[10]. This section comprises the development of the B cell lineage, its regulation, production of the B cell receptor, B cell subsets and B cell metabolism.

1.2.1 B cell development

B cells start to form from extra-haematopoietic precursors in the yolk sac at embryonic day E7 and then from haematopoietic precursors in the foetal aorta-gonad-mesonephros region, foetal liver and post-natal BM[10]. The earliest B cells derived from the foetus are B1 cells while B2 cells mainly develop post-natally[10]. B cells circulate within the foetus by week 12 of gestation and independent foetal IgM responses have been detected at week 24[10]. B1 cells gather in the peritoneal and pleural cavities 2 weeks after birth and are highly receptive to innate stimuli and harbour sentinel function[10]. Final maturation occurs when transitional B

cells enter the spleen[30] where they undergo selection which results in autoreactive B cell elimination[10]. The B cell repertoire diversifies with age[10].

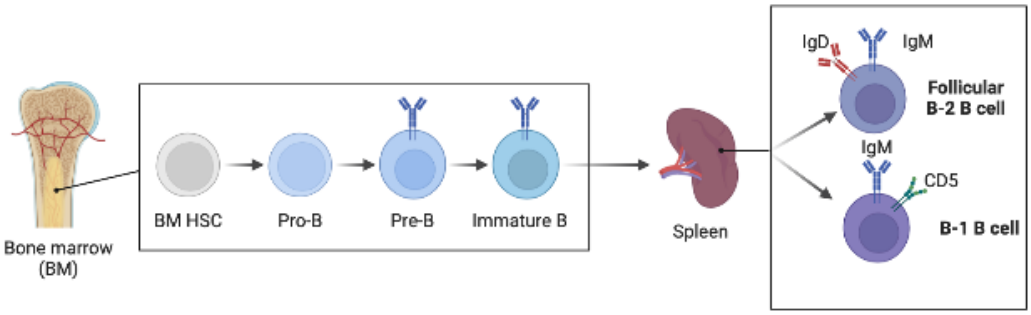

Figure 3. ***B cells develop from precursors in the bone marrow and undergo differentiation through pro-B and pre-B to form immature B cells.*** *These cells travel to the spleen where they undergo final maturation into B1 and B2 cells. Created using BioRender.com template made by Akiko Iwasaki, PhD and Ruslan Medzhitov, PhD.*

Immunoglobulin gene rearrangement during differentiation generates the pre-B cell receptor (BCR) and mature antigen-binding BCR[31]. The recombination process is dependent on RAG1 and RAG2 which bind recombination signal sequences either side of each gene segment[32]. Pro-B cells undergo IgH chain D and J gene rearrangement on both alleles with further rearrangement of the upstream V gene afterwards[33] on one allele only[34]. If this produces a non-functional BCR, the second allele will also be subject to VDJ recombination[34]. At the pre-B stage, $V_HD_HJ_H$ recombination triggers formation of the pre-BCR (IgM) whereby the newly synthesised heavy chain is tested for light chain association fitness at the first checkpoint[35]. The first instance of antigen detection is when pre-B cells initially express immunoglobulin light chain genes which can assemble with the heavy chain to form membrane-bound IgM[36]. The pre-BCR has autonomous signalling capabilities and can be activated by self-antigens within the BM[37]. Pre-BCR signalling enables early B cell maturation and initiates light chain gene rearrangement[37]. Signalling through the pre-BCR temporarily suppresses recombination-activating gene (RAG) expression[38] prohibiting the occurrence of 2 heavy chains with different specificities within one cell[33]. The second checkpoint involves examination of the heavy chain for autoreactivity and once passed, IgM is expressed as the BCR on immature B cells[39]. It is vital that the final BCR does not exceed a certain signalling threshold otherwise RAG expression and function will continue to rearrange light chains of the V genes[38].

VDJ recombination is intrinsically random, thus producing some self-reactive or non-productive antibodies[36]. The outcome of RAG-dependent recombination of the V, D and J

genes expands immunoglobulin diversity to recognition of $5x10^{13}$ molecules[40]. These BCRs can be replaced through continuation of light chain rearrangement or undergo apoptosis if self-reactivity is detected[36]. Autoreactive B cell clonal deletion occurs at the immature B cell stage[33] and is dependent on Bim. At the third checkpoint, autoantigen is presented and those BCRs with high affinity, i.e. autoreactive immature B cells, are deleted, around 85%[39], in a Bim-dependent manner[41]. Those BCRs with low affinity are positively selected for BM exit[39] and migration and maturation in secondary lymphoid organs (SLOs) into marginal zone (MZ) B cells or mature follicular B cells[10].

Interleukin (IL) 7R is essential to the formation of pro-B cells as it stimulates proliferation via protein kinase B (PKB) pathway-induced phosphatidylinositol 3-kinase (PI3K) expression[42], expansion and expression of CD19 and Pax5[43]. Signalling via pre-BCR dampens IL7 signalling preventing the clonal expansion of pre-B cells[44]. Large pre-B cells become unresponsive to IL7 signalling and move to low IL7 concentrations enabling their exit from the cell cycle and development into pre-B cells[44]. IL7-mediated signal transducer and activator of transcription (STAT)5 activation causes Ccnd3 activation which encodes cyclin D3 and is necessary for pro- and pre-B cell proliferation[42].

1.2.1.1 Regulation of B cell development

Pax5 is expressed solely by the B cell lineage and is key to B cell commitment and development[45]. It binds to numerous sites within the deoxyribonucleic acid (DNA) of follicular B cells enabling initial commitment of lymphoid progenitors to the B cell fate[8] by modulating the BCR, CD19, CD21, Bach2, interferon regulatory factor 4 (IRF4), IRF8 and SpiB[8]. Through use of histone modifying complexes to remodel the chromatin, Pax5 facilitates active chromatin at gene targets, including transcription factors downstream of BCR signalling, and represses chromatin at all other sites (i.e. non B lineage genes)[45]. Pax5 favours class-switch recombination (CSR) to IgG1 through induction of open chromatin at the IgG1 promoter and activation of its transcription[45]. Loss of Pax5 results in B cell gene downregulation and upregulation of non-B cell genes thus converting B cells into T cells via dedifferentiation[45]. Pax5-deficient follicular (FO) B cells are reduced in number and longevity partly due to

defective PI3K signalling[45]. Furthermore, the MZ B cell and B1a cell populations are lost along with the GC and PC populations[45].

Interferon-induced transmembrane protein 3 (IFITM3) is critical for affinity maturation in B cells and is induced by the activity of the PI3K pathway[46]. BCR engagement results in SRC-facilitated Y20 phosphorylation of IFITM3 causing a build-up of IFITM3 at the plasma membrane[46]. Here, IFITM3 has a scaffold function for LYN and CD19 to allow for BCR signal amplification[46]. IFITM3 augments PI3K signalling by upregulating phosphatidylinositol (3,4,5)-trisphosphate (PIP3) and facilitating PIP3 integration into lipid raft signalling complexes[46]. This IFITM3-dependent enhancement of PI3K signalling is necessary for rapid proliferation of high affinity B cells[46].

CCL2 is key in the homeostasis of peripheral B cells[47]. CCL2 modulates BCR signalling and actin reorganisation facilitated by dedicator of cytokinesis (DOCK)8-Wiskott-Aldrich syndrome protein (WASP) through MST-mammalian target of rapamycin complex (mTORC)1[47]. This prevents BCR clustering at the plasma membrane and consequent BCR signalling[47]. CCL2 prevents MZ and GC B cell differentiation by decreasing the activity of the PI3K-AKT-mTORC1 metabolic signalling pathway[47].

B cell activating factor (BAFF), expressed on macrophages and follicular dendritic cells (FDCs)[48], prevents spontaneous apoptosis in naïve mature B cells and requires BAFF receptor (BAFFR) to transduce survival signals within B cells[49]. The level of BAFF determines the population of mature B cells as it regulates the entry of immature B cells into the mature B cell population[49].

MTor plays a key role in B cell differentiation and function as it is critical for the development from early pro B cell to the immature small pre-B cell stage[51]. MTor deficiency in pre-B cell progenitors results in a B cell developmental block leading to the absence of immature and mature B cell populations[51]. B cells deficient in mTOR showed blunted proliferative capacity and elevated levels of apoptosis as well as defective antibody responses[51].

IL21R expression increases progressively with B cell maturation and its expression is augmented by toll-like receptor (TLR) and CD40 activation[52]. IL21 enhances survival and proliferation of activated B cells which respond to antigen and acquire T cell help[52]. The cytokine prevents proliferation and induces apoptosis of B cells that receive non-specific BCR signals[52].

Deficiency in complement factor H causes strong BCR signalling which results in dysregulated splenic B2 cell development[53]. Additionally, complement factor H (CFH) KO results in uncontrolled complement activation and disrupted spleen architecture[53]. Furthermore, absence of CFH results in autoreactivity of GCs and PCs, spontaneous GC formation, increased numbers of GC B and T follicular helper (Tfh) cells as well as PCs and plasmablasts (PBs) in spleen and LNs[53]. Thus, CFH deficiency encourages B cell autoimmunity through elevated BCR signalling with augmented double stranded (ds)DNA autoantibody levels[53].

1.2.2 BCR

Individual B cells have unique BCRs, comprised of duplicate light and heavy chain assembly, which are cell surface bound immunoglobulins containing unique epitope binding sites for antigen attachment[30]. The BCR is part of a signalling complex containing B220, CD19, CD22, CD79a (α chain) and CD79b (β chain) which transduces signalling via mitogen-activated protein kinase (MAPK), nuclear factor κ-light chain-enhancer of activated B cell (NFκB) and PI3K[30]. The antigenic specificities of the BCRs are determined by the complementarity determining region (CDR) regions of the Ig heavy and light chains with CDR-H3 providing the most diversity and functioning as a highly antigen-specific loop[54].

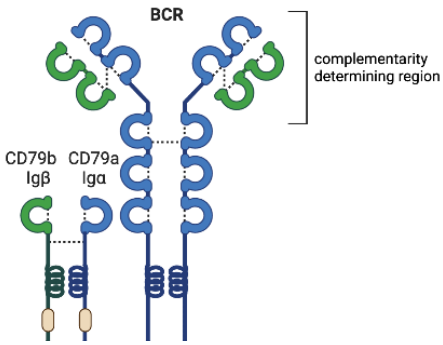

*Figure 4.**B cell receptor is composed of duplicate light and heavy chains along with CD79a and CD79b for signalling.** The complementarity determining region is responsible for the antigen specificity of each individual BCR. Created using BioRender.com template made by Akiko Iwasaki, PhD and Ruslan Medzhitov, PhD.*

In resting mature B cells, the BCR is isolated from cholesterol rafts while antigen-induced crosslinking of the BCR facilitates its recruitment to rafts[55]. Antigen engagement activates the BCR and triggers the BCR signalling cascade inducing immunoreceptor tyrosine based activation motif (ITAM) phosphorylation by LYN[56]. Through the Src homology (SH)2 domain, SYK is recruited to the phosphorylated Igα-Igβ heterodimer[56]. SYK activation enables the BCR signal to be transduced via BLNK-associated proteins[56]. The BCR signalling cascade enables BCR signalosome reorganisation and antigen internalisation, loading of antigen onto major histocompatibility class (MHC)II, increased gene transcription for survival and cell cycle entry, B cell migration to the T:B border and increased expression of MHCII, co-stimulatory molecules and chemokines to enhance the B-T cell interaction[10].

SHP-1 is an important inhibitor of BCR signalling by binding immunoreceptor tyrosine based inhibitory motif (ITIM)-containing receptors – CD22, CD72, FcγRIIb, Fc receptor-like protein (FCRL)3 and paired immunoglobulin-like receptor (PIR)-B[57]. This is critical as excessive BCR signalling can cause elevated levels of apoptosis in the extrafollicular (EF)-derived PC population[57]. The absence of SHP-1 within the GC enables greater levels of Syk phosphorylation leading to upregulated signalling in GC B cells and consequently, their death[57]. Mechanistically, CD22 and CD72 limit antigen-induced phosphorylation of extracellular signal-regulated kinase (ERK)1 and ERK2 for IgM and IgD isotypes[58]. This is not the case for IgG isotypes likely due to the presence of the IgG cytoplasmic tail[58]. Through inhibiting BCR signalling, CD22 prevents GC B cell apoptosis and promotes their survival and selection[59].

CD45 is a protein tyrosine phosphatase that augments antigen-mediated signalling and is needed for pro-survival molecule expression[60] in B cells by inducing Src family kinase members[61]. CD45-induced Syk signalling induces B lymphocyte-induced maturation protein-1 (Blimp1) and Irf4 transcription[61] and, thus, is critical for the production of a normal ASC population[60]. Indeed, high CD45 phosphatase activity defined a high affinity subset of PC precursors within the GC[61]. Thus, CD45 acts as an identifier of cells which have received T cell help via CD40L connecting BCR affinity with phosphatase activity and PC differentiation downstream[61]. Deletion of CD45 in B cells results in dysregulation of Src family kinase

activity, blockade of B cell maturation at the T2 transitional stage in the spleen[60] and autoantibody production and autoimmunity ensue[61].

1.2.3 B cell subsets

B cells can be categorised into two main lineages – B1 and B2 cells. The B2 cell lineage can be further defined into subsets based on function and include follicular B cells and marginal zone B cells. It is still unclear to which lineage B regulatory cells belong to. Each subset is described in detail below.

1.2.3.1 B1 cells

The naturally occurring antibody repertoire of B1 cells is based on evolutionary key epitopes[62] that are infection independent[30]. B1a cells are produced from foetal liver and neonatal progenitor cells while adult precursor cells tend to produce B1b cells only[30]. B1 cells are positively selected for self-antigen recognition[10]. They monitor mucosal surfaces providing a first line defence against pathogens and an initial source of antibody[30]. B1 cells can rapidly differentiate into short-lived plasma cells (SLPCs) and MBCs in response to infection[10]. The majority of circulating IgM is B1-derived[10] and B1 cells majorly contribute throughout life to IgA+ PB populations within the intestine[10]. B1 cell PD-L2 expression dampens T cell production of IL5 thus inhibiting B1 cell ability for ASC differentiation and consequent antibody production[63].

Siglec-G is an inhibitor of the B1a cell population by dampening BCR signalling[64]. Deficiency in Siglec-G in LDL receptor (LDLr) KO causes the proliferation of the B1a cell population along with elevated IgM levels especially those against oxidation-specific epitopes (OSEs)[64]. In KO mice, atherosclerotic plaque size is reduced by 50% characterised by decreased number of macrophages and reduced necrotic core area[64].

1.2.3.2 B2 cells

B2 cells develop from BM precursors resulting in maturation from immature B cells to follicular and MZ B cells in the spleen[30]. BAFF interaction with BAFFR is critical for the maturation of B2 cells[65]. BM-derived c-Myb is a key effector of atherosclerosis through its expression in B cells where it supplies survival and proliferation signals to B2 cells[63].

1.2.3.3 Follicular B cells

Follicular B cells migrate to lymphoid follicles and can recirculate between follicular organs[10]. NFκB subunits p50 and p65 influence follicular B cell fate and BAFF is required for follicular B cell differentiation[31]. Follicular B cells bind antigen coupled to complement or antigen-antibody complexes via complement receptors and carry the antigen to FDCs[10]. Upon antigen uptake, follicular B cells increase CCR7 expression, migrate to the T:B border and secrete CCL4 to attract T cells[10]. Upregulation of CXCR5 on T cells, as occurs in T follicular helper cells, enables T cell migration to the T:B border[10]. Follicular B cells interact with T follicular helper cells and differentiate into GC B cells which go on to form the GC reaction[30].

1.2.3.4 Marginal zone B cells

MZ B cells secrete large amounts of IgM[66] and harbour polyreactive BCRs enabling rapid differentiation into PBs[10] upon recognition of blood-borne pathogens[67]. They can transport antigens into the follicle[30] for FDC antigen presentation[10] within a T cell-dependent immune response[66]. MZ B cell differentiation is dependent on neurogenic locus notch homolog protein (NOTCH)2 signalling[30] as Notch2 engages PDL1 which triggers Notch2 cleavage enabling Notch2 migration to the nucleus[31]. In the nucleus, Notch2 engages mastermind-like protein 1 (MAML1) and RBP-Jκ transcription factors triggering MZ B cell fate commitment[31]. Through NFκB activation, BAFF-BAFFR engagement provides survival signals to MZ B cells[31].

MZBs must be in the marginal zone to induce and sustain SIGN-R1 expression on marginal zone macrophages (MZMs)[68]. These SIGN-R1+ MZMs require MZBs to trigger the production of molecules needed for capturing antigens within the spleen[68].

Within the low S1P concentration of the follicle, MZBs rescue S1PR1 expression enabling their migration back to the MZ resulting in shuttling action[20]. MZ B cells are important in the promotion of GC B cell differentiation[69].

1.2.3.5 B Regulatory cells

B regulatory cells (Bregs) secrete anti-inflammatory cytokines such as IL10, IL35 and transforming growth factor (TGF)β and can dampen the activity of T helper (Th)1 and Th2 cells preventing proinflammatory cytokine secretion[71] and antigen presentation by macrophages[72].

1.2.4 Metabolism

Downstream signalling from the BCR via the PI3K-AKT pathway elevates glucose transport 1 (GLUT1) expression increasing glycolysis in B cells[37]. Once activated, B cells increase lactate secretion and oxygen consumption using both glycolysis and oxidative phosphorylation[73]. Increased mitochondrial mass and respiratory capacity boost B cell energy supply enabling them to carry out heightened demands exerting their effector functions[37]. High expression of protein kinase C β (PKCβ) due to BCR-mediated PI3K signalling increases c-Myc activity and consequent mTORC1 metabolic activity which endorses the transcription of proliferation genes enabling a proliferative burst from B cells[74]. A deficiency in PKCβ reportedly reduced mTORC1 activation in B cells impairing metabolism and leading to reduced formation of GCs and generation of PCs[75]. Inhibition of glycolysis, acetyl-coenzyme A (CoA) synthesis or mitochondrial respiration impairs B cell proliferation and survival[73].

1.3 Germinal centre

A major role of B cells is the secretion of antibody and the ability to form immunological memory. These capacities are developed in the germinal centre. The GC reaction generates high affinity class switched antibodies secreted from PCs and long-lived memory B cells through an iterative process of somatic hypermutation (SHM) and proliferation rounds[30]. The

process selects for mutants with higher antigen affinity and enables a diversified response from single clones up to families of clones which differ by various mutations from the parent cell[76]. GC B cells can either differentiate, undergo apoptosis or enter into another round of selection and SHM[76]. The GC produces 2 populations of antibody-forming cells (AFCs) – short-lived PBs which seed the spleen and long-lived PCs which inhabit the BM[76].

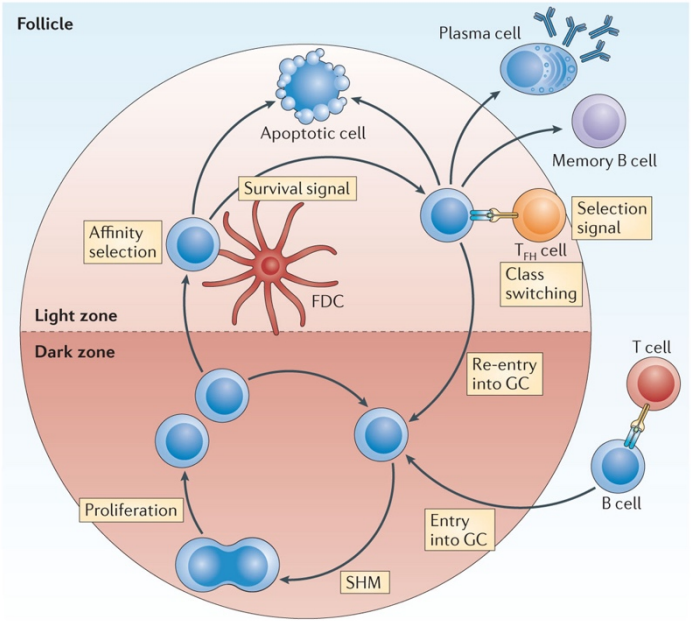

Figure 5. ***The germinal centre response.*** *A B cell is activated by antigen presented on a T cell triggering entry into the GC. GC B cells undergo SHM and proliferation within the DZ before migrating to the LZ to test antigen affinity against immune complexes captured on FDCs. If GC B cells fail this test, they undergo apoptosis. Cells that pass the test present their antibody to antigen on Tfh cells which provide survival and positive selection signals to those of appropriate affinity. These cells can either differentiate into plasma cells and memory B cells and leave the GC or re-enter the DZ to undergo further rounds of SHM and proliferation. Diagram from Heesters et al. doi:10.1038/nri3689.*

Naïve B cells are primed for rapid GC induction and respond to activation signals by homing to the desired lymphoid organ[77]. Naïve B cells express $CXCR5^{hi}CCR7^{lo}$ promoting chemotaxis toward FDC-produced CXCL13[49]. Antigen-coupled follicular B cells reduce their velocity by half that of naïve B cells[78].

Within 6 hours of antigen interaction, activated B cells migrate to the follicle perimeter guided by CCR7 and react to T zone stromal cell production of CCL21 and CCL19[79]. CCR7 is upregulated by antigen binding, correlated with antigen affinity[48], and directs migration of activated B cells towards an EBI2/CXCR5/CCR7 gradient located between the T and B cell border zone[80]. Antigen-engaged follicular B cells downregulate S1P within 6 hours to prevent lymphoid tissue exit and retain the cells at a location where T cells can encounter them[78]. Interactions between B and T cells within the T-B zone leads to BCR engagement-induced[81]

upregulation of EBI2 which guides activated B cells to the outer follicle areas where they start their initial proliferation[80]. The antigen-BCR interaction is critical in determining whether an activated B cell enters the GC reaction or rapidly differentiates into a PC in an extrafollicular reaction[57]. BCR occupancy is the sum of antigen concentration and BCR affinity with antigen concentration controlled by negative feedback[57]. The B cells present peptide-MHC complexes to specific CD4 T cells and receive activation signals critical for B cells to proceed further in the GC response[82].

Low affinity cells fated for a GC response lose EBI2 expression and induce Tfh cell differentiation[48]. Antigen encounter stimulates B cell lymphoma 6 (BCL6) expression through myocyte-specific enhancer factor (MEF)2C[83] and is key to the formation of B-T conjugates before commitment to the GC[84]. BCL6 inhibits S1PR1 and EBI2 expression thus elevating S1PR2 expression to confine B cells within the GC[85]. The concentration of S1P is highest at the GC boundary forcing GC B cells to reduce their speed and, thus, stay within the GC[14].

Thus, the CCR7: CXCR5 ratio is higher maintaining high affinity B cells in the outer follicle away from the GC developing in the inner follicle[48]. Those B cells with high CCR7, indicating high affinity due to strong interaction with the antigen, are poised to undergo PC differentiation and prevent Tfh differentiation[48] enabling the EF response and providing the early antibody production phase[57]. These cells retain EBI2 expression which also helps to maintain localisation in the outer follicle[48].

EBI2 is critical for supporting CD4 T cell and B cell proliferation as well as early GC and PC production in response to blood-borne antigens[86]. High expression of EBI2 is found in naïve B cells which is further augmented upon B cell activation[87]. EBI2 facilitates B cell migration, in conjunction with 7α25-HC and CCR7[79], towards the periphery of follicles particularly to EF regions[49] of lymphoid organs[86]. Downregulation of EBI2 induced by BCL6 expression[81], while maintaining CXCR4 and CXCR5 expression, is a necessary step enabling GC cells to migrate into the central follicular areas, associated with the FDC network[80], for the GC process[87]. If EBI2 expression remains high, GC B cell differentiation is blocked[49]. EBI2-deficient B cells are no longer able to localise to the outer follicle, instead favouring the centre of the follicle colocalising with FDCs[81] thus displaying defective migration within the GC[49]. EBI2 deficiency

causes diminished EF PB[49], PC and CD4 DC numbers and consequent blunted antibody production while overexpression of EBI2 leads to augmented antibody responses[87]. A single nucleotide polymorphism (SNP) in the Ebi2 promoter has been associated with inflammation of the heart[88].

The formation of the dark zone (DZ) and light zone (LZ) requires lymphotoxin β (LTB) and tumour necrosis factor (TNF)α production by activated B cells[15]. Binding CXCL13 at the B cell surface instigates a positive feedback loop enhancing LTB expression by B cells[15]. IL21 facilitates the kinetics of zone formation within the GC by determining the ratio of LZ to DZ GC B cells partly through promoting LZ GC B cell migration to the DZ[89]. The GC architecture provides a unique situation in which mitogenic stimuli are separated from the proliferation they induce[90].

The LZ contains FDCs, Tfh cells, stromal cells as well as GC B cells[82]. Only the B cells which compete for antigen successfully and can present antigen for Tfh cell engagement are able to undergo further rounds of proliferation[10]. Peptide-MHCII complexes travel via the actin cytoskeleton to the cell membrane where they cluster to acquire T cell help[91]. Tfh cell help to GC B cells is delivered through repeated frequent rapid cell-cell contacts, the duration of which increases after positive selection[92]. MHCII-mediated antigen presentation by B cells triggers intracellular Tfh calcium release enabling CD40L localisation to the cell surface[48]. BCL6 regulates the delivery of T cell contact-dependent help through modulating antigen-induced calcium signalling genes in T cells[93]. Through CD40L, Tfh cells engage the CD40 receptor on B cells inducing growth and proliferation signals, augmented by IL21[48], via Myc and mTOR[82]. IL21 enhances GC B cell proliferation by increasing S6 and AKT phosphorylation downstream of BCR engagement[89] leading to phosphorylation of cell cycle proteins[94]. IL21 increases CD86 expression on B cells enhancing T cell costimulatory capability[95]. Through upregulation of Blimp1 and Bcl6, IL21 triggers activation-induced cytidine deaminase (AID) expression, modulates isotype class switching to IgA and IgG and promotes PC differentiation[52]. Deficiency of the IL21 receptor dampens T-dependent antibody production reducing total and specific immunoglobulins[95]. MYC is induced synergistically by CD40 and BCR activation[96]. As a result of CD40L engagement with CD40 on the B cell surface, NFκB p65 and p52 pathways are activated[97] and B cell survival and proliferation is promoted[98]. The interaction is vital for

T cell-dependent B cell differentiation and consequent results including GC differentiation, memory cell and PC generation and class switching[99]. IRF4 is induced immediately following CD40 or BCR stimulation and is critical to the instigation of the GC by triggering the expression of OBF1 and Bcl6[85]. Dampening of CD40 signalling, via TNF receptor-associated factor 2 (TRAF2) phosphorylation, alters balance of IRF4 to BCL6 in favour of BCL6 promoting cells towards the GC identity[100].

Higher affinity BCRs allow B cells to present more antigen resulting in more CD40L expressed on the Tfh cell surface leading to stronger CD40 signalling[48]. Thus CD40 signalling influences cell fate[101]. CD40 engagement triggers ICOSL surface expression on B cells activating ICOS on Tfh and elevating Tfh cell calcium signalling[48]. GC B cell and Tfh cell encounter keeps cells in the LZ for up to 12hrs followed by DZ migration which can last for several days[76]. Tfh cell signal strength, and thus quantity of the presented antigen, provided in the LZ determines the degree of Myc upregulation and the number of cell divisions which take place[102] as well as the duration spent in the DZ[103]. As c-Myc levels are diluted with each cell division, GC B cells can only undergo a further 2 rounds of cell division[90] before they must migrate back to the LZ for cognate antigen interaction to initiate another cycle of selection[75]. Thus, the T cell interaction seems to set an intrinsic timer determining the number of cell divisions in the DZ hence regulating clonal expansion and affinity maturation[103].

Signalling lymphocytic activation molecule (SLAM) family members are critical to restrain GC expansion and augment T-cell dependent antibody responses[104]. The proteins dampen the T cell receptor (TCR) signal strength to avoid excessive stimulation of Tfh cells thus limiting the activation of GC B cells[104]. Death-associated protein kinase 2 (Dapk2) is an inhibitor of T cell help in the context of GC formation through blocking T cell interaction with cognate antigen-presenting B cells by preventing Raptor-induced mTORC1 functions[105]. GC formation is increased when T cells are deficient for Dapk2 through the enhanced conjugate formation of B and T cells while Dapk2 overexpression resulted in reduced number of T-B contacts[105].

In the presence of high levels of Tfh help, lower affinity GC B cells can be positively selected[106]. NUR77 is induced by antigen stimulation in lymphocytes[107] and its transcription is directly proportional to the affinity and concentration of antigen encountered by the BCR when T cell

help is limited[108]. NUR77 is expressed by GC B cells undergoing selection in the LZ[109] and facilitates BCR-induced B cell apoptosis thus restricting B cell proliferation[108]. Through this mechanism, NUR77 limits clonal immunodominance in early GCs[109] in this way allowing lower affinity B cell clones to compete in the GC reaction[109].

CCL22 is upregulated on B cells after BCR or CD40 stimulation which augments the provision of help from CCR4+ Tfh cells[110]. The degree of CCL22 expression reflects the extent of Tfh cell help received by the GC B cell and correlates with the cellular antigen affinity[110]. This implies that CCL22 acts as a marker of affinity which Tfh cells can detect at distance[110]. The interaction between CCR4 and CCL22 enables an increased contact frequency between antigen-specific B and T cells to enhance GC formation[110]. Deficiency in CCL22 results in defective Tfh cell help leading to reduced cellularity of the GC and PC pool along with compromised affinity maturation[110]. Thus, CCL22 is key in enhancing positive selection within the GC through creation of a positive feedback loop recruiting additional T cell help to those cells which have already undergone positive selection[110].

10-30% of GC B cells at one time and up to 50% of GC B cell clones every 6 hours undergo apoptosis[106] due to active negative selection or failed positive selection[76]. Negative selection of GC B cells occurs to those with antigen affinity that does not pass a certain threshold[106]. Failed positive selection is either due to an inadequate BCR affinity or inactivating BCR mutations producing a defective BCR[76]. B cells with defective BCRs have defective migration[106] and are fated to undergo apoptosis by tingible body macrophages[10]. Some GC B cell clones that have self-reactivity are permitted to survive so long as they simultaneously have affinity for foreign antigen[106]. In the LZ, Bcl6 inhibits Bcl2 causing high rates of apoptosis within GC B cells facilitating affinity-based selection[92]. Due to rapidly declining levels of cellular flice-inhibitory protein (cFLIP), GC B cells undergo apoptosis without requiring death signals[111]. Interaction with FDCs or CD40 signals can prevent apoptotic pathways through sustaining cFLIP expression levels[111].

Ell-associated factor 2 (EAF2) is an apoptosis initiator with high expression in GC B cells partly via regulating the Bcl2 family gene expression[112]. EAF2 plays a role in inhibiting antibody responses by removing autoreactive GC B cells which is essential to avoid autoimmunity[113].

In Eaf2 KO mice, GC B cells have increased survival rates resulting in larger GCs and an increased memory B cell population along with elevated antibody responses including self-reactive antibodies[113]. A blockage of apoptosis results in the accumulation of autoreactive antibodies and an autoimmune phenotype[113]. Caspase 9 facilitates the removal of GC B cells through apoptosis but maintains the GC B cell homeostasis by preventing excessive necroptosis[114].

Follicular B cells transport immune complexes through follicles to be captured by FDCs[15]. B cells test their BCR affinity on an antigen captured by FDC through force application using myosin II motors through a specialised GC synapse[115]. GC B cells use myosin contractility transducing pulling forces[116] to extract antigen by applying short repetitive bursts of force followed by endocytosis[117]. Antigen binding induces BCR clustering, aggregated in ezrin-rich and F-actin pod-like structures[116] on the smooth membrane surface which is equipped with clathrin lattices[91], within lipid rafts. An immunological synapse is formed between the GC B cells and antigen-presenting surface[118]. This is proceeded by clustering of antigen and its transport towards the middle of the synapse[115]. The actin structures also facilitate spreading of GC B cells, by enlarging the contact zone between B cell and APC and mediating their attachment[118]. WASp is a critical component as it produces and maintains actin structures which provide support to sustain membrane protrusions in the middle of the synapse[117] thus enhancing cell spreading and BCR clustering leading to greater BCR activation[118].

The casitase B-lineage lymphoma (Cbl) proteins are necessary for the B cell's ability to uptake and process antigen via the BCR in order to present it for T cell help as they control BCR-mediated antigen endocytosis and trafficking to lysosomes by ubiquination of CD79A and CD79B in BCR complexes[119]. The Cbl proteins determine the entry and proliferation of B cells within the GC[119]. Cbl proteins regulate affinity maturation of antibodies, through positive selection of high affinity GC B cells during the GC process, and total antibody production[120]. Cbls enhance ubiquitination and consequent degradation of IRF4 in GC B cells thus maintaining the GC state and preventing progression to the PC fate[120]. Double KO of Cbl and Cbl-b in mice results in a reduced MZB cell population, Tfh cell population, GC B cell population and PC population along with a defective quantitative and qualitative antibody response to immunisation[119].

B cell activation induces MHCII recruitment to lysosomes and endosomes[91]. MHCII is acidified through a Syk-dependent mechanism which enables the extraction and proteolytic processing of antigen[91]. Thus, they signal more strongly via the BCR and acquire more antigen to present to T cells[118]. Antigen internalisation facilitated by the BCR dictates the fate of B cell responses by regulating the number and repertoire of MHCII-loaded molecules presented to T cells[121].

Positive selection is the process by which cells compete for FDC-deposited antigen[106] resulting in the expansion of progressively higher affinity B cell clones through reduced apoptosis and increased proliferation[76]. BCR signalling triggers the expression of anti-apoptotic factors increasing the chance of GC B cells gaining selection signals from T cells[76]. Positive selection signals from T cells reduce the length of time spent in S phase and result in quicker cell cycles[111] leading to increased proliferation in the DZ[76]. Myc expression, induced by positive selection activation of mTORC1[122], is protective against apoptosis[123] and stimulates the cell cycle[102]. C-Myc is essential for the initiation and maintenance of the GC[124].

mTORC1 signalling is essential for CD40-dependent positive selection of GC LZ B cells[75] as well as enhancing stable T-B interactions and GC initiation[105]. Positively selected GC B cells express both MYC and MIZ1[96] which form a transcriptional repressor complex[85]. The complex suppresses MIZ1 target genes promoting cell cycle entry of GC B cells receiving T cell help[85]. The complex represses MBC genes thus preventing MBC differentiation and enabling DZ re-entry, further affinity maturation[74] and PC differentiation[96]. Positively selected LZ GC B cells strongly express CD69 after BCR or CD40 stimulation[125]. Antigen interaction stimulates IRF4 expression in LZ GC B cells and those with highest affinity will differentiate into PCs with Tfh cell help[116]. Genes involved in activation, i.e. c-Myc and mTORC1, BCR and CD40 ligation are strongly upregulated in LZ B cells[92]. Forkhead box protein O1 (Foxo1) is blocked by BCR signalling in the LZ preventing Foxo1-induced activation of cyclin D3 and therefore preventing proliferation[126]. In the LZ, CXCR5 and CXCL13 are key chemoattractants for GC B cells[127].

Once positively selected, 10-30% of LZ GC B cells[128] transition from G1 to S phase and migrate, with the help of REL[83], to the DZ promoted into cell cycle by IL21[48]. Driven by NFκB signalling, REL can induce IRF4 and MYC expression and is essential to GC maintenance through

enhancing metabolic pathways supporting cellular proliferation[74]. Signalling via PI3K and AKT using Syk-dependent pathways, BCR signalling modulates the DZ to LZ transition in a Foxo1-dependent manner[129]. CXCR4 is necessary for maintaining a subset of GC B cells in the DZ[130]. Additionally, CXCR4 is required for the separation of the DZ and LZ as CXCR4 inhibition resulted in altered organisation[131]. Syk is important for regulating the cyclic re-entry process within GCs as its degradation limits the duration of BCR signalling enabling B cell migration into the DZ[132]. If Syk is not degraded, signalling is prolonged facilitating the differentiation into PCs[132].

In the DZ, successfully mutated B cells (centroblasts) undergo proliferative G2 and M phases[90]. BCL6 represses p53 and p21 transcription to prevent cell cycle arrest and apoptosis enabling many rounds of proliferation within the DZ[48]. In the DZ, GC B cells enter the cell cycle twice as much as they do in the LZ through Tfh cell enhanced DNA synthesis rate during S phase[92]. Per cell division, there is on average 1 mutation[76] and daughter GC B cells can inherit antigen complexes[102]. Thus they maintain the ability to recruit T cell help[102]. Activity of mTORC1 is dose-dependent and, therefore, decreases exponentially with each round of cell division[122]. Cell cycling within the DZ is critical for the production of clonal bursts which are responsible for the proliferation of high affinity B cell clones[90]. In the DZ, GC B cells undergo apoptosis due to deleterious BCR rearrangements[111]. The activity of AID introduces these insertions, deletions or stop codons within the BCR genes[123]. Bcl6 inhibits DNA damage sensor expression i.e. ataxia and telangictasia and Rad3-related protein (ATR) and p53, thus improving B cell tolerance to DNA breaks induced by SHM[92]. GC B cells replace their antigen receptors after SHM within the DZ which prevents the build-up of non-functional BCRs and enables selection within the LZ[133].

Foxo1 is a key transcription factor involved in the regulation of GC DZ cell differentiation, class switching and affinity maturation[129]. Furthermore, Foxo1 suppresses the LZ program[92]. Late in the cell cycle, S phase and mitosis gene expression is confined to DZ B cells[92]. Glycogen synthase kinase (GSK)3 controls proliferation programs including reactive oxygen species (ROS) formation and mitochondrial synthesis[74]. Phosphorylated Gsk3 can be found in c-Myc+ GC B cells and is vital for the maintenance of the GC B cell and PC populations[134]. This suggests that Gsk3 inactivation is critical to the formation of PCs from positively selected GC B cells[134].

DZ GC B cells upregulate CXCR5 to allow for LZ chemotactic migration[135] helped by IL4[48]. By decreasing CXCR4 and the DZ gene expression program alongside a simultaneous increase in LZ-associated genes, cells are able to migrate into the LZ[83].

Recently, a new zone has been described within the DZ, termed the grey zone[18]. The LZ, DZ and grey zone (GZ) are transcriptionally unique with specific epigenetic landscapes[136]. The grey zone is the major site for proliferation within the GC while the DZ is responsible for differentiation[136]. GC B cells that are selected in the LZ migrate into the grey zone to divide and proliferate and then move into the DZ for differentiation[136]. The GZ acts as a checkpoint to remove any cells that were not positively selected in the LZ before proliferation occurs[136].

MYC is key to cellular proliferation, it induces the expression of cyclin D2 and D3 which promote the cell cycle[85]. MYC also triggers E2F1 expression which induces enhancer of zeste homolog 2 (EZH2) and this promotes GC B cell proliferation through inhibiting cyclin-dependent kinase inhibitors[85]. Cyclins D2 and D3 drive proliferation within B cells; cyclin D3 is critical for the expansion of pre B cells in the BM while cyclin D2 facilitates mature B cell proliferation[126]. Cyclin D3, regulated by BCR signalling, is critical for the proliferation of GC B cells within the DZ[126] and dose-dependently determines the number of cell divisions to be undertaken in the DZ[90] following transient c-Myc induction via Tfh signals[111]. Cell division rates within the GC are rapid averaging 4-6 hours with up to a third of cells in the cell cycle at any one time[123].

Leukocyte emigration from lymphoid organs occurs via G protein coupled receptor (GPCR)-facilitated active cell migration followed by reverse transmigration across endothelial cell layers[5]. The process is highly dependent on S1P which is highly concentrated in circulation and found at low concentrations within the lymphoid organ interstitium[5].

The rate of emigration is predicted to be low; around 0.01% for PCs and 2% for memory B cells[123]. In the centrocyte to memory cell transition, expression levels of genes associated with proliferation, DNA metabolism and activation returned to levels seen in naïve B cells suggesting that memory B cells become quiescent[77]. Anti-apoptotic, cytokine responsiveness and chemotaxis genes were upregulated[77]. Polyreactivity of B cells is greater in the GC than

in the naïve B cell pool but is subsequently eliminated once within the memory compartment[137]. Soluble antibodies can feedback positively or negatively to the GC reaction[111].

1.3.1 AID

Activation-induced cytidine deaminase (AID) is the lynchpin of the GC response vital in the creation of highly diverse antibody repertoires through regulating class switching and somatic hypermutation. The AID enzyme is composed of 198-210 amino acids[138] and is a DNA mutating enzyme key to the instigation of SHM in the BCR[30] and CSR of C_H genes[139]. Pax5 augments AID expression and its downregulation during PB differentiation suppresses AID[10]. Aicda messenger RNA (mRNA) transcription is triggered synergistically by IL4 and CD40 signalling through Stat6 and NFκB induction[140]. Lipopolysaccharide (LPS) can bind to TLR4 and crosslink BCRs; it uses both pathways to stimulate AID transcription by inducing NFκB p52 recruitment to the AID promoter and p65 to an upstream enhancer element[140]. Its expression is augmented by STAT6-dependent IL4 and IL13[141]. Achaete-scute complex homolog 2 (Ascl2) is specifically expressed in GC B cells and enhances GC B cell proliferation and antibody production through control of AID expression[140].

AID targeting to immunoglobulin genes is strong[138], functioning on single stranded (ss)DNA structures created as a result of a transcription bubble or in R loops[138]. AID attachment to immunoglobulin genes is dependent on interaction with RNA polymerase II (RNAPII) and Spt5 located downstream of transcriptional start sites (TSSs)[142]. AID recruitment is also aided by the RNAPII associated polymerase associated factor[142]. AID-induced mutations amass at a rate of 1 in 1000 base pairs per cellular generation, approximately a million times higher than the genome-wide baseline mutation rate[92]. AID preferentially targets WRCY motifs[92].

The activity of AID is required to eliminate autoreactive B cell clones through genotoxic stress and apoptosis induction[141]. AID triggers SHM and CSR by inducing damage at cytosines producing deoxy-uracil (deamination) which stimulates the base excision repair (BER) and mismatch repair (MMR) pathways[143] thus escaping faithful DNA repair instead triggering

mutagenic DNA repair[143]. The BER and MMR processes use low fidelity DNA polymerases which introduce small insertions, deletions and point mutations all of which adjust the antibody affinity[144].

In AID-deficient mice, class-switched antibodies are nearly absent and there is hyperproliferation of the GC B cell population, partly due to reduced apoptosis rates[145], including expansion of autoreactive B cell clones[146].

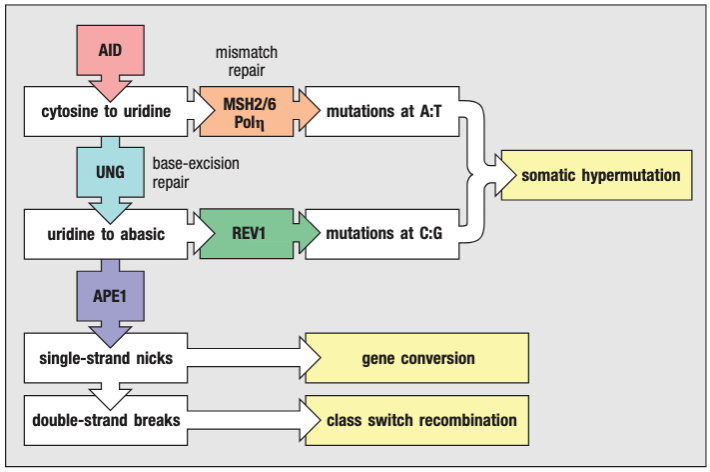

Figure 6. ***The mechanism of action for AID.*** *AID converts a cytidine to a uridine within immunoglobulin genes. Use of mismatch repair causes mutations at A:T using MSH2/6 Poln results in somatic hypermutation while base excision repair using UNG removes the uridine base while REV1 will synthesise a new base forming in mutations at C:G which results in somatic hypermutation. APE1 will produce single stranded nicks from an abasic site which will be converted to double stranded breaks enabling class switch recombination. Diagram from p414 Janeway's Immunology, 9th Edition.*

1.3.1.1 The role of AID in class switching

CSR is a region-specific intrachromosomal looping recombination[143] process involving the exchange of constant immunoglobulin heavy chains[141]. In this way, it changes the antibody isotype, the receptors it can interact with and thus its effector functions[141]. Activation of AID expression by T-dependent or independent stimuli through NFκB induces CSR as the primary stimuli[147]. Secondary stimuli, i.e. cytokines, are necessary for determining the target isotype switch[140] and enable BCR activation beyond the minimal threshold resulting in metabolic activity[74]. Without this secondary signal, B cells will undergo apoptosis as a consequence of mitochondrial dysfunction[74]. Prior to the establishment of the GC, B cells exhibit a brief period of AID enabling CSR to mark the appropriate isotype onto the responding B cells[148]. Class-switched B cells are produced by day 2.5, corroborating the finding that CSR occurs before the GC reaction[149].

The antigen-binding variable region of IgH and IgL is in the NH_2 terminus while the COOH-terminus of IgH harbours specialised antibody effector functions[150]. The process of CSR reassembles the IgH gene to excise the Cμ/Cδ coding exons and replace them with alternative coding exons Cα, Cε or Cγ[151]. Replacement of heavy chain constant region creates an antibody with the same specificity but different effector function[152].

The target region for AID-induced mutations is between 200-1500 base pairs downstream of the transcriptional start site and spans to the intronic J sequence-containing regions[153]. Switch (S) repeat regions are upstream of the constant coding exons (except Cδ)[151] at the 5' end of the IgH locus[144]. They have G:C rich[150] DNA sequences which promote transcription-mediated R loop generation[150]. These single-stranded DNA structures are composed of palindromic AGCT sequences[150] which are the ideal target for AID[144]. Localisation of AID to these regions is dependent on the spliceosome[151].

AID converts the cytosine (C) base to a uracil (U) base by deamination and repair mechanisms result in a single stranded break which is converted into a double stranded break via MMR[143] within preceding donor and proceeding recipient S segments[151]. Double-stranded breaks (DSBs) are ligated through non-homologous end joining (NHEJ) and the region between each S region is eliminated as a circular extrachromosomal DNA fragment[151] thus resulting in intrachromosomal DNA recombination[140].

BER is triggered by the recognition and eradication of damaged bases by DNA glycosylases producing apurinic/apyrimidinic (AP) sites[143]. APs are extremely mutagenic and have to be processed by AP endonucleases[143]. The process produces single-stranded DNA nicks which are converted into DSBs[143]. MMR begins as the mismatch is recognised by MutS homolog heterodimers[143]. MuTL homolog 1 and homolog 2 heterodimers and exonuclease 1 are recruited to remove the damaged base[143]. DNA polymerases are then recruited to synthesise the missing DNA[143].

DNA glycosylases recognise and remove the damaged DNA base[143]. Uracil DNA glycosylase (UNG)2 is the major glycosylase to remove U bases and can act on single and double stranded

DNA[143]. Meanwhile thymine DNA glycosylase (TDG) and methyl-CpG binding domain protein (MBD)4 act on double stranded DNA and single strand selective monofunctional uracil DNA glycosylase 1 (SMUG1) on single stranded DNA[143]. UNG is needed for the generation of DSBs in immunoglobulin S regions where it replaces damaged U bases with DNA nicks[143]. APE2 creates DSBs in the S region during CSR[143]. DNA polymerase β (POLB) can repair AID-generated DNA nicks in the S region thus preventing CSR[143]. DNA ligase III seals nicks in short-patch BER while DNA ligase I functions in long-patch BER[143].

During an immune response, cytokines, in combination with T cell help[154], initiate C_H gene transcription resulting in specific antibody isotype production[150]. Cytokines activate transcription of particular isotypes by binding upstream germline promoters which contain cytokine-responsive elements[155]. CSR needs 2 rounds of cell division to switch to the IgG isotype[140]. IgG2a/c antibody production is driven by interferon (IFN)γ Th1 lymphocytes while IgG1 and IgE responses are driven by IL4-producing Th2 lymphocytes[149] and TGFβ promotes switching to IgG2b and IgA[140]. In conjunction with TGFβ, LPS stimulates high titre levels of IgG2b while CD40L induces high titre levels of IgA[155]. Intrinsic TLR7 signalling in B cells is important for isotype switching to IgG2b and IgG2c whilst also augmenting SHM and antibody diversity[156].

1.3.1.2 The role of AID in SHM

SHM occurs predominantly during G1 concurrently with a peak in transcriptional activity[102] and up to 40% of DZ GC B cells can be involved at any one time[102]. AID facilitates the process of SHM[157] whereby point mutations are inserted into the V, D and J regions of the immunoglobulin light and heavy chains, the antibody variable region, at a high frequency enabling positive selection of immunoglobulin mutants with higher affinity for antigen[158]. AID deaminates U bases in recombined VDJ segments[151] resulting in a dU: dG mismatch which triggers the MMR pathway to form nicks in the DNA[40] and carry out error-prone repair to drive SHM[151]. MMR recruits error-prone DNA polymerase ε (POLH) which mutates A and T bases, UNG causes transversion of C and guanine (G) bases and MBD4 removes Ts from T:G mismatches and Us from U:G mismatches[143].

1.3.2 GC kinetics

Moderately autoreactive follicular B cells can be found in SLOs prepared to react to foreign antigen[54]. These cells are the product of strong tonic BCR signalling during development and lessening of tonic signalling through IgD expression maintains this cell state[54]. Polyreactive antibodies are involved at the start of an immune response using their ability to bind a variety of viral and bacterial antigens enabling effective neutralisation and opsonisation of the pathogen[54]. Within 1-2 days after immunisation, B cells that capture antigen are found at the border of the T zone[159]. The interaction between an antigen-coupled B cell and a T helper cell that have non-cognate antigen specificity typically lasts for under 10 minutes[78]. The engagement of B and T cells with cognate antigen specificity, augmented by BCL6 upregulation via integrins[83], form longer-lasting connections anywhere from 20 minutes[78] to over an 1hr in some cases[82]. The interaction between a Tfh and a GC B cell is shorter, seldom over 10 minutes[82]. At day 4 after immunisation, GC precursors begin to proliferate and polarise with complete segregation into the light and dark zones[160] by day 7[84]. GC B cells tend to move around their zone following random walk patterns while occasionally migrating to the other zone[82]. The migration from the DZ to the LZ happens quickly as 50% of DZ B cells enter the LZ over 4-6 hours while the opposite trip is much slower with only 10% of LZ GC B cells having arrived at the DZ within 6 hours[82].

Newly formed GCs are seeded by tens to hundreds of founder B cell clones[161] making it highly oligoclonal[162]. At GC initiation high antigen concentration allows GCs to be tolerant in selection of lower affinity cells early in positive selection process within the LZ[163]. This allows both low and high affinity clones to survive[159]. Later on in the response, antigen concentration is limited thus B cell clonality diminishes over time[82] with only the highest affinity B cells surviving[159]. These cells undergo clonal burst, periods of strong positive selection, characterised by intensive proliferation[82]. Intraclonal competition is the evolution of lower affinity clones being replaced by higher affinity clones over time[164]. Interclonal competition enables immunodominance and is responsible for the global specificity and clonal diversity of an antibody response[82]. Multiple clones are output from the GC with divergence towards high affinity over the evolution of the GC response[30]. The GC response modifies the B cell

repertoire through expansion of more diverse B cell clones producing MBCs which can in turn, feed back into EF responses[10].

Affinity maturation is the product of many individual GC reactions occurring concurrently and independently[82]. Affinity maturation occurs through simple alterations in the CDRs of IgHV region enabling cells to quickly gain neutralising function[162]. By generating diversity in GCs, pools of B cells are available which recognise similar but different epitopes enabling secondary immune responses and the ability to react to viral mutants[162]. Clonal diversity is created by allowing low, moderate and high affinity receptors to survive within the GC whilst the mean antibody affinity is always improving over time[162]. IgM B cells predominate the output of early GCs but wane as the response continues[147]. High affinity IgG B cells are maintained within the GC to a greater extent than high affinity IgM B cells[147]. IgG GC B cells underwent cell cycle division at a greater rate and had a greater frequency in the DZ than those of IgM isotype[147]. Within GC clones, around half produced only 1 cell type output (i.e. plasma cell OR memory) demonstrating that antigen affinity influences cell fate choice[124]. However, the other half of clones gave rise to both PCs and memory cells[124]. The probability of a clone having multiple fates was strongly associated with clone size[124].

In the nascent stages of GC development, an expansion phase is undertaken which primarily consists of lymphocyte proliferation proceeded by a contraction phase[165] due to differentiation, emigration and apoptosis[166]. As the GC reaches its peak, an equilibrium between apoptosis and proliferation is achieved which can be maintained for weeks or months depending on the context[76]. Over the course of an immune response, the GC size and number of cells within the LN decreases signifying that the extent of the GC response has influence on the total cell population of the lymphoid organ[167].

The repertoires of PCs tend to have higher frequencies of SHM than those of MBCs as PCs are produced later in the GC response when the average GC B cell has higher BCR affinity[76] while MBCs are produced early in the response and tend to be lower affinity[8]. The clonality of the GC and memory compartments display limited overlap with 90% of GC B cells and only 6% of memory cells deriving from expanded clones[166].

Upon rechallenge, secondary GCs are almost entirely seeded with precursors with no prior GC experience[82] displaying rates of SHM much reduced compared to those cells derived from the primary GC[165]. Only a small subset of primary GC-derived dominant MBC clones are recruited into a secondary GC response[92] and contribute considerably to the PC output[165]. This subset contains cells with high germline affinity thus showing that the initial VDJ rearrangement of a clone is the deterministic factor for whether that MBC participates in a secondary GC recall response[165]. IgG1 memory B cells have a high proclivity to differentiate into PCs within the secondary response[168]. During secondary immunisation, plasma cells and memory B cells with identical CDR3 sequences have been identified in the blood demonstrating that secondary memory B cells and plasma cells have a shared clonal relative[169]. The majority of memory cells produced in the secondary immunisation reaction continue to divide and participate in further SHM rounds[169]. Thus, the SHM burden and clonal diversity of secondary GCs reflects that of early primary GCs rather than the product of established primary GCs[165]. Chronic infection causes GC B cell responses with increased cell numbers and sustained PC, antibody and MBC production for a longer period than that of acute infection[170].

1.3.3 Stromal cell control of GC

The GC is a highly complex microenvironment which critically depends on the correct positioning of cells and the ability for cellular interaction with antigen. Stromal cells enable antigen transport, lymphocyte travel and coordinated interactions with DCs, Tfh, B cells and macrophages[93]. Stromal cells are the main producer and quencher of EBI2 within lymphoid organs[23]. Lymphatic and vascular endothelial cells facilitate lymphocyte entry and exit from LNs[22]. Fibroblastic reticular cells (FRCs) produce BAFF to sustain primary B cell follicular structure[22]. CXCL13 FRCs are restricted to medullary cords and B cell follicles and facilitate B cell migration and the formation of the follicle[15]. CXCL12-producing reticular cells (CRCs) facilitate GC B cell shuttling between light and dark zone via CXCR4/CXCR5 chemotaxis[22]. CXCL12 facilitates communication between reticular cells and B cells to remodel the FDC network within the GC thus determining the effectiveness of the GC response by directing B and T cell interactions[125]. The FDC and CXCR cellular networks increase to allow zonal formation within the GC[22].

The induction of the FDC population is dependent on B cell-derived LTα1β2 occurring after the appearance of B cells within follicles[171]. CXCL13-producing FDCs enable B cell localisation and are key to GC function[22]. Using their long slender processes FDCs form a network throughout the GC through which lymphocytes can travel freely[172]. FDCs secrete chemokines which retain lymphocytes in the GC to aid in cellular organisation as well as the GC reaction itself[172].

FDCs within the LZ express high complement, CD21, CD35[135], Fc receptor levels and genes important in intracellular stiffness which support GC B cell antigen sampling[15]. FDCs capture antigen using CR1/2 and/or FcγRIIB depending on the nature of activation and complement protein availability[173]. FcγRIIb expression is increased on FDCs following creation of the GC and contributes to FDC immune complex (IC) capture capacity[174] in a non-degradative fashion[78]. IC engagement by FDCs stimulates IL6 production, augments AID production and affinity maturation[172]. ICs acquired by FDCs are quickly internalised taking around 36 minutes and reappear on the FDC surface for approximately 21 mins[173]. ICs can undergo numerous rounds of cycling within FDCs whilst a significant quantity of antigen remains intact[173]. FDCs can maintain antigen on their cell surface for long periods enabling B cells to scan the network of FDCs for antigen[135]. Cycling is beneficial as it enables antigen redistribution on FDC surface which can augment the GC reaction resulting in a greater total volume, lifespan and increased PC output[173]. Additionally, FDCs enhance B cell migration increasing the B cell chance of antigen encounter[171]. GC B cell integrins αLβ2 and α4β1 bind intracellular adhesion molecule (ICAM) and VCAM respectively which are upregulated on FDC processes[175] by IC deposition via a FcγRIIb-dependent mechanism[176].

FDCs maintain the centre of the B cell area with low EBI2 production capacity which enables EBI2-mediated segregation of B cells of the inner and outer follicle[23]. Within follicles, FDCs upregulate CXCL13 and BAFF to maintain the LZ and secrete milk fat globule EGF and factor V/VII domain containing (Mfge)8 and IL15 to augment SHM and IgG production as well as providing support for B cell proliferation[22]. Expression of IL4Ra on FDCs is important in limiting IL4 availability within the GC thus encouraging GC B cell differentiation and affinity maturation[177].

Murine spleens contain a set number of FDC clusters that are assembled prior to immunisation and is unchanged by microbiota or chronic inflammation[136]. Pre-existing GC B cells must be removed from FDC niches in order to begin a new GC response[178].

1.3.4 Microenvironment and Metabolism

Thanks to the rapid proliferation and poor vascularisation[179] which occurs in the GC, the microenvironment (mainly LZ[140]) is hypoxic and nutrient poor[180]. Hypoxia enhances antibody class switching[181] towards IgG1 and plasma cell differentiation[182]. Consequently, hypoxia induced factor (HIF)1α levels are upregulated in GC B cells[181] and HIF1α increases expression of glycolytic enzymes in GC B cells[75]. GC B cell hypoxia is inversely correlated with the rate of proliferation and positively correlated with the rate of apoptosis[181] as demonstrated by increased apoptosis and reduced GC B cell and PC populations that accompany HIF1α deficiency[130]. Furthermore, the deficiency resulted in a defective antibody response due to impaired CSR[130].

B cells must increase their glycolytic rate to enable proliferation and antibody production[181]. Low oxygen concentrations within the LZ stimulates a high glycolytic rate and LZ GC B cells are enriched in genes required for glycolysis and hypoxia[51]. Glycolytic gene expression peaks during the transition from LZ to DZ and is linked with G1 to S phase transition[183]. Selection signals conferred by T cells stimulate cMyc and mTORC1 leading to increased cellular mass which in turn determines the number of cell divisions the cell will partake in within the DZ[73]. mTORC1 activates PI3K[73] inducing key transcription factors for GC B cells as well as class switching gene targets[184]. mTORC1 activation induces a pathway involving ribosomal production and anabolic cell proliferation in positively selected cells once they enter the DZ[122] which is critical to maintain rapid cell division rates[85]. Proliferative DZ GC B cells are non-glycolytic showing very low glycolytic extracellular acidification rate and minimal glycolytic reserve[185]. Glycolysis related pathways are downregulated and instead they use mitochondria to facilitate oxidative phosphorylation[179] and indeed mitochondrial mass is increased[179]. Through this process, GC B cells rely on oxidising endogenous and exogeneous sources[179] of

long chain fatty acids, in mitochondria and peroxisomes for energy requirements[82]. This reliance increases as GCs mature[75].

OXPHOS and fatty acid oxidation (FAO)[51] gene expression peaked in the DZ and was associated with G2 and M cell cycle phases[183]. The OXPHOS and FAO pathways were increased in higher affinity GC B cells that had undergone greater levels of proliferation[183]. Elevated OXPHOS activity during an immune response can enhance affinity maturation by promoting positive selection of high affinity B cell clones[183]. Increased mitochondrial mass predisposes activated B cells to undergo CSR while reduced mitochondrial mass favours PC differentiation[37].

1.3.5 Regulation of germinal centre

Regulation of the GC is vital to enable smooth coordination of the various cell types involved in the response and to decide the fate of each GC cell based on antigen experience and affinity. This section details the functions of 3 key regulators of the GC programme – BCL6, IRF4 and CD40.

1.3.5.1 BCL6

BCL6 is a master regulator of the GC gene programme[186]. It inhibits genes involved in signalling through CD40 and BCR, PC differentiation, cell cycle and DNA damage response[186]. Bcl6 expression is essential for GC maintenance enabling affinity maturation while preventing premature activation[186]. BCL6 regulates gene expression for B cell activation, survival and cell cycle arrest[187]. NFκB signalling following BCR activation is vital for GC formation[178] as it modulates expression of IRF4 and BCL6[84]. IRF4 triggers Bcl6 expression by binding to a transcriptional start site 24kB[17] upstream of the Bcl6 promoter[83]. IRF8 triggers Bcl6 transcription through a complex with PU.1 and maintains GC B cell survival by inducing mouse double minute (MDM)2[85]. Bcl6 is downregulated upon PC and memory B cell differentiation through suppression of IRF4 which is stimulated by CD40-mediated induction of NFκB[187].

1.3.5.2 IRF4

Low levels of IRF4 stimulate Bcl6 transcription, GC B cell differentiation and suppression of PC fate[188] through transcription of Aicda, OBF1 and Bcl6[158]. In contrast, high levels stimulate Prdm1 transcription, PC differentiation and suppression of GC B cell fate[188]. Haploinsufficiency of IRF4 results in defective affinity maturation, impaired Blimp1 expression and reduced capacity to recruit T cell help[188]. IRF4 deficiency severely reduces GC cell generation as IRF4 regulates the differentiation of early antigen-specific GC B cells[189].

1.3.5.3 CD40

Binding of CD40 to its ligand CD40L triggers receptor trimerization and TRAF recruitment stimulating CD40 signalling[190]. The CD40 cytoplasmic tail has 2 TRAF-binding domains with the proximal region binding to TRAF6 and the distal region binding TRAF2 and TRAF3 and indirectly TRAF5[98]. CD40 can activate the NFκB, c-Jun N-terminal kinase (JNK) or MAPK pathway depending on the TRAFs recruited[191]. CD40 signalling triggers JNK and p28 which induce expression of JUN and JUNB to promote the GC response[85]. Through activation of the canonical NFκB pathway, CD40 can induce c-Myc in a Syk-dependent manner[95]. CD40 ligation in GC B cells suppresses AKT and ERK pathways[129] markedly blunting PI3K signals[76]. CD40 signalling lengthens the duration of proliferation in B cells prolonging their survival[192]. However with increased number of cellular divisions the phenotypic plasticity of B cells reduces while likelihood of differentiation increases[192]. CD40 deletion in the B cell population results in reduced levels of atherosclerosis and GC populations[193].

1.3.6 Extrafollicular responses

Although the majority of plasma cells are producing in the GC reaction, there is an initial wave of PBs produced upon antigen recognition in the extrafollicular regions of the spleen. EF responses are essential for the neutralisation and opsonisation of pathogens driving humoral immunity while the GC response shapes the peripheral B cell pool[10]. EF responses augment pre-existing antibody responses and are the main eliminator of infections[10]. High affinity B

cells favour an EF response, through suppression of BCL6 and induction of IRF4, which occurs in splenic bridging channels or LN medulla[48]. In the EF response, proliferation and survival signals come from IL6 and a proliferation-inducing ligand (APRIL) produced by DCs and macrophages[48]. EF B cells can generate PBs[49] producing IgG and IgA through CSR[48] but affinity maturation cannot occur[30].

1.4 Memory B cell differentiation

The memory B cell is one of 2 fates a GC B cell can differentiate into. Memory precursors are quiescent, show signs of somatic mutation and have elevated expression of survival proteins i.e. Bcl2[128]. Low levels of T cell help (weak CD40 signalling[101]) in low affinity GC LZ B cells, negatively associated with Bach2[194], result in increased Bach2 expression and suppression of mTORC1-facilitated metabolism and c-Myc-induced cell growth[195] thus poising these cells to become MBCs[85]. Bach2 haploinsufficiency prevents memory B cell development, instead skewing toward PC differentiation[168]. These cells congregate at the edge of the LZ[128] and are characterised by reduced S1PR2 and Bcl6 expression and elevated expression of CCR6, CD38[196] and EBI2[197]. Downregulation of Bcl6 is a key step toward memory differentiation[195] enabling MBC precursors to efficiently exit the GC[85].

Memory B cells give the immune system the ability to respond much more rapidly and specifically if a pathogen is seen multiple times[30]. Memory B cells are produced throughout the course of an immune response[198] and mutated cells accumulate over the course of primary immune response into the memory subset[199]. The peak of MBC production occurs early during a GC response when clonal diversity is at its peak before the majority of affinity maturation has taken place thus providing a highly diverse repertoire for the MBC population[200]. Consequently, most memory cells don't share clonality with the dominant clones produced by a mature GC[201]. Memory B cells reside at sites of antigen drainage and pathogen entry[128] i.e. splenic marginal zone and BM, with the spleen as the preferred location for long-lived memory cells[202] enabling detection of pathogens which have breached both skin and lymph node barriers[128]. As memory B cells tend to exhibit lower antigen affinity and

reduced rates of SHM, they have broader reactivity for a wide range of pathogens[85] compared to PCs[203] and provide protection against pathogens and potential variants[204].

The transcription factor Hhex acts in GC B cells to induce MBC differentiation by binding Tle3[106] and dampening c-Myc activity[200]. Furthermore, Hhex can modulate the responsiveness of MBCs to antigen re-exposure[196]. Tfh cells provide IL9 which promotes the differentiation of GC B cells to memory B cells[197]. Increased expression of key survival genes e.g. Bcl2, and proliferative genes e.g. cyclin E2, can be found in memory B cells along with reduced expression of cell cycle inhibitors e.g. p21, KLF4 and KLF9[25]. The signalling pathway for Bmpr1a is consistently expressed in memory B cells enabling the self-renewal capacity of this cell type[24]. Long-lived memory B cells have an elevated mitochondrial respiratory capacity and can use catabolic metabolism to use nutrients in the TCA cycle and use adenosine trisphosphate (ATP) produced via OXPHOS to ensure long term survival[185].

MBCs can be identified by CD38, B220, CD19 and CD95/GL7/peanut agglutinase (PNA) markers in mice[205]. After immunisation, B cell CD80 expression, dependent on strong Tfh-induced CD40 signals[204], is increased significantly representing a memory subset[202]. Memory cells have increased MHCII, CD95, CD62L and CD73 compared to naïve B cells[199]. Programmed death ligand (PDL)2 is upregulated in memory B cells[199] and over time, the number of MBCs positive for PDL1 increases[206].

MBC subsets in mice are characterised by differential expression of CD73, CD80 and PD-L2[195]. $CD80^{+}PD\text{-}L2^{+}$ MBCs are poised for PC differentiation upon recall while $CD80^{-}PD\text{-}L2^{-}$ MBCs participate in the GC response[207]. $T\text{-}bet^{-}$ and $T\text{-}bet^{lo}$ MBCs originate in SLOs and travel freely through the circulation while $T\text{-}bet^{hi}$ MBCs are produced and confined in the spleen[207]. $T\text{-}bet^{-}$ and $T\text{-}bet^{+}$ MBCs arise from a common ancestor but diverge after antigen experience and remain as separate independent MBC pools[207]. Those CD80+ cells with low CD35 expression were characterised as a mutated memory population as they had high mutation load whereas those with high CD35 expression comprised an unmutated memory cell subset[199].

Upon antigen rechallenge and recognition from subcapsular sinus macrophages, MBCs proliferate and differentiate either into PCs or GC B cells[208]. Memory B cells generated early

in the GC response function as evolutionary templates for SHM and selection in secondary GCs where they cultivate high affinity BCR repertoires[201]. MBCs have a lower threshold for activation, expansion and antibody secretion than naïve B cells do[194]. This enables them to respond more sensitively and quickly to secondary infection[194]. MBCs can recognise a variant epitope and can expand in response to secondary challenge without the need for SHM[209]. Tissue-resident high affinity $CD80^{hi}$ IgG MBCs exhibit high mutational load[210] and are poised to produce rapid ASC responses while recirculating $CD80^{lo}$ IgM MBCs[194] display high V region germline identity[210] and will re-enter the GC upon secondary challenge[209]. MBCs can enter the GC as a source of increased diversity and serve as a higher affinity starting point for the GC reaction[76].

Memory PCs are dependent on contact via $\alpha4\beta1$ integrin VLA-4 and $\alpha L\beta2$ integrin LFA-1 with stromal cell ligands VCAM1 and ICAM1[206]. The cell-cell contact induces the PI3K/AKT signalling pathway resulting in the downregulation of FOXO1 and FOXO3, key requirements for memory PC survival as well as preventing caspase activation hence providing mitochondrial protection[9]. Bach2 suppression is an important part of the increased predisposition of memory B cells to differentiate into ASCs after antigen re-exposure[177]. Memory PC survival is also dependent on BAFF and APRIL as if these are blocked, PCs are absent from the BM[9].

1.5 Plasma cell differentiation

The plasma cell is the second of the two fates that beholds a germinal centre B cell. PCs are defined by downregulation of CD19, IgM, IgD and B220 and upregulation of CD138[200]. Plasma cells produced from follicular B cells are long-lived while those derived from B1 cells, MZ B cells or the EF reaction are short-lived[30]. PBs are proliferative ASCs which secrete lower antibody levels than PCs and tend to be short-lived[211]. PBs retain CD19 expression and occupy a state between activated B cell and fully differentiated PC[211]. SLPCs tend to be short lived and of lower antigen affinity while long-lived plasma cells (LLPCs) are produced later in the GC reaction after undergoing rounds of SHM thus providing higher antigen affinity and increased longevity[211].

Only GC B cells with high antigen affinity are chosen to complete PC differentiation[9] - increased signalling BCR strength is directly proportion to IRF4 expression which predisposes GC cells to PC differentiation[17]. Strong T cell help and CD40 signalling[101], via positive selection, result in IL4 and IL21 production which encourages PC differentiation of LZ B cells and aids with migration into and through the DZ[106]. PC precursors within the LZ have been identified as $Bcl6^{lo}CD69^{hi}$ with enriched expression of IRF4 and c-Myc and display high affinity BCRs[212]. GC genes are downregulated in these cells including Bach2, S1pr2 and Efnb1 while PC and IRF4 target genes[213] are upregulated[212]. A Blimp1+ cell subset within the GC has high rates of proliferation and are primed for the PC cell state[214]. PC precursors are enriched in the CD23- LZ GC B cell population and temporarily express MYC enabling cell proliferation into PBs[215]. IgG GC B cells have a higher propensity to differentiate into PCs than IgM GC B cells[102].

Short-lived PCs aggregate in the red pulp and only exist until infection has been cleared[6]. IgG PCs do not express a functional BCR on the cell surface but secrete more immunoglobulin than IgM PCs[8]. PB differentiation is associated with downregulation of CXCR5 facilitating PB movement away from the B cell follicle toward CXCL12-expressing stromal cells in EF regions[49]. EF PB differentiation can be observed 3-5 days after immunisation in the bridging channels of the spleen[204]. IL21R is induced by the EF reaction to B cell activation and its expression is further upregulated after GC formation[216]. IL21 is a major player is the induction of GC-produced PBs[216].

Activated B cells reduce mitochondrial mass and reactive oxygen species as they begin PB differentiation while mitochondrial mass and aerobic metabolic capacity is increased again as cells differentiate from short to long lived PCs[217]. Plasma cells have increased uptake of amino acids[218]. Their glucose metabolism is key to survival and antibody secretion[74] through glycosylation of antibodies[218]. LLPCs have a high glucose and oxygen consumption rate and show reduced spare respiratory capacity compared to SLPCs in the BM[75].

Around 70% of the PC transcriptome is allocated to immunoglobulin synthesis while the other 30% is dedicated to metabolic rewiring including endoplasm reticulum (ER) synthesis and nutrient uptake to enable the high antibody secretion rate that PCs achieve[219]. Elongation factor for RNA polymerase II (ELL2) and cleavage stimulating factor (CSTF)64 reduce

ribonucleic acid (RNA) transcription rate at immunoglobulin loci and stop transcription before the transmembrane region thus shifting from membrane bound BCR to secreted antibody[74]. The cytoplasm, ER and Golgi of ASCs expand, at cost of nucleus size, to facilitate antibody synthesis and secretion[220].

Upon BCR engagement, IRF4 expression is increased as its transcription is driven by c-Rel downstream of PI3K signalling[74]. During B cell activation, IRF4 can form complexes with PU.1 or basic leucine zipper ATF-like transcription factor (BATF) to target AP-1 and Ets motifs and augment B cell activation and GC-related genes[74]. High IRF4 levels are necessary for PC differentiation and survival which requires downregulation of Cbl/Cbl-b, via strong BCR signalling, as these molecules degrade IRF4[106]. High IRF4 expression inhibits Bcl6 and initiates Blimp1 expression mediating ASC differentiation[8]. IRF4 is responsible for PC identity modulating the PC gene signature and transcriptional program[217]. IRF4^{high} cells are detectable at the T:B border hinting that PC output of the GC occurs in this location[216]. Deletion of IRF4 reduced follicular and GC B cell numbers[221], induced apoptosis in PCs[217], dysregulated mitochondrial control, resulted in defective ER structure[211] and impaired IgM and IgG secretion[217] as well as reducing PC generation and resulting in loss of PC identity genes[211].

PAX5 stimulates Bach2 which inhibits Blimp1 preventing early exit of cells from the GC reaction and consequent PC differentiation[222]. PAX5 suppression is required for PC differentiation as this transcription factor maintains cells in the B cell lineage[221].

Antigen-stimulated B cells increase Blimp1 expression and undergo chromatin remodelling at Blimp1 binding sites before PC differentiation[223]. Blimp1 abolishes a gene expression program which comprises B cell identity, cell surface marker expression, BCR signalling and B cell activation genes[224] thus terminating the GC reaction[224]. Blimp1 also inhibits proliferation, c-Myc induced growth[224] and DNA synthesis and repair enabling B cell terminal differentiation[112]. BLIMP1 plays a critical role in regulating mTOR which is required for the synthesis and secretion of antibodies[217]. BLIMP1 controls expression of unfolded protein response (UPR) components activating transcription factor 6 (ATF6), Ell2, Ern1[74] and X-box binding protein (XBP)1[211] which are key to antibody secretion[225]. Furthermore Blimp1 attaches to the immunoglobulin heavy chain enhancer region to promote transcription[225].

IFNγ regulates the elevation in levels of Blimp1, Irf1 and T-bet and is key to PC development[223]. Blimp1 is essential to PC differentiation and in its absence, plasma cells numbers are greatly decreased, antibody titres reduced and atherosclerosis was ameliorated[193].

Xbp1 enhances IgH mRNA processing, ER remodelling and the secretion of antibodies[8]. Inositol-requiring enzyme 1 (IRE1) converts XBP-1 to its spliced isoform XBP-1s which facilitates PC remodelling for antibody secretion[74]. XBP-1s upregulates chaperone expression and other protein folding associated components of the ER[74]. High XBP1 levels are dependent on IRF4 and loss of XBP1 severely reduces antigen-specific immunoglobulin production[211] and results in loss of ER structure and mass[217]. Global[30] and B-cell specific[226] loss of XBP1 exacerbated atherosclerosis.

S1PR2 is critical for emigration of ASCs from SLOs into circulation[8] and Myb induces the egress of GC-produced PCs from lymphoid organs to the BM[227]. Recruitment to the BM requires CXCL12 and CXCR4 while CXCL9, CXCL10 and CXCL11 facilitate homing of PCs to inflammation sites[8].

1.6 Antibodies

Antibody production is the key role of a plasma cell and antibodies can be classified into 5 subtypes – IgA, IgG, IgD, IgE and IgM.

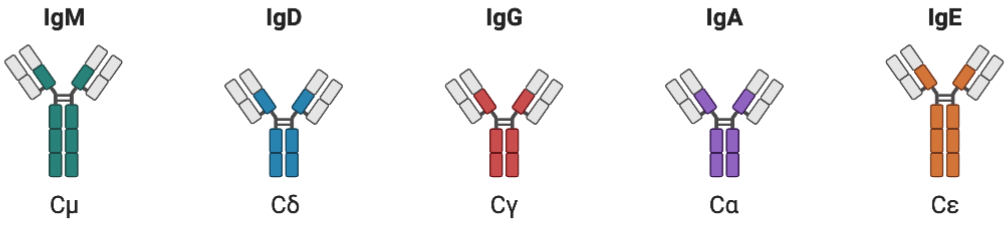

Figure 7. ***Structure of antibody subtypes encoded for by constant (C) region – IgM is encoded by Cμ, IgD by Cδ, IgG by Cγ, IgA and Cα and IgE by Cε.*** *Created using BioRender.com template made by Akiko Iwasaki, PhD and Ruslan Medzhitov, PhD.*

1.6.1 IgA

IgA is the major antibody isotype produced in the body and is vital for maintaining intestinal homeostasis through its secretion along the epithelia of the intestine[128]. IgA PCs migrate and stay within mucosal tissues through use of CCR9, CCR10 and $\alpha4\beta7$[228]. These intestinal PCs are similar to BM IgA PCs in terms of clonality[228]. A positive correlation between cardiovascular outcomes and IgA titres has been found in humans[30].

1.6.2 IgG

The IgG antibody class contains 4 subclasses – IgG1, IgG2a/c, IgG2b and IgG3 in mice while in humans they comprise IgG1, IgG2, IgG3 and IgG4[30]. IgG antibodies trigger a diversity of cellular effector mechanisms including antigen presentation, antibody-mediated cell toxicity, inflammatory mediator release, and induction of innate cell phagocytosis[30]. IgG antibodies have a flexible hinge region which allows movement of Fab fragments promoting high avidity engagement of antigen[229]. The structure of IgG harbours optional glycans at the terminus attached to the Fc tail and glycan patterns can vary dramatically impacting effector function[230]. Cytokines within the microenvironment can influence these glycan patterns through modulation of glycosylation enzymes; IFNγ restructures the carbohydrate bestowing pathogenicity while IL17A and IL21 instil both anti- and pro-inflammatory glycan patterns[230].

IgG B cells have a quicker response time to antigens than IgM or IgD due to their longer cytoplasmic tail which enables stronger signalling through the BCR[228]. The membrane tail of IgG enhances antibody production and augments T cell-dependent formation of PBs[231]. When comparing IgM B cells to IgG B cells, IgG B cells produced 100-fold more ASCs and elevated IgG titres to a greater extent[140]. The clonal expansion of IgG B cells is more significant than that of IgM B cells suggesting that IgM B cells must have undergone an increased rate of apoptosis[231]. Thus, IgG BCRs, the membrane tail specifically, bestow an enhanced clonal burst capacity during T cell-dependent extrafollicular antibody response providing evidence as to why IgG isotypes dominate in the memory recall response to T cell-dependent antigens[231].

1.6.2.1 IgG1

After cross-linking IgG1 creates immune synapses mediated by synapse associated protein (SAP)97 recruitment to the SSVV motif in its cytoplasmic tail resulting in the activation of MAPK[147]. The importance of the IgG1 cytoplasmic domain is demonstrated by the observation that its truncation led to poorly specific antibody responses[232]. IgG1 is internalised through ubiquitination which inhibits IgG1 recycling to cell surface[232].

1.6.2.2 IgG2c

For class switching to IgG2c, myeloid differentiation primary response (MyD)88-dependent activation of B cells is critical as B cell-intrinsic MyD88 signals induce T cell-derived IFNγ production[123]. In the absence of IFNγ signalling, IgG2c class switching is severely impaired[233]. Indeed, recombinant IFNγ can recover the IgG2c class switching impairment seen in MyD88 KO mice[234].

1.6.3 IgD

IgD usually doesn't exist in a secreted form[30] and its expression is non-existent on immature B cells, low on transitional B cells and upregulated on mature follicular B cells[234]. Peripheral B cells express simultaneously IgM and IgD BCRs which are identical in specificity[235]. Activation of the IgD BCR requires polyvalent antigens as the stimulation threshold is higher than that of IgM[235]. Monovalent antigens can bind IgD but cannot induce signalling due to being outcompeted by polyvalent antigens[235].

1.6.4 IgE

Upon antigen encounter, IgE triggers FcεR1 activation causing cellular degranulation of mast cells and basophils[226]. IgE can mediate its pathogenic effects through activation of macrophages to release proinflammatory cytokines such as IFNγ and TNFα[235].

Plasma IgE levels are an independent risk factor for cardiovascular disease (CVD)[236] and its elevated levels correlate with atherosclerosis, abdominal aortic aneurysm, and heart failure[236]. Expression levels of IgE and its receptor FcεR1 are elevated in human and mouse atherosclerotic plaques particularly in macrophage-rich areas[236]. IgE is pro-atherogenic through activation of macrophages and mast cells in the plaque and surrounding area[30]. Deletion of FcεR1 was atheroprotective in the Apoe$^{-/-}$ mouse model[236] including decreased necrotic core size[30]. Apoe$^{-/-}$ mice with IgE deficiency had limited atherosclerotic plaque development particularly the number of intraplaque smooth muscle cells (SMCs)[236]. Total cholesterol and triglyceride levels were diminished[236].

1.6.5 IgM

Surface bound IgM exists as a monomer[30]. The antibodies facilitate the induction of the complement cascade[237] by interacting strongly with C1q leading to cell lysis or opsonisation and phagocytosis[226] . IgM antibodies are produced early in life by B1 cells, the secreted form binds to cellular debris and apoptotic cells both of which are self-antigen sources thus limiting autoreactivity[140]. Natural IgM antibodies augment apoptotic cell clearance, inhibit proinflammatory pathways[238] and prevent endothelial activation[30]. The natural IgM repertoire is mainly composed of germline VDJ gene segments skewed toward autoantigen specificities[238]. Indeed 30% of B1-produced IgM recognises OSEs present on apoptotic cells, microvesicles and oxidised LDL (oxLDL)[30] including malondialdehyde and phosphorylcholine (PC)[238]. B cell expression of PD-L2 sustains total serum IgM levels and restricts production of IgM antibodies against PC[239].

1.7 Atherosclerosis as an inflammatory disease

Atherosclerosis is the most common cause of ischaemic heart disease and stroke which represent a global health concern responsible for significant levels of morbidity and mortality worldwide[30]. Increased incidence of diabetes and obesity as well as shifts toward the Western diet partly account for elevated risk of CVD[240]. The prevalence of ischaemic heart disease has increased from 100 million people in 1990 to over 180 million people in 2019[240]. LDL causes

atherosclerosis; the extent and duration of exposure to high LDL concentrations is associated with atherosclerotic disease[240]. Inflammatory biomarkers predict the risk of CVD development independently of all other risk factors[240].

Atherosclerosis is a chronic inflammatory disease characterised by the accumulation of atheromas, fatty plaques, within arteries[30]. Elevated plasma LDL levels are the main driver of atherosclerosis; its accrual in the intima initiates atherogenesis[30] with the formation of a fatty streak[241]. Within the intima, LDL undergoes lipid peroxidation and produces neoantigens termed oxidative specific epitopes[30] which are recognised by multiple innate pattern recognition receptors (PRRs) as endogenous DAMPs[242]. Examples include oxidised phospholipids harbouring phosphorylcholine (PC) and its degraded counterpart malondialdehyde (MDA)[30].

In response to LDL accumulation and oxidation, the endothelial lining upregulates leukocyte adhesion molecules resulting in leukocyte accumulation in the intima[241]. The hyperlipidaemia-induced activation of endothelium permits immunoglobulin to access to the atherosclerotic plaque[30]. OxLDL stimulates an inflammatory cascade including activation of endothelial cells and recruitment of monocytes and T cells into the vascular wall[30]. Once inside the intima, monocytes proliferate in response to hypercholesterolemia[243]. Oxidised phospholipids can stimulate macrophages via scavenger receptors[62], including CD36, TLR1, 2 and 6 and TLR4/CD14, elucidating a wide range of responses. OxLDL uptake by macrophages induces ROS production and stimulates NFκB signalling leading to phosphorylation of p38, Erk1/2 and JNK1/2 which upregulate mRNA transcript levels of IL6 and TNFα[244]. Monocyte recruitment into the intima begins early in life and the initial stages of plaque formation can be observed in infants less than 12 months old[245]. Macrophages augment inflammation by secreting proinflammatory cytokines and extracellular matrix (ECM) constituents enhancing lipoprotein retention[245] and contributing to lipoprotein modification and accumulation[241]. Furthermore, macrophages have the ability to rupture plaques through secretion of matrix metalloproteinases (MMPs), proteases and cytokines[246]. Plaque macrophages have impaired motility which results in defective inflammation resolution, instead promoting unstable atherogenic plaque formation[245]. The inflammatory nature of the plaque induces macrophage cell death (via apoptosis and necrosis and potentially other pathways) resulting in debris

accumulation and formation of the necrotic core[245]. Cholesterol also contributes to macrophage apoptosis through overwhelming the ER leading to excessive stiffness of the ER membrane and activation of the UPR stress pathway[244].

Within humans, it appears that atherosclerotic plaques undergo acute periods of expansion followed by long periods of stability[241]. Acute events can be triggered by infection which augments leukocyte recruitment and activation of VSMCs within the plaque[241]. Infection also stimulates damage-associated molecular patterns (DAMPs) and PAMPs which can enhance the inflammatory nature of the plaque[241]. Ischaemic injury induces release of soluble mediators from myocardial cells and leukocytes which amplify atherogenesis[241]. Chronic inflammatory diseases such as rheumatoid arthritis (RA) and systemic lupus erythematous (SLE) result in pro-inflammatory mediator production from joints among other sites which promote inflammation within the arteries thus contributing to the progression of atherosclerosis[241].

Microparticles are small phospholipid vesicles shed from activated or dying cells. Levels of microparticles are elevated in CVD[247]. Microparticles have been identified in atherosclerotic plaques where they facilitate monocyte adhesion to endothelial cells via ICAM1[247]. A subset of microparticles has been found to express OSEs which can be targeted by anti-IgM MDA-LDL antibodies thus dampening the inflammatory nature of microparticles[247].

Thinning of the fibrous cap occurs as a result of reduced collagen synthesis and increased collagen degradation by proinflammatory cytokine-induced activation[241] of immune cell-produced collagenases[240]. During thrombosis, platelets produce TGFβ and platelet-derived growth factor (PDGF) which induce SMC migration and matrix production[241]. Thrombus formation is triggered by the interaction of coagulation proteins with lipid core materials when the plaque fibrous cap ruptures[241].

The engagement of CD40 and CD40L augments leukocyte recruitment to vascular inflammation spots partly through CD40L-mediated endothelial cell activation which increases the expression of adhesion molecules such as vascular cell adhesion molecule (VCAM)1, ICAM1 and E-selectin[99] enabling leukocyte infiltration into the arterial wall[98].

Macrophages activated by CD40 produce MMPs which contribute to plaque destabilisation and rupture[248] and CD40L expression induces monocyte differentiation into macrophages and the formation of foam cells[190]. The CD40-TRAF6 interaction is key in the formation of the neointima and TRAF6 inhibition resulted in an anti-inflammatory phenotype along with decreased atherosclerotic plaque size[190]. Absence of CD40L limits autoantibody titres against oxidised lipids and shifts the balance of B cells towards more anti-inflammatory subsets e.g. B regulatory cells[129]. CD40 deficiency leads to smaller atherosclerotic plaques which contain more collagen and SMC content and less macrophage content[190] as a consequence of impaired macrophage migration and M2 phenotype polarisation[249]. Absence of CD40 reduces the formation of neointima after carotid artery ligation[98] which was accompanied by decreased inflammatory cell recruitment, production of proinflammatory mediators and MMPs with elevated collagen production[98]. In human subjects, a SNP in the CD40 gene increased surface CD40 expression by 87% and correlated with increased risk of atherosclerosis[248]. Soluble CD40L in circulation is a potential new biomarker for atherosclerotic CVD as elevated levels have been linked with major adverse cardiovascular events[248].

1.7.1 Autoimmunity

Autoimmunity drives chronic inflammation and specifically B cell autoimmunity drives immunopathology in many autoimmune conditions and can be pro-atherogenic[30]. SLE mouse models show higher atherosclerotic plaque burden[30]. Furthermore, patients with RA or SLE, consisting of a major B cell pathology, develop atherosclerosis prematurely[30] and have an increased CV risk associated suggesting a key role for B cells in CVD[226].

Atherogenic hyperlipidaemia exacerbates autoimmune lupus[250]. $LDLr^{-/-}$ SLE mice had elevated IgG and IgG2c titres and greater autoantibody production[251]. Thus, the atherogenic background of $LDLr^{-/-}$ and $Apoe^{-/-}$ enhances pathogenic IgG2c autoantibodies resulting in SLE[251].

Deficiency in either CD95 (Fas) or CD178 (Fas ligand), responsible for initiation of apoptosis, causes defective apoptotic cell clearance, autoantibody production and elevated atherosclerosis[30] including elevated anti-oxLDL antibody titres in Apoe$^{-/-}$CD95$^{-/-}$ mice[252].

1.8 Role of B cells in atherosclerosis

B cells play numerous roles in atherosclerosis through both protective and pathogenic mechanisms. Lifelong B cell deficiency is atheroprotective as CD4 T cell numbers are decreased by 85% and thus T cell recruitment to plaques is also reduced[253]. Additionally antibody[253] and cytokine levels are reduced and HFD-induced insulin resistance is prevented[71]. Bone marrow transfer from B cell deficient (μMT) mice into LDLr$^{-/-}$ mice induced a greater degree of atherosclerosis compared to controls[30]. However, Kyaw et al showed decreased atherosclerosis in μMT Apoe$^{-/-}$ in which there was global deletion of B cells and immunoglobulins and defective GC formation[253]. Splenectomy in Apoe$^{-/-}$ mice augmented atherosclerosis and anti-MDA-LDL IgG antibody levels decreased[254] while adoptive total splenic B cell transfer back into these mice limited atherosclerosis progression[72], decreased plasma cholesterol levels and antibodies against MDA-LDL were rescued. This demonstrates that immune responses to oxLDL are associated with atheroprotection[254].

B1 cells produce natural IgM antibodies against oxidation-specific epitopes both on apoptotic cells and within atherosclerotic lesions[62] which are atheroprotective due to the prevention of macrophage lipid uptake and foam cell formation[72]. These natural antibodies induce apoptotic cell phagocytosis by macrophages[62] thus promoting apoptotic cell clearance[72]. B1 cell CXCR4 expression expands IgM titres against OSEs in murine and human studies and expression levels are negatively associated with coronary artery plaque volume in humans[72]. Increased IgM titres and B1 cell numbers are atheroprotective while their depletion exacerbates atherosclerosis[226].

Follicular B2 cells are atherogenic primarily through their interaction with Tfh cells mediated by CD40 and MHCII to produce pathogenic IgG-producing plasma cells[193]. B2 cell depletion through CD20 and BAFFR deficiency blunted atherosclerosis progression[30] while adoptive

transfer of B2 cells but not B1 cells enhanced atherosclerosis in HFD-fed Apoe$^{-/-}$ mice[65]. Depletion of B2 cells dampened T cell IFNγ production, CD4 T cell proliferation and proinflammatory cytokine production[72].

An induced deletion of Apoe$^{-/-}$ in adult mice causes severe hyperlipidaemia accompanied by inflammation and atherosclerosis[255]. Specifically under hyperlipidaemic conditions, levels of antibodies against atherosclerosis-associated autoantigens were increased[255]. In the kidneys, widespread deposition of IgM and IgG was observed indicating an autoimmune-like phenotype of these mice[255]. The inflammatory response occurred prior to the formation of atherosclerotic plaques demonstrating that metabolic changes directly impact immunity and that the GC response to hyperlipidaemia exacerbates atherogenesis[255].

TNFα has been detected in atherosclerotic plaques of Apoe$^{-/-}$ mice[65]. B cell-derived TNFα increases macrophage TNFα production leading to enhanced macrophage recruitment to the plaque, apoptosis-mediated expansion of the necrotic core, production of proinflammatory cytokines and the progression of atherosclerosis with a more rupture-prone phenotype[65]. A global genetic deficiency and an antibody-mediated blockade of TNFα are atheroprotective, reducing atherosclerotic lesion size[65] with concurrent reduction in lipid and macrophage accumulation, apoptosis and necrotic core size[65].

Genome wide association studies (GWAS) and transcriptomic studies have identified a positive correlation between activated CD19+CD86+ B cells and stroke risk and a negative correlation between IgM+ memory B cells and CVD risk[30]. B cell activation genes are expressed at higher levels in healthy controls compared to coronary heart disease (CHD) patients[256]. In coronary artery disease patients, B cells have been found in the intima and adventitia[28] with large numbers clustered in the epicardial adipose tissue[71]. IgG and IgA B cells secreting proinflammatory cytokines including granulocyte macrophage colony stimulating factor (GM-CSF), IL6 and TNFα[256] have been observed in the vasculature of human atherosclerotic plaques[30].

To summarise, B cells are a double-edged sword in the context of atherosclerosis providing both protective and pathogenic functionality.

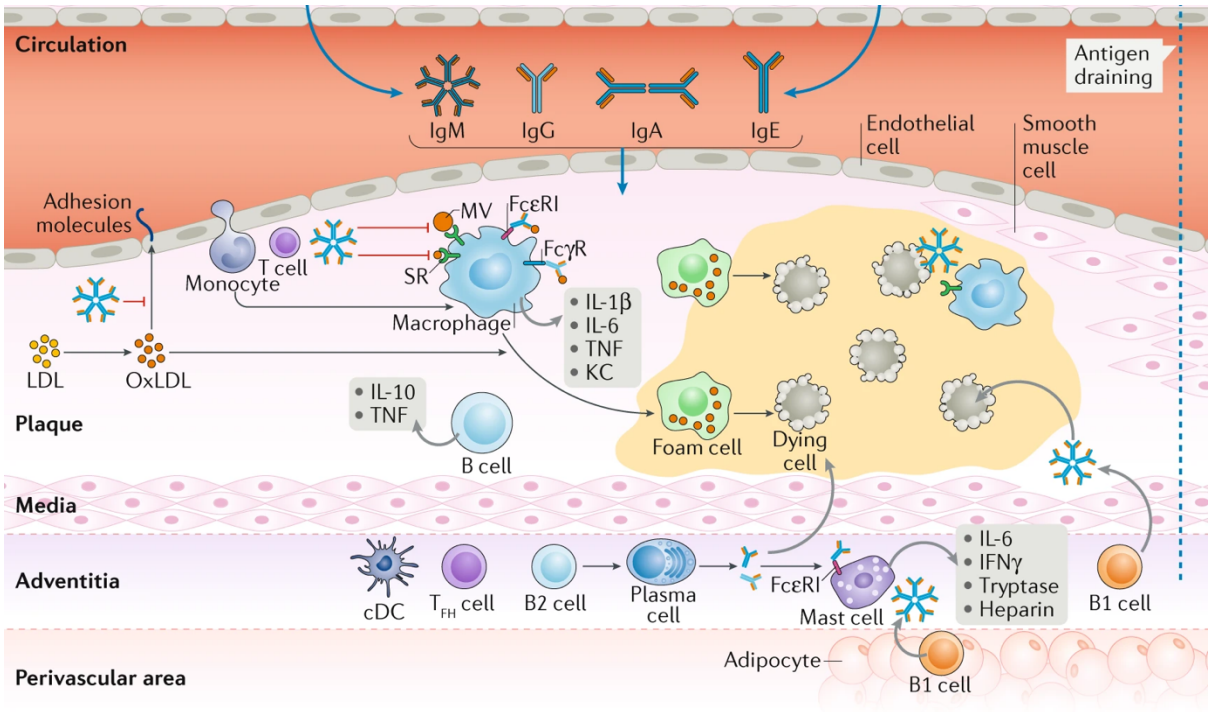

Figure 8. ***The role of B cells in atherosclerosis.*** *In the presence of dyslipidaemia, activated endothelium overlying atherosclerotic plaques allows the entry of different immunoglobulins into the plaque area. In advanced stages of plaque formation, artery tertiary lymphoid organs are also formed, which include plasma cell formation in situ, leading to production of immunoglobulins in the adventitia. A large proportion of immunoglobulin M (IgM) antibodies have the capacity to recognize oxidation-specific epitopes, which are present on oxidized LDL (OxLDL), apoptotic cells, and microvesicles (MVs). Thereby, IgM antibodies limit OxLDL-induced endothelial activation and foam cell formation via scavenger receptors (SRs), as well as MV-triggered pro-inflammatory responses by macrophages. Conversely, IgG antibodies form immune complexes with OxLDL and promote macrophage inflammatory responses. IgE has strong proatherogenic properties by stimulating macrophages and mast cells both in the plaque and in the perivascular area. B1 cells also produce various cytokines such as proatherogenic tumour necrosis factor (TNF) and antiatherogenic IL-10. Diagram from Sage et al[30].*

1.8.1.1 Role of germinal centre in atherosclerosis

There has been increasing evidence that the GC and its products, memory cells and antibody-producing plasma cells, are pathogenically dysregulated during atherosclerosis. During the progression of atherosclerosis, the frequency of GCs within the spleen and LNs increases[222]. Defective GC formation[257] and selective deletion of the GC response ameliorated atherosclerosis with reduced titres of antibodies against autoantigens[255]. There is a strong positive correlation between atherogenesis and the size of the GC B cell pool within SLOs[222]. In the absence of AID, Apoe$^{-/-}$ mice lose their ability to class switch antibody isotype and atherosclerotic lesions are reduced[250]. Aid$^{-/-}$Apoe$^{-/-}$ mice did not exhibit the Apoe$^{-/-}$ induced B cell expansion showing that this population contributes to the increased atherosclerosis in

this model[250]. The loss of PAX5 in AID+ cells reduced splenic GC and plasma cell numbers and loss of PAX5 in CD23+ cells led to a diminished B2 cell population[222]. Aicda-mediated genetic deletion of the GC resulted in lack of IgG responses[222]. As a consequence, atherosclerosis decreased by 48% and SMC proliferation was compromised[222].

By knocking out Prdm1 (Blimp1), the splenic B1 cell population expands while the plasma cell pool contracts[222]. Consequently, there are significant drops in antibody titres especially those of anti-Cu-oxLDL IgG and anti-MDA-LDL IgM[222]. This genetic deficiency is atheroprotective as the extent of atherosclerosis is reduced 4-fold by 33 weeks and plaques lack the characteristic antibody deposition and become more lipid laden[222]. Thus, plasma cells enhance atherosclerotic plaque size[222] and are pro-atherogenic[29].

In Apoe$^{-/-}$, high IgG1 levels were detected before HFD administration while IgM levels were enhanced by the diet[250]. Apoe$^{-/-}$ mice with GC cell depletion and absence of OSE-reactive IgG had decreased plaque formation[226]. In aged Apoe$^{-/-}$ mice, GC B cell and Tfh cell populations are expanded as Tfh regulation by CD8 T regulatory cells (Tregs) is impaired[29] and antibody titres are increased[251]. Dysregulation of the Tfh population resulted in increased IgG antibody deposition in atherosclerotic lesions[29]. Anti-ICOSL treatment or genetic Tfh cell depletion[30], blocking the Tfh-GC interaction, decreased the Tfh cell population and the GC reaction leading to reduction in lesion size[29] as well as limited accumulation of B cells in the adventitia[29]. Antibody treatment also decreased the frequency of memory B cell mutations and the quantity of IgG1 antibodies produced[258].

LDLr$^{-/-}$ fed a HFD have a higher proportion of the IgG2c isotype and lower proportion of the IgG3 isotype accompanied by a higher rate of SHM[259]. A third of antibodies detected in the serum of HFD-fed mice were reactive against atherosclerotic lesions compared with only 8% of antibodies from LDLr$^{+/+}$ mice fed chow diet[259].

1.8.1.1.1 Role of antibodies in atherosclerosis

Immunoglobulin can be detected in atherosclerotic lesions and shows reactivity toward OSEs in both mice and humans[30]. Classical autoantigens in CVD have been proposed to include

lipoproteins and vascular wall components[226]. High IgG levels are positively associated while IgM levels are negatively associated with increased intraplaque lipid concentration[28].

APOB is a component of LDL and acquires the majority of OSEs[30]. ApoB peptides p45 and p210 have been identified as neoantigens[226] and IgG antibodies against these epitopes have been shown to be atheroprotective[28], negatively associated with atherosclerosis[226]. Immunisation of Apoe$^{-/-}$ mice with MDA-45 a MDA-modified ApoB100 peptide, a recombinant IgG antibody, decreased atherosclerotic plaque size by 50%[260]. In pre-clinical testing, treatment with human anti-APOB100 antibodies impaired atherosclerosis development[30]. An immunogenic epitope found on APOA1 is detectable at very low levels in circulation of patients with coronary artery disease (CAD), yet comprised for 20% of APOA1 found in atherosclerotic arteries[261].

Splenic autoimmune response to OSEs produces a protective B cell response which ameliorates atherosclerotic plaque development and heightened lipid levels[262]. Anti-OSE antibodies sequester OSEs preventing their inflammatory action on macrophages[238] including consequent foam cell formation[64]. Immunising against oxLDL or native LDL significantly lowers atherosclerotic plaque formation[28]. Immunisation with MDA-LDL is atheroprotective and triggers a Th2-biased response with high levels of IgG1 as well as anti-OSE antibody production[28]. Antigen-induced clonal expansion of B cells has been detected in atherosclerotic plaques[28]. The V_H5 and V_H7 BCR families, reactive to PC, were clonally expanded in hypercholesterolemic Apoe$^{-/-}$ mice[262]. Anti-PC and anti-oxLDL antibodies of both IgG and IgM isotypes were increased in Apoe$^{-/-}$ and also elevated with age[262]. Therapeutic application of anti-phosphorylcholine IgM reduced atherosclerosis progression while IgG from Apoe$^{-/-}$ accelerated atherosclerosis[250]. In elderly patients anti-OSE antibodies were induced moderately decreasing CVD-related events[226].

Transfer of IgG antibodies from atherosclerotic mice enhances atherogenesis and expands the necrotic core of the plaque[193]. A meta-analysis found anti-oxLDL IgG titres positively associated with risk of CV events[30]. MDA-oxLDL immunisation limited atherosclerosis by augmented IgG levels[250].

The humoral IgM response is linked with hypercholesterolemia in Apoe$^{-/-}$ mice and the spleen is the main producer of total IgM and oxLDL-specific IgM within these mice[239]. However, IgM production was not limited to within GCs[239]. Instead there was significant IgM production from EF reactions and EF-derived IgM PCs could be detected in the BM[239]. IgM can be found within atherosclerotic plaques in LDLr$^{-/-}$ mice[263]. Anti-OSE[239] and anti-oxLDL IgM levels increase in Apoe$^{-/-}$ by 16 weeks and further increase by 24 weeks compared to WT mice[263]. IgM antibodies reactive to PC and MDA epitopes are significantly increased in atherosclerosis and are atheroprotective through neutralisation preventing proinflammatory effects of oxidised lipids[30]. Anti-OSE IgM treatment is anti-inflammatory in cholesterol-dependent hepatic inflammation[30]. Polyclonal IgM infusion is atheroprotective in hyperlipidaemic Apoe$^{-/-}$ mice[226]. Furthermore, IgM-secreting B1a cell transfer ameliorated atherosclerotic lesion and necrosis in splenectomised Apoe$^{-/-}$[30]. OxLDL immunisation elevated anti-oxLDL IgM titres and reduced atherosclerotic plaque size[226]. Mice deficient in serum IgM on the LDLr background have exacerbated atherosclerosis and the frequency of apoptotic cells was increased alongside IgG autoantibody production[263].

High MDA-LDL IgM levels are negatively associated with autoantibody titers[226]. Anti-oxLDL IgM antibodies are negatively associated with carotid artery intima media thickness[28]. Increased anti-MDA-LDL IgM antibody levels correlated with reduced incidence of coronary artery disease, reduced atherosclerotic plaque burden[226] and fewer cardiovascular events in a CVD patient cohort[238].

The E06 antibody was cloned from hyperlipidaemic murine spleens and has shown reactivity against oxidised phospholipids[30]. It has the same CDR3 region as B1-produced T15 clone[30] which recognises both the PC head group of the immunodominant epitope on Streptococcus pneumoniae and atherosclerotic intraplaque oxidised phospholipids[238]. The E06 antibody reduces adhesion molecule expression[226] and oxLDL uptake by macrophages thus lowering macrophage cholesterol content and serum amyloid alpha (SAA) levels[242]. Streptococcus pneumoniae immunisation of LDLr$^{-/-}$ resulted in increased anti-PC[226] and T15 IgM titres[30] and a reduction in atherosclerotic plaque formation, in both humans and mice, by exploiting the molecular mimicry between oxLDL and Streptococcus. Overexpression of the E06 antibody is protective against atherosclerosis, and reduced TNFα and IL6 levels[242] in hyperlipidaemic

LDLr$^{-/-}$ mice[30]. Plaques had reduced necrotic core with increased collagen content suggesting a more stable phenotype[242].

In CVD patients, B and T-lymphocyte attenuator (BTLA) is highly expressed on circulating B cells while expression is absent within atherosclerotic plaques[238]. Activation of BTLA reduces early atherosclerosis with decreases in the follicular B2 cell population and concurrent increases in atheroprotective B cell subsets (B1, MZ and Breg)[264]. Atherosclerotic plaques were more collagenous and decreased in size demonstrating the atheroprotective nature of BTLA activation[264].

In the canakinumab anti-inflammatory thrombosis outcome study (CANTOS) trial, a neutralising antibody against IL1β reduced risk of recurrent MI, cardiac or stroke death in CAD patients following myocardial infarction (MI) with 26% reduction in C-reactive protein (CRP) levels[240]. The CANTOS trial proved that inflammatory processes are central to the pathology of atherosclerosis[30].

In summary, B cells and their effector functions play a plethora of roles in the progression of atherosclerosis. The germinal centre response is a keystone of the adaptive immune response playing critical roles in health and disease. Its contribution to atherosclerosis has not yet been fully elucidated and this PhD aims to further characterise and understand the involvement of the GC response in atherosclerosis paving the way for novel therapeutic possibilities.

This PhD thesis has four main aims:

1. **Validate the AEL model for use in tracking germinal centre responses in atherosclerosis**
    a. Optimise a labelling strategy to be able to track germinal centre cells and their progeny during atherosclerosis
    b. Culture germinal centre B cells *in vitro*

2. **Characterise germinal centre responses occurring within atherosclerotic mice**
    a. Determine the impact of genotype, diet and time on germinal centre responses in atherosclerosis
    b. Determine the time course and output of atherosclerotic germinal centres using lineage tracing

3. **Investigate the mechanism underlying elevated germinal centre responses in atherosclerosis**
    a. Investigate the impact of cholesterol on the germinal centre response
    b. Investigate the impact of inflammation on the germinal centre response

4. **Investigate the importance of IgG2c and its receptor FcγRIV in atherosclerosis**
    a. Investigate the potential for IgG2c to directly affect atherosclerotic cell types
    b. Determine the effect of FcγRIV deficiency on atherosclerosis

2 Methods

2.1 Mice

AID-Cre-ERT2 mice were bred with Rosa26-loxP-enahncer yellow fluorescent protein (EYFP) reporter mice to generate heterozygous AID reporter mice termed AID-CreERT2-EYFP mice[30]. These were brought into the lab and crossed with the *LDLr*$^{-/-}$ mouse strain (originally bought from Jackson labs) in a specific pathogen-free facility at the University of Cambridge. These produced AID-Cre-ERT2-Rosa26-loxP-EYFPxLDLr$^{-/-}$ mice. FcγRIV deficient mice were a gift from Falk Nimmerjahn. All experimental studies were regulated under the Animals Scientific Procedures Act 1986 following ethical review by the University of Cambridge Animal Welfare and Ethical Review Body (PPL PA4BDF775 and PP9485757).

2.1.1 Breeding and maintenance

Breeding and maintenance were conducted by Toni Bray, Magdalena Ridley and Dr Andrew Sage and I was also involved in maintenance. For breeding, 2 females were co-housed with 1 male for 1 week before males were boxed out into individual cages. AID-Cre-ERT2-Rosa26-loxP-EYFPxLDLr$^{-/-}$ mice, termed AEL mice, were bred with C57/Bl/6 mice to produce AID-Cre-ERT2-Rosa26-loxP-EYFPxLDLr$^{+/-}$ mice, termed WT AEL mice, for experimental usage. (Both LDLr deficient and LDLr heterozygous mice termed AEL due to some level of LDLr absence). AEL male mice were bred with LDLr$^{-/-}$ female mice to produce AID$^{CreERT2/+}$ male offspring for experiments, termed *LDLr*$^{-/-}$. Pups were maintained with their mother for 3 weeks after birth before weaning and moving into separate cages. Ear notching enabled identification of individual mice within cages. Cages contained up to 6 mice and one sex only. Experimental groups were mixed between cages where possible. Mice were kept under a standard 12/12-hour day/night cycle with access to food and water ad libitum.

2.1.2 Diets

From 8 weeks of age, some mice were fed a high fat or 'western' diet (21% fat; 0.15% cholesterol; Scientific Diet Services or Envigo) for up to 8 weeks with weekly weighing to ensure mouse health and that HFD was inducing weight gain. In some studies, a high fat (HF) only diet was used (21% fat, 0.05% cholesterol from fat; Envigo). In some instances, fasting was undertaken with food removed 12 hours prior to harvest for the purposes of regulating blood concentrations of biomolecules.

2.1.3 Dosing

Tamoxifen was administered by intraperitoneal injection (3mg) or oral gavage (9mg) with timing varied throughout studies. For the 3mg dose, 120mg tamoxifen and for the 9mg dose, 480mg was added to 0.8ml prewarmed 100% ethanol. The mixture was dissolved by incubation at 55°C (with shaking) for a few minutes and thorough mixing using a vortex. 7.2ml pre-warmed corn oil was added and again incubated at 55°C (with shaking) with mixing using vortex at regular intervals until completely dissolved and no crystals remained. The solution was divided into 800μl aliquots and protected from light using tin foil before storage at -20°C. Tamoxifen was thawed and thoroughly mixed before administration.

Bio X Cell InVivoMab anti-mouse IL6 clone MP-20F3 (catalogue no. BE0046) was diluted from stock concentration of 6.81mg/ml to a working concentration of 1μg/μl in sterile phosphate buffered saline (PBS). The Bio X Cell InVivoMab rat IgG1 isotype control anti-horseradish peroxidase clone HRPN (catalogue no. BE0088) was used as a control and diluted from stock concentration of 9.25mg/ml to working concentration of 1μg/μl in sterile PBS. Mice were injected i.v. with 200μl weekly for 2-4 weeks.

Lomitapide (Sigma) had a stock concentration of 25μg/μl which was diluted to 125μg/ml working concentration to give a final dose of 1mg/kg in 200μl 0.5% dimethylsulfoxide (DMSO) PBS. For control dosing, 0.5% DMSO PBS was used. Mice were dosed via oral gavage with 200μl 3x per week for 2-4 weeks.

2.1.4 Bone marrow transfer

Bone marrow transfer studies were conducted for the FcγRIV mouse strain. 6–8-week-old male LDLr$^{-/-}$ mice were lethally irradiated (9.5 Gy) followed by i.v. injection via the lateral tail vein with 1x10^{7} bone marrow cells from FcγRIV$^{-/-}$ donor femurs on the same day. Mice were given a 4-week recovery period with antibiotic (Baytril) supplemented water. Mice were weighed and health checked 3 times a week during recovery. After this period, mice were started on HFD for 8 weeks.

2.1.5 Tissue collection

After euthanasia, blood was collected through cardiac puncture of the left ventricle and between 0.1-0.9ml was withdrawn. Blood was contained within heparin coated tubes.

Mice were pinned by their limbs to a corkboard to allow for easy dissection and sprayed with ethanol to reduce interference from hair. The skin was cut from abdomen near the hips all the way up to the throat allowing the body cavity to be opened. The spleen and lymph nodes (inguinal and para-aortic) were removed using scissors and tweezers. To access the inguinal lymph nodes the skin was pulled away from the lining of the abdomen. The small intestine was removed, and individual Peyer's patches were collected. Para-aortic lymph nodes were collected after removal of the small intestine and reproductive organs. To harvest the bones, the skin from around the hip was removed and the leg was cut at the knee joint. Muscle was removed to expose the bone and the joints were snipped. To eradicate remnant blood, mice were perfused with 5ml PBS via the circulatory system. The heart was exposed and harvested by cutting through the sternum up to the ribcage using scissors. Spleen, BM, LNs, para-aortic lymph nodes (PALNs) and PPs were kept in 1ml PBS/5% foetal bovine serum (FBS) on ice until processing. Heart was stored in 4% PFA before processing.

2.2 Flow cytometry

Spleen was filtered through 70μm nylon mesh and washed through with 10ml PBS/3% FBS. LNs, PALNs and PPs were filtered through 30μm nylon mesh and washed through with 1ml PBS/3% FBS. Samples were centrifuged for 5 minutes at 400 x g and supernatant discarded. Red blood cells were lysed from spleen using 4ml red blood cell lysis buffer followed by dilution with 4ml PBS/3% FBS and centrifugation at 400 x g for 5 minutes before supernatant discard. Red blood cell lysis (RBC) buffer was made up with 4.14g ammonium chloride, 0.5g potassium bicarbonate and 0.1ml 0.5M ethylenediaminetetraacetic acid (EDTA) in 500ml distilled water. Single cell spleen suspensions were resuspended in 5ml PBS/3% FBS. LNs, PALNs and PPs were resuspended in 200μl PBS/3% FBS.

5-10 volumes of RBC lysis were added to whole blood and incubated for 5 minutes. Samples were centrifuged and resuspended in 3 volumes RBC lysis buffer for 1 minute before equal volume of PBS/3% FBS added. Samples were centrifuged and washed with PBS before resuspension at 50μl.

Bones were cleaned of tissue and ends cut off. Bone marrow was flushed from bone using 25G needle with 1ml syringe filled with PBS/3% FBS into a 30μm sieve.

Cell counting was conducted for the spleen by adding 10μl of the final 5ml cell suspension to 100μl A solution, 100μl B solution (both from Chemometec) and 90μl PBS which was analysed by aspiration of mixture into a nucleocassette using a Nucleocounter automated cell counter (Chemometec). For the LNs and PALNs, 10μl of final cell suspension was added to 10μl PBS and 90μl trypan blue for LNs and 190μl for PALNs. 20μl of the cell counting solution was pipetted into a counting chamber and cells enumerated under a microscope.

Single cell suspension aliquots (up to 200μl) of bone marrow, spleen, blood, para-aortic lymph nodes, lymph nodes and Peyer's patches were added to a 96 well V-bottom plate and spun for 5 minutes at 400 x g. The supernatant was discarded and 50-200μl 1:100 fluorescently labelled antibody mix diluted in 0.5% bovine serum albumin (BSA)/PBS was added and cells

stained for 20 mins at 4°C in the dark. After a PBS wash, zombie aqua solution was incubated with cells for 5 minutes before final wash. Prior to intracellular staining, cells were stained with cell surface antigens and then fixed with IC fixation buffer (Thermofisher). Samples were resuspended in 200µl PBS/3% FBS if flow cytometry was being run on the same day. If cells were being run on flow cytometer another day, cells were resuspended in 100µl CellFix (BD) for 1hr before wash and resuspension in 200µl PBS. Cells were kept at 4°C until analysis when samples were filtered using a filter plate and diluted to a final volume of 400-600µl before running on flow cytometer. Single stain controls were included for each fluorophore used. Live single cells were gated on the basis of forward side scatter (FSc), side scatter (SSc) and negative Zombie Aqua live/dead staining. Different flow cytometry antibody panels were created to identify GC-related cells (Table 1) and myeloid cells (Table 2). Schematic for how GC cells were identified can be seen (Figure 9). The BD Fortessa flow cytometer was used to acquire samples and all analysis was conducted using FlowJo software and GraphPad 7.0.

Table 1. Flow cytometry antibodies used to identify germinal centre, memory, and plasma cells

Antibody marker	Dilution	Fluorophore	Wavelength
B220	1:200	APCVio770	Red 780/60
CD138	1:200	PE	Yellow 585/15
IgM	1:100	APC	Red 670/14
CD95	1:100	PECy7	Yellow 780/60
GL7	1:200	eF450	Violet 450/50
Zombie Aqua	1:400	N/A	Violet 525/50

Table 2. Flow cytometry antibodies used to identify cell types in FcyRIV-/- studies

Cell type	Antibody marker	Dilution	Fluorophore	Wavelength
B cell subsets	B220	1:200	APCVio770	Red 780/60
	CD19	1:200	BV650	Violet 655/8
	CD21	1:100	FITC	Blue 530/30
	CD23	1:200	PECy7	Yellow 780/60
	CD43	1:200	BV510	Violet 525/50
	CD138	1:200	PE	Yellow 585/15
	GL7	1:200	eF450	Violet 450/50
	IgD	1:20	PerCP Cy5.5	Blue 695/40
	IgM	1:100	APC	Red 670/14
Cytokines	IFNγ	1:100	PeCy7	Yellow 780/60
	IL10	1:100	APC	Red 670/14
	IL17	1:100	BV605	Violet 605/12
cDC	CD8a	1:100	PerCP	Blue 695/40
	CD11b	1:100	AF488	Blue 530/30
	CD11c	1:100	PE-Cy7	Yellow 780/60
	CD40	1:100	APC	Red 670/14
	CD80	1:100	PE	Yellow 585/15
	CD86	1:15	VioBlue	Violet 450/50
	MHCII	1:100	APC-Vio770	Red 780/60
Monocytes	CD11b	1:400	AF488	Blue 530/30
	CD115	1:200	PE	Yellow 585/15
	FcγRI	1:100	APC-Vio770	Red 780/60
	FcγRII/III	1:100	PE-Cy7	Yellow 780/60
	FcγRIV	1:200	BV650	Violet 655/8
	Ly6C	1:200	AF647	Red 670/14
	Ly6G	1:400	Pacific Blue	Violet 450/50
Tregs	CD4	1:200	Pacific Blue	Violet 450/50
	CD25	1:200	APC	Red 670/14
	GITR	1:100	FITC	Blue 530/30
	Foxp3	1:100	PE	Yellow 585/15
Tfh	CD3	1:200	APC	Red 670/14
	CD4	1:200	AF700	Red 730/45
	CD8	1:100	PerCP	Blue 695/40
	CD44	1:200	BV605	Violet 605/12
	CD62L	1:100	Pacific Blue	Violet 450/50
	CXCR5	1:100	PE	Yellow 585/15
	PD1	1:100	Pe-Cy7	Yellow 780/60
	Zombie Aqua	1:400	N/A	Violet 525/50

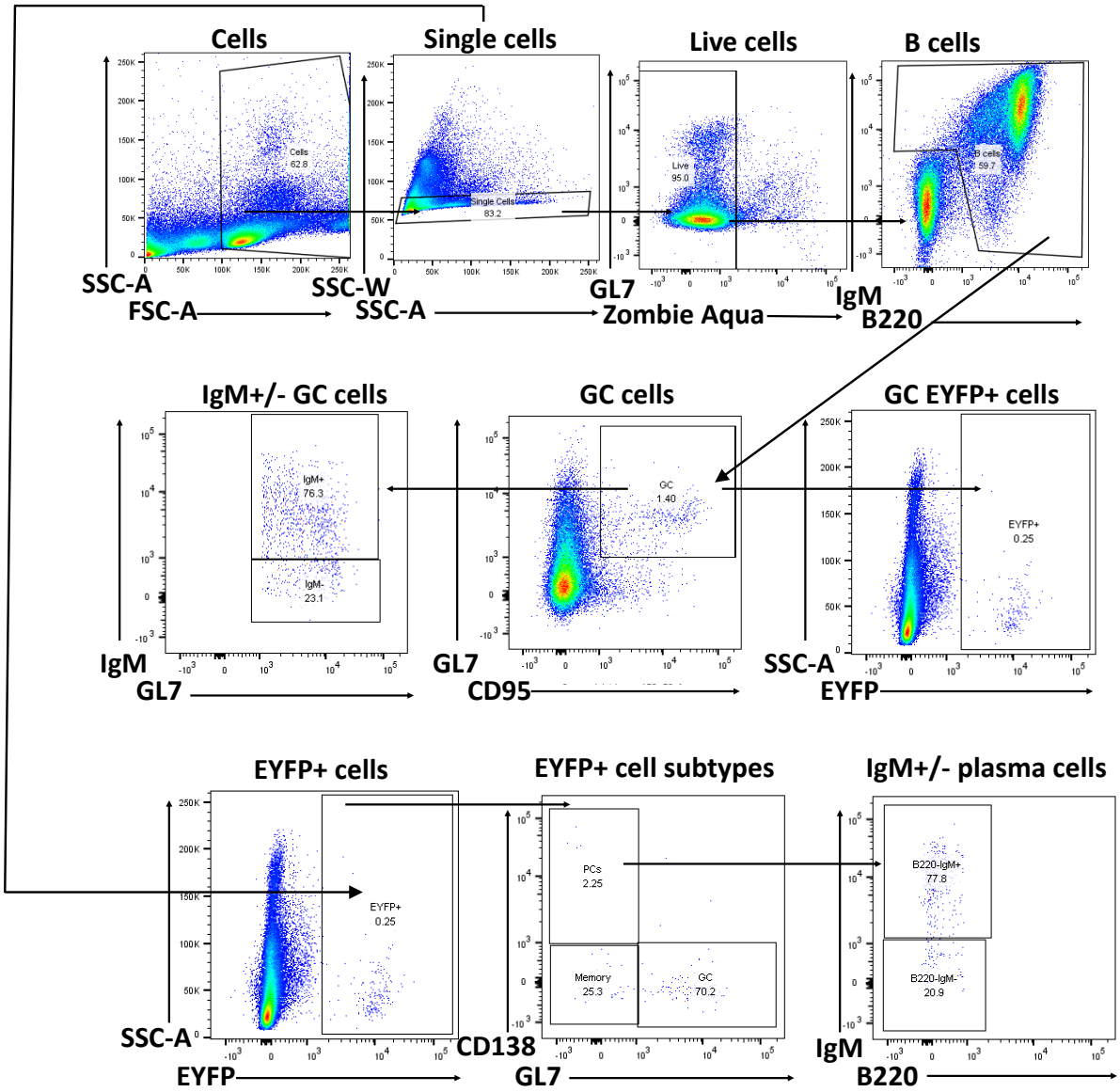

Figure 9. ***Flow cytometry gating strategy illustrated through FlowJo plots.*** *All cells are gated on forward scatter area (FSC-A) and side scatter area (SSC-A), and doublets are removed by gating on single cells using side scatter width (SSC-W) and SSC-A. From the single cell gate, live cells are gated on the basis of negative zombie aqua staining. B cells are gated within the live cell gate, using B220 APCVio770 and IgM APC. Within this gate, GC B cells are identified as CD95+(PECy7) GL7+(eF450). GC cells are further characterised by EYFP expression and IgM status. The total number of EYFP+ cells is also found from the single cell gate. EYFP+ cells are further categorised as plasma cells (PC) CD138+GL7-, GC cells (CD138-GL7+) or memory cells (CD138-GL7-). PCs are further gated on IgM status.*

2.3 Cell culture

Bone marrow cells were isolated from wildtype mouse femurs and tibias and cultured in RPMI supplemented with 10% foetal bovine serum and 1% penicillin/streptomycin in Petri dishes. GM-CSF and macrophage colony stimulating factor (M-CSF) (both at 1μg/ml) were used to differentiate cells into dendritic cells or macrophages, respectively. Cell media was refreshed

on day 4 and macrophages reached maturity at day 7 while dendritic cells reached maturity at day 10. IFNγ (100ng/ml) was added to media for 24 hours as an activating treatment which could mimic atherosclerotic plaque microenvironment conditions. All cells were grown at 37°C and 5% CO_2 in a humidified environment.

For coating experiments, 96 well culture plates were coated with mouse IgG2c or IgG1 antibody (Biolegend) one day before cell maturity and cells were seeded the following day. For the bead experiments, cells were seeded the day before maturity and beads added to culture the following days. After treatment, cells were harvested 48 hours later *(Figure 10)*.

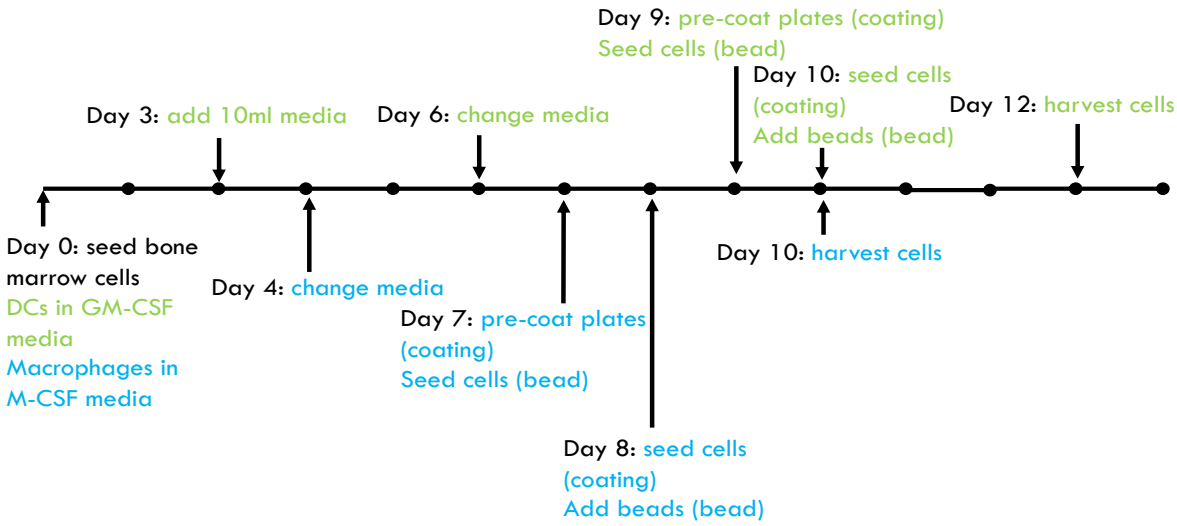

Figure 10. ***Timeline of in vitro experimental setup with DCs depicted in green and macrophages depicted in blue.***

For the culture of GC B cells *in vitro*, spleens were harvested and dissociated to form a single cell suspension in MACS buffer. Biotin antibody cocktail from B cell isolation kit was added at 1:4 ratio with cells and incubated for 5 minutes. MACS buffer and beads from B cell isolation kit were added at ratio of 3:2 and incubated for 10 minutes. Sample was run on autoMACS using depletes programme and enriched purified B cell population collected in the negative fraction at position B of autoMACS. Cell culture plates were coated with BAFF (2μg/ml) and CD40 (10μg/ml) prior to cell seeding. The purified B cell population was seeded and IL21 (10ng/ml) was added to culture at day 5 and cells were harvested between days 6-9.

2.4 RNA extraction

RNA was harvested using TRIzol and extracted using DirectZOL RNA extraction kit (Zymo). Liquid nitrogen-frozen liver was added to tubes containing 2 beads and 750µl QIAzol on ice in a fume hood and emulsified using a homogenizer at 50Hz for 3 minutes. For cell cultures, media was removed through aspiration and washed with PBS before addition of TRIzol and scrapping to remove cells. TRIzol containing samples were centrifuged for 1 minute before transfer to a new tube. Equal volume of 100% ethanol was added and vortexed. 650µl was transferred to a column in a 2ml tube. If the total volume was more than 650µl, this step was repeated until all volume had been processed. The column was washed with 400µl RNA wash buffer. 800µl DNase mix was added and incubated for 15 minutes. DNase mix contained 5µl DNase, 8µl 10x buffer, 64µl RNA wash buffer and 3µl RNase free water per sample. 400µl RNA pre-wash was added, and this step repeated. 700µl RNA wash buffer was added. After each step, sample was centrifuged for 1 minute at 500g. The column was spun again to dry and transferred to a 1.5ml tube. 20µl RNase-free water was added and centrifuged to elute. RNA purity and concentration was quantified using the Nanodrop. RNA was stored at -80°C.

2.5 cDNA synthesis

Isolated RNA was converted to cDNA using the Quantitect reverse transcription kit (Qiagen). 1µg RNA was diluted in RNase-free water and adjusted to total volume of 13µl. 1µl gDNA wipeout buffer was added per sample followed by 2-minute incubation at 42°C using the thermocycler to remove genomic DNA. On ice, per sample 1µl reverse transcriptase (RT), 4µl 5X RT buffer and 1µl RT primer mix were mixed to create the reverse transcription master mix. 6µl master mix was then added to the RNA sample and left in the thermocycler at 42°C for 20 minutes to generate cDNA. Finally, to inhibit the reverse transcriptase, a 3-minute incubation at 95°C was performed, and cDNA was stored at -20°C.

2.6 Quantitative polymerase chain reaction

For quantitative reverse transcription polymerase chain reaction (PCR), cDNA samples were diluted by 5-fold in nuclease free water. The qRT-PCR reaction mix consisted of 1μl of forward and reverse primer mixes at 3μM concentration, 1.5μl nuclease free water and 7.5μl 2X SYBR Green qRT-PCR Master Mix (Eurogentec). 5μl of diluted cDNA was added to 10μl of reaction mix and prepared in triplicate on LightCycler 480 96-well plates with LightCycler sealing foil to seal the plates. Plates were spun using a centrifuge for 30s at 500 x g before initiating LightCycler program. The LightCycler program consisted of an initial 95°C incubation for 2 minutes followed by 40 cycles of denaturation at 95°C for 10s, annealing at 60°C for 30s and extension at 72°C for 10s. Each PCR reaction contained 12.5μl GoTaq PCR master mix, 1μl extracted DNA, 0.1μM each of forward and reverse primer and 9.5μl nuclease free water. At the end of the run, 5 minutes of extension at 72°C was conducted.

For qRT-PCR data analysis, the LightCycler program set a background threshold from which to measure signal cutting out background noise. Calculation of the cycle number (CT) at which the fluorescence from each sample exceeded that of the threshold could then be conducted. The 2^-(ΔΔCT) method was used for data analysis and data was presented as the target gene expression fold change normalised against a housekeeping reference gene, either 36B4 or hypoxanthine-guanine phosphoribosyltransferase (HPRT).

2.7 ELISAs

96 well enzyme-linked immunosorbent assay (ELISA) plates were coated with capture antibody *(Table 3)* diluted 1:100 (1:120 for IL6) in SSC buffer and sealed overnight at room temperature followed by 3x PBS-T washes. Plates were blocked with PBS/1%BSA for 30 minutes at room temperature followed by 3x PBS-T washes. The top standard was generated and serially diluted to form the standard range of concentrations *(Table 3)*. 50μl of each was added to wells in duplicate. Mouse serum samples were diluted *(Table 3)* in PBS-T/0.1%BSA and 50μl added in duplicate per concentrations. 2 concentrations were used for most ELISAs. Following 1hr incubation (2hrs for SAA and IL6) on shaker, plates were washed 3x with PBS-

T. The appropriate detection antibody *(Table 3)* was added for 1hr on shaker, 50µl/well, (again 2hrs for SAA and IL6) before 3x PBS-T washes. The SAA ELISA required a 20-minute Streptavidin-horse radish peroxidase (HRP) step, 50µl/well, at this stage and was diluted 1:40 in PBS-T/0.1% BSA. Plates were washed 3x with PBS-T. The antibody ELISAs did not require this step. Substrate solution (Thermofisher) was prepared by mixing substrate solution A and B in 1:1 ratio and added, 50µl/well, for up to 20 minutes or when colour had developed (blue) in the dark. 50µl stop solution (2M sulphuric acid) was added to change colour from blue to yellow. Plates were analysed on microplate reader at 450nm and 570nm.

Table 3. Dilutions for capture and detection antibodies and standard curve range for ELISA antibodies used

ELISA type	Sample dilution	Detection antibody dilution	Standard curve range
IgM	1:5000, 1:10000	1: 150,000	15.6 – 1000ng/ml
IgG1	1:2000, 1:5000	1: 100,000	15.6 – 100ng/ml
IgG2c	1: 250, 1:500	1: 100,000	15.6 – 1000ng/ml
IL6	1:5	1: 120	250 – 1000pg/ml
SAA	1:500, 1:5000	1: 60	500-32,000pg/ml
TNF	1:2	1: 60	31.2-2000ng/ml

To detect dsDNA within samples, an ELISA plate was coated with 5µg/ml calf thymus DNA (Sigma) in SSC buffer for 18hrs at 37°C. SSC buffer was made using 8.74g 0.15M NaCl and 1ml 0.1% 0.015M citric acid in 1L of filtered water. Following incubation, plates were washed 3x with PBS-T and blocked with PBS/1%BSA for 30 minutes. Serum was diluted 1:50 in PBST/0.1% BSA and added for 2hrs. Plates were washed 3x with PBS-T and anti-mouse total IgG-HRP 1:75000 (Bethyl Labs) was incubated for 1hr. Plates were washed 3x and substrate added for 10 minutes before addition of stop solution. Plates were analysed at 450nm, and quantity was calculated by removing blank value from the absorbance value of each sample.

The Core Biochemical Assay Laboratory conducted the MSD mouse cytokine array proinflammatory panel 1 10-plex assay for IFNγ, IL1β, IL2, IL4, IL5, IL6, KC/GROα, IL10, IL12 and TNFα.

2.8 Cholesterol quantitation

The Sigma Aldrich cholesterol quantitation kit (MAK043) was used to carry out a colorimetric assay in 96 well tissue culture flat bottomed plate. Cholesterol esterase and enzyme mix were reconstituted with 200μl cholesterol assay buffer before use. The 2μg/μl cholesterol standard solution was diluted with 140μl cholesterol assay buffer to produce 0.25μg/ml standard solution. 0, 4, 8, 12, 16 and 20μl of 0.25μg/μl cholesterol standard solution was added to 96 well plate generating a 0, 0.1, 0.2, 0.3, 0.4 and 0.5μg/well standards. Cholesterol assay buffer was added to each well to bring total volume to 50μl. Standard was replicated to have duplicate values. 50μl mouse serum samples were added at a dilution of 1:100 with cholesterol assay buffer. The reaction mix comprised of 44μl cholesterol assay buffer, 2μl cholesterol probe, 2μl cholesterol enzyme mix and 2μl cholesterol esterase. 50μl reaction mix was added per well and mixed thoroughly. Plate was protected from light and incubated at 37°C for 15 minutes. Absorbance was measured at 570nm using the Perkin Elmer microplate reader. The absorbance value of the 0 (blank) cholesterol standard was used as the background which was subtracted from all readings. Sample cholesterol content was determined from the linear standard curve which was produced from the values of the appropriate cholesterol standards.

The Core Biochemical Assay Laboratory conducted lipidomic analysis on a subset of samples providing quantitation of total cholesterol, LDL, high density lipoprotein (HDL), and TGs.

2.9 Immunostaining

2.9.1 Tissue and slide preparation

Hearts were harvested and fixed using 5ml 4% paraformaldehyde (PFA) and left on shaker for 6hrs at room temperature. Samples were then stored overnight at 4°C. At this point, tissues were bathed in PBS followed by 30% sucrose solution for 24hrs (or until tissue had sunk, whichever came last) before embedding. Forceps were used to rinse the heart in OCT then placed into fresh optimal cutting temperature compound (OCT) in an embedding cassette

with the aortic root horizontal. Embedding cassettes were bathed in isopentane and dry ice to slowly freeze. Samples were stored in the freezer at -80°C. Samples were trimmed by 50μm until the tissue was visible. At this point, the tissue was trimmed at 10μm steps until the aortic valves could be seen. Cryosections were produced at 10μm thick sequentially, air dried for 30 minutes at room temperature and stored at -80°C.

2.9.2 Immunofluorescent staining

For staining, sections were thawed for 10 minutes followed by a 10-minute PBS wash. Sections were fixed using 4% PFA for 10 minutes followed by 5-minute washes in PBS and then PBS-T. Samples were blocked using 1%BSA/5% goat serum for 30 minutes followed by 5-minute PBS wash. Slides were incubated with primary antibodies (diluted in 0.05% PBST/1% goat serum) for 1hr at room temperature followed by 3x 5-minute washes with PBS-T. Secondary antibody (diluted in 0.05% PBST/1% goat serum) was applied for 1hr at room temperature followed by 3x 5-minute washes with PBS-T. Sections were counterstained with Hoechst nuclear stain (1:2000 in water) and mounted using CC mount. Imaging of slides was conducted on a Leica DM6000B microscope and associated software. Image analysis was performed using ImageJ. Primary antibodies were used at 1:100 and were anti-mouse and included αSMA (Sigma C6198), CD68 (abcam ab76308), IgG2c (abcam ab97254). Secondary antibodies were anti-rabbit or anti-rat within the green 488nm range (Thermofisher A11006 and A11008).

2.9.3 Oil Red O staining

Oil Red O stain was prepared using stock solution of 0.5% Oil Red O powder dye (Sigma Aldrich) in 100% isopropanol and dissolved at 55°C. Working solution was composed of 3 parts Oil Red O stock solution in 2 parts water which was filtered before use. Oil Red O staining first comprised samples being incubated for 5 minutes in PBS and 5 minutes in water. Slides were then incubated for 1 minute in 60% isopropanol before 15-minute incubation in the working Oil Red O solution. Following this, slides were rinsed briefly (5s) in 60% isopropanol

and lightly stained with diluted (1:10) haematoxylin for 30s. Slides were washed for 5 minutes in tap water prior to mounting using CC mount.

For haematoxylin and eosin (H&E) staining, slides were rinsed in PBS before 5-minute incubation in haematoxylin (Sigma). Slides were dipped 5x in destain solution, which was comprised of 250ml methanol, 250ml filtered water and 5ml concentrated HCl. Slides were placed in Scott's Solution for 5 minutes which was made from 20g magnesium sulphate and 2g sodium bicarbonate in 1L of filtered water. Following this, slides were bathed in eosin (Sigma) solution for 10 minutes and then dipped in MilliQ water twice. Slides were rapidly dehydrated through 90% and 100% alcohols for 1 minute each followed by 2 incubations in xylene lasting 2.5 minutes each. Coverslips were adhered to the slides and mounted with DPX.

For analysis of both plaque size and composition, aortic root cryosections were stained with Oil Red O, haemotoxylin and eosin or with anti-α smooth muscle actin (Sigma) or CD68 (Biorad). Cell density was calculated by determining the area stained with nuclei within plaques as a proportion of total plaque size.

2.10 Statistics

Data were analysed in GraphPad Prism 7.0 (La Jolla, CA); using two-tailed unpaired t test or Mann Whitney U test for data sets which failed normality tests. The D'Agostino-Pearson omnibus normality test was used to test datasets for normal distribution. Results were presented as mean +/- SD. A p value of <0.05 was considered significant. The Grubbs' test (ESD method; extreme studentised deviate) was used to determine the presence of significant ($\alpha = 0.05$) outliers which were excluded. The two-tailed Spearman correlation was used for correlation analysis with 95% confidence interval.

3 The AEL mouse model can be used to track GC responses in atherosclerosis

3.1 Abstract

The GC response relies heavily on the AID enzyme which was used to track the fate of GC B cells in a genetic lineage tracing system. The AID-Cre-ERT2-Rosa26-lox-EYFP mouse model was imported and crossed with the LDLr$^{-/-}$ mouse model to investigate the fate of AID expressing cells during the course of atherosclerosis. This tamoxifen-inducible mouse model enables fluorescent EYFP labelling of any cells expressing AID at the time of tamoxifen administration. Validation of this model has been completed showing that EYFP cells are only detected after tamoxifen administration and can be identified as GC-derived cells demonstrating specificity of the model. Furthermore, genotype, time and diet do not impact the labelling efficiency which is ~5-20% of GC B cells corroborating existing literature. This model inducibly and specifically EYFP labels GC B cells and their progeny, plasma cells and memory B cells, using tamoxifen which enables tracking of atherosclerosis-specific B cell clones.

3.2 Background

This PhD project relies on genetic lineage tracing to track labelled cells within the murine system. As previously discussed, AID is a key enzyme in the GC reaction responsible for isotype class switching and somatic hypermutation. Thus, this enzyme robustly marks GC B cells and can be harnessed for tracking the fate and location of GC derived cells.

Genetic lineage tracing is a method of DNA site-specific recombination which permanently labels cells enabling tracking of cellular movements and interactions[248]. Recombinase is used to control the system whereby the recombined cells can be identified using previously decided upon genetic markers[265], in this particular model AID is used. Cre recombinase removes a specific sequence which is flanked by loxP sites which the enzyme recognises[265]. In this model the EYFP gene, flanked by loxP sites, is in the ROSA locus; a 'safe' locus for

transgene insertion. A STOP construct is inserted such that prior to the first loxP site there is a promoter and stop codon and a STOP codon is present between loxP sites thus blocking EYFP translation. When Cre recombinase is activated, the loxP sites are removed and EYFP expression is induced. Inducible systems have been created through use of the oestrogen receptor (ER) which can be fused with Cre[265]. In the deactivated state, CreER recombinase is located in the cytoplasm bound to HSPs[265]. Once activated through application and binding of the ER ligand tamoxifen, CreER dissociates from HSPs and translocates to the nucleus where it facilitates Cre-loxP recombination[265].

Mice carrying a tamoxifen-inducible Cre under control of the Aicda locus and a floxed EYFP gene were crossed onto the atherosclerotic LDLr$^{-/-}$ background. The triple mutant mice will be referred to as AEL from now on. At the time of tamoxifen dosing, cells expressing AID will be labelled with EYFP. Labelling is permanent and irreversible. Thus, the fate of GC B cells in terms of final phenotype, progeny, and location, can be tracked over time.

3.2.1 EYFP expression is tamoxifen inducible and detectable by flow cytometry and immunofluorescence

The AID-Cre-ERT2-ROSA26-lox-EYFP mouse was designed to enable inducible EYFP+ labelling of AID-expressing cells upon tamoxifen dosing. This lineage tracing model has been used to investigate B cell memory and has been validated in the literature[266]. Dogan et al. intraperitoneally immunised AID-Cre-EYFP mice with sheep red blood cell suspension (SRBC) at day 0 and boosted them at day 30. Tamoxifen was administered at day 7, 12 and 31. They show that an EYFP+ population is only present in the presence of tamoxifen and when GC B cells are induced by immunisation *(Figure 11A)*. This demonstrates that EYFP+ expression is dependent on tamoxifen and is only expressed in GC B cells. Additionally, they showed that EYFP+ cells in the spleen are also PNA+ thus confirming the GC phenotype of EYFP+ labelled cells *(Figure 11B)*.

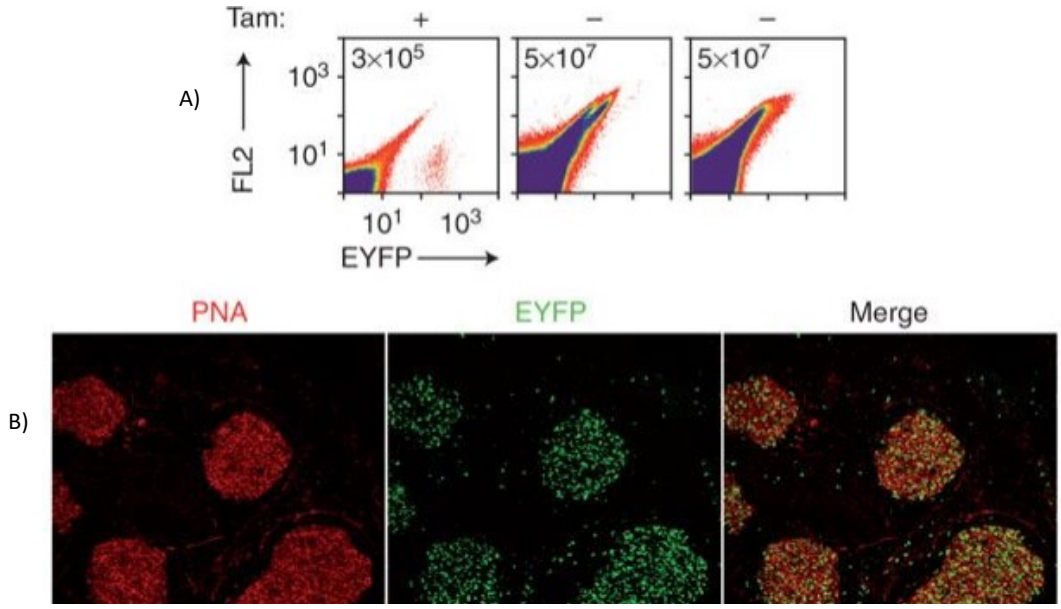

*Figure 11.**Tamoxifen-dependent EYFP labelling in GC B cells from AID-Cre-EYFP mice after antigen challenge. A)** Flow cytometry of splenic cells 8 d after the secondary immunization, with (Tam +; left) or without (Tam –; middle) the three-dose tamoxifen regimen, and of splenic cells from an 18-month-old mouse not treated with tamoxifen or immunized (right). Top left, number of cells analysed. **(B)** confocal analysis of GC PNA$^+$ B cells expressing EYFP, 4 d after secondary immunization. Scale bar 200µm. Figure taken from Dogan et al[266].*

To validate the model initially, splenic cells from male LDLr$^{-/-}$ AEL mice were dosed with either vehicle (PBS) or tamoxifen and were analysed by flow cytometry. A readily detectable EYFP+ cell population was induced in the spleen of male LDLr$^{-/-}$ AEL mice after tamoxifen administration while no EYFP+ cells were identified in the absence of tamoxifen *(Figure 12A, Figure 13)*. At 3 days post-tamoxifen administration (5 days since first injection), EYFP+ cells of the spleen were 99% B220+ B cells with more than 60% expressing the GC marker GL7 *(Figure 12A)*. Under homeostatic conditions, it is likely that cells will only harbour the GC phenotype for a short period of time thus many more EYFP+ cells would have been GC cells at the time of labelling. The remaining 1% of EYFP+ cells were identified as CD138+ plasma cells at this timepoint. EYFP labelling was also detected using anti-EYFP immunofluorescent antibodies within the spleen; clusters of EYFP+ cells were detected within the B cell follicle where GC formation takes place *(Figure 12B)*. This data shows that tamoxifen can induce EYFP expression within B cells and a significant proportion of the EYFP+ B cell population has a GC phenotype thus validating this model for investigating the GC response. The aim is to track atherosclerosis-specific B cell clones using the AEL lineage tracing strategy.

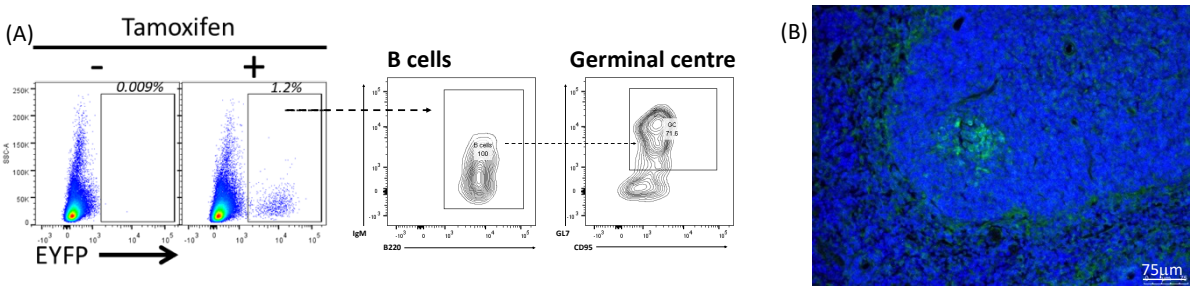

Figure 12. ***The majority of tamoxifen-inducible EYFP cells have GC phenotype and can be seen within splenic GCs. (A)*** *Representative FACS profiles of murine splenic cell suspensions gated for side scatter area (SSC-A) and EYFP (blue 530/30 laser). Within the EYFP+ gate, 99.1% of EYFP+ cells are B cells using B220 (APCVio770, red 780/60 laser) and IgM (APC, red 670/14 laser. A subset of EYFP+ B cells (B220+IgM+/-) can be further classified as GC B cells as identified by CD95+ (PECy7, yellow 780/60) and GL7+ (eF450, violet 450/50 laser).* ***(B)*** *Immunofluorescence of paraformaldehyde fixed spleen cryosection using chicken polyclonal anti-EFYP primary antibody and goat anti-chicken IgY AlexaFluor 488 (green) secondary antibody. Hoechst staining used to depict nuclei (blue) – brighter staining demonstrates higher cell density and the follicle region of the spleen.*

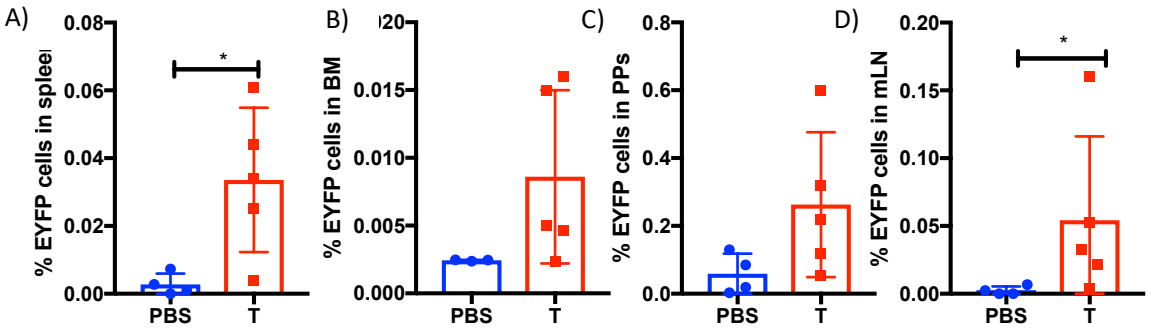

Figure 13. ***EYFP-labelled cells are only detectable upon tamoxifen administration.*** *The proportion of EYFP+ cells within the total sample population assessed by flow cytometry in* ***(A)*** *spleen,* ***(B)*** *bone marrow (BM),* ***(C)*** *Peyer's patches (PP) and* ***(D)*** *mesenteric lymph nodes (mLN). A significant EYFP cell population is only seen in mice which received a tamoxifen dose rather than the control PBS dose. Each dot represents 1 mouse; data depict mean +/- SD. Statistics carried out using Mann-Whitney test, * P < 0.05; ** P < 0.01; *** P < 0.001; **** P < 0.0001.*

3.3 Aims

1. Validate the AEL model
    a. *Optimise dosing strategy for labelling efficiency and study design*
    b. *Investigate impact of tamoxifen on GC responses*

2. Culture GC B cells in vitro

3.4 Results

3.4.1 Dosing strategies and labelling efficiency

Labelling efficiency is defined as the proportion of GC cells (GL7+CD95+) that are EYFP+. Existing literature has determined that the labelling efficiency of this genetic lineage tracing model is between 5-20% of AID expressing cells i.e., 5-20% of AID+ (GC B cells) will be EYFP+ labelled when tamoxifen is administered. To determine the labelling efficiency, 4 different dosing strategies were trialled which varied by tamoxifen dosage and timing of dosage *(Figure 14)*.

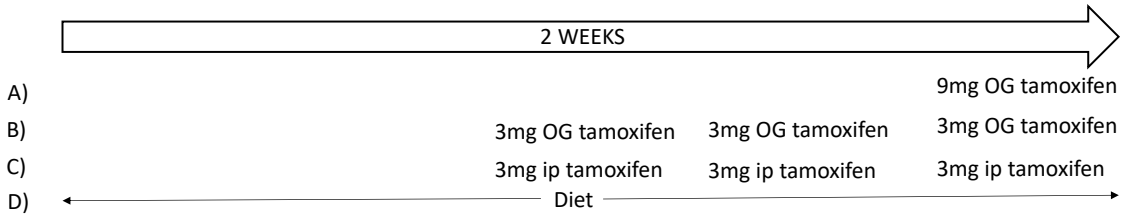

*Figure 14**. Dosing strategies used to optimise labelling efficiency**. **(A)** 1x 9mg oral gavage (OG) tamoxifen dose at the end of the 2 weeks. **(B)** 3x 3mg OG tamoxifen dose within the second week of study, **(C)** 3x 3mg intra-peritoneal (i.p.) dose within the second week of study and **(D)** tamoxifen containing diet (40mg/kg) refreshed daily for 2 weeks.*

All male LDLr$^{-/-}$ AEL mice received 9mg tamoxifen over the course of the study, however repeated dosing results in elevated numbers of EYFP labelled AID+ cells as multiple timepoints are labelled in which more cells have passed through the GC and acquired AID expression. The labelling efficiency of cells in the Peyer's patches was used as control as these lymphoid tissues harbour chronic GCs. The diet resulted in the highest absolute numbers of EYFP cells as well as proportion of GC labelled EYFP in both the spleen and PPs *(Figure 15)*. 3 doses of

3mg tamoxifen delivered via oral gavage was more effective than the same dose delivered via intraperitoneal injection in the PPs *(Figure 15B, D)*. As the PPs are constantly sampling from the gut, this result is logical as the PPs will encounter tamoxifen more efficiently via the oral gavage method. Meanwhile, the delivery method of the 3x 3mg tamoxifen did not affect the total number of EYFP cells and EYFP GC population in the spleen *(Figure 15A, C)*. Delivery of the 9mg tamoxifen by one oral gavage dose resulted in the lowest labelling efficiency (EYFP+ of GC) in both spleen and PPs *(Figure 15C, D)* and the smallest total EYFP population in the PPs *(Figure 15B)*. However, the total EYFP population in the spleen was similar via all routes trialled *(Figure 15A)*. This optimisation study has demonstrated that the duration of labelling positively correlates with the number of EYFP labelled cells.

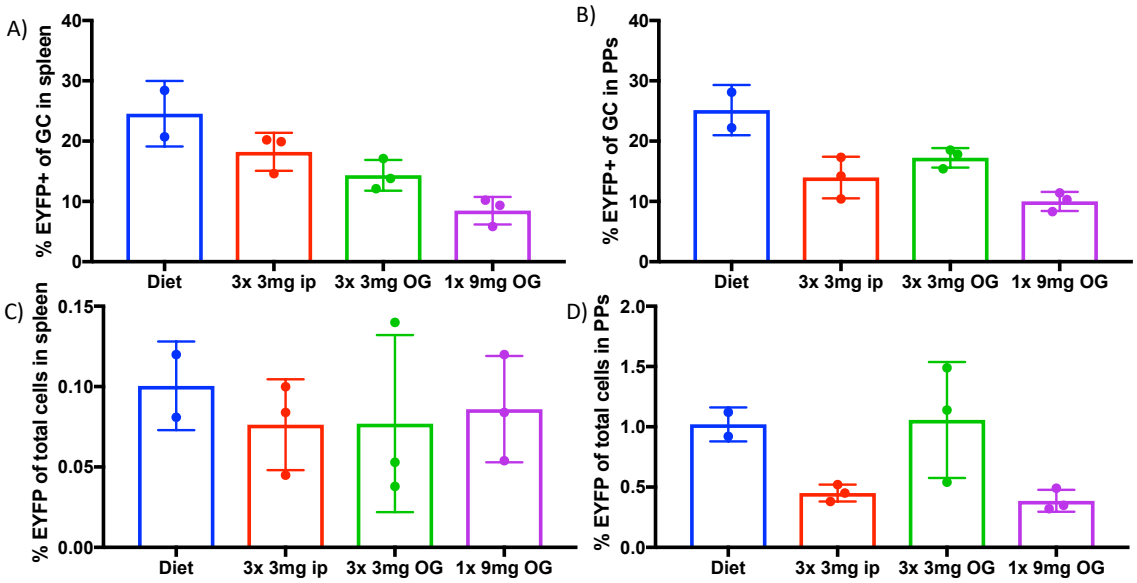

Figure 15. ***Size of EYFP population varies depending on dosing strategy.*** *Over the course of 2 weeks mice were either fed a tamoxifen diet (red) or dosed with 3x intraperitoneal injection of 3mg tamoxifen (red), 3x oral gavage of 3mg tamoxifen (green) or 1x oral gavage of 9mg tamoxifen (purple). Using flow cytometry analysis, the percentage of EYFP+ cells within the GC (GL7+CD95+) population is depicted in* ***(A)*** *the spleen and* ***(B)*** *the Peyer's patches (PP). The total number of EYFP+ cells within the sample is depicted in* ***(C)*** *the spleen and* ***(D)*** *the PPs. Each dot represents one mouse, data depicted as mean +/- SD.*

With one oral gavage dose of 9mg, labelling efficiency in the PPs tended to be up to 20% matching results previously reported in the literature *(Figure 16)*. Labelling efficiency was not impacted by diet or time in the PPs *(Figure 16)*.

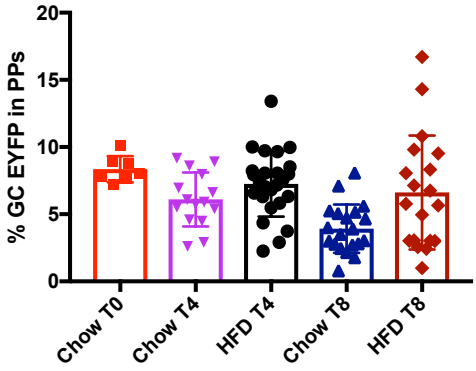

Figure 16. ***Labelling efficiency is not impacted by time or diet.*** *Percentage of germinal centre (GC) cells (GL7+CD95+) which are EYFP+ in the Peyer's patches (PPs) as determined using flow cytometry in chow and high fat diet (HFD) fed AEL mice. Diet was given for either 0 weeks (T0), 4 weeks (T4) or 8 weeks (T8). Each dot represents one mouse and average of group +/- SD is depicted.*

3.5 Impact of tamoxifen on GC responses

To determine any potential impact of tamoxifen on GC responses, female LDLr$^{-/-}$ AEL mice fed chow diet were dosed either with 150µl 9mg tamoxifen or 150µl PBS via oral gavage. Upon sacrifice 48hrs later, spleen, PPs, BM and mesenteric lymph nodes (around stomach) were harvested. The spleen is the major site of immune responses while the PPs and mesenteric lymph nodes (mLNs) surround the gastrointestinal (GI) tract and are exposed to tamoxifen first. The bone marrow is the location for GC-derived long-lived PCs to reside. Tamoxifen did not significantly impact the viability of cells in any tissues analysed *(Figure 17)*.

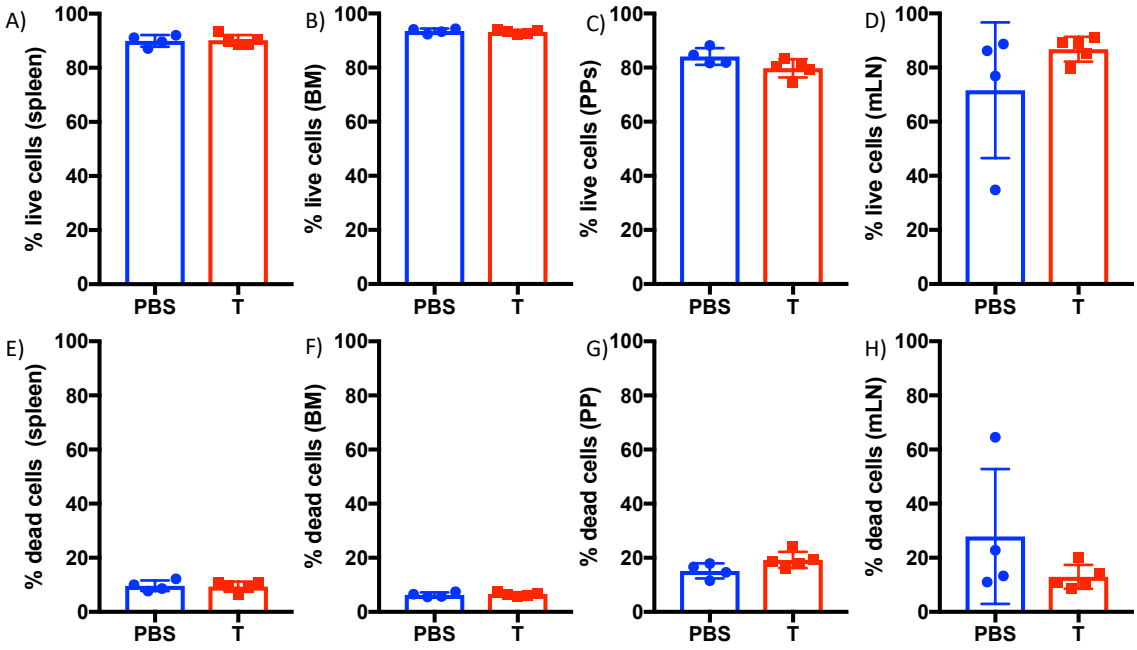

Figure 17. ***Tamoxifen does not impact cell viability.*** *Mice were dosed with PBS control or 9mg tamoxifen (T). The viability of cells was assessed using Zombie Aqua (ZA) fluorescent dye which is only taken up by dying cells; therefore, dead cells can be categorised as ZA+ while live cells are ZA-. The proportion of total cells which are live (ZA-) assessed by flow cytometry seen in the (A) spleen, (B) bone marrow (BM), (C) Peyer's patches (PP) and (D) mesenteric lymph nodes (mLN). The proportion of total cells which are dead (ZA+) assessed by flow cytometry seen in the (E) spleen, (F) BM, (G) PP and (H) mLN. Each dot represents one mouse and data are depicted with mean +/- SD.*

Tamoxifen did not impact on the population of B cells *(Figure 18)*, plasma cells *(Figure 19A-D)*, plasmablasts *(Figure 19E-H)* or IgM status of the plasma cell pool *(Figure 20)* or GC B cell pool *(Figure 21)* within the spleen, BM, PPs and mLNs.

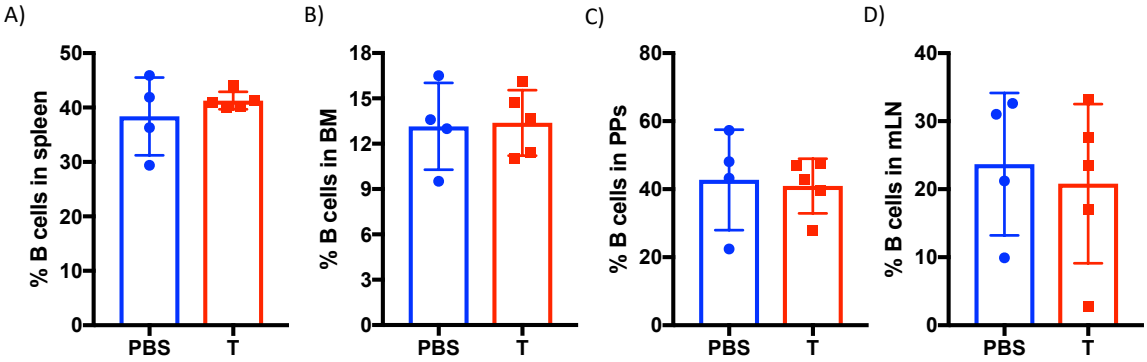

Figure 18. ***Tamoxifen does not impact B cell populations.*** *Mice were dosed with PBS control or 9mg tamoxifen (T). Flow cytometric analysis of proportion of B cells (B220+) in* ***(A)*** *spleen,* ***(B)*** *bone marrow (BM),* ***(C)*** *Peyer's patches (PP) and* ***(D)*** *mesenteric lymph nodes (mLN). Each dot represents one mouse and data are depicted with mean +/- SD.*

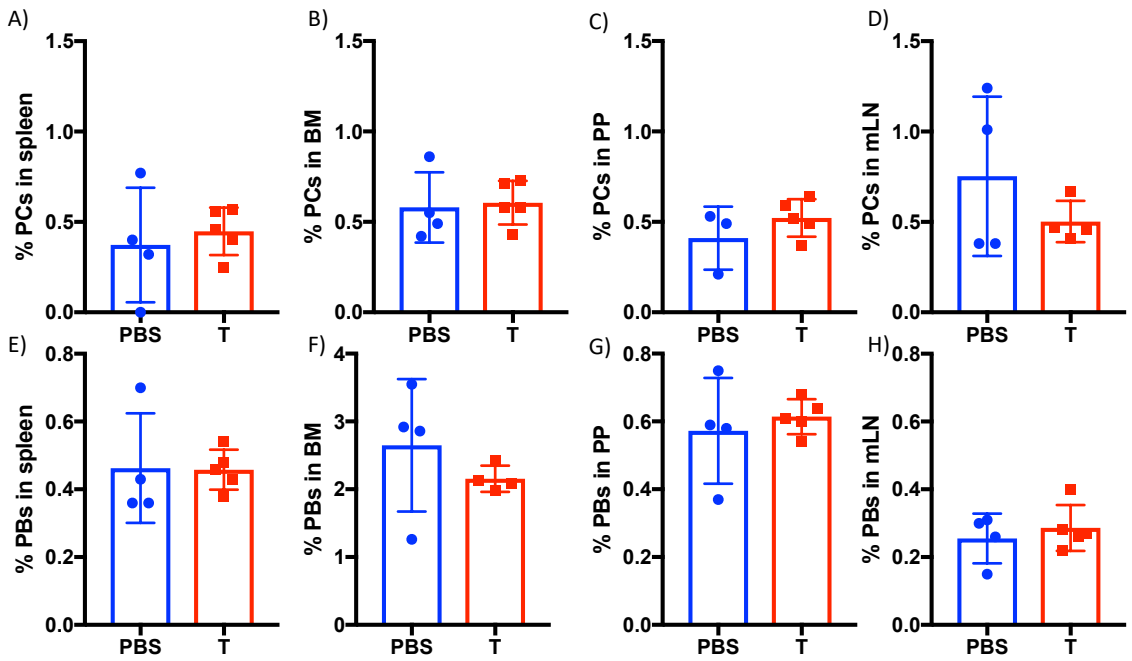

Figure 19. ***Tamoxifen does not impact plasma cell or plasmablast populations.*** *Mice were dosed with PBS control or 9mg tamoxifen (T). Flow cytometric analysis of proportion of plasma cells (PCs; CD138+B220-) in* ***(A)*** *spleen,* ***(B)*** *bone marrow (BM),* ***(C)*** *Peyer's patches (PP) and* ***(D)*** *mesenteric lymph nodes (mLN). Flow cytometric analysis of proportion of plasmablasts (PBs; CD138+B220+) in* ***(E)*** *spleen,* ***(F)*** *bone marrow (BM),* ***(G)*** *PP and* ***(H)*** *mLN. Each dot represents one mouse and data are depicted with mean +/- SD.*

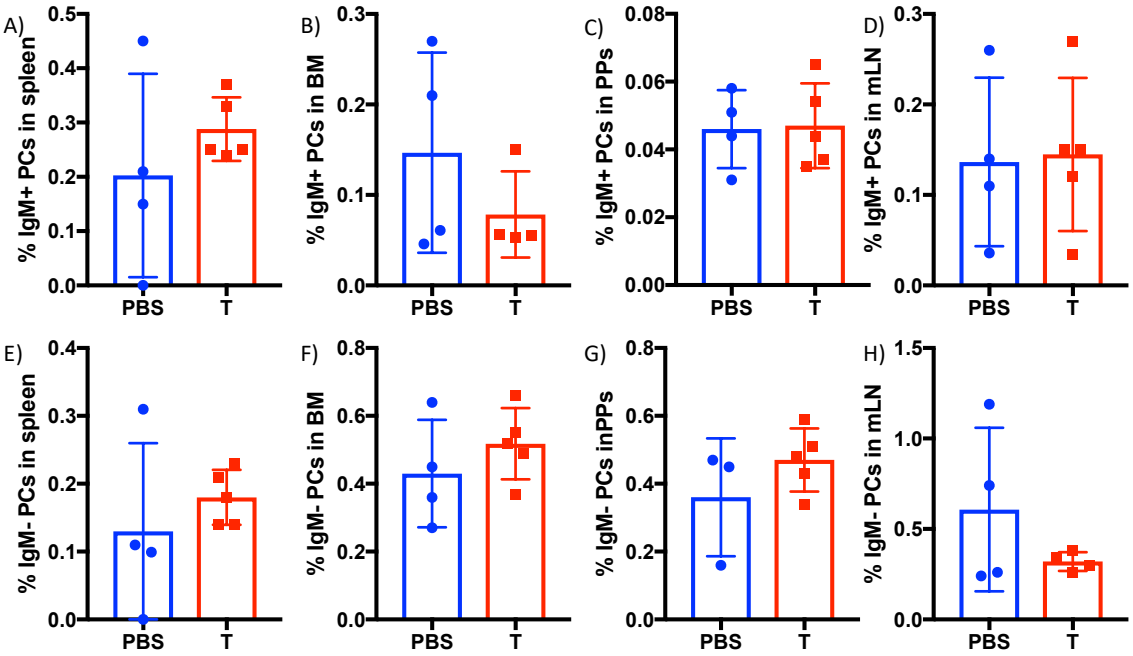

Figure 20. ***Tamoxifen does not impact plasma cell antibody isotype.*** *Mice were dosed with PBS control or 9mg tamoxifen (T). Flow cytometric analysis of proportion of IgM+ plasma cells (PCs; CD138+B220-) in* ***(A)*** *spleen,* ***(B)*** *bone marrow (BM),* ***(C)*** *Peyer's patches (PP) and* ***(D)*** *mesenteric lymph nodes (mLN). Flow cytometric analysis of proportion of IgM- PCs in* ***(E)*** *spleen,* ***(F)*** *bone marrow (BM),* ***(G)*** *PP and* ***(H)*** *mLN. Each dot represents one mouse and data are depicted with mean +/- SD.*

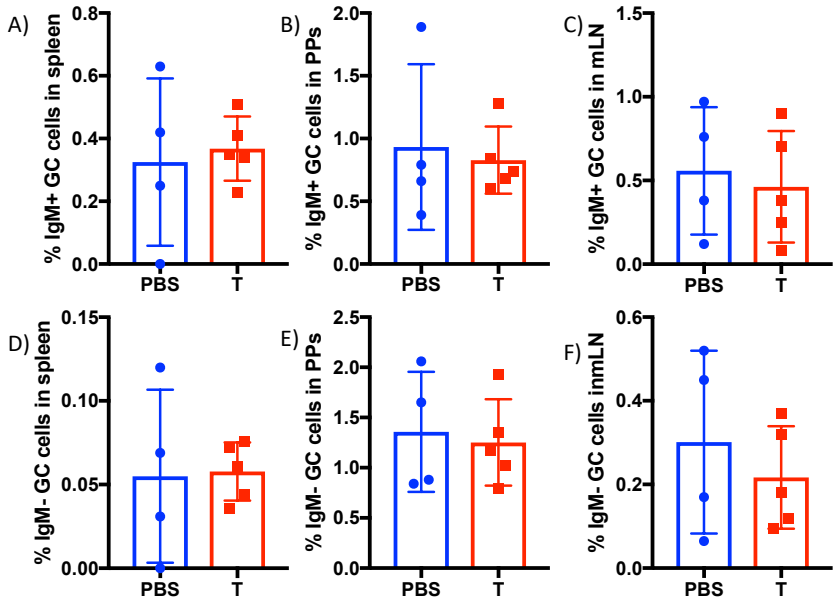

Figure 21. ***Tamoxifen does not impact GC cell antibody isotype.*** *Mice were dosed with PBS control or 9mg tamoxifen (T). Flow cytometric analysis of proportion of IgM+ germinal centre B cells (GC; GL7+CD95+) in* ***(A)*** *spleen,* ***(B)****) Peyer's patches (PP) and* ***(C)*** *mesenteric lymph nodes (mLN). Flow cytometric analysis of proportion of IgM- GC cells in* ***(D)*** *spleen,* ***(E)*** *PPs and* ***(F)*** *mLNs. Each dot represents one mouse and data are depicted with mean +/- SD.*

Tamoxifen did not induce a germinal centre response in any of the lymphoid organs *(Figure 22A-C)*. EYFP labelled GC B cells could only be detected in spleen, PPs and mLNs of the tamoxifen-treated group of female $LDLr^{-/-}$ AEL mice demonstrating the specificity of the mouse model system *(Figure 22D-F)*.

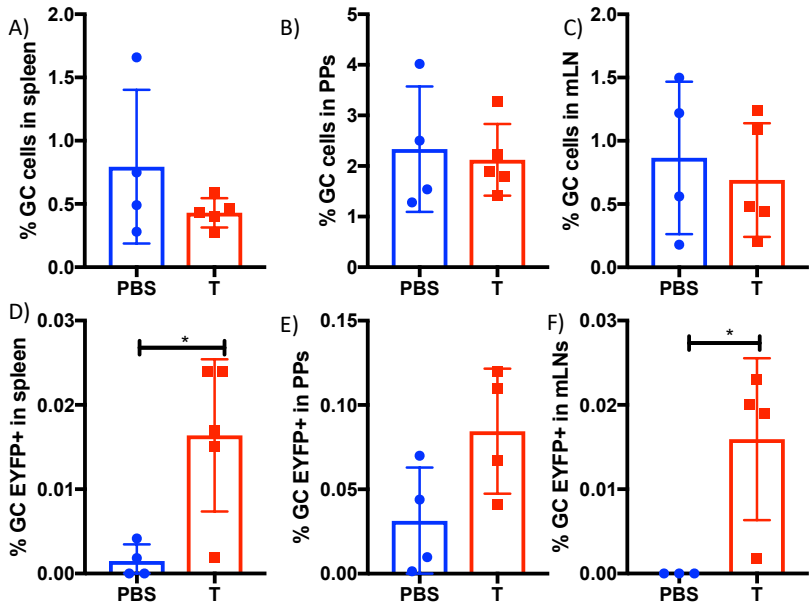

Figure 22. ***Tamoxifen does not induce a GC response and EYFP+ GC cells are only detectable upon tamoxifen administration.*** *Mice were dosed with PBS control or 9mg tamoxifen (T). Flow cytometric analysis of proportion of germinal centre B cells (GC; GL7+CD95+) in (A) spleen, (B) Peyer's patches (PP) and (C) mesenteric lymph nodes (mLNs). Flow cytometric analysis of proportion of GC cells labelled with EYFP (GC EYFP) in (D) spleen, (E) PPs and (F) mLNs. Each dot represents one mouse and data are depicted with mean +/- SD. Statistics carried out using Mann-Whitney test, * P < 0.05; ** P < 0.01; *** P < 0.001; **** P < 0.0001.*

Tamoxifen had no impact on serum IgG1 and IL6 but did reduce titres of serum IgM and IgG2c while serum SAA levels were elevated *(Figure 23)*.

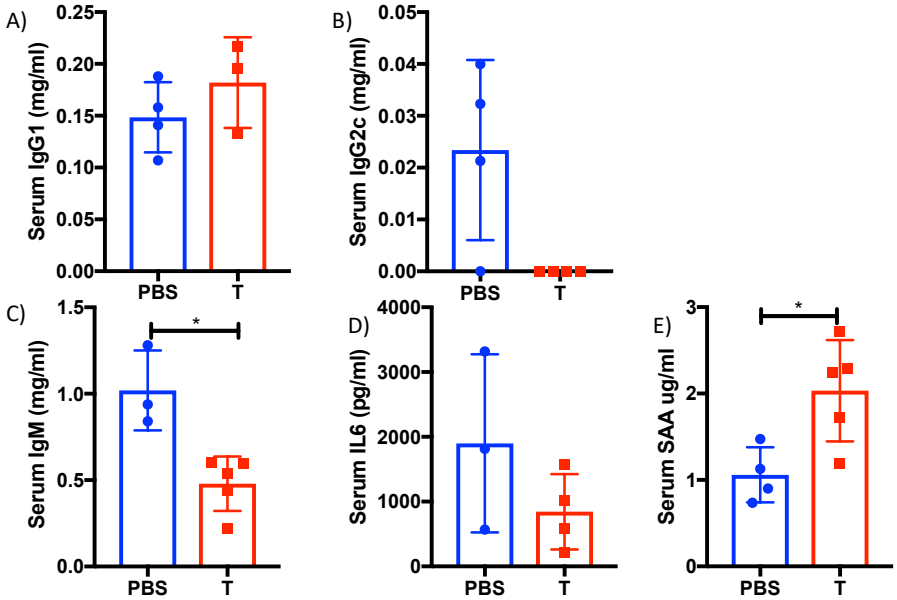

Figure 23. ***Tamoxifen impacts levels of some serum antibodies.*** *Serum from mice dosed with either PBS control or 9mg tamoxifen was analysed by ELISA for titres of* ***(A)*** *IgG1,* ***(B)*** *IgG2c,* ***(C)*** *IgM,* ***(D)*** *IL6 and* ***(E)*** *SAA. Each dot represents one mouse and data are depicted with mean +/- SD. Statistics carried out using Mann-Whitney test, * P < 0.05; ** P < 0.01; *** P < 0.001; **** P < 0.0001. Data represent n = 4 for PBS-treated mice and n = 5 for tamoxifen-treated mice, where these numbers are not reflected in the graphs this is due to values for mice being below limit for detection threshold.*

3.6 In vitro GC culture

In vitro culture of GC B cells has been challenging for many years making it hard to elucidate the regulation of GC B cells. However, a method has been described in recent literature by Haniuda et al[267] *(Figure 24)*. They used a fibroblast feeder cell line which expressed endogenous CD40L and BAFF critical for B cell survival and proliferation. Provision of BAFF enabled the memory phenotype to be acquired[268]. Cultured on this layer with addition of IL4 for the first 4 days followed by IL21 for days 4-8, naïve B cells proliferated exponentially, displayed GC phenotypic markers GL7, PNA and Bcl6, and had capacity to class switch. IL21 increased the proliferative capacity of the cultured cells and increased Bcl6 expression[268].

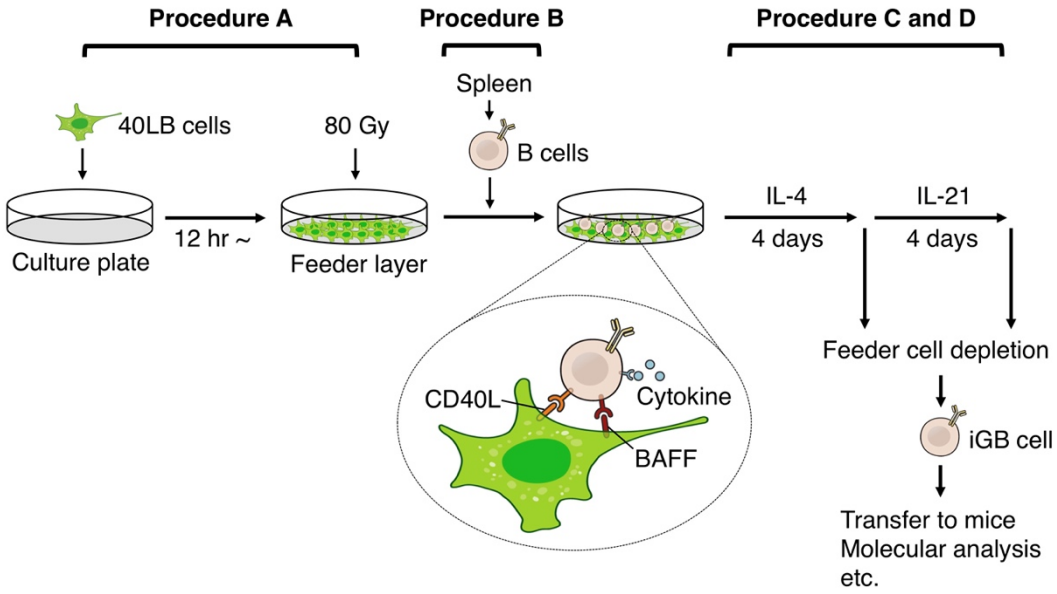

Figure 24. ***Method for culture of induced-germinal centre B cells (iGB) as created by Haniuda et al.*** *40LB cells were a feeder cell line generated from Balb/c 3T3 cell line with exogenous expression of CD40L and BAFF. 40LB cells were seeded in 10cm culture dishes for around 12 hours to allow cells to attach and spread out before irradiation with 80 Gy of γ-ray to stop proliferation. B cells were isolated and purified from mouse spleen and seeded on 40LB feeder layer. Once they started to proliferate the cells were termed 'iGB cells'. Cells were cultured with IL4 for 4 days with the option of following with IL21 for 4 days. The feeder cell layer is depleted using an antibody depletion cocktail to allow harvest of pure iGC cell population which can then be transferred to mice or for molecular analysis.*

To determine whether it was possible to culture GC B cells without the feeder layer, an adapted method was created. ELISA plates were coated overnight at 4°C with anti-CD40 (2μg/ml) and BAFF (2μg/ml). A spleen was harvested from a mouse and B cells were isolated using the AutoMACS machine and B cell isolation kit. Isolated B cells were seeded at $1x10^5$/well on ELISA plate in IL4 (1ng/ml) supplemented media. After 3 days, media was

refreshed with addition of soluble anti-CD40 (10μg/ml) and BAFF (20ng/ml) and cells were harvested between days 6-9.

The proportion of cells identified as B cells remained >90% at days 6 and 7 in all treatment groups *(Figure 25A)*. By day 9, this proportion had reduced in all conditions however presence of coated anti-CD40 and BAFF in either coated or soluble form maintained the highest proportion of B cells in the population of cells *(Figure 25A)*. A similar trend can be observed for GC cells *(Figure 25B)*. The combination of coated anti-CD40 and BAFF gave rise to the highest percentage of IgM+ GC cells *(Figure 25C)*. Plasma cells were most abundant when plates were coated with anti-CD40, and media was supplemented with soluble BAFF *(Figure 25D)*. The proportion of IgM+ PCs rose over time as would be expected as differentiation occurs and the coated CD40 plates with no BAFF supplementation appeared to produce the most IgM+ PCs *(Figure 25F)*.

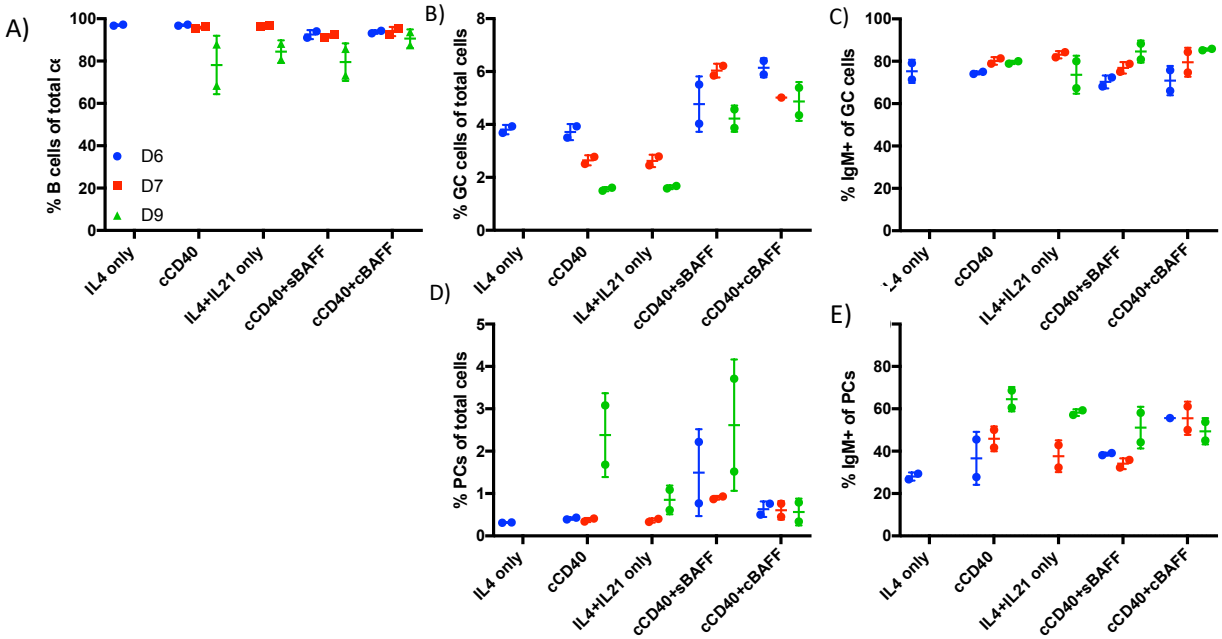

Figure 25. ***Phenotypic characterisation of cells cultured to form induced GC cells.*** *Cells were collected at day 6, 7 and 9 (D6, D7 and D9) and stained with antibodies for identification by flow cytometry. Cells were treated with IL4 supplemented media, addition of IL21 to media (all treatments except for IL4 only), anti-CD40 coated on plates (cCD40) and BAFF in either coated form (cBAFF) or soluble form (sBAFF). Proportion of cells identified as* ***(A)*** *B cells using B220,* ***(B)*** *GC cells using CD95 and GL7,* ***(C)*** *IgM+ GC cells using CD95, GL7 and IgM,* ***(D)*** *plasma cells using CD138 and* ***(E)*** *IgM+ plasma cells using CD138 and IgM. Each dot represents one treatment well.*

3.7 Discussion

3.7.1 AEL validation

The data presented in this chapter provides validation of the AEL mouse model as EYFP expression was only detectable by flow cytometry when tamoxifen was administered to the animals. Furthermore, EYFP labelled cells could be visualised within the spleen of a high fat diet fed mouse by immunofluorescence staining. The trialling of dosing strategies demonstrated that labelling efficiency increases as the duration of dosing increases. The 3 doses by oral gavage regimen induced a similar EYFP population size to that of the tamoxifen diet while 3 doses by intraperitoneal injection and 1 dose by oral gavage produced similar EYFP population sizes. This study highlighted that each dosing strategy has its benefits; the diet does label the greatest number of cells however specificity of the GC response is lost as dosing occurs over 2 weeks. On the contrary, there was a trade off in labelling efficiency with 1 dose of tamoxifen via oral gavage as a much smaller EYFP cell population was produced yet this strategy had the advantage that a single snapshot in time had been captured. Thus, the dosing strategy chosen was aligned with the aims of each study i.e., whether maximum labelling or a single snapshot was more important.

The data show that EYFP+ labelling efficiency remains stable up to 20% of GC B cells and is reliable as it is not affected by diet or time. This gives confidence that any differences in EYFP labelling are due to differences in GC dynamics related to the pathology occurring in the different mice. The low labelling efficiency is sub optimal and must be taken into account when interpreting results as not all GC cells are captured through labelling. An open question remains whether the lack of complete labelling of the GC cells is due to lack of Cre activity (low tamoxifen dose received by some cells or other failure of CreER2) despite adequate AID expression or due to some of the expression of AID being cyclical and insufficient to induce recombination at the time of labelling in all GC cells.

The toxicity of the tamoxifen was investigated and found not to impact viability of cells or any of the following populations: B cells, plasma cells, plasmablasts and GC B cells. Additionally,

isotype class switching was not affected as proportions of IgM+ and IgM- cells remained the same in the plasma cell and germinal centre B cell pools. The specificity of the model was again demonstrated by the presence of EYFP+ labelled GC B cells only in the tamoxifen treated condition. Serum IgG1 and IL6 were not impacted by tamoxifen, however serum IgM and IgG2c levels were diminished. This could explain why IgG2c titre levels were so variable across studies and therefore data was not included in the thesis for the majority. Future validatory experiments should compare IgM and IgG2c levels between mice with and without a tamoxifen dose at the different timepoints and with different diets included in this thesis. It is possible that with reduced concentrations of serum IgG2c and IgM this has a causal impact on atherosclerosis. Contrastingly, serum SAA levels were increased suggesting that tamoxifen is either detected by the liver directly or indirectly and induces an early acute phase response resulting in inflammation. However, as all of the mice in experimental cohorts were dosed with tamoxifen these effects are unlikely to influence the results significantly.

It has recently been discovered that the majority of class switching occurs before a cell enters the GC response and as such, not all AID-expressing cells are GC cells. However, the majority of class switched cells will go on to participate in the GC reaction with a small proportion forming the extrafollicular response. Additionally, CD138+ plasma cells are the major output of extrafollicular responses, but the EYFP labelled cells which are not of GC phenotype, GL7+, are not CD138+ plasma cells. As AID is expressed during CSR as well as the GC response, it is possible that some AID-expressing cells will be labelled with EYFP despite never having entered a GC reaction. This is a limitation of the lineage tracing model and will be taken into consideration when interpreting results. Furthermore, given the low labelling efficiency it appears that high AID expression, not just any expression level, is required for tamoxifen-inducible Cre recombinase to work and hence turn on EYFP expression. In previous experiments, EYFP labelling was shown to be very low in extrafollicular populations[266].

3.7.2 In vitro GC culture

The pilot studies to culture GC B cells *in vitro* without the CD40LB feeder layer showed promise with GC B cells and PCs identified by flow cytometry. However, there were large shortcomings compared to the *in vivo* system as only simple aspects of the GC reaction could

be recapitulated. Due to time constraints, further optimisation of these methods was not conducted but could be done to enable experiments such as analysing the impact of particular antigens, i.e., oxLDL, on the GC response and output.

In future, a 3D cell culture system such as organoids could be developed as this would provide the 3D architecture and signals required by a GC response. Potentially this method would simulate the *in vivo* conditions to a better degree and thus reduce the need for animal usage. This could be beneficial as *in vivo* models come with layers of complexity which can be stripped back with a simpler cell culture system.

3.7.3 Future work

There is the possibility that clones produced in the PPs travel to the spleen to seed further rounds of SHM. If PP-derived GC clones (i.e., external) could be differentiated from spleen-derived GC clones (i.e., internal) within the spleen this could be of interest. Furthermore, it would be interesting to determine which tissues contribute to and by how much to the cell populations within the BM.

Initial optimisation of intracellular antibody isotypes was conducted, however due to time constraints this flow cytometry antibody panel was not utilised. In order to detect a significant population of each antibody isotype, large cell populations must be used with more time allowed for each sample to run on the flow cytometer. Thus, experiments specifically designed to analyse isotype dynamics should be conducted for this purpose.

4 GC responses increase in atherosclerotic conditions

4.1 Abstract

In order to characterise the GC response under atherosclerotic conditions, this chapter provides an extensive characterisation, including isotype dynamics and cellular outputs, of GC responses varied by genotype, time and diet type in order to disentangle the impact of each variable and its contribution to the GC response. The WT model was used to determine the impact of time in male chow diet-fed AEL mice, and to determine the impact of diet in male HFD-fed AEL mice. The LDLr$^{-/-}$ model was used to determine the impact of genotype in male chow diet-fed AEL mice and the combination of the LDLr$^{-/-}$ genotype and HFD replicated hyperlipidaemic conditions to determine the GC contribution to atherosclerosis. The data showed that there was an time-dependent increase in GC responses, however class-switching was not present at baseline. It was found that absence of LDL receptors, even in male chow diet-fed AEL mice, resulted in elevated serum cholesterol levels which caused an expansion in the GC response and a degree of class-switching. The feeding of HFD augmented the GC response inducing pathogenicity in the form of increased numbers of class-switched GC-derived clones. Combining HFD with the LDLr$^{-/-}$ genotype resulted in lymphoid organ hypertrophy at least partly due to increased GC B cell numbers, with greater progeny production and elevated class-switching. This data points towards the finding that serum cholesterol levels exacerbate and have a pathogenic impact on the GC response thus contributing to the chronic inflammatory conditions present in the context of atherosclerosis.

4.2 Background

In order to determine the impact of the GC response on atherosclerosis, a thorough characterisation of the response was required at key stages in the progression of the disease. In this chapter, the GC response and its cellular output, memory, and plasma cells, are described throughout the course of atherosclerosis creating a large body of data varied in genotype, time, and diet.

4.3 Aims

1. Characterise the GC response at baseline in WT mice
    a. *Using chow diet to determine the impact of time on GC responses*
    b. *Using high fat diet to determine the impact of diet alone on GC responses*

2. Characterise the GC response under atherosclerotic conditions in LDLr$^{-/-}$ mice
    a. *Using chow diet to determine the impact of LDLr deficiency on GC responses*
    b. *Using high fat diet to determine the impact of atherosclerosis on GC responses*

4.4 Results

Throughout experiments in this thesis, diet and time have been the main variables investigated. To determine the role played by the GC response during the course of atherosclerosis, the LDLr$^{-/-}$ background was utilised to induce hyperlipidaemia. However, as this adds an additional variable to the model, the GC response was initially characterised in male WT AEL mice to disentangle the impact of time and diet from the hyperlipidaemic conditions present in the LDLr$^{-/-}$ mouse model. Next, the differences observed between the WT and LDLr$^{-/-}$ mouse models are discussed to elucidate the impact that deficiency of the LDL receptor plays in the GC response. Then, the results for the LDLr$^{-/-}$ mouse model are investigated, first looking at chow diet to determine the impact of time in combination with the LDLr deficiency and finally looking at HFD which together with the genetic deletion of the LDL receptor results in atherosclerotic conditions. As such, some data is shown on more than one occasion in order to address one variable at a time. In this way, the results contribute to a clear picture of the interplay between all the variables and how they contribute to the phenotype observed.

4.4.1 Characterisation of the GC response at baseline in WT mice

Male WT AEL mice were fed either a chow diet or high fat diet (HFD) from 8 weeks of age (T0) for either 4 weeks (T4) or 8 weeks (T8) until 12 weeks and 16 weeks of age respectively *(Figure 26)*.

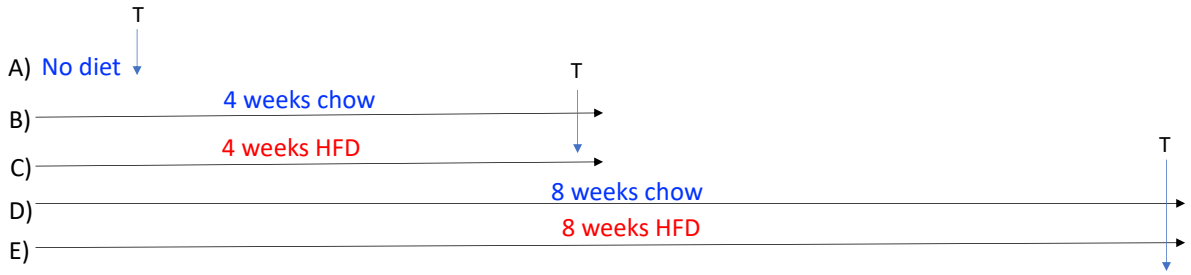

*Figure 26. **Standard experimental design.** Diagram of experimental setup – WT AEL male mice (LDLr$^{+/-}$) were **(A)** dosed with 9mg tamoxifen (T) via oral gavage at 8 weeks old 48hrs prior to sacrifice. Mice were started on chow diet and either kept on chow diet or put onto high fat diet (HFD) at 8 weeks old for either **(B, C)** 4 weeks or **(D, E)** 8 weeks until 12 weeks and 16 weeks old respectively. Mice were dosed with 9mg tamoxifen via oral gavage 48hrs prior to sacrifice.*

The spleen and para-aortic lymph nodes were chosen for analysis because the spleen gives a measure of systemic inflammation as it filters antigens from throughout the blood while the para-aortic lymph nodes provide a look at local inflammation as these lymphoid organs filter lymph. Both organs showed hypercellularity after 4 weeks of HFD feeding, significantly more so compared to chow diet feeding *(Figure 27A, D)*. The cell counts reduced again after 8 weeks of HFD feeding *(Figure 27A, D)*. Apart from this timepoint, cellularity was not impacted by diet type or time. The GC B cell population was only marginally increased after 4 weeks of diet in the spleen but expanded significantly at 8 weeks of diet compared to the 4-week timepoint *(Figure 27B)*. Furthermore, HFD caused a greater expansion of the GC population compared to chow diet at 8 weeks *(Figure 27B)*. In the PALN, the GC population was also only induced significantly at the 8-week timepoint and although not significant, there was a trend towards a greater GC population in HFD compared to chow diet-fed WT male mice *(Figure 27E)*. This expansion in the GC response was primarily driven by IgM- clones in both organs demonstrating that class switching has occurred *(Figure 27C, F)*.

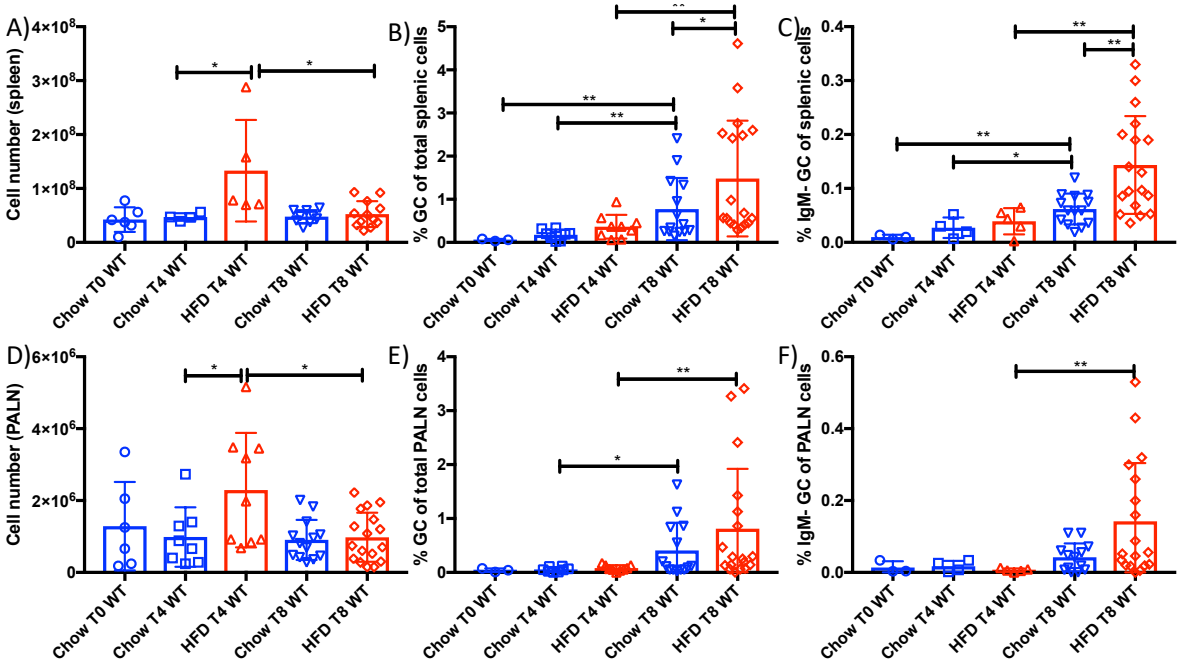

Figure 27. ***Changes in cell numbers and GC population over time in WT mice.*** *WT AEL male mice were fed either chow diet (blue) or high fat diet (HFD; red) for 0 (T0), 4 (T4) or 8 (T8) weeks. Total cellularity was shown in* ***(A)*** *spleen and* ***(D)*** *para-aortic lymph node (PALN) while proportion of cells identified as GC through flow cytometry analysis was shown in* ***(B)*** *spleen and* ***(E)*** *PALN. The proportion of GC cells which have IgM- isotype was shown for* ***(C)*** *spleen and* ***(F)*** *PALN. Each dot represents one mouse, graphs show mean +/- SD. Statistics carried out using Mann-Whitney test, * P < 0.05; ** P < 0.01; *** P < 0.001; **** P < 0.0001.*

The class switch ratio was used throughout this thesis as a measure of the extent of class switching occurring i.e., what proportion of GC clones, which all start out as IgM+, have undergone CSR to become different isotypes (IgM-). This was calculated by dividing the proportion of IgM- GC clones by the proportion of IgM+ GC clones. Thus, the higher the ratio value, the greater the amount of class switching occurring.

Analysis of both the inguinal and para-aortic lymph nodes showed that, at the 4-week timepoint, class switching was occurring more so in the chow diet-fed than the HFD-fed WT male mice *(Figure 28A, C)*. After 8 weeks of HFD, the extent of class switching was greater compared to the 4 weeks of HFD in both lymphoid organs *(Figure 28A, C)*. As the lineage tracing model permanently labels AID expressing cells with EYFP in the presence of tamoxifen, any cells detected with EYFP expression must have expressed AID at the time of tamoxifen-induced labelling. This comprises GC B cells, memory B cells and plasma cells. As can be seen below, it is possible to analyse both EYFP labelled and the total GC population (the total will include both labelled and non EYFP-labelled cells). The EYFP label on the GC B cells demonstrates that these cells were expressing AID at the time of labelling while the total GC

population will also include cells which have entered the GC reaction since the time of labelling. Class-switching within the EYFP GC B cell population was much greater after 8 weeks compared to 4 weeks HFD in both lymph node types *(Figure 28B, D)*.

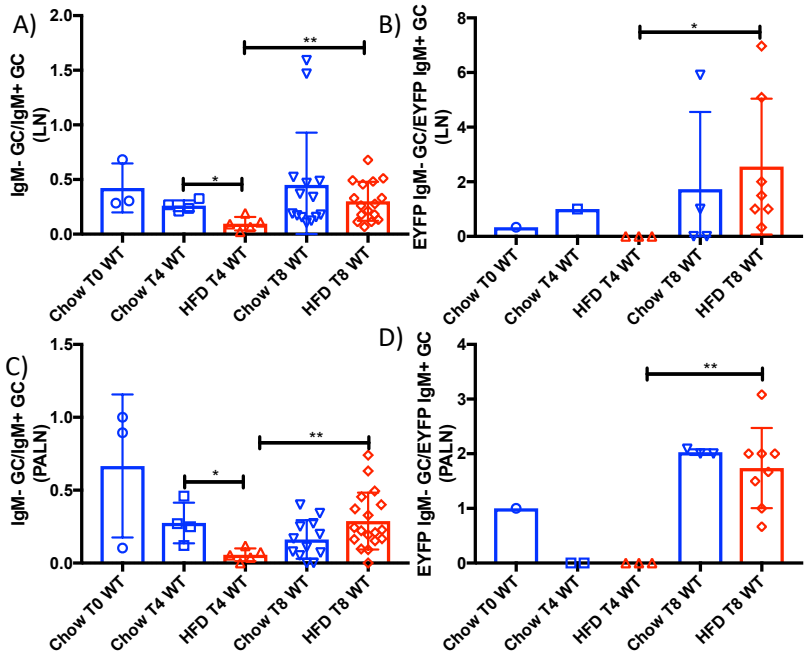

Figure 28. ***Class switching occurs more with time in HFD-fed WT mice.*** *WT AEL male mice were fed either chow diet (blue) or high fat diet (HFD; red) for 0 (T0), 4 (T4) or 8 (T8) weeks and 9mg tamoxifen was administered via oral gavage 48hrs prior to sacrifice. The class switch ratio was depicted in the* ***(A)*** *inguinal lymph node* ***(LN)*** *and (C) para-aortic lymph node (PALN). The EYFP class switch ratio (i.e., the amount of class switching between labelled clones) was shown for* ***(B)*** *LN and* ***(D)*** *PALN. Each dot represents one mouse, graphs show mean +/- SD. Statistics carried out using Mann-Whitney test, * P < 0.05; ** P < 0.01; *** P < 0.001; **** P < 0.0001.*

The level of EYFP labelling gradually increased over time in the spleen, both in proportional and absolute terms, and by the 8-week timepoint, male WT AEL HFD-fed mice had a significantly greater proportion of EYFP cells than male chow diet-fed WT AEL mice *(Figure 29A, D)*. In both sets of lymph nodes, the extent of EYFP labelling was only significant at the 8-week timepoint both in proportion and absolute terms *(Figure 29B, C, E, F)*.

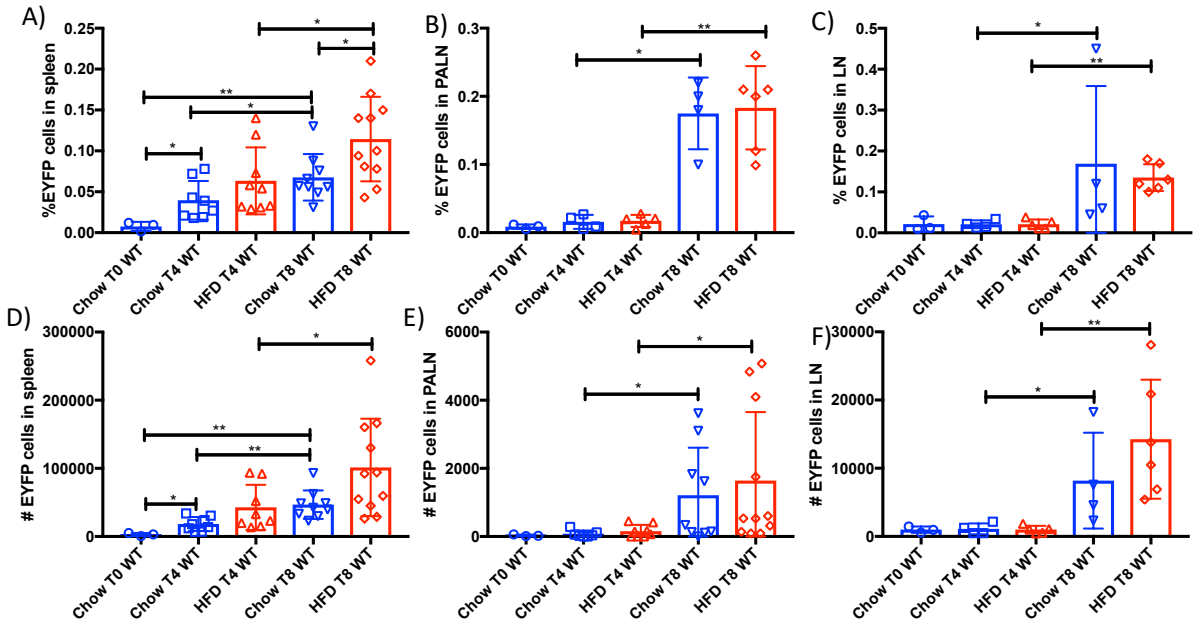

Figure 29. ***Presence of EYFP cells increases over time in WT mice.*** *WT AEL male mice were fed either chow diet (blue) or high fat diet (HFD; red) for 0 (T0), 4 (T4) or 8 (T8) weeks and 9mg tamoxifen was administered via oral gavage 48hrs prior to sacrifice. The proportion of cells labelled with EYFP was shown in* ***(A)*** *spleen,* ***(B)*** *para-aortic lymph node (PALN) and* ***(C)*** *inguinal lymph node (LN). The absolute number of EYFP+ cells was depicted in* ***(D)*** *spleen,* ***(E)*** *PALN and* ***(F)*** *LN. Each dot represents one mouse, graphs show mean +/- SD. Statistics carried out using Mann-Whitney test, * P < 0.05; ** P < 0.01; *** P < 0.001; **** P < 0.0001.*

The proportion of EYFP cells was also significantly greater at the 8-week timepoint compared to the 4-week timepoint regardless of diet in the bone marrow and blood of male WT AEL mice *(Figure 30)*. This showed that clones labelled after 8 weeks of diet are in circulation and homing to the bone marrow more so than at earlier time points.

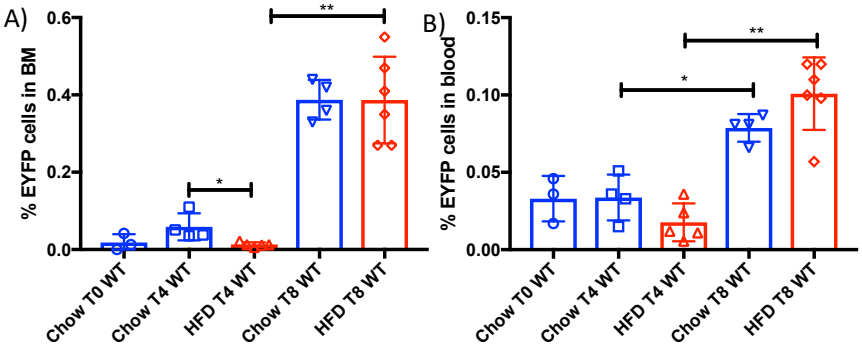

Figure 30. ***Presence of EYFP cells increases over time in WT mice.*** *WT AEL male mice were fed either chow diet (blue) or high fat diet (HFD; red) for 0 (T0), 4 (T4) or 8 (T8) weeks and 9mg tamoxifen was administered via oral gavage 48hrs prior to sacrifice. The proportion of cells labelled with EYFP was shown in* ***(A)*** *the bone marrow (BM) and* ***(B)*** *blood. Each dot represents one mouse, graphs show mean +/- SD. Statistics carried out using Mann-Whitney test, * P < 0.05; ** P < 0.01; *** P < 0.001; **** P < 0.0001.*

By looking more in depth at the EYFP population within the PALN, it can be seen that the EYFP GC population was significantly greater after 8 weeks of HFD feeding compared to both 8 weeks of chow diet feeding and 4 weeks of HFD feeding in male WT AEL mice *(Figure 31A)*. This was not isotype-specific as both IgM+ and IgM- clonal populations were significantly increased in the 8-week HFD group *(Figure 31B, C)*. As the 8-week chow diet group also showed a significant expansion of the EYFP GC IgM- clones *(Figure 31C)*, this implies that class switching of EYFP labelled cells occurs more over time even at baseline.

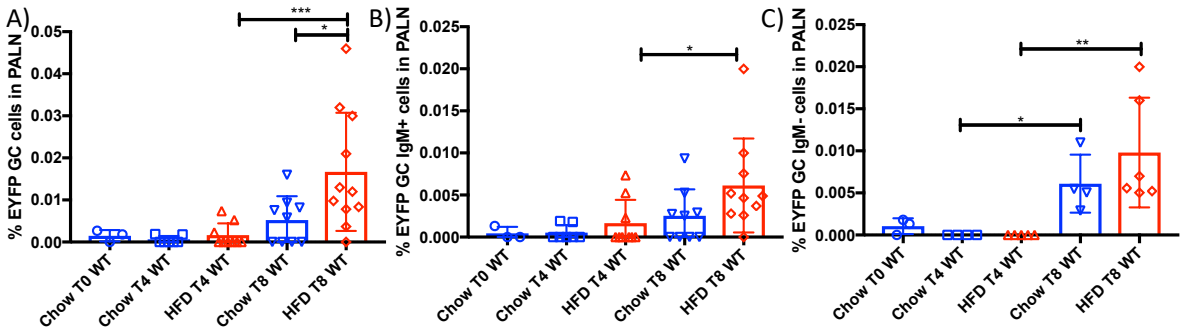

Figure 31. ***The EYFP GC population increases with HFD feeding in WT mice.*** *WT AEL male mice were fed either chow diet (blue) or high fat diet (HFD; red) for 0 (T0), 4 (T4) or 8 (T8) weeks and 9mg tamoxifen was administered via oral gavage 48hrs prior to sacrifice. Within the para-aortic lymph nodes (PALN), graphs show the proportion of EYFP cells which are* ***(A)*** *GC phenotype,* ***(B)*** *GC IgM+ phenotype and* ***(C)*** *GC IgM- phenotype. Each dot represents one mouse, graphs show mean +/- SD. Statistics carried out using Mann-Whitney test, * P < 0.05; ** P < 0.01; *** P < 0.001; **** P < 0.0001.*

In the spleen, both EYFP GC and memory cell populations increased over time as 8 weeks of chow diet feeding resulted in significantly larger populations compared to the zero timepoint in male WT AEL mice *(Figure 32A, B)*. Furthermore, both cell types were more common upon HFD feeding compared to chow diet feeding at the 4-week timepoint *(Figure 32A, B)*. This effect was also seen after 8 weeks of HFD compared to chow diet in the EYFP GC population *(Figure 32A)*.

The fate of every GC reaction was to produce memory and plasma cells before its demise. With flow cytometric analysis, it was impossible to know whether EYFP GC clones belong to the same or different GC reactions. Hence a greater number of EYFP GC cells could mean each GC was larger or there are more individual GCs ongoing. As a proxy, I have implemented the use of a parameter I term 'the GC to memory ratio'. By dividing the number of EYFP+ GC cells by the number of EYFP+ memory cells, a measure of the longevity of each GC was provided. A greater number of GC cells suggests that the GC reaction was still ongoing and therefore longer while if there was a greater number of memory cells it was suggestive that the GC

reaction was diminishing and therefore shorter. As can be seen, the GC to memory ratio within the spleen was significantly higher after 8 weeks of HFD compared to chow diet in male WT AEL mice suggesting that even in control conditions HFD causes greater and longer lasting GC reactions *(Figure 32C)*.

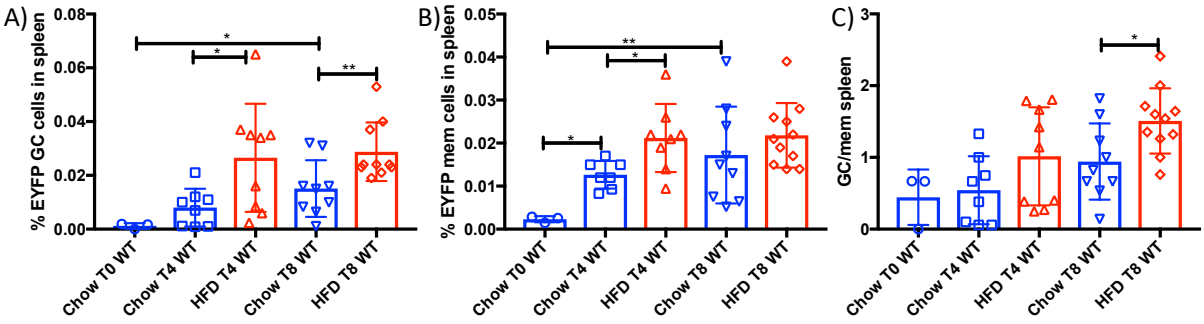

Figure 32. ***Increased splenic GC and memory cells over time in WT mice.*** *WT AEL male mice were fed either chow diet (blue) or high fat diet (HFD; red) for 0 (T0), 4 (T4) or 8 (T8) weeks and 9mg tamoxifen was administered via oral gavage 48hrs prior to sacrifice. Within the spleen, graphs depict the proportion of EYFP cells which are* ***(A)*** *GC phenotype and* ***(B)*** *memory (mem) phenotype. In* ***(C)*** *the splenic GC to memory (GC/mem) ratio was depicted. Each dot represents one mouse, graphs show mean +/- SD. Statistics carried out using Mann-Whitney test, * P < 0.05; ** P < 0.01; *** P < 0.001; **** P < 0.0001.*

The production of EYFP memory cells was seen at the 8-week timepoint in both inguinal and para-aortic lymph nodes and was significantly greater than that of the 4-week timepoint in both proportional and absolute terms *(Figure 33)*. Although not significant, there was a trend toward greater EYFP memory cell production upon HFD feeding compared to chow diet feeding in male WT AEL mice *(Figure 33)*.

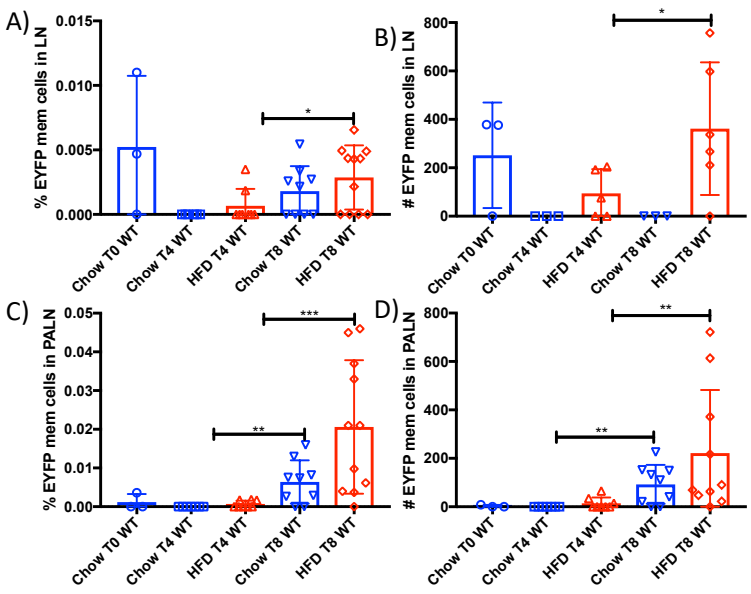

Figure 33. ***EYFP memory cell production increases over time in WT mice.*** *WT AEL male mice were fed either chow diet (blue) or high fat diet (HFD; red) for 0 (T0), 4 (T4) or 8 (T8) weeks and 9mg tamoxifen was administered via oral gavage 48hrs prior to sacrifice. In the lymph node (LN), the EYFP memory (mem) cell population was depicted in* ***(A)*** *proportional terms and* ***(B)*** *absolute terms. In the para-aortic lymph node (PALN), the EYFP memory (mem) cell population was depicted in* ***(C)*** *proportional terms and* ***(D)*** *absolute terms. Each dot represents one mouse, graphs show mean +/- SD. Statistics carried out using Mann-Whitney test, * P < 0.05; ** P < 0.01; *** P < 0.001; **** P < 0.0001.*

In the spleen, production of EYFP memory clones, both IgM+ and IgM-, increased with time as 8-week male chow diet-fed WT AEL mice had a significantly greater population than those at T0 *(Figure 34A, B)*. The IgM+ EYFP memory cell population was greater upon HFD feeding compared to chow diet feeding after 4 weeks in the spleen *(Figure 34A)*. The switched (IgM-) EYFP population was significantly expanded after 8 weeks compared to 4 weeks of HFD feeding in both the spleen and PALN *(Figure 34C, D)*. In the para-aortic lymph nodes, EYFP memory cell production was not detectable until the 8-week timepoint for both unswitched and switched clones *(Figure 34B, D)*.

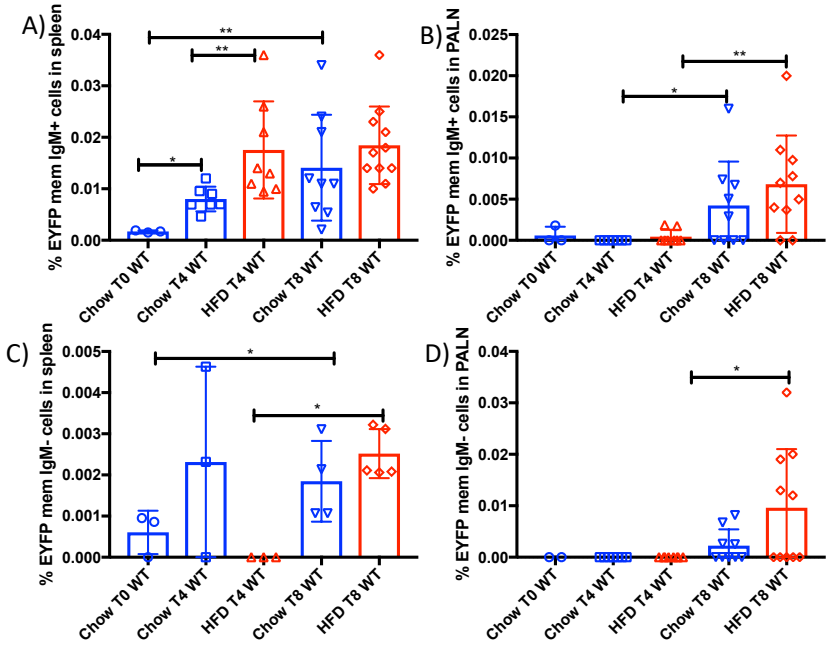

Figure 34. ***Increased presence of EYFP IgM- memory cell clones with time in WT mice.*** *WT AEL male mice were fed either chow diet (blue) or high fat diet (HFD; red) for 0 (T0), 4 (T4) or 8 (T8) weeks and 9mg tamoxifen was administered via oral gavage 48hrs prior to sacrifice. The proportion of total cells which are EYFP memory (mem) cells and are IgM+ was depicted in* ***(A)*** *spleen and* ***(B)*** *para-aortic lymph node (PALN). The proportion of total cells which are EYFP mem cells and are IgM- was depicted in* ***(C)*** *spleen and* ***(D)*** *PALN. Each dot represents one mouse, graphs show mean +/- SD. Statistics carried out using Mann-Whitney test, * P < 0.05; ** P < 0.01; *** P < 0.001; **** P < 0.0001.*

Within the spleen, 4 weeks of HFD resulted in a significant expansion of the plasma cell pool compared to both 4 weeks of chow diet and 8 weeks of HFD feeding in male WT AEL mice *(Figure 35A)*. The IgM+ plasma cell pool expanded with time as 8 weeks of chow diet resulted in a greater proportion of IgM+ PCs compared to the T0 timepoint *(Figure 35B)*. By the 8-week time point, HFD was responsible for a significantly bigger IgM+ plasma cell population compared to chow diet *(Figure 35B)*. Production of switched IgM- plasma cells was significantly greater at the 4-week timepoint compared to the 8-week timepoint for both diet types *(Figure 35C)*. These data suggest that plasma cells, and specifically IgM- clones, are responsible for the increased total splenic cellularity seen at the 4-week timepoint.

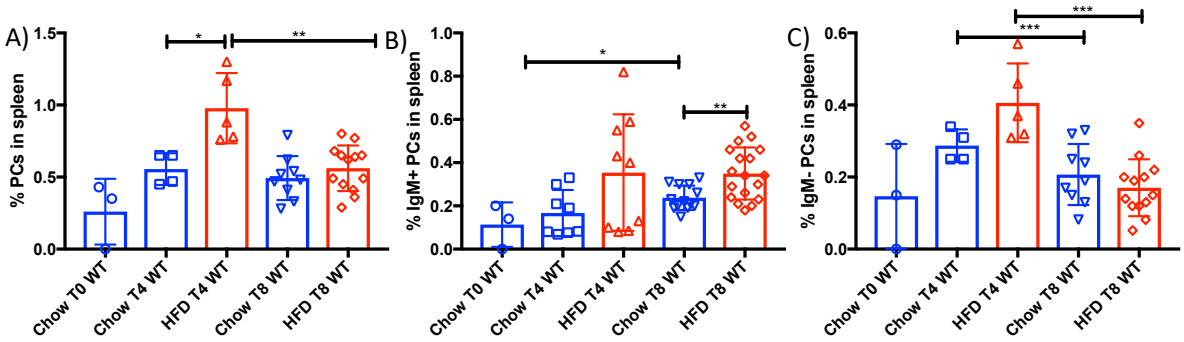

Figure 35. ***Increased splenic PC population at 4 week timepoint in WT mice.*** *WT AEL male mice were fed either chow diet (blue) or high fat diet (HFD; red) for 0 (T0), 4 (T4) or 8 (T8) weeks. Graphs depict the splenic proportion of* ***(A)*** *total plasma cells (PCs),* ***(B)*** *IgM+ PCs and* ***(C)*** *IgM- PCs. Each dot represents one mouse, graphs show mean +/- SD. Statistics carried out using Mann-Whitney test, * P < 0.05; ** P < 0.01; *** P < 0.001; **** P < 0.0001.*

The generation of EYFP labelled plasma cells was only significantly detectable at the 8-week timepoint in the spleen, PALN and LN of male WT AEL mice *(Figure 36A, D, G)*. This was not isotype specific as both IgM+ and IgM- EYFP plasma cell clones were expanded *(Figure 36B, C, E, F, H, I).* In the inguinal lymph nodes, HFD caused significantly greater EYFP plasma cell production than chow diet at the 8-week timepoint *(Figure 36G)*. This showed that the generation of EYFP labelled plasma cells increases with time in male WT AEL mice.

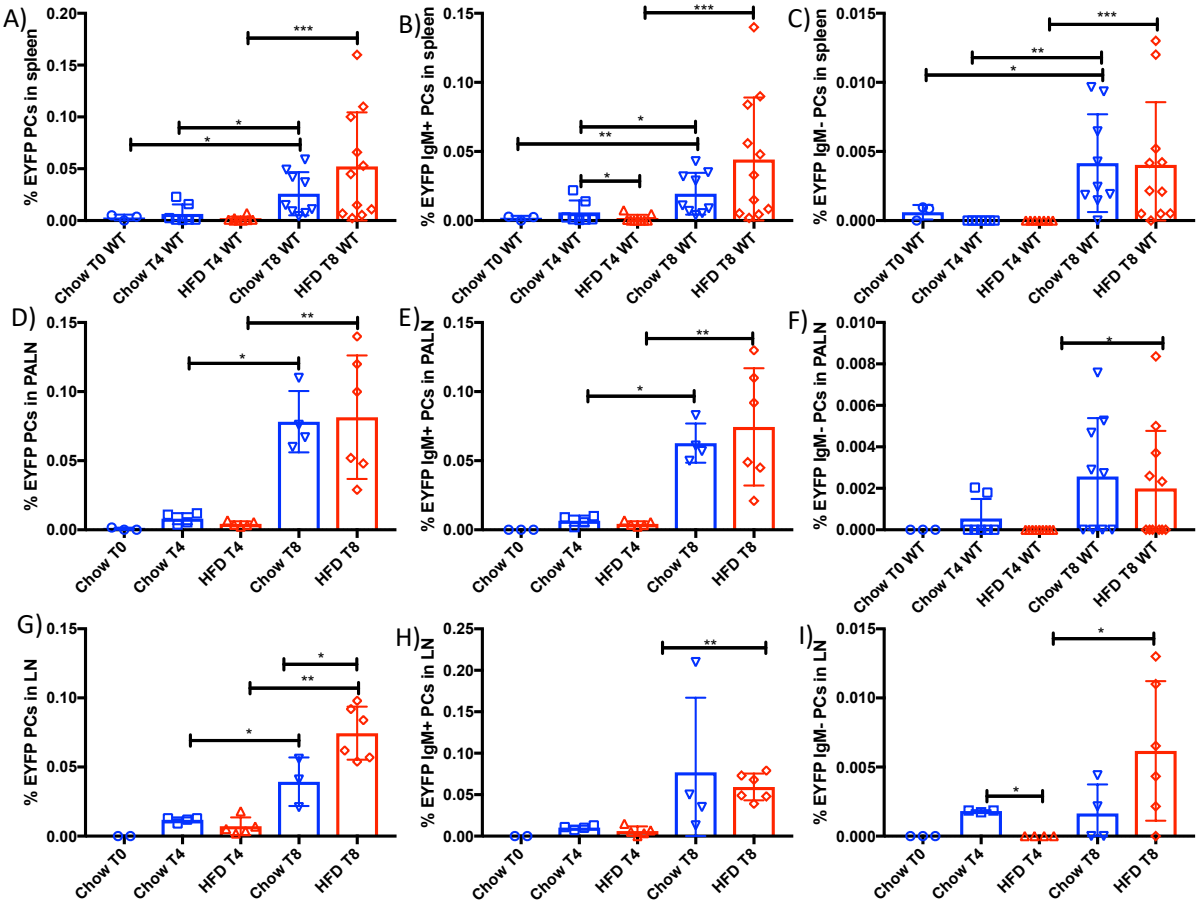

Figure 36. ***Increased presence of EYFP PCs over time in WT mice.*** *WT AEL male mice were fed either chow diet (blue) or high fat diet (HFD; red) for 0 (T0), 4 (T4) or 8 (T8) weeks and 9mg tamoxifen was administered via oral gavage 48hrs prior to sacrifice. Graphs depict the proportion of total EYFP plasma cells (PCs) in* ***(A)*** *spleen,* ***(D)*** *para-aortic lymph node (PALN) and* ***(G)*** *lymph node (LN). The proportion of EYFP PCs which are IgM+ was depicted in* ***(B)*** *spleen,* ***(E)*** *PALN and* ***(H)*** *LN. The proportion of EYFP PCs which are IgM+ was depicted in* ***(C)*** *spleen,* ***(F)*** *PALN and* ***(I)*** *LN. Each dot represents one mouse, graphs show mean +/- SD. Statistics carried out using Mann-Whitney test, * P < 0.05; ** P < 0.01; *** P < 0.001; **** P < 0.0001.*

Production of total splenic plasma cells was at its highest at the 4-week timepoint which did not align with the peak of splenic EYFP PC production at the 8-week timepoint; this suggests one of two possibilities – either GC reactions are quicker at the 8 week timepoint resulting in PC production within the 48hrs after labelling, or at the 8 week diet timepoint the GCs of male WT mice are more likely to produce PCs. As the proportion of EYFP memory cells exported

from splenic GCs was not significantly different between the 4 and 8 week timepoints *(Figure 32A)*, this would support the latter hypothesis as a quicker GC reaction would result in increased EYFP memory cell production at the 8-week timepoint. Furthermore, the splenic GC to memory ratio which measures GC longevity was not signficantly different between the 4 and 8 week timepoints *(Figure 32C)*. As PCs tend to be produced at later stages of the GC response when antibody affinity is high, this suggests that the GC cells which were labelled with EYFP at the 8 week timepoint (and differentiated into the EYFP labelled PCs) were of high affinity and therefore had likely undergone multiple rounds of SHM within the GC prior to labelling. This could be tested using BCR sequencing to determine the extent of mutation within EYFP GC cells and PCs at this timepoint compared to the 4 week timepoint and analysis could focus on overlap in sequence simiarlity between the cell types. In both inguinal and para-aortic lymph nodes, significant detection of EYFP cells only occurred after 8 weeks of diet *(Figure 29)* in line with the expansion of the GC population *(Figure 27)*. This then mirrored the significant increase in proportions of EYFP PCs and memory cells detected in these LNs at the 8 week timepoint implying that the increased GC activity was responsible for the increased production of GC-exported cells.

Analysis of the EYFP plasma cell pool within the BM showed similar results with greatest influx of labelled PCs, both IgM+ and IgM-, at the 8-week time point *(Figure 37)*. This suggests that the increased numbers of EYFP plasma cells across the lymphoid organs migrate and reside in the BM.

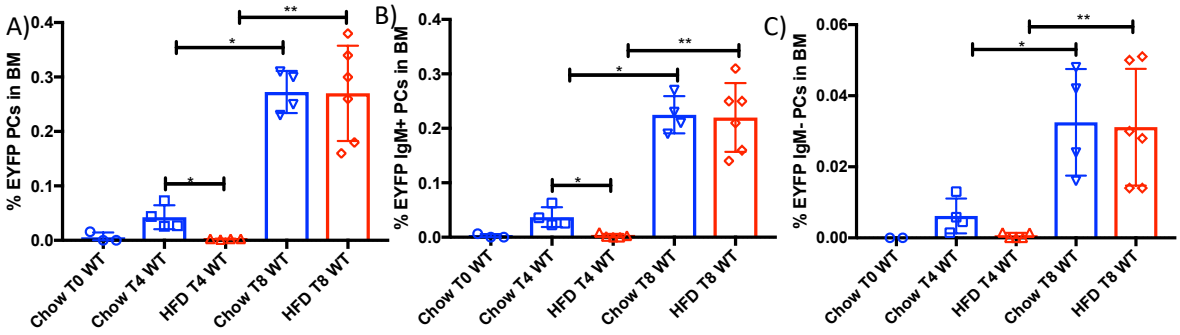

Figure 37. ***Increased presence of EYFP PCs in BM of WT mice with time.*** *WT AEL male mice were fed either chow diet (blue) or high fat diet (HFD; red) for 0 (T0), 4 (T4) or 8 (T8) weeks and 9mg tamoxifen was administered via oral gavage 48hrs prior to sacrifice. Within the BM, graphs depict* ***(A)*** *total EYFP plasma cell (PC) population,* ***(B)*** *IgM+ EYFP PCs and* ***(C)*** *IgM- EYFP PCs. Each dot represents one mouse, graphs show mean +/- SD. Statistics carried out using Mann-Whitney test, * P < 0.05; ** P < 0.01; *** P < 0.001; **** P < 0.0001.*

4.4.2 Differences between the WT and LDLr$^{-/-}$ mouse model

To understand the differences between the WT and LDLr$^{-/-}$ mouse background, the 2 strains were compared using the same experimental setup as shown in *(Figure 26)*. Across the spleen, LN and PALN there was a trend towards increased cellularity in the LDLr$^{-/-}$ mouse model compared to the WT background *(Figure 38)*. This reached statistical significance at the 4-week timepoint for both total and B cell numbers in the spleen *(Figure 38A, D)* and LN of chow diet and HFD-fed male LDLr$^{-/-}$ AEL mice *(Figure 38B, E)*. In both the inguinal and para-aortic lymph nodes, HFD resulted in increased total and B cell numbers after 8 weeks in the male LDLr$^{-/-}$ AEL mice compared to male WT AEL mice *(Figure 38B, C, E, F)*.

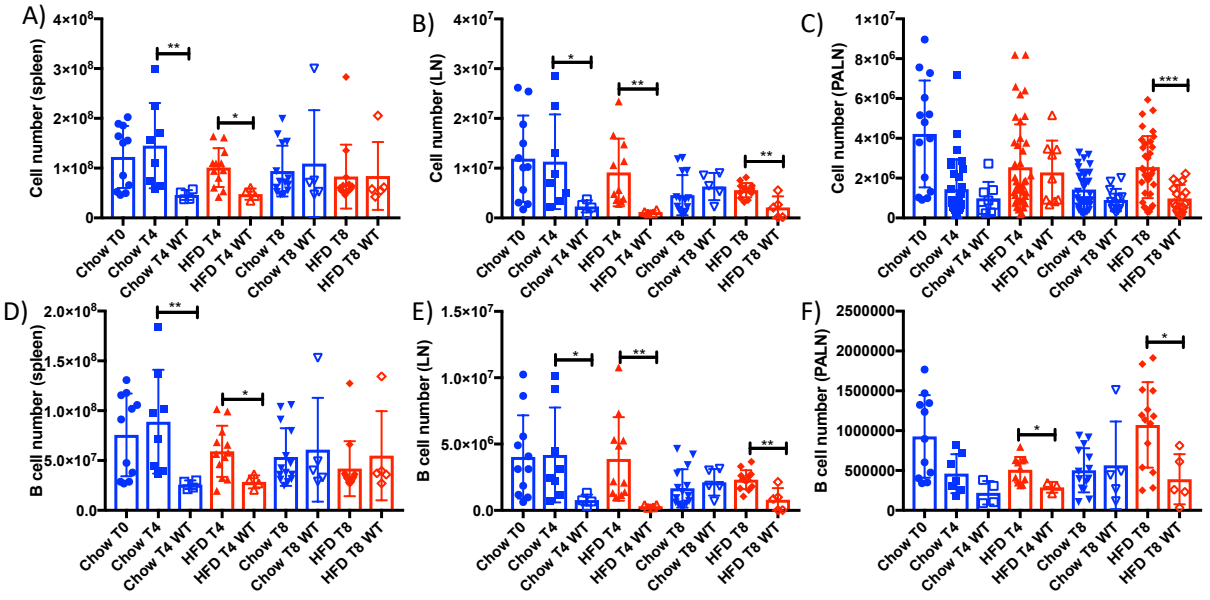

Figure 38. ***LDLr$^{-/-}$ tend to have increased cell numbers compared to WT mice.*** *WT (open symbols) and LDLr$^{-/-}$ (closed symbols) AEL male mice were fed either chow diet (blue) or high fat diet (HFD; red) for 0 (T0), 4 (T4) or 8 (T8) weeks. Graphs display total cell numbers for* ***(A)*** *spleen,* ***(B)*** *lymph node (LN) and* ***(C)*** *para-aortic lymph node (PALN). Graphs* ***(D-F)*** *display total B cell numbers for respective tissues. Each dot represents one mouse, graphs show mean +/- SD. Statistics carried out using Mann-Whitney test, * P < 0.05; ** P < 0.01; *** P < 0.001; **** P < 0.0001.*

The GC population was significantly bigger as a proportion of total cells within the spleen, LN and PALN after 4 weeks of diet in the LDLr$^{-/-}$ compared to WT AEL mouse model *(Figure 39A, B, C)*. This was also reflected at the 8-week timepoint in both the LN and PALN *(Figure 39B, C)*. The total number of GC cells was significantly higher after 4 weeks of diet in both the spleen and PALN while the same was true at 8 weeks of diet in the LN and PALN in male LDLr$^{-/-}$ AEL mice compared to male WT AEL mice *(Figure 39D, E, F)*.

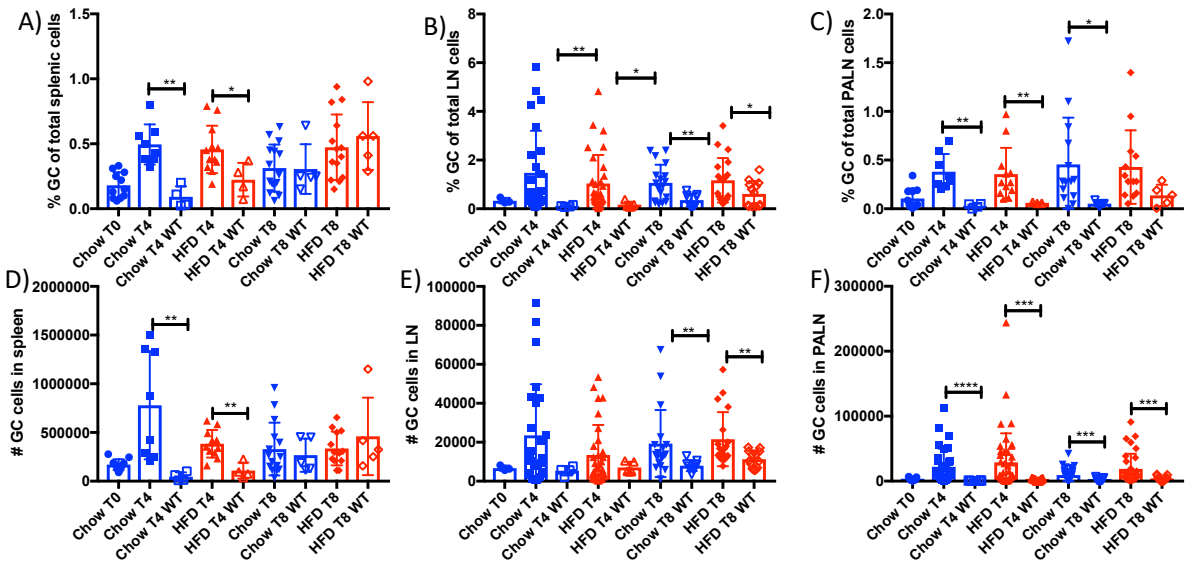

Figure 39. ***LDLr$^{-/-}$ have a bigger GC population compared to WT mice.*** *WT (open symbols) and LDLr$^{-/-}$ (closed symbols) AEL male mice were fed either chow diet (blue) or high fat diet (HFD; red) for 0 (T0), 4 (T4) or 8 (T8) weeks. Graphs display proportion of cells with GC phenotype in* ***(A)*** *spleen,* ***(B)*** *lymph node (LN) and* ***(C)*** *para-aortic lymph node (PALN). Graphs* ***(D-F)*** *display total GC B cell numbers for respective tissues. Each dot represents one mouse, graphs show mean +/- SD. Statistics carried out using Mann-Whitney test, * P < 0.05; ** P < 0.01; *** P < 0.001; **** P < 0.0001.*

Comparison of the GC clone isotypes revealed that there was significantly greater production of IgM+ GC clones at the pre-diet timepoint (chow T0) and after 8 weeks HFD in the spleen of male LDLr$^{-/-}$ AEL mice compared to male WT AEL mice *(Figure 40A)*. In the inguinal and para-aortic lymph nodes, IgM+ GC B cell populations were significantly greater at the 4-week timepoint regardless of diet and after 8 weeks of chow in the LN of male LDLr$^{-/-}$ AEL mice compared to male WT AEL mice *(Figure 40B, C)*. IgM- GC clone production was significantly greater at the 8-week timepoint in the spleen and LN regardless of diet in male LDLr$^{-/-}$ AEL mice compared to male WT AEL mice *(Figure 40D, E)*. Furthermore, the IgM- GC B cell population was significantly bigger after 4 weeks HFD in the LN and PALN in male LDLr$^{-/-}$ AEL mice compared to male WT AEL mice *(Figure 40E, F)*. Additionally, IgM- GC B cell production was significantly greater after 4 and 8 weeks of chow diet in the PALN in male LDLr$^{-/-}$ AEL mice compared to male WT AEL mice *(Figure 40F)*. This data show that both unswitched and class-switched GC B cells contribute to the enlargement of the GC seen in male LDLr$^{-/-}$ compared to male WT AEL mice.

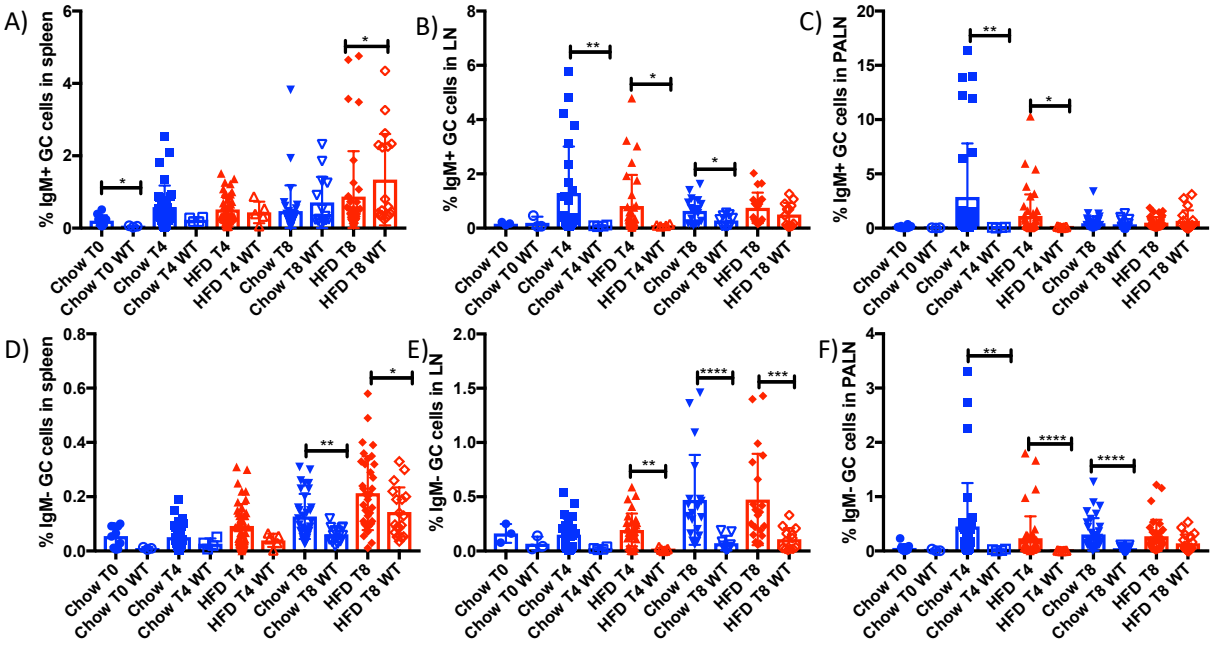

Figure 40. ***Increased production of IgM+ and IgM- GC clones in LDLr$^{-/-}$ compared to WT mice.*** *WT (open symbols) and LDLr$^{-/-}$ (closed symbols) AEL male mice were fed either chow diet (blue) or high fat diet (HFD; red) for 0 (T0), 4 (T4) or 8 (T8) weeks. Graphs display proportion of GC cells that are IgM+ in* ***(A)*** *spleen,* ***(B)*** *lymph node (LN) and* ***(C)*** *para-aortic lymph node (PALN). Graphs* ***(D-F)*** *display proportion of GC cells that are IgM- for respective tissues. Each dot represents one mouse, graphs show mean +/- SD. Statistics carried out using Mann-Whitney test, * P < 0.05; ** P < 0.01; *** P < 0.001; **** P < 0.0001.*

Despite this finding, it was not the case that production of IgM+ and IgM- GC clones increased proportionally as the class switch ratio was significantly increased in the LDLr$^{-/-}$ mouse model indicating that the ratio of IgM- GC clone production to IgM+ GC clone production was significantly higher in the male LDLr$^{-/-}$ AEL mice compared to the male WT AEL mice. The class switch ratio was significantly higher after 8 weeks of diet in all lymphoid organs analysed *(Figure 41)*. Furthermore, this result was also evident after 4 weeks of HFD in the inguinal and para-aortic lymph nodes showing that the high fat diet plays a pathogenic role in these organs which are more responsive to local inflammatory stimuli *(Figure 41C, D)*. This demonstrates that the LDLr$^{-/-}$ background provides a more pathogenic environment which induces greater class switching away from the IgM isotype.

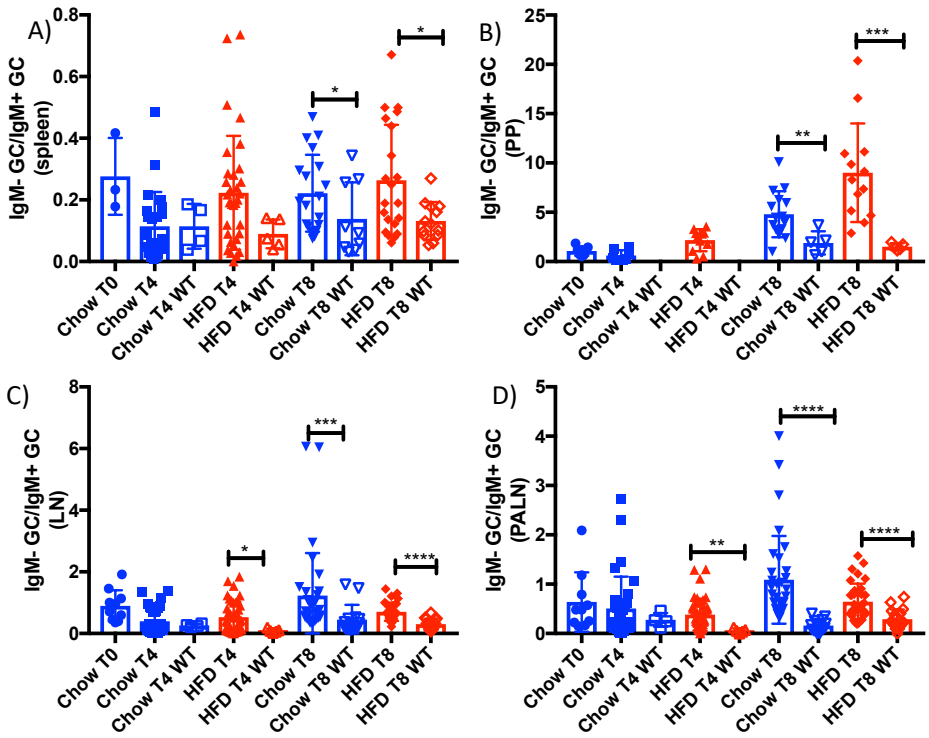

Figure 41. ***Increased class switching in LDLr$^{-/-}$ compared to WT mice. WT*** *(open symbols) and LDLr$^{-/-}$ (closed symbols) AEL male mice were fed either chow diet (blue) or high fat diet (HFD; red) for 0 (T0), 4 (T4) or 8 (T8) weeks. Graphs display the class switch ratio (i.e., proportion of IgM- GC cells divided by IgM+ GC cells) in* ***(A)*** *spleen,* ***(B)*** *Peyer's patches (PP),* ***(C)*** *lymph node (LN) and* ***(D)*** *para-aortic lymph node (PALN). Each dot represents one mouse, graphs show mean +/- SD. Statistics carried out using Mann-Whitney test, * P < 0.05; ** P < 0.01; *** P < 0.001; **** P < 0.0001.*

The proportion of cells labelled with EYFP was significantly greater after 4 weeks of HFD feeding in both sets of LNs and additionally after 8 weeks of chow diet in the inguinal lymph nodes in male LDLr$^{-/-}$ AEL mice compared to male WT AEL mice *(Figure 42A, B)*. Although not statistically significantly, there was a trend towards increased EYFP proportion at other timepoints across both tissues *(Figure 42A, B)*. The absolute number of EYFP labelled cells was significantly higher after 4 and 8 weeks of HFD feeding in both inguinal and para-aortic lymph nodes as well as after 4 weeks of chow diet feeding in the PALN of male LDLr$^{-/-}$ AEL mice compared to male WT AEL mice *(Figure 42C, D)*.

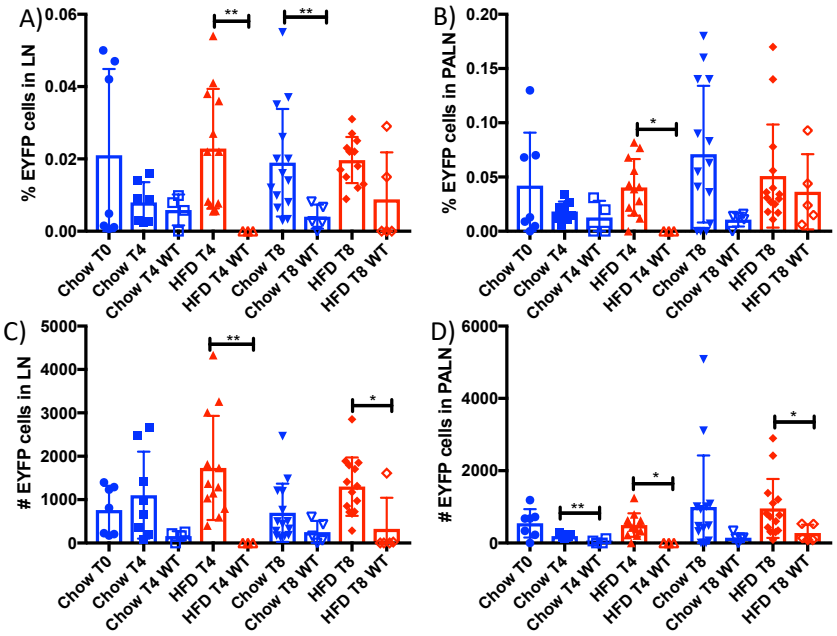

Figure 42. ***Increased EYFP population in LDLr$^{-/-}$ compared to WT mice.*** *WT (open symbols) and LDLr$^{-/-}$ (closed symbols) AEL male mice were fed either chow diet (blue) or high fat diet (HFD; red) for 0 (T0), 4 (T4) or 8 (T8) weeks and 9mg tamoxifen was administered via oral gavage 48hrs prior to sacrifice. Graphs display proportion of EYFP cells in* ***(A)*** *lymph node (LN) and* ***(B)*** *para-aortic lymph node (PALN). Graphs* ***(C, D)*** *display absolute number of GC cells for respective tissues. Each dot represents one mouse, graphs show mean +/- SD. Statistics carried out using Mann-Whitney test, * P < 0.05; ** P < 0.01; *** P < 0.001; **** P < 0.0001.*

On the LDLr$^{-/-}$ background after 4 weeks of HFD, there was a greater number of class switched IgM- EYFP GC clones in the PALN and PPs in male LDLr$^{-/-}$ AEL mice compared to male WT AEL mice *(Figure 43)*. This effect was also seen after 4 weeks of chow diet in the PPs.

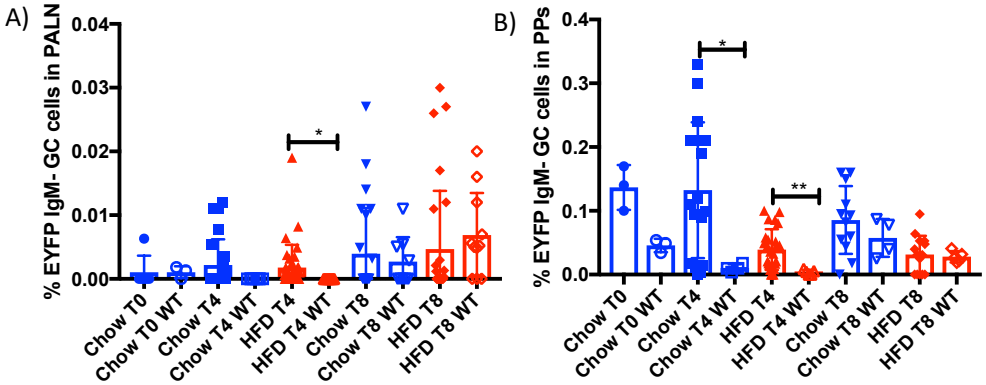

Figure 43. ***Increased EYFP IgM- GC production in LDLr$^{-/-}$ compared to WT mice.*** *WT (open symbols) and LDLr$^{-/-}$ (closed symbols) AEL male mice were fed either chow diet (blue) or high fat diet (HFD; red) for 0 (T0), 4 (T4) or 8 (T8) weeks and 9mg tamoxifen was administered via oral gavage 48hrs prior to sacrifice. Graphs display proportion of EYFP GC cells which are IgM- in* ***(A)*** *para-aortic lymph node (PALN) and* ***(B)*** *Peyer's patches (PPs). Each dot represents one mouse, graphs show mean +/- SD. Statistics carried out using Mann-Whitney test, * P < 0.05; ** P < 0.01; *** P < 0.001; **** P < 0.0001.*

The LDLr$^{-/-}$ mouse model had greater production of EYFP labelled memory cells compared to the WT mouse model. After 4 weeks of diet, the proportion and absolute number of EYFP memory cells produced was significantly greater in the LN and PALN of male LDLr$^{-/-}$ AEL mice compared to male WT AEL mice *(Figure 44B, C, E, F)*. This effect was also seen in the spleen and in the total number of EYFP memory cells across all 3 tissues after 8 weeks of HFD *(Figure 44A, D, E, F)*.

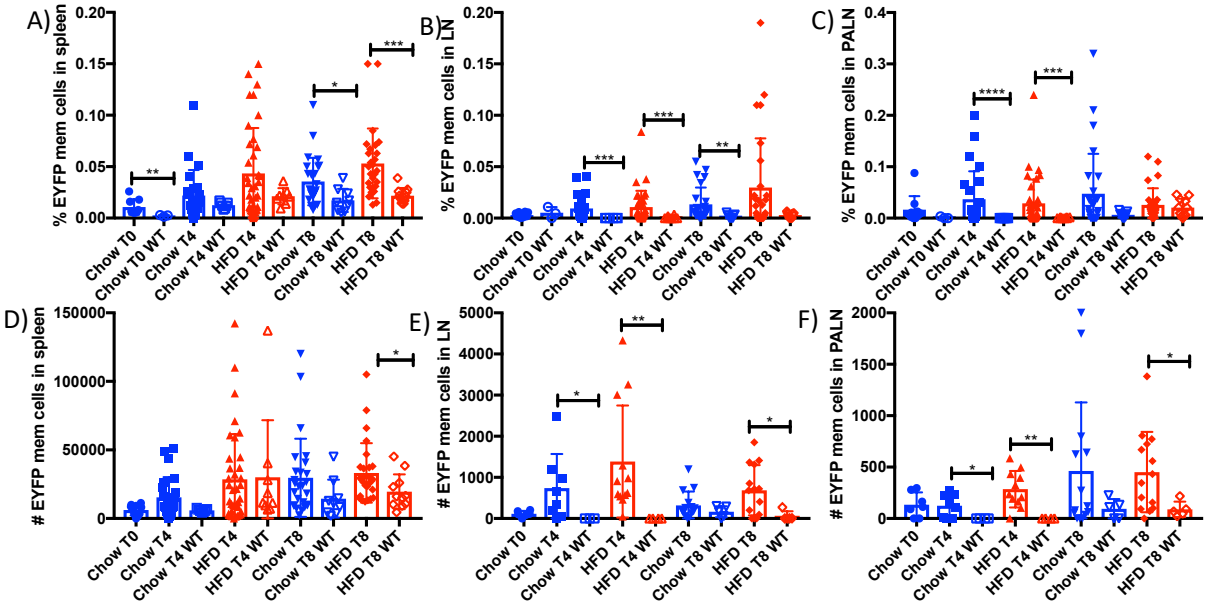

Figure 44. ***Increased EYFP memory presence in LDLr$^{-/-}$ compared to WT mice.*** *WT (open symbols) and LDLr$^{-/-}$ (closed symbols) AEL male mice were fed either chow diet (blue) or high fat diet (HFD; red) for 0 (T0), 4 (T4) or 8 (T8) weeks and 9mg tamoxifen was administered via oral gavage 48hrs prior to sacrifice. Graphs display proportion of EYFP memory (mem) cells in* ***(A)*** *spleen,* ***(B)*** *lymph node (LN) and* ***(C)*** *para-aortic lymph node (PALN). Graphs* ***(D-F)*** *display absolute number of EYFP memory cells for respective tissues. Each dot represents one mouse, graphs show mean +/- SD. Statistics carried out using Mann-Whitney test, * P < 0.05; ** P < 0.01; *** P < 0.001; **** P < 0.0001.*

Further analysis of the EYFP memory compartment revealed that EYFP IgM+ memory cell production was significantly greater after 4 weeks of diet in the PALN and after 8 weeks of HFD in the LN and PPs of male LDLr$^{-/-}$ AEL mice compared to male WT AEL mice *(Figure 45B, C, D)*. The EYFP labelled switched (IgM-) memory cell population was significantly expanded at the 4-week timepoint in both inguinal and para-aortic lymph nodes regardless of diet and after 4 weeks of HFD in the spleen of LDLr$^{-/-}$ compared to male WT AEL mice *(Figure 45E, F, G)*. In the PPs, IgM- EYFP memory cell production was significantly higher in male LDLr$^{-/-}$ AEL mice compared to male WT AEL mice after 8 weeks of diet *(Figure 45H)*.

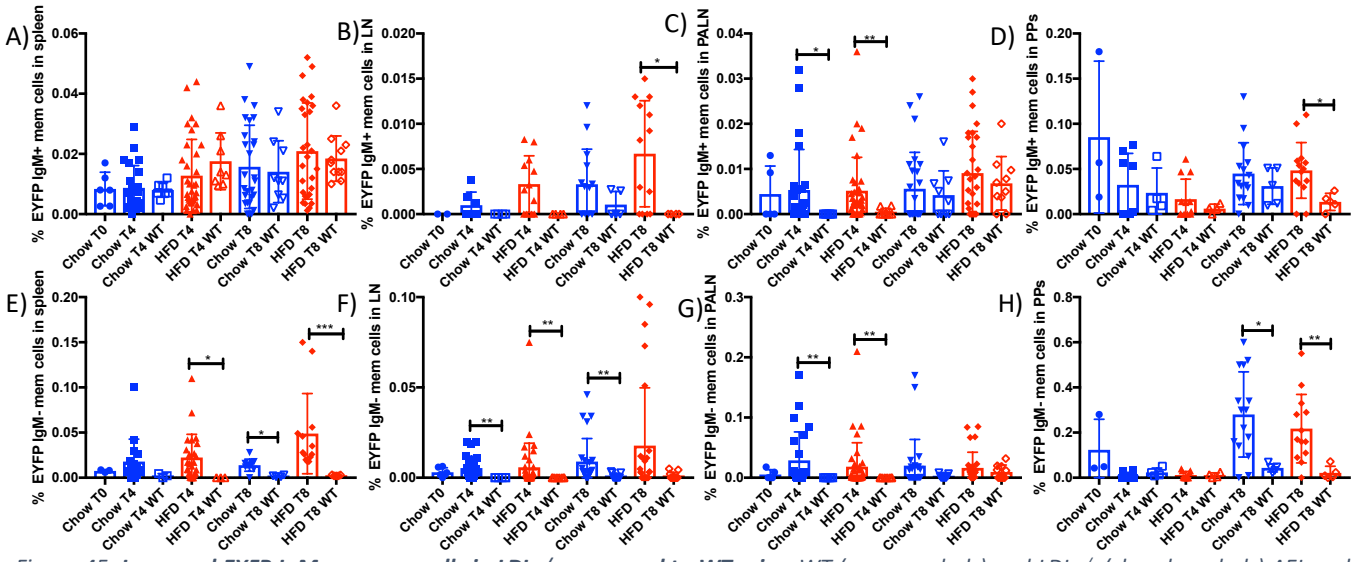

Figure 45. ***Increased EYFP IgM- memory cells in LDLr$^{-/-}$ compared to WT mice.*** *WT (open symbols) and LDLr$^{-/-}$ (closed symbols) AEL male mice were fed either chow diet (blue) or high fat diet (HFD; red) for 0 (T0), 4 (T4) or 8 (T8) weeks and 9mg tamoxifen was administered via oral gavage 48hrs prior to sacrifice. Graphs display proportion of EYFP IgM+ memory (mem) cells in* ***(A)*** *spleen,* ***(B)*** *lymph node (LN)* ***(C)*** *para-aortic lymph node (PALN) and* ***(D)*** *Peyer's patches (PPs). Graphs* ***(E-H)*** *display proportion of EYFP IgM- memory cells for respective tissues. Each dot represents one mouse, graphs show mean +/- SD. Statistics carried out using Mann-Whitney test, * P < 0.05; ** P < 0.01; *** P < 0.001; **** P < 0.0001.*

Analysis of the plasma cell output from the GC showed that 8 weeks of HFD resulted in increased plasma cell production across the spleen, LN, PALN and PPs of male LDLr$^{-/-}$ AEL mice compared to male WT AEL mice *(Figure 46)*. The plasma cell population was bigger after 4 weeks of diet in the spleen and 8 weeks of diet in the LN of male LDLr$^{-/-}$ AEL mice compared to male WT AEL mice *(Figure 46A, C)*. Additionally, 4 weeks of HFD resulted in an expanded plasma cell pool in the PPs on the LDLr$^{-/-}$ background compared to WT background *(Figure 46B)*.

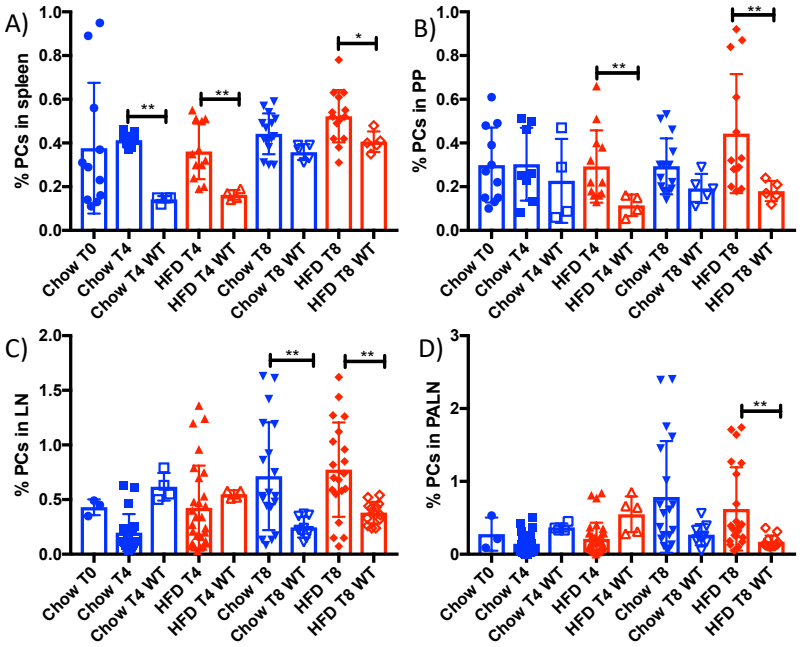

Figure 46. ***Increased PC populations in LDLr$^{-/-}$ compared to WT mice.*** *WT (open symbols) and LDLr$^{-/-}$ (closed symbols) AEL male mice were fed either chow diet (blue) or high fat diet (HFD; red) for 0 (T0), 4 (T4) or 8 (T8) weeks Graphs display proportion of plasma cells (PCs) in* ***(A)*** *spleen,* ***(B)*** *Peyer's patches (PPs),* ***(C)*** *lymph node (LN) and* ***(D)*** *para-aortic lymph node (PALN). Each dot represents one mouse, graphs show mean +/- SD. Statistics carried out using Mann-Whitney test, * P < 0.05; ** P < 0.01; *** P < 0.001; **** P < 0.0001.*

Characterisation of the isotype balance in the plasma cell pool revealed that in both the spleen and PPs, IgM+ plasma cell production was significantly higher after 4 weeks of diet in the male LDLr$^{-/-}$ AEL mice compared to male WT AEL mice *(Figure 47)*.

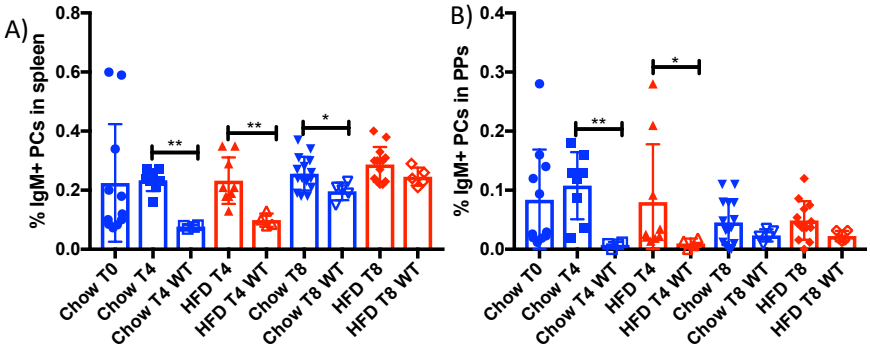

Figure 47. ***Increased presence of IgM+ PCs in LDLr$^{-/-}$ compared to WT mice.*** *WT (open symbols) and LDLr$^{-/-}$ (closed symbols) AEL male mice were fed either chow diet (blue) or high fat diet (HFD; red) for 0 (T0), 4 (T4) or 8 (T8) weeks Graphs display proportion of IgM+ plasma cells (PCs) in* ***(A)*** *spleen and* ***(B)*** *Peyer's patches (PPs). Each dot represents one mouse, graphs show mean +/- SD. Statistics carried out using Mann-Whitney test, * P < 0.05; ** P < 0.01; *** P < 0.001; **** P < 0.0001.*

Analysis of class switched plasma cell clones revealed that the IgM- plasma cell population was significantly bigger at the 4-week timepoint in the spleen and at the 8-week timepoint in the inguinal and para-aortic lymph nodes in male LDLr$^{-/-}$ AEL mice compared to male WT AEL

mice *(Figure 48A, C, D)*. Additionally, 8 weeks of HFD induced greater IgM- plasma cell production in the PPs of male LDLr$^{-/-}$ AEL mice compared to male WT AEL mice *(Figure 48B)*.

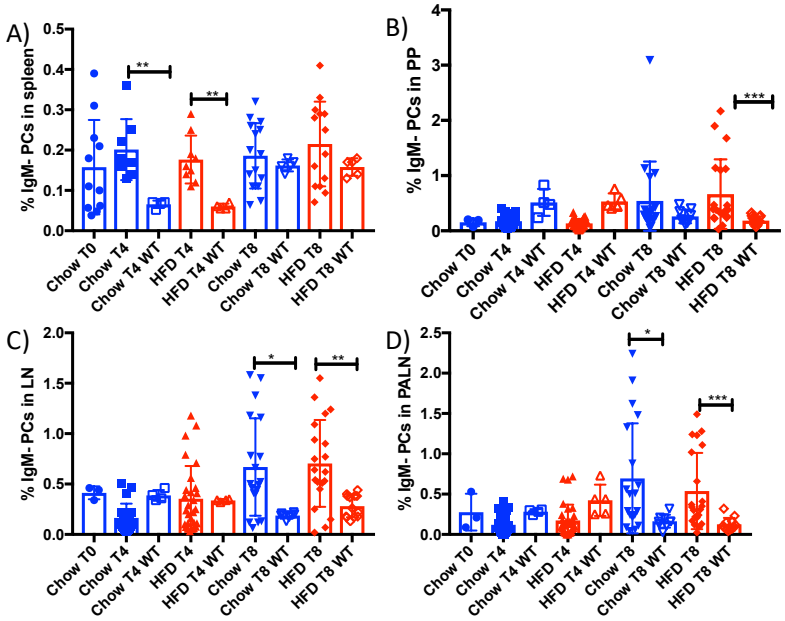

Figure 48. ***Increased presence of IgM- PCs in LDLr$^{-/-}$ compared to WT mice.*** *WT (open symbols) and LDLr$^{-/-}$ (closed symbols) AEL male mice were fed either chow diet (blue) or high fat diet (HFD; red) for 0 (T0), 4 (T4) or 8 (T8) weeks. Graphs display proportion of IgM- plasma cells (PCs) in* ***(A)*** *spleen,* ***(B)*** *Peyer's patches (PPs),* ***(C)*** *lymph node (LN) and* ***(D)*** *para-aortic lymph node (PALN). Each dot represents one mouse, graphs show mean +/- SD. Statistics carried out using Mann-Whitney test, * P < 0.05; ** P < 0.01; *** P < 0.001; **** P < 0.0001.*

Analysis of mouse weights revealed that mice gain weight over time as shown by significant increases in weight gained between 4 and 8 weeks of chow and HFD diet in male WT and LDLr$^{-/-}$ AEL mice showing that this effect was independent of genotype *(Figure 49A, B)*. HFD feeding resulted in significantly more weight gain compared to chow diet at both 4 and 8 weeks in both WT and LDLr$^{-/-}$ mouse models *(Figure 49A, B)*. Comparison between the two models revealed significantly greater weight gain in the LDLr$^{-/-}$ mice compared to WT mice demonstrating that absence of the LDL receptor and the consequent elevation in serum cholesterol levels resulted in weight gain *(Figure 49A, C)*.

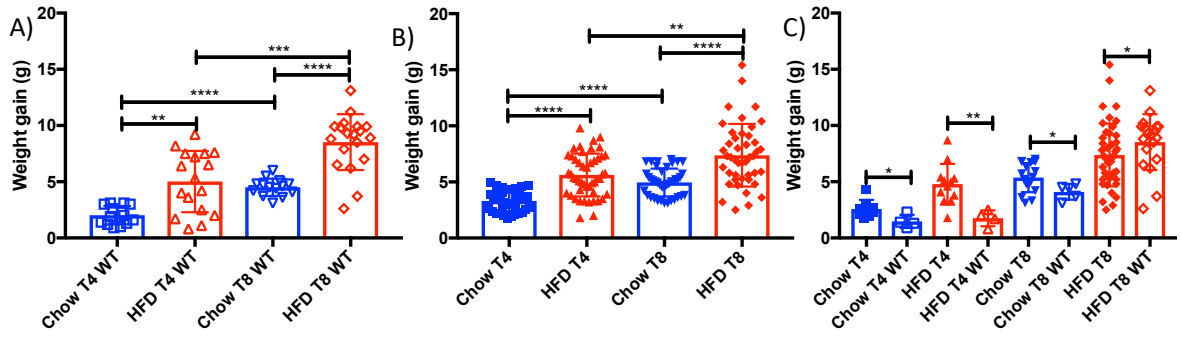

Figure 49. ***HFD resulted in increased weight gain compared to chow diet in LDLr$^{-/-}$ and LDLr$^{-/-}$ consistently put on more weight than WT mice.*** *WT (open symbols) and LDLr$^{-/-}$ (closed symbols) AEL male mice were fed either chow diet (blue) or high fat diet (HFD; red) for 0 (T0), 4 (T4) or 8 (T8) weeks. Graphs display difference in weight from start to end of study measured in grams (g) for* ***(A)*** *WT mice,* ***(B)*** *LDLr$^{-/-}$ mice and* ***(C)*** *WT and LDLr$^{-/-}$ combined. Each dot represents one mouse, graphs show mean +/- SD. Statistics carried out using Mann-Whitney test, * P < 0.05; ** P < 0.01; *** P < 0.001; **** P < 0.0001.*

Analysis of plasma cholesterol levels revealed that HFD caused a significantly increased cholesterol concentration in male WT AEL mice at both 4- and 8-week timepoints *(Figure 50A)*. Combination of the LDLr$^{-/-}$ background and HFD had a synergistic effect resulting in significantly higher total cholesterol levels *(Figure 50B)*. Comparison of total plasma cholesterol levels in both genotypes demonstrated that the LDLr$^{-/-}$ background resulted in increased cholesterol levels across all groups, even in male chow diet-fed AEL mice *(Figure 50C)*.

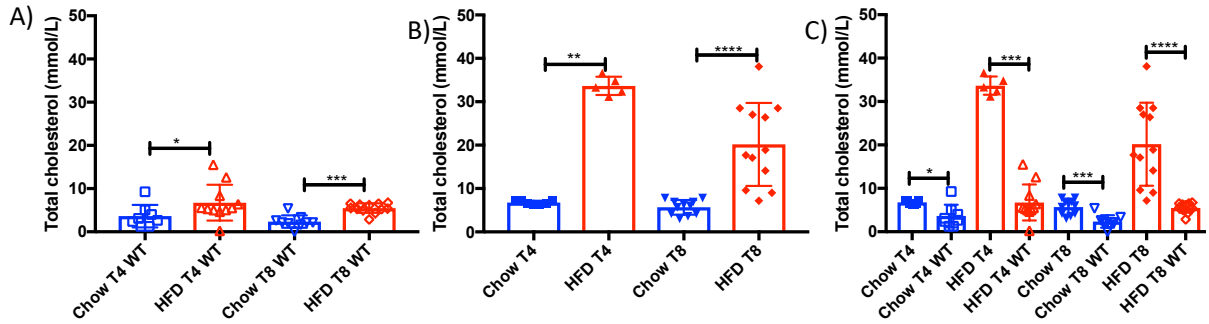

Figure 50. ***Serum cholesterol levels were higher after HFD compared to chow diet feeding and on the LDLr$^{-/-}$ background compared to WT.*** *WT (open symbols) and LDLr$^{-/-}$ (closed symbols) AEL male mice were fed either chow diet (blue) or high fat diet (HFD; red) for 0 (T0), 4 (T4) or 8 (T8) weeks. Graphs display total plasma cholesterol levels for* ***(A)*** *WT mice,* ***(B)*** *LDLr$^{-/-}$ mice and* ***(C)*** *WT and LDLr$^{-/-}$ combined. Each dot represents one mouse, graphs show mean +/- SD. Statistics carried out using Mann-Whitney test, * P < 0.05; ** P < 0.01; *** P < 0.001; **** P < 0.0001.*

4.4.3 Characterisation of the GC response under atherosclerotic conditions in LDLr$^{-/-}$ mice

Male LDLr$^{-/-}$ AEL mice were exposed to the same experimental setup as shown in Figure 26. In the LDLr$^{-/-}$ AEL mouse model, both total and B cell numbers in the PALN were significantly increased upon HFD feeding compared to chow diet feeding at 4 and 8 weeks *(Figure 51)*.

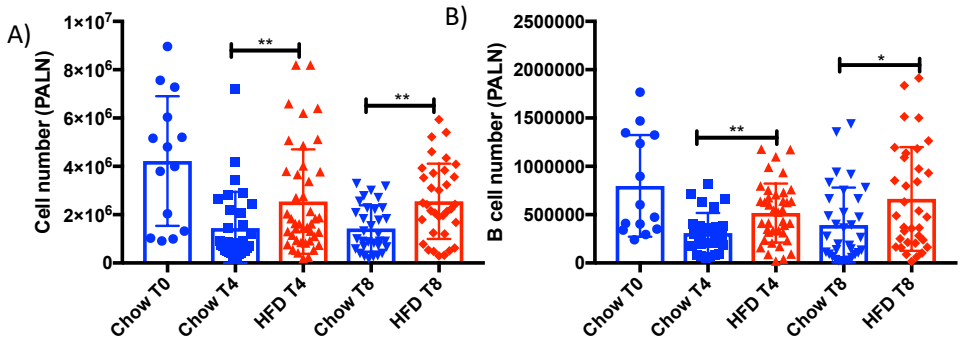

Figure 51. ***HFD resulted in greater total and B cell numbers in PALN compared to chow diet in LDLr$^{-/-}$.*** *LDLr$^{-/-}$ AEL male mice were fed either chow diet (blue) or high fat diet (HFD; red) for 0 (T0), 4 (T4) or 8 (T8) weeks. Within the para-aortic lymph node (PALN), graphs display* ***(A)*** *total cell number and* ***(B)*** *B cell number. Each dot represents one mouse, graphs show mean +/- SD. Statistics carried out using Mann-Whitney test, * P < 0.05; ** P < 0.01; *** P < 0.001; **** P < 0.0001.*

Within the spleen, the proportion of cells identified with GC phenotype increased significantly over time as seen by the increase from prior to diet (chow T0) to 4 and 8 weeks of chow diet *(Figure 52A)*. Furthermore, by 8 weeks of HFD feeding the GC population expanded significantly more compared to chow diet feeding in male LDLr$^{-/-}$ AEL mice *(Figure 52A)*. Analysis of IgM+ GC clones revealed that this population was expanded after 4 weeks of chow diet compared to before diet (T0) and decreased again by 8 weeks of chow diet *(Figure 52B)*. The production of IgM+ GC clones also decreased significantly from 4 to 8 weeks of HFD feeding *(Figure 52B)*. Contrastingly, IgM- GC clone production increased with time; there was a significant expansion in the IgM- GC clone population at 8 weeks of chow diet compared to 4 weeks of chow diet and compared to 0 weeks of diet *(Figure 52C)*. HFD caused further expansion of the IgM- GC cell population compared to chow diet at both 4 and 8 weeks *(Figure 52C)*. Additionally, production of IgM- GC cells was significantly greater after 8 weeks of HFD compared to 4 weeks of HFD *(Figure 52C)*.

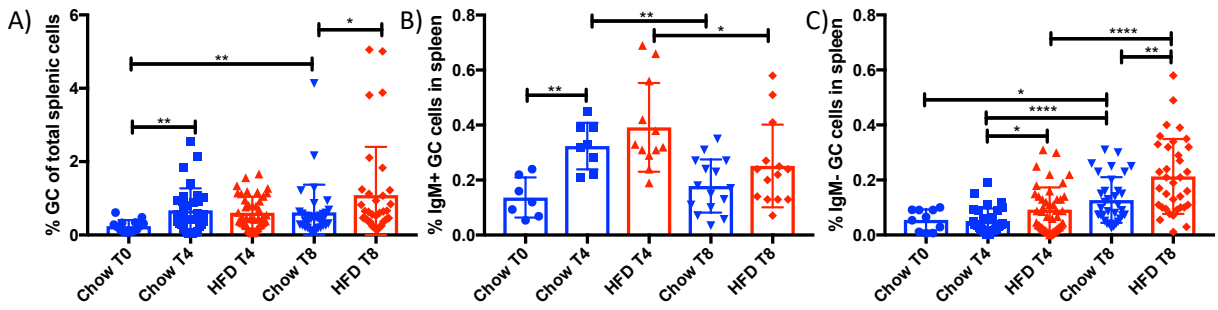

Figure 52. ***Greater GC population after HFD compared to chow diet feeding in LDLr$^{-/-}$.*** *LDLr$^{-/-}$ AEL male mice were fed either chow diet (blue) or high fat diet (HFD; red) for 0 (T0), 4 (T4) or 8 (T8) weeks. Within the spleen, graphs display* ***(A)*** *proportion of GC cells,* ***(B)*** *proportion of IgM+ GC cells and* ***(C)*** *proportion of IgM- GC cells. Each dot represents one mouse, graphs show mean +/- SD. Statistics carried out using Mann-Whitney test, * P < 0.05; ** P < 0.01; *** P < 0.001; **** P < 0.0001.*

Analysis of the class switch ratio demonstrated that production of IgM- clones increased over time in the spleen, PPs, LNs and PALNs regardless of diet *(Figure 53)*. Furthermore, after 4 weeks of HFD the ratio was significantly higher in male HFD-fed compared to chow diet-fed LDLr$^{-/-}$ AEL mice in the spleen and PPs *(Figure 53A, B)*.

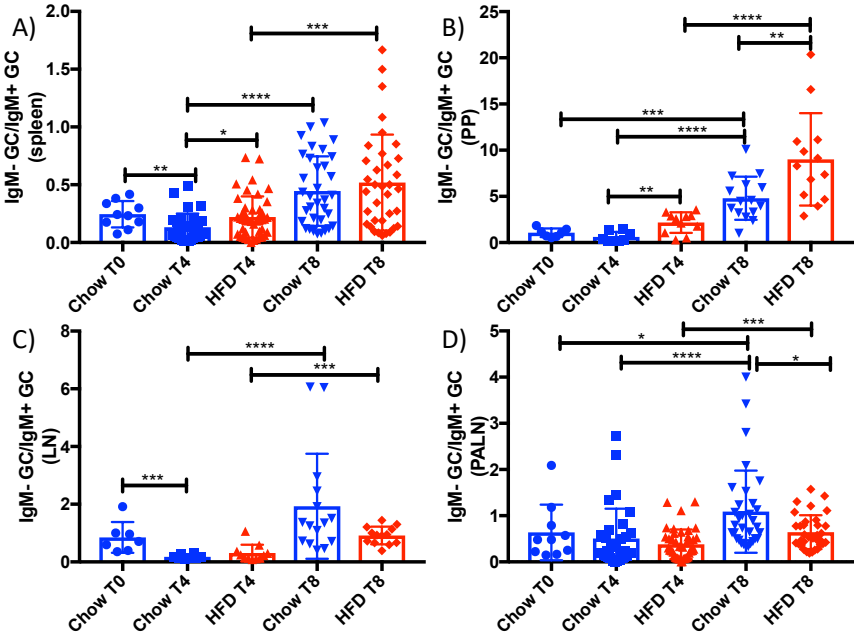

Figure 53. ***Greater degree of class-switching in HFD compared to chow diet-fed LDLr$^{-/-}$.*** *LDLr$^{-/-}$ AEL male mice were fed either chow diet (blue) or high fat diet (HFD; red) for 0 (T0), 4 (T4) or 8 (T8) weeks. The class switch ratio (IgM- GC cells/ IgM+ GC cells) was depicted in* ***(A)*** *spleen,* ***(B)*** *Peyer's patches,* ***(C)*** *lymph node (LN) and* ***(D)*** *para-aortic lymph node (PALN). Each dot represents one mouse, graphs show mean +/- SD. Statistics carried out using Mann-Whitney test, * P < 0.05; ** P < 0.01; *** P < 0.001; **** P < 0.0001.*

The proportion and absolute number of cells labelled with EYFP, and therefore expressing AID at time of labelling, increased over time in the spleen *(Figure 54A, D)*. In the lymph node, the proportion and absolute number of EYFP cells was significantly greater after 8 weeks compared to 4 weeks of HFD *(Figure 54B, E)*. The total number of EYFP cells within the LN was significantly higher in HFD compared to male chow diet-fed LDLr$^{-/-}$ AEL mice *(Figure 54E)*. In the PALN, the EYFP population, both proportionally and in absolute terms, was significantly expanded in response to HFD at 4 weeks compared to chow diet in male LDLr$^{-/-}$ AEL mice *(Figure 54C, F)*.

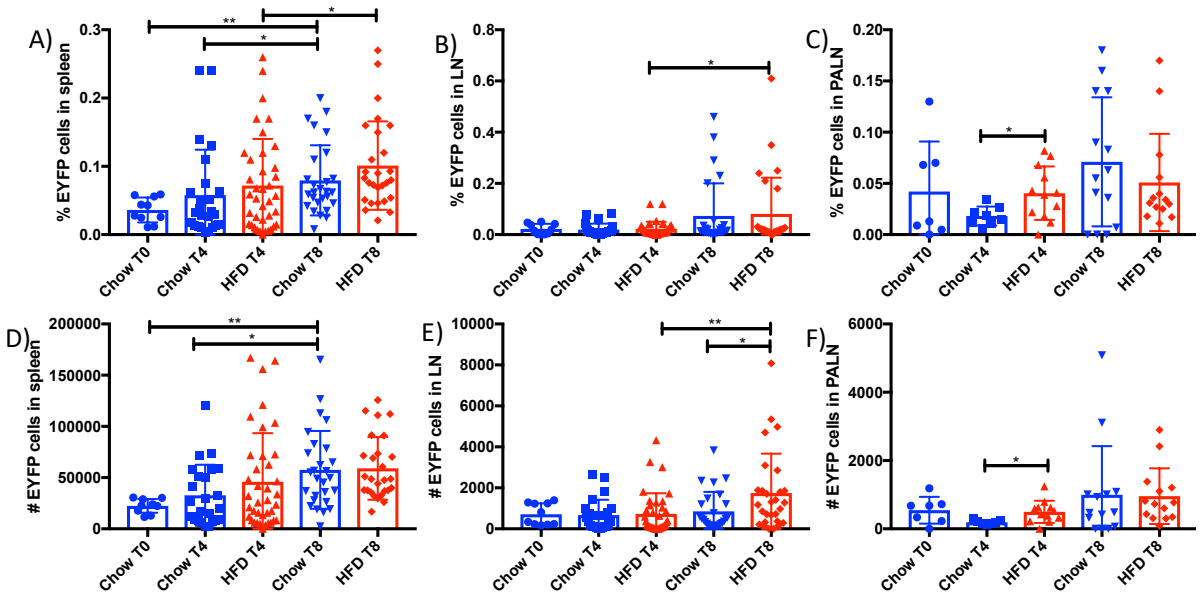

Figure 54. ***Increased EYFP population upon HFD compared to chow diet feeding in LDLr$^{-/-}$.*** *LDLr$^{-/-}$ AEL male mice were fed either chow diet (blue) or high fat diet (HFD; red) for 0 (T0), 4 (T4) or 8 (T8) weeks and 9mg tamoxifen was administered via oral gavage 48hrs prior to sacrifice. The proportion of EYFP cells was depicted in* ***(A)*** *spleen,* ***(B)*** *lymph node (LN) and* ***(C)*** *para-aortic lymph node (PALN). Graphs* ***(D-F)*** *depict absolute EYFP cell numbers for respective tissues. Each dot represents one mouse, graphs show mean +/- SD. Statistics carried out using Mann-Whitney test, * P < 0.05; ** P < 0.01; *** P < 0.001; **** P < 0.0001.*

Analysis of EYFP cell populations within the bone marrow demonstrated that the EYFP cell population was at its highest after 4 weeks of HFD *(Figure 55A)*. This was significantly more so than 4 weeks of chow diet and 8 weeks of HFD *(Figure 55A)*. These dynamics reflect those of the EYFP memory cell population whereby there was a significantly bigger EYFP memory cell population after 4 weeks of HFD compared to 4 weeks of chow diet and 8 weeks of HFD *(Figure 55B)*.

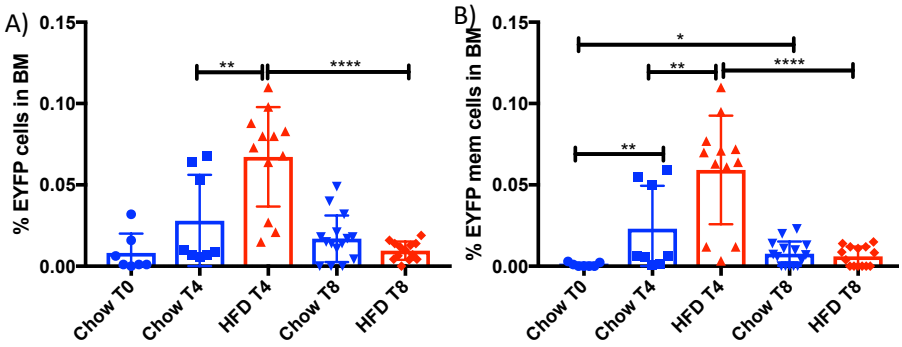

Figure 55. ***Peak of EYFP population due to memory cells in the BM after 4 weeks HFD in LDLr$^{-/-}$.*** *LDLr$^{-/-}$ AEL male mice were fed either chow diet (blue) or high fat diet (HFD; red) for 0 (T0), 4 (T4) or 8 (T8) weeks and 9mg tamoxifen was administered via oral gavage 48hrs prior to sacrifice. In the bone marrow (BM), graphs depict* ***(A)*** *total proportion of EYFP cells and* ***(B)*** *EYFP memory cell population. Each dot represents one mouse, graphs show mean +/- SD. Statistics carried out using Mann-Whitney test, * P < 0.05; ** P < 0.01; *** P < 0.001; **** P < 0.0001.*

In the spleen and PPs, EYFP class switched GC, memory and plasma cell populations increased over time as seen by the comparison of 8 weeks to 4 weeks of chow diet *(Figure 56)*. The same

result could be seen within the PPs of HFD-fed male LDLr$^{-/-}$ AEL animals *(Figure 56D, E, F)*. Production of EYFP IgM- clones in the splenic memory and PC compartments also increased in male HFD-fed LDLr$^{-/-}$ AEL mice after 8 weeks compared to 4 weeks *(Figure 56B, C, E, F)*. Additionally, HFD induced a bigger population of EYFP IgM- GC clones after 4 weeks in the spleen *(Figure 56A)*. Meanwhile, HFD resulted in an expanded splenic EYFP IgM- memory cell population compared to chow diet after 8 weeks *(Figure 56B)*.

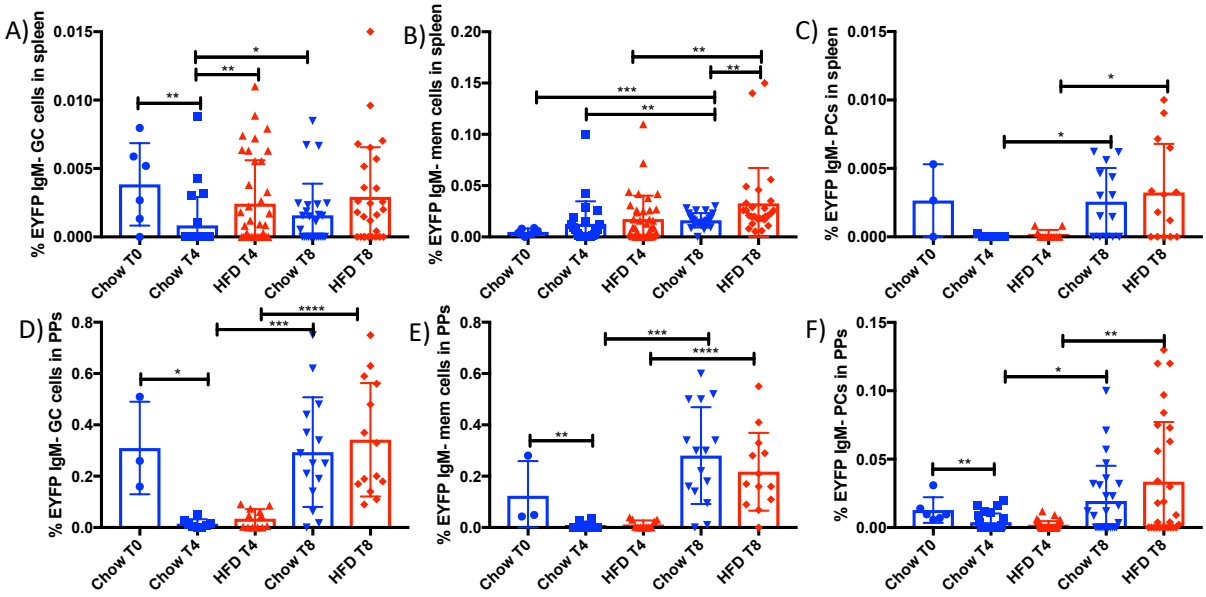

Figure 56. ***Greater presence of IgM- GC-derived clones in spleen and PPs of HFD compared to chow diet-fed LDLr$^{-/-}$.*** *LDLr$^{-/-}$ AEL male mice were fed either chow diet (blue) or high fat diet (HFD; red) for 0 (T0), 4 (T4) or 8 (T8) weeks and 9mg tamoxifen was administered via oral gavage 48hrs prior to sacrifice. Graphs depict EYFP IgM- populations in the spleen of* ***(A)*** *GC cells,* ***(B)*** *memory (mem) cells and* ***(C)*** *plasma cells (PCs). Graphs depict EYFP IgM- populations in the Peyer's patches (PPs) of* ***(D)*** *GC cells,* ***(E)*** *memory (mem) cells and* ***(F)*** *plasma cells (PCs). Each dot represents one mouse, graphs show mean +/- SD. Statistics carried out using Mann-Whitney test, * P < 0.05; ** P < 0.01; *** P < 0.001; **** P < 0.0001.*

HFD resulted in an expanded EYFP memory cell population after 4 weeks compared to chow diet in both the inguinal and para-aortic lymph nodes *(Figure 57B, C)*. In the spleen, EYFP memory cell production increased over time regardless of diet *(Figure 57A)*. By 8 weeks, HFD caused a bigger proportion of EYFP memory cells compared to chow diet in the spleen *(Figure 57A)*.

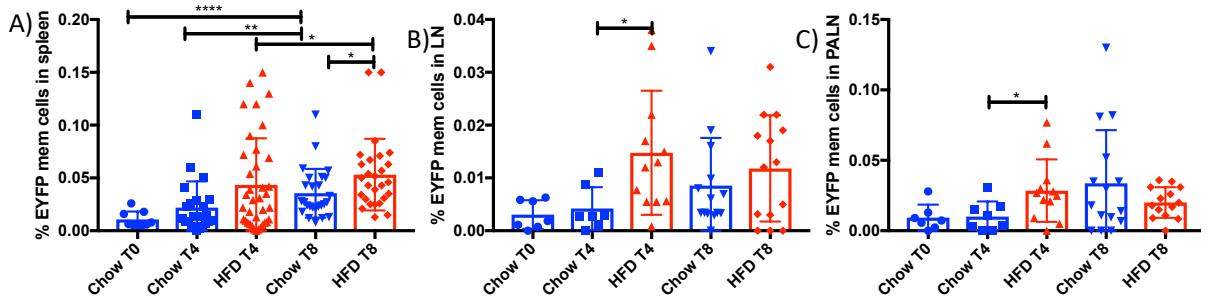

Figure 57. ***Increased presence of EYFP memory cells after HFD compared to chow diet feeding in LDLr$^{-/-}$.*** *LDLr$^{-/-}$ AEL male mice were fed either chow diet (blue) or high fat diet (HFD; red) for 0 (T0), 4 (T4) or 8 (T8) weeks and 9mg tamoxifen was administered via oral gavage 48hrs prior to sacrifice. Graphs depict EYFP memory (mem) populations in the* ***(A)****spleen,* ***(B)*** *lymph nodes (LN) and* ***(C)*** *para-aortic lymph nodes (PALN). Each dot represents one mouse, graphs show mean +/- SD. Statistics carried out using Mann-Whitney test, * P < 0.05; ** P < 0.01; *** P < 0.001; **** P < 0.0001.*

Production of EYFP labelled IgM+ memory cells was higher after 8 weeks of HFD compared to 4 weeks of HFD in the PALN, PPs and blood of male LDLr$^{-/-}$ AEL mice *(Figure 58)*. The same was true for the PALNs of chow diet-fed male LDLr$^{-/-}$ AEL mice *(Figure 58A)*. In the PALN, HFD resulted in an expanded EYFP IgM+ memory cell population compared to chow diet after 4 weeks *(Figure 58A)*.

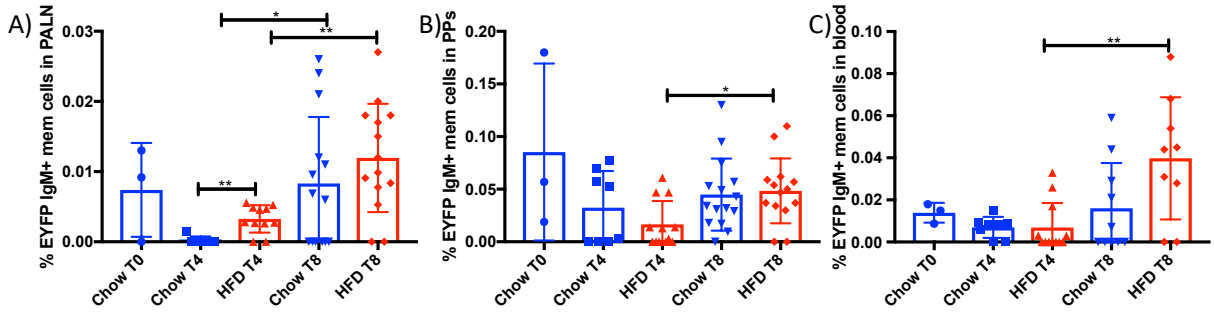

Figure 58. ***Presence of EYFP IgM+ memory cells increases with time in HFD-fed LDLr$^{-/-}$.*** *LDLr$^{-/-}$ AEL male mice were fed either chow diet (blue) or high fat diet (HFD; red) for 0 (T0), 4 (T4) or 8 (T8) weeks and 9mg tamoxifen was administered via oral gavage 48hrs prior to sacrifice. Graphs depict EYFP IgM+ memory (mem) populations in the* ***(A)*** *para-aortic lymph nodes (PALN),* ***(B)*** *Peyer's patches (PP) and* ***(C)*** *blood. Each dot represents one mouse, graphs show mean +/- SD. Statistics carried out using Mann-Whitney test, * P < 0.05; ** P < 0.01; *** P < 0.001; **** P < 0.0001.*

Within the spleen, the total plasma cell population increased significantly from 4 to 8 weeks regardless of diet and isotype *(Figure 59A, B, C)*. By 8 weeks of HFD, the splenic plasma cell population was significantly larger than that of male chow diet-fed LDLr$^{-/-}$ AEL mice *(Figure 59A)*. In the LN and PALN, total plasma cell proportion also increased over time regardless of diet *(Figure 59D, G)*. However, IgM+ PC production peaked at 4 weeks and was diminished by 8 weeks of diet in the LN and PALN irrespective of diet *(Figure 59E, H)*. Meanwhile, IgM- PC production was significantly greater after 8 weeks of diet compared to 4 weeks of diet in the LN and PALN showing that IgM+ clones dominate at 4 weeks and are replaced by class

switched IgM- clones by 8 weeks of diet in the LN and PALN *(Figure 59F, I)*. Additionally, after 4 weeks of HFD the IgM- PC pool of the LN was significantly larger than that of male LDLr$^{-/-}$ AEL mice fed chow diet *(Figure 59I)*.

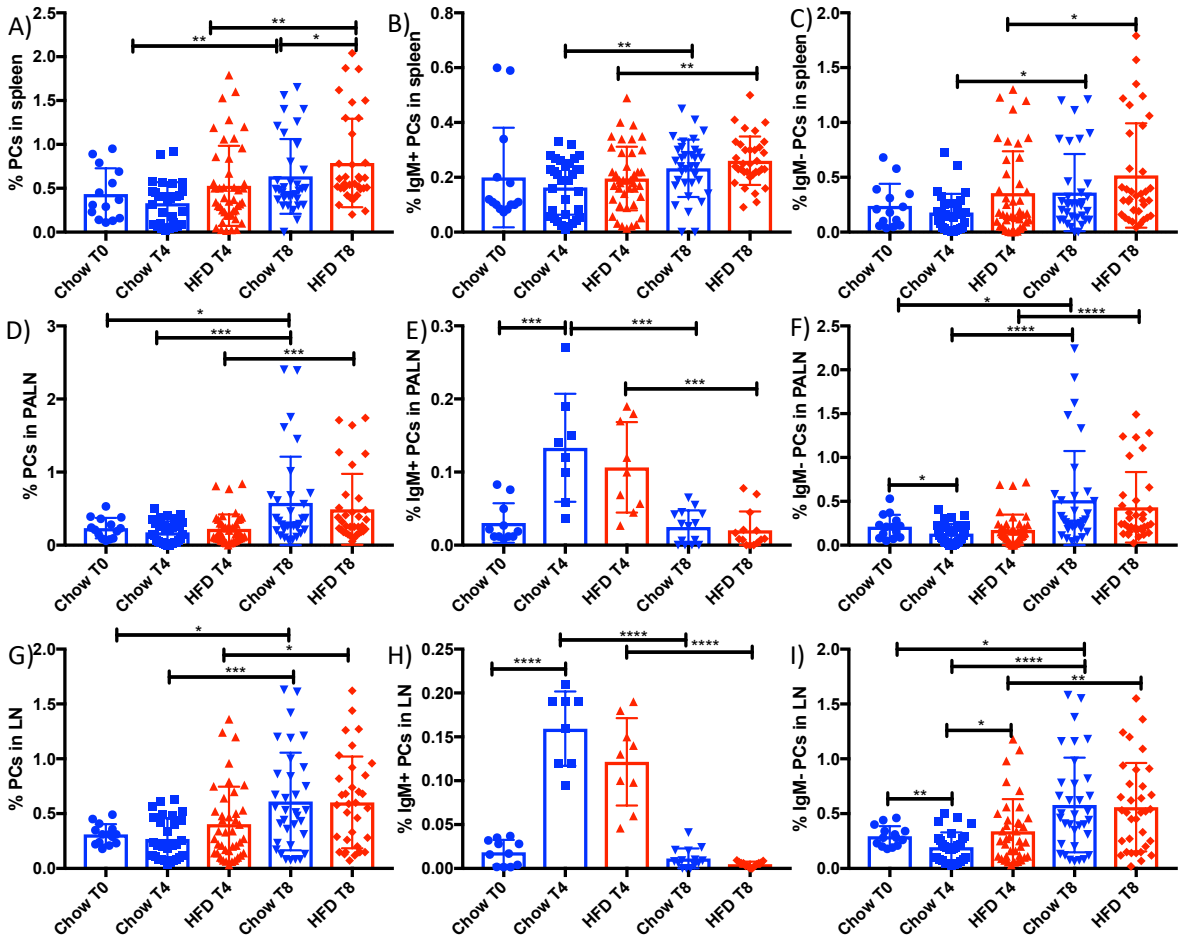

Figure 59. ***Changing plasma cell dynamics with respect to time and diet in LDLr$^{-/-}$.*** *LDLr$^{-/-}$ AEL male mice were fed either chow diet (blue) or high fat diet (HFD; red) for 0 (T0), 4 (T4) or 8 (T8) weeks. In the spleen, graphs depict* ***(A)*** *total plasma cell (PC) population,* ***(B)*** *IgM+ PC population and* ***(C)*** *IgM- PC population. In the para-aortic lymph node (PALN), graphs depict* ***(D)*** *total plasma cell (PC) population,* ***(E)*** *IgM+ PC population and* ***(F)*** *IgM- PC population. In the lymph node (LN), graphs depict* ***(G)*** *total plasma cell (PC) population,* ***(H)*** *IgM+ PC population and* ***(I)*** *IgM- PC population. Each dot represents one mouse, graphs show mean +/- SD. Statistics carried out using Mann-Whitney test, * P < 0.05; ** P < 0.01; *** P < 0.001; **** P <*

Having investigated the organs of plasma cell production, I next turned to analyse the locations where plasma cells migrate and home to, the blood and bone marrow respectively. Over time, the plasma cell population increased significantly regardless of diet in both the bone marrow and blood *(Figure 60A, D)*. In the bone marrow, both IgM+ and IgM- plasma cell pools expanded significantly after 8 weeks compared to 4 weeks regardless of diet type *(Figure 60B, C)*. However, in the blood, migration of IgM+ plasma cells decreased from 4 to 8 weeks in both diet types while IgM- plasma cell migration increased from 4 to 8 weeks irrespective of diet *(Figure 60E, F)*. This was in line with the increased IgM- plasma cell

production from lymph nodes at the 8-week timepoint which then migrate to the bone marrow niche.

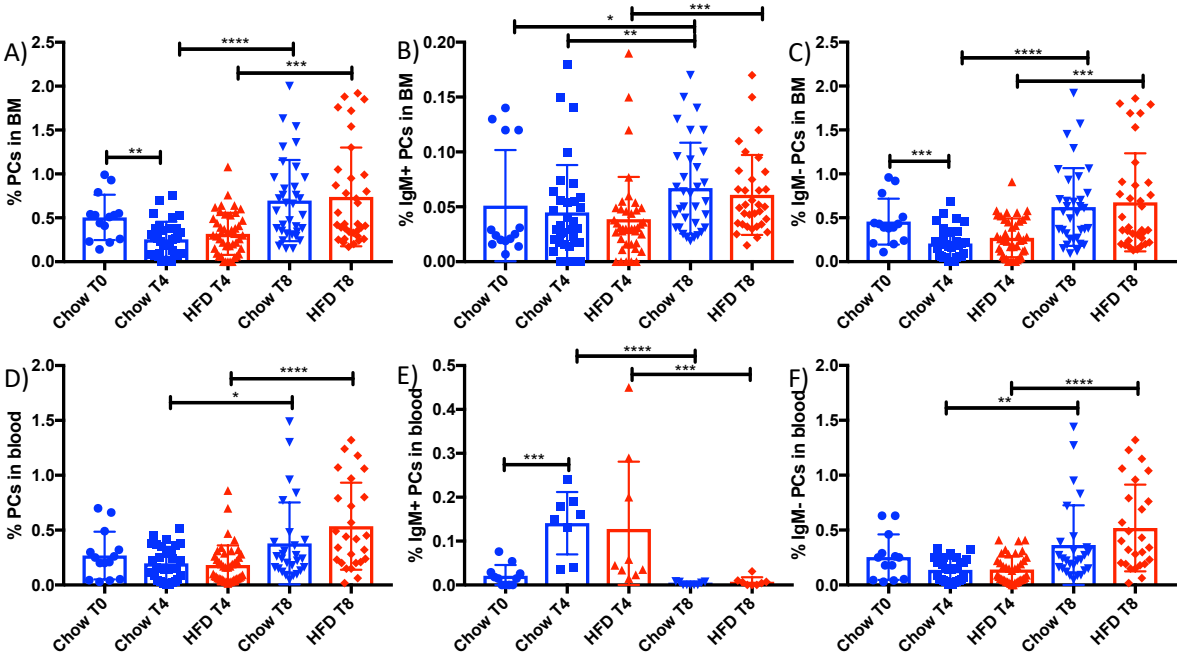

Figure 60. ***Changing plasma cell dynamics with respect to time and diet in LDLr$^{-/-}$.*** *LDLr$^{-/-}$ AEL male mice were fed either chow diet (blue) or high fat diet (HFD; red) for 0 (T0), 4 (T4) or 8 (T8) weeks. In the bone marrow (BM), graphs depict* ***(A)*** *total plasma cell (PC) population,* ***(B)*** *IgM+ PC population and* ***(C)*** *IgM- PC population. In the blood, graphs depict* ***(D)*** *total plasma cell (PC) population,* ***(E)*** *IgM+ PC population and* ***(F)*** *IgM- PC population. Each dot represents one mouse, graphs show mean +/- SD. Statistics carried out using Mann-Whitney test, * P < 0.05; ** P < 0.01; *** P < 0.001; **** P < 0.0001.*

Analyses of serum for antibody titres revealed that male LDLr$^{-/-}$ AEL mice fed chow diet for 4 weeks had the greatest level of IgG1 antibodies, significantly more so than pre-diet, 4 weeks of HFD and 8 weeks of chow diet *(Figure 61A)*. The same trends were seen for IgM titres *(Figure 61B)*. Furthermore, after 8 weeks of chow diet IgG1 titres were significantly higher than those of 8 weeks HFD-fed male LDLr$^{-/-}$ AEL mice *(Figure 61A)*. Meanwhile, serum IgM levels were significantly higher after 8 weeks of HFD compared to 8 weeks of chow diet feeding in male LDLr$^{-/-}$ AEL mice *(Figure 61B)*. Serum IL6 levels were significantly higher after 4 weeks of HFD compared to chow diet and also higher than after 8 weeks of HFD feeding in male LDLr$^{-/-}$ AEL mice *(Figure 61C)*. However, as cytokines are less stable than antibodies comparison between the groups is not as reliable despite the fact samples were analysed together. Therefore, the reduction in serum IL6 from 4 to 8 weeks of HFD could be a technical error as titres are expected to increase during atherosclerosis as inflammation increases. This could be addressed by analysing serum immediately after collection prior to freezing of the sample.

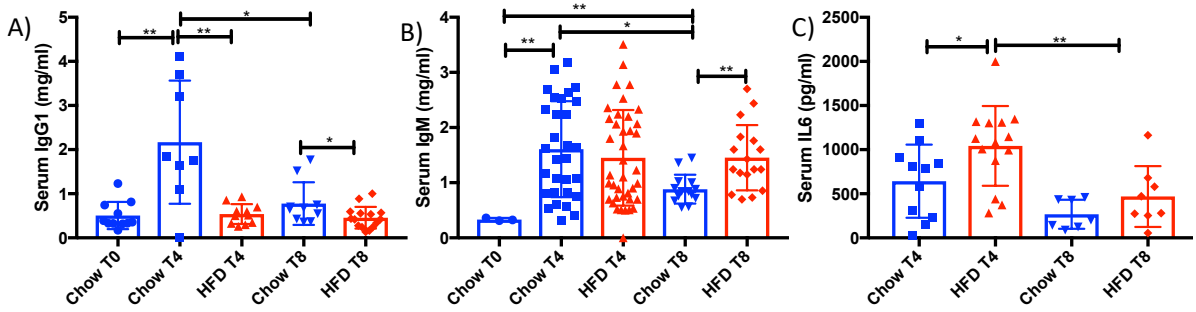

Figure 61. ***Serum antibody titres varied over time and with diet in LDLr$^{-/-}$.*** *LDLr$^{-/-}$ AEL male mice were fed either chow diet (blue) or high fat diet (HFD; red) for 0 (T0), 4 (T4) or 8 (T8) weeks. Plasma was analysed using ELISA for* ***(A)*** *IgG1,* ***(B)*** *IgM and* ***(C)*** *IL6. Each dot represents one mouse, graphs show mean +/- SD. Statistics carried out using Mann-Whitney test, * P < 0.05; ** P < 0.01; *** P < 0.001; **** P < 0.0001.*

4.4.4 Impact of HFD on lymphoid organs proximal to intestines

The mesenteric lymph nodes are the first lymphoid organs to filter food components and microbial species as they travel in the lymph through the intestinal lamina propria. These LNs are the primary site for oral tolerance induction as well as maintaining systemic ignorance to commensals within the gut. Additionally, dietary lipids travel through the mLNs on their way from the small intestine to the thoracic duct[269]. As such, the impact of HFD on mesenteric lymph nodes was investigated. After 2 weeks, HFD caused an expansion in the GC population of the mLN particularly of IgM+ clones as these were significantly increased compared to 2 weeks of chow diet and 1 week of HFD *(Figure 62A, B)*. IgM- clones were also elevated after 2 weeks of HFD compared to 1 week *(Figure 62C)*. This demonstrates that the components of the HFD have immunogenic properties.

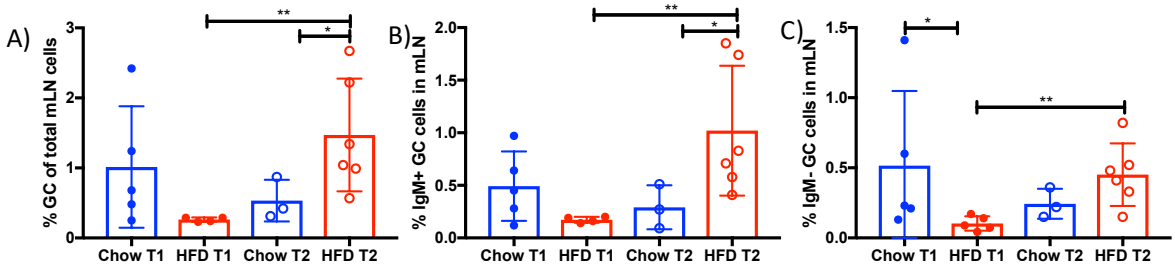

Figure 62. ***HFD impacted the GC population of the mLN in LDLr$^{-/-}$.*** *LDLr$^{-/-}$ AEL male mice were fed either chow diet (blue) or high fat diet (HFD; red) for 1 (T1; closed circles) or 2 weeks (T2; open circles). Data showed within the mesenteric lymph nodes (mLN)* ***(A)*** *the proportion of GC cells,* ***(B)*** *the proportion of IgM+ GC cells and* ***(C)*** *the proportion of IgM- GC cells. Each dot represents 1 mouse, graphs show mean +/- SD. Statistics carried out using Mann-Whitney test, * P < 0.05; ** P < 0.01; *** P < 0.001; **** P < 0.0001.*

In the Peyer's patches, HFD had a suppressive effect on the total GC population, independent of isotype, at both 4 and 8 weeks of diet with significantly diminished populations compared

to chow diet *(Figure 63A, B, C)*. This was true also of clones which had been EYFP labelled *(Figure 63D, E, F)*. Additionally, the GC response was of greater magnitude after 4 weeks of chow diet compared to 8 weeks of chow diet, regardless of isotype *(Figure 63A, D)*. Interestingly, the EYFP labelled total GC and IgM+ GC populations expanded over time upon chow diet feeding *(Figure 63D, E)*. The EYFP labelled IgM- GC population was significantly greater at 8 weeks compared to 4 weeks of chow diet feeding in WT male mice *(Figure 63F)*.

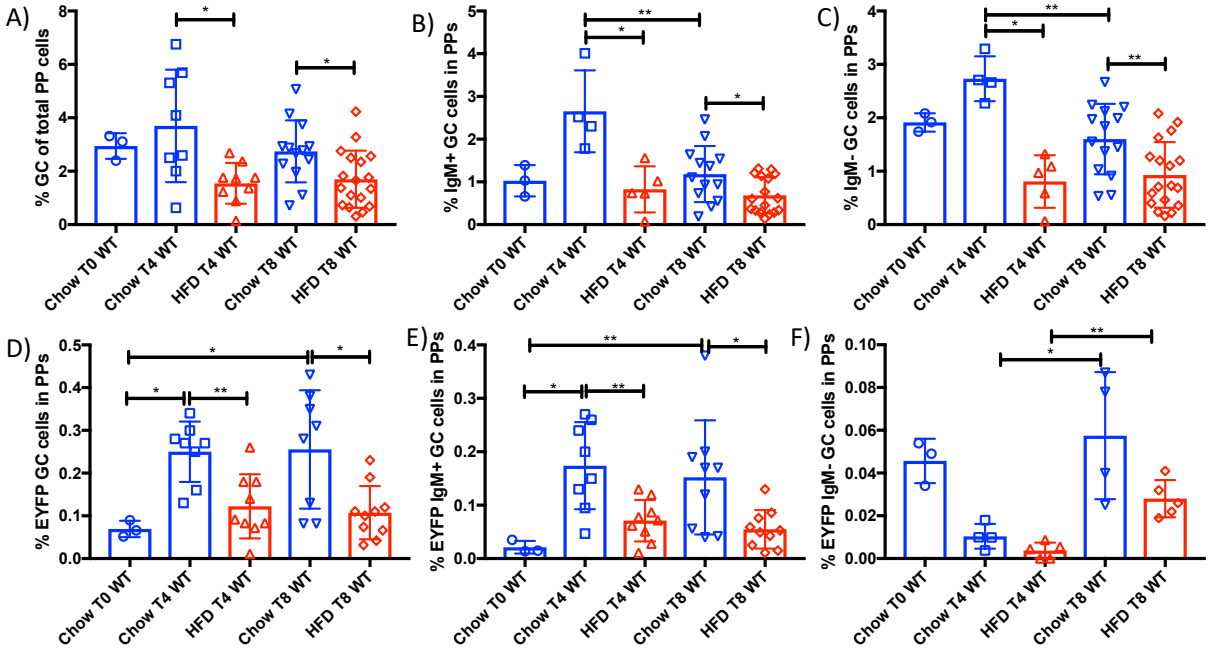

*Figure 63.**HFD suppresses GC responses in the PPs of WT mice.** WT AEL male mice were fed either chow diet (blue) or high fat diet (HFD; red) for 0 (T0), 4 (T4) or 8 (T8) weeks and 9mg tamoxifen was administered via oral gavage 48hrs prior to sacrifice. Within the Peyer's patches (PP) graphs depict **(A)** total GC population, **(B)** IgM+ GC population and **(C)** IgM- GC population. **(D-F)** depict the EYFP labelled clones within the same populations. Each dot represents one mouse, graphs show mean +/- SD. Statistics carried out using Mann-Whitney test, * P < 0.05; ** P < 0.01; *** P < 0.001; **** P < 0.0001.*

By investigating the other EYFP populations of the PPs, it could be seen that the suppressive action of HFD was also evident in IgM+ memory cells as this population was significantly diminished in HFD-fed WT male mice compared to chow diet-fed WT male mice at both 4 and 8-week timepoints *(Figure 64A)*. Meanwhile, the EYFP plasma cell pool followed trends seen for other tissues whereby they were only significantly detectable at the 8-week timepoint *(Figure 64B, C)*. Interestingly, HFD induced greater production of IgM+ EYFP labelled PCs compared to chow diet at 8 weeks *(Figure 64B)*. Thus, HFD suppresses both GC and memory cell formation resulting in reduced EYFP labelling while plasma cell populations were not impacted by this suppressive action.

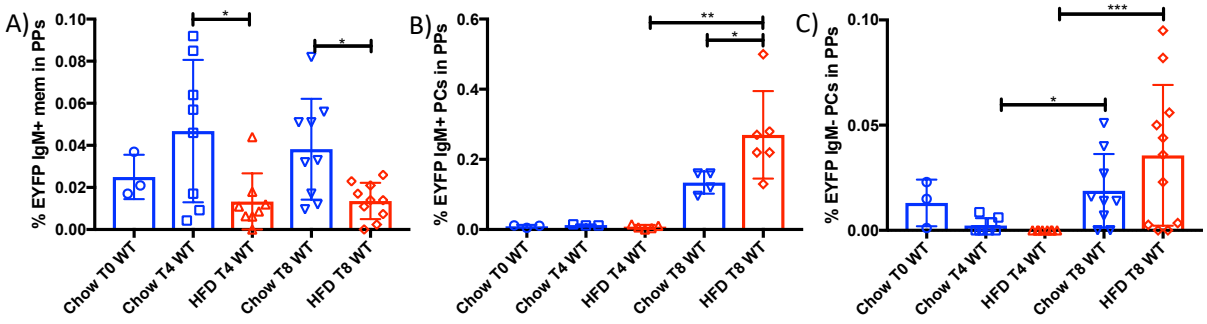

Figure 64. ***EYFP cell subsets show different responses to HFD in the PPs of WT mice.*** *WT AEL male mice were fed either chow diet (blue) or high fat diet (HFD; red) for 0 (T0), 4 (T4) or 8 (T8) weeks and 9mg tamoxifen was administered via oral gavage 48hrs prior to sacrifice. Within the Peyer's patches, graphs depict EYFP labelled* ***(A)*** *IgM+ memory (mem) cells,* ***(B)*** *IgM+ plasma cells (PCs) and* ***(C)*** *IgM- PCs. Each dot represents one mouse, graphs show mean +/- SD. Statistics carried out using Mann-Whitney test, * P < 0.05; ** P < 0.01; *** P < 0.001; **** P < 0.0001.*

The suppressive nature of HFD on Peyer's patches GC responses was also seen in the LDLr$^{-/-}$ mouse model. The GC population, both in proportional and absolute terms, was significantly diminished in HFD-fed male AEL mice at 4 and 8 weeks compared to chow diet *(Figure 65)*. Production of IgM+ GC clones was significantly greater at 4 weeks compared to 8 weeks in both chow diet and HFD-fed male AEL mice *(Figure 65B)*. At both 4 and 8 weeks of diet, chow diet-fed male AEL mice had a bigger population of IgM+ GC clones compared to HFD-fed male AEL mice *(Figure 65B)*.

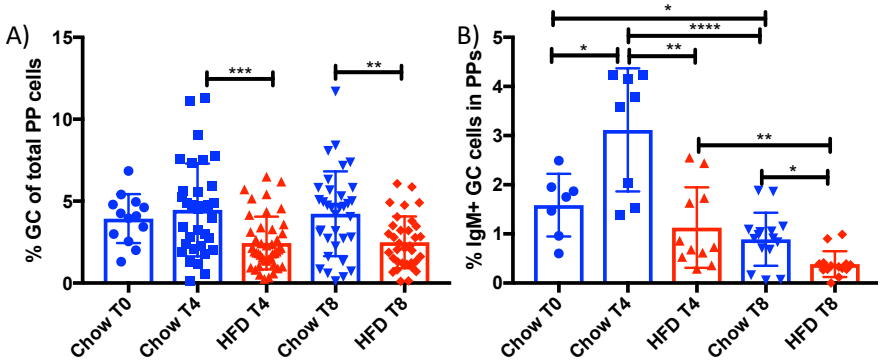

Figure 65. ***HFD suppresses GC responses in the PPs of LDLr-/- mice.*** *LDLr$^{-/-}$ AEL male mice were fed either chow diet (blue) or high fat diet (HFD; red) for 0 (T0), 4 (T4) or 8 (T8) weeks. Within the Peyer's patches (PPs), graphs depict* ***(A)*** *proportion of GC cells and* ***(B)*** *proportion of IgM+ GC cells. Each dot represents one mouse, graphs show mean +/- SD. Statistics carried out using Mann-Whitney test, * P < 0.05; ** P < 0.01; *** P < 0.001; **** P < 0.0001.*

4.4.5 GC response to regression

To determine the lasting impact of HFD, the regression model was used whereby mice fed HFD were swapped back to the chow diet. Previous literature has shown that in this scenario, plaques reduce in size and become more stable i.e. they regress[245]. These experiments would determine whether exposure to HFD early in life permanently affects GC responses within mice.

Male LDLr$^{-/-}$ AEL mice were fed chow for 8 weeks or HFD for either 4 or 8 weeks. Male LDLr$^{-/-}$ AEL mice were either sacrificed after 4 weeks of HFD and or were switched back to chow at this timepoint for a further 4 weeks. Tamoxifen was administered 48hrs prior to sacrifice *(Figure 66)*.

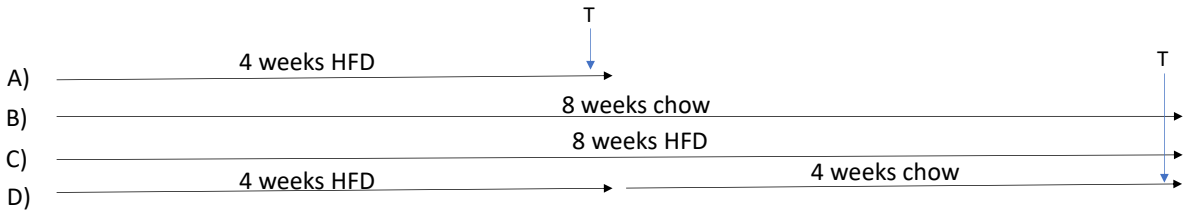

Figure 66. ***Schematic showing experimental design for regression study.*** *LDLr$^{-/-}$ AEL male mice were fed either* ***(A)*** *high fat diet (HFD) for 4 weeks before sacrifice (blue),* ***(B)*** *8 weeks of chow diet (red),* ***(C)*** *8 weeks of HFD (green) or* ***(D)*** *4 weeks of HFD followed by chow diet for 4 weeks (purple). Mice were dosed with 9mg tamoxifen (T) via oral gavage 48hrs prior to sacrifice.*

Total cell numbers and B cell numbers of both the inguinal and para-aortic lymph nodes, responsive to local immune stimuli, were significantly increased after 8 weeks compared to 4 weeks of HFD *(Figure 67A, B, E, F)*. The regression group in both lymphoid organs also showed elevated total and B cell numbers compared to 4 weeks of HFD but to a lower extent than 8 weeks of HFD *(Figure 67A, B, E, F)*. Indeed, the male LDLr$^{-/-}$ AEL mice fed HFD for 8 weeks had significantly greater total and B cell numbers than the regression group in the PALN *(Figure 67E, F)*. In both the LN and the PALN the total number of GC B cells was significantly increased after 8 weeks compared to 4 weeks of HFD *(Figure 67C, G)*. Furthermore, even in the regression group the number of GC B cells was greater than after only 4 weeks HFD in the LNs while in the PALN the size of the GC population stayed similar to that of those fed HFD for 4 weeks *(Figure 67C, G)*. Plasma cell numbers increased significantly in the LN and PALN after 8 weeks of HFD compared to 4 weeks of HFD and this observation was also true of the regression group although to a lesser degree *(Figure 67D, H)*.

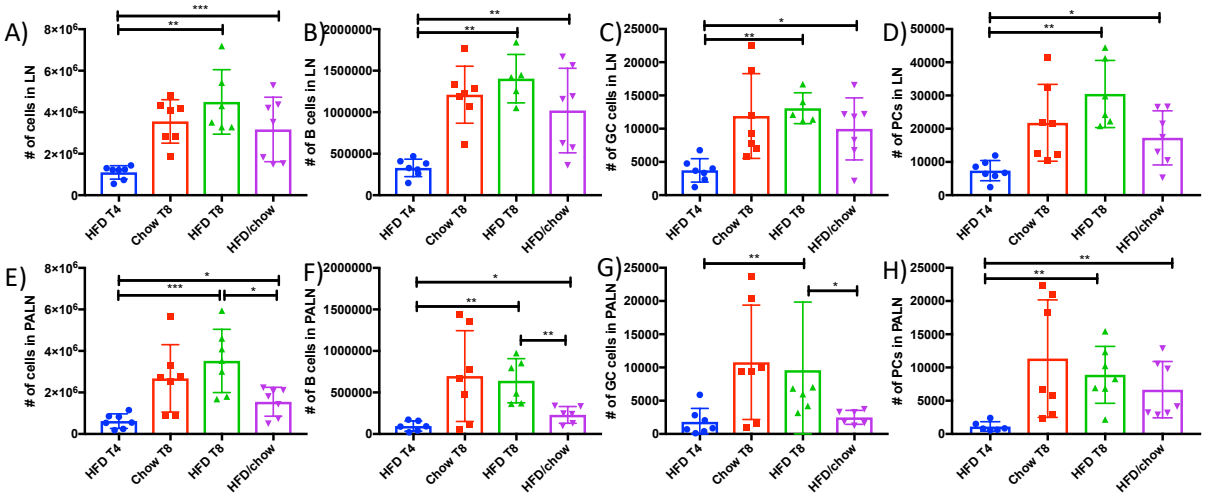

Figure 67. ***Impact of regression on cell numbers in the LN and PALN of LDLr$^{-/-}$ mice.*** *LDLr$^{-/-}$ AEL male mice were fed either high fat diet (HFD) for 4 weeks before sacrifice (blue), 8 weeks of chow diet (red), 8 weeks of HFD (green) or 4 weeks of HFD followed by chow diet for 4 weeks (purple). Total cell numbers displayed in* ***(A)*** *lymph node (LN) and* ***(E)*** *para-aortic lymph node (PALN). Flow cytometric analysis of total B cell (B220+) numbers displayed in* ***(B)*** *LN and* ***(F)*** *PALN, total GC B cell numbers in* ***(C)*** *LN and* ***(G)*** *PALN and total plasma cell (PC) numbers in* ***(D)*** *LN and* ***(H)*** *PALN. Each dot represents 1 mouse, graphs show mean +/- SD. Statistics carried out using Mann-Whitney test, * P < 0.05; ** P < 0.01; *** P < 0.001; **** P < 0.0001.*

4.4.5.1 PP response to regression

In the Peyer's patches, the GC population increased in the regression group compared to 4 weeks of HFD only *(Figure 68A)*. Although not significant, the GC population was diminished in response to 8 weeks of HFD compared to 8 weeks of chow diet *(Figure 68A)*. This was reflected in the EYFP population which was significantly smaller in the 8-week HFD-fed compared to 8-week chow diet-fed male LDLr$^{-/-}$ AEL mice *(Figure 68B)*. The proportion of EYFP cells increased significantly in both male LDLr$^{-/-}$ AEL mice fed HFD for 8 weeks and the regression group compared to the 4-week HFD group *(Figure 68B)*. Of note, the EYFP population was significantly greater in the regression group compared to the 8-week HFD-fed group *(Figure 68B)*.

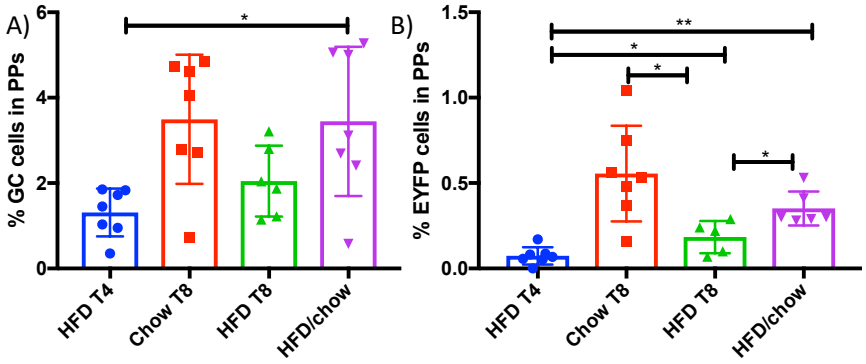

Figure 68. ***Effect of regression on GC cells in the PPs of LDLr$^{-/-}$ mice.*** *LDLr$^{-/-}$ AEL male mice were fed either high fat diet (HFD) for 4 weeks before sacrifice (blue), 8 weeks of chow diet (red), 8 weeks of HFD (green) or 4 weeks of HFD followed by chow diet for 4 weeks (purple). Proportion of cells within Peyer's patches (PP) which were (A) GC phenotype and (B) EYFP positive. Each dot represents 1 mouse, graphs show mean +/- SD. Statistics carried out using Mann-Whitney test, * P < 0.05; ** P < 0.01; *** P < 0.001; **** P < 0.0001.*

Within the EYFP cells of the Peyer's patches, the populations of all 3 cell types were increased after the regression intervention compared to 4 weeks of HFD, driven by an expansion of IgM- clones *(Figure 69)*.

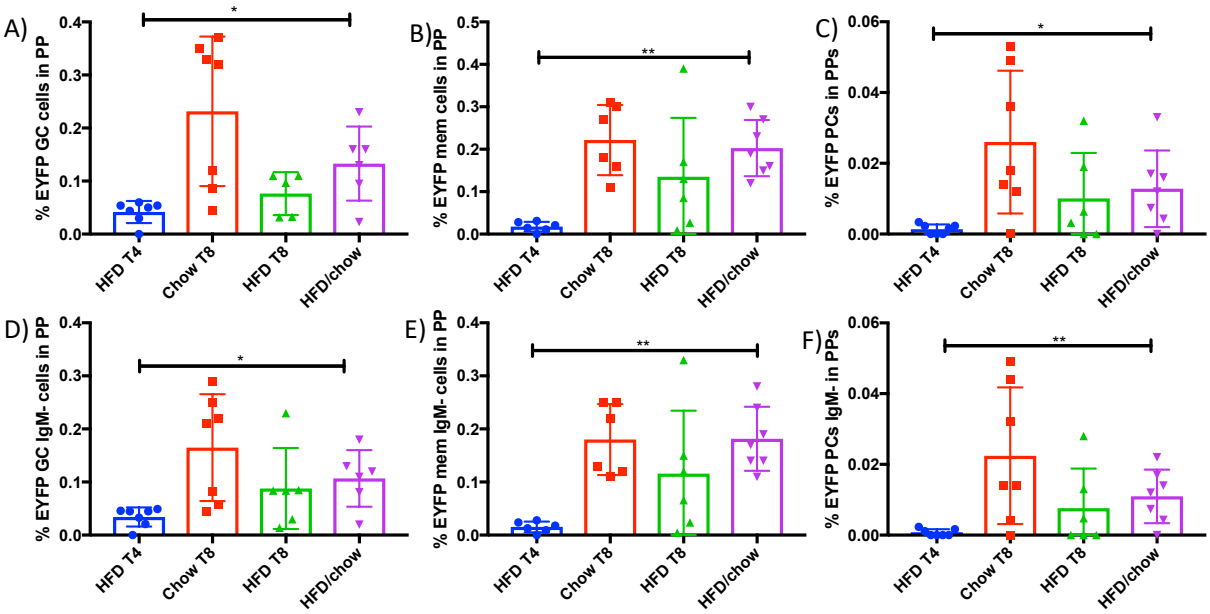

Figure 69. ***Increased EYFP populations, driven by IgM- clones, after regression in PPs of LDLr$^{-/-}$ mice.*** *LDLr$^{-/-}$ AEL male mice were fed either high fat diet (HFD) for 4 weeks before sacrifice (blue), 8 weeks of chow diet (red), 8 weeks of HFD (green) or 4 weeks of HFD followed by chow diet for 4 weeks (purple). The proportion of EYFP cells within the Peyer's patches (PPs) that are* ***(A)*** *GC cells,* ***(B)*** *memory (mem) cells and* ***(C)*** *plasma cells (PCs).* ***(D-F)*** *show the IgM- cells within each of these populations. Each dot represents 1 mouse, graphs show mean +/- SD. Statistics carried out using Mann-Whitney test, * P < 0.05; ** P < 0.01; *** P < 0.001; **** P < 0.0001.*

4.4.5.2 Antibody and lipid response to regression

Analysis of serum revealed that IgG1 production was significantly higher after 8 weeks of chow diet compared to the regression group (HFD/chow) in LDLr$^{-/-}$ AEL males *(Figure 70A)*.

IgM titres were significantly greater in mice fed HFD for 8 weeks compared to all other groups of LDLr$^{-/-}$ AEL males *(Figure 70B)*. Anti-double stranded DNA IgG antibody levels, characteristic of autoimmunity, were significantly raised after 8 weeks of HFD compared to both 8 weeks of chow diet and the regression group in LDLr$^{-/-}$ AEL males *(Figure 70C)*. Plasma cholesterol levels were significantly lower in the regression group compared to both 4 and 8 weeks of chow diet *(Figure 70D)*. Additionally, cholesterol levels were significantly greater after 8 weeks of HFD compared to chow diet in LDLr$^{-/-}$ AEL males *(Figure 70D)*.

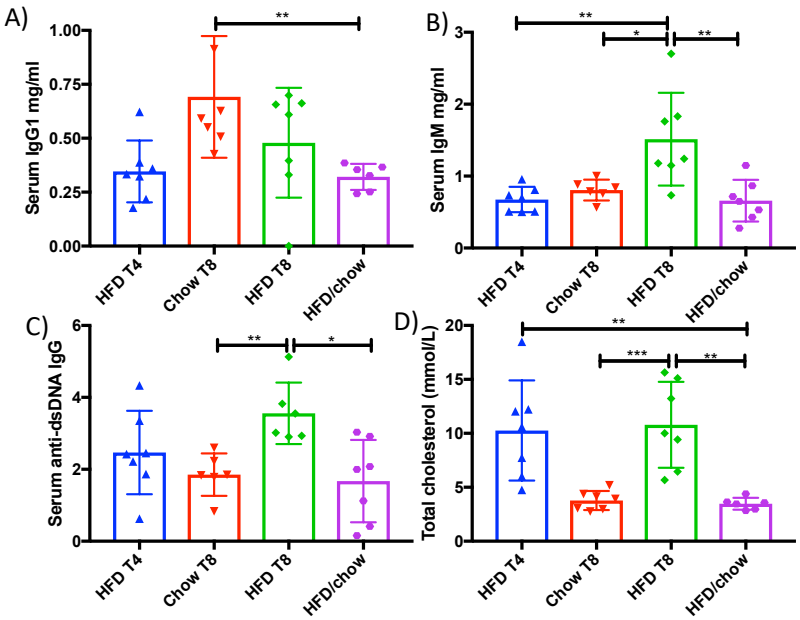

Figure 70. ***Serum antibody levels were altered in response to regression in LDLr$^{-/-}$ mice.*** *LDLr$^{-/-}$ AEL male mice were fed either high fat diet (HFD) for 4 weeks before sacrifice (blue), 8 weeks of chow diet (red), 8 weeks of HFD (green) or 4 weeks of HFD followed by chow diet for 4 weeks (purple). Plasma was analysed for* ***(A)*** *IgG1 antibodies,* ***(B)*** *IgM antibodies,* ***(C)*** *anti-double stranded DNA (dsDNA) IgG antibodies and* ***(D)*** *total cholesterol. Each dot represents 1 mouse, graphs show mean +/- SD. Statistics carried out using Mann-Whitney test, * P < 0.05; ** P < 0.01; *** P < 0.001; **** P < 0.0001.*

4.5 Discussion

4.5.1 Characterisation of GC response at baseline in WT mice

Through use of WT mice, I was able to investigate the impact of time and diet variables without the confounding variable of genotype provided by the LDLr$^{-/-}$ background. Thus, on the WT background, chow diet enabled investigation of the impact of time on GC responses while HFD allowed analysis of the diet variable on GC responses.

4.5.1.1 Effect of time on GC responses and output (WT chow)

In male WT AEL mice fed a chow diet, there were no changes in splenic or para-aortic cell numbers over time. The GC population of both the spleen and PALN showed an time-dependent expansion, as it was significantly increased following 8 weeks of chow diet. The total class-switched GC clone population also showed a time-dependent increase after 8 weeks of chow diet in the spleen while EYFP labelled class-switched GC B cells were detected after 8 weeks of chow in the PALN. Furthermore, the para-aortic EYFP memory cell population was expanded upon 8 weeks of chow diet feeding.

The presence of EYFP labelled cells increased with time in the spleen, inguinal and para-aortic lymph nodes, and blood. Within the spleen, both GC and memory EYFP-labelled populations expanded over time in chow diet-fed WT AEL male mice. In the PALN, only IgM+ EYFP labelled memory cells were increased with time.

Although the plasma cell pool remained stable over time in the spleen, the isotype profile switched from being dominated by IgM- clones after 4 weeks to IgM+ clones by 8 weeks of chow diet. EYFP labelled plasma cells increased with time across the lymphoid organs, blood, and BM. Only IgM+ EYFP labelled PCs within the LN showed a significant increase with time. This demonstrates that labelled PCs are exported from lymphoid organs, circulate in the blood and home to the BM.

These data reveal that there was a time-dependent increase in GC responses with class switching of GC cells occurring more at later timepoints. In tandem, EYFP cell populations expand with time although only IgM+ clones are detected as memory and plasma cells. This reveals that limited class switching occurs by 8 weeks of chow diet feeding and has not resulted in any functional output at this timepoint. Le Gallou et al found a tamoxifen-induced EYFP-labelled B cell population in the absence of immunisation which diminished over a 2 week period[270]. To determine the longevity of EYFP-labelled GC-derived cells in this model, sacrifice could be conducted 2 weeks after tamoxifen labelling. Dogan et al found a small but consistent IgM+ GC B cell population in control unimmunised mice along with occasional germinal centre-like structures within B cell follicles[266]. They suggested that these cells were

the results of stimulation from microbial or environmental antigens which is also likely the case in the male WT AEL mice fed chow diet[266].

The results confirm that EYFP labelling can capture the expansion of the GC population and the consequent increased production of memory and plasma cells. Additionally, these data display the sensitivity of the lineage tracing system as the dynamics of GC cells and their progeny can be analysed in a system where GC activity was minimal.

4.5.1.2 Effect of diet on GC responses and output (WT HFD)

In response to 4 weeks of HFD, total cell numbers were expanded in the spleen and PALN in WT AEL male mice compared to chow diet. The population of GC B cells was significantly increased after 8 weeks of HFD in both the spleen and PALN compared to 4 weeks of HFD, driven by the expansion of IgM- clones. Furthermore, the splenic GC population was significantly bigger after 8 weeks of HFD compared to chow diet. This was reflected in the splenic EYFP cell population. Evidence of increased class switching was also detected in the LN and PALN in both total and EYFP labelled populations after 8 weeks of HFD.

The total EYFP cell population was expanded in the spleen, inguinal and para-aortic lymph nodes, blood, and BM after 8 weeks of HFD. Although this trend also occurred in the chow diet-fed WT AEL male mice, it happened to a greater degree in HFD-fed male WT AEL mice. Within the PALN, the EYFP labelled GC B cell population expanded after 8 weeks of HFD with an increase in IgM+ clones and an even greater increase in IgM- clones. Within the spleen, HFD consistently resulted in a greater population of EYFP labelled GC clones compared to chow diet and EYFP memory cell production was significantly greater, driven by IgM+ clones, in 4-week HFD-fed compared to 4-week chow diet-fed male WT AEL mice. By 8 weeks of HFD, EYFP memory cell production had switched to IgM- clones. There was a significant increase in the splenic EYFP GC cell population in 8-week HFD compared to 8-week chow diet-fed male WT AEL mice which was not observed for the splenic EYFP memory cell population. This resulted in a significantly elevated GC to memory ratio, indicating that GCs were longer lasting upon HFD feeding compared to chow diet feeding in male WT AEL mice.

Production of EYFP labelled memory cells was also significantly greater after 8 weeks compared to 4 weeks of HFD feeding in both the inguinal and para-aortic lymph nodes. Both IgM+ and IgM- clones contributed to this memory expansion in the PALN.

Splenic plasma cell production reached a peak after 4 weeks of HFD, primarily due to IgM- clones. By 8 weeks of diet, HFD induced a significantly bigger pool of IgM+ PCs compared to chow diet. Meanwhile the pool of EYFP labelled PCs within the spleen, LN, PALN and BM was greatest after 8 weeks of HFD, regardless of isotype.

HFD resulted in an exacerbated GC response beyond that of time-related impacts alone. This response was longer in duration and more pathogenic with greater class switching and IgM- clonal output. The result was an expanded EYFP population of memory and plasma cells exported from all lymphoid organs leading to greater presence of EYFP cells in circulation and within the BM. Thus, HFD itself was immunogenic eliciting an adaptive B cell response presumably partly due to food antigens and partly due to elevated lipid levels within the blood. Trottier et al showed increased frequencies of B cells residing in the BM in response to HFD which could have a knock-on effect to other B cell populations[271]. Additionally, in response to HFD, B cells secrete pro-inflammatory cytokines, pathogenic IgG antibodies and natural self-reactive IgM autoantibodies demonstrating an adaptive B cell response[272]. Under hyperlipidaemic conditions[273], the gut microbiome can expand the B2 cell population via TLR signalling pathways resulting in induction of B2 cell proinflammatory cytokine gene expression[274].

HFD feeding reduces gut microbial diversity resulting in microbial dysbiosis[275]. In particular, Lactobacillaceae, Proteobacteria and Betaproteobacteria were all decreased in HFD-fed LDLr$^{-/-}$ mice while Staphylococcaceae, Bacillales, Streptococcaceae and Clostridiaceae were increased[275]. Furthermore, the microbiome encourages arterial thrombus growth by increasing platelet activation[275]. Immunisation against specific microbial species can reduce the ratio of Firmicutes: Bacteriodetes, which results in decreased macrophage levels within the plaque and reducing proinflammatory cytokines in the blood[276]. HFD has been shown to increase the presence of Gram-negative bacteria in the gut such as *Enterobacteriaceae*, which can elevate intestinal LPS levels[277]. As LPS is a major inducer of systemic inflammation, this

could contribute to the enhanced B cell response. HFD feeding causes stress to the epithelial lining of the intestine resulting in increased permeability and reduced gene expression of tight junction proteins ZO-1 and claudin-1[273] leading to reduced barrier function[71]. This facilitates greater diffusion of microbiome-derived endotoxins i.e. gut bacterial antigen components[71], into the blood which leads to metabolic endotoxemia[278]. Foods such as red meat, poultry, fish, eggs and milk are rich in lipid phosphatidylcholine which is broken down into choline, converted to TMA and oxidised to form trimethylamine N-oxide (TMAO)[279]. High levels of plasma TMAO are associated with higher risk of atherosclerosis, indicative of a key role in atherosclerosis for the gut microbiome[280].

The impact of the gut microbiome can be investigated through administration of antibiotics to wipe out microbial species or by using germ-free conditions to prevent any microbiome from ever developing. Antibiotic treatment during HFD feeding reduced the size of atherosclerotic lesions partly through repair of the intestinal barrier reducing the leaky gut phenotype[273]. Additionally, the therapeutic intervention prevented HFD-induced increase in the follicular B cell population and increased the MZ B cell population whilst also dampening antibody responses[274].

High serum cholesterol levels result in the accumulation of LDL within the intima where it undergoes lipid peroxidation producing immunogenic oxidation-specific epitopes which induce both innate and adaptive immune responses[281]. Constituents of LDL act as autoantigens and can activate macrophages and B cells resulting in the production of modified LDL antibodies[255]. In the subsequent Chapter 4, cholesterol was removed from the HFD, and no differences are seen in GC levels within WT mice. This suggests that the high cholesterol content of HFD was the main driver of the greater GC responses seen in WT AEL male mice despite the presence of LDL receptors available for cellular cholesterol uptake. Of note, although these mice are referred to as 'WT', they are in fact heterozygous for the LDL receptor ($LDLr^{+/-}$) and are likely to have a diminished LDLr protein product as observed by Ishibashi et al[282]. This could influence the ability to take up cholesterol into cells and thus impact serum cholesterol concentrations. Indeed, mice heterozygous for the LDL receptor had raised cholesterol concentrations, by 35%, compared to WT littermates. When placed on a 0.2% cholesterol supplemented chow diet, these heterozygous mice had a small but

significant increase in plasma LDL cholesterol levels[282]. Therefore, in the future, experiments should also be conducted on a true WT background with $LDLr^{+/+}$ to compare the two wildtype strains to determine the impact of LDL receptor heterozygosity on serum cholesterol concentrations and GC responses.

4.5.2 Differences between the WT and $LDLr^{-/-}$ mouse model

To elucidate the impact of the $LDLr^{-/-}$ genotype on GC responses, a direct comparison between the WT and $LDLr^{-/-}$ strains has been conducted for both diet types.

4.5.2.1 Effect of genotype on GC responses and output in chow diet-fed mice ($LDLr^{-/-}$ v WT)

The $LDLr^{-/-}$ background resulted in elevated total and B cell numbers in the spleen and LNs after 4 weeks of chow diet.

The GC population was significantly expanded in male $LDLr^{-/-}$ AEL mice compared to male WT AEL mice after 4 and 8 weeks in the LN and PALN and after 4 weeks only in the spleen. Furthermore, the EYFP cell populations within the LN and PALN were significantly bigger in chow diet-fed male $LDLr^{-/-}$ AEL compared to male WT AEL mice after 4 weeks. Production of IgM+ GC B cell clones within inguinal and para-aortic lymph nodes was significantly higher in male $LDLr^{-/-}$ AEL compared to chow diet-fed male WT AEL mice after 4 weeks and after 8 weeks only in the inguinal LNs. The presence of class switched GC B cells was higher in male $LDLr^{-/-}$ AEL compared to chow diet-fed male WT AEL mice after 8 weeks in both sets of LNs and spleen and after 4 weeks in the PALN. This was confirmed by the significantly higher-class switch ratio in all lymphoid organs analysed in male $LDLr^{-/-}$ AEL compared to male WT AEL mice on chow diet for 8 weeks. Production of class-switched EYFP labelled GC clones was greater after 4 weeks of chow diet in PPs of male $LDLr^{-/-}$ AEL compared to male WT AEL mice.

EYFP labelled memory cell populations were expanded significantly in the inguinal and para-aortic lymph nodes of male $LDLr^{-/-}$ AEL fed chow diet for 4 weeks compared to male WT AEL mice. Within the PALN, both IgM+ and IgM- memory cell production was superior on the $LDLr^{-}$

$^{/-}$ background compared to WT in AEL mice fed chow diet for 4 weeks. Populations of IgM-EYFP labelled memory cells were significantly bigger after 4 weeks of chow diet in the inguinal LNs and after 8 weeks of chow diet in the spleen and PPs of male LDLr$^{-/-}$ AEL mice compared to male WT AEL mice.

Plasma cell populations were increased within the spleen at 4 weeks and the LN at 8 weeks of chow diet in male LDLr$^{-/-}$ AEL compared to male WT AEL mice. The production of both IgM+ and IgM- plasma cells was significantly higher in male LDLr$^{-/-}$ AEL compared to male WT AEL mice after 4 weeks of chow diet in the spleen. In both inguinal and para-aortic lymph nodes, the IgM- PC pool was significantly expanded after 8 weeks of chow diet in the LDLr$^{-/-}$ mouse model compared to the WT model.

These results suggest absence of LDL receptors resulted in an augmented GC response across the spleen and both sets of LNs even in male chow diet-fed mice with more EYFP-labelled cells participating in GC reactions than in male WT AEL mice. As the GC to memory ratio was not significantly different between the 2 genotypes (GC and memory cell production are both increased on the LDLr$^{-/-}$ background), GCs do not last longer. This means that lymphoid organs must either contain more individual GCs or each GC contains more cells. Flow cytometry cannot provide clarity on this and thus immunofluorescence of lymphoid organ sections could be carried out to determine which option was true. Production of GC clones was elevated across all timepoints analysed, however IgM+ clones dominate after 4 weeks and class switching occurs mainly at later stages resulting in a majority of IgM- clones by 8 weeks. Thus, while the GC showed the starkest difference between genotypes at 4 weeks, this mainly comprises non-class switched cells outputting PCs from the spleen and memory cells from both sets of LNs. Although the GC response was comparatively smaller by 8 weeks, it has skewed towards more pathogenic isotypes with mainly PCs exported from the inguinal and para-aortic LNs.

This mirrors existing literature regarding GC dynamics whereby Weisel and colleagues conducted BrdU pulse chase experiments showing that memory cell production occurred earlier on in the response with clones tending to be low affinity and have undergone little class switching[283]. An initial wave of memory B cell (MBC) production was observed between

D0-2 with 40% of MBC created by day 5 post-immunisation[283]. The peak of IgG1 MBC production was mainly between D6-8 of the immunisation response and 50% of all IgG1 MBCs had exited the GC by day 11[283]. Later on in the GC response, plasma cell production dominated after successive rounds of SHM and class switching for affinity maturation have taken place[283]. Disruption of the GC in the day 12-14 window greatly diminished the BM IgG1 AFC population 8 weeks later accompanied by 90% loss of high affinity LLPCs demonstrating that LLPC production is predominantly later in the GC lifespan[283]. Through mutational content analysis of the V region of the BCR they showed that MBCs had similar amount of mutations to GC B cells from days 6-8 of the GC reaction while the mutational content of PCs matched that of GC B cells from days 18-20[283].

As male LDLr$^{-/-}$ AEL mice on chow diet exhibit increased cholesterol levels compared to male WT AEL mice on chow diet, this data corroborates the findings of the male WT AEL mice fed a HFD whereby the increased serum cholesterol levels result in enhanced GC responses.

4.5.2.2 Effect of genotype on GC responses and output in HFD-fed mice (LDLr$^{-/-}$ v WT)

After 4 weeks of HFD, total and B cell numbers within the spleen and LN were significantly higher in male LDLr$^{-/-}$ AEL mice compared to male WT AEL mice. After 8 weeks of HFD, total and B cell numbers within inguinal and para-aortic LNs were significantly higher in male LDLr$^{-/-}$ AEL mice compared to male WT AEL mice.

The GC population was significantly expanded after 4 and 8 weeks of HFD in both sets of LNs and after 4 weeks only of HFD in the spleen of male LDLr$^{-/-}$ AEL mice compared to male WT AEL mice. This result was confirmed by the expanded EYFP cell pool seen after 4 and 8 weeks of HFD in the inguinal and para-aortic lymph nodes on the LDLr$^{-/-}$ background compared to WT background. The production of IgM+ and IgM- GC clones was greater after 4 weeks HFD in both lymph nodes of male LDLr$^{-/-}$ AEL mice compared to male WT AEL mice. The pool of splenic IgM+, splenic and inguinal lymph node IgM- GC B cells was bigger after 8 weeks HFD on the LDLr$^{-/-}$ AEL background compared to WT AEL background. The class switch ratio was higher after both 4 and 8 weeks of HFD in both sets of LNs and after 8 weeks only of HFD in the spleen and PPs of male LDLr$^{-/-}$ AEL mice compared to male WT AEL mice. Clearly the HFD

has a pathogenic influence on the GC response even early on in the LNs as these are sensitive to local inflammatory changes. Although the spleen reacts to systemic changes and therefore doesn't show signs of increased class-switching after 4 weeks, this organ has skewed towards a pathogenic GC response by 8 weeks of diet. In germ-free conditions, the number of GC B cells present in the spleen remained unchanged while the GC population was drastically reduced in LNs indicating that endogenous antigens drive GC reactions within the spleen but that GCs within LNs are activated by foreign antigen[284].

The population of class-switched EYFP labelled GC clones were expanded after 4 weeks HFD in the PALN and PPs of male LDLr$^{-/-}$ AEL compared to male WT AEL mice. As the PPs react to food antigens, this showed that the immunogenic nature of HFD resulted in the production of pathogenic GC clones. As the EYFP GC pool was expanded in the PALN but not the LN, this reveals the specificity of the EYFP labelled GC response as the PALNs react to the ongoing process of atherogenesis in the aorta while this stimulus was absent from the LNs.

Besides GC cells, memory production was also responsible for the increased proportion of EYFP cells in both sets of LNs as EYFP memory cell production was significantly higher after 4 and 8 weeks of HFD against the male LDLr$^{-/-}$ AEL compared to male WT AEL background. The class-switched EYFP memory cell pool was significantly bigger after 4 and 8 weeks of HFD in the spleen on the male LDLr$^{-/-}$ AEL compared to male WT AEL background. Both IgM+ and IgM- clones contributed to the expanded EYFP memory cell pool in the PALN after 4 weeks of HFD. Meanwhile in the LN, IgM- EYFP memory cells predominated after 4 weeks of HFD followed by dominance of IgM+ EYFP memory clones by 8 weeks of HFD in male LDLr$^{-/-}$ AEL compared to male WT AEL mice.

Plasma cell production was augmented by the LDLr$^{-/-}$ background after 4 weeks and 8 weeks of HFD in the spleen regardless of isotype. By 8 weeks of HFD, the male LDLr$^{-/-}$ AEL mice showed increased plasma cell pools, mainly due to expansion of IgM- clones, in the PP, LN and PALN compared to WT mice.

Analyses of serum cholesterol revealed that HFD induces significantly elevated cholesterol levels even in male WT mice at both 4 and 8 weeks compared to chow diet. This effect was

augmented upon the LDLr$^{-/-}$ background where the differences in serum cholesterol levels between chow and HFD-fed AEL mice were even more significant. Comparison between the 2 genotypes revealed that the LDLr$^{-/-}$ background resulted in elevated cholesterol levels at baseline as chow diet-fed male LDLr$^{-/-}$ AEL mice had significantly higher serum cholesterol levels than those of chow diet-fed male WT AEL mice at both 4 and 8 weeks. Upon HFD feeding, there was a very significant increase in serum cholesterol levels in male LDLr$^{-/-}$ AEL mice compared to male WT AEL mice. This finding has previously been reported in the literature whereby young LDLr$^{-/-}$ mice fed a chow diet had plasma cholesterol levels twice as high as C57BL/6 around 5.2 mmol/L (200mg/dL) which increased gradually to 9 mmol/L (350mg/dL) over time[285].

Absence of the LDL receptor resulted in hypercholesterolemia due to the incapacity of cells to take up cholesterol. Compared to HFD feeding in male WT AEL mice, HFD feeding in male LDLr$^{-/-}$ AEL mice resulted in hypercellularity of the spleen and hypertrophic LNs. This was due to increases in GC related populations, GC B cells, memory cells and plasma cells. Hyperlipidaemic conditions result in bigger populations of GC B cells, Th1 and Treg cell populations[255]. Additionally, plasma cell populations have been found to be increased with corresponding increases in IgM and IgG titres[255]. In Apoe$^{-/-}$ mice, PCs reactive to T15 were elevated and increased with age[262]. Other cell populations are likely to also be expanded but were not included in the analysis. For instance, macrophages can increase up to 20-fold within the aorta during the progression of atherosclerosis[245]. A large fraction of monocytes recruited to the atherosclerotic plaque originate from the spleen which is an important reservoir and producer of Ly6C^{high} monocytes; indeed the spleen contains considerable pools of proliferative myeloid progenitors under atherosclerotic conditions[286]. Absence of the LDL receptor also resulted in enhanced GC responses with proportionally increased cellular output and greater extent of class switching. Although there was an increase in the EYFP cell population in both sets of LNs, there were no significant differences in EYFP cell populations between the genotypes in the spleen, BM, and blood. The spleen of male LDLr$^{-/-}$ AEL mice had an increased GC population after 4 weeks of HFD resulting in a lower proportion of GC cells with the EYFP label compared to male WT AEL mice as the male WT AEL mice had a similar EYFP population but smaller GC size. This suggests that in the spleens of male LDLr$^{-/-}$ AEL mice, there was a greater rate of GC initiation thus replacing EYFP clones when fed HFD. The finding

that there was not an increase in EYFP cells in circulation and the BM suggests that the increased EYFP cellular output from lymphoid organs was not homing to the BM and perhaps instead was homing towards ATLOs and the aorta. Given time constraints the aorta was not analysed for GC-derived cells, however this could be conducted to determine if EYFP cells are travelling to these locations. Hypercholesterolemia induced significant expansion of memory and plasma cell populations and a substantial degree of class-switching by 8 weeks demonstrating the pathogenic impact of high plasma cholesterol levels.

4.5.3 Characterisation of the GC response under atherosclerotic conditions In LDLr$^{-/-}$ mice

The LDLr$^{-/-}$ mouse model prevents cellular uptake of cholesterol due to the absence of LDL receptors thus creating high blood cholesterol concentrations characteristic of atherosclerosis. First, the impact of this genotype was analysed in male AEL mice fed the chow diet. Finally using the LDLr$^{-/-}$ mouse model and HFD in combination, the GC response was characterised under atherosclerotic conditions.

4.5.3.1 Effect of genotype on GC responses and output in chow diet-fed mice (LDLr$^{-/-}$ chow)

The splenic GC population increased over time with a significant increase in IgM+ clones after 4 weeks of chow diet and a significant increase in IgM- clones after 8 weeks of chow diet. As such, the class switch ratio showed a time-dependent increase in all lymphoid tissues analysed. As a result of the expansion of the GC population, the EYFP cell population increased over time in the spleen.

The splenic EYFP memory cell population expanded with time driven by an increase in IgM- clones. The EYFP memory cell pool residing in the BM was at its biggest after 4 weeks of chow diet and had diminished by 8 weeks of chow diet although still significantly higher than prior to diet. This suggests that the greatest memory cell influx was at the 4-week timepoint despite memory cell production within the spleen being highest after 8 weeks. Plasma and memory B cells that arrive and embed in the BM lose their migration ability, thus resulting in a finite niche for cells to migrate to[287]. GC-derived cells have long lifespans within the BM and are

only displaced and replaced when a new clone can outcompete[288]. Thus, over time the cellular competition increases as space becomes more limited and antigen affinity increases[288]. Therefore, it was possible that there was no more space for additional memory cells at the 8-week timepoint. Further research could be conducted to test this hypothesis. Additionally, the EYFP labelled IgM+ memory cell pool expanded over time in the PALN.

The plasma cell population expanded with time in the spleen, LN, PALN, BM and blood with IgM+ clones dominating after 4 weeks and class-switched IgM- clones dominating after 8 weeks of chow diet.

The EYFP GC populations of the spleen and PPs as well as the EYFP memory population of the PPs was significantly reduced after 4 weeks of chow diet compared to prior to diet. This could be due to the maturation of the immune system and perhaps natural immunity was still being compiled at this early time point (T0).

These data confirm the time-related increases in GC responses reported for the WT mice fed a chow diet but showed that on the $LDLr^{-/-}$ background male AEL mice display a greater degree of class-switching, across all GC-derived cell populations, even on chow diet. Thus, even the small increase in plasma cholesterol levels, induced by absence of LDL receptors, has a pathogenic impact on the GC response. This could be partly facilitated by the microbiome as in germ free conditions, $Apoe^{-/-}$ mice fed a chow diet developed less atherosclerotic plaque characterised by reduced lipid and macrophages accumulation[278]. Furthermore, these mice have reduced LPS, IL6 and TNFα levels along with reduced levels of other pro-inflammatory chemokines[278].

Obviously, the absence of the LDL receptor leads to increased circulating levels of plasma LDL due to its inability to be taken up cellularly via LDLr[289]. These high plasma LDL levels increase the likelihood of LDL oxidation which is a central driver of pathology in atherosclerosis[289]. Furthermore, when Ishibashi et al first developed and characterised the $LDLr^{-/-}$ mouse model, they noted that deficiency in the LDL receptor resulted in augmented responses to dietary cholesterol[282]. Additionally, the LDL receptor may have an important role in LDL antigen presentation within B cells and thus, in its absence there would be altered antigen

presentation and as a consequence altered B cell responses[289]. These factors contribute to the inflammation key to atherosclerosis and could therefore help to explain the pathogenic impact of LDLr deficiency on the GC response in chow diet-fed male LDLr$^{-/-}$ AEL mice.

4.5.3.2 Effect of atherosclerosis on GC response and output (LDLr$^{-/-}$ HFD)

Total and B cell numbers in the PALN were significantly higher after HFD feeding compared to chow diet feeding at both 4 and 8 weeks. This backs up existing literature which found that LNs in Apoe$^{-/-}$ became hypertrophic with age and this effect was exacerbated by the presence of western diet (WD) to the extent that hypertrophy was seen by 16 weeks of age[290].

The GC population was significantly greater after 8 weeks of HFD compared to chow diet in the spleen and there was a time-dependent increase in the presence of IgM- GC clones. This increase was significantly greater than that of chow diet-fed mice at both 4 and 8 weeks. After 4 weeks of HFD, a greater number of EYFP IgM- GC cells were detected compared to chow diet in the spleen.

The class switch ratio was greater after 8 weeks compared to 4 weeks HFD in all lymphoid tissues analysed. The class-switch (CS) ratio was significantly higher in mice fed HFD compared to chow diet for 4 and 8 weeks in the PPs and for 4 weeks HFD only in the spleen. Class switched EYFP populations of memory and plasma cells were significantly greater after 8 weeks compared to 4 weeks of HFD in the spleen and PPs.

The EYFP cell population was expanded after 8 weeks compared to 4 weeks HFD in the spleen and LN. After 4 weeks, HFD induced a greater pool of EYFP cells in the PALN compared to chow diet. The EYFP cell population, primarily those cells with memory phenotype, was at its highest after 4 weeks of HFD in the BM; significantly greater than 4 weeks of chow diet and 8 weeks of HFD. After 8 weeks, HFD resulted in a higher absolute number of EYFP cells in the LN compared to chow diet.

The EYFP memory cell pool was greater after 8 weeks compared to 4 weeks of HFD in the spleen. At the 4-week timepoint, HFD induced a bigger EYFP memory cell pool compared to

chow diet in the inguinal and para-aortic lymph nodes. In the PALN, this was due to expansion of IgM+ clones. The production of EYFP IgM+ memory cells was greater after 8 weeks compared to 4 weeks of HFD in the PALN, PPs and blood. Production of EYFP IgM- memory cells was greater after 8 weeks of HFD compared to chow diet in the spleen.

After 4 weeks of diet, HFD resulted in a significantly larger population of IgM- plasma cells compared to chow diet in the LNs. The production of plasma cells was significantly greater, primarily due to expansion of IgM- clones, after 8 weeks compared to 4 weeks of HFD in all tissues. In the spleen and BM, the IgM+ PC pool expanded from 4 to 8 weeks of HFD suggesting that there was great migration of IgM+ plasma cells to the BM solely from the spleen at the 8-week timepoint. Contrastingly, the IgM+ plasma cell population shrank in both sets of LNs and the blood. In the spleen specifically, the plasma cell population was significantly larger upon HFD feeding compared to chow diet feeding after 8 weeks.

Serum analysis for antibody titres revealed that IgG1 production was highest after 4 weeks of chow diet and diminished to pre-diet levels by 8 weeks of chow diet. The quantity of IgG1 detected in serum was significantly greater after 8 weeks of chow diet compared to HFD. IgM production was highest after 4 weeks of chow diet, significantly more so than pre-diet, and was significantly reduced by 8 weeks of chow diet. Serum titres of IgM were significantly higher after 8 weeks of HFD feeding compared to chow diet feeding. Serum IL6 titres were significantly greater after 4 weeks of HFD compared to 4 weeks of chow diet and 8 weeks of HFD.

These data show that the combination of the LDLr knock-out and HFD resulted in LN hypertrophy with an enlarged PC population in $LDLr^{-/-}$ mice which was reported to contribute to hypertrophic LNs in $apoE^{-/-}$ mice previously by Khoo et al.[239]. Thus hypercholesterolemia has a hypertrophic impact on lymph nodes accounted for by expansion of the pre-existing lymphatic network and impaired lymphocyte egress as reported by Srikakulapu et al[12]. Immunoflurorescence staining could be conducted to validate these findings in experimental $LDLr^{-/-}$ mice. The combination of HFD and $LDLr^{-/-}$ genotype had a synergestic impact eliciting an enlarged GC response dominated by class-switched clones leading to output of class-switched memory and plasma cells. The response was larger than the impact of either HFD or

LDLr$^{-/-}$ genotype alone. Class-switching occurred earlier and to a greater extent than either chow diet-fed male LDLr$^{-/-}$ or HFD-fed male WT mice. There were greater EYFP cell populations showing that labelled cells are retained within the lymphoid organs and primarily contribute to the memory response. Somewhat surprisingly, EYFP labelled GC populations were not expanded in line with the expansion of the total GC populations suggesting that there was a high turnover in individual GCs resulting in the creation of non-labelled GC cells which contribute to the increased GC population. Data from the inguinal and para-aortic lymph nodes suggests that PC production was characterised by an initial wave of IgM+ clones followed by a secondary wave of class-switched PC clones demonstrating that the GC output becomes more pathogenic over time augmented by the presence of HFD. Antibody analyses suggests that the peak antibody response was after 4 weeks of diet and while HFD had a suppressive effect on IgG1 titres, it resulted in increased serum concentrations of IgM and IL6. This suggests a higher antigenic load likely partly a result of foreign antigens within HFD itself and partly due to the hypercholesterolemic environment resulting in exposure of immunogenic epitopes such as oxLDL.

The gut microbiota has been implicated in cardiometabolic disorders including the pathology of atherosclerosis[278]. Endotoxemia as a consequence of HFD-induced leaky gut, has been associated with decreased expression of ATP-binding cassette transporter 1 (ABCA1)/ABCG1, key genes involved in cholesterol efflux[276]. Previously it has been shown that there was a significant correlation between the gut microbiome and serum lipid levels[291]. Furthermore, the microbiota can influence liver cholesterol and fatty acid synthesis as β-hydroxy β-methylglutaryl (HMG)-coA synthase 1, HMG-CoA reductase, LDLr and sterol regulatory element-binding protein (SREBP)2 were reduced in the livers of germ-free Apoe$^{-/-}$ mice[278]. In germ free mice, IgM levels persist while IgG levels are reduced demonstrating that gut microbial species are vital for B2 cell-derived IgG production[273].

In human subjects, changes to the gut metagenome have been linked with atherosclerosis[280] and up to 50 bacterial species have been identified in plaques as atheromas accumulate bacteria from passing blood[273]. As such the frequency of microbial molecular signatures increases progressively as lesions advance e.g. C. pneumonia has been detected in atherosclerotic plaques of humans who have had previous infection[273].

4.5.4 Impact of HFD on lymphoid organs proximal to intestines

The HFD had an immunogenic effect on the mLN as characterised by the enlarged GC population after 2 weeks, skewed towards class-switched IgM- clones. HFD had a suppressive effect on GC responses within the PPs as the GC population was significantly smaller compared to chow diet at both 4 and 8 weeks in male WT and LDLr$^{-/-}$ AEL mice. In male LDLr$^{-/-}$ AEL mice, production of IgM+ GC B cell clones was significantly reduced upon HFD feeding compared to chow diet feeding at both 4 and 8 weeks. Furthermore, IgM+ clone production was significantly reduced after 8 weeks compared to 4 weeks in both diet types. This fits with the fact that immunological memory was built up over time thus antibody and memory responses are developed at early stages in order to neutralise gut-related antigens and thus IgM+ production wanes over time. Additionally, IgM- clones increase over time in the PPs (data not shown) adding additional layers of affinity maturation. The overall proportion of IgM+ and IgM- GC B cells reduced over time from 4 to 8 weeks in chow diet-fed WT AEL male mice while the proportion of EYFP+ IgM- GC clones increased. This showed that while the number of IgM- GC clones was reducing, a greater proportion of them were EYFP labelled indicating the presence of prolonged chronic GC responses. IgM- memory cell populations expanded from 4 to 8 weeks of chow diet as shown previously demonstrating that over time GCs within the PPs become more productive with increasing cellular output. Indeed, both IgM+ and IgM- EYFP labelled plasma cell pools expanded by 8 weeks of diet. The presence of IgM- memory cells could indicate that the GC response was against similar diet-related antigens and low affinity memory cells are present to provide a template for affinity maturation and undergo further rounds of SHM as would be expected in secondary immune challenges. Of note, the presence of IgM- GC B cells significantly increased from 4 to 8 weeks of HFD feeding while this was not evident in chow diet-fed WT male mice demonstrating the inflammatory nature of HFD in stimulating production of class-switched pathogenic GC responses.

4.5.5 GC response to regression

Use of the regression model in experimental design enabled me to investigate the long-term impact of HFD on GC responses and whether early exposure to HFD permanently altered the behaviour of GC-derived cells. If the 8 weeks HFD group and regression group showed similar values, then one could assume that the early exposure to HFD had pre-programmed cells in a more pathological setting. However, if these 2 groups did not show similar values, it could be assumed that HFD did not have a long-lasting impact on cellular behaviour.

Total and B cell populations of both inguinal and para-aortic lymph nodes were increased in the regression group compared to 4 weeks of HFD only, yet to a smaller degree than after 8 weeks of HFD. This suggests that early HFD exposure resulted in elevated cell numbers over time, however stimulus of HFD for an additional 4 weeks directly influences cell populations by augmenting the total and B cell numbers.

The GC B cell population was smaller in the regression group compared to 8 weeks of HFD in both sets of LNs demonstrating that GCs respond to the atherogenic conditions provided by the HFD. Thus, GCs are not permanently programmed to be more active in mice who have been fed HFD for 4 weeks. The plasma cell population of the inguinal lymph nodes was expanded to a lesser degree after 8 weeks of HFD compared to 4 weeks of HFD demonstrating that plasma cell production was augmented in response to continuous HFD. In contrast, the plasma cell pool was similar in the regression group compared to both 8 weeks of HFD and chow diet in the PALN suggesting that the main driver of plasma cell population expansion in this tissue type was time.

These results show that the inguinal and para-aortic lymph nodes are sensitive to and adapt quickly to changes in diet as they are responsive to local changes in inflammation.

4.5.5.1 PP response to regression

As described previously, the HFD had a suppressive effect on GC responses of the Peyer's patches. In line with this evidence, the regression group of mice had a greater GC B cell population compared to mice fed HFD for 8 weeks and in fact it was similar to that of chow diet-fed mice. Furthermore, the EYFP cell population was greater in the regression group

compared to the 8-week HFD group with IgM- clones dominating the elevated EYFP populations of GC, memory, and plasma cell types. These results show that the HFD does not permanently suppress the GC response, merely affecting GC reactions while the HFD stimulus was present. Meanwhile, the presence of IgM- clones in all GC-derived populations demonstrates that class switched responses have occurred and dominate GC reactions by the 8-week timepoint.

4.5.5.2 Antibody and lipid response to regression

Analysis of serum antibodies revealed that titres of IgG1, IgM and anti-dsDNA IgG remained at the levels for mice fed HFD for 4 weeks and mice on the regression programme. There was a trend towards reduced IgG1 titres after 8 weeks of HFD compared to chow diet which was further exacerbated by the regression setup. This showed that while chow diet resulted in elevated IgG1 levels, this effect was suppressed in mice which have received HFD for 4 weeks prior to 4 weeks of chow diet. As seen in previous analyses, the majority of IgG1 produced in chow diet-fed male LDLr$^{-/-}$ AEL mice occurred within the first 4 weeks explaining these results. Serum IgM levels were significantly lower in the regression group compared to mice fed 8 weeks of HFD suggesting that changes which occur mainly between weeks 4 and 8 of HFD feeding are responsible for the elevated IgM production. As IgM has a circulating half-life of around 4 days, it is not an accumulation of IgM over the 4-week period that is responsible. As the inflammatory milieu increases as atherosclerosis progresses, this is likely to induce greater IgM production. There was a greater difference between anti-dsDNA IgG titres comparing 8 weeks of chow diet to 8 weeks of HFD than regression group to 8 weeks of HFD. This demonstrates the HFD induces autoimmunity as anti-dsDNA IgG antibodies are a key measure of this pathology and the diet was required continuously to elevate anti-dsDNA IgG titres. To surmise, antibody production was determined by diet present at time of analysis and HFD feeding for 4 weeks did not have any predisposing impact on antibody titres as regression group antibody levels did not reach those of 8 weeks HFD.

Male LDLr$^{-/-}$ AEL mice in the regression group showed cholesterol levels similar to those mice fed chow diet for 8 weeks, corroborating findings from Wang et al.[292], significantly lower than

both 4 and 8 weeks of HFD. This demonstrates that HFD presence was required for hypercholesterolemia and that without this stimulus, cholesterol levels drop.

4.5.6 Future work

With more time, the regression studies should be conducted in WT mice to distinguish the impact of diet and genotype on GC responses in this experimental setup. Additionally, it would be interesting to add a group whereby mice are fed chow diet for 4 weeks followed by HFD for 4 weeks. This would enable analysis of the magnitude of HFD impact at different timepoints e.g., does HFD have a more inflammatory role earlier or later in the progression of atherosclerosis?

To investigate in more granular detail the mechanisms at play in the regression studies, it would be interesting to sequence cells from the 4 weeks HFD group to determine whether early HFD exposure predisposes cells to increased proliferation i.e., increased proliferation gene expression. Furthermore, GC B cells could be sequenced to determine the extent of SHM in cells from the regression group compared to that of the HFD for 4 and 8 weeks. In conjunction, assays to determine average antibody affinity should be conducted and compared across groups to see whether antibody maturation was impacted by early exposure to HFD i.e., whether antibody affinity was higher in the regression group than the 4-week HFD group.

The presence of high concentrations of fat and cholesterol within the HFD has been shown to increase serum LPS levels. Indeed, in a 5 year epidemiological study of over 500 middle-aged patients, plasma LPS levels over 50pg/ml increased risk of atherosclerosis by 3-fold[273]. LPS facilitates its pathogenic function by activating TLRs and the consequent inflammatory cascade including NFκB activation[273]. The consequent inflammatory cytokine production acts in a paracrine manner within the PVAT to augment vascular inflammation[273]. As LPS was a major stimulant for systemic inflammation this could be influencing responses seen to HFD. Therefore, in the future serum should be analysed for LPS concentrations to determine the impact of HFD. As LPS was ubiquitous throughout the immune system it would be difficult to

remove LPS from the murine system to analyse the impact of HFD without the confounding variable of LPS concentrations.

As the gut microbiome has a significant impact on the progression of atherosclerosis, experiments could be conducted to determine what effect this variable has in the model characterised within this chapter. As HFD-fed mice are likely to exhibit gut dysbiosis, this was another confounding variable within the model. Thus, by use of germ-free conditions or antibiotics to wipe out the gut bacterial species, the impact of the microbiome could be disentangled from the time, diet, and genotype variables.

As increased salt intake can be a major driver of hypertension and CVD, it was possible that salt content within the HFD has a pathogenic impact on the GC response. Due to time constraints this was not investigated during the course of this PhD, however use of a HFD without salt could be administered to determine its impact in the GC response.

5 EYFP clones are longer-lived under hyperlipidaemic conditions

5.1 Abstract

By labelling AID+ cells with EYFP and tracking them over time at various points in the process of atherogenesis, this chapter determines that HFD-induced hyperlipidaemia causes EYFP clones to be longer lived and more persistent. Labelled clones retained in the GC tended to have undergone class switching demonstrating the HFD skewed GC responses to be more pathogenic. HFD resulted in greater output of EYFP labelled memory and plasma cells from the spleen and PALN. These results demonstrate that not only are GC responses greater in magnitude, both in cellularity and output, but they are also longer lasting and skewed toward pathogenic switched responses. The results are persistent chronic GC responses which could exacerbate the inflammatory phenotype of atherosclerosis.

5.2 Background

As the animal tracking model utilised throughout this thesis enables permanent and irreversible EYFP labelling of cells expressing AID at the time of labelling, it is possible to trace the fates of previously AID expressing cells as they proliferate and differentiate into plasma cells and memory B cells. Using this feature and varying the time of dosing, in this chapter I investigated the movement, persistence and dynamics of EYFP labelled cells over time and the impact of atherosclerosis on these cells.

5.3 Aims

1. Track EYFP-labelled cells over the course of atherosclerosis by investigating labelling at different timepoints during the progression of atherosclerosis

5.4 Results

To determine any acute effects of HFD on EYFP labelled cells, male LDLr$^{-/-}$ AEL mice aged 8 weeks old were dosed with 9mg tamoxifen via oral gavage and then sacrificed either 48hrs later after chow diet or after 1 week of either chow or HFD *(Figure 71)*. No significant differences were seen in any EYFP parameters after 1 week between chow and HFD (data not shown). This demonstrates that there were no acute effects of HFD on labelled cells.

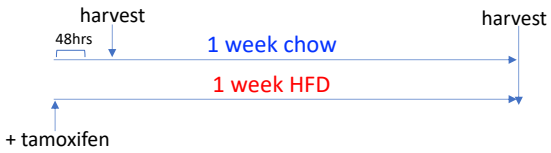

Figure 71. ***Experimental design with 1 week labelling window before diet.*** *Male AEL mice aged 8 weeks old were dosed with 9mg tamoxifen via oral gavage and sacrificed either 48hrs later after only chow diet or 7 days later after 1 week of either chow or high fat diet (HFD).*

5.4.1 Labelling prior to 8 weeks of diet in male LDLr$^{-/-}$ AEL mice

To determine whether the type of diet after labelling had an impact on EYFP labelled cells, male LDLr$^{-/-}$ AEL mice were dosed with tamoxifen at 8 weeks old and put on either chow or HFD for 8 weeks *(Figure 72)*.

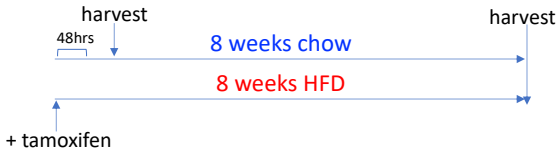

Figure 72. ***Experimental design with 8 week labelling window.*** *Male AEL mice aged 8 weeks old were dosed with 9mg tamoxifen via oral gavage and sacrificed either 48hrs later after only chow diet or after 8 weeks of chow or high fat diet (HFD).*

The EYFP population expanded within the spleen regardless of diet suggesting that whatever reactivity is present at 8 weeks of age prior to diet remains throughout the time course with active GCs ongoing *(Figure 73A)*. In both the inguinal and para-aortic lymph nodes, the EYFP population shrank over the 8 weeks regardless of diet demonstrating that individual GCs resolve more quickly in these organs than in the spleen *(Figure 73B, C)*. In the PPs, the proportion of EYFP labelled cells remained constant in male mice fed the chow diet but in the HFD-fed male mice the population expanded greatly *(Figure 73D)*. It appears that labelled GC clones generated prior to diet intervention within the PPs have greater reactivity against components of the HFD than to chow diet. While the proportion of BM EYFP labelled cells grew marginally in chow diet-fed male mice, the EYFP population diminished over time in those male LDLr$^{-/-}$ AEL mice fed the HFD *(Figure 73E)*. As the BM has a finite niche, this suggests that the EYFP clones have been replaced by non-labelled GC-derived cells, i.e., produced after the labelling in response to the HFD. Finally, the proportion of EYFP cells migrating through circulation was reduced in response to both diet types, however to a lesser degree in male LDLr$^{-/-}$ AEL mice fed the HFD *(Figure 73F)*. This suggests that EYFP labelled clones present in HFD-fed male LDLr$^{-/-}$ AEL mice have an extended lifespan and travel in the blood for longer periods of time.

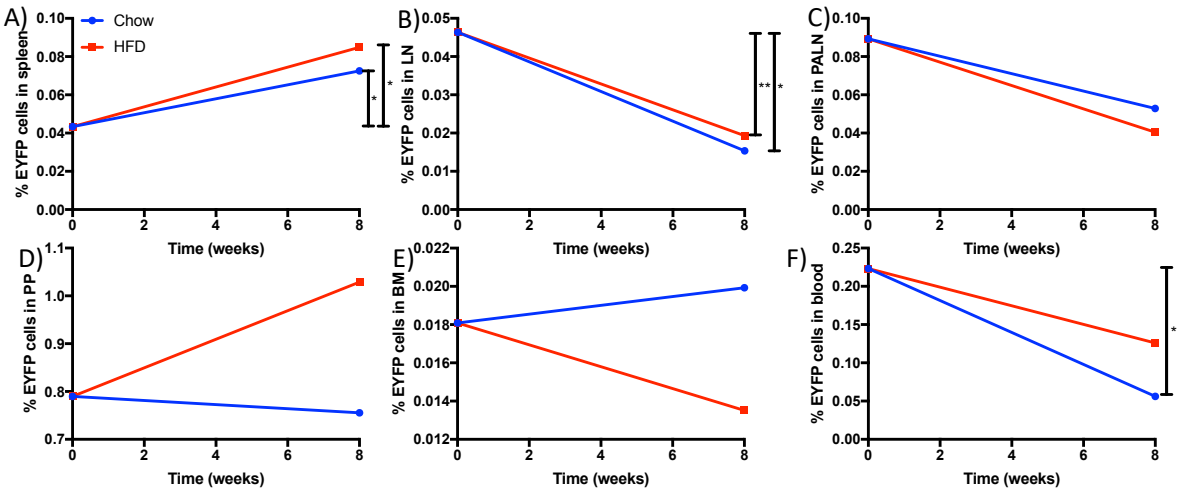

Figure 73. ***EYFP cell populations change over 8 weeks depending on tissue.*** *Male AEL mice were dosed with 9mg tamoxifen via oral gavage at 8 weeks old and fed chow diet (blue) or high fat diet (HFD; red) for 8 weeks. The EYFP population can be seen in* ***(A)*** *spleen,* ***(B)*** *lymph nodes (LN),* ***(C)*** *para-aortic lymph nodes (PALN),* ***(D)*** *Peyer's patches (PP),* ***(E)*** *bone marrow (BM) and* ***(F)*** *blood. Each dot represents the average for each group. Statistics carried out using Mann-Whitney test, * P < 0.05; ** P < 0.01; *** P < 0.001; **** P < 0.0001.*

The study further discriminated IgM+ and IgM- GC cells at the timepoints analysed. Both splenic and para-aortic IgM+ EYFP GC clones diminished over time regardless of diet *(Figure 74A, B)*. In the Peyer's patches, the proportion of EYFP IgM+ GC cells reduced to a greater

extent in HFD-fed male mice compared to chow diet highlighting the suppressive nature of HFD on GC responses within the PPs *(Figure 74C)*. In the spleen, IgM- EYFP GC clones also reduced to the same extent independent of diet *(Figure 74D)*. Chow diet-fed male LDLr$^{-/-}$ AEL mice had stable levels of IgM- EYFP GC clones in the PALN and PPs *(Figure 74E, F)*. In contrast, in response to HFD, both PP and para-aortic IgM- EYFP GC cells expanded demonstrating that the HFD skews toward pathogenic GC responses *(Figure 74E, F)*.

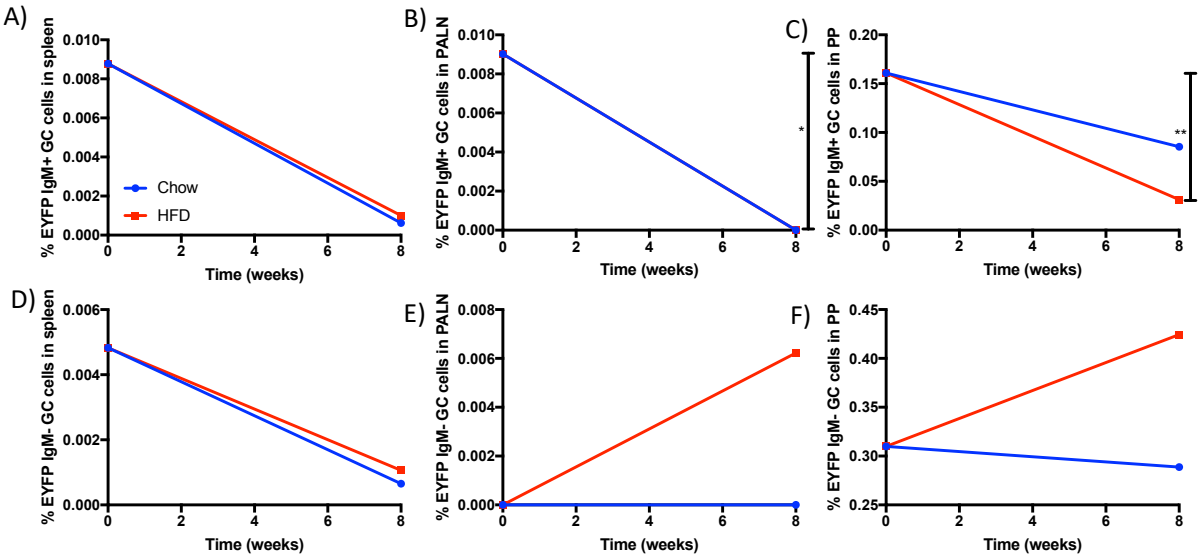

Figure 74. ***Populations of IgM+ and IgM- EYFP GC cells change over time depending on tissue****. Male AEL mice were dosed with 9mg tamoxifen via oral gavage at 8 weeks old and fed chow diet (blue) or high fat diet (HFD; red) for 8 weeks. The EYFP IgM+ GC population can be seen in* ***(A)*** *spleen,* ***(B)*** *para-aortic lymph nodes (PALN) and* ***(C)*** *Peyer's patches (PP).* ***The EYFP*** *IgM- GC population can be seen in* ***(D)*** *spleen,* ***(E)*** *PALN and* ***(F)*** *PP.* ***Each*** *dot represents the average for each group. Statistics carried out using Mann-Whitney test, * P < 0.05; ** P < 0.01; *** P < 0.001; **** P < 0.0001.*

The EYFP labelled IgM+ memory population within the spleen and LNs was significantly expanded after 8 weeks of diet, and this was significantly greater in HFD-fed compared to chow diet-fed male LDLr$^{-/-}$ AEL mice *(Figure 75)*.

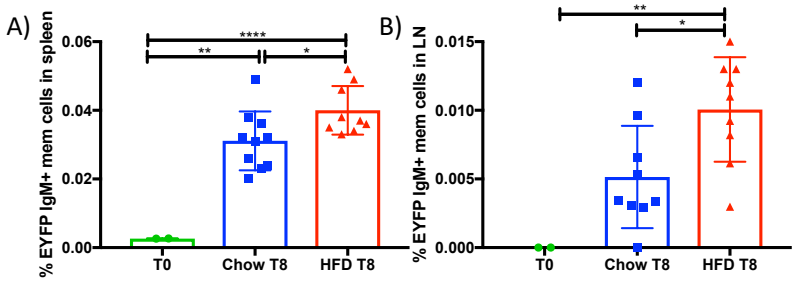

Figure 75. ***EYFP memory cell populations expand in the spleen and LN after 8 weeks.*** *Male AEL mice were dosed with 9mg tamoxifen via oral gavage at 8 weeks old and fed chow diet (blue) or high fat diet (HFD; red) for 8 weeks. Mice were sacrificed at 8 weeks old prior to diet (T0) and at 16 weeks old after 8 weeks of diet (T8). The proportion of EYFP labelled memory (mem) cells which are IgM+ are depicted in* ***(A)*** *spleen and* ***(B)*** *lymph node (LN). Each dot represents one mouse, graphs show mean +/- SD. Statistics carried out using Mann-Whitney test, * P < 0.05; ** P < 0.01; *** P < 0.001; **** P < 0.0001.*

Similarly, the proportion of EYFP IgM- memory cells increased across all tissues analysed but no diet dependent effect was observed in the spleen or PPs *(Figure 76)*. However, in the LNs, PALNs, BM and blood, this population expanded to a greater extent in the HFD-fed male LDLr$^{-/-}$ AEL mice compared to those on chow diet *(Figure 76B, C, E, F)*.

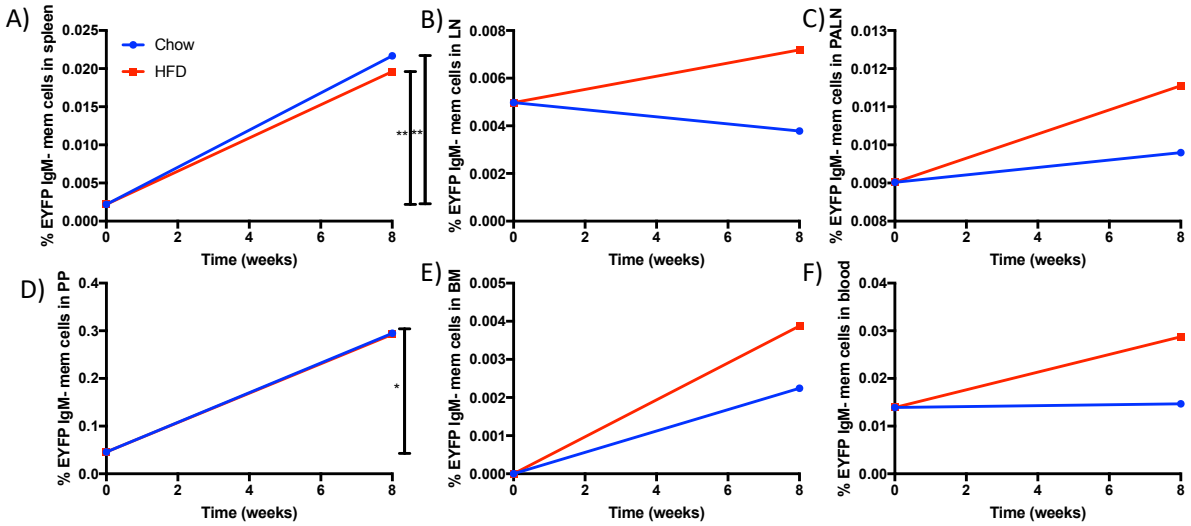

Figure 76. ***EYFP IgM- memory cell populations expand over time in all tissues.*** *Male AEL mice were dosed with 9mg tamoxifen via oral gavage at 8 weeks old and fed chow diet (blue) or high fat diet (HFD; red) for 8 weeks. The EYFP IgM- memory (mem) population can be seen in* ***(A)*** *spleen,* ***(B)*** *lymph nodes (LN),* ***(C)*** *para-aortic lymph nodes (PALN),* ***(D)*** *Peyer's patches (PP),* ***(E)*** *bone marrow (BM) and* ***(F)*** *blood. Each dot represents the average for each group. Statistics carried out using Mann-Whitney test, * P < 0.05; ** P < 0.01; *** P < 0.001; **** P < 0.0001.*

The HFD caused an expansion of both IgM+ and IgM- EYFP PCs in the spleen compared to that of chow diet in male LDLr$^{-/-}$ AEL mice *(Figure 77A, D)*. In the Peyer's patch, the IgM+ EYFP PC population remained relatively stable upon HFD feeding while chow feeding caused a reduction in the population *(Figure 77B)*. Meanwhile more IgM- EYFP PCs were produced in the PPs after HFD feeding in contrast to the stable proportion of IgM- EYFP PCs in chow diet-fed male LDLr$^{-/-}$ AEL mice *(Figure 77E)*. In the BM, both IgM+ and IgM- EYFP PC populations expanded after 8 weeks but to a greater extent in chow diet compared to HFD-fed male LDLr$^{-/-}$ AEL mice *(Figure 77C, F)*.

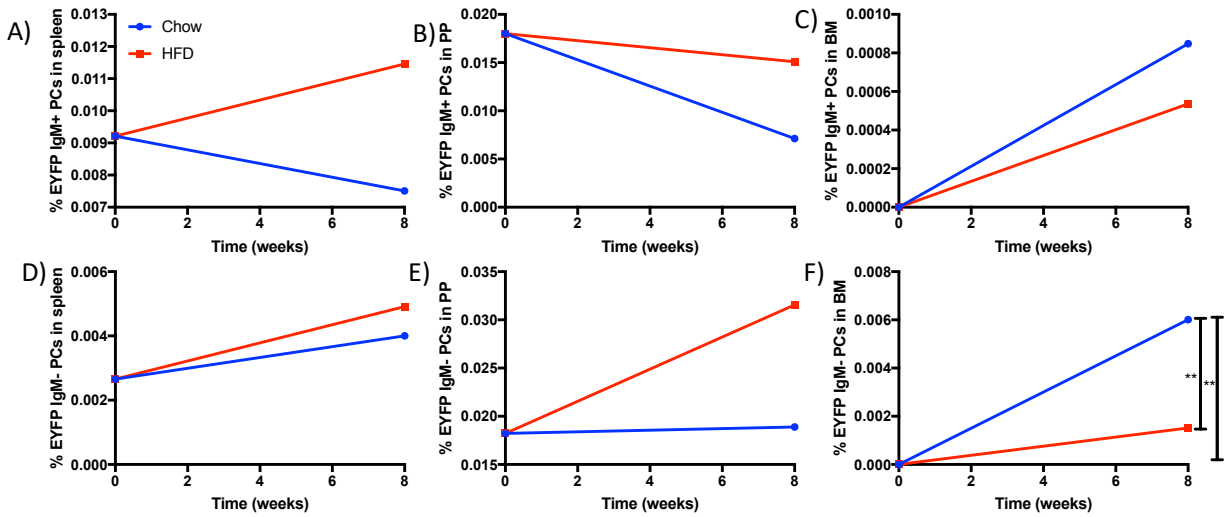

Figure 77. ***EYFP plasma cell populations change over duration of 8 weeks.*** *Male AEL mice were dosed with 9mg tamoxifen via oral gavage at 8 weeks old and fed chow diet (blue) or high fat diet (HFD; red) for 8 weeks. The EYFP IgM+ plasma cell (PC) population can be seen in* ***(A)*** *spleen,* ***(B)*** *Peyer's patches (PP) and* ***(C)*** *bone marrow (BM).* ***The EYFP IgM- plasma cell (PC) population can be seen in (D)*** *spleen,* ***(E)*** *PP and* ***(F)*** *BM. Each dot represents the average for each group. Statistics carried out using Mann-Whitney test, * P < 0.05; ** P < 0.01; *** P < 0.001; **** P < 0.0001.*

5.4.2 Labelling at 4 weeks of diet in male LDLr$^{-/-}$ AEL mice

Next, I investigated whether any significant change of labelled cells could be observed 1 week after labelling in male LDLr$^{-/-}$ AEL mice which had already been on 4 weeks of chow diet or HFD *(Figure 78)*.

Figure 78. ***Experimental design with 1 week labelling window after 4 weeks of diet.*** *Male AEL mice were put on chow or high fat diet (HFD) at 8 weeks old and dosed with 9mg tamoxifen via oral gavage at 12 weeks old after 4 weeks of diet. Mice were sacrificed either 48hrs later or after 1 week more of diet.*

The splenic EYFP cell population was greater in both proportion and absolute terms in male LDLr$^{-/-}$ AEL mice which had been fed HFD for 4 weeks previously compared to that of chow-fed mice *(Figure 79)*. In the 1-week timeframe, the percentage and total number of splenic EYFP labelled cells increased significantly in the HFD-fed group while maintaining a stable level in the chow diet-fed group of male LDLr$^{-/-}$ AEL mice (*Figure 79)*.

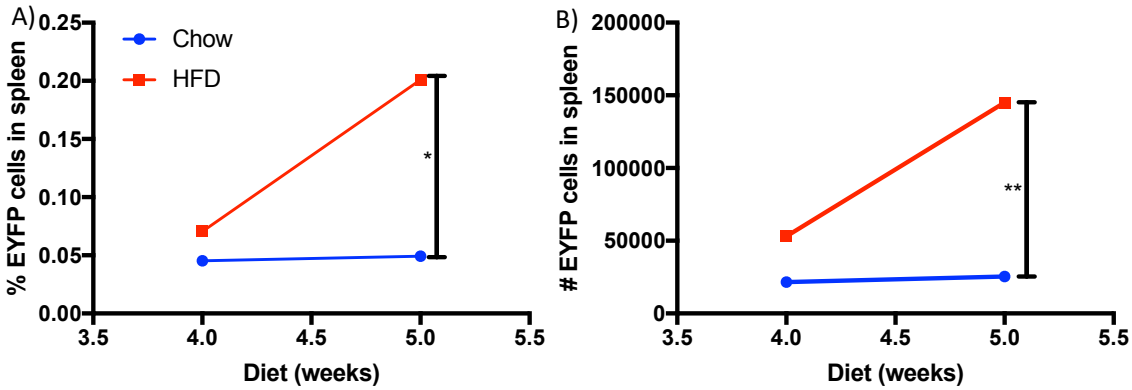

Figure 79. ***Splenic EYFP cell populations expand over 1 week after 4 weeks of diet.*** *Male AEL mice were fed either chow (blue) or high fat (HFD; red) diets for 4 weeks before oral gavage dosing of 9mg tamoxifen. Mice were sacrificed either 48hrs later (4 weeks of diet) or 1 week later (5 weeks of diet). The EYFP population in the spleen depicted in* ***(A)*** *proportion and* ***(B)*** *absolute numbers. Each dot represents the average for each group. Statistics carried out using Mann-Whitney test, * P < 0.05; ** P < 0.01; *** P < 0.001; **** P < 0.0001.*

In the spleen, both the GC and memory populations labelled with EYFP were expanded in male LDLr$^{-/-}$ AEL mice fed HFD compared to chow diet, both in proportion and absolute terms *(Figure 80)*.

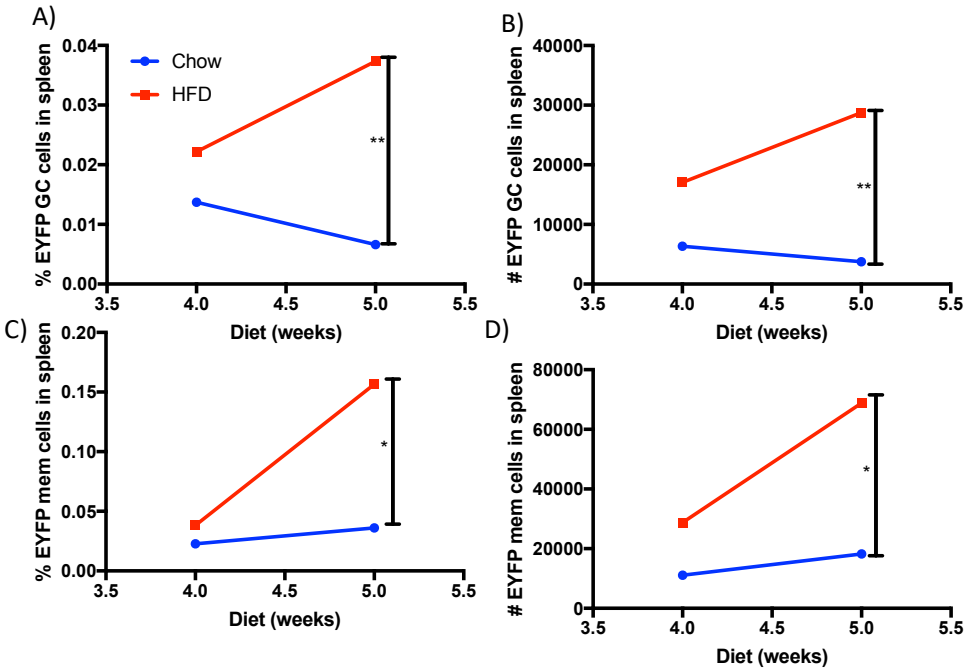

Figure 80. ***Splenic EYFP GC and memory cell populations are expanded after 1 week.*** *Male AEL mice were fed either chow (blue) or high fat (HFD; red) diets for 4 weeks before oral gavage dosing of 9mg tamoxifen. Mice were sacrificed either 48hrs later (4 weeks of diet) or 1 week later (5 weeks of diet). The splenic EYFP GC population is depicted in* ***(A)*** *proportional and* ***(B)*** *absolute terms. The splenic EYFP memory (mem) population is depicted in* ***(C)*** *proportional and* ***(D)*** *absolute terms. Each dot represents the average for each group. Statistics carried out using Mann-Whitney test, * P < 0.05; ** P < 0.01; *** P < 0.001; **** P < 0.0001.*

This effect was seen in both IgM+ and IgM- clonotypes across the EYFP labelled GC and memory compartments of the spleen *(Figure 81)*.

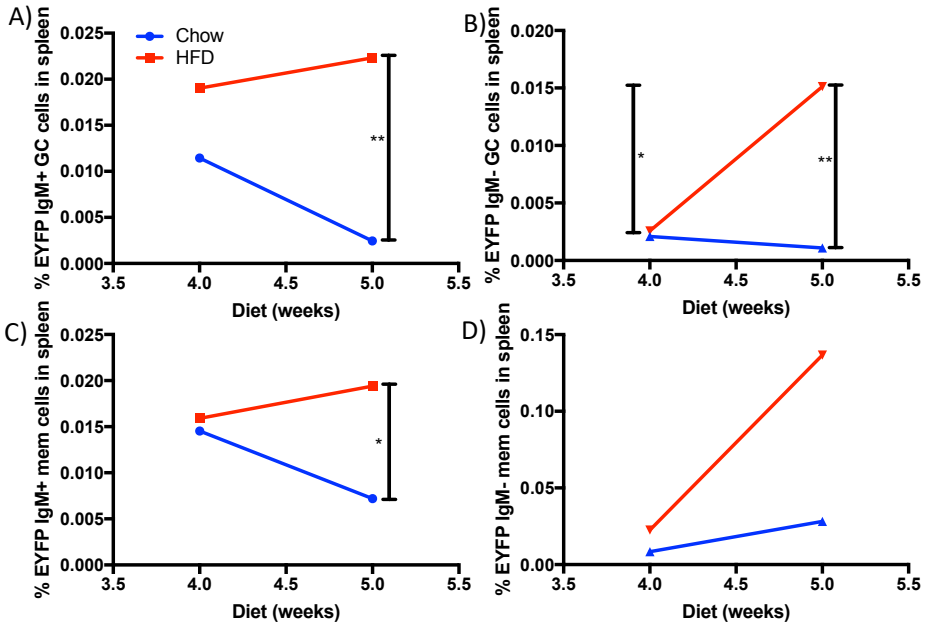

Figure 81. ***HFD induced greater expansion of EYFP population over 1 week labelling after 4 weeks of diet.*** *Male AEL mice were fed either chow or high fat (HFD) diets for 4 weeks before oral gavage dosing of 9mg tamoxifen. Mice were sacrificed either 48hrs later (4 weeks of diet) or 1 week later (5 weeks of diet). The splenic EYFP GC population is depicted in* ***(A)*** *IgM+ and* ***(B)*** *IgM- clonotypes. The splenic EYFP memory (mem) population is depicted in* ***(C)*** *IgM+ and* ***(D)*** *IgM- clonotypes. Each dot represents the average for each group. Statistics carried out using Mann-Whitney test, * P < 0.05; ** P < 0.01; *** P < 0.001; **** P < 0.0001.*

5.4.3 Labelling at 4 weeks of diet in female LDLr$^{-/-}$ AEL mice

To determine any sex-specific differences, the same experimental setup was used in female AEL LDLr$^{-/-}$ mice. In the spleen, both sets of lymph nodes and the BM, HFD induced greater expansion and proliferation of the total EYFP population compared to chow over the 1-week period despite the 48hr labelling (4-week timepoint) showing similar levels of EYFP labelling in both diet types *(Figure 82)*.

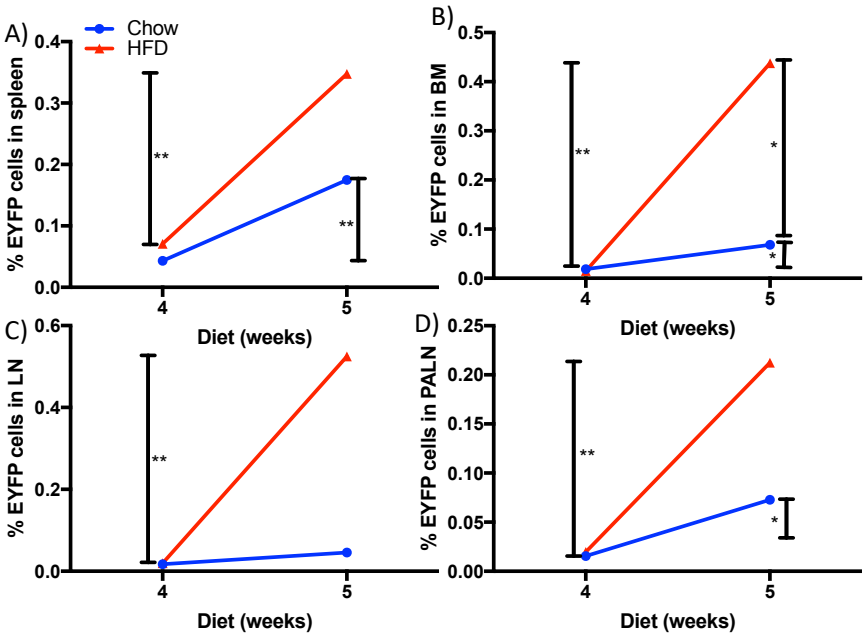

Figure 82. ***HFD induced a greater proliferation of EYFP cells after 1 week.*** *Female AEL mice were fed either chow (blue) or high fat (HFD; red) diets for 4 weeks before oral gavage dosing of 9mg tamoxifen. Mice were sacrificed either 48hrs later (4 weeks of diet) or 1 week later (5 weeks of diet). The proportion of total cells which were labelled with EYFP is shown in the* ***(A)*** *spleen,* ***(B)*** *bone marrow (BM),* ***(C)*** *lymph node (LN) and* ***(D)*** *para-aortic lymph node (PALN). Each dot represents the average for each group. Statistics carried out using Mann-Whitney test, * P < 0.05; ** P < 0.01; *** P < 0.001; **** P < 0.0001.*

By investigating the cell phenotypes within the EYFP population, it was discovered that a greater proportion of EYFP cells were of GC phenotype in the HFD-fed female LDLr$^{-/-}$ AEL mice after 4 weeks and this expanded upon a further week of diet within the spleen, LN and PALN *(Figure 83)*.

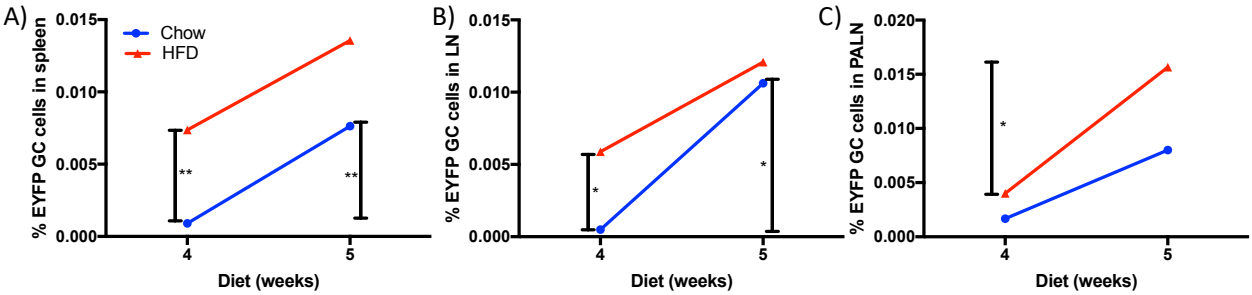

Figure 83. ***Greater EYFP GC population in HFD-mice which expands over 1 week.*** *Female AEL mice were fed either chow (blue) or high fat (HFD; red) diets for 4 weeks before oral gavage dosing of 9mg tamoxifen. Mice were sacrificed either 48hrs later (4 weeks of diet) or 1 week later (5 weeks of diet). The proportion of EYFP cells which were of GC phenotype is shown in* ***(A)*** *spleen,* ***(B)*** *lymph node (LN) and* ***(C)*** *para-aortic lymph node (PALN). Each dot represents the average for each group. Statistics carried out using Mann-Whitney test, * P < 0.05; ** P < 0.01; *** P < 0.001; **** P < 0.0001.*

Investigation of the EYFP memory compartment revealed that the extent of labelling was independent of diet after 48hrs in both inguinal and para-aortic lymph nodes as well as the bone marrow, but labelling was slightly higher in HFD-fed compared to chow diet-fed female LDLr$^{-/-}$ AEL mice in the spleen *(Figure 84)*. However, after 1 week the EYFP memory population

was expanded significantly in HFD-fed compared to chow diet-fed female LDLr$^{-/-}$ AEL mice in the spleen, BM, LN and PALN *(Figure 84)*.

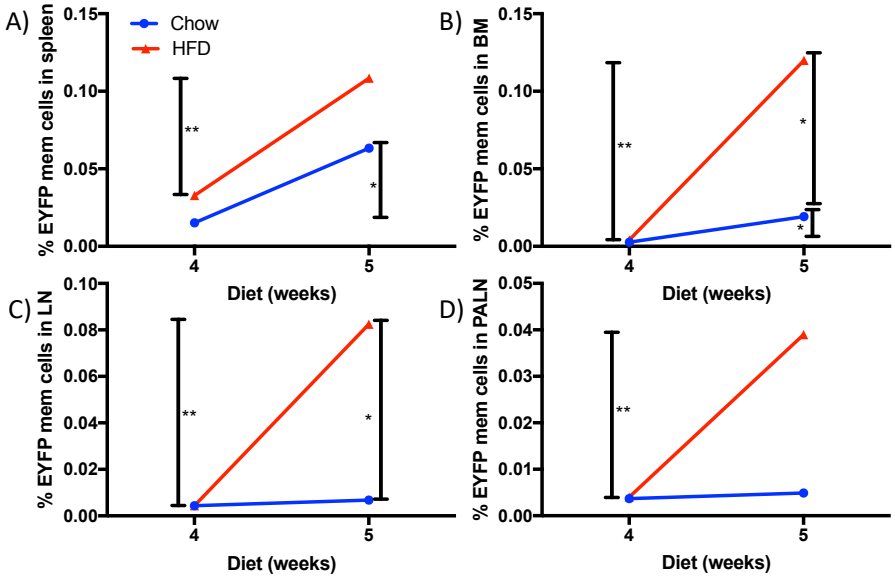

Figure 84. ***EYFP memory cell population is expanded after 1 week.*** *Female AEL mice were fed either chow (blue) or high fat (HFD; red) diets for 4 weeks before oral gavage dosing of 9mg tamoxifen. Mice were sacrificed either 48hrs later (4 weeks of diet) or 1 week later (5 weeks of diet). The proportion of EYFP cells which were of memory (mem) phenotype is shown in* ***(A)*** *spleen,* ***(B)*** *bone marrow (BM),* ***(C)*** *lymph node (LN) and* ***(D)*** *para-aortic lymph node (PALN). Each dot represents the average for each group. Statistics carried out using Mann-Whitney test, * P < 0.05; ** P < 0.01; *** P < 0.001; **** P < 0.0001.*

This was not isotype dependent as both IgM+ and IgM- memory cells labelled with EYFP across these tissues were present at a greater extent in HFD-fed compared to chow diet-fed female LDLr$^{-/-}$ AEL mice *(Figure 85)*. One exception was the proportion of IgM+ EYFP+ memory cells in the spleen which decreased over one week *(Figure 85A)*. This effect was more significant in HFD compared to chow diet-fed female LDLr$^{-/-}$ AEL mice *(Figure 85A)*. This implies that splenic memory formation is skewed away from the IgM antibody class in response to HFD.

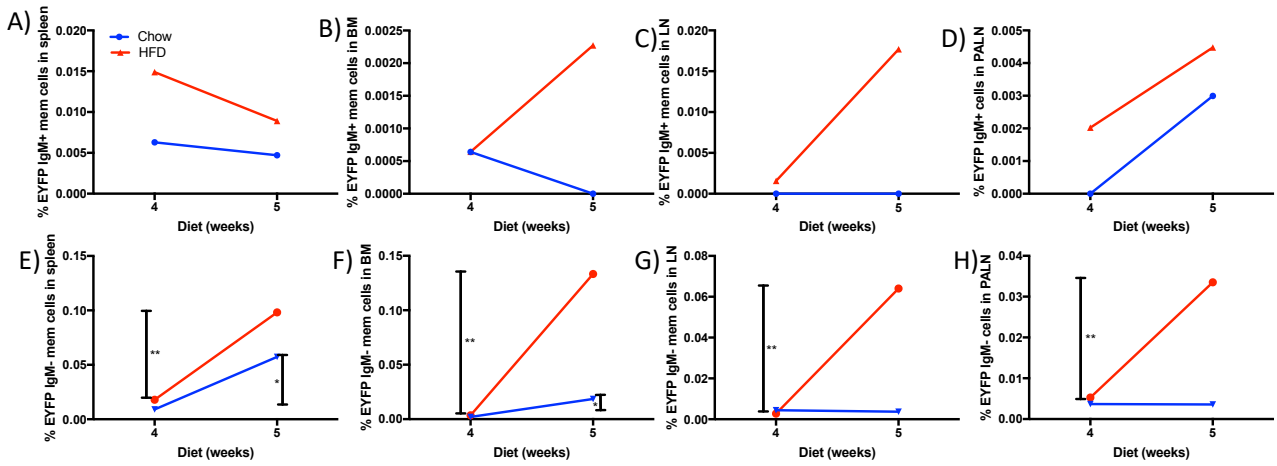

Figure 85. ***The expansion in EYFP memory cell population is mainly isotype-independent.*** *Female AEL mice were fed either chow (blue) or high fat (HFD; red) diets for 4 weeks before oral gavage dosing of 9mg tamoxifen. Mice were sacrificed either 48hrs later (4 weeks of diet) or 1 week later (5 weeks of diet). The proportion of EYFP memory (mem) cells which were IgM+ is shown in* ***(A)*** *spleen,* ***(B)*** *bone marrow (BM),* ***(C)*** *lymph node (LN) and* ***(D)*** *para-aortic lymph node (PALN). The proportion of EYFP mem cells which were IgM- is shown in* ***(E)*** *spleen,* ***(F)*** *BM,* ***(G)*** *LN and* ***(H)*** *PALN. Each dot represents the average for each group. Statistics carried out using Mann-Whitney test, * P < 0.05; ** P < 0.01; *** P < 0.001; **** P < 0.0001.*

Similar results were observed for plasma cells within the EYFP labelled population whereby initial labelling was independent of diet after 48hrs, but HFD caused greater expansion of the population after 1 week in the spleen, BM, LN and PALN *(Figure 86)*.

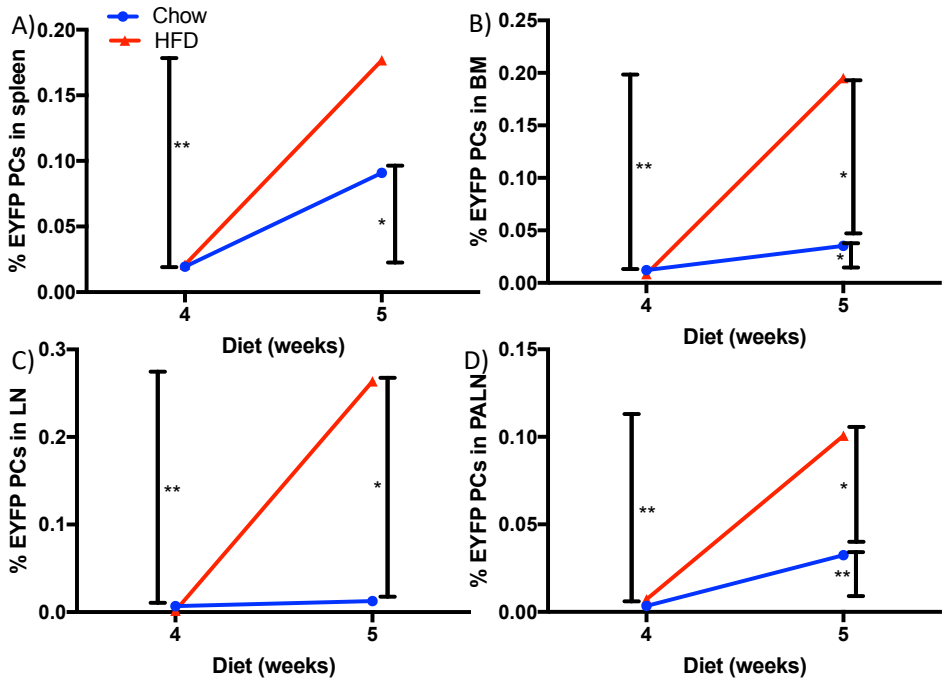

Figure 86. ***HFD caused greater expansion of the EYFP PC population after 1 week.*** *Female AEL mice were fed either chow (blue) or high fat (HFD; red) diets for 4 weeks before oral gavage dosing of 9mg tamoxifen. Mice were sacrificed either 48hrs later (4 weeks of diet) or 1 week later (5 weeks of diet). The proportion of EYFP cells which were of plasma cell (PC) phenotype is shown in* ***(A)*** *spleen,* ***(B)*** *bone marrow (BM),* ***(C)*** *lymph node (LN) and* ***(D)*** *para-aortic lymph node (PALN). Each dot represents the average for each group. Statistics carried out using Mann-Whitney test, * P < 0.05; ** P < 0.01; *** P < 0.001; **** P < 0.0001.*

Again, this effect was not antibody isotype specific as both IgM+ and IgM- EYFP+ plasma cell populations were expanded to a much greater extent in the context of HFD compared to chow diet across these tissues in female LDLr$^{-/-}$ AEL mice *(Figure 87)*.

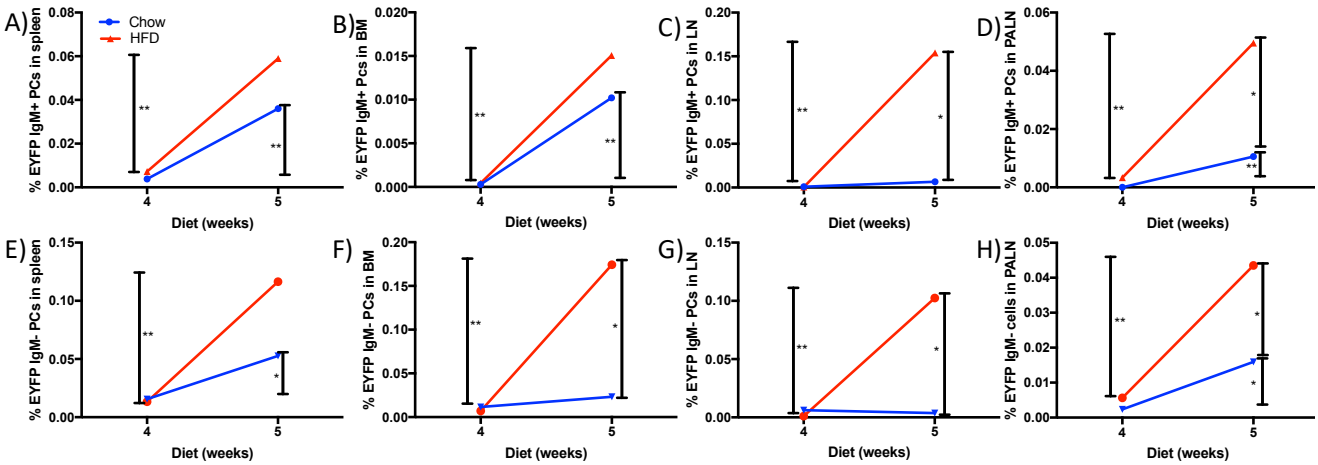

Figure 87. ***The expansion of EYFP PC population is isotype-independent.*** *Female AEL mice were fed either chow (blue) or high fat (HFD; red) diets for 4 weeks before oral gavage dosing of 9mg tamoxifen. Mice were sacrificed either 48hrs later (4 weeks of diet) or 1 week later (5 weeks of diet). The proportion of EYFP plasma cells (PCs) which were IgM+ is shown in* ***(A)*** *spleen,* ***(B)*** *bone marrow (BM),* ***(C)*** *lymph node (LN) and* ***(D)*** *para-aortic lymph node (PALN). The proportion of EYFP PCs which were IgM- is shown in* ***(E)*** *spleen,* ***(F)*** *BM,* ***(G)*** *LN and* ***(H)*** *PALN. Each dot represents the average for each group. Statistics carried out using Mann-Whitney test, * P < 0.05; ** P < 0.01; *** P < 0.001; **** P < 0.0001.*

The dynamics of EYFP cell populations differed within the PPs. The EYFP GC population was greater in chow diet-fed compared to HFD-fed female LDLr$^{-/-}$ AEL mice after 48hrs showcasing a suppressive effect of HFD on GC responses within the PPs *(Figure 88A)*. There was very little change in the proportion of total EYFP GC cells of the PPs upon HFD feeding over the course of the week in female LDLr$^{-/-}$ AEL mice *(Figure 88A)*. IgM- GC populations remained relatively stable, only increasing marginally regardless of diet over the duration of a week in the PPs of female LDLr$^{-/-}$ AEL mice *(Figure 88B)*. Over the week, EYFP plasma cell populations of both isotypes expanded in both diet types within the PPs *(Figure 88C, D, E)*. The increase was slightly greater in HFD-fed female LDLr$^{-/-}$ AEL mice except for the IgM+ EYFP+ PCs *(Figure 88E)*. This data suggests that while GC responses are suppressed in the PPs of HFD-fed female LDLr$^{-/-}$ AEL mice, this does not impact strongly on the plasma cell population.

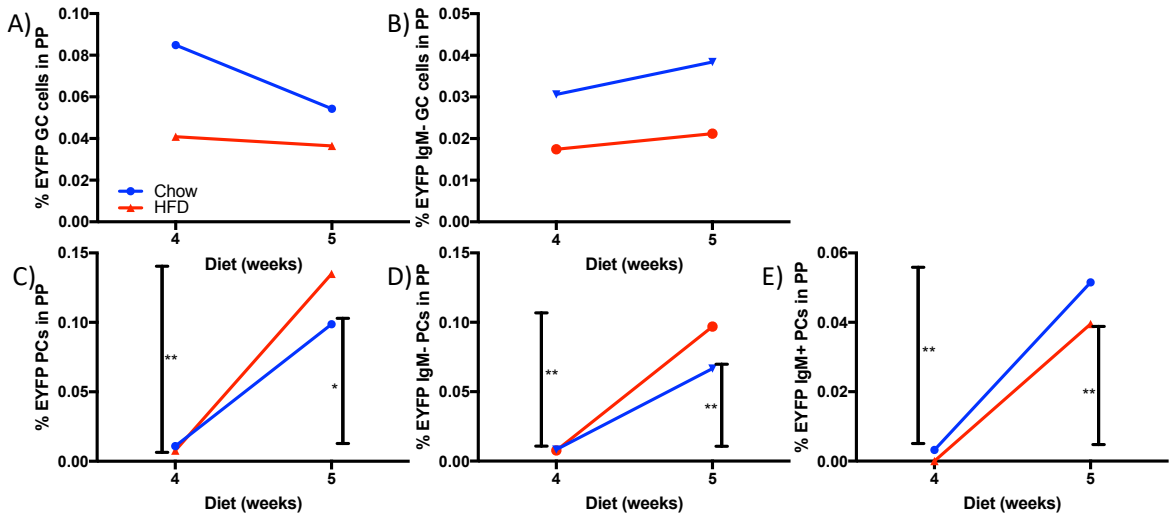

Figure 88. ***EYFP cell dynamics differed within the PPs.*** *Female AEL mice were fed either chow (blue) or high fat (HFD; red) diets for 4 weeks before oral gavage dosing of 9mg tamoxifen. Mice were sacrificed either 48hrs later (4 weeks of diet) or 1 week later (5 weeks of diet). The proportion of EYFP cells within the Peyer's patches (PP) which are* ***(A)*** *germinal centre (GC),* ***(B)*** *IgM- GC,* ***(C)*** *plasma cells (PCs),* ***(D)*** *IgM- PCs and* ***(E)*** *IgM+ PCs are depicted. Each dot represents the average for each group. Statistics carried out using Mann-Whitney test, * P < 0.05; ** P < 0.01; *** P < 0.001; **** P < 0.0001.*

5.4.4 Labelling at 8 weeks of diet in male LDLr$^{-/-}$ AEL mice

To investigate the dynamics of GC-derived cells at more advanced stages of atherosclerosis, male LDLr$^{-/-}$ AEL mice were fed either chow diet or HFD for 8 weeks and dosed with tamoxifen at 16 weeks of age before sacrifice either 48hrs or 7 days later *(Figure 89)*.

Figure 89. ***Experimental design with 1 week labelling window after 8 weeks of diet.*** *Male AEL mice were put on chow or high fat diet (HFD) at 8 weeks old and dosed with 9mg tamoxifen via oral gavage at 16 weeks old after 8 weeks of diet. Mice were sacrificed either 48hrs later or after 1 week more of diet.*

After 1 week of labelling, EYFP labelled GC cells had proliferated more in HFD-fed male LDLr$^{-/-}$ AEL mice compared to chow diet in both the spleen and PALN *(Figure 90A, D)*. The EYFP memory cell population was significantly greater in the PALN after HFD compared to chow diet *(Figure 90F)* while in the spleen, the EYFP memory population declined only slightly after HFD compared to a greater decrease in population size upon chow diet feeding in male LDLr$^{-/-}$ AEL mice *(Figure 90C)*. In particular, IgM+ EYFP+ GC cells were responsible for the expansion of EYFP GC population in both tissues *(Figure 90B, E)*.

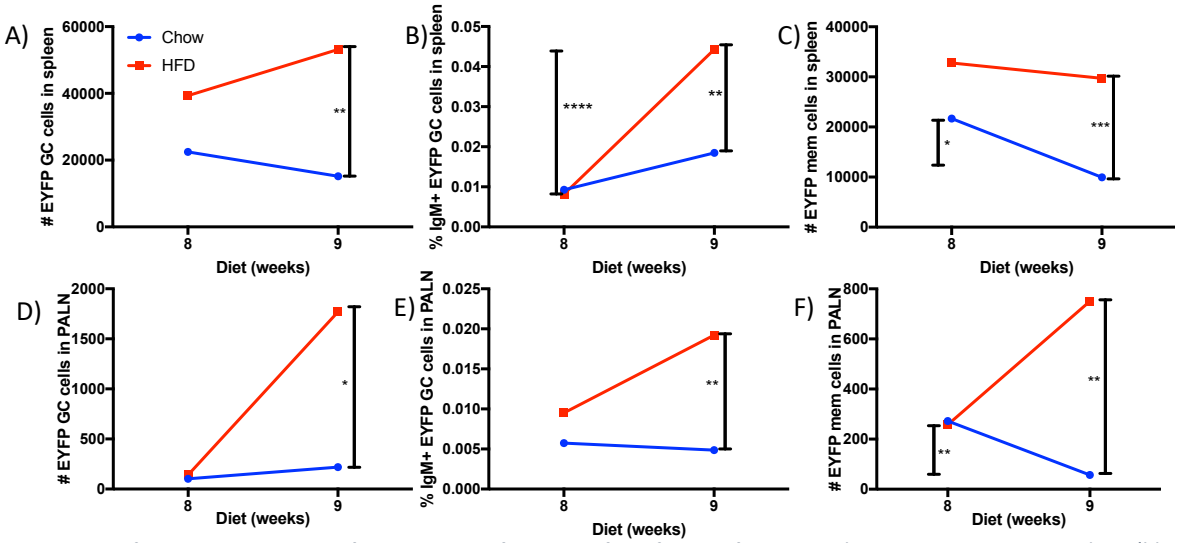

*Figure 90.**Changes in EYFP GC and memory populations in the spleen and PALN.** Male AEL mice were put on chow (blue) or high fat diet (HFD, red) at 8 weeks old and dosed with 9mg tamoxifen via oral gavage at 16 weeks old after 8 weeks of diet. Mice were sacrificed either 48hrs later (8 weeks of diet) or 7 days later (9 weeks of diet). In the spleen, graphs depict **(A)** total number of EYFP GC cells, **(B)** IgM+ proportion of EYFP GC cells and **(C)** total number of EYFP memory (mem) cells. In the para-aortic lymph node (PALN), graphs depict **(D)** total number of EYFP GC cells, **(E)** IgM+ proportion of EYFP GC cells and **(F)** total number of EYFP mem cells. Each dot represents the average for each group. Statistics carried out using Mann-Whitney test, * P < 0.05; ** P < 0.01; *** P < 0.001; **** P < 0.0001.*

In the spleen, the proportion and number of total EYFP cells reduced 1 week after labelling in both diet types *(Figure 91A, B)*. However, the reduction was less dramatic in HFD-fed male LDLr$^{-/-}$ AEL mice *(Figure 91A, B)*. Meanwhile, the proportion of splenic EYFP GC cells expanded 1 week after labelling independent of diet *(Figure 91C)*. In the LN, the EYFP population shrank in both proportion and absolute terms 1 week after labelling regardless of diet *(Figure 91D, E)*. In the PALN, although the proportion of EYFP cells reduced 1 week after labelling regardless of diet, the absolute number of EYFP cells, primarily due to the EYFP GC population, was markedly expanded upon HFD-feeding in male LDLr$^{-/-}$ AEL mice compared to chow diet *(Figure 91G, H, I)*.

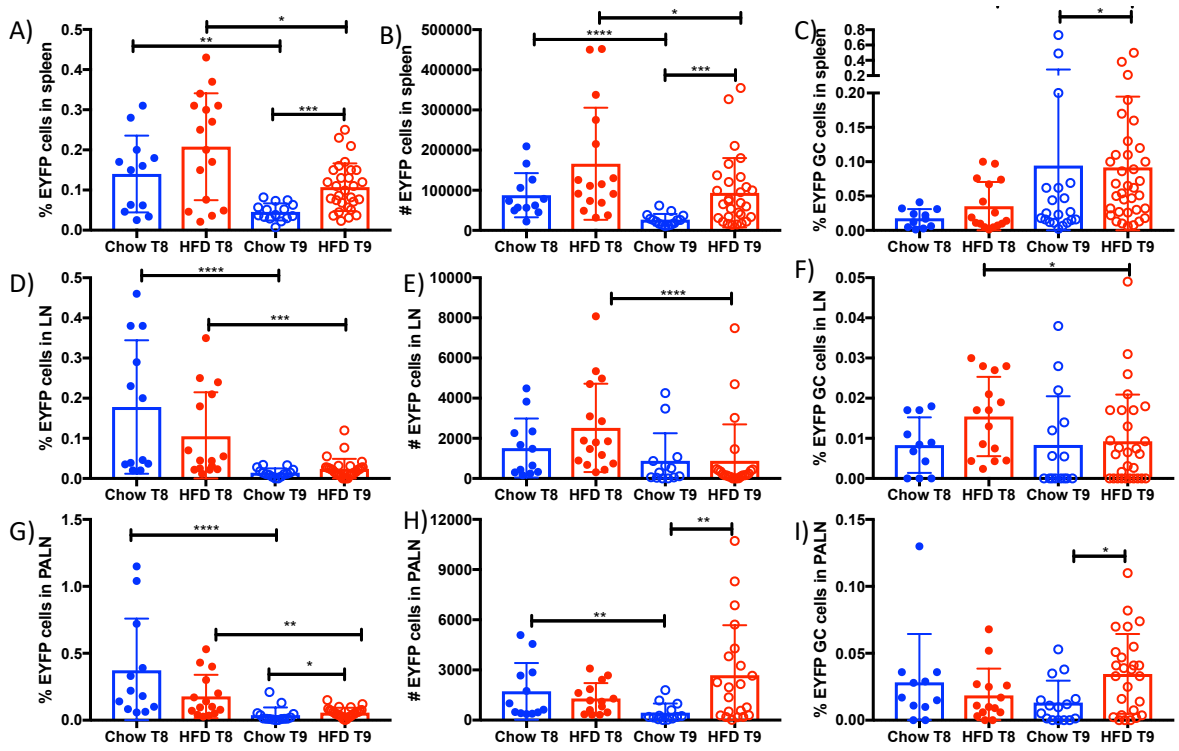

Figure 91. ***Total EYFP populations declined after 1 week labelling while EYFP GC populations increased in HFD-fed mice.*** *Male AEL mice were put on chow (blue) or high fat diet (HFD; red) at 8 weeks old and dosed with 9mg tamoxifen via oral gavage at 16 weeks old after 8 weeks of diet. Mice were sacrificed either 48hrs later (8 weeks of diet; T8; closed circles) or 7 days later (9 weeks of diet; T9; open circles). Within the spleen, graphs depict* ***(A)*** *proportion of EYFP cells,* ***(B)*** *absolute number of EYFP cells and* ***(C)*** *proportion of EYFP GC cells. Within the lymph node (LN), graphs depict* ***(D)*** *proportion of EYFP cells,* ***(E)*** *absolute number of EYFP cells and* ***(F)*** *proportion of EYFP GC cells. Within the para-aortic lymph node (PALN), graphs depict* ***(G)*** *proportion of EYFP cells,* ***(H)*** *absolute number of EYFP cells and* ***(I)*** *proportion of EYFP GC cells. Each dot represents one mouse, graphs show mean +/- SD. Statistics carried out using Mann-Whitney test, * P < 0.05; ** P < 0.01; *** P < 0.001; **** P < 0.0001.*

Within the spleen, inguinal and para-aortic lymph nodes, the IgM+ EYFP memory cell population was greater 1 week after labelling in HFD-fed compared to chow diet-fed male LDLr$^{-/-}$ AEL mice *(Figure 92A, B, C)*. The IgM- EYFP memory cell population was greater in HFD-fed male LDLr$^{-/-}$ AEL mice compared to chow diet-fed male LDLr$^{-/-}$ AEL mice at both timepoints analysed within the spleen *(Figure 92D)*. However, the overall splenic IgM- EYFP memory cell population was reduced at 9 weeks compared to 8 weeks independent of diet *(Figure 92D)*. In the LN, the IgM- EYFP memory cell population was significantly smaller 1 week after compared to 48hrs after labelling in chow-fed male LDLr$^{-/-}$ AEL mice *(Figure 92E)*. In the PALN, both the IgM+ and IgM- EYFP memory populations shrank 1 week after labelling regardless of diet compared to 48hrs after labelling *(Figure 92C, F)*.

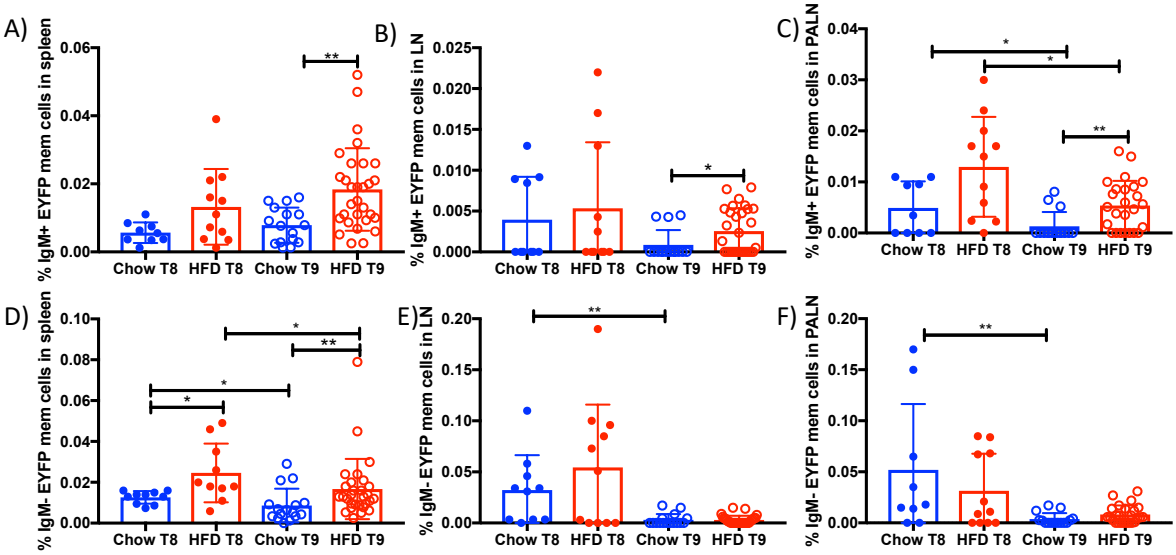

Figure 92. ***Changes in EYFP memory cell populations after 1 week labelling.*** *Male AEL mice were put on chow (blue) or high fat diet (HFD; red) at 8 weeks old and dosed with 9mg tamoxifen via oral gavage at 16 weeks old after 8 weeks of diet. Mice were sacrificed either 48hrs later (8 weeks of diet; T8; closed circles) or 7 days later (9 weeks of diet; T9; open circles). The proportion of IgM+ EYFP memory (mem) cells are depicted in* ***(A)*** *spleen,* ***(B)*** *lymph node (LN) and* ***(C)*** *para-aortic lymph node (PALN). The proportion of IgM+ EYFP memory (mem) cells are depicted in* ***(D)*** *spleen,* ***(E)*** *LN and* ***(F)*** *PALN. Each dot represents one mouse, graphs show mean +/- SD. Statistics carried out using Mann-Whitney test, * P < 0.05; ** P < 0.01; *** P < 0.001; **** P < 0.0001.*

In the spleen, the EYFP labelled plasma cell population was at its largest proportionally and in absolute terms in HFD-fed male LDLr$^{-/-}$ AEL mice after 48 hours labelling *(Figure 93A, C)*. The EYFP PC pool was significantly reduced in the spleen 1 week after labelling *(Figure 93A, C)*. In the LN, there was also a significant reduction in the size of the EYFP plasma cell population after 1 week of labelling compared to 48 hours regardless of diet in male LDLr$^{-/-}$ AEL mice *(Figure 93B, D)*.

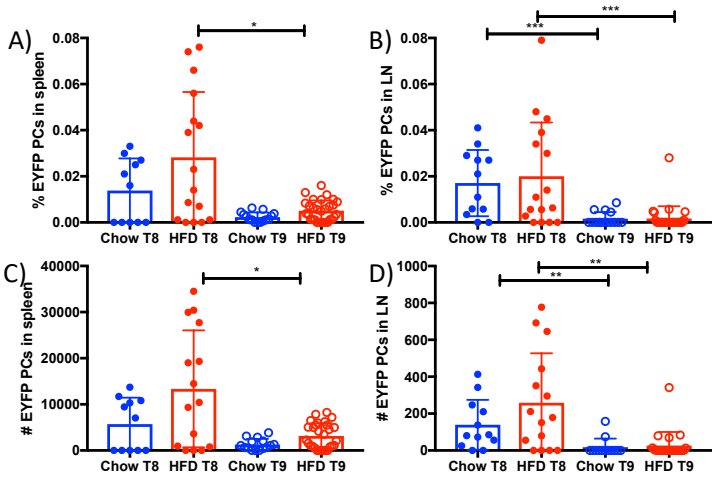

Figure 93. ***EYFP PC populations shrank 1 week after labelling.*** *Male AEL mice were put on chow (blue) or high fat diet (HFD; red) at 8 weeks old and dosed with 9mg tamoxifen via oral gavage at 16 weeks old after 8 weeks of diet. Mice were sacrificed either 48hrs later (8 weeks of diet; T8; closed circles) or 7 days later (9 weeks of diet; T9; open circles). The proportion of EYFP plasma cells (PCs) are depicted in* ***(A)*** *spleen and* ***(B)*** *lymph node (LN). The absolute number of EYFP PCs are depicted in* ***(C)*** *spleen and* ***(D)*** *LN. Each dot represents one mouse, graphs show mean +/- SD. Statistics carried out using Mann-Whitney test, * P < 0.05; ** P < 0.01; *** P < 0.001; **** P < 0.0001.*

The detection of IgM- EYFP labelled plasma cells was greatest at 48hrs of labelling and was significantly reduced by 1 week post labelling in the spleen, LN, PP and BM of HFD-fed male LDLr$^{-/-}$ AEL mice *(Figure 94)*. This effect could also be seen significantly within the LN and BM of chow-fed male LDLr$^{-/-}$ AEL mice *(Figure 94B, D)*.

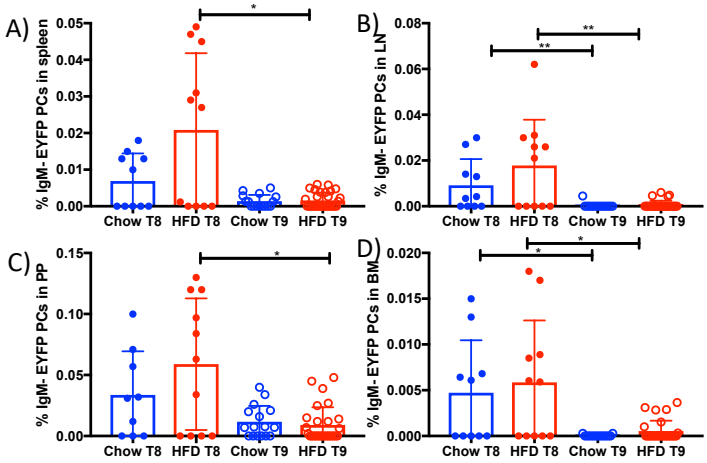

Figure 94. ***Production of EYFP IgM- PCs reduced after 1 week labelling.*** *Male AEL mice were put on chow (blue) or high fat diet (HFD; red) at 8 weeks old and dosed with 9mg tamoxifen via oral gavage at 16 weeks old after 8 weeks of diet. Mice were sacrificed either 48hrs later (8 weeks of diet; T8; closed circles) or 7 days later (9 weeks of diet; T9; open circles). The proportion of IgM- EYFP plasma cells (PCs) are depicted in* ***(A)*** *spleen,* ***(B)*** *lymph node (LN),* ***(C)*** *Peyer's patches (PP) and* ***(D)*** *bone marrow (BM). Each dot represents one mouse, graphs show mean +/- SD. Statistics carried out using Mann-Whitney test, * P < 0.05; ** P < 0.01; *** P < 0.001; **** P < 0.0001.*

5.5 Discussion

5.5.1 Labelling prior to 8 weeks diet

Labelling AID cells when male LDLr$^{-/-}$ AEL mice were 8 weeks old and analysing after 8 weeks of diet showed that the EYFP population expanded in the spleen implying that clones generated prior to diet are still present in 16-week-old mice which have received 8 weeks of diet. While the EYFP GC population (both IgM+ and IgM-) within the spleen shrank over the 8-week duration, both EYFP labelled plasma cell and memory B cell compartments expanded demonstrating that these GC-derived cells are responsible for the increased overall EYFP cell content within the spleen at 16 weeks. Additionally, there could be migration of EYFP+ cells from the PPs into the spleen as the PPs also exhibited increased EYFP cell content after 8 weeks of HFD. This expansion of the EYFP cell population within the PPs, primarily due to proliferation of IgM- EYFP GC cell clones, in response to HFD highlights the immunogenicity of HFD within the PPs resulting in a greater degree of class-switching.

The total EYFP population was decreased 8 weeks after labelling regardless of diet in both the inguinal and para-aortic LNs. This suggests that the antigens fuelling GC responses at the time of labelling are no longer present and thus EYFP-labelled GC B cells are replaced with non-labelled GC B cells. Compared to the spleen, this data implies that individual GC reactions are shorter-lived in lymph nodes perhaps as a consequence of their local function. However, in the PALN the HFD resulted in extensive proliferation of IgM- EYFP GC clones while this cell type was absent from chow-fed male LDLr$^{-/-}$ AEL mice suggesting that presence of HFD is a major stimulus for class-switching.

HFD induced greater production of IgM+ EYFP memory cells in the spleen and LN compared to chow diet suggesting a more productive GC response. This suggests that there has been a greater number of GCs over the 8 weeks of HFD compared to chow diet resulting in elevated memory cell production. Within all tissues analysed, IgM- EYFP memory cell populations expanded regardless of diet. The presence of IgM- EYFP memory cells was further increased upon HFD compared to chow diet feeding in both types of LN, the BM, and the blood. This

shows that EYFP labelled GC cells export mainly switched memory cells after 8 weeks and HFD augments this effect through increased class-switching demonstrating a bias towards pathogenic GC output. The increased presence of memory cells in the blood could be a result of memory cells travelling to the BM and LNs. It is known that memory B cells will return to lymphoid organs to either initiate new GC reactions with the same clonal specificity or to quench antigen deposited on FDCs to shut down a GC response[1]. With the available data, it is impossible to determine which function the memory cells are carrying out but perhaps using immunofluorescent staining it could be determined whether memory cells are colocalised with FDCs.

In the BM, the EYFP cell population increased slightly in chow diet-fed male $LDLr^{-/-}$ AEL mice while it decreased in HFD-fed male $LDLr^{-/-}$ AEL mice. This was further evident from the decreased IgM+ and IgM- EYFP PC populations after 8 weeks of HFD compared to chow diet in the BM. As the BM is a finite niche, the data suggests that EYFP PC clones are continuously being replaced by newer non-EYFP labelled PCs in the HFD-fed male mice while this process isn't occurring to the same extent in chow-fed male $LDLr^{-/-}$ AEL mice potentially due to the smaller plasma cell pool (data not shown). Additionally, data obtained for the BM 48hrs after labelling (i.e., chow T0) could be unreliable as this is a short timeframe for cells to migrate from lymphoid organs to the BM.

In the blood, EYFP cell circulation reduced over the 8-week diet period but to a greater degree in chow diet-fed compared to HFD-fed male $LDLr^{-/-}$ AEL mice. This could be due to the increased production of EYFP cells observed in the spleen and PPs of HFD-fed mice – indeed EYFP cells from the PPs may be migrating to the spleen as previously mentioned. Perhaps using luminescence or radioactivity, it would be possible to visualise individual EYFP cells and track their movements to see whether migration is occurring from the PPs to the spleen. An additional strategy to investigate this possibility would be to conduct BCR sequencing of EYFP clones from the PPs and spleen to determine whether there is any clonal overlap suggestive of migration between the sites. It is possible that EYFP cells migrate more to other lymphoid sites or to the plaque under the hyperlipidaemia conditions induced by the HFD. Aortic root and lymphoid organ sections could be analysed using immunofluorescence staining for EYFP

and CD138 to determine whether there are EYFP cells present and if so, whether there are greater numbers in mice fed HFD compared to chow diet.

The EYFP PC pool, both IgM+ and IgM- isotypes, was expanded after 8 weeks of HFD compared to chow diet in the spleen. In chow-diet fed male LDLr$^{-/-}$ AEL mice, the proportion of EYFP PCs which were IgM+ reduced while the IgM- proportion increased. This data suggests that antigens present prior to diet are still driving splenic plasma cell production 8 weeks later although HFD is responsible for the increased production of IgM+ EYFP plasma cells. In the PPs, production of IgM+ EYFP PCs reduced over time in 8-week chow diet-fed male LDLr$^{-/-}$ AEL mice while IgM- EYFP PC production remained minimal. Therefore, HFD resulted in maintenance of the IgM+ EYFP PC population and production of class-switched EYFP labelled PCs. Although this data shows that HFD-fed male LDLr$^{-/-}$ AEL mice have higher numbers of EYFP plasma cells, this could be due to greater production or longer lifespan of individual EYFP labelled plasma cells. To determine which possibility is true, an experiment using BrdU could be conducted. As BrdU is a proliferation dye, any cells with strong signal demonstrate little proliferation while weak signal is indicative of increased proliferation as the dye fades with each cellular division. Thus, if EYFP plasma cells from HFD-fed mice have stronger BrdU staining this would suggest that these cells have a longer lifespan than EYFP PCs from chow diet-fed mice. As the plasma cells themselves aren't subject to proliferation, EYFP labelled GC B cells would have to be investigated for proliferation as a proxy. If the EYFP GC B cells from HFD-fed mice have weaker BrdU staining this would suggest that these cells have undergone greater proliferation than EYFP GC B cells from chow diet-fed mice. A greater proliferation rate could indicate an increased production of PCs; to measure this the number of EYFP PCs could be divided by the number of EYFP GC B cells to give a measure of how many plasma cells are produced per GC B cell. In any case, this suggests that the hyperlipidaemic conditions induced by HFD create an inflammatory environment, perhaps with greater antigenic stimulation, which retains the presence of GC-derived EYFP labelled cells, skewed toward switched (IgM-) clones, in the form of PCs and memory B cells.

5.5.2 Labelling at 4 weeks of diet

There was no effect on EYFP populations when GC B cells were EYFP-labelled prior to 1 week of diet. This implies that there is no acute effect of HFD on the GC response and rather it is the atherogenic conditions and environment created by HFD, that has a pathogenic impact. Labelling AID cells with EYFP after 4 weeks of diet enabled me to investigate the impact of early stages of atherosclerosis on GC-derived cells. In male LDLr$^{-/-}$ AEL mice, the splenic EYFP cell population expanded in the 1-week period after labelling upon HFD feeding compared to chow diet feeding. Both GC and memory cell subsets within the labelled splenic population were increased, in proportion and absolute terms, independent of antibody isotype as both IgM+ and IgM- clones within each compartment were elevated in HFD-fed male LDLr$^{-/-}$ AEL mice 1 week after labelling. As HFD results in a greater number of EYFP GC B cells within the spleen, this implies that EYFP labelled GC clones are either longer-lived and/or replicate more in mice fed a HFD compared to chow diet. The GC to memory ratio, measuring GC longevity, was not significantly different between diet types (data not shown) favouring the latter hypothesis. To investigate the extent of replication within EYFP GC B cells, BrdU could be used, and its signal intensity measured and compared between diet types.

In female LDLr$^{-/-}$ AEL mice fed HFD, greater expansion of the EYFP population 1 week after labelling was also observed in the spleen, BM, inguinal and para-aortic lymph nodes compared to chow diet feeding. In these tissues, all EYFP labelled GC-derived cell type populations (GC B cell, memory cells and plasma cells) were increased 1 week after labelling in HFD compared to chow diet-fed female LDLr$^{-/-}$ AEL mice. This excludes a GC population in the BM as these cells do not reside in the BM nor do they migrate to the BM. This effect was not isotype dependent as both IgM+ and IgM- memory and plasma cell clone populations were expanded 1 week after labelling in HFD-fed female mice. In the chow-fed female LDLr$^{-/-}$ AEL mice, the EYFP labelled memory cell population remained relatively unchanged after 1 week apart from in the spleen where it had increased to a lesser degree than the HFD induction. There was a small time-dependent increase in EYFP labelled PCs in chow diet-fed female LDLr$^{-/-}$ AEL mice. These data demonstrate that the HFD-induced increased GC activity correlates with increased GC output in lymphoid organs. This is indicative of productive GC responses whereby GC cells undergo differentiation rather than apoptosis due to insufficient

antigen affinity. There was significant migration of EYFP plasma and memory cell populations to the BM as these cell types were also increased in the BM upon HFD feeding.

Within the PPs, the EYFP GC population, including IgM- clones, remained stable 1 week after labelling in HFD-fed female LDLr$^{-/-}$ AEL mice. Regardless of diet, the EYFP PC population, both IgM+ and IgM- clonotypes, expanded 1 week after labelling. This demonstrates that the HFD has a suppressive effect on GC responses within the PPs and that GC output is not influenced by diet to the same extent as it is in other organs analysed.

In male LDLr$^{-/-}$ AEL mice, chow diet resulted either in no change or decrease in EYFP cell populations 1 week after labelling. In female mice, chow diet resulted in a slight increase in the proportion of EYFP cells, primarily due to GC clones, with smaller contributions from memory and PC pools. As detailed above, HFD resulted in expansion of the total EYFP cell pool with GC, memory and plasma cells all contributing. Thus, there was a small time-dependent increase in EYFP GC responses, but this was overshadowed by the impact of HFD which significantly enlarged EYFP GC responses and its output. Immunogenic epitopes of LDL and intraplaque apoptotic cells could provide increased antigen deposits on FDCs within lymphoid organs resulting in longer time spent in the GC undergoing rounds of SHM and replication resulting in greater cellular output.

5.5.3 Labelling at 8 weeks of diet

Analysing EYFP cell dynamics after 8 weeks of diet provided a snapshot of GC responses once atherosclerosis is established. The proportion and absolute number of cells labelled with EYFP reduced 1 week after labelling in the spleen and LN regardless of diet. In both the spleen and PALN the total EYFP and the EYFP GC cell populations, especially IgM+ clones, were greater in HFD-fed than in chow diet-fed male mice after 1 week. Thus, EYFP GC cells made up a greater proportion of the remaining EYFP cells in HFD-fed mice after 1 week compared to chow diet. Under homeostatic conditions, individual GCs tend to resolve within 3 weeks and in any lymphoid tissue, GCs will be found at all stages spanning this timeframe. Thus, in chow diet-fed male LDLr$^{-/-}$ AEL mice, EYFP labelled GCs will be replaced over time with non-EYFP labelled GCs with specificity against another antigen. This process would account for the reduction in

the EYFP cell population seen over the course of 1 week. Using this framework, the finding that EYFP GC cells are still present at higher levels in HFD compared to chow diet-fed male LDLr$^{-/-}$ AEL mice after 1 week suggests that GCs are longer-lasting and not replaced as quickly under hyperlipidaemic conditions. This implies that GCs are resolved more quickly in chow-fed male mice strengthening the hypothesis that HFD causes an exacerbated, persistent, more chronic set of GC responses.

After 48hrs labelling, splenic EYFP IgM- memory cell production was higher in HFD compared to chow diet-fed male LDLr$^{-/-}$ AEL mice. By the 1-week timepoint, both IgM+ and IgM- EYFP splenic memory cell populations were significantly bigger in HFD compared to chow diet-fed male LDLr$^{-/-}$ AEL mice. EYFP IgM- memory cell pools were also significantly larger in the LN and PALN 1 week after labelling in HFD compared to chow diet-fed male LDLr$^{-/-}$ AEL mice. These data show that the hyperlipidaemic conditions created by HFD result in greater production of memory cells due to the increased and longer-lasting GC reaction and these cells are skewed towards pathogenic class-switched isotypes.

EYFP labelled PC populations were diminished 1 week after labelling independent of diet in the spleen and LNs both in proportional and absolute terms. Presence of EYFP class-switched PCs was also reduced 1 week after labelling in the spleen, LN, PP and BM. This result may just be indicative of the fact that PCs tend to migrate quickly out of tissues, into circulation and home to the BM after differentiation and thus would no longer be detected in lymphoid organs 1 week after labelling.

These experiments have shown that HFD results in increased numbers of EYFP-labelled GC-derived cells after labelling. Labelling at both 4 and 8 weeks with 1 week prior to sacrifice showed that HFD resulted in a greater number of EYFP GC cells demonstrating that EYFP labelled clones persist and replicate more compared to chow diet. As 1 week of diet had no impact, this shows that it is not solely the week since labelling that has this effect but rather the build-up of HFD which is pathogenic. To determine whether this is solely diet related or whether it is atherosclerosis-related and impacted by the LDLr$^{-/-}$ genotype, these experiments should be conducted within WT mice. In the regression studies, 8 weeks of HFD and 4 weeks of HFD followed by 4 weeks of chow diet resulted in similar sized populations of EYFP GC

clones (data not shown). If GC clonal lifespan was not impacted by diet, then one would expect the EYFP GC population in the regression group to decline once mice are fed a chow diet. As this is not the case, it suggests that clones generated during HFD feeding have extended lifespan enabling them to persist until the 8-week timepoint. Furthermore, labelling prior to 8 weeks of diet resulted in mainly EYFP-labelled GC exported memory and plasma cells demonstrating that GC reactions present prior to diet are mainly completed and all that remains is the product of those GC reactions.

5.5.4 Limitations

From the experiments presented in this chapter, it was shown that LDLr$^{-/-}$ mice fed a HFD exhibited prolonged GC responses compared to chow diet-fed LDLr$^{-/-}$ mice indicative of the inflammatory environment induced by hyperlipidaemic conditions. As a result of low labelling efficiency, the number of cells labelled with EYFP is smaller than optimal. Thus, the number of EYFP cells detected in progressively narrower flow cytometry gates is very small meaning that a small number of cells can have a large influence on the relative proportion of labelled cells. This is a limitation of the work. With more time, more cells could be captured during flow cytometry to offset this limitation.

5.5.5 Future work

These experiments do not distinguish the impact of diet and the hyperlipidaemic conditions facilitated by the absence of LDL receptor. To investigate the impact of the hyperlipidaemia context, these experiments could be repeated in WT AEL mice where the LDL receptor is present. As shown in the previous chapter, WT mice show much reduced populations of GC cells thus it is expected that the absence of hyperlipidaemia would result in comparable EYFP cell dynamics between chow and HFD feeding. These experiments could also be repeated in mice fed the HF only diet to determine the specific impact that dietary fat has on EYFP labelled cells. To determine whether the HFD programs GC cells to be longer-lived or whether the surrounding environment is sufficient, EYFP cells from HFD-fed mice could be collected and transferred to chow-fed mice and dynamics observed.

6 High dietary cholesterol required for induction of GC responses in atherosclerotic mice

6.1 Abstract

Germinal centre responses are enhanced in atherosclerotic mice which could be due to hypercholesterolemia or the inflammatory nature of atherosclerosis. Using a cholesterol uptake inhibitor drug and cholesterol free diet, this chapter demonstrates that dietary cholesterol is required for GC responses in atherosclerotic mice at early stages i.e., 4 weeks. Dampening inflammation using a cytokine inhibitor dampens GC responses at later time points of atherosclerosis i.e., 8 weeks, suggesting that inflammation is key as atherosclerosis develops. The model proposed is that dietary cholesterol is critical early on in atherosclerosis as disrupted lipid homeostasis results in autoimmune B cell responses with GCs primarily reacting to accumulated oxidised LDL while at later stages, the inflammation associated with atherosclerosis fuels pathogenic GC responses.

6.2 Background

As seen in previous chapters, the high fat diet results in an expansion of the GC B cell population. As atherosclerosis is characterised as an inflammatory disease caused by hypercholesterolemia, I sought to investigate the impact of cholesterol and inflammation on the GC response.

6.2.1 Cholesterol

Cholesterol is a key component of mammalian cells comprising 25% of total membrane lipid[293]. It provides stability to the plasma membrane and deters movement thanks to its rigid hydrophobic structure[293]. Cholesterol is important as a precursor in the synthesis of vitamin D, steroid hormones, oxysterols and bile acids[293]. Lipids rafts are critical structures for the recruitment and signalling of immune receptors[294]. Insufficient cholesterol content within

lipid rafts disrupts the structure and stability, restricts TLR4 and TCR-facilitated immune activation and is inflammatory[294]. Meanwhile, increased cholesterol content within the plasma membrane fosters production of TLR4-MD2 and TLR4-CD14 complexes which increase responsiveness to TLR4 ligands i.e. LPS[261].

In addition to absorption of cholesterol via the intestinal cholesterol transporter Niemann-Pick C1-like 1 (NCP1L1), cholesterol is synthesised in the liver and intestines[295]. In mice, the liver is responsible for 21-38% of native cholesterol while the small intestines account for 12-24%[295]. Cholesterol synthesis is regulated by sterol accumulation in the liver which negatively feeds back to prevent more synthesis through inhibition of SREBP[296].

In response to low intracellular cholesterol levels, SREBPs are activated and modulate cholesterol metabolism through uptake or synthesis of cholesterol[293]. SREBP1a and SREBP1c induce fatty acid (FA) synthesis gene expression while SREBP2 is involved with cholesterol synthesis[297].

Global regulation of cholesterol metabolism genes by LXRs is vital for sterol homeostasis as they modulate fatty acid, phospholipid and cholesterol metabolism[298]. LXRα is expressed in the intestine, liver and adipose tissue while LXRβ is expressed globally[299]. LXRs are activated by intracellular hyperaccumulation of cholesterol[298] resulting in binding through the LXR binding domain of oxidised cholesterol, oxysterols and cholesterol precursors[299]. LXR activation results in heterodimerisation with RXR enabling binding to LXR responsive elements[299] within target gene regulatory regions[296]. Cholesterol overload stimulates ABCA1 and ABCG1 transcription induced by LXRs[299]. ABCA1 and ABCG1 initiate reverse cholesterol transport (RCT) which restrains cholesterol-enriched lipid raft formation in the plasma membrane[299]. This prevents MyD88-dependent TLR trafficking by reducing free cholesterol content and thus dampens macrophage inflammatory responses[299]. LXRs have anti-inflammatory properties in their capacity to prevent transcription of genes induced by transcription factors NFκB, AP-1 and STAT1[299]. The LXRs initiate cholesterol export, via RCT[299], to HDL and ApoA-I acceptors through transcription of Abca1 and Abcg1[298]. LXR activation also stimulates inducible degrader of LDL (IDOL) expression which reduces LDLr expression on the cell surface thereby reducing cellular LDL uptake[299].

ABCA1 mediates excess cholesterol and phospholipid transfer to apolipoprotein receptors, apoA-I and apoE, forming nascent preβ HDL[300]. This comprises the first step of RCT which is critical for atheroprotection[300]. ABCA1 overexpression in C57BL/6 mice elevated total plasma and HDL cholesterol levels demonstrating that liver ABCA1 is key to modulating HDL cholesterol levels[300]. Hepatic ABCA1 overexpression in LDLr$^{-/-}$ resulted in increased aortic atherosclerosis along with increased plasma concentrations of TGs, HDL and total cholesterol[300].

Disruption to the liver X receptor (LXR) pathway results in cholesterol overload systemically and intracellularly and development of atherosclerosis[298] as well as an autoimmune phenotype[298]. LXRβ deficiency prevents excessive cholesterol accumulation which results in disruption of immune homeostasis including immune complex deposition and immune cell infiltration within the kidneys, increased autoantibodies titres and B cell proliferation[298]. LXR agonism within LDLr$^{-/-}$ mice prevents atherogenesis[301].

Excessive cholesterol can also feedforward to enable cholesterol conversion to bile acid[296]. Cholesterol that has been accepted by HDL is transported to the liver for excretion via the reverse cholesterol transport pathway[298], scavenger receptor class B type I (SR-BI) receptor, and packaged into bile acid[55]. CYP7A facilitates the conversion of cholesterol into 7α-hydroxycholesterol which is the initial bile acid synthesis step[296]. ApoE, induced by cholesterol uptake[296], facilitates lipoprotein clearance within the liver and mediates macrophage cholesterol efflux[296]. ApoA-I reduces cholesterol content of plasma membrane lipid rafts[292]. Therapeutic treatment with ApoA-I decreased lipid staining within the aorta and restored impaired lymphatic transport in HFD-fed LDLr$^{-/-}$ mice[292].

Modified LDL is inflammatory as it acts as PAMP for macrophages PRRs including TLRs initiating proinflammatory signalling pathways such as inflammasome activation[261]. Jnk phosphorylation induced by CD36 is key to oxLDL uptake and the subsequent foam cell formation[302]. Engulfment of modified LDL by macrophages results in accumulation of cholesterol primarily in lysosomes[301] which augments TLR signalling[261]. Elevated TLR signalling exacerbates production of cytokines and chemokines[261] and can inhibit the action of LXRs

preventing cholesterol efflux[261]. A reduced capacity for cholesterol efflux is correlated with SAA accumulation within HDL[261]. OxLDL has been found to increase LXRα expression in human THP1 macrophages[296] which stimulates ABCA1 expression and the consequent cholesterol efflux to avoid build-up of cholesteryl esters which drive atherogenesis[296].

Dietary cholesterol excess triggers inflammation within the liver as it triggers JNK1-dependent mitochondrial hepatocyte cell death causing HMGB1 release and the induction of TLR4 and consequent hepatocyte injury[303]. Furthermore, inflammation is augmented through expression of SAA, F4/80, Mac2, TNFα and IL6[304]. Dietary cholesterol elevated levels of apoptosis and circulating free fatty acids (FFAs)[304].

The typical Western diet has high levels of oxidative lipid products; oxidation occurs when cholesterol and fatty acids are exposed to heat, air, light and oxidising agents[305]. Dietary fat is absorbed in the small intestine, enters the bloodstream as chylomicrons and is taken up by the liver[305]. Dietary cholesterol compromises endothelial function[306]. Oxidised cholesterol and fatty acids present within a diet accelerate the formation of fatty streaks within the aorta, a 32% increase in one study using $LDLr^{-/-}$, demonstrating the atherogenic nature of these compounds[305].

Oxidation of cholesterol produces oxysterol metabolites catalysed by hydroxylases and ROS oxidation[293]. Oxysterols regulate intracellular cholesterol levels via LXR and SREBP[293]. Oxysterols are oxidised derivatives of cholesterol, concentrated in LDL and are linked with increased CVD risk[301]. In WD, 1% of the sterol is oxidised. 70-90% of oxysterols in the plasma are present as fatty acyl esters within lipoprotein[301]. 27-OHC is the most plentiful oxysterol in human atherosclerotic plaques and its concentration shows a positive correlation with lesional cholesterol content and extent of atherosclerosis[301].

Intracellular cholesterol homeostasis regulation modulates immune responses[299]. The CD11c+MHCII+ myeloid cell population was expanded and showed lipid accumulation stimulating BAFF and APRIL production which induced B cell proliferation[298]. In the hypercholesterolemic environment, antigen presentation by CD11c+ cells was increased[298]. Thus CD11c+ cells were the main driving force of the autoimmune phenotype demonstrating

that impaired cholesterol homeostasis can play a role in dysregulation of the immune response[298].

6.2.2 IL6

IL6 is produced, by macrophages and monocytes among other cell types involved in CVD including endothelial cells and fibroblasts in response to inflammation, oxidative stress and vascular injury[307]. The IL6 gene contains transcription factor binding sites for AP-1, C/EBPβ, cAMP-responsive elements and STAT3[308]. IL6 gene transcription is initiated by TLR ligands, IL1, TNFα and reactive oxygen species[308]. The IL6 receptor (IL6R) is comprised of an IL6 binding receptor molecule, IL6Rα and the signal transducer gp130[308] which in combination trigger intracellular signalling[307]. Cell surface expression of IL6Rα and gp130 are essential to IL6 signalling thus restricting the effects of IL6 to lymphocytes, hepatocytes and myeloid cells[308]. IL6 signals via 3 pathways – secreted IL6 can bind to surface IL6R, or soluble IL6R to form a soluble IL6R-IL6 complex or an interaction between DCs and receiver T cells[307]. In conjunction with sIL6Rα, IL6 can act on endothelial cells to activate STAT3 leading to chemokine expression and local inflammation through leukocyte recruitment[308]. Within the vessel wall, IL6 increases expression of cell adhesion molecules increasing vascular permeability resulting in loss of the endothelium's barrier function[307]. IL6 is proatherogenic with a destabilising effect on the plaque as well as having a thrombotic role through increasing blood platelet counts and monocyte procoagulant capacity[307]. After atherosclerotic plaque rupture, local IL6 production is elevated[307].

IL6 augments B cell maturation[172] and antibody production[308] through its modulation of RAG[309]. Autoantigen binding to BCR together with IL6 production and IL7R signalling results in RAG gene transcription and editing of the light chain[309]. Consequently IL6 is responsible for BCR editing through regulation of IL7 and its receptor[309]. IL6 is necessary for the re-induction of RAG expression in antigen-activated B cells as seen by the reduction in RAG protein when mice are administered an anti-IL6 antibody[309].

Mice with ablation of IL6 have disrupted GC formation with reduced number and size of GCs[309]. Genetic deficiency and inhibitory antibody treatment of IL6 prevents SHM[172]. Overexpression of human IL6 in mice elevates IgG and autoantibody titres along with PC numbers[309] and increased risk of atherosclerosis[310]. Genetic variants in the IL6R signalling pathway result in increased risk of CVD over the course of a lifetime and indeed IL6 levels predict the risk of cardiovascular events[310]. In the CANTOS trial, atherosclerosis prevention by canakinumab was directly correlated with the extent of IL6 reduction[310]. Zilitivekimab is a monoclonal therapeutic antibody against the IL6 ligand which reduced plasma CRP and SAA levels over the course of 12 weeks in a phase 2 trial[310]. Furthermore, lipoprotein(a) levels were reduced by 16-25% and small but significant increases in APOB, HDL and APOA1 were measured[310].

6.3 Aims

1. Investigate the impact of cholesterol on the GC response through use of cholesterol uptake inhibitor lomitapide and through cholesterol-free diet in AEL mice

2. Investigate the impact of inflammation on the GC response through use of anti-inflammatory anti-IL6 treatment in AEL mice

6.4 Results

6.4.1 Dietary cholesterol is key for induction of GC responses in atherosclerotic mice

6.4.1.1 Impact of blocking cholesterol uptake on GC responses

Lomitapide is a drug which binds and inhibits the activity of the microsomal triglyceride transfer protein (MTP) in the ER of liver hepatocytes and intestinal enterocytes[311] *(Figure 95)*. MTP plays a crucial role in early chylomicron and very low density lipoprotein (VLDL) assembly, using a shuttle mechanism to transfer triglycerides to triglyceride-rich lipoproteins onto VLDL precursor, apoB as it enters the lumen of the ER[311]. Thus, MTP regulates the

number of ApoB lipoproteins in the blood[311]. By inhibiting the MTP enzyme, lomitapide inhibits lipoprotein production[312] thereby lowering levels of all ApoB-containing lipoproteins including VLDL, LDL and chylomicrons[311] *(Figure 95)*. LDLr$^{-/-}$ mice fed a standard chow diet showed reduced atherosclerotic plaque development, decreased cholesterol content within monocyte-derived cells and reduced inflammation when administered with lomitapide[313]. Lomitapide is clinically licensed only for the treatment of homozygous familial hypercholesterolaemia, patients who present with no LDL receptor[312]. The disease results in increased LDL levels to as much as 13.0 mmol/L if left untreated and leads to premature atherosclerosis[312]. As a consequence of MTP inhibition, LDL production rate dropped by 70% in one study[312]. In a clinical trial, after 26 weeks LDL-C and apoB had reduced by 50% while Lp(a) had decreased by 15%[312]. Adding lomitapide to a combination of lipid-lowering drugs reduced LDL-C further by 56.8% compared to lipid-lowering drugs alone[312]. In one cohort, up to 68% of patients with familial hypercholesterolaemia achieved the European Atherosclerosis Society (EAS) recommended adult LDL-C target of less than 100mg/dL with 40% even managing to maintain LDL-C levels below 70mg/dL[311].

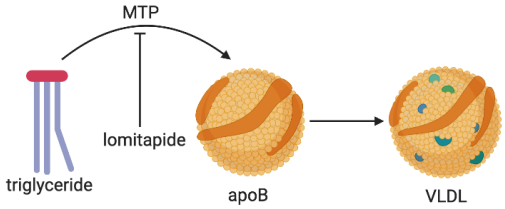

Figure 95. ***Lomitapide mechanism of action.*** *Lomitapide blocks the microsomal triglyceride transfer protein (MTP) enzyme from shuttling triglycerides to apoB which is a very low density lipoprotein (VLDL) precursor.*

6.4.1.1.1 2-week lomitapide study in female AEL LDLr$^{-/-}$ mice

As a pilot study, lomitapide was administered over the course of 1 week as part of a 2-week diet study in female LDLr$^{-/-}$ AEL mice *(Figure 96)*. Blood samples were taken following 4 hour fast after 3 doses (halfway through study) and at sacrifice after 18 hours fast.

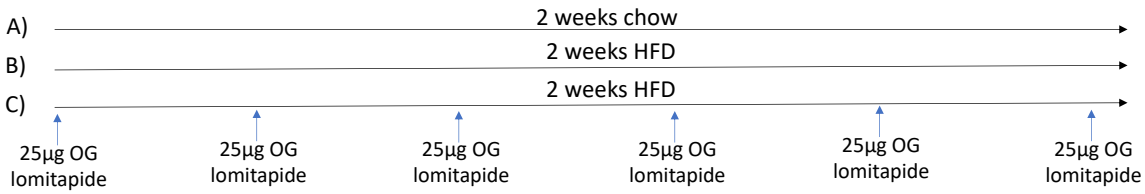

Figure 96. ***Lomitapide study design for 2 weeks.*** *Female AEL mice aged 8 weeks old were fed either* ***(A)*** *chow or* ***(B, C)*** *high fat diet (HFD) for 2 weeks.* ***(C)*** *Lomitapide treatment of 25µg by oral gavage (OG) was administered 3 times within the final*

After 1 week of lomitapide treatment, total cholesterol and LDL levels were significantly reduced compared to both untreated chow and HFD-fed female LDLr$^{-/-}$ AEL mice *(Figure 97A, B)*. After the second week, both HFD-fed groups of female LDLr$^{-/-}$ AEL mice had elevated total cholesterol and LDL compared to the chow group *(Figure 97A, B)*. HDL levels were unaffected by diet, drug treatment or time in female LDLr$^{-/-}$ AEL mice *(Figure 97C)*. Triglyceride levels were unaltered after 1 week of the study, however triglyceride levels in the lomitapide-treated HFD-fed group were significantly higher after 2 weeks compared to 1 week and compared to the HFD and chow groups without treatment in female LDLr$^{-/-}$ AEL mice *(Figure 97D)*. The ratio of total cholesterol to HDL and LDL to HDL reflected changes seen in total cholesterol and LDL levels in female LDLr$^{-/-}$ AEL mice *(Figure 97E, F)*. From these results, it would appear that the lomitapide was working well after 1 week but not after 2 weeks in female LDLr$^{-/-}$ AEL mice. With hindsight, the study was not well designed. The second blood sample was taken after an 18 hour fast and 2 days after the final dose, whereas the first blood sample was taken after a 4 hour fast following a dose of lomitapide. Therefore, it was hypothesised that too much time had passed for the drug to still be having an impact for the second timepoint. This caveat was fixed in the next study.

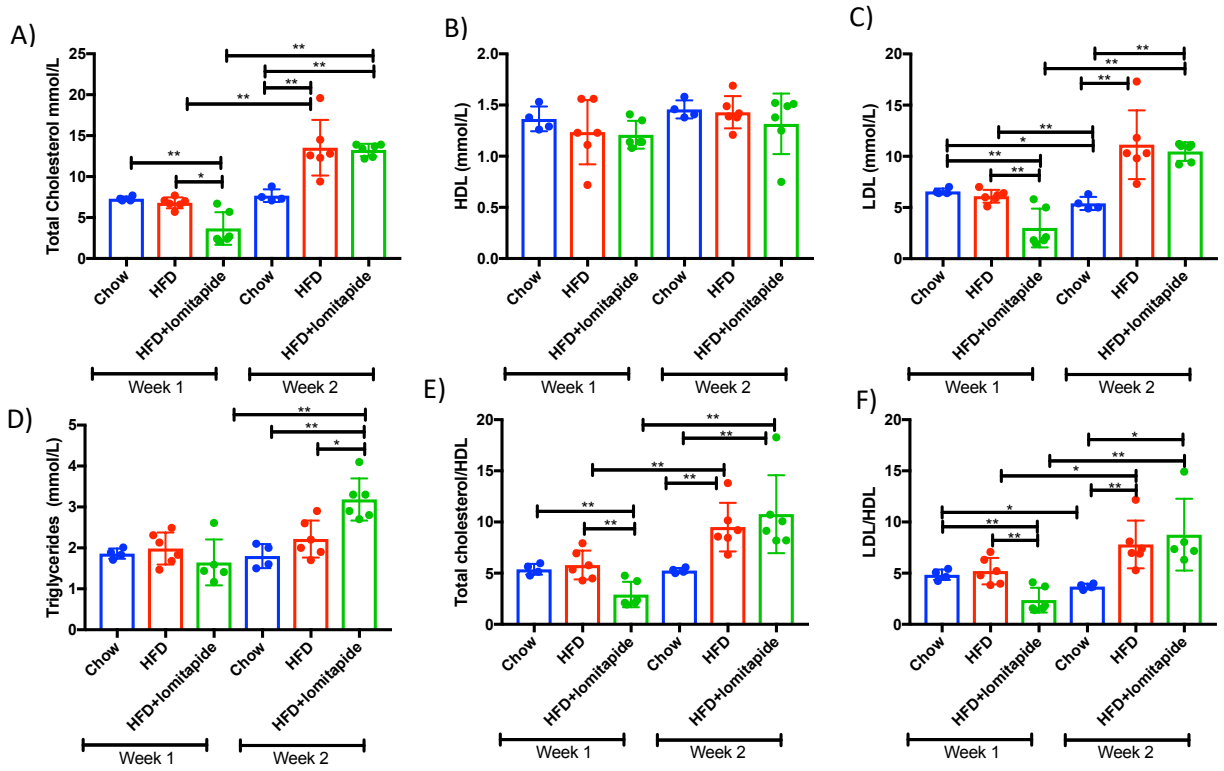

Figure 97. ***Effect of lomitapide on serum lipid levels in female AEL mice after 2 weeks.*** *Female AEL mice were fed either chow (blue) or high fat diet (HFD, red) for 2 weeks and one group of HFD-fed mice were treated with25μg oral gavage lomitapide (green) 3 times per week. Blood samples were taken for lipid analysis after 1 and 2 weeks with a 4hr and 18hr fast respectively. Serum was analysed for* ***(A)*** *total cholesterol,* ***(B)*** *high density lipoprotein (HDL),* ***(C)*** *low density lipoprotein (LDL) and* ***(D)*** *triglycerides. The ratio was total cholesterol: HDL was calculated* ***(E)*** *as was the LDL: HDL ratio* ***(F)****. Each dot represents one mouse, graphs show mean +/- SD. Statistics carried out using Mann-Whitney test, * P < 0.05; ** P < 0.01; *** P < 0.001; **** P < 0.0001.*

Average weight was not altered by drug treatment nor were cell numbers (data not shown) in female LDLr$^{-/-}$ AEL mice. The proportion of GC cells in the spleen and PALN was not impacted in female LDLr$^{-/-}$ AEL mice *(Figure 98)*.

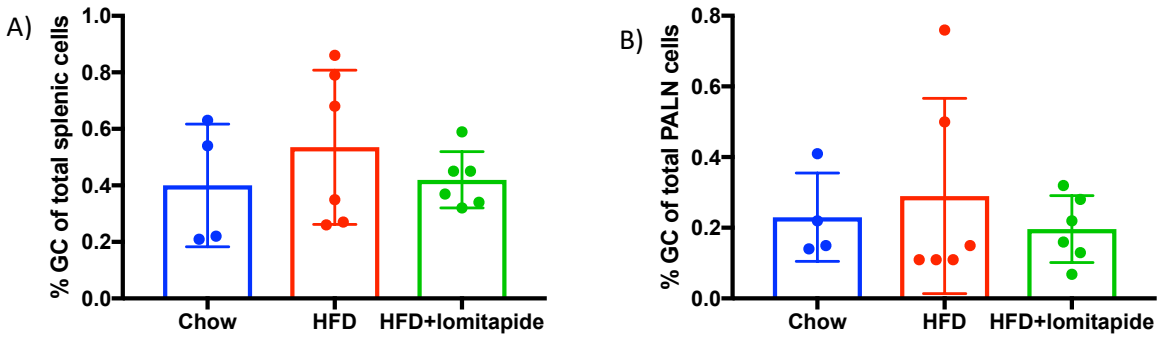

*Figure 98.****Lomitapide had no effect on the GC population in female AEL mice after 2 weeks.*** *Female AEL mice were fed either chow (blue) or high fat diet (HFD, red) for 2 weeks and one group of HFD-fed mice were treated with25μg oral gavage lomitapide (green) 3 times per week. The proportion of GC B cells (CD95+GL7+) as identified by flow cytometry of total cells in* ***(A)*** *the spleen and* ***(B)*** *the para-aortic lymph nodes (PALN). Each dot represents 1 mouse, graphs show mean +/- SD. Statistics carried out using Mann-Whitney test, * P < 0.05; ** P < 0.01; *** P < 0.001; **** P < 0.0001.*

The monocyte population within the spleen was increased in response to lomitapide treatment compared to HFD alone or chow diet in female LDLr$^{-/-}$ AEL mice *(Figure 99A)*. Contrastingly, the neutrophil population was diminished in the spleen when lomitapide was administered compared to chow and HFD-fed untreated female LDLr$^{-/-}$ AEL mice *(Figure 99B)*.

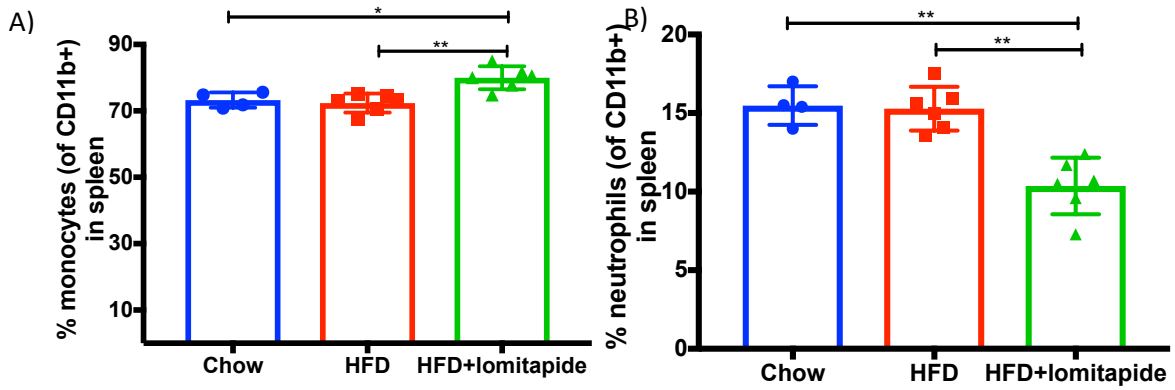

*Figure 99.**Impact of lomitapide on CD11b+ cells in spleen of female AEL mice after 2 weeks.** Female AEL mice were fed either chow (blue) or high fat diet (HFD, red) for 2 weeks and one group of HFD-fed mice were treated with25μg oral gavage lomitapide (green) 3 times per week. The splenic proportion as identified by flow cytometry of **(A)** monocytes and **(B)** neutrophils of total CD11b+ population. Each dot represents 1 mouse, graphs show mean +/- SD. Statistics carried out using Mann-Whitney test, * P < 0.05; ** P < 0.01; *** P < 0.001; **** P < 0.0001.*

The Ly6C^{hi} and Ly6C^{int} monocyte populations were expanded in response to HFD while the Ly6C^{lo} monocyte population was increased only in the presence of lomitapide in the spleen of female LDLr$^{-/-}$ AEL mice *(Figure 100A, B, C)*. While in the BM of female LDLr$^{-/-}$ AEL mice, HFD and lomitapide reduced the Ly6C^{hi} monocyte population but increased the Ly6C^{lo} population *(Figure 100D, F)*. The Ly6C^{int} monocyte population expanded in response to HFD in the BM of female LDLr$^{-/-}$ AEL mice *(Figure 100E)*.

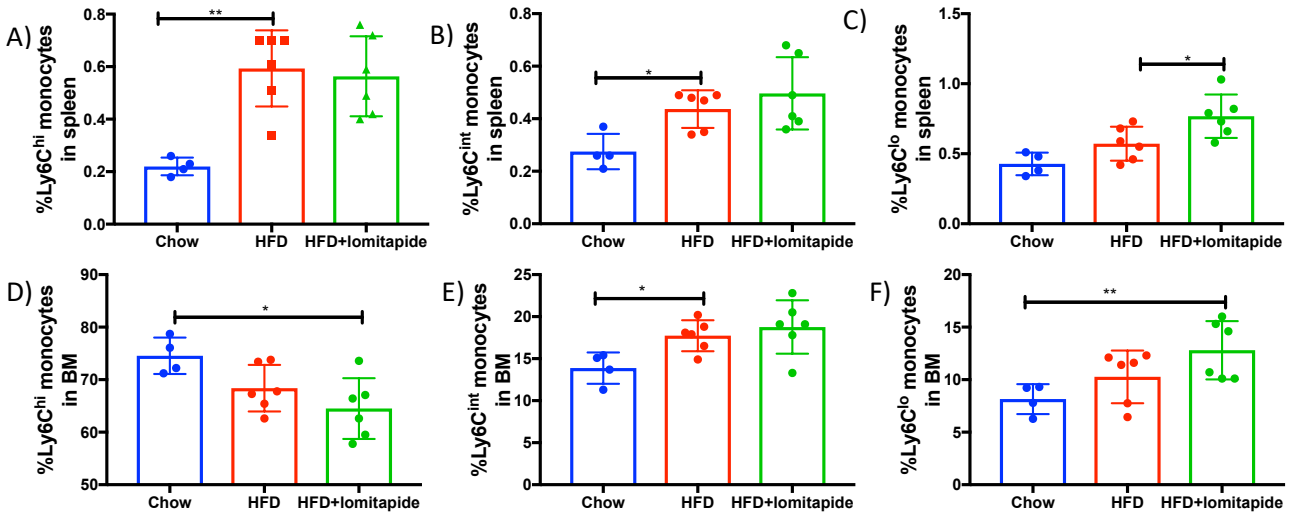

Figure 100. ***Impact of lomitapide on monocytes in female AEL mice after 2 weeks.*** *Female AEL mice were fed either chow (blue) or high fat diet (HFD, red) for 2 weeks and one group of HFD-fed mice were treated with 25μg oral gavage lomitapide (green) 3 times per week. The total proportion of splenic* ***(A)*** *Ly6C^{hi},* ***(B)*** *Ly6C^{int}, and* ***(C)*** *Ly6C^{lo} monocytes as determined by flow cytometry. The total proportion of BM* ***(D)*** *Ly6C^{hi},* ***(E)*** *Ly6C^{int}, and* ***(F)*** *Ly6C^{lo} monocytes as determined by flow cytometry. Each dot represents 1 mouse, graphs show mean +/- SD. Statistics carried out using Mann-Whitney test, * P < 0.05; ** P < 0.01; *** P < 0.001; **** P < 0.0001.*

6.4.1.1.2 4-week lomitapide study in female AEL mice

After this optimisation study, lomitapide was used again in female LDLr$^{-/-}$ AEL mice. Female LDLr$^{-/-}$ AEL mice were fed diet for a total of 4 weeks with treatment in the second two weeks. Control groups of female LDLr$^{-/-}$ AEL mice were treated with vehicle *(Figure 101)*. Female LDLr$^{-/-}$ AEL mice were fasted for 4hrs after a dose at both blood sampling timepoints for consistency.

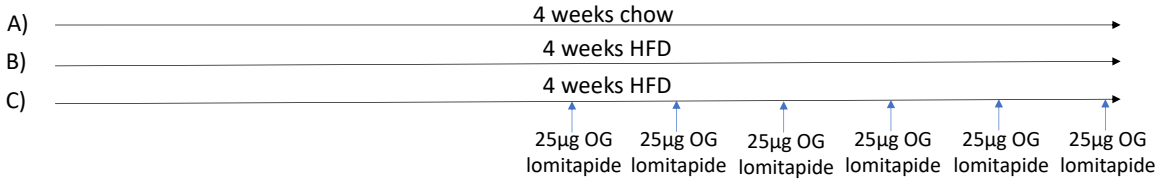

Figure 101. ***Lomitapide study design for 4 weeks.*** *Female AEL mice aged 8 weeks old were fed either* ***(A)*** *chow or* ***(B, C)*** *high fat diet (HFD) for 4 weeks.* ***(C)*** *Lomitapide treatment of 25μg by oral gavage (OG) was administered 3 times within the final 2 weeks.*

HFD-fed female LDLr$^{-/-}$ AEL mice put on more weight than chow-fed mice over the 4-week period as expected, however lomitapide-treated HFD-fed female LDLr$^{-/-}$ AEL mice had blunted

weight gain in comparison *(Figure 102)*. This suggests that cholesterol absorption and uptake into circulation contributes to weight gain in HFD-fed female LDLr$^{-/-}$ AEL animals.

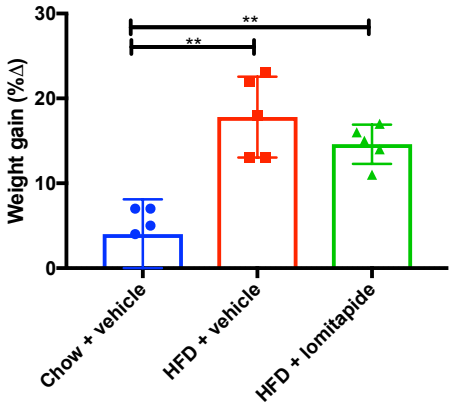

Figure 102. ***Impact of lomitapide on weight in female AEL mice after 4 weeks.*** *Female AEL mice were weighed weekly from start of study (8 weeks old) over 4 week time course until study end (12 weeks old). The percentage change from starting weight to final weight is shown for chow (blue), high fat diet (HFD; red) and HFD + lomitapide treated animals (lom; green). Each dot represents one mouse, graphs show mean +/- SD. Statistics carried out using Mann-Whitney test, * P < 0.05; ** P < 0.01; *** P < 0.001; **** P < 0.0001.*

HFD induced elevations in total cholesterol, LDL, HDL, and triglycerides compared to chow-fed female LDLr$^{-/-}$ AEL mice as expected at both time points analysed *(Figure 103A, B, C, D)*. Lomitapide blunted the HFD-induced increase at both time points of total cholesterol, LDL, HDL, and triglycerides in female LDLr$^{-/-}$ AEL mice *(Figure 103A, B, C, D)*. The ratios of total cholesterol to HDL and LDL to HDL were significantly higher in HFD-fed female LDLr$^{-/-}$ AEL mice compared to those fed chow at both time points *(Figure 103E, F)*. Thus, lomitapide worked effectively to lower plasma cholesterol levels in female LDLr$^{-/-}$ AEL mice.

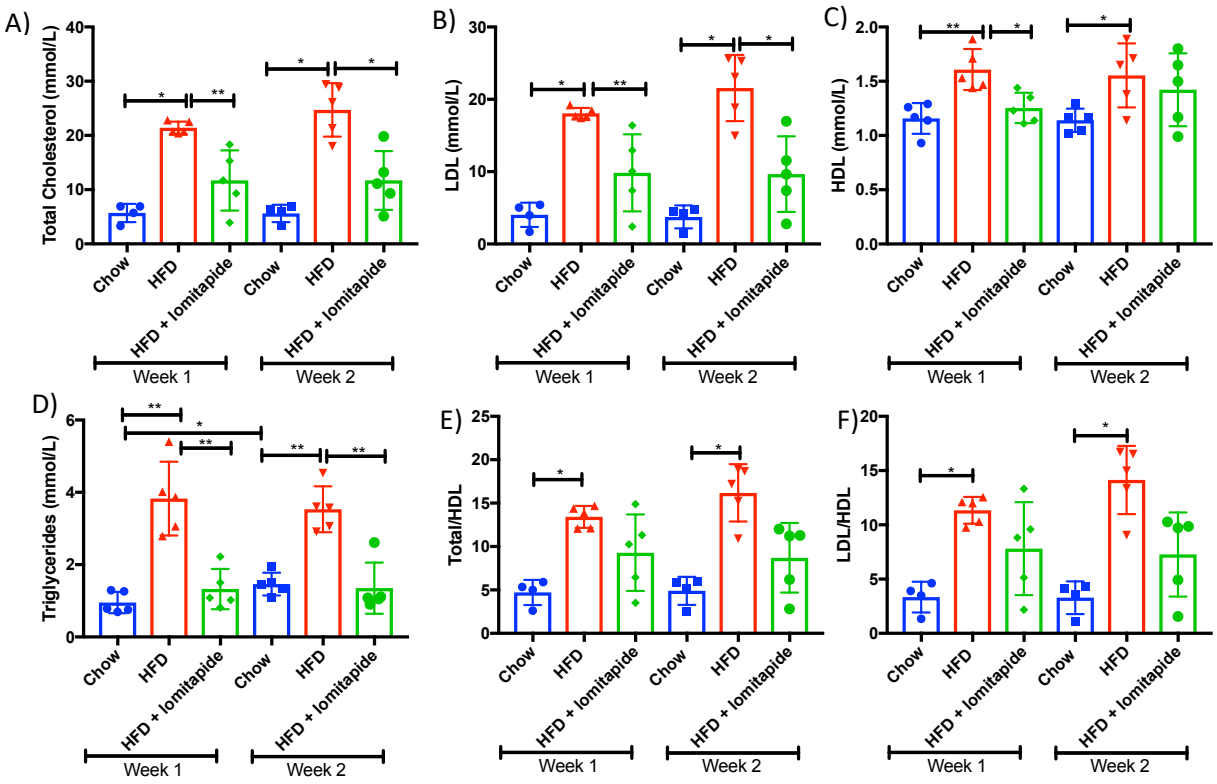

Figure 103. ***Impact of lomitapide on serum lipid levels in female AEL mice after 4 weeks.*** *Female AEL mice were fed either chow (blue) or high fat diet (HFD; red) for 4 weeks and one group of HFD-fed mice were treated with25μg oral gavage lomitapide (green) 3 times per week for 2 weeks. Blood samples were taken for lipid analysis after 1 and 2 weeks treatment with 4hr fast between dose and blood sample. Serum was analysed for* ***(A)*** *total cholesterol,* ***(B)*** *high density lipoprotein (HDL),* ***(C)*** *low density lipoprotein (LDL) and* ***(D)*** *triglycerides. The ratio was total cholesterol: HDL was calculated* ***(E)*** *as was the LDL: HDL ratio* ***(F)****. Each dot represents one mouse, graphs show mean +/- SD. Statistics carried out using Mann-Whitney test, * P < 0.05; ** P < 0.01; *** P < 0.001; **** P < 0.0001.*

The proportion and absolute number of cells within the spleen which were identified as GC was expanded by HFD, but this effect was restricted by use of lomitapide in female LDLr$^{-/-}$ AEL mice *(Figure 104A, B)*. Both splenic IgM+ and IgM- GC B cells were reduced in lomitapide treated female LDLr$^{-/-}$ AEL mice *(Figure 104C, F)* This effect was not seen in the PALN; this lymphoid organ was unaffected by lomitapide treatment in female LDLr$^{-/-}$ AEL mice *(Figure 104D, E)*.

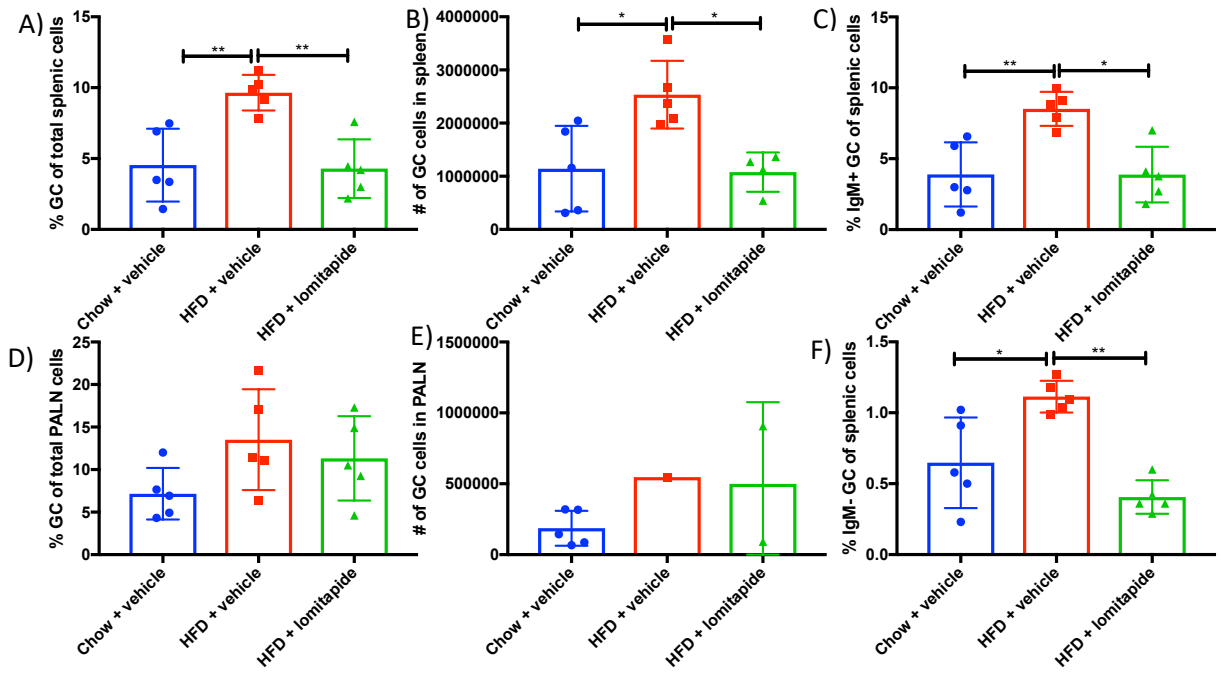

Figure 104. ***Impact of lomitapide on GC populations after 4 weeks in female AEL mice.*** *Female AEL mice were fed either chow (blue) or high fat diet (HFD, red) for 4 weeks and one group of HFD-fed mice were treated with25μg oral gavage lomitapide (green) 3 times per week. The proportion of GC B cells (CD95+GL7+) as identified by flow cytometry of total cells in* ***(A)*** *the spleen and* ***(D)*** *the para-aortic lymph nodes (PALN). The total number of GC B cells in the* ***(B)*** *spleen and* ***(E)*** *PALN. The proportion of GC cells in the spleen which were* ***(C)*** *IgM+ and* ***(F)*** *IgM-. Each dot represents 1 mouse, graphs show mean +/- SD. Statistics carried out using Mann-Whitney test, * P < 0.05; ** P < 0.01; *** P < 0.001; **** P < 0.0001.*

Within the splenic monocyte population, lomitapide treatment reduced Ly6C^{int} and Ly6C^{lo} monocyte levels back toward chow diet-fed levels in female LDLr$^{-/-}$ AEL mice *(Figure 105)*.

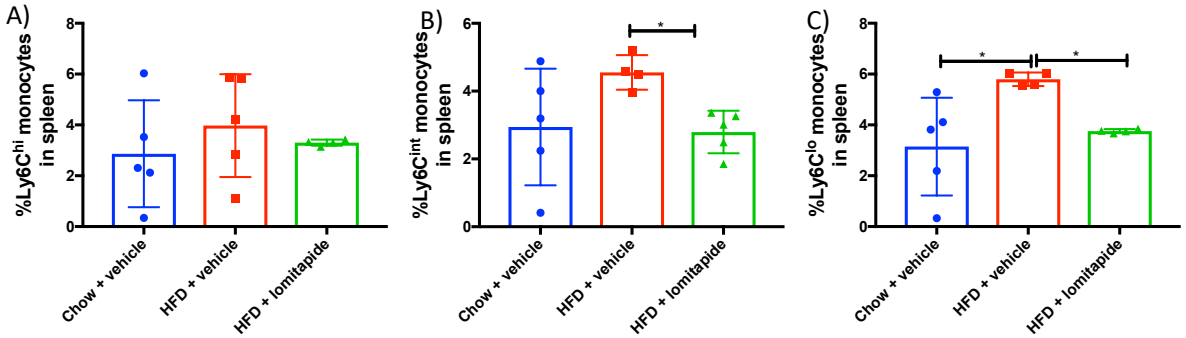

Figure 105. ***Impact of lomitapide on monocytes in female AEL mice after 4 weeks.*** *Female AEL mice were fed either chow (blue) or high fat diet (HFD, red) for 4 weeks and one group of HFD-fed mice were treated with25μg oral gavage lomitapide (green) 3 times per week. The total proportion of splenic* ***(A)*** *Ly6C^{hi},* ***(B)*** *Ly6C^{int}, and* ***(C)*** *Ly6C^{lo} monocytes as determined by flow cytometry. Each dot represents 1 mouse, graphs show mean +/- SD. Statistics carried out using Mann-Whitney test, * P < 0.05; ** P < 0.01; *** P < 0.001; **** P < 0.0001.*

Furthermore, lomitapide treatment lowered serum IgM levels in HFD-fed female LDLr$^{-/-}$ AEL mice *(Figure 106)*.

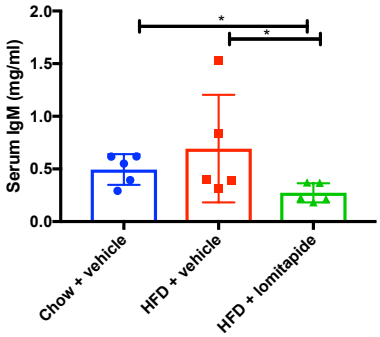

Figure 106. ***4 weeks of lomitapide treatment reduces serum IgM in female AEL mice.*** *Female AEL mice were fed either chow (blue) or high fat diet (HFD, red) for 4 weeks and one group of HFD-fed mice were treated with25μg oral gavage lomitapide (green) 3 times per week. Serum IgM levels were measured in the serum using ELISA. Each dot represents 1 mouse, graphs show mean +/- SD. Statistics carried out using Mann-Whitney test, * P < 0.05; ** P < 0.01; *** P < 0.001; **** P < 0.0001.*

To determine the impact of lomitapide in a normolipidemic environment, the study was also carried out in female WT AEL mice following the same design as previously *(Figure 101)*. Weights were not impacted by diet or treatment *(Figure 107)*.

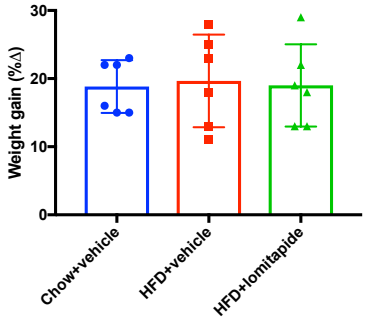

Figure 107. ***Lomitapide does not impact weight in female WT AEL mice after 4 weeks.*** *Female WT AEL mice were weighed weekly from start of study (8 weeks old) over 4 week time course until study end (12 weeks old). The percentage change from starting weight to final weight is shown for chow (blue), high fat diet (HFD; red and HFD + lomitapide treated animals (lom; green). Each dot represents one mouse, graphs show mean +/- SD.*

Serum analysis confirmed that lomitapide did not impact lipid levels under conditions of normal cholesterol homeostasis (low levels) and did not blunt HFD-induced elevations in total cholesterol, LDL and HDL in female WT AEL mice *(Figure 108)*.

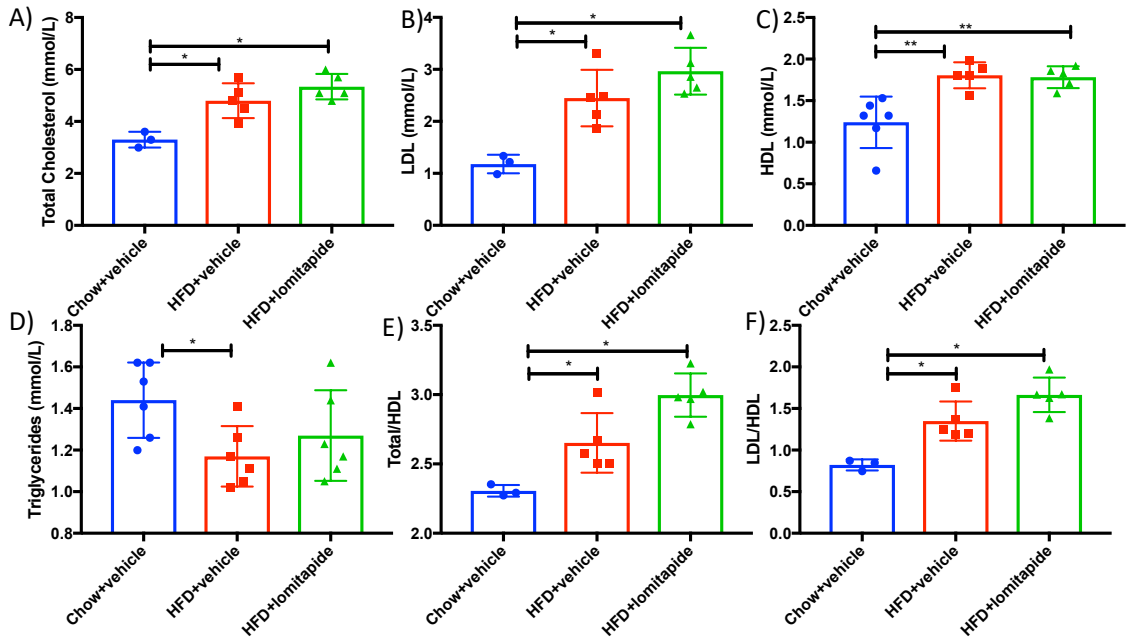

*Figure 108.**Lomitapide did not impact serum lipid levels in female AEL WT mice after 4 weeks.** Female AEL WT (LDLr$^{+/-}$) mice were fed either chow or high fat diet (HFD) for 4 weeks and one group of HFD-fed mice were treated with25μg oral gavage lomitapide 3 times per week for 2 weeks. Serum was analysed at study end after 4hr fast for **(A)** total cholesterol, **(B)** high density lipoprotein (HDL), **(C)** low density lipoprotein (LDL) and **(D)** triglycerides. The ratio was total cholesterol: HDL was calculated **(E)** as was the LDL: HDL ratio **(F)**. Each dot represents one mouse, graphs show mean +/- SD. Statistics carried out using Mann-Whitney test, * P < 0.05; ** P < 0.01; *** P < 0.001; **** P < 0.0001.*

The proportion and absolute number of GC B cells within the spleen and PALN were unaffected by diet or lomitapide treatment in female WT AEL mice *(Figure 109)*.

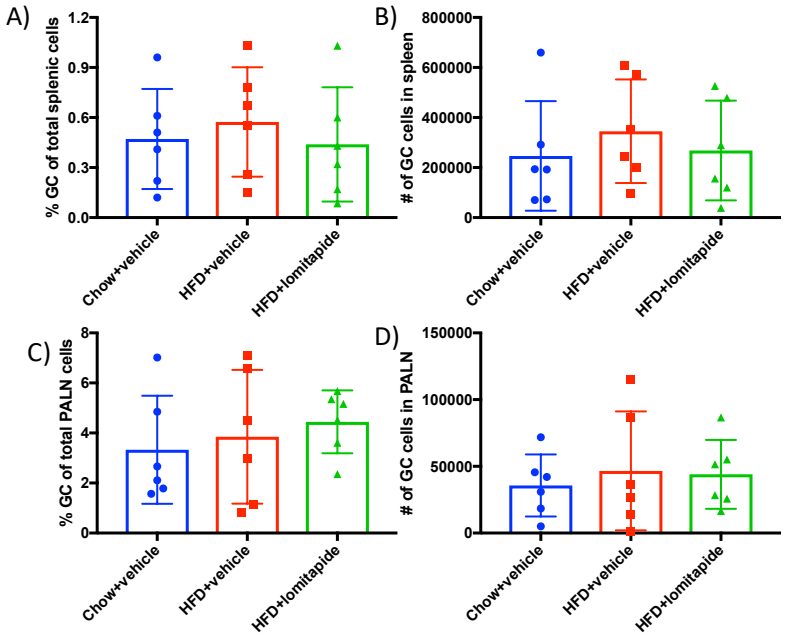

*Figure 109. **Lomitapide had no impact on GC populations in female AEL WT mice after 4 weeks.** Female AEL WT (LDLr$^{+/-}$) mice were fed either chow (blue) or high fat diet (HFD, red) for 4 weeks and one group of HFD-fed mice were treated with 25μg oral gavage lomitapide (green) 3 times per week. The proportion of GC B cells (CD95+GL7+) as identified by flow cytometry of total cells in **(A)** the spleen and **(C)** the para-aortic lymph nodes (PALN). The total number of GC B cells in the **(B)** spleen and **(D)** PALN. Each dot represents 1 mouse, graphs show mean +/- SD.*

Curiously, the proportion of plasma cells within the bone marrow and para-aortic lymph nodes was increased with lomitapide treatment due to an increase in the proportion of IgM- plasma cells in female WT AEL mice *(Figure 110)*.

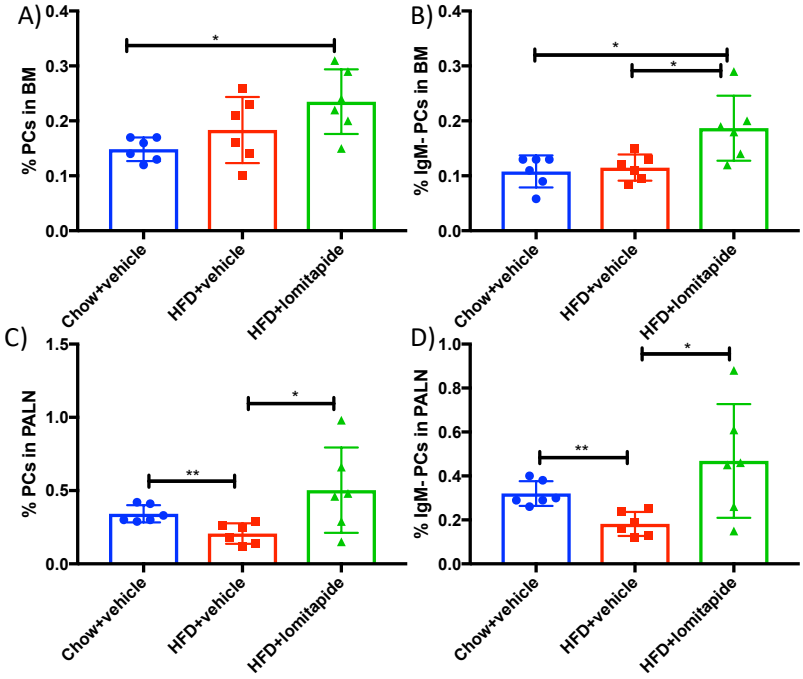

Figure 110. ***Increased PC populations with lomitapide treatment in female AEL WT mice after 4 weeks.*** *Female AEL WT (LDLr$^{+/-}$) mice were fed either chow (blue) or high fat diet (HFD, red) for 4 weeks and one group of HFD-fed mice were treated with 25μg oral gavage lomitapide (green) 3 times per week. The proportion of plasma cells CD138+) as identified by flow cytometry in the* ***(A)*** *bone marrow (BM) and* ***(C)*** *para-aortic lymph nodes. The absolute number of plasma cells shown in* ***(B)*** *BM and* ***(D)*** *PALN. Each dot represents one mouse, graphs show mean +/- SD. Statistics carried out using Mann-Whitney test, * P < 0.05; ** P < 0.01; *** P < 0.001; **** P < 0.0001.*

6.4.1.1.3 4-week lomitapide study in male AEL LDLr$^{-/-}$ mice

Having determined a link between GC response and hypercholesterolemia in females, lomitapide was administered to male LDLr$^{-/-}$ AEL mice. In this study, a diet without added cholesterol was also used (HF only) to separate the effect of lomitapide on dietary cholesterol compared to endogenous cholesterol *(Figure 111)*.

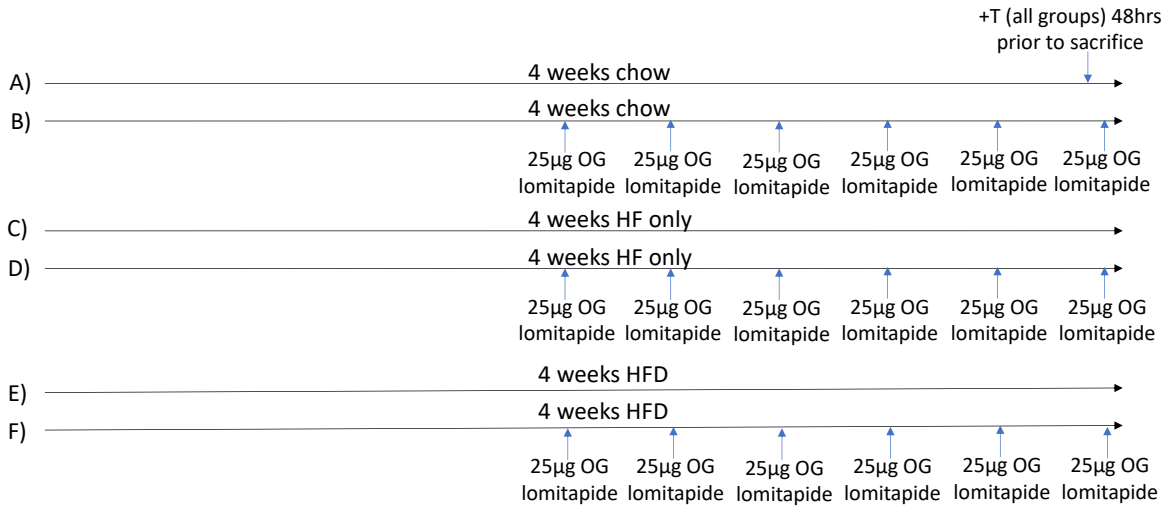

Figure 111. ***Experimental study design using male AEL mice aged 8 weeks old.*** *Mice were fed either chow* ***(A, B)****, high fat only diet (HF only;* ***C, D****) or high fat high cholesterol diet (HFHC; aka HFD;* ***E, F****) for 4 weeks. Mice were either treated via oral gavage 3 times a week for the final 2 weeks with either vehicle* ***(A, C, E)*** *or 25µg lomitapide* ***(B, D, F)****. 48hrs prior to sacrifice all groups were dosed with 9mg tamoxifen via oral gavage to induce EYFP labelling.*

Both HF only and high fat high cholesterol (HFHC) diets increased weight gain beyond that of chow diet with HFHC diet having a greater impact in male LDLr$^{-/-}$ AEL mice. Lomitapide had little impact on weight gain in male LDLr$^{-/-}$ AEL mice *(Figure 112)*.

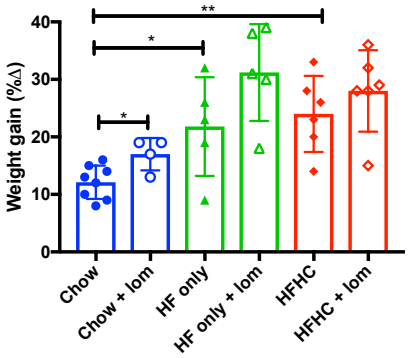

Figure 112. ***Lomitapide had little impact on weight in male AEL mice after 4 weeks.*** *Male AEL mice were weighed weekly from start of study (8 weeks old) over 4 week time course until study end (12 weeks old). The percentage change from starting weight to final weight is shown for chow (blue), high fat only diet (HF only; green) and high fat high cholesterol diet (HFHC; red) and lomitapide (lom) treated animals (open circles). Each dot represents one mouse, graphs show mean +/- SD. Statistics carried out using Mann-Whitney test, * P < 0.05; ** P < 0.01; *** P < 0.001; **** P < 0.0001.*

In hyperlipidaemic male LDLr$^{-/-}$ AEL mice, lomitapide reduced cholesterol levels – both total and LDL as well as triglycerides in chow diet-fed mice *(Figure 113A, B, D)*. Total cholesterol, LDL and triglycerides were significantly increased in HF only and HFHC diet-fed male LDLr$^{-/-}$ AEL mice compared to chow diet-fed male LDLr$^{-/-}$ AEL mice *(Figure 113A, B, D)*. The HFHC diet elevated total cholesterol and LDL levels beyond that of the HF only diet both in treated and control groups of male LDLr$^{-/-}$ AEL mice *(Figure 113A, B)*. In the HF only diet-fed male LDLr$^{-/-}$

AEL mice, lomitapide reduced total cholesterol, LDL, and triglycerides levels but not significantly *(Figure 113A, B, D)*. Strangely, lomitapide appeared to elevate total cholesterol, LDL, and triglyceride levels in male LDLr$^{-/-}$ AEL mice fed the HFHC diet *(Figure 113A, B, D)*. HDL levels were not impacted by diet type or treatment in male LDLr$^{-/-}$ AEL mice *(Figure 113C)*.

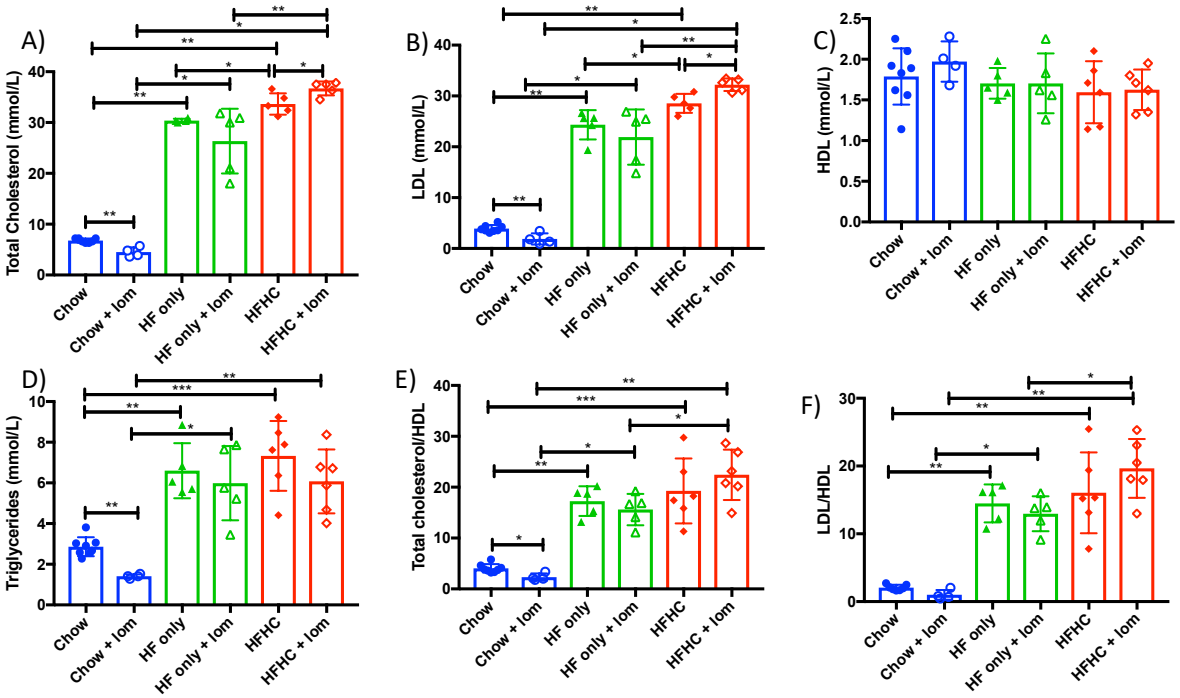

Figure 113. ***Impact of lomitapide on serum lipids levels in male AEL mice after 4 weeks.*** *Male AEL mice were fed either chow (blue), high fat only (HF only; green) or high fat diet (HFD, red) for 4 weeks and half of each diet type were treated with 25μg oral gavage lomitapide (lom) 3 times per week for 2 weeks (open circles). Serum was analysed at study end after 4hr fast for* ***(A)*** *total cholesterol,* ***(B)*** *high density lipoprotein (HDL),* ***(C)*** *low density lipoprotein (LDL) and* ***(D)*** *triglycerides. The ratio of total cholesterol: HDL was calculated* ***(E)*** *as was the LDL: HDL ratio* ***(F)****. Each dot represents one mouse, graphs show mean +/- SD. Statistics carried out using Mann-Whitney test, * P < 0.05; ** P < 0.01; *** P < 0.001; **** P < 0.0001.*

In male LDLr$^{-/-}$ AEL mice, the GC response was unaffected by diet or treatment in the spleen and PALN *(Figure 114)*.

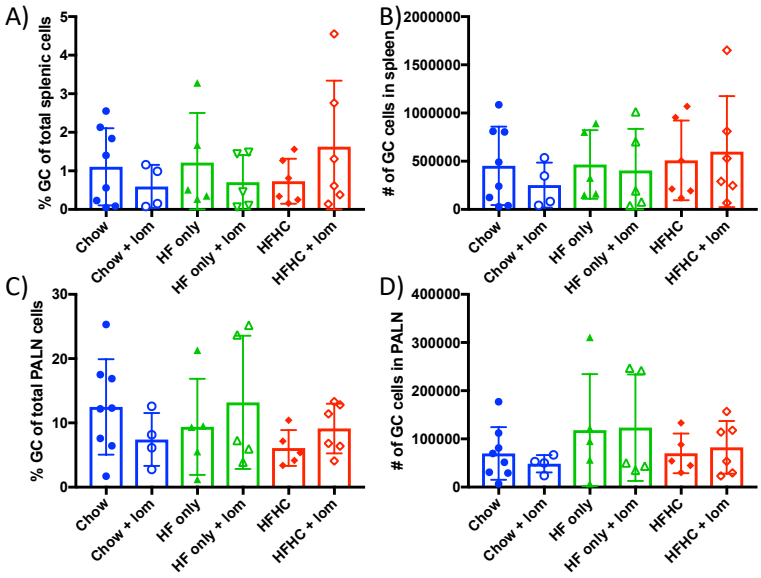

Figure 114. ***Lomitapide had no impact on GC populations in male AEL mice after 4 weeks.*** *Male AEL mice were fed either chow (blue and red), high fat only (HF only; green and purple) or high fat diet (HFD, orange and black) for 4 weeks and half of each diet type were treated with 25μg oral gavage lomitapide (lom) 3 times per week for 2 weeks (red, purple, black). The proportion of GC B cells (CD95+GL7+) as identified by flow cytometry of total cells in* ***(A)*** *the spleen and* ***(C)*** *the para-aortic lymph nodes (PALN). The total number of GC B cells in the* ***(B)*** *spleen and* ***(D)*** *PALN. Each dot represents*

6.4.1.2 Impact of cholesterol free diet on GC responses

As an alternative approach for removing dietary cholesterol, a cholesterol free diet was used. This was identical to the high fat and high cholesterol (HFHC) standard Western diet but without the added 0.15% cholesterol. The diet contained 0.05% cholesterol, but this was derived from dietary fat.

6.4.1.2.1 4-week cholesterol free diet in female AEL mice

Diet was fed to female LDLr$^{-/-}$ AEL mice for a total of 4 weeks as females show increased differences between chow and HFD feeding at 4 weeks in regard to GC responses. As expected, HFHC diet-fed female LDLr$^{-/-}$ AEL mice gained more weight than chow diet-fed female LDLr$^{-/-}$ AEL mice however the HF only diet-fed female LDLr$^{-/-}$ AEL mice gained even more weight both in absolute and proportional terms *(Figure 115)*.

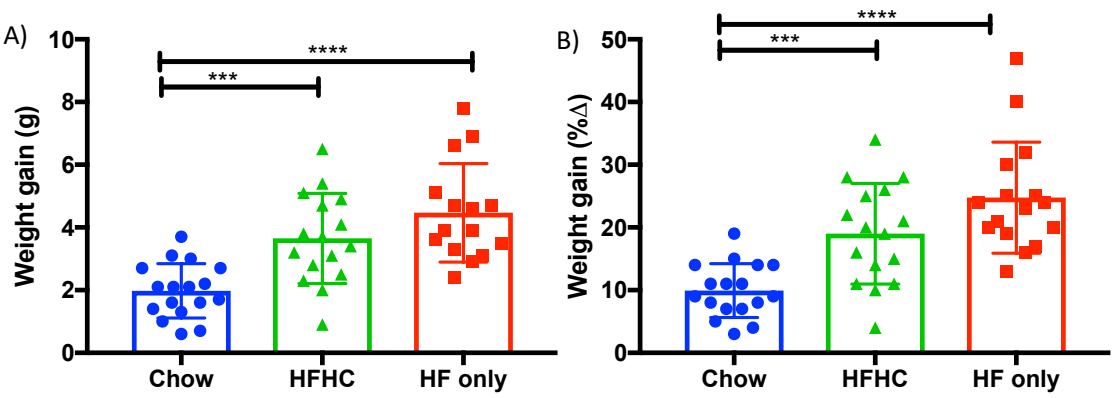

Figure 115. ***Weight gain with high fat-containing diets in female AEL mice after 4 weeks.*** *Difference in weight from start of experiment, female AEL mice aged 8 weeks old, to end of experiment after 4 weeks of diet (mice aged 12 weeks old) of either chow (blue), high fat high cholesterol (HFHC; green) or high fat only (HF only; red) in* ***(A)*** *absolute terms and* ***(B)*** *as proportion. Each dot represents 1 mouse, graphs show mean +/- SD. Statistics carried out using Mann-Whitney test, * P < 0.05; ** P < 0.01; *** P < 0.001; **** P < 0.0001.*

The HF only diet prevented the HFHC-induced elevations in total cholesterol, LDL, and triglycerides *(Figure 116A, C, D)*. Interestingly, HDL was increased in the HF only diet-fed female LDLr$^{-/-}$ AEL mice more so than in the HFHC diet-fed female LDLr$^{-/-}$ AEL mice *(Figure 116B)*. As can be observed, the HF only group split into a group whose cholesterol levels were not impacted and a group whose lipid levels were downregulated – the reason for this is unknown; differences were split across cages. It was hypothesised that there could have been a mix up with genotypes at some point as the LDLr$^{-/-}$ genotype is not regularly checked, but when tested these mice were indeed LDLr$^{-/-}$. Other members of the laboratory did find that mice which should have been LDLr$^{-/-}$ were actually LDLr$^{+/-}$ however so this could be the reason for the split in cholesterol levels. Thus, dietary cholesterol is responsible for elevated plasma lipid levels and a high dietary fat concentration is insufficient on its own in female LDLr$^{-/-}$ AEL mice.

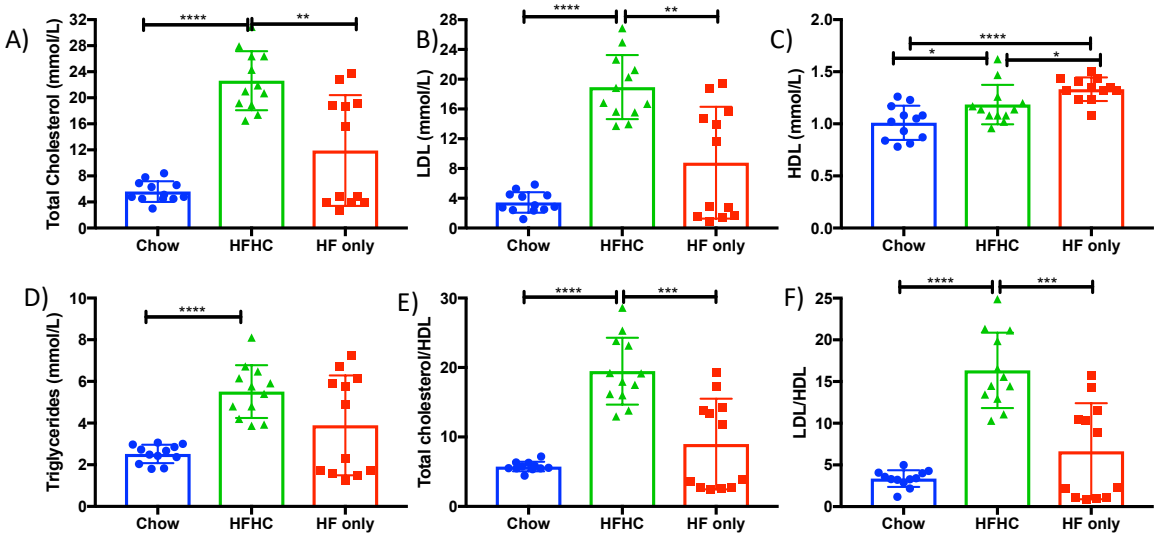

Figure 116. ***Reduced serum lipid levels with HF only diet in female AEL mice after 4 weeks.*** *Female AEL mice were fed either chow (blue), high fat and high cholesterol (HFHC; green) or high fat only diet (HF only; red) for 4 weeks. Serum was analysed at study end after 4hr fast for* ***(A)*** *total cholesterol,* ***(B)*** *high density lipoprotein (HDL),* ***(C)*** *low density lipoprotein (LDL) and* ***(D)*** *triglycerides. The ratio of total cholesterol: HDL was calculated* ***(E)*** *as was the LDL: HDL ratio* ***(F)****. Each dot represents one mouse, graphs show mean +/- SD. Statistics carried out using Mann-Whitney test, * P < 0.05; ** P < 0.01; *** P < 0.001; **** P < 0.0001.*

The HFHC diet resulted in hypertrophy of the PALN which was absent when dietary cholesterol was missing from diet (HF only) *(Figure 117B)*. HFD induced an expansion in the B cell population within the spleen and PALN which was blunted when female LDLr$^{-/-}$ AEL mice were fed the HF only diet *(Figure 117C, D)*. This suggests that dietary cholesterol is required for the expansion in B cells as well as total PALN cell number in HFD-fed female LDLr$^{-/-}$ AEL animals.

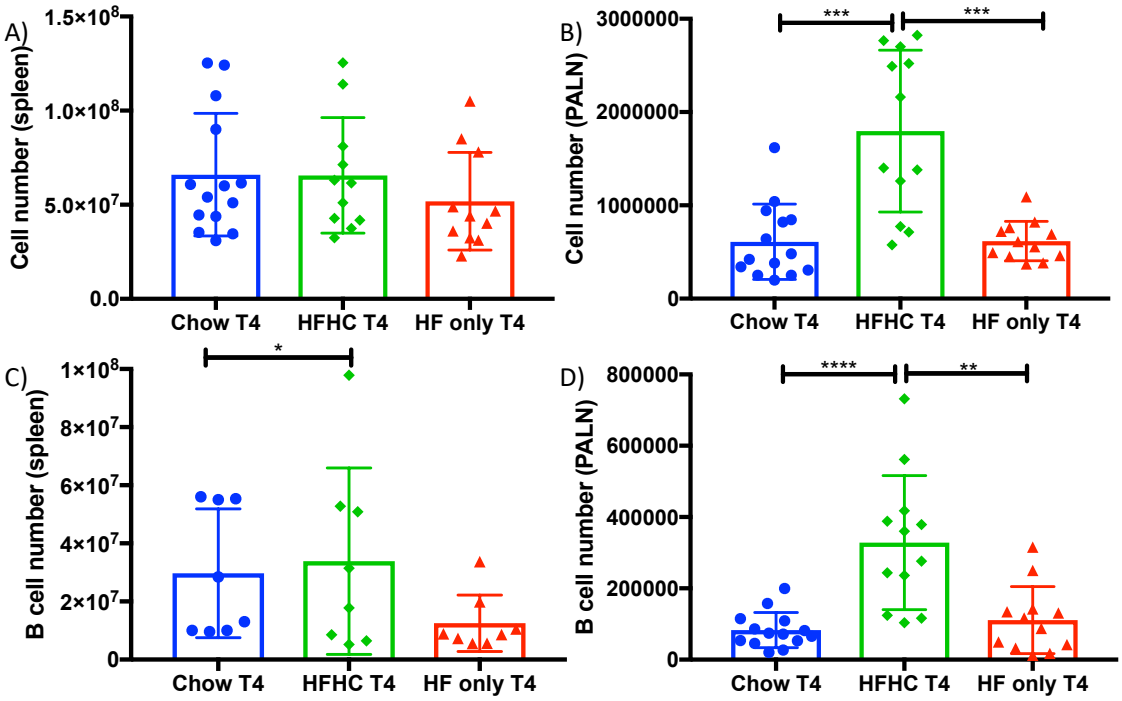

Figure 117. ***No PALN hypertrophy after HF only diet in female AEL mice after 4 weeks.*** *Female AEL mice were fed either (chow), high fat and high cholesterol (HFHC; green) or high fat only diet (HF only; red) for 4 weeks (T4). Total cell number was calculated for (A) spleen and (B) PALN. Total B cell number was calculated for (C) spleen and (D) PALN. Each dot represents one mouse, graphs show mean +/- SD. Statistics carried out using Mann-Whitney test, * P < 0.05; ** P < 0.01; *** P < 0.001; **** P < 0.0001.*

As seen previously, HFHC diet induced an increase in the proportion of GC cells significantly in the spleen whilst the increase did not quite reach significance in the PALN *(Figure 118A, D)*. The absolute number of GC cells was also elevated in the spleen and PALN of HFHC diet-fed female LDLr$^{-/-}$ AEL mice *(Figure 118B, E)*. This result was not isotype specific as both splenic IgM+ and IgM- GC cells were increased in the HFHC diet-fed female LDLr$^{-/-}$ AEL mice compared with both chow and HF only diet-fed female LDLr$^{-/-}$ AEL mice *(Figure 118C, F)*. This effect was blunted in HF only diet-fed female LDLr$^{-/-}$ AEL mice in both absolute and proportion of GC cells in the spleen and PALN *(Figure 118)*.

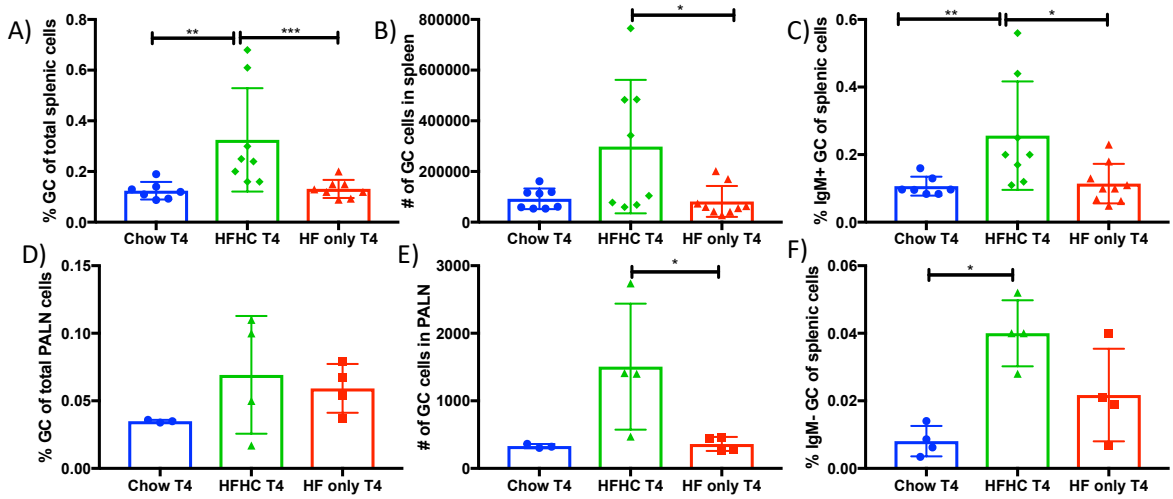

Figure 118. ***Reduced GC population upon HF only diet feeding in female AEL mice after 4 weeks.*** *Female AEL mice were fed either chow (blue), high fat high cholesterol diet (HFHC; green) or high fat only diet (HF only; red) for 4 weeks (T4). The proportion of GC cells as assessed by flow cytometry in the* ***(A)*** *spleen and* ***(D)*** *PALN. The total number of GC B cells calculated in* ***(B)*** *spleen and* ***(E)*** *PALN. The proportion of GC cells within spleen which are* ***(C)*** *IgM+ and* ***(F)*** *IgM- is depicted. Each dot represents one mouse, graphs show mean +/- SD. Statistics carried out using Mann-Whitney test, * P < 0.05; ** P < 0.01; *** P < 0.001; **** P < 0.0001.*

Looking at the relationship between plasma LDL levels and the splenic GC population, there was a direct correlation between these 2 variables in female LDLr$^{-/-}$ AEL mice fed HFHC diet for 4 weeks while this was absent from the other 2 diet types demonstrating that dietary cholesterol has a direct impact on GC responses within the spleen *(Figure 119)*.

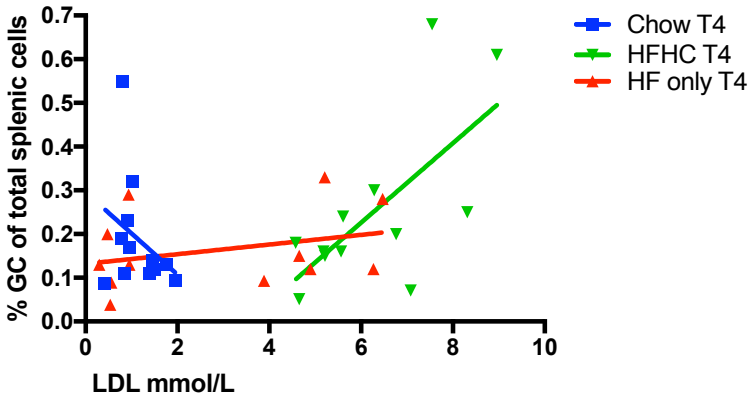

Figure 119. ***Relationship between GC population and LDL levels in female AEL mice after 4 weeks.*** *Female AEL mice were fed either chow (blue), high fat high cholesterol diet (HFHC; green) or high fat only diet (HF only; red) for 4 weeks (T4). Graph depicts the relationship between plasma LDL cholesterol and splenic GC population.*

The total number of EYFP cells, a measure of GC activity, was increased in mice fed the HFHC but not in the HF only diet-fed female LDLr$^{-/-}$ AEL mice in the spleen and PALN *(Figure 120)*. This demonstrates that dietary cholesterol exacerbates the GC response in female LDLr$^{-/-}$ AEL mice.

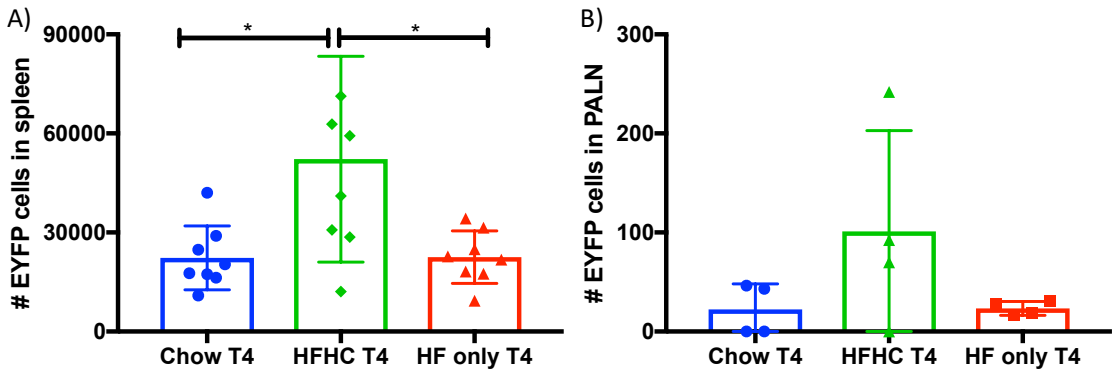

Figure 120. ***No increase in EYFP cell numbers after HF only diet in female AEL mice after 4 weeks.*** *Female AEL mice were fed either chow (blue), high fat high cholesterol (HFHC; green) or high fat only (HF only; red) diets for 4 weeks (T4). Tamoxifen was administered, 9mg via oral gavage, 48hrs prior to sacrifice to induce EYFP labelling. The absolute number of EYFP cells was assessed by flow cytometry and calculated using total cell numbers for the (A) spleen and (B) PALN. Each dot represents one mouse, graphs show mean +/- SD. Statistics carried out using Mann-Whitney test, * P < 0.05; ** P < 0.01; *** P < 0.001; **** P < 0.0001.*

The high fat high cholesterol diet induced expansion of the proportion and absolute number of EYFP GC cells in the spleen which was blunted when female LDLr$^{-/-}$ AEL mice were fed the HF only diet *(Figure 121A, B)*. Similar results were observed for EYFP memory cells in the spleen *(Figure 121D)*. Both HFHC and HF only diets resulted in expansion of the proportion of splenic EYFP GC cells which were IgM+ *(Figure 121C)*.

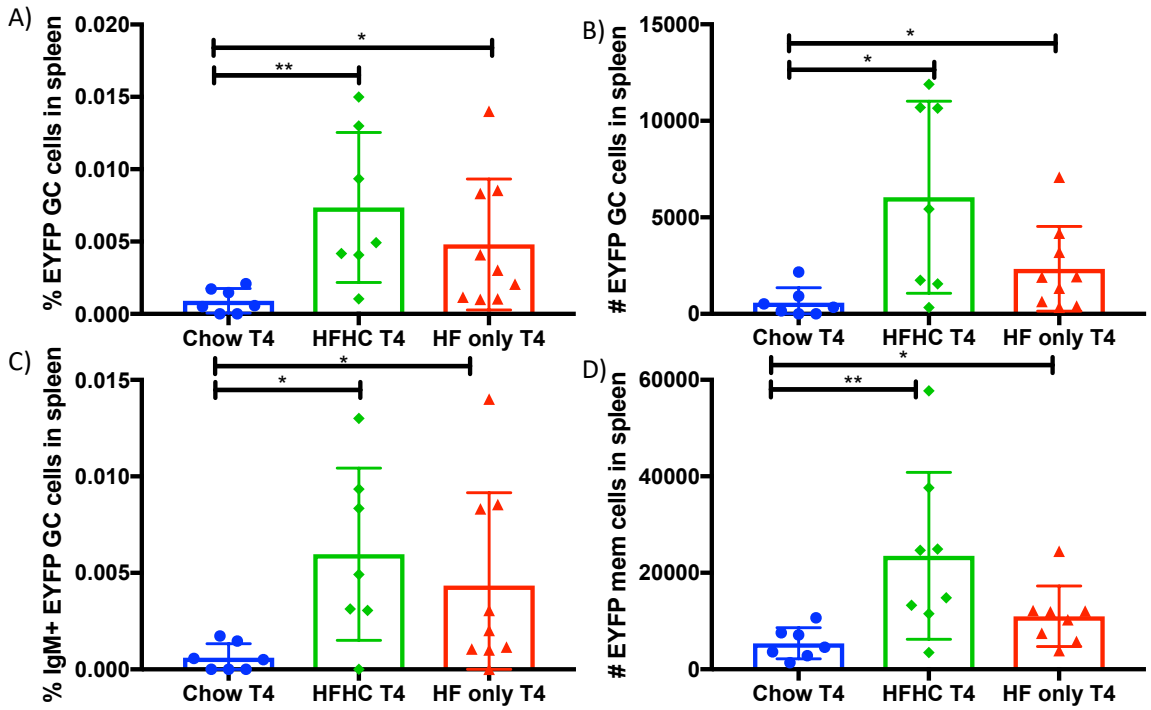

Figure 121. ***Increased EYFP GC cells in both high fat-containing diets in female AEL mice after 4 weeks.*** *Female AEL mice were fed either chow (blue), high fat high cholesterol (HFHC; green) or high fat only (HF only; red) diets for 4 weeks (T4). Tamoxifen was administered, 9mg via oral gavage, 48hrs prior to sacrifice to induce EYFP labelling. Within the spleen (A) The percentage and (B) the absolute number of EYFP cells with GC phenotype and (C) those EYFP GC cells which are IgM+. (D) shows the number of EYFP memory cells. Each dot represents one mouse, graphs show mean +/- SD. Statistics carried out using Mann-Whitney test, * P < 0.05; ** P < 0.01; *** P < 0.001; **** P < 0.0001.*

In the PALNs, HFHC diet induced expansion of the PC population, both total and EYFP labelled, while the EYFP memory population, especially IgM+ isotype, was diminished in both high fat containing diets *(Figure 122)*.

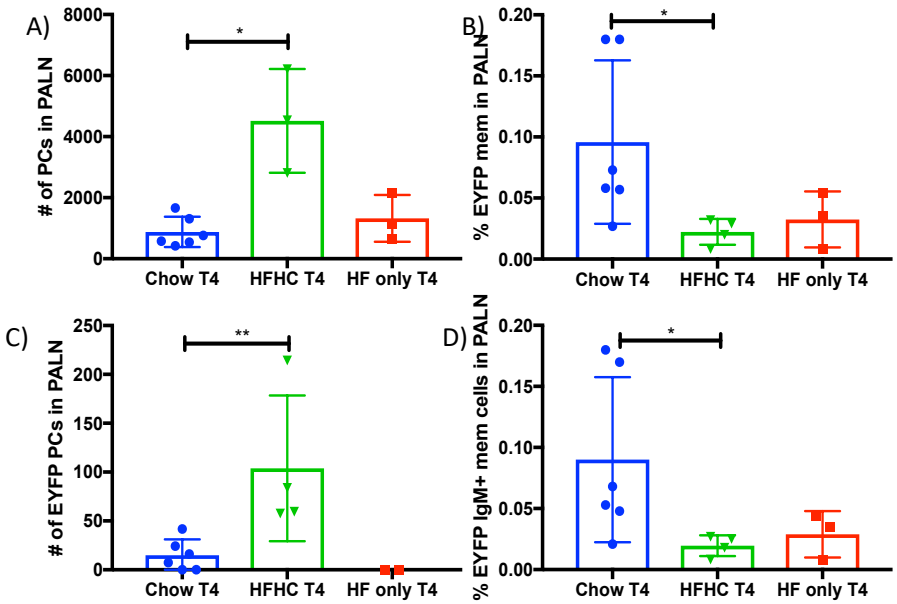

Figure 122. ***Impact of diet on GC-derived cells of the PALN in female AEL mice after 4 weeks.*** *Female AEL mice were either fed chow (blue), high fat high cholesterol (HFHC; green) or high fat only (HF only; red) diets for 4 weeks (T4). Tamoxifen was administered, 9mg via oral gavage, 48hrs prior to sacrifice to induce EYFP labelling. Within the para-aortic lymph nodes (PALN), the number of* ***(A)*** *plasma cells (PC) and those which are* ***(C)*** *EYFP labelled. The proportion of cells which are* ***(B)*** *EYFP memory and those which are* ***(D)*** *IgM+ EYFP memory cells. Each dot represents one mouse, graphs show mean +/- SD. Statistics carried out using Mann-Whitney test, * P < 0.05; ** P < 0.01; *** P < 0.001; **** P < 0.0001.*

The GC population within the PPs was suppressed by the presence of HF containing diets compared to chow diet, mainly due to the IgM isotype *(Figure 123)*.

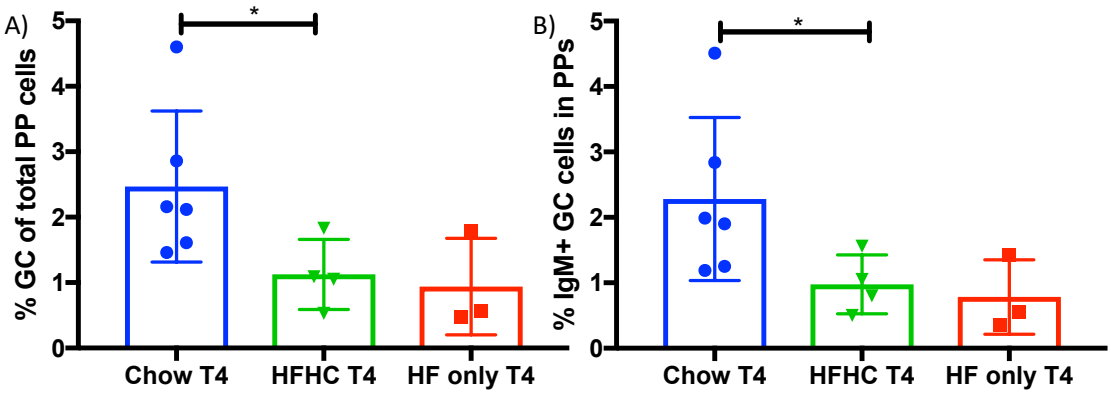

Figure 123. ***Reduced GC population in PPs upon high fat-containing diet feeding in female AEL mice after 4 weeks.*** *Female AEL mice were either fed chow (blue), high fat high cholesterol (HFHC; green) or high fat only (HF only; red) diets for 4 weeks (T4). Within the Peyer's patches (PP), the proportion of* ***(A)*** *GC cells and* ***(B)*** *IgM+ GC cells is depicted using flow cytometry. Each dot represents one mouse, graphs show mean +/- SD. Statistics carried out using Mann-Whitney test, * P < 0.05; ** P < 0.01; *** P < 0.001; **** P < 0.0001.*

In the Peyer's patches, the proportion of EYFP cells, and those which were of GC and memory phenotype, were diminished upon HFHC and HF only feeding *(Figure 124A, B, C)*. Both IgM+ and IgM- EYFP memory cells were reduced in high fat containing diets *(Figure 124D, E)*. IgM+ EYFP PCs showed the same result *(Figure 124F)*.

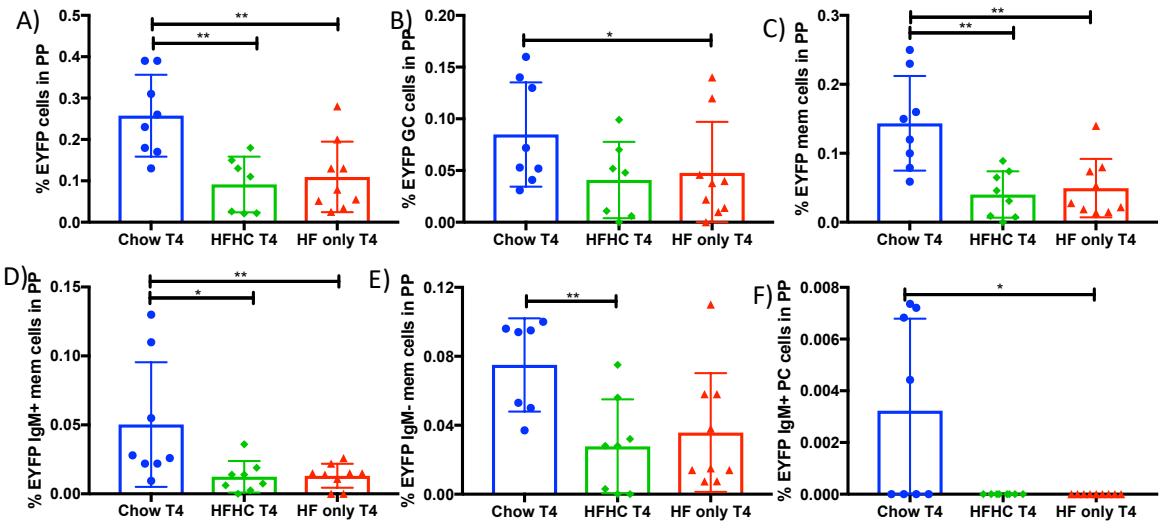

Figure 124. ***Impact of diet on EYFP cells of the PPs in female AEL mice after 4 weeks.*** *Female AEL mice were fed either chow (blue), high fat high cholesterol (HFHC; green) or high fat only (HF only; red) diets for 4 weeks (T4). Tamoxifen was administered, 9mg via oral gavage, 48hrs prior to sacrifice to induce EYFP labelling. Within the Peyer's patches (PP), (A) proportion of EYFP cells, (B) percentage of EYFP GC, (C) percentage of EYFP memory (mem), percentage of EYFP memory cells which are (D) IgM+ and (E) IgM- and the proportion of EYFP IgM+ plasma cells (PCs). Each dot represents one mouse, graphs show mean +/- SD. Statistics carried out using Mann-Whitney test, * P < 0.05; ** P < 0.01; *** P < 0.001; **** P < 0.0001.*

The class switch ratio was reduced in HFHC diet-fed female mice compared to chow diet-fed female LDLr$^{-/-}$ AEL mice, yet class switching was not impacted by HF only feeding in both the LN and PALN *(Figure 125)*.

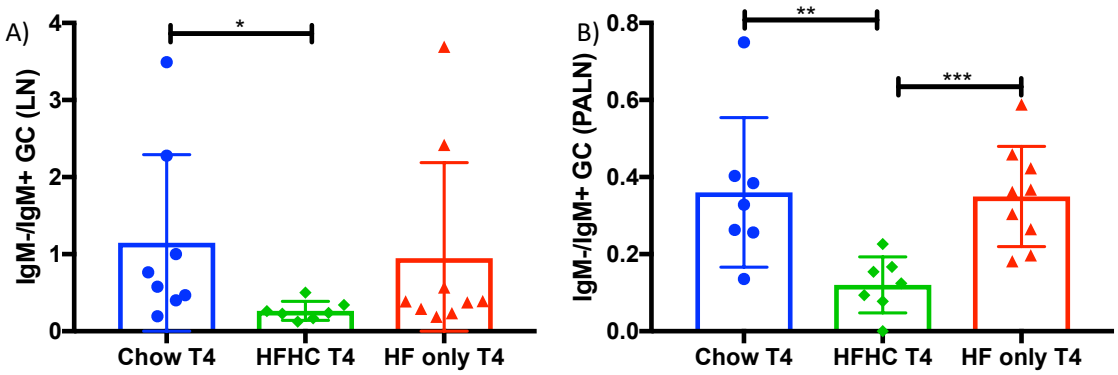

Figure 125. ***The class switch ratio was not reduced in HF only diet-fed female AEL mice after 4 weeks.*** *Female AEL mice were fed either chow (blue), high fat high cholesterol (HFHC; green) or high fat only (HF only; red) diets for 4 weeks (T4). The class switch ratio (IgM- GC/IgM+ GC) is shown for (A) the inguinal lymph nodes (LN) and (B) para-aortic lymph nodes (PALN). Each dot represents one mouse, graphs show mean +/- SD. Statistics carried out using Mann-Whitney test, * P < 0.05; ** P < 0.01; *** P < 0.001; **** P < 0.0001.*

The GC to memory ratio, which provides a measure of GC longevity, increased in the PALN and PPs of female LDLr$^{-/-}$ AEL mice fed the HFHC diet compared to those fed chow *(Figure 126)*. This effect was reduced in HF only diet-fed female LDLr$^{-/-}$ AEL mice *(Figure 126)*.

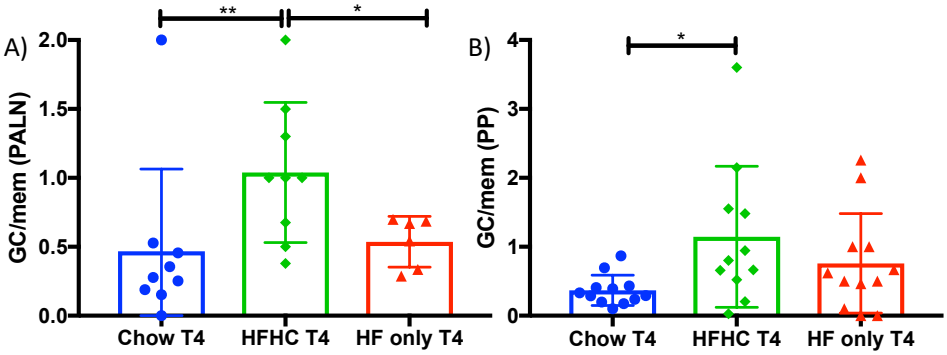

Figure 126. ***Reduced GC to memory ratio in HF only diet compared to HFHC diet in female AEL mice after 4 weeks.*** *Female AEL mice were fed either chow (blue), high fat high cholesterol (HFHC; green) or high fat only (HF only; red) diets for 4 weeks (T4). Tamoxifen was administered, 9mg via oral gavage, 48hrs prior to sacrifice to induce EYFP labelling. The GC to memory ratio was calculated by dividing the EYFP GC proportion by the EYFP memory proportion and shown for* ***(A)*** *para-aortic lymph nodes (PALN) and* ***(B)*** *Peyer's patches (PP). Each dot represents one mouse, graphs show mean +/- SD. Statistics carried out using Mann-Whitney test, * P < 0.05; ** P < 0.01; *** P < 0.001; **** P < 0.0001.*

In the spleen and PALN, HFHC diet induced expansion of the plasma cell pool. This effect was diminished in female LDLr$^{-/-}$ AEL mice fed the HF only diet *(Figure 127)*.

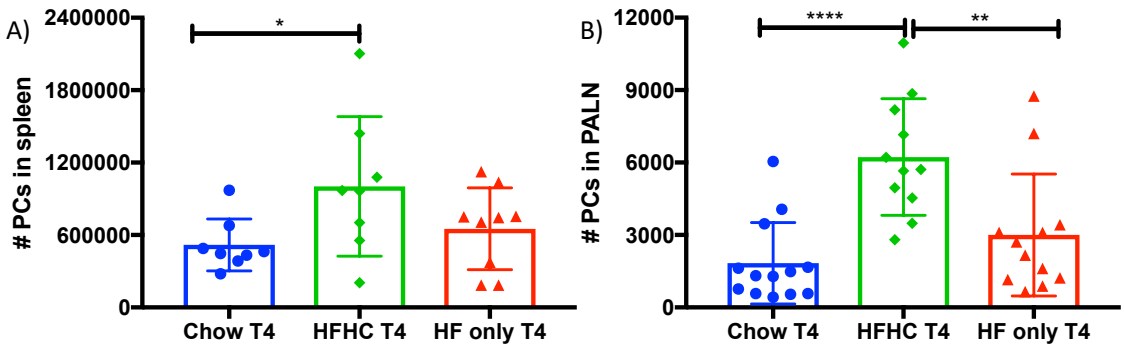

Figure 127. ***Plasma cell pool not expanded to same extent as HFHC in HF only diet-fed female AEL mice after 4 weeks.*** *Female AEL mice were fed either chow (blue), high fat high cholesterol (HFHC; green) or high fat only (HF only; red) diets for 4 weeks (T4). The proportion of plasma cells as determined by flow cytometry was multiplied by the total cell number to give a total plasma cell (PC) number in* ***(A)*** *the spleen and* ***(B)*** *the para-aortic lymph nodes (PALN). Each dot represents one mouse, graphs show mean +/- SD. Statistics carried out using Mann-Whitney test, * P < 0.05; ** P < 0.01; *** P < 0.001; **** P < 0.0001.*

In the serum, IgG1 was suppressed when female LDLr$^{-/-}$ AEL mice were fed both HF containing diets, but this effect was smaller when female LDLr$^{-/-}$ AEL mice were fed HF only diet *(Figure 128A)*. IgM titres were increased upon HFHC feeding and to a lesser extent upon HF only feeding *(Figure 128B)*. IgG titres against double stranded DNA, a classic autoantigen, were elevated in HFHC diet-fed female LDLr$^{-/-}$ AEL mice only; this was not observed in HF only diet-fed female mice *(Figure 128C)*.

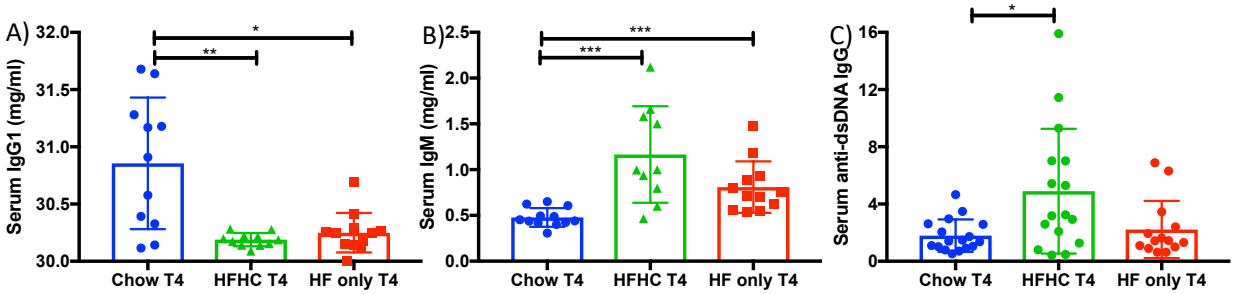

Figure 128. ***Impact of diet on serum antibody levels in female AEL mice after 4 weeks.*** *Female AEL mice were fed either chow (blue), high fat high cholesterol (HFHC; green) or high fat only (HF only; red) diets for 4 weeks (T4). Serum antibodies were measured by ELISA for* ***(A)*** *IgG1,* ***(B)*** *IgM and* ***(C)*** *anti-double stranded DNA (dsDNA) IgG. Each dot represents one mouse, graphs show mean +/- SD. Statistics carried out using Mann-Whitney test, * P < 0.05; ** P < 0.01; *** P < 0.001; **** P < 0.0001.*

Serum analysis was also conducted using a multiplex array for other cytokines. Serum levels of CXCL1 and IL1β were increased significantly in female LDLr$^{-/-}$ AEL mice fed both the high fat high cholesterol diet and high fat only diet *(Figure 129A, B)*. Meanwhile, serum IL6 and IL10 levels were significantly elevated in HFHC diet-fed female LDLr$^{-/-}$ AEL mice but not in HF only diet-fed female LDLr$^{-/-}$ AEL mice *(Figure 129C, D)*.

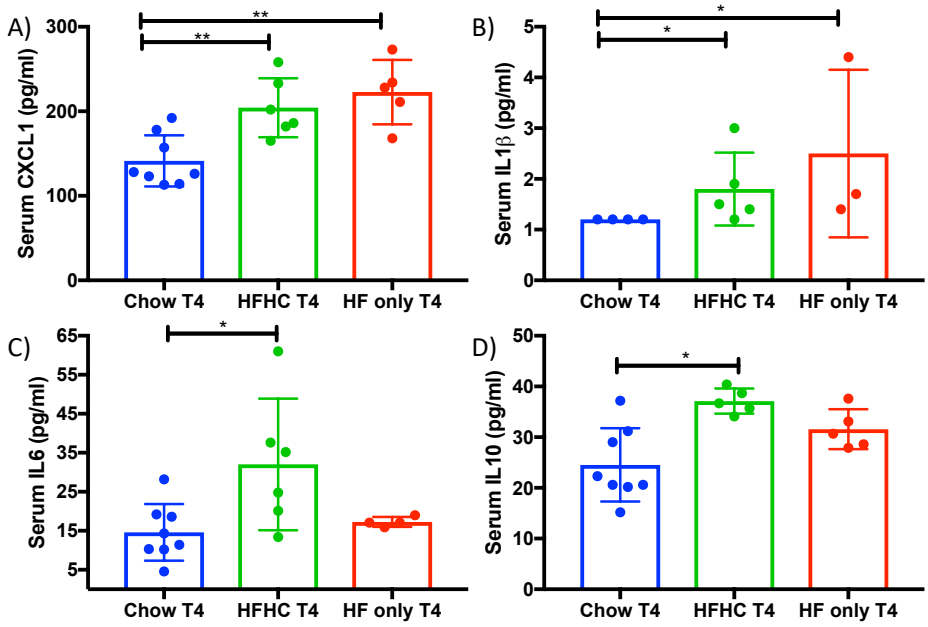

Figure 129. ***Impact of diet on serum cytokine levels in female AEL mice after 4 weeks.*** *Female AEL mice were fed either chow (blue), high fat high cholesterol (HFHC; green) or high fat only (HF only; red) diets for 4 weeks (T4). Serum was analysed using MSD multiplex array for* ***(A)*** *CXCL1,* ***(B)*** *IL1β,* ***(C)*** *IL6 and* ***(D)*** *IL10. Each dot represents one mouse, graphs show mean +/- SD. Statistics carried out using Mann-Whitney test, * P < 0.05; ** P < 0.01; *** P < 0.001; **** P < 0.0001.*

Furthermore, plasma IL6 and LDL levels showed a direct correlation indicating a link between hypercholesterolemia and systemic inflammation *(Figure 130)*.

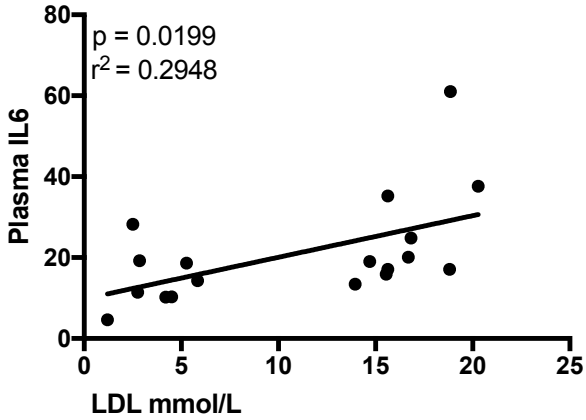

Figure 130. ***Relationship between IL6 and LDL in female AEL mice after 4 weeks.*** *Correlation between plasma LDL levels and IL6 levels in female mice fed chow, high fat high cholesterol or high fat only diets for 4 weeks. Each dot represents one mouse.*

Dietary cholesterol is known to induce liver inflammation. Thus, expression of inflammatory genes within the liver was analysed. HFHC diet induced upregulation of CXCL1, F4/80 and MCP1 significantly and also Mac2 and TNF but these did not reach significance *(Figure 131A, B, E)*. HF only diet prevented this upregulation of F4/80 and Mac2 significantly and also CXCL1 and MCP1 but not significantly *(Figure 131B, D, A, E)*. Intriguingly, IL6 gene expression was

downregulated in the HFHC diet-fed group while the effect was absent from HF only diet-fed female LDLr$^{-/-}$ AEL mice *(Figure 131C)*.

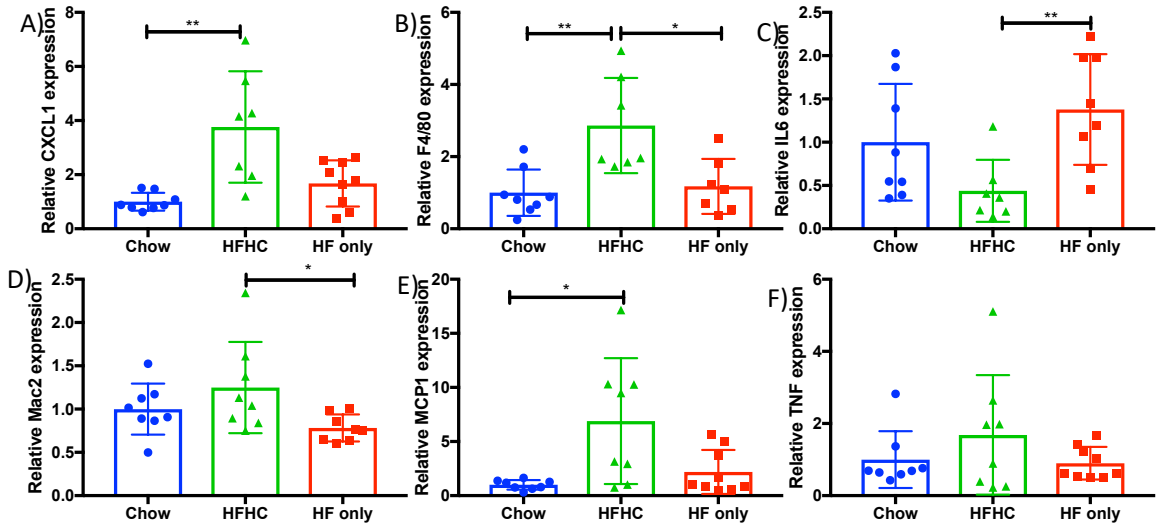

*Figure 131.**Impact of diet on inflammatory gene expression in the liver of female AEL mice after 4 weeks.** Female AEL mice were fed either chow (blue), high fat high cholesterol (HFHC; green) or high fat only (HF only; red) diets for 4 weeks (T4). Liver tissue was analysed by qPCR for gene expression of (A) CXCL1, (B) F4/80, (C) IL6, (D) Mac2, (E) MCP1 and (F) TNF. Each dot represents one mouse, graphs show mean +/- SD. Statistics carried out using Mann-Whitney test, * P < 0.05: ** P < 0.01: *** P < 0.001: **** P < 0.0001.*

Both CXCL1 and MCP1 transcript levels showed a positive correlation with plasma LDL levels indicating a link between hepatic inflammation and hypercholesterolemia *(Figure 132)*.

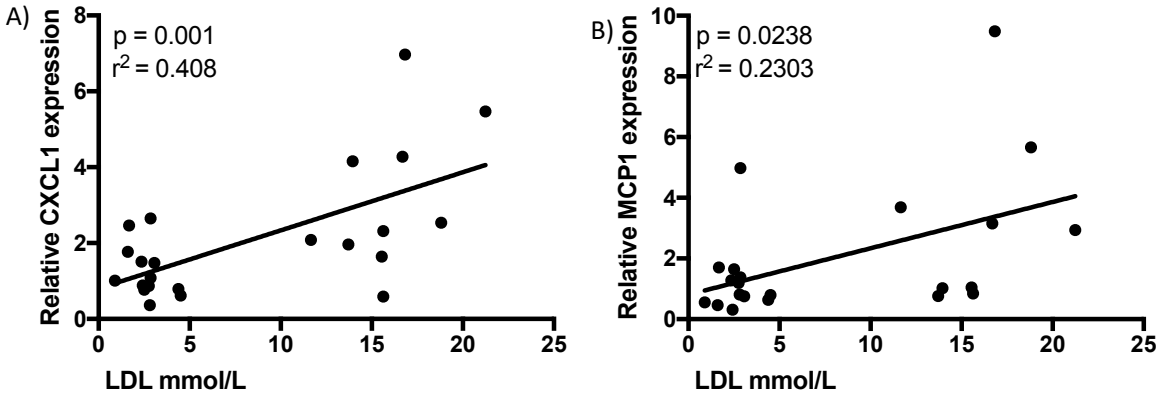

*Figure 132.**Relationship between inflammatory gene expression and plasma LDL levels after 4 weeks.** Correlation between plasma LDL and hepatic (A) CXCL1 expression (B) MCP1 expression in female mice fed chow, high fat high cholesterol or high fat only diets for 4 weeks. Each dot represents one mouse.*

To determine the role of dietary cholesterol without the atherosclerosis-prone LDLr$^{-/-}$ background, experiments were also conducted in female WT AEL mice. In female WT AEL mice after 4 weeks of diet, there was no significant difference in weight or cholesterol levels between different diet groups *(Figure 133)*.

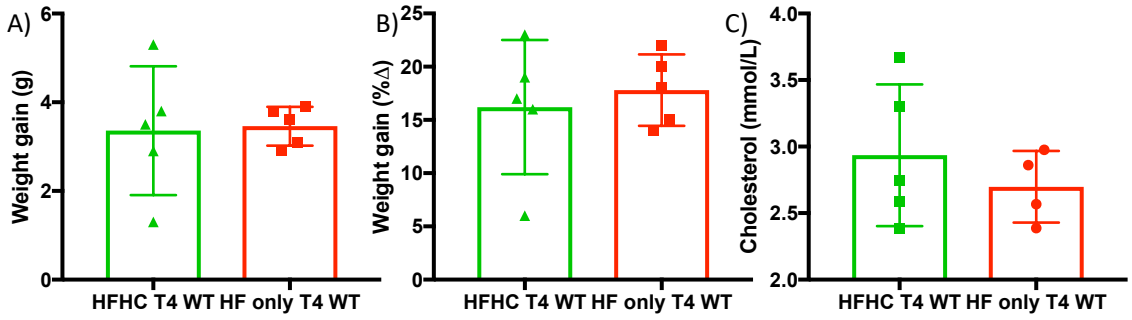

Figure 133. ***No diet-related difference in weight or cholesterol levels in female WT AEL mice after 4 weeks.*** *Difference in weight from start of experiment, female WT AEL mice aged 8 weeks old, to end of experiment after 4 weeks of diet (T4; mice aged 12 weeks old) of either high fat high cholesterol (HFHC; green) or high fat only (HF only; red) in* ***(A)*** *absolute terms and* ***(B)*** *as proportion. Each dot represents 1 mouse, graphs show mean +/- SD.* ***(C)*** *Total cholesterol was measured using colorimetric assay. Statistics carried out using Mann-Whitney test, * P < 0.05; ** P < 0.01; *** P < 0.001; **** P < 0.0001.*

Total cell number and B cell number was not significantly affected in either the spleen or PALNs of female WT AEL mice on diet for 4 weeks *(Figure 134)*.

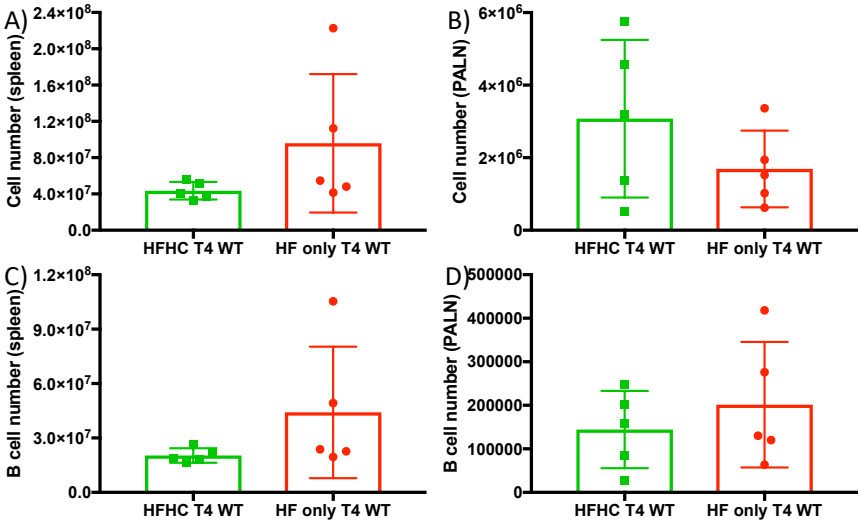

Figure 134. ***Total and B cell numbers unaffected by diet in female WT AEL mice after 4 weeks.*** *Female WT AEL mice were fed either high fat and high cholesterol (HFHC; green) or high fat only diet (HF only; red) for 4 weeks (T4). Total cell number was calculated for* ***(A)*** *spleen and* ***(B)*** *PALN. Total B cell number was calculated for* ***(C)*** *spleen and* ***(D)*** *PALN. Each dot represents one mouse, graphs show mean +/- SD.*

The proportion and absolute number of GC B cells was not significantly impacted by diet type in the spleen and PALN of female WT AEL mice after 4 weeks *(Figure 135)*.

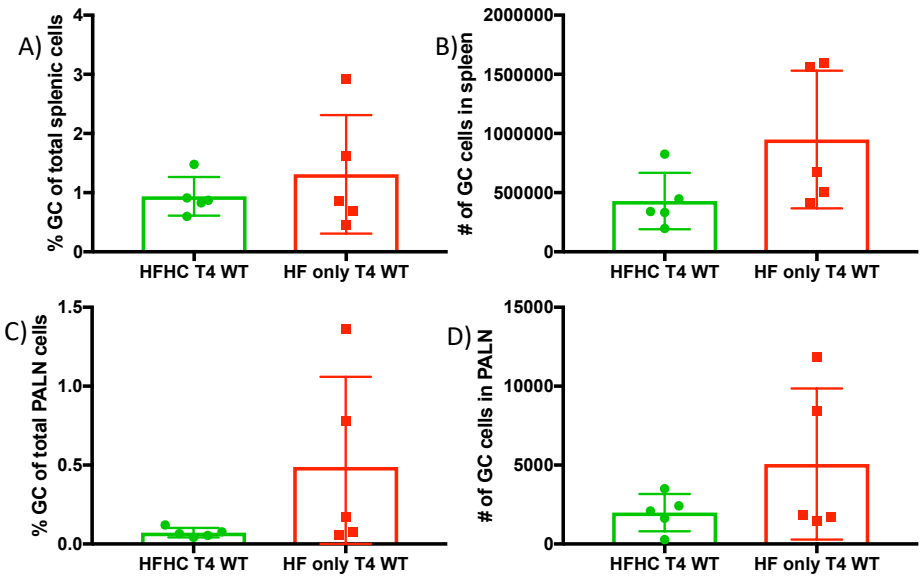

Figure 135. ***Impact of 4 week diet on GC population in female AEL WT mice.*** *Female AEL WT mice were fed either high fat high cholesterol diet (HFHC; green) or high fat only diet (HF only; red) for 8 weeks (T4). The proportion of GC cells as assessed by flow cytometry in the* ***(A)*** *spleen and* ***(C)*** *PALN. The total number of GC B cells calculated in* ***(B)*** *spleen and* ***(D)*** *PALN. Each dot represents one mouse, graphs show mean +/- SD.*

6.4.1.2.2 8-week cholesterol free diet in female LDLr$^{-/-}$ AEL mice

The experiment was repeated in LDLr$^{-/-}$ females for a duration of 8 weeks to determine whether dietary cholesterol had a similar effect at a later timepoint. Both high fat containing diets induced weight gain greater than that of chow in absolute and proportional terms *(Figure 136)*.

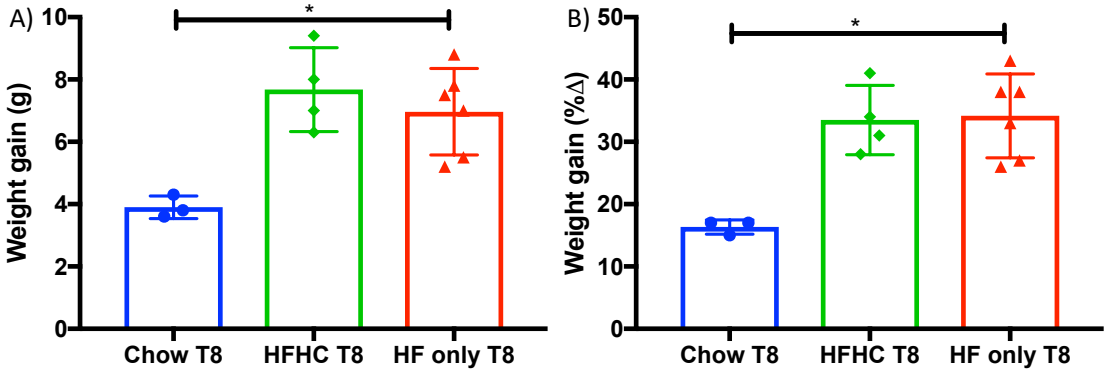

Figure 136. ***Diet-related weight gain after 8 weeks in female AEL mice.*** *Difference in weight from start of experiment, female AEL mice aged 8 weeks old, to end of experiment after 8 weeks of diet (mice aged 16 weeks old) of either chow (blue), high fat high cholesterol (HFHC; green) or high fat only (HF only; red) in* ***(A)*** *absolute terms and* ***(B)*** *as proportion. Each dot represents 1 mouse, graphs show mean +/- SD. Statistics carried out using Mann-Whitney test, * P < 0.05; ** P < 0.01; *** P < 0.001; **** P < 0.0001.*

The HFHC and HF only diets did not show any significant differences in any of the cholesterol parameters measured *(Figure 137)*. As results were so variable, this experiment would need repeating to determine if this result is true. Furthermore, after 8 weeks of diet it is expected that there would be greater differences between chow and HFHC diets.

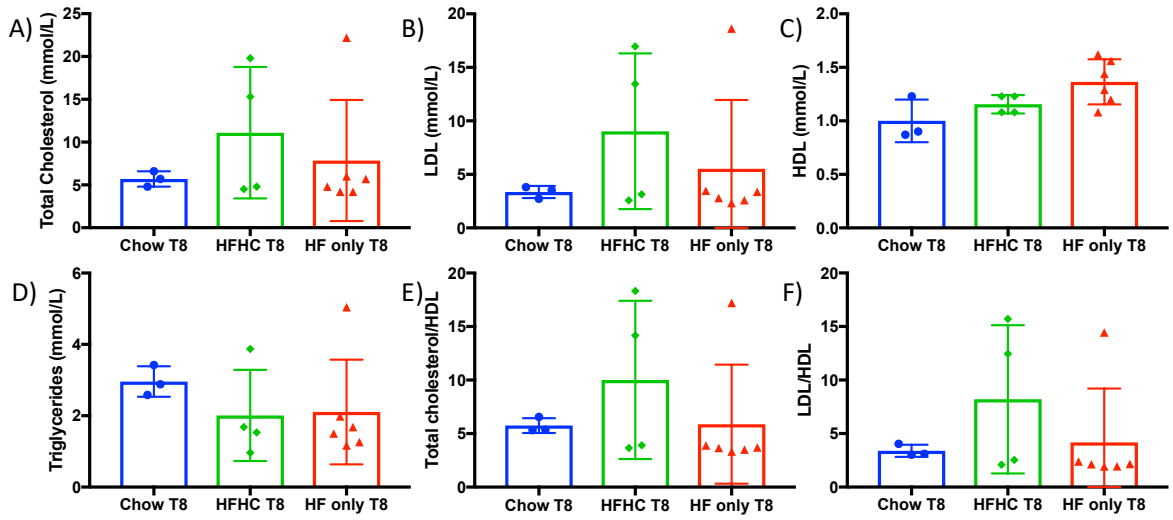

Figure 137. ***No impact of diet on serum lipid levels in female AEL mice after 8 weeks.*** *Female AEL mice were fed either chow (blue), high fat and high cholesterol (HFHC; green) or high fat only diet (HF only; red) for 8 weeks. Serum was analysed at study end after 4hr fast for* ***(A)*** *total cholesterol,* ***(B)*** *high density lipoprotein (HDL),* ***(C)*** *low density lipoprotein (LDL) and* ***(D)*** *triglycerides. The ratio of total cholesterol: HDL was calculated* ***(E)*** *as was the LDL: HDL ratio* ***(F)****. Each dot represents one mouse, graphs show mean +/- SD. Statistics carried out using Mann-Whitney test, * P < 0.05; ** P < 0.01; *** P < 0.001; **** P < 0.0001.*

Both high fat containing diets induced hypercellularity and B cell expansion of the spleen and PALN after 8 weeks compared to chow diet *(Figure 138)*. There was a trend toward smaller total and B cell number in the spleen and PALN in female LDLr$^{-/-}$ AEL mice fed HF only diet compared to HFHC diet *(Figure 138)*. Of note, the chow diet-fed female LDLr$^{-/-}$ AEL mice in this study had abnormally small spleens and therefore the data obtained from, and comparisons made to the chow diet-fed female LDLr$^{-/-}$ AEL mice were not reliable. Data was included to show that chow diet group was present, but the study would need repeating to draw solid conclusions about the differences between chow diet and high fat-containing diet feeding after 8 weeks in female LDLr$^{-/-}$ AEL mice.

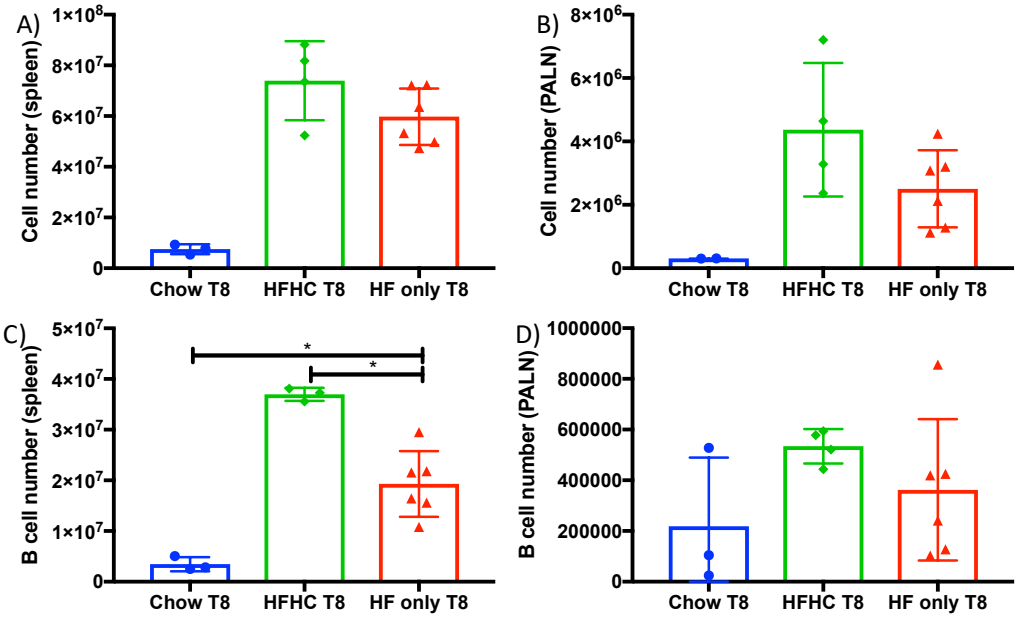

Figure 138. ***Impact of diet after 8 weeks on cell numbers in female AEL mice.*** *Female AEL mice were fed either chow (blue), high fat and high cholesterol (HFHC; green) or high fat only diet (HF only; red) for 4 weeks (T4). Total cell number was calculated for (A) spleen and (B) PALN. Total B cell number was calculated for (C) spleen and (D) PALN. Each dot represents one mouse, graphs show mean +/- SD. Statistics carried out using Mann-Whitney test, * P < 0.05; ** P < 0.01; *** P < 0.001; **** P < 0.0001.*

Both HF only and HFHC diets resulted in expansion of the GC population both in proportional and absolute terms compared to chow diet in the spleen *(Figure 139)*. In the spleen, the total number of GC cells was slightly lower in HF only diet-fed female LDLr$^{-/-}$ AEL mice compared to HFHC diet-fed female LDLr$^{-/-}$ AEL mice *(Figure 139B)*. There were no differences in the PALN *(Figure 139D)*.

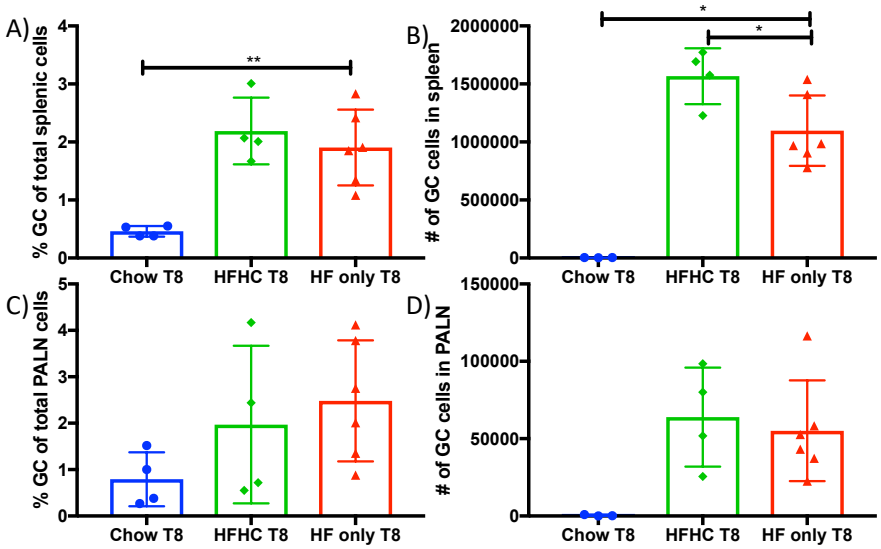

Figure 139. ***Impact of diet after 8 weeks on GC population in female AEL mice.*** *Female AEL mice were fed either chow (blue), high fat high cholesterol diet (HFHC; green) or high fat only diet (HF only; red) for 8 weeks (T8). The proportion of GC cells as assessed by flow cytometry in the* ***(A)*** *spleen and* ***(C)*** *PALN. The total number of GC B cells calculated in* ***(B)*** *spleen and* ***(D)*** *PALN. Each dot represents one mouse, graphs show mean +/- SD. Statistics carried out using Mann-Whitney test, * P < 0.05; ** P < 0.01; *** P < 0.001; **** P < 0.0001.*

Interestingly, both in the PALN and PPs the plasma cell population was increased upon HF only diet feeding compared to HFHC diet feeding *(Figure 140A, B)*. Furthermore, IgM- plasma cells were responsible for this increase *(Figure 140D, E)*. Contrastingly, in the BM the HF only diet-fed female LDLr$^{-/-}$ AEL mice had reduced proportions of EYFP+ PCs as a result of an IgM- reduction *(Figure 140C, F)*.

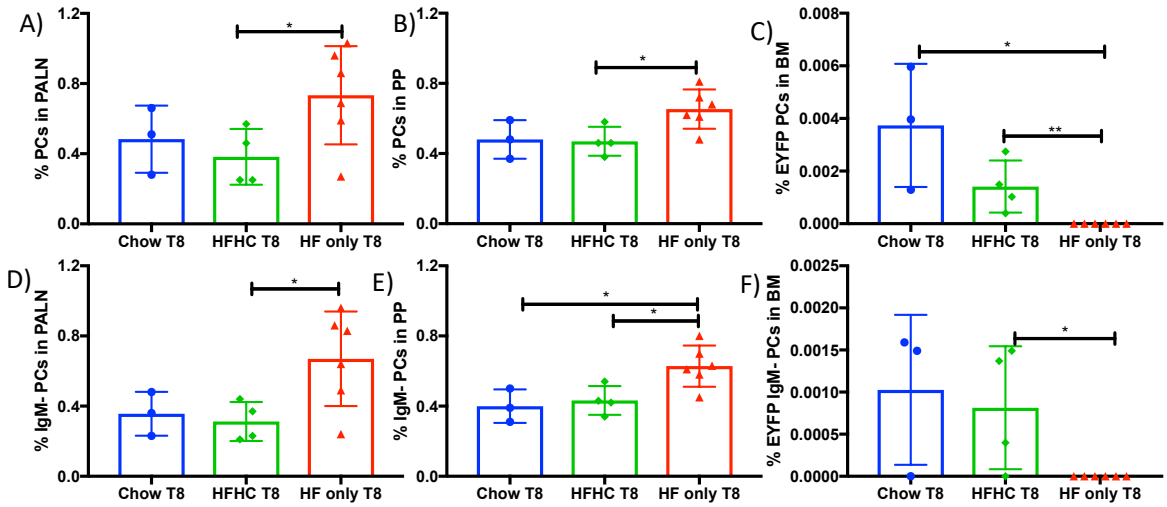

Figure 140. ***Impact of 8 weeks diet on PCs in female AEL mice.*** *Female AEL mice were fed either chow (blue), high fat high cholesterol (HFHC; green) or high fat only (HF only; red) diets for 8 weeks (T8). Tamoxifen was administered, 9mg via oral gavage, 48hrs prior to sacrifice to induce EYFP labelling. Flow cytometric analysis of plasma cells (PCs) and those which are IgM- in* ***(A)*** *para-aortic lymph nodes (PALN),* ***(B)*** *Peyer's patches (PP),* ***(D)*** *PALN and* ***(E)*** *PP can be observed respectively.* ***(C)*** *shows EYFP PCs in the bone marrow (BM) and* ***(F)*** *shows EYFP IgM- PCs in the BM. Each dot represents one mouse, graphs show mean +/- SD. Statistics carried out using Mann-Whitney test, * P < 0.05; ** P < 0.01; *** P < 0.001; **** P < 0.0001.*

Similarly, to the 4-week timepoint, serum IgG1 levels were reduced in HFHC diet-fed female LDLr$^{-/-}$ AEL mice compared to chow diet-fed female LDLr$^{-/-}$ AEL mice, but this effect was less pronounced in HF only diet-fed female LDLr$^{-/-}$ AEL mice *(Figure 141)*.

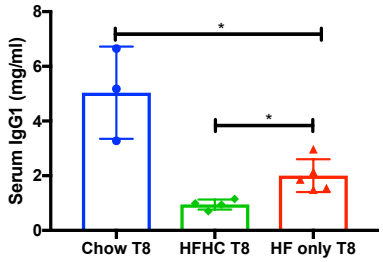

Figure 141. ***Effect of diet on serum IgG1 in female AEL mice after 8 weeks.*** *Female AEL mice were fed either chow (blue), high fat high cholesterol (HFHC; green) or high fat only (HF only; red) diets for 8 weeks (T8). Serum antibodies were measured by ELISA for IgG1. Each dot represents one mouse, graphs show mean +/- SD. Statistics carried out using Mann-Whitney test, * P < 0.05; ** P < 0.01; *** P < 0.001; **** P < 0.0001.*

6.4.1.2.3 4-week cholesterol free diet in male LDLr$^{-/-}$ AEL mice

In male LDLr$^{-/-}$ AEL mice, both high fat containing diets increased weight but only the HF only diet did so significantly *(Figure 142A, B)*. Total cholesterol levels in the blood were significantly increased in both HFHC and HF only diet-fed male LDLr$^{-/-}$ AEL mice compared to chow diet-fed male LDLr$^{-/-}$ AEL mice *(Figure 142C)*.

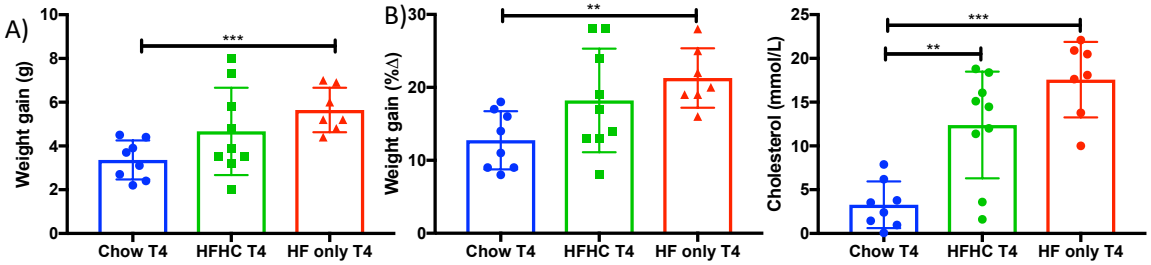

Figure 142. ***Impact of diet after 4 weeks on weight gain in male AEL mice.*** *Difference in weight from start of experiment, male AEL mice aged 8 weeks old, to end of experiment after 4 weeks of diet (T4; mice aged 12 weeks old) of either chow (blue), high fat high cholesterol (HFHC; green) or high fat only (HF only; red) in* ***(A)*** *absolute terms and* ***(B)*** *as proportion.* ***(C)*** *Total cholesterol was measured using colorimetric assay. Each dot represents one mouse, graphs show mean +/- SD. Statistics carried out using Mann-Whitney test, * P < 0.05; ** P < 0.01; *** P < 0.001; **** P < 0.0001.*

The GC population was unaffected in the spleen by diet type in male LDLr$^{-/-}$ AEL mice *(Figure 143A, B)*. The proportion of the GC population was increased significantly in the HF only diet-fed male LDLr$^{-/-}$ AEL mice while absolute numbers of GC cells was increased in both high fat containing diets but to a greater extent in the HF only diet within the PALN *(Figure 143C, D)*.

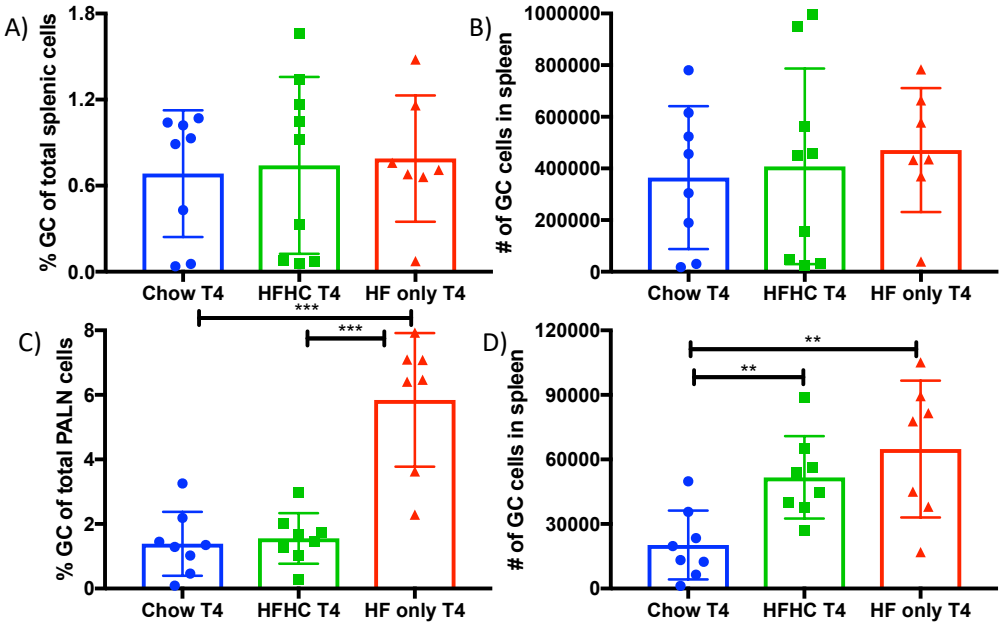

Figure 143. ***Impact of diet on GC population after 4 weeks in male AEL mice.*** *Male AEL mice were fed either chow (blue), high fat high cholesterol diet (HFHC; green) or high fat only diet (HF only; red) for 4 weeks (T4). The proportion of GC cells as assessed by flow cytometry in the* ***(A)*** *spleen and* ***(C)*** *PALN. The total number of GC B cells calculated in* ***(B)*** *spleen and* ***(D)*** *PALN. Each dot represents one mouse, graphs show mean +/- SD. Statistics carried out using Mann-Whitney test, * P < 0.05; ** P < 0.01; *** P < 0.001; **** P < 0.0001.*

Both IgM+ and IgM- GC cells were expanded within the LNs and PALNs of HF only diet-fed male LDLr$^{-/-}$ AEL mice *(Figure 144)*.

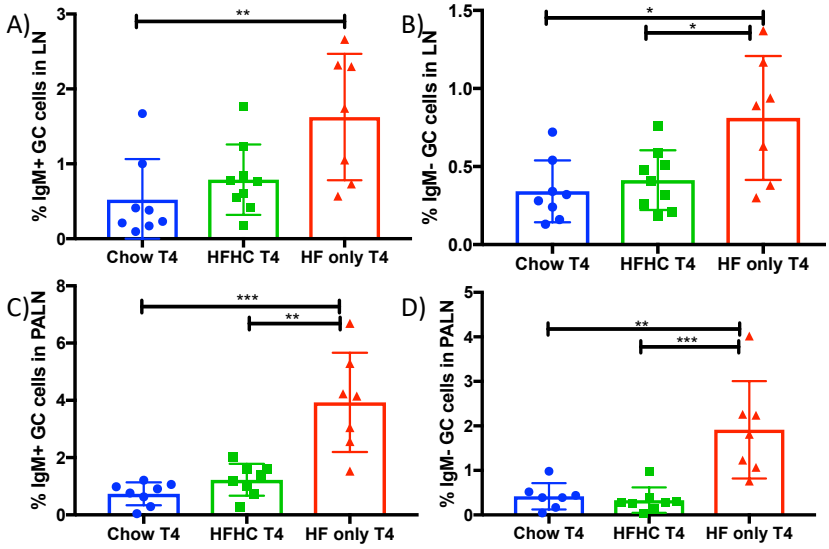

Figure 144. ***Expansion of IgM+ and IgM- GC clones after 4 weeks of HF only diet in male AEL mice.*** *Male AEL mice were fed either chow (blue), high fat high cholesterol diet (HFHC; green) or high fat only diet (HF only; red) for 4 weeks (T4). The proportion of IgM+ GC cells as assessed by flow cytometry in the* ***(A)*** *lymph nodes (LN) and* ***(C)*** *para-aortic lymph nodes (PALN). The proportion of IgM- GC cells in the* ***(B)*** *LN and* ***(D)*** *PALN. Each dot represents one mouse, graphs show mean +/- SD. Statistics carried out using Mann-Whitney test, * P < 0.05; ** P < 0.01; *** P < 0.001; **** P < 0.0001.*

In the Peyer's patches, the HFHC diet suppressed GC responses; both total and EYFP labelled and affected both IgM+ and IgM- cells *(Figure 145)*. The HF only diet-fed male LDLr$^{-/-}$ AEL mice did not show this total GC suppression but did show reduced levels of EYFP labelled IgM+ and IgM- GC cells *(Figure 145E, F)*.

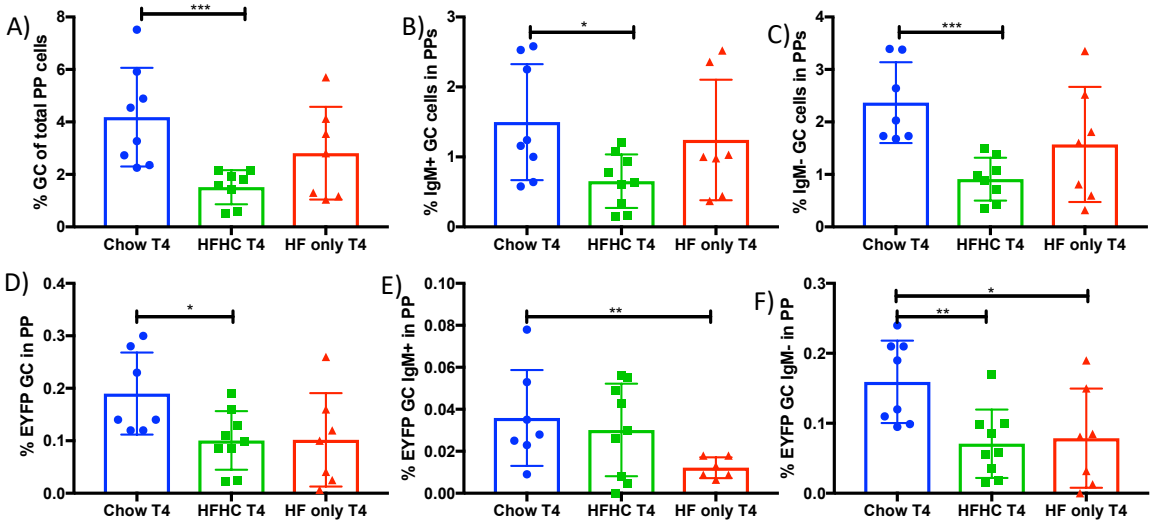

Figure 145. ***Impact of diet on GC responses of the PPs after 4 weeks in male AEL mice.*** *Male AEL mice were fed either chow (blue), high fat high cholesterol diet (HFHC; green) or high fat only diet (HF only; red) for 4 weeks (T4). Tamoxifen was administered, 9mg via oral gavage, 48hrs prior to sacrifice to induce EYFP labelling. The proportion of cells within the Peyer's patches (PP) which were* ***(A)*** *total GC,* ***(B)*** *IgM+ GC,* ***(C)*** *IgM- GC,* ***(D)*** *EYFP GC,* ***(E)*** *EYFP GC IgM+ and* ***(F)*** *EYFP GC IgM-. Each dot represents one mouse, graphs show mean +/- SD. Statistics carried out using Mann-Whitney test, * P < 0.05; ** P < 0.01; *** P < 0.001; **** P < 0.0001.*

The proportion of cells which were labelled with EYFP was significantly increased upon HF only diet feeding in the LNs, PALNs and blood compared to both chow and HFHC diets *(Figure 146)*.

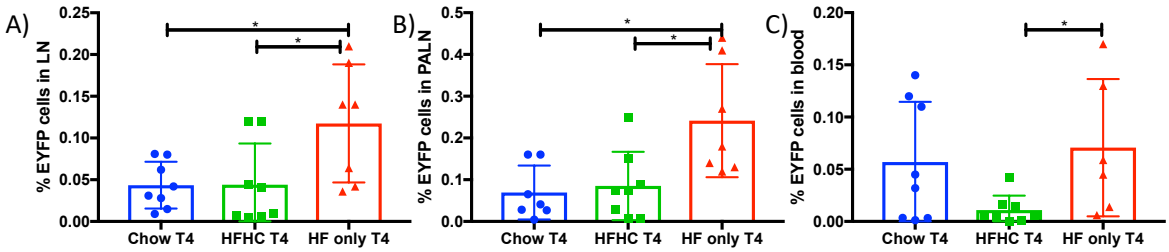

Figure 146. ***Increased EYFP population after 4 weeks of HF only diet in male AEL mice.*** *Male AEL mice were fed either chow (blue), high fat high cholesterol diet (HFHC; green) or high fat only diet (HF only; red) for 4 weeks (T4). Tamoxifen was administered, 9mg via oral gavage, 48hrs prior to sacrifice to induce EYFP labelling. The proportion of EYFP cells within the* ***(A)*** *lymph nodes (LN),* ***(B)*** *para-aortic lymph nodes (PALN) and* ***(C)*** *blood. Each dot represents one mouse, graphs show mean +/- SD. Statistics carried out using Mann-Whitney test, * P < 0.05; ** P < 0.01; *** P < 0.001; **** P < 0.0001.*

The class switch ratio was impacted by diet type – both in the inguinal and para-aortic lymph nodes it was reduced upon HFHC and HF only diet feeding compared to chow *(Figure 147A, B)*. However, in the PALN, the class switch ratio was slightly but significantly increased in the HF only compared to HFHC diet-fed male LDLr$^{-/-}$ AEL mice *(Figure 147B)*. Meanwhile, in the PPs HF only diet reduced the ratio compared to that of the HFHC diet *(Figure 147C)*.

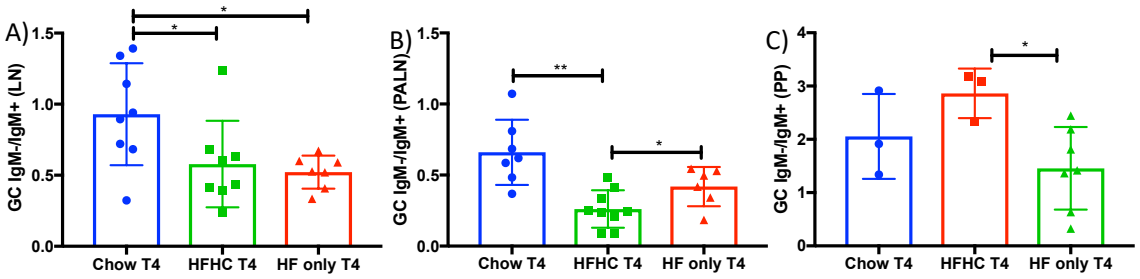

Figure 147. ***Impact of diet on class switch ratio after 4 weeks in male AEL mice.*** *Male AEL mice were fed either chow (blue), high fat high cholesterol diet (HFHC; green) or high fat only diet (HF only; red) for 4 weeks (T4). The class switch ratio (GC IgM-/IgM+) shown within the* ***(A)*** *lymph nodes (LN),* ***(B)*** *para-aortic lymph nodes (PALN) and* ***(C)*** *Peyer's patches (PP). Each dot represents one mouse, graphs show mean +/- SD. Statistics carried out using Mann-Whitney test, * P < 0.05; ** P < 0.01; *** P < 0.001; **** P < 0.0001.*

The HF only diet reduced the GC to memory ratio in the LN and PP compared to chow diet while in the PALN, the GC to memory ratio was reduced upon HF only diet feeding compared to HFHC diet feeding *(Figure 148)*.

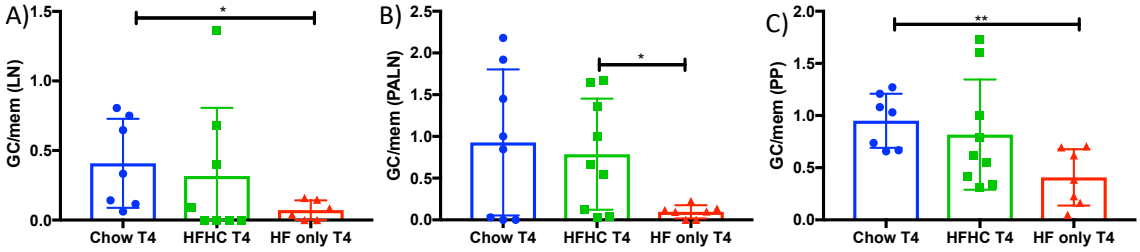

Figure 148. ***Reduced GC to memory ratio after 4 weeks HF only diet in male AEL mice.*** *Male AEL mice were fed either chow (blue), high fat high cholesterol diet (HFHC; green) or high fat only diet (HF only; red) for 4 weeks (T4). Tamoxifen was administered, 9mg via oral gavage, 48hrs prior to sacrifice to induce EYFP labelling. The GC to memory (EYFP) cell ratio shown within the* ***(A)*** *lymph nodes (LN),* ***(B)*** *para-aortic lymph nodes (PALN) and* ***(C)*** *Peyer's patches (PP). Each dot represents one mouse, graphs show mean +/- SD. Statistics carried out using Mann-Whitney test, * P < 0.05; ** P < 0.01; *** P < 0.001; **** P < 0.0001.*

In the spleen and PALN, the proportion of plasma cells was elevated upon HF only diet feeding primarily due to IgM- PCs compared to chow diet *(Figure 149)*. The total number of PCs was greatest upon HF only diet feeding in the spleen whereas the HFHC diet induced the biggest number of PCs in the PALN *(Figure 149B, E)*.

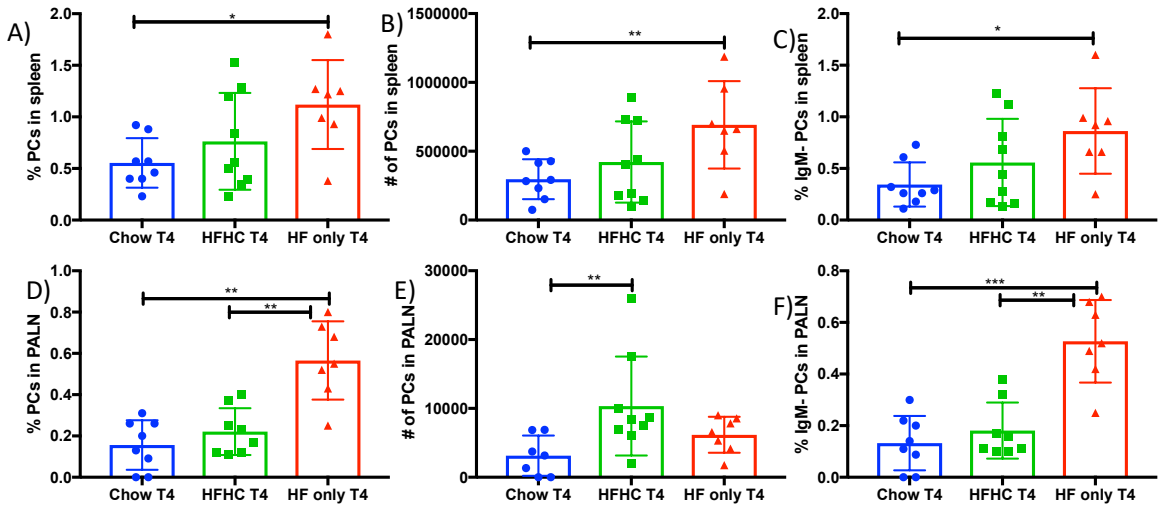

Figure 149. ***Impact of diet on plasma cell populations after 4 weeks in male AEL mice.*** *Male AEL mice were fed either chow (blue), high fat high cholesterol diet (HFHC; green) or high fat only diet (HF only; red) for 4 weeks (T4). The proportion of plasma cells is shown in the* ***(A)*** *spleen and* ***(D)*** *para-aortic lymph nodes (PALN) while the total number of plasma cells is shown in* ***(B)*** *spleen and* ***(E)*** *PALN. The proportion of IgM- PCs is shown in the* ***(C)*** *spleen and* ***(F)*** *PALN. Each dot represents one mouse, graphs show mean +/- SD. Statistics carried out using Mann-Whitney test, * P < 0.05; ** P < 0.01; *** P < 0.001; **** P < 0.0001.*

The HF only diet resulted in an expanded EYFP plasma cell population within the spleen, PALN, PPs, BM and blood compared to both the chow and HFHC diets *(Figure 150, Figure 151)*. This expansion was seen in both the IgM+ and IgM- isotypes *(Figure 150, Figure 151)*.

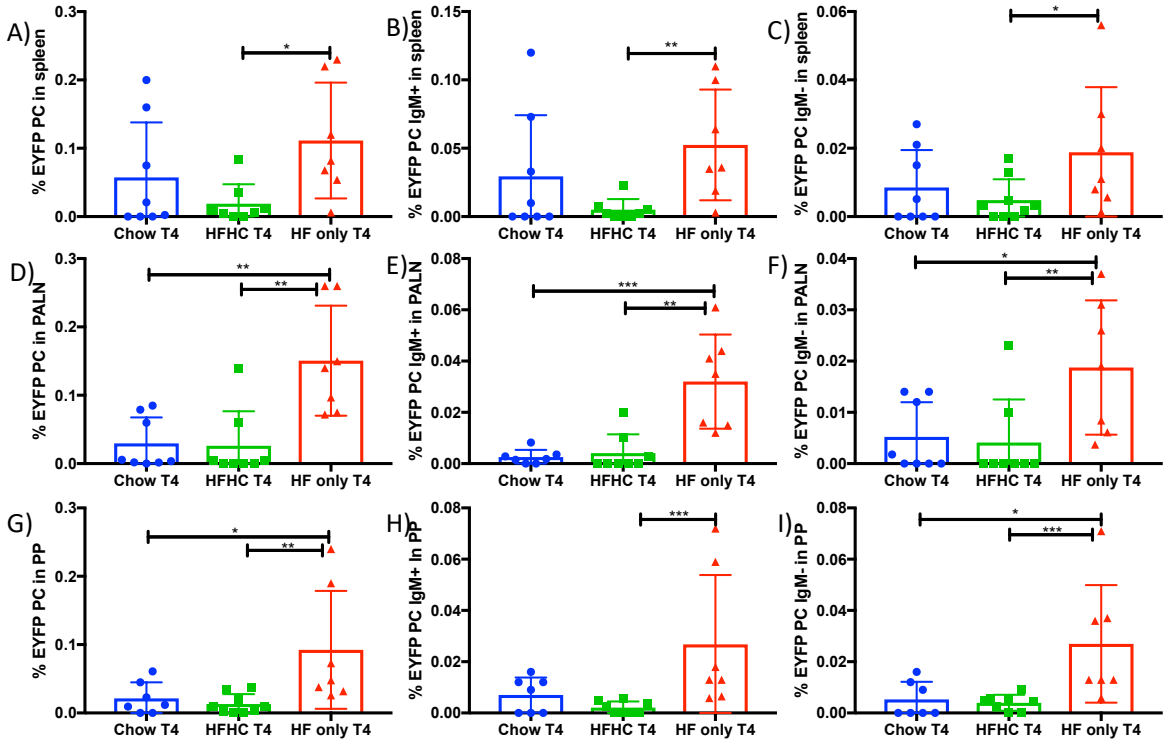

Figure 150. ***Expansion of EYFP PCs after 4 weeks HF only diet in male AEL mice.*** *Male AEL mice were fed either chow (blue), high fat high cholesterol diet (HFHC; green) or high fat only diet (HF only; red) for 4 weeks (T4). Tamoxifen was administered, 9mg via oral gavage, 48hrs prior to sacrifice to induce EYFP labelling. The proportion of EYFP plasma cells is shown in the* ***(A)*** *spleen and* ***(D)*** *para-aortic lymph nodes (PALN) and (G) Peyer's patches (PP). IgM+ EYFP PCs are show in* ***(B)*** *spleen,* ***(E)*** *PALN and* ***(H)*** *BM. IgM- EYFP PCs are shown in* ***(C)*** *spleen,* ***(F)*** *PALN and* ***(I)*** *BM. Each dot represents one mouse, graphs show mean +/- SD. Statistics carried out using Mann-Whitney test, * P < 0.05; ** P < 0.01; *** P < 0.001; **** P < 0.0001.*

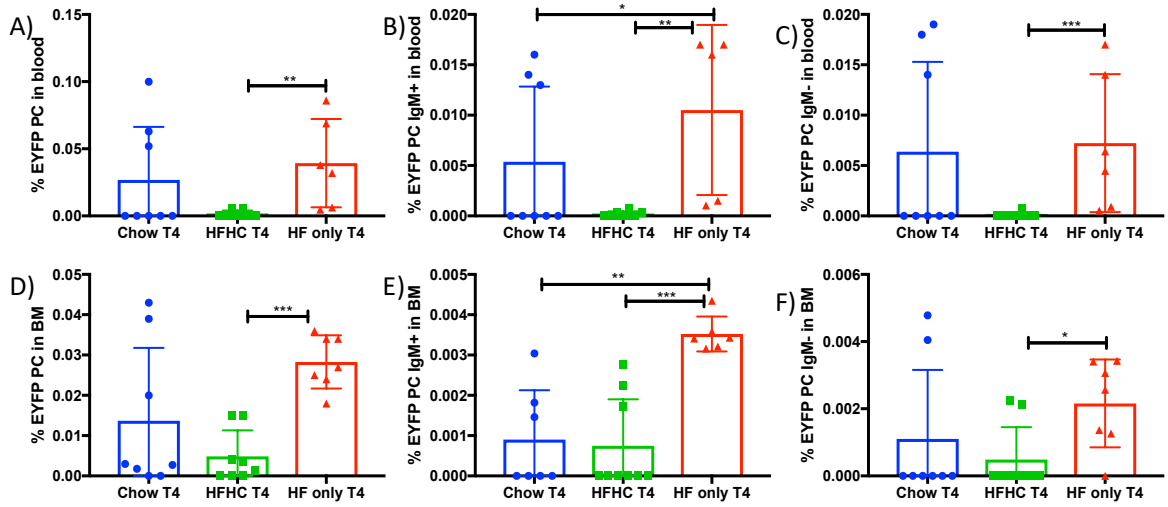

Figure 151. ***Expansion of EYFP PCs after 4 weeks HF only diet in male AEL mice.*** *Male AEL mice were fed either chow (blue), high fat high cholesterol diet (HFHC; green) or high fat only diet (HF only; red) for 4 weeks (T4). Tamoxifen was administered, 9mg via oral gavage, 48hrs prior to sacrifice to induce EYFP labelling. The proportion of EYFP plasma cells is shown in the* ***(A)*** *blood and* ***(D)*** *bone marrow. IgM+ EYFP PCs are show in* ***(B)*** *blood and* ***(E)*** *BM, IgM- EYFP PCs are shown in* ***(C)*** *blood and* ***(F)*** *BM. Each dot represents one mouse, graphs show mean +/- SD. Statistics carried out using Mann-Whitney test, * P < 0.05; ** P < 0.01; *** P < 0.001; **** P < 0.0001.*

6.4.1.2.4 8-week cholesterol free diet in male LDLr$^{-/-}$ AEL mice

After 8 weeks of diet in male LDLr$^{-/-}$ AEL mice, total cholesterol, LDL, HDL, and triglyceride levels were significantly upregulated in both high fat containing diets compared to chow diet *(Figure 152)*.

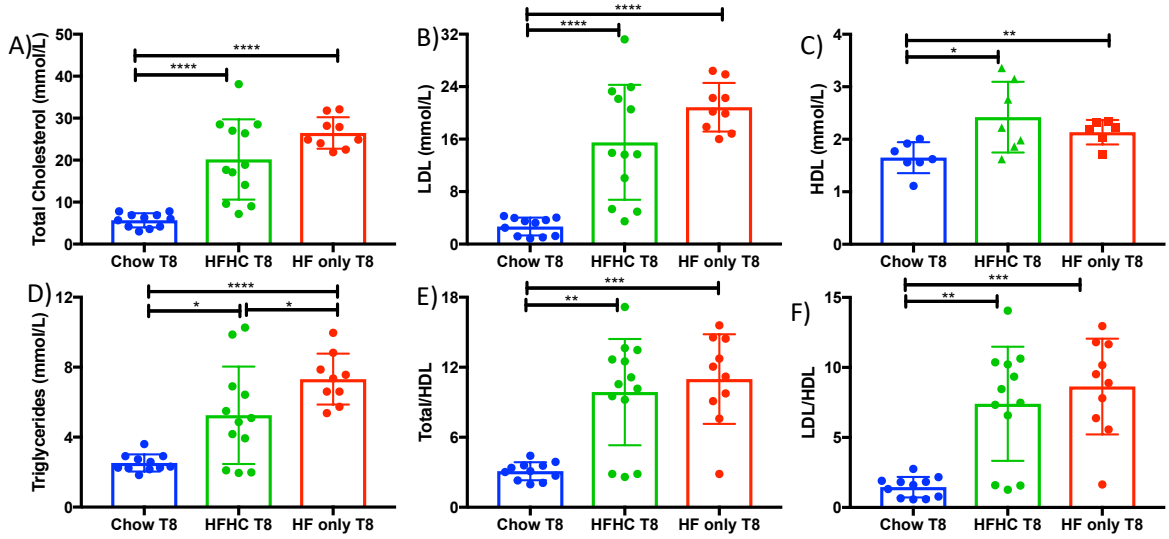

Figure 152. ***Increased serum lipid levels after 8 weeks of high fat-containing diet in male AEL mice.*** *Male AEL mice were fed either chow (blue), high fat and high cholesterol (HFHC; green) or high fat only diet (HF only; red) for 8 weeks (T8). Serum was analysed at study end after 4hr fast for* ***(A)*** *total cholesterol,* ***(B)*** *low density lipoprotein (LDL),* ***(C)*** *high density lipoprotein (HDL) and* ***(D)*** *triglycerides. The ratio of total cholesterol: HDL was calculated* ***(E)*** *as was the LDL: HDL ratio* ***(F)****. Each dot represents one mouse, graphs show mean +/- SD. Statistics carried out using Mann-Whitney test, * P < 0.05; ** P < 0.01; *** P < 0.001; **** P < 0.0001.*

High fat containing diets caused a similar increase in weight gain compared to chow diet over the course of 8 weeks *(Figure 153)*.

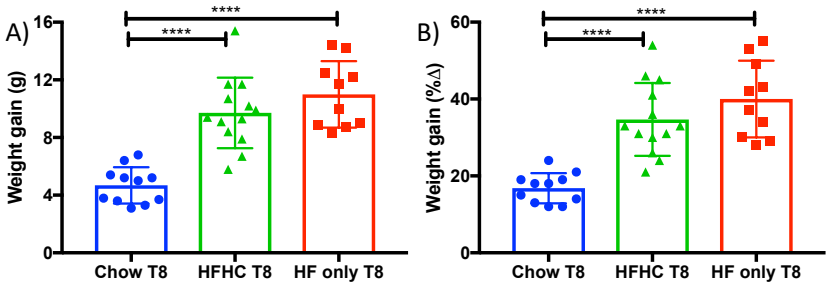

Figure 153. ***Similar weight gain on high fat-containing diets after 8 weeks in male AEL mice.*** *Difference in weight from start of experiment, male AEL mice aged 8 weeks old, to end of experiment after 8 weeks of diet (T8; mice aged 12 weeks old) of either chow (blue), high fat high cholesterol (HFHC; green) or high fat only (HF only; red) in* ***(A)*** *absolute terms and* ***(B)*** *as proportion. Each dot represents one mouse, graphs show mean +/- SD. Statistics carried out using Mann-Whitney test, * P < 0.05; ** P < 0.01; *** P < 0.001; **** P < 0.0001.*

Splenic total and B cell numbers were unchanged by diet type, however there was a trend toward increased cell numbers in the PALN upon HFHC diet feeding *(Figure 154A, B, C)*. The total number of B cells in the PALN was significantly increased in male LDLr$^{-/-}$ AEL mice fed the HFHC diet for 8 weeks compared to chow and HF only diets *(Figure 154D)*.

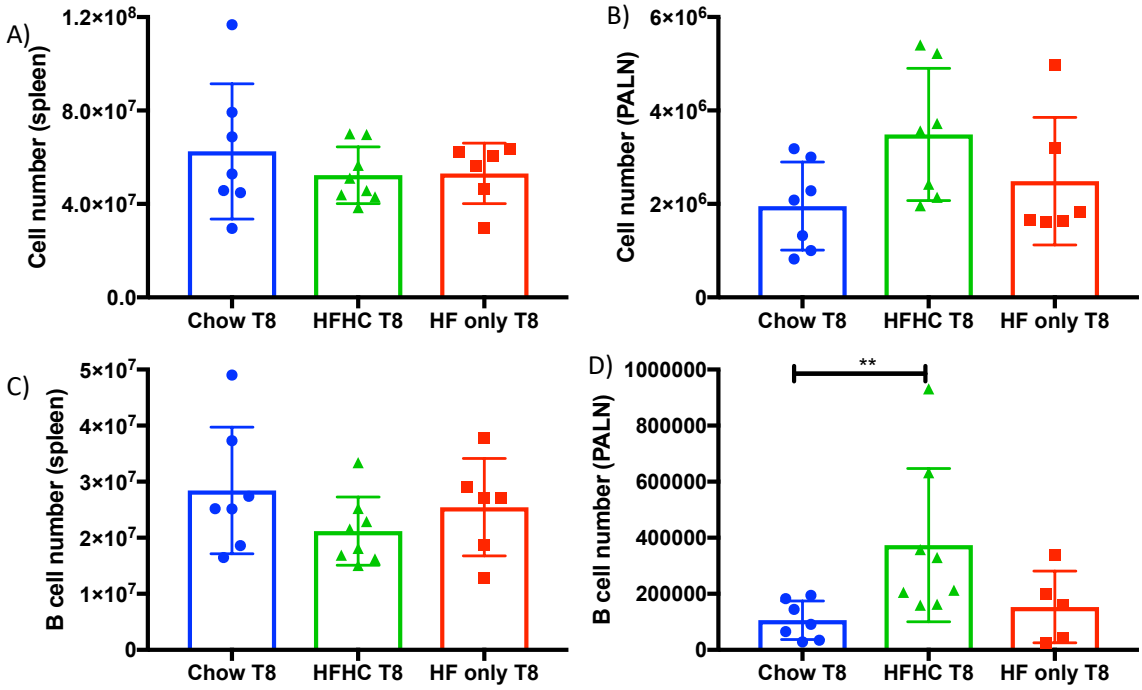

Figure 154. ***Impact of diet on cell numbers after 8 weeks in male AEL mice.*** *Male AEL mice were fed either chow (blue), high fat and high cholesterol (HFHC; green) or high fat only diet (HF only; red) for 8 weeks (T8). Total cell number was calculated for* ***(A)*** *spleen and* ***(B)*** *para-aortic lymph nodes (PALN). Total B cell number was calculated for* ***(C)*** *spleen and* ***(D)*** *PALN. Each dot represents one mouse, graphs show mean +/- SD. Statistics carried out using Mann-Whitney test, * P < 0.05; ** P < 0.01; *** P < 0.001; **** P < 0.0001.*

The GC proportion within the spleen and PALN was not significantly altered by diet *(Figure 155)*. In the spleen, the total number of GC cells was significantly more in the HF only diet-fed male LDLr$^{-/-}$ AEL mice compared to other diet types while in the PALN, the HFHC diet induced the greatest expansion in GC B cell numbers compared to other diet types *(Figure 155)*.

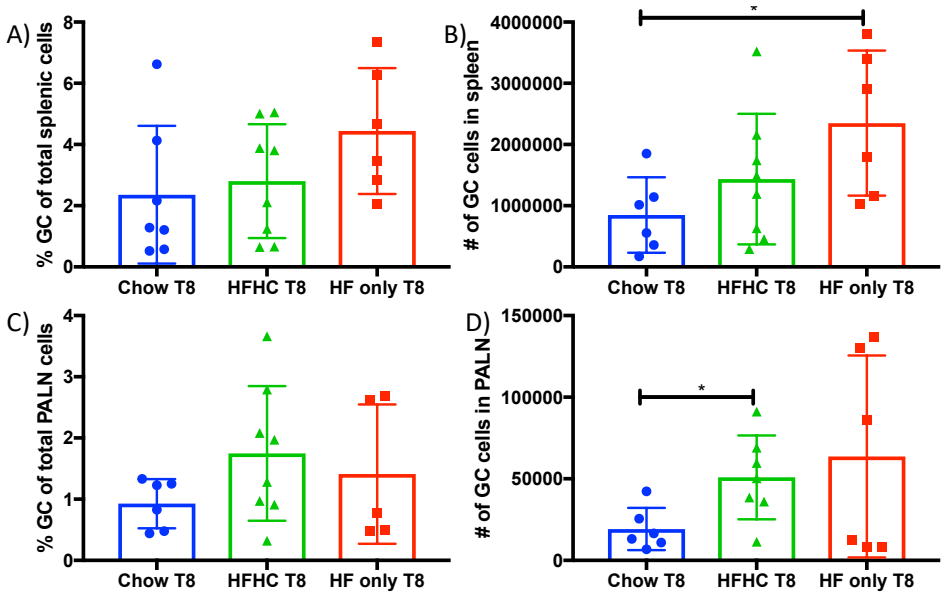

Figure 155. ***Impact of 8 weeks diet on GC populations in male AEL mice.*** *Male AEL mice were fed either chow (blue), high fat high cholesterol diet (HFHC; green) or high fat only diet (HF only; red) for 8 weeks (T8). The proportion of GC cells as assessed by flow cytometry in the* ***(A)*** *spleen and* ***(C)*** *para-aortic lymph nodes (PALN). The total number of GC B cells calculated in* ***(B)*** *spleen and* ***(D)*** *PALN. Each dot represents one mouse, graphs show mean +/- SD. Statistics carried out using Mann-Whitney test, * P < 0.05; ** P < 0.01; *** P < 0.001; **** P < 0.0001.*

Within the EYFP labelled population of the spleen, the HF only diet induced expansion of the EYFP GC cells mainly due to the IgM+ isotype *(Figure 156A, B)*. Total EYFP memory cell production was greatest in those male LDLr$^{-/-}$ AEL mice fed the HFHC diet as a result of IgM- memory cell expansion *(Figure 156C, E)*. However, in the HF only diet-fed male LDLr$^{-/-}$ AEL mice, EYFP IgM+ memory cells were increased *(Figure 156D)*.

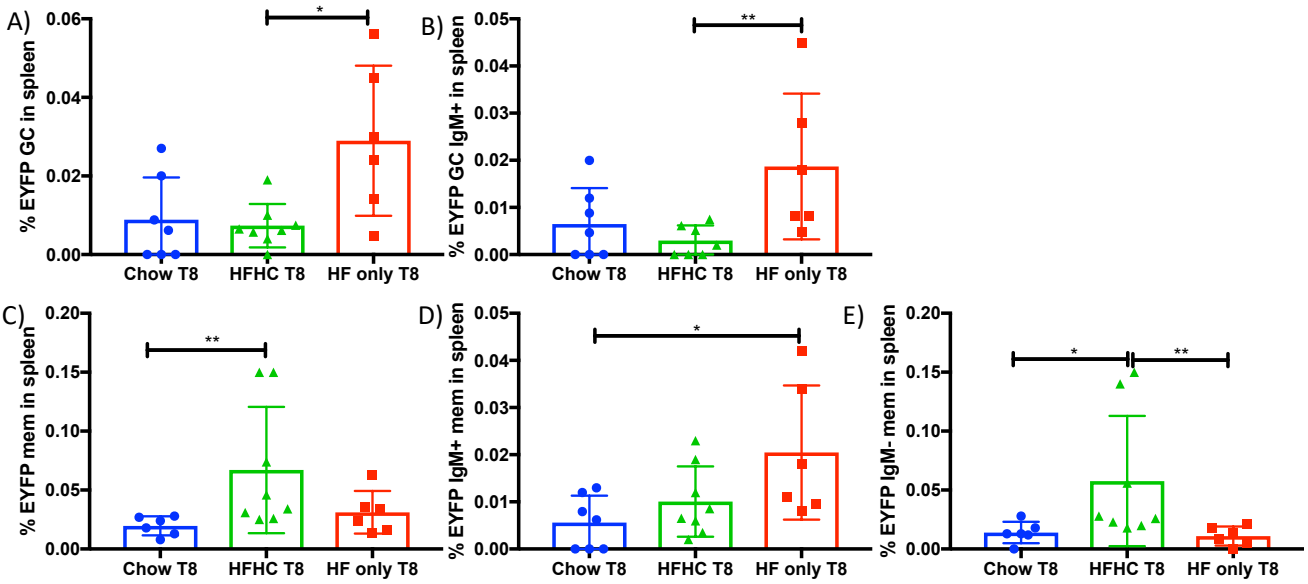

Figure 156. ***Impact of diet on EYFP populations of the spleen in male AEL mice.*** *Male AEL mice were fed either chow (blue), high fat high cholesterol diet (HFHC; green) or high fat only diet (HF only; red) for 8 weeks (T8). Tamoxifen was administered, 9mg via oral gavage, 48hrs prior to sacrifice to induce EYFP labelling. The total proportion of splenic* ***(A)*** *EYFP GC cells,* ***(B)*** *EYFP GC IgM+ cells,* ***(C)*** *EYFP memory cells,* ***(D)*** *EYFP IgM+ memory cells and* ***(E)*** *EYFP IgM- memory cells. Each dot represents one mouse, graphs show mean +/- SD. Statistics carried out using Mann-Whitney test, * P < 0.05; ** P < 0.01; *** P < 0.001; **** P < 0.0001.*

Serum was analysed for cytokine levels and the serum levels of CXCL1 and TNFα were increased in HF only diet-fed male LDLr$^{-/-}$ AEL mice compared to that of chow diet-fed male LDLr$^{-/-}$ AEL mice *(Figure 157A, E)*. The HFHC diet also induced upregulation of TNFα levels within serum *(Figure 157E)*. The levels of IFNγ and IL2 were reduced upon HFHC diet feeding compared to chow diet while HF only diet also caused reduction in IFNγ serum levels *(Figure 157B, C)*. Serum IL5 was reduced in HF only compared to the HFHC diet-fed male LDLr$^{-/-}$ AEL mice *(Figure 157D)*.

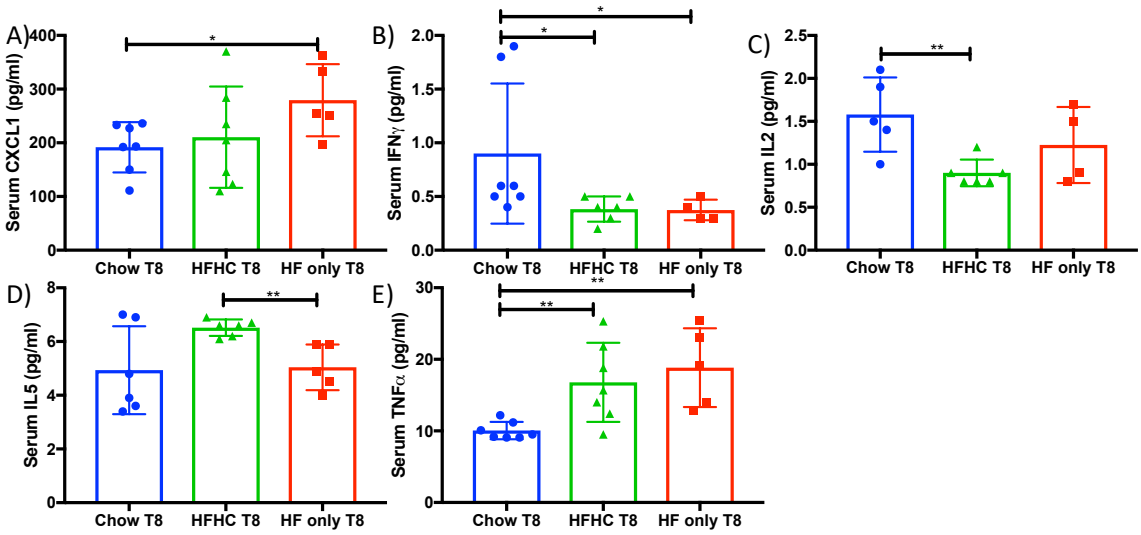

Figure 157. ***Impact of 8 weeks diet on serum cytokine levels in male AEL mice.*** *Male AEL mice were fed either chow (blue), high fat high cholesterol diet (HFHC; green) or high fat only diet (HF only; red) for 8 weeks (T8). Serum was analysed using multiplex array for* ***(A)*** *CXCL1,* ***(B)*** *IFNγ,* ***(C)*** *IL2,* ***(D)*** *IL5 and* ***(E)*** *TNFα. Each dot represents one mouse, graphs show mean +/- SD. Statistics carried out using Mann-Whitney test, * P < 0.05; ** P < 0.01; *** P < 0.001; **** P < 0.0001.*

Serum IgG1 was decreased in response to both high fat containing diets but to a lesser extent with the HF only diet in male LDLr$^{-/-}$ AEL mice *(Figure 158A)*. The HF only diet induced a significant increase in IgM titres compared to chow diet *(Figure 158A)*.

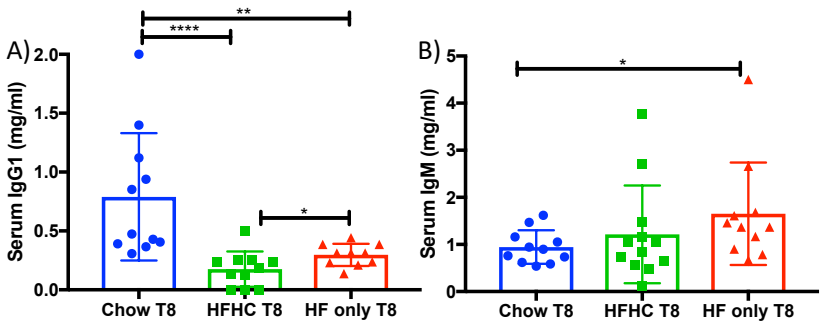

Figure 158. ***Reduced IgG1 after 8 weeks of both high fat-containing diets in male AEL mice.*** *Male AEL mice were fed either chow (blue), high fat high cholesterol diet (HFHC; green) or high fat only diet (HF only; red) for 8 weeks (T8). Serum was analysed using ELISA for* ***(A)*** *IgG1 and* ***(B)*** *IgM. Each dot represents one mouse, graphs show mean +/- SD. Statistics carried out using Mann-Whitney test, * P < 0.05; ** P < 0.01; *** P < 0.001; **** P < 0.0001.*

6.4.2 Impact of blocking IL6 on GC responses

To determine the impact of inflammation on the GC response, an antagonist to IL6 was administered as this cytokine is a key driver of atherosclerosis and has been implicated in regulation of the GC.

6.4.2.1 4-week anti-IL6 study in female LDLr$^{-/-}$ AEL mice

The anti-IL6 antibody or an isotype control was given on a weekly basis *(Figure 159)*.

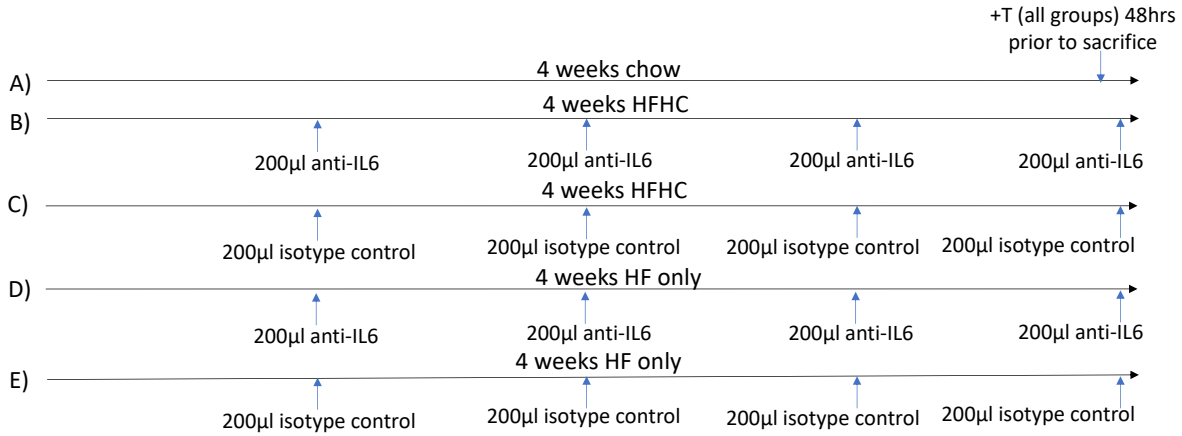

Figure 159. ***Experimental design for blocking IL6 for 4 weeks in female AEL mice.*** *Female AEL mice were fed either chow, high fat high cholesterol (HFHC) or high fat only (HF only) diet for 4 weeks. The HFHC and HF only diet fed female mice were injected intraperitoneally with either 200µl of anti-IL6 or isotype control weekly. 48hrs prior to sacrifice all groups were dosed with 9mg tamoxifen via oral gavage to induce EYFP labelling.*

In the spleen, cell numbers were largely unaffected by diet or antibody treatment except for the significant increase in total and B cell numbers in HFHC diet-fed compared to HF only diet-fed female LDLr$^{-/-}$ AEL mice treated with anti-IL6 antibody *(Figure 160A, B)*. In the PALN, HFHC diet induced a significant expansion in total and B cell numbers compared with chow and HF only diet-fed female LDLr$^{-/-}$ AEL mice *(Figure 160C, D)*. Furthermore, total and B cell numbers were higher in the spleen and PALN of HFHC diet-fed compared to HF only diet-fed female LDLr$^{-/-}$ AEL mice treated with anti-IL6 *(Figure 160)*.

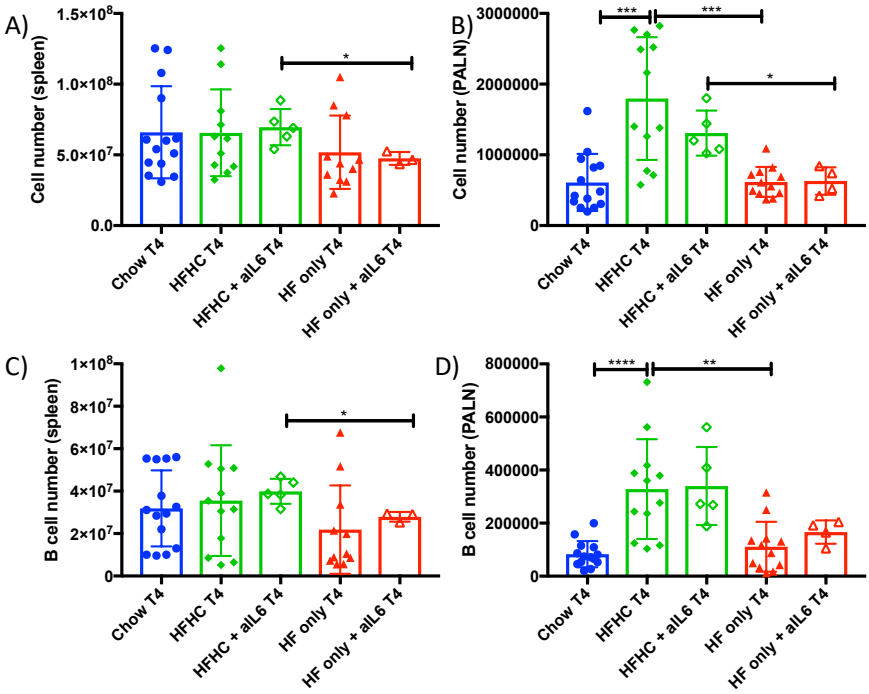

Figure 160. ***Impact of anti-IL6 on cell numbers after 4 weeks in female AEL mice.*** *Female AEL mice were fed either chow (blue), high fat high cholesterol (HFHC; green) or high fat only (HF only; red) diets for 4 weeks (T4) and treated with either isotype control (closed symbols) or anti-IL6 (aIL6; open circles).* ***(A)*** *Total and* ***(C)*** *B cell numbers in spleen and* ***(B)*** *total and* ***(D)*** *B cell numbers in para-aortic lymph nodes (PALN). Each dot represents one mouse, graphs show mean +/- SD. Statistics carried out using Mann-Whitney test, * P < 0.05; ** P < 0.01; *** P < 0.001; **** P < 0.0001.*

Treatment with the anti-IL6 antibody significantly increased the proportion and absolute number of GC B cells in the spleen in both HFHC and HF only diet-fed female LDLr$^{-/-}$ AEL mice *(Figure 161A, B)*. No significant changes were observed in the PALN *(Figure 161C, D)*.

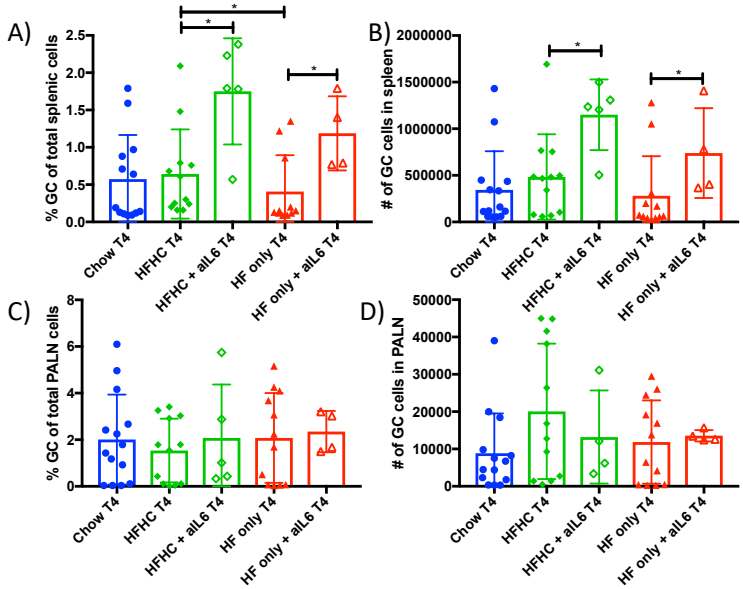

Figure 161. ***Impact of anti-IL6 treatment on GC responses after 4 weeks in female AEL mice.*** *Female AEL mice were fed either chow (blue), high fat high cholesterol (HFHC; green) or high fat only (HF only; red) diets for 4 weeks (T4) and treated with either isotype control (closed symbols) or anti-IL6 (aIL6; open circles).* ***(A)*** *Proportion and* ***(B)*** *absolute numbers of GC B cells in spleen and* ***(C)*** *proportion and* ***(D)*** *absolute numbers of GC B cells in para-aortic lymph nodes (PALN). Each dot represents one mouse, graphs show mean +/- SD. Statistics carried out using Mann-Whitney test, * P < 0.05; ** P < 0.01; *** P < 0.001; **** P < 0.0001.*

Within the EYFP labelled GC population of the spleen, anti-IL6 treatment significantly increased the total population in proportion and absolute terms, and this was in both the IgM+ and IgM- isotypes in HFHC diet-fed female LDLr$^{-/-}$ AEL mice *(Figure 162)*. Furthermore, the proportion and absolute number of EYFP GC cells in the spleen was significantly greater in HFHC diet-fed female LDLr$^{-/-}$ AEL mice compared with HF only diet-fed female LDLr$^{-/-}$ AEL mice treated with anti-IL6 *(Figure 162A, B)*. The proportion of IgM- EYFP GC splenic cells was also significantly increased in HF only diet-fed female LDLr$^{-/-}$ AEL mice treated with anti-IL6 compared to isotype control *(Figure 162D)*.

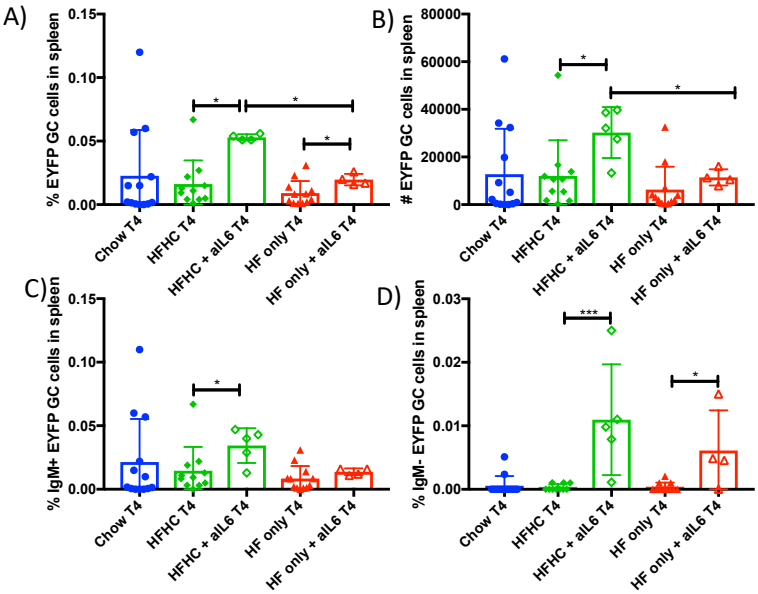

Figure 162. ***Increased EYFP GC in spleen after anti-IL6 in HFHC diet-fed female AEL mice after 4 weeks.*** *Female AEL mice were fed either chow (blue), high fat high cholesterol (HFHC; green) or high fat only (HF only; red) diets for 4 weeks (T4) and treated with either isotype control (closed symbols) or anti-IL6 (aIL6; open circles). Tamoxifen was administered, 9mg via oral gavage, 48hrs prior to sacrifice to induce EYFP labelling.* ***(A)*** *Proportion,* ***(B)*** *total number,* ***(C)*** *IgM+ and* ***(D)*** *IgM- EYFP GC B cells in spleen. Each dot represents one mouse, graphs show mean +/- SD. Statistics carried out using Mann-Whitney test, * P < 0.05; ** P < 0.01; *** P < 0.001; **** P < 0.0001.*

Within the PALNs, the EYFP GC population, specifically IgM+, was significantly increased upon anti-IL6 treatment compared with isotype control in HFHC diet-fed female LDLr$^{-/-}$ AEL mice *(Figure 163A, B)*. These populations were also significantly greater than those of HF only diet-fed female LDLr$^{-/-}$ AEL mice treated with anti-IL6 *(Figure 163A, B)*. The same results were recapitulated for the EYFP memory cell population within the PALN *(Figure 163C, D)*.

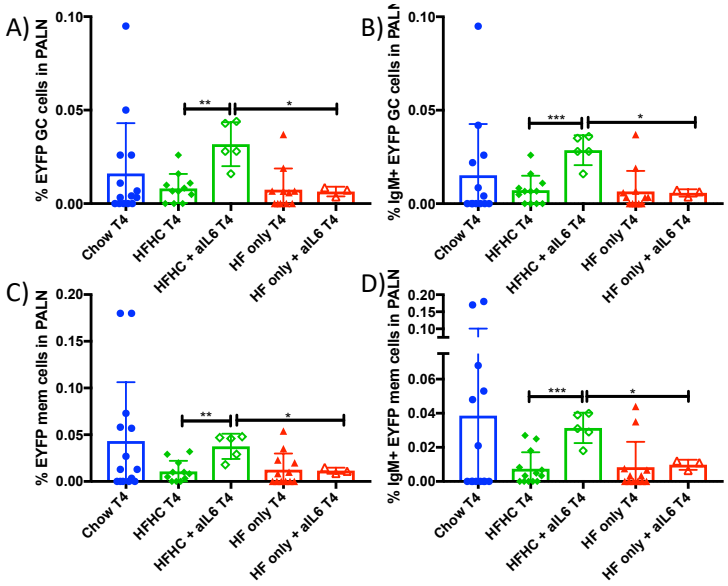

Figure 163. ***Increased EYFP memory after anti-IL6 treatment in HFHC diet-fed female AEL mice after 4 weeks.*** *Female AEL mice were fed either chow (blue), high fat high cholesterol (HFHC; green) or high fat only (HF only; red) diets for 4 weeks (T4) and treated with either isotype control (closed symbols) or anti-IL6 (aIL6; open circles). Tamoxifen was administered, 9mg via oral gavage, 48hrs prior to sacrifice to induce EYFP labelling.* ***(A)*** *total proportion and* ***(B)*** *IgM+ proportion of EYFP GC cells in para-aortic lymph node (PALN).* ***(C)*** *total proportion and* ***(D)*** *IgM+ proportion of EYFP memory (mem) cells in PALN. Each dot represents one mouse, graphs show mean +/- SD. Statistics carried out using Mann-Whitney test, * P < 0.05; ** P < 0.01; *** P < 0.001; **** P < 0.0001.*

In the PPs, both HF containing diets had reduced proportion of total and memory EYFP cell populations compared to chow diet while anti-IL6 treatment reduced the proportion of these populations compared to isotype control in the HFHC diet-fed female LDLr$^{-/-}$ AEL mice *(Figure 164)*.

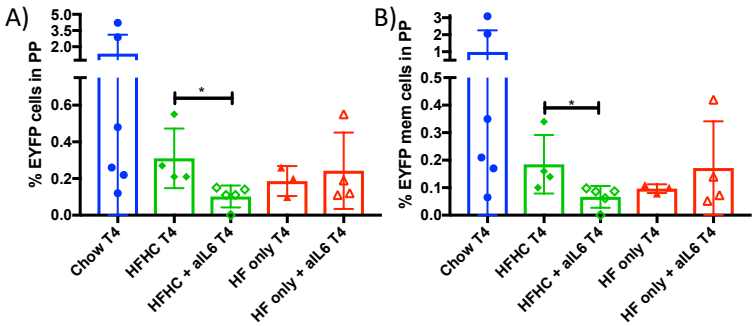

Figure 164. ***Reduced EYFP cells after anti-IL6 in HFHC diet-fed female AEL mice after 4 weeks in PPs.*** *Female AEL mice were fed either chow (blue), high fat high cholesterol (HFHC; green) or high fat only (HF only; red) diets for 4 weeks (T4) and treated with either isotype control (closed symbols) or anti-IL6 (aIL6; open circles). Tamoxifen was administered, 9mg via oral gavage, 48hrs prior to sacrifice to induce EYFP labelling. In the Peyer's patches (PP), the proportion of* ***(A)*** *total EYFP and* ***(B)*** *EYFP memory cells can be seen. Each dot represents one mouse, graphs show mean +/- SD. Statistics carried out using Mann-Whitney test, * P < 0.05; ** P < 0.01; *** P < 0.001; **** P < 0.0001.*

Within the spleen, the GC to memory ratio was increased in HF only diet-fed female LDLr$^{-/-}$ AEL mice treated with anti-IL6 compared with isotype control showing a prolonged GC response *(Figure 165A)*. While in the PPs, the GC to memory ratio was significantly higher in

HFHC treated with isotype control compared with both HFHC treated with anti-IL6 and chow diet-fed female LDLr$^{-/-}$ AEL mice *(Figure 165B)*.

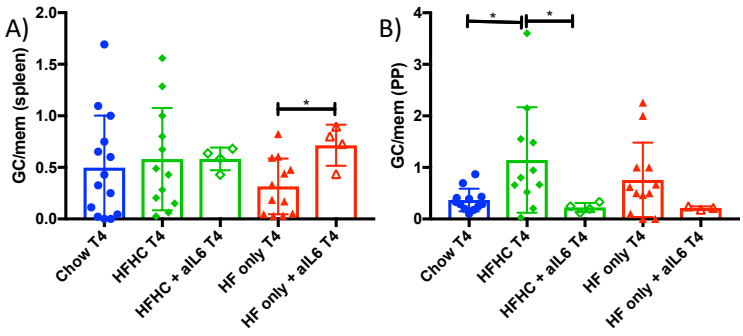

Figure 165. ***Impact of anti-IL6 on GC to memory ratio in female AEL mice after 4 weeks.*** *Female AEL mice were fed either chow (blue), high fat high cholesterol (HFHC; green) or high fat only (HF only; red) diets for 4 weeks (T4) and treated with either isotype control (closed symbols) or anti-IL6 (aIL6; open circles). The proportion of EYFP GC to EYFP memory cells (GC/mem) can be seen in the* ***(A)*** *spleen and* ***(B)*** *Peyer's patches (PP). Each dot represents one mouse, graphs show mean +/- SD. Statistics carried out using Mann-Whitney test, * P < 0.05; ** P < 0.01; *** P < 0.001; **** P < 0.0001.*

In terms of functional output from the GC, anti-IL6 treatment reduced the absolute, total and IgM-proportion of plasma cells produced in the spleen of HFHC and HF only diet-fed female LDLr$^{-/-}$ AEL animals *(Figure 166)*.

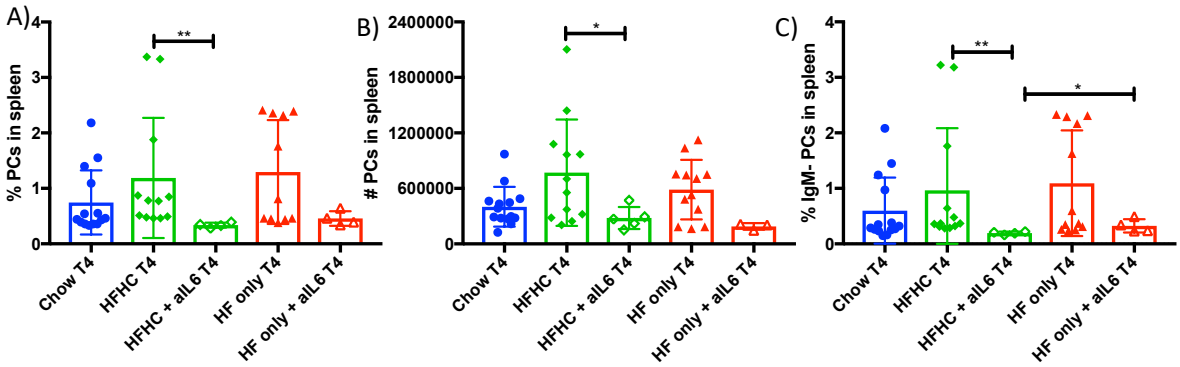

Figure 166. ***Reduced PC populations after anti-IL6 treatment in female AEL mice after 4 weeks.*** *Female AEL mice were fed either chow (blue), high fat high cholesterol (HFHC; green) or high fat only (HF only; red) diets for 4 weeks (T4) and treated with either isotype control (closed symbols) or anti-IL6 (aIL6; open circles). The splenic plasma cell (PC) population in terms of* ***(A)*** *proportion,* ***(B)*** *absolute number and* ***(C)*** *IgM- proportion. Each dot represents one mouse, graphs show mean +/- SD. Statistics carried out using Mann-Whitney test, * P < 0.05; ** P < 0.01; *** P < 0.001; **** P < 0.0001.*

Contrastingly, IgM+ plasma cell proportions were significantly increased upon anti-IL6 treatment compared with isotype control in the PPs of both HFHC and HF only diet-fed female LDLr$^{-/-}$ AEL mice *(Figure 167A)*. The proportion of IgM- plasma cells in the PPs was reduced in anti-IL6 treated HF only diet-fed female LDLr$^{-/-}$ AEL mice compared to those treated with isotype control *(Figure 167B)*.

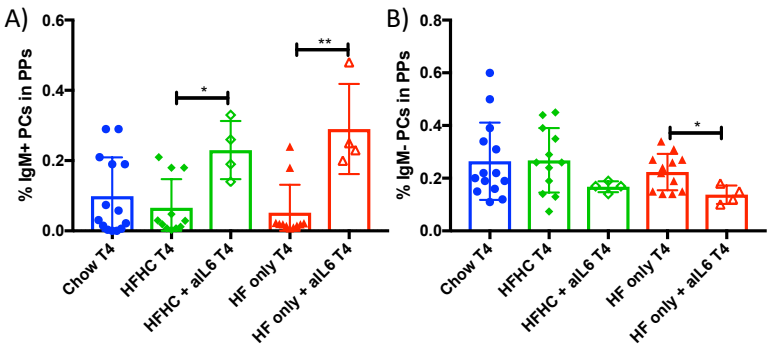

Figure 167. ***Impact of anti-IL6 treatment on PCs of the PPs in female AEL mice after 4 weeks.*** *Female AEL mice were fed either chow (blue), high fat high cholesterol (HFHC; green) or high fat only (HF only; red) diets for 4 weeks (T4) and treated with either isotype control (closed symbols) or anti-IL6 (aIL6; open circles). The Peyer's patches (PP) plasma cell (PC) population in terms of* ***(A)*** *IgM+ and* ***(B)*** *IgM- isotypes. Each dot represents one mouse, graphs show mean +/- SD. Statistics carried out using Mann-Whitney test, * P < 0.05; ** P < 0.01; *** P < 0.001; **** P < 0.0001.*

6.4.2.2 8-week anti-IL6 study in female LDLr$^{-/-}$ AEL mice

To investigate the impact of anti-IL6 treatment at later stages of atherosclerosis, female LDLr$^{-/-}$ AEL mice were put on diet for 8 weeks and administered anti-IL6 for the later 4 weeks *(Figure 168)*.

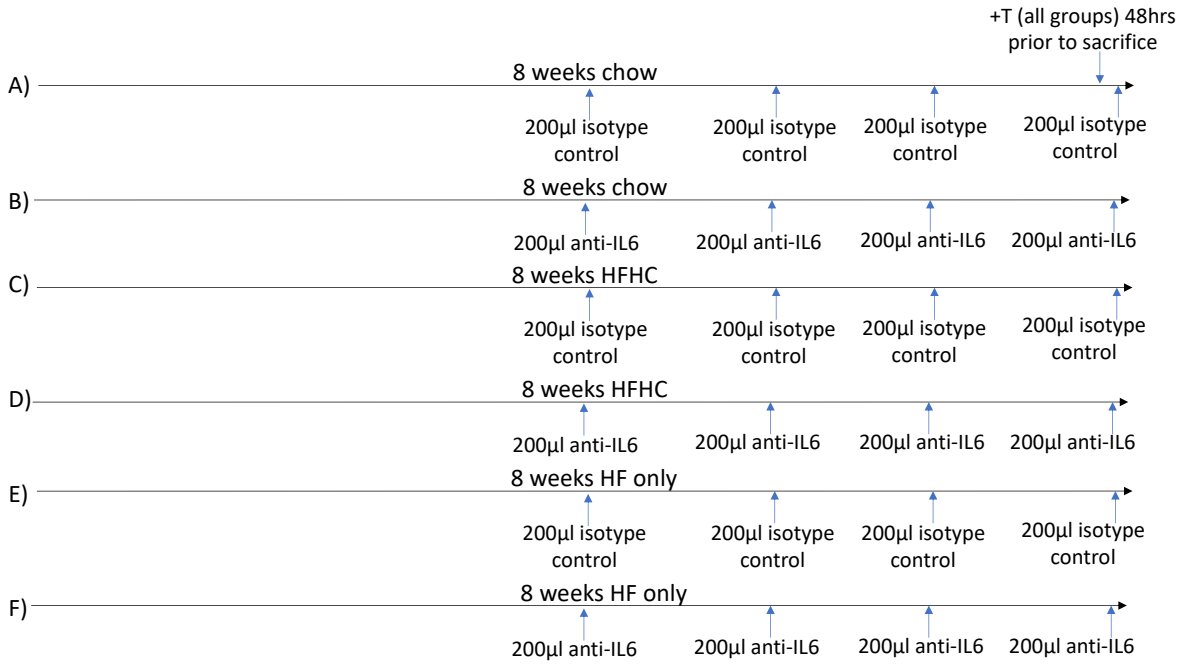

Figure 168. ***Experimental design for blocking IL6 for 8 weeks in female AEL mice.*** *Female AEL mice were fed either chow, high fat high cholesterol (HFHC) or high fat only (HF only) diet for 8 weeks and treated via intraperitoneal injection with either 200µl anti-IL6 or isotype control weekly from week 4. 48hrs prior to sacrifice all groups were dosed with 9mg tamoxifen via oral gavage to induce EYFP labelling.*

Serum titres of total cholesterol and LDL cholesterol were significantly increased upon HF only diet feeding compared to chow diet after 8 weeks in female LDLr$^{-/-}$ AEL mice treated with anti-IL6 *(Figure 169A, B)*. Anti-IL6 treatment elevated levels of total and LDL cholesterol as well as triglycerides in HF only diet-fed female LDLr$^{-/-}$ AEL mice compared to isotype control *(Figure 169A, B)*. HDL levels were unaltered by diet or treatment type *(Figure 169C)*. The observation that both HF only diet-fed female LDLr$^{-/-}$ AEL mice had similarly high cholesterol levels by 8 weeks to those fed HFHC diet suggests that dietary cholesterol plays a more influential role at earlier stages of atherosclerosis and its role wanes by the 8-week timepoint.

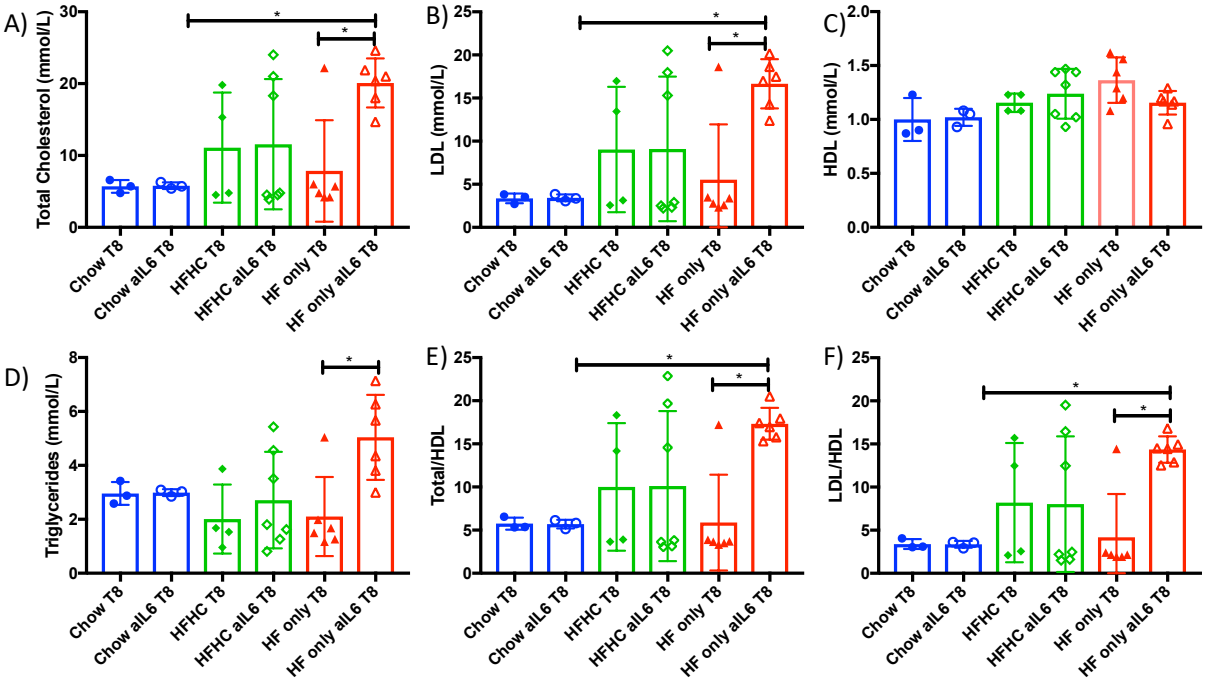

Figure 169. ***Impact of anti-IL6 treatment after 8 weeks on serum lipid levels in female AEL mice.*** *Female AEL mice were fed either chow (blue), high fat and high cholesterol (HFHC; green) or high fat only diet (HF only; red) for 8 weeks (T8) and treated for the final 4 weeks with either 200µl isotype control (closed circles) or anti-IL6 (open circles). Serum was analysed at study end after 4hr fast for* ***(A)*** *total cholesterol,* ***(B)*** *low density lipoprotein (LDL),* ***(C)*** *high density lipoprotein (HDL) and* ***(D)*** *triglycerides. The ratio of total cholesterol: HDL was calculated* ***(E)*** *as was the LDL: HDL ratio* ***(F)****. Each dot represents one mouse, graphs show mean +/- SD. Statistics carried out using Mann-Whitney test, * P < 0.05; ** P < 0.01; *** P < 0.001; **** P < 0.0001.*

Anti-IL6 treatment did not impact total cell number in the spleen or PALN after 8 weeks of diet in female LDLr$^{-/-}$ AEL mice *(Figure 170A, B)*. Anti-IL6 treatment reduced the total B cell number in female LDLr$^{-/-}$ AEL mice fed the HFHC diet for 8 weeks in the spleen but had no impact on the B cell population in the PALN *(Figure 170C, D)*. Both HFHC and HF only diets induced increased total and B cell numbers in the spleen and PALN compared to chow diet after 8 weeks in female LDLr$^{-/-}$ AEL mice *(Figure 170)*.

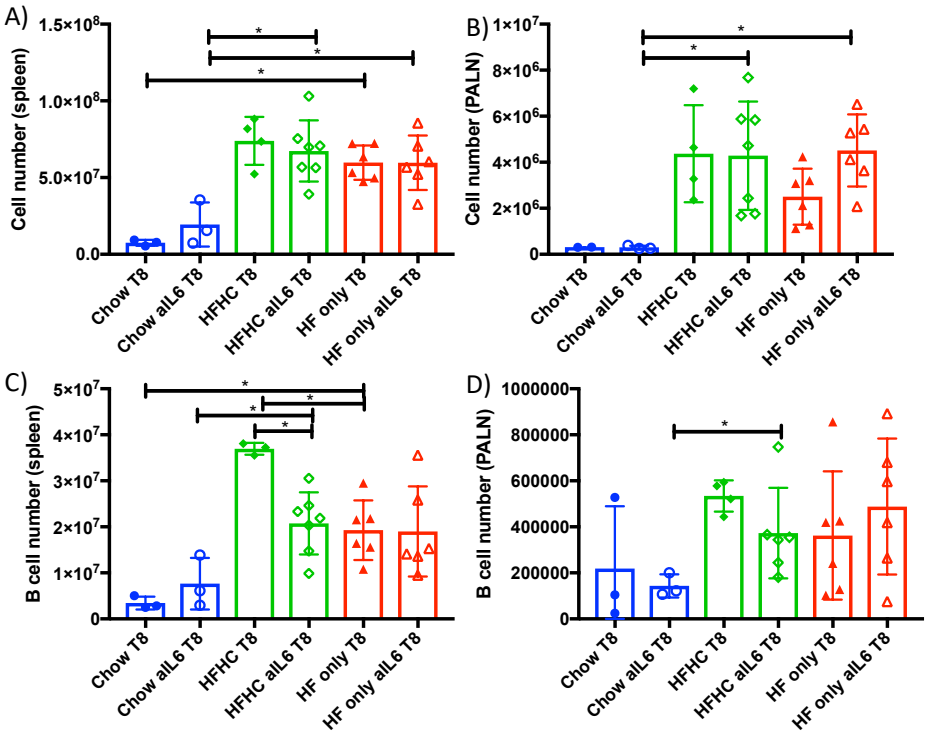

Figure 170. ***Impact of 8 weeks anti-IL6 treatment on cell numbers in female AEL mice.*** *Female AEL mice were fed either chow (blue), high fat high cholesterol (HFHC; green) or high fat only (HF only; red) diets for 8 weeks (T8) and treated for the final 4 weeks with either 200μl isotype control (closed circles) or anti-IL6 (open circles).* ***(A)*** *Total and* ***(C)*** *B cell numbers in spleen and* ***(B)*** *total and* ***(D)*** *B cell numbers in para-aortic lymph nodes (PALN). Each dot represents one mouse, graphs show mean +/- SD. Statistics carried out using Mann-Whitney test, * P < 0.05; ** P < 0.01; *** P < 0.001; **** P < 0.0001.*

After 8 weeks of high fat containing-diet, the proportion and absolute number of splenic GC cells was significantly expanded compared to chow diet *(Figure 171A, B)*. In the spleen, anti-IL6 treatment caused reduction in the proportion and number of GC B cells in the HFHC diet-fed female LDLr$^{-/-}$ AEL mice *(Figure 171A, B)*. The total number of splenic GC cells was reduced upon IL6 blockade in the spleen of HF only diet-fed female LDLr$^{-/-}$ AEL mice compared to isotype control while the HFHC diet induced greater expansion of the GC population than did the HF only diet *(Figure 171A, B)*. As splenic GC responses were more greatly impacted in HFHC than HF only diet-fed female LDLr$^{-/-}$ AEL mice, this suggests that IL6 has a more influential role when dietary cholesterol is present.

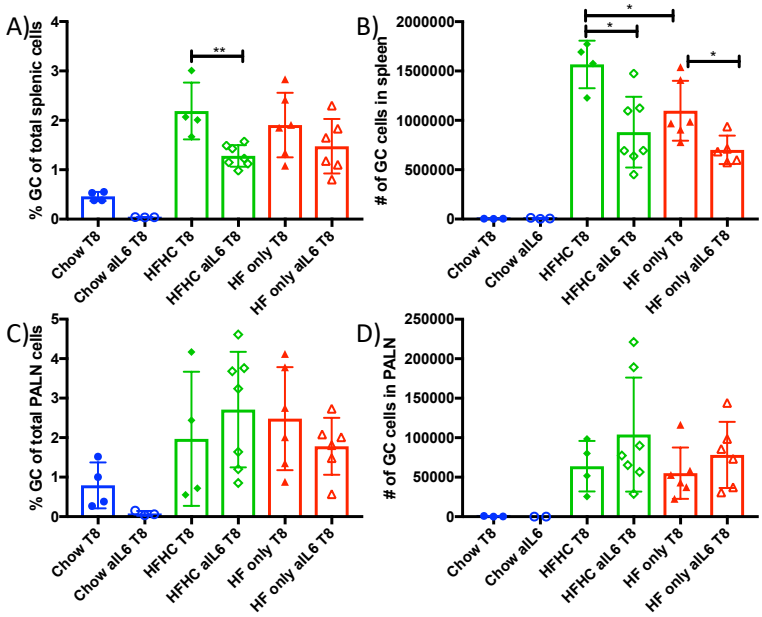

Figure 171. ***Impact of anti-IL6 on GC responses after 8 weeks in female AEL mice.*** *Female AEL mice were fed either chow (blue), high fat high cholesterol (HFHC; green) or high fat only (HF only; red) diets for 4 weeks (T4) and treated with either isotype control (closed symbols) or anti-IL6 (aIL6; open circles).* ***(A)*** *Proportion and* ***(B)*** *absolute numbers of GC B cells in spleen and* ***(C)*** *proportion and* ***(D)*** *absolute numbers of GC B cells in para-aortic lymph nodes (PALN). Each dot represents one mouse, graphs show mean +/- SD. Statistics carried out using Mann-Whitney test, * P < 0.05; ** P < 0.01; *** P < 0.001; **** P < 0.0001.*

Anti-IL6 treatment reduced expansion of the EYFP labelled GC population both in relative and absolute terms, mainly due to the IgM+ isotype, in both the spleen and LN compared to isotype control in female LDLr$^{-/-}$ AEL mice fed HFHC diet for 8 weeks *(Figure 172)*. Anti-IL6 treatment in female LDLr$^{-/-}$ AEL mice fed the HF only diet also reduced the proportion of EYFP GC cells, particularly those of IgM+ isotype, in the LN *(Figure 172D, F)*.

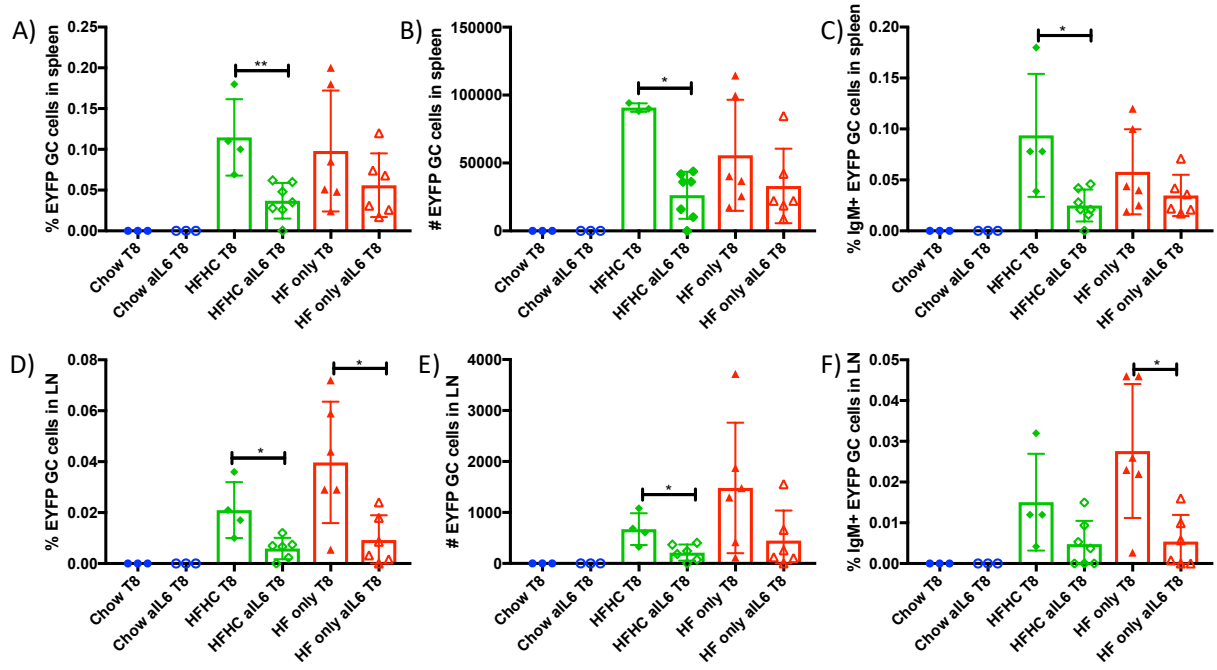

Figure 172. ***Impact of anti-IL6 treatment on EYFP GC populations after 8 weeks in female AEL mice.*** *Female AEL mice were fed either chow (blue), high fat high cholesterol (HFHC; green) or high fat only (HF only; red) diets for 8 weeks (T8) and treated with either isotype control (closed symbols) or anti-IL6 (aIL6; open circles). Tamoxifen was administered, 9mg via oral gavage, 48hrs prior to sacrifice to induce EYFP labelling. Proportion of EYFP+ GC cells in* ***(A)*** *spleen and* ***(D)*** *lymph node (LN); number of EYFP+ GC cells in* ***(B)*** *spleen and* ***(E)*** *LN and proportion of IgM+ EYFP GC cells in* ***(C)*** *spleen and* ***(F)*** *LN. Each dot represents one mouse, graphs show mean +/- SD. Statistics carried out using Mann-Whitney test, * P < 0.05; ** P < 0.01; *** P < 0.001; **** P < 0.0001.*

6.4.2.3 4-week anti-IL6 study in male LDLr$^{-/-}$ AEL mice

The effect of anti-IL6 treatment was also tested in male LDLr$^{-/-}$ AEL mice on chow or HFD *(Figure 173)*.

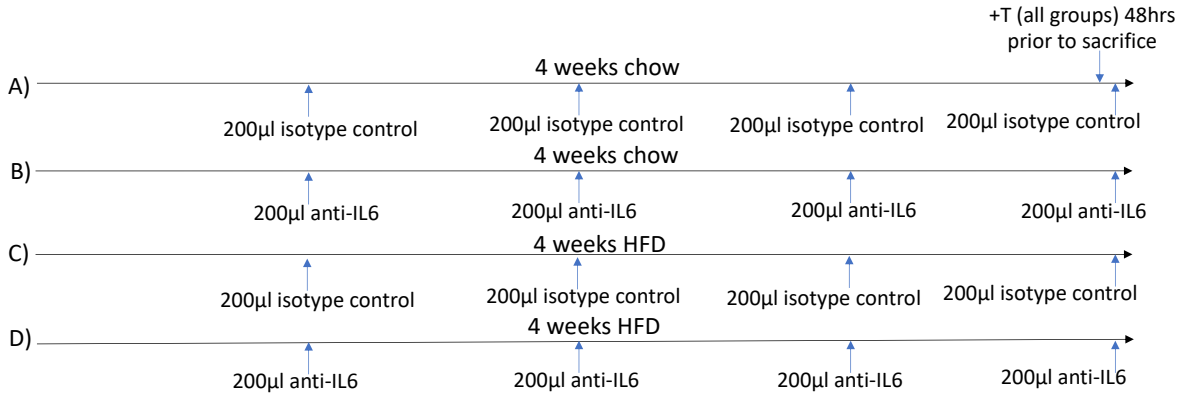

Figure 173. ***Experimental design for blocking IL6 for 4 weeks in male AEL mice.*** *Male AEL mice were fed either chow or high fat diet (HFD) for 4 weeks with weekly treatment of 200µl intraperitoneal injection with anti-IL6 or isotype control. 48hrs prior to sacrifice all groups were dosed with 9mg tamoxifen via oral gavage to induce EYFP labelling.*

In male LDLr$^{-/-}$ AEL mice, anti-IL6 treatment did not impact cholesterol levels after 4 weeks of either chow or HFD *(Figure 174)*. As expected, HFD-fed groups had significantly increased cholesterol levels *(Figure 174)*.

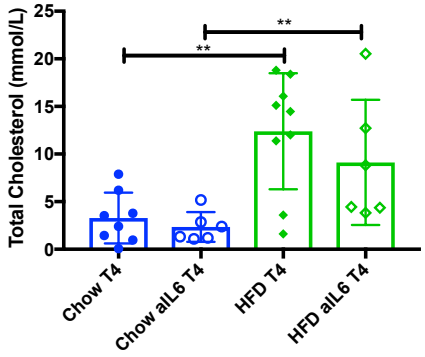

Figure 174. ***Anti-IL6 treatment did not impact cholesterol levels after 4 weeks in male AEL mice.*** *Male AEL mice were fed either chow (blue) or high fat diet (HFD; green) for 4 weeks (T4) and treated with either isotype control (closed symbols) or anti-IL6 (aIL6; open circles). Total cholesterol was measured using a colorimetric assay. Each dot represents one mouse, graphs show mean +/- SD. Statistics carried out using Mann-Whitney test, * P < 0.05; ** P < 0.01; *** P < 0.001; **** P < 0.0001.*

Total and B cell numbers of the spleen were not impacted by diet or treatment type after 4 weeks in male LDLr$^{-/-}$ AEL mice *(Figure 175A, C)*. In the PALN, anti-IL6 treatment significantly increased the total and B cell numbers in chow diet-fed male LDLr$^{-/-}$ AEL mice *(Figure 175B, D)*. The HFD-fed male mice had greater total and B cell numbers in the PALN compared to chow diet-fed male LDLr$^{-/-}$ AEL mice *(Figure 175B, D)*.

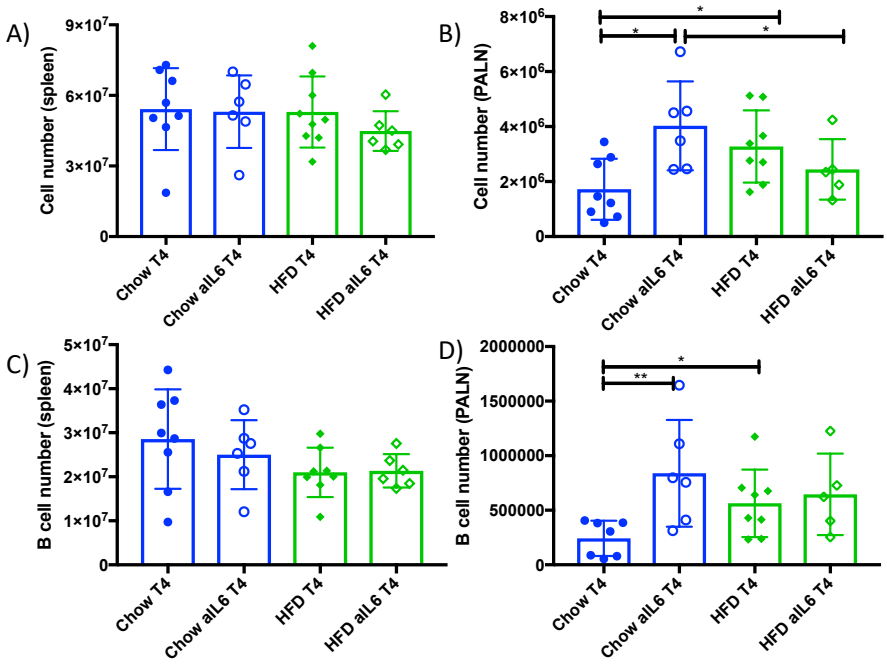

Figure 175. ***Increased PALN cell numbers after anti-IL6 treatment in chow diet-fed male AEL mice after 4 weeks.*** *Male AEL mice were fed either chow (blue) or high fat diet (HFD; green) for 4 weeks (T4) and treated weekly with either 200µl isotype control (closed circles) or anti-IL6 (open circles).* ***(A)*** *Total and* ***(C)*** *B cell numbers in spleen and* ***(B)*** *total and* ***(D)*** *B cell numbers in para-aortic lymph nodes (PALN). Each dot represents one mouse, graphs show mean +/- SD. Statistics carried out using Mann-Whitney test, * P < 0.05; ** P < 0.01; *** P < 0.001; **** P < 0.0001.*

The relative and absolute proportion of cells identifiable as GC was not altered by diet or treatment type in the spleen nor was the proportion of GC cells in the PALN *(Figure 176A, B, C)*. However, as expected HFD induced a significant expansion in the number of GC B cells in the PALN compared to chow diet *(Figure 176D)*.

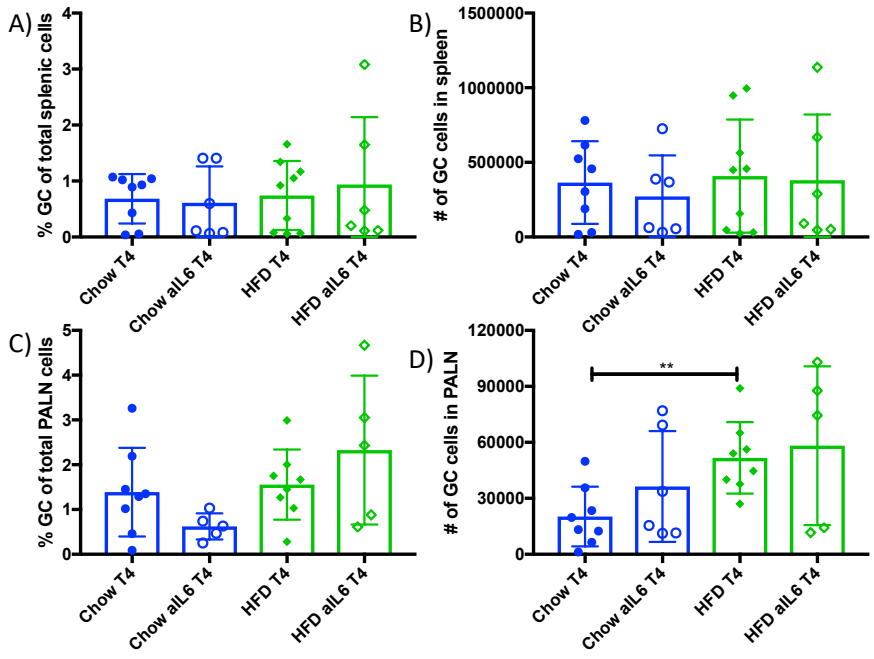

Figure 176. ***No impact of anti-IL6 on GC responses after 4 weeks in male AEL mice.*** *Male AEL mice were fed either chow (blue or high fat diet (HFD; green) for 4 weeks (T4) and treated weekly with either isotype control (closed symbols) or anti-IL6 (aIL6; open circles).* ***(A)*** *Proportion and* ***(B)*** *absolute numbers of GC B cells in spleen and* ***(C)*** *proportion and* ***(D)*** *absolute numbers of GC B cells in para-aortic lymph nodes (PALN). Each dot represents one mouse, graphs show mean +/- SD. Statistics carried out using Mann-Whitney test, * P < 0.05; ** P < 0.01; *** P < 0.001; **** P < 0.0001.*

The total number of cells in the LN labelled with EYFP was reduced in chow diet-fed male LDLr$^{-/-}$ AEL mice by IL6 blockade and this was most apparent in the EYFP plasma cells of both IgM+ and IgM- isotypes *(Figure 177)*. Similar trends were seen in HFD-fed male LDLr$^{-/-}$ AEL mice but did not reach significance *(Figure 177)*.

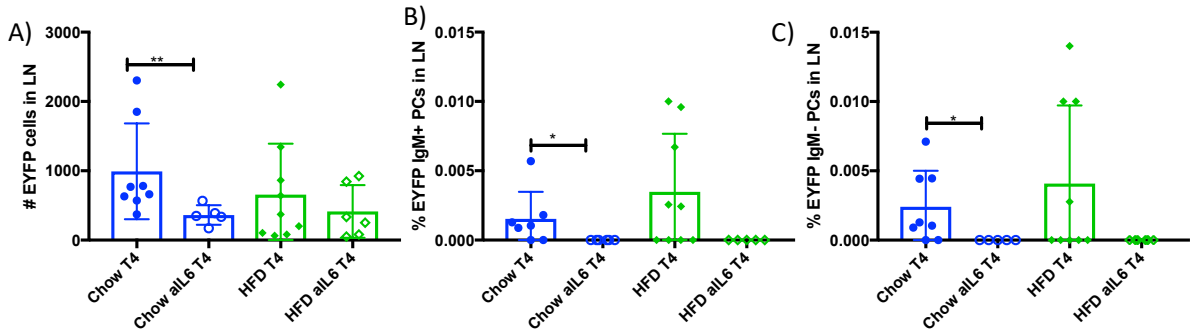

Figure 177. ***Reduced EYFP cell numbers after anti-IL6 treatment in chow diet-fed male AEL mice after 4 weeks.*** *Male AEL mice were fed either chow (blue or high fat diet (HFD; green) for 4 weeks (T4) and treated weekly with either isotype control (closed symbols) or anti-IL6 (aIL6; open circles). Tamoxifen was administered, 9mg via oral gavage, 48hrs prior to sacrifice to induce EYFP labelling. In the lymph node (LN)* ***(A)*** *Total number of EYFP cells,* ***(B)*** *EYFP IgM+ plasma cells (PCs) and* ***(C)*** *EYFP IgM- PCs. Each dot represents one mouse, graphs show mean +/- SD. Statistics carried out using Mann-Whitney test, * P < 0.05; ** P < 0.01; *** P < 0.001; **** P < 0.0001.*

Therapeutic antagonism of IL6 reduced the proportion of EYFP memory cells identified in the blood, specifically those of IgM- isotype in male LDLr$^{-/-}$ AEL mice *(Figure 178)*.

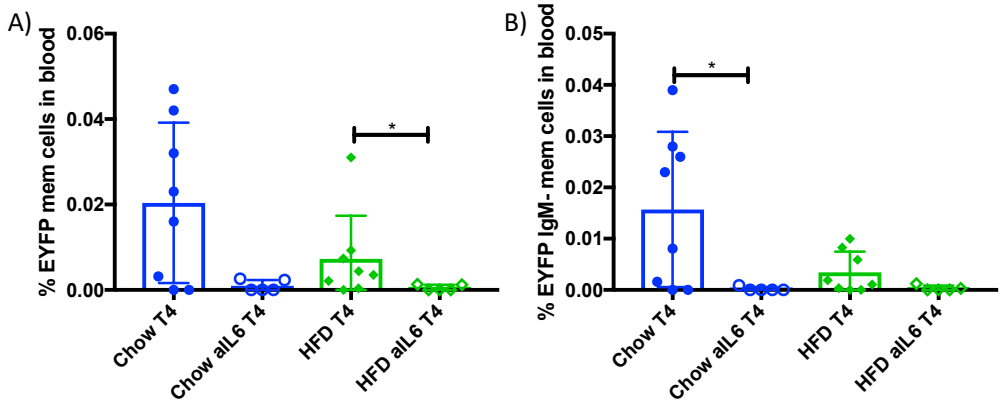

Figure 178. ***Reduced EYFP memory cells in blood after anti-IL6 treatment in male AEL mice after 4 weeks.*** *Male AEL mice were fed either chow (blue or high fat diet (HFD; green) for 4 weeks (T4) and treated weekly with either isotype control (closed symbols) or anti-IL6 (aIL6; open circles). Tamoxifen was administered, 9mg via oral gavage, 48hrs prior to sacrifice to induce EYFP labelling. In the blood* ***(A)*** *proportion of EYFP memory (mem) cells and* ***(B)*** *those EYFP memory cells which are IgM-. Each dot represents one mouse, graphs show mean +/- SD. Statistics carried out using Mann-Whitney test, * P < 0.05; ** P < 0.01; *** P < 0.001; **** P < 0.0001.*

In the Peyer's patches, anti-IL6 treatment caused a reduction in the GC population as well as the EYFP cell population, particularly the EYFP PC population, in chow diet-fed male LDLr$^{-/-}$ AEL mice *(Figure 179A, B, F)*. In HFD-fed male LDLr$^{-/-}$ AEL mice, anti-IL6 treatment also reduced the proportion of EYFP cells compared to isotype control especially those of GC and memory phenotype *(Figure 179B, D, E)*. Additionally anti-IL6 administration reduced the class switch ratio in chow diet-fed male LDLr$^{-/-}$ AEL mice compared to isotype control *(Figure 179C)*.

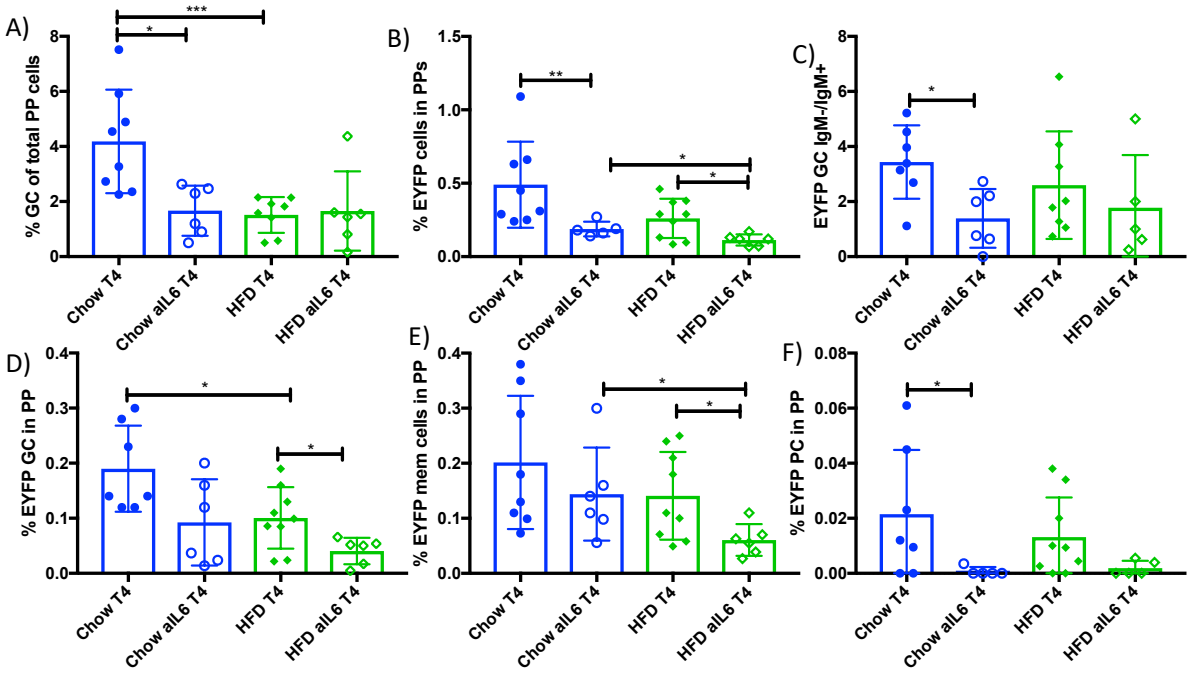

Figure 179. ***Impact of anti-IL6 treatment on GC responses of PPs after 4 weeks in male AEL mice.*** *Male AEL mice were fed either chow (blue or high fat diet (HFD; green) for 4 weeks (T4) and treated weekly with either isotype control (closed symbols) or anti-IL6 (aIL6; open circles). Tamoxifen was administered, 9mg via oral gavage, 48hrs prior to sacrifice to induce EYFP labelling. In the Peyer's patches (PP)* ***(A)*** *proportion of GC cells,* ***(B)*** *EYFP cells,* ***(C)*** *class switch ratio,* ***(D)*** *EYFP GC cells,* ***(E)*** *EYFP memory (mem) cells and* ***(F)*** *EYFP plasma cells (PCs). Each dot represents one mouse, graphs show mean +/- SD. Statistics carried out using Mann-Whitney test, * P < 0.05; ** P < 0.01; *** P < 0.001; **** P < 0.0001.*

6.5 Discussion

6.5.1 Impact of blocking cholesterol uptake on GC responses

Lomitapide was validated for experimental use by the finding that total cholesterol and LDL levels within the plasma of mice was reduced in the presence of the drug only. Further studies demonstrated that lomitapide also lowered HDL and triglyceride levels when the final dose was administered 4 hours prior to sacrifice. The total cholesterol to HDL ratio is used clinically to determine a patient's risk of cardiovascular disease; a value of greater than 5 is categorised as unhealthy. Lomitapide lowered the total cholesterol to HDL ratio demonstrating that it provides health benefits. As HDL is protective against atherosclerosis, calculating the ratio of LDL to HDL provides a risk profile; a value greater than 3 is pathogenic. Lomitapide lowered the LDL to HDL ratio demonstrating its protective function. In $LDLr^{+/-}$ mice, homeostatic cholesterol levels are lower as there are more LDL receptors available to uptake LDL into cells – in $LDLr^{-/-}$ total cholesterol levels were ~5mmol/L while $LDLr^{+/-}$ total cholesterol levels were ~3mmol/L. Furthermore, HFD had a lesser impact in $LDLr^{+/-}$; total cholesterol levels increased

to ~5mmol/L while in LDLr$^{-/-}$ total cholesterol levels rose to ~20mmol/L. Differences of the same magnitude were observed for LDL levels. Lomitapide had no effect on any cholesterol parameters within female WT AEL mice suggesting that the drug only functions within hyperlipidaemic environments provided by LDLr deficiency. In male LDLr$^{-/-}$ AEL mice, lomitapide reduced total cholesterol and LDL levels even in mice fed a chow diet suggesting that LDLr deficiency raises cholesterol levels in chow diet. This finding has previously been reported in the literature whereby young LDLr$^{-/-}$ mice fed a chow diet had plasma cholesterol levels twice as high as C57BL/6 around 5.2 mmol/L (200mg/dL) which increased gradually to 9 mmol/L (350mg/dL) over time[285]. Despite lacking in additional cholesterol, the HF only diet increased total cholesterol, LDL and triglyceride levels showing that a high lipid concentration within circulation can elevate cholesterol levels. Lomitapide lowered cholesterol parameters slightly but not significantly in HF only diet-fed mice while it appeared to elevate levels in HFHC diet-fed mice. This was an unexpected result, and its reason is unknown currently. Repeat experiments should be conducted to determine whether this was a true result.

In the pilot study, the GC population was unaffected; however as previously mentioned the tissue collection took place 3 days after the last dose when the lomitapide would no longer have much effect so it is possible that the GC population had been affected and had already returned to baseline. In the 4-week female LDLr$^{-/-}$ AEL study, the GC population was reduced by lomitapide in the spleen both in proportion and absolute terms while it was unaffected in the PALN. Both IgM+ and IgM- GC B cells were reduced in response to lomitapide demonstrating that the reduction in GC was not isotype specific. This implies that the spleen is more responsive to changes in cholesterol levels which go on to influence the GC response while the PALN is less responsive possibly due to its hyper localised function. In the female WT AEL mice, the proportion and absolute number of GC B cells was not affected by diet or treatment in the spleen or PALN demonstrating that the GC population changes in response to cholesterol levels as these were also not impacted in female WT AEL mice. This was also observed in male LDLr$^{-/-}$ AEL mice where cholesterol parameters were not significantly impacted by lomitapide treatment, and neither were GC levels.

Curiously, in the pilot study the monocyte population was increased in the spleen in the treated group. The neutrophil population was reduced in response to lomitapide in the

spleen. Lomitapide resulted in an expanded Ly6C^{lo} monocyte population within the spleen and BM while it reduced the Ly6C^{hi} monocyte population in the BM. In the 4-week study however, both Ly6C^{int} and Ly6C^{lo} monocyte populations were decreased in response to lomitapide treatment within the spleen. As the monocyte population was not the focus of the PhD, this was not investigated further but could prove an interesting direction for future research.

Serum IgM was reduced in the lomitapide treated HFD-fed group demonstrating an impact on the output of the GC. Possibly, lowering of cholesterol concentrations reduces the concentration of antigen available thus less IgM is required. In support of this hypothesis, IgM- plasma cells were increased in the BM and PALN in response to lomitapide treatment as was the proportion of total plasma cells.

In summary, lomitapide lowered total and LDL cholesterol as well as triglyceride levels in female LDLr$^{-/-}$ AEL mice after 4 weeks of diet and 2 weeks of treatment. In response the GC population was diminished suggesting a link between cholesterol homeostasis and the GC reaction. This effect was not seen in males possibly due to sex hormone differences.

6.5.2 Impact of cholesterol free diet on GC responses

In these studies, a cholesterol free (HF only) diet was used to elucidate the impact of dietary cholesterol on the GC response in atherosclerotic mice. The HF only diet induced similar weight gain to that of the HFHC diet after 4 weeks in female LDLr$^{-/-}$ AEL mice, however it did not elevate plasma lipid levels implying that dietary cholesterol is required for the increased plasma lipid content observed in atherosclerotic female mice. The HF only diet also prevented hypertrophy of the PALNs induced by HFHC diet, both in total cellularity and B cell population size suggesting that dietary cholesterol is responsible for the expansion of the PALNs within female LDLr$^{-/-}$ AEL mice. Within both the spleen and PALN, the GC population remained comparable with chow diet upon HF only diet feeding both in relative and absolute terms and this was seen across IgM+ and IgM- clones in female LDLr$^{-/-}$ AEL mice suggesting that plasma LDL levels were not sufficient to stimulate GC responses. There was a direct correlation between plasma LDL levels and extent of splenic GC responses in the spleen in female LDLr$^{-/-}$

AEL mice fed HFHC diet while there were no clear correlations between lipid levels and splenic GC proportion in either of the other diet types demonstrating that dietary cholesterol is key to enhanced GC responses in atherosclerotic female LDLr$^{-/-}$ AEL mice.

At 4 weeks in female LDLr$^{-/-}$ AEL mice, the HF only diet also prevented the HFHC diet-induced expansion of the EYFP population in the spleen and PALN suggesting that dietary cholesterol causes an increase in cells actively which are AID positive; undergoing SHM and class switching within the GC. The HF only diet induced increases in the EYFP GC, particularly those which were IgM+, and memory cell populations to a smaller extent than that of the HFHC diet demonstrating reduced GC output upon HF only diet feeding.

The plasma cell population was expanded in response to 4 weeks of HFHC diet in the spleen and PALN while in the HF only diet-fed female LDLr$^{-/-}$ AEL mice this effect was blunted. Furthermore, the EYFP labelled plasma cell pool was expanded in response to 4 weeks of HFHC diet in female LDLr$^{-/-}$ AEL mice while this effect was absent in HF only diet-fed female LDLr$^{-/-}$ AEL mice. The total EYFP memory, particularly IgM+ clones, population was reduced in PALN upon feeding both HFHC and HF only diets compared to chow. This would suggest that memory populations are less impacted by dietary cholesterol than plasma cell populations; potentially more PCs are produced in response to the HFHC diet in order to produce more antibody. This suggests that the HFHC diet induces a more productive splenic and para-aortic GC response with greater output of plasma cells prepared to mobilise in response to the high dietary concentration of cholesterol which is not seen in response to high dietary fat concentration.

As seen previously (earlier chapters), HFHC diet suppresses GC responses within the PPs and this effect was observed for the HF only diet also, mainly due to a decrease in IgM+ clones. This was reflected in the EYFP cell populations which were also suppressed upon feeding HF only and HFHC diets compared to chow diet for 4 weeks in female LDLr$^{-/-}$ AEL mice. This shows that dietary cholesterol is not required for the suppressive function of the HFHC diet on GC responses within the PPs and thus suggests that high concentrations of dietary fat could be responsible.

The reduction in the class switch ratio both in the LN and the PALN in female LDLr$^{-/-}$ AEL mice fed HFHC diet for 4 weeks demonstrates that more IgM+ GC clones were produced in response to the diet compared to both chow and HF only diets. This corroborates the previous hypothesis suggesting that the increased IgM titres seen in atherosclerotic mice are in response to dietary cholesterol.

GC responses were longer lasting, as measured by the GC: memory ratio, both in the PALN and PPs of female LDLr$^{-/-}$ AEL mice fed HFHC diet. This effect was blunted in HF only diet-fed female LDLr$^{-/-}$ AEL mice suggesting that individual GCs resolve at a faster rate in response to high fat only compared to the addition of high cholesterol.

While IgG1 antibody titres were diminished in response to both high fat containing diet types after 4 weeks in female LDLr$^{-/-}$ AEL mice, IgM antibody levels were increased in both diet types after 4 weeks. IgG1 levels were also reduced at the 8-week timepoint for both HF only and HFHC diets but to a lesser extent in the HF only diet. Serum levels of anti-dsDNA antibodies were elevated in HFHC diet-fed female LDLr$^{-/-}$ AEL mice but not in HF only diet-fed female LDLr$^{-/-}$ AEL mice after 4 weeks implying that dietary cholesterol is responsible for autoimmune responses while dietary fat is not. Furthermore, serum levels of CXCL1 and IL1β were amplified by both HFHC and HF only diets while serum IL6 and IL10 levels were only raised by 4 weeks of HFHC diet in female LDLr$^{-/-}$ AEL mice. This suggests that while the HF only diet can induce some level of inflammation through cytokine biomarkers, dietary cholesterol induces inflammation to a greater degree. This was confirmed by the finding that plasma IL6 and LDL levels were directly correlated.

These cytokines were chosen for analysis due to their roles in atherosclerosis. Binding to IL1R, IL1 stimulates production of wide variety of cytokines and chemokines along with endothelial cell adhesion molecules ultimately causing inflammatory cell recruitment and vascular damage through MMP production[314]. IL6 contributes to a positive feedback mechanism exacerbating vascular mitochondrial dysfunction leading to augmented atherosclerosis[315]. A deficiency in KC/GROα is accompanied by absence of intimal macrophages and reduced atherogenesis[316].

In the liver, 4 weeks of HFHC diet induced hepatic inflammation as seen in the increased expression of CXCL1, F4/80 and MCP1. Meanwhile, the HF only diet only increased transcript levels of IL6. MCP1 is a major driver of macrophage recruitment through adhesion and chemotaxis to atherosclerosis lesions using its receptor, CCR2, which is expressed on circulating monocytes[316]. Previous reports in the literature have determined a direct correlation between the degree of hepatic inflammation and total plasma cholesterol[317] and indeed in this study it was seen that there was a positive correlation between plasma cholesterol and transcript levels of both MCP1 and CXCL1. Western diet-fed LDLr$^{-/-}$ mice have been reported to have increased liver mass up by 45-65% with signs of hepatic steatosis and accumulation of cholesterol and TGs[285] as well as augmented inflammation as evidenced by elevated expression levels of Mcp1, CD68 and TNF[317].

In female WT AEL mice, no changes in weight gain, plasma lipid levels, cell numbers or GC levels were observed after 4 weeks of diet demonstrating that dietary cholesterol has little impact in a normolipidemic environment.

After 8 weeks of diet, weight gain was similar between HFHC and HF only diet-fed female LDLr$^{-/-}$ AEL mice and no differences in lipid levels were apparent. Both diets induced expansion in total and B cell numbers within the spleen and PALN yet only B cell numbers in the spleen were blunted in the HF only diet compared to the HFHC diet-fed female LDLr$^{-/-}$ AEL mice. Relative and absolute proportions of GC cells were increased to similar degree in both high fat containing diets compared to chow diet after 8 weeks while the absolute number of GC cells was significantly less in the spleen of female LDLr$^{-/-}$ AEL mice fed the HF only diet compared to the HFHC diet. These data demonstrate that the HF only diet had less impact on dietary cholesterol after 8 weeks and therefore had minor impact on the GC population thus highlighting those differences in lipid levels are key to modulating the GC population rather than specific dietary components alone.

Surprisingly, the HF only diet stimulated production of greater plasma cell pools, mainly those which were IgM-, within the PALN and PPs after 8 weeks compared to either the chow or HFHC diet in female LDLr$^{-/-}$ AEL mice. Contrastingly, no EYFP labelled plasma cells were detected in the BM of those female mice fed the HF only diet. This suggests that GCs are

skewed towards high affinity plasma cell production at the 8-week timepoint after HF only diet feeding, indeed plasma cell production does occur at later stages of a GC response, but EYFP labelled plasma cells are not homing to the BM niche.

In male LDLr$^{-/-}$ AEL mice, increases in weight gain and cholesterol levels were comparable between HFHC and HF only diets after 4 weeks. GC responses within the spleen were unaffected by diet type, however in the PALN the HF only diet induced greater expansion of the GC population than did the HFHC diet after 4 weeks. This was not isotype specific as both IgM+ and IgM- GC clones were expanded in the HF only diet-fed male mice and similar results were found in the LNs. Again, high fat containing diets reduced PPs GC responses, including labelled cells, although this effect was blunted slightly but not significantly in the HF only diet-fed male LDLr$^{-/-}$ AEL mice. Thus, dietary cholesterol has an immunosuppressive function on GC responses of the PPs. The HF only diet also resulted in an increased number of cells expressing AID at time of labelling expanding the EYFP cell population within the LN, PALN and blood after 4 weeks in male LDLr$^{-/-}$ AEL mice. The class switch ratio was reduced in both HF containing diet types compared to chow diet in the LNs while it was slightly increased compared to HFHC diet in the PALN. The opposite was true for the PPs where the HFHC diet class switch ratio was higher than that of the HF only diet after 4 weeks in male LDLr$^{-/-}$ AEL mice. Across the LN, PALN and PP, the GC longevity was reduced in HF only diet-fed male LDLr$^{-/-}$ AEL mice compared to HFHC diet for 4 weeks in male LDLr$^{-/-}$ AEL mice. These data suggest that dietary cholesterol has little impact on the spleen but greater impact on the PALN after 4 weeks in male LDLr$^{-/-}$ AEL mice. Absence of dietary cholesterol led to increased AID activity, however GCs resolved more quickly suggesting a more acute rather than chronic response compared to the HFHC diet.

Plasma cell production was greatest in HF only diet-fed male LDLr$^{-/-}$ AEL mice in the spleen and PALN after 4 weeks, mainly due to IgM- clones. The EYFP labelled plasma cell population, both IgM+ and IgM- isotypes, was expanded in HF only diet-fed male LDLr$^{-/-}$ AEL mice compared to other diet types across the spleen, PALN, PPs, BM and blood suggesting that dietary cholesterol suppresses PC production after 4 weeks in male LDLr$^{-/-}$ AEL mice.

Plasma lipid levels and weight were significantly increased in response to both HF only and HFHC diets compared to chow diet after 8 weeks in male LDLr$^{-/-}$ AEL mice. While 8 weeks of HFHC diet in male LDLr$^{-/-}$ AEL mice induced an expansion of the para-aortic B cell population, there was no impact of diet type on total cell numbers in spleen or PALN nor on splenic B cell numbers. The total number of splenic GC cells was significantly greater in HF only diet-fed male LDLr$^{-/-}$ AEL mice after 8 weeks while the HFHC diet induced the greatest proliferation of para-aortic GC B cells after 8 weeks. The EYFP GC population was greater in HF only diet-fed male LDLr$^{-/-}$ AEL mice while the EYFP memory population was the biggest in HFHC diet-fed male LDLr$^{-/-}$ AEL mice after 8 weeks. The HF only diet induced expansion of IgM+ clones visible in both the GC and memory labelled compartments while HFHC diet induced production of IgM- memory cells. Thus, dietary cholesterol plays a less significant role after 8 weeks in male LDLr$^{-/-}$ AEL mice and appears to skew GC output toward memory production while HF only diet skews toward PC production.

Serum analysis demonstrated that both CXCL1 and TNFα levels were augmented in HF only diet-fed male LDLr$^{-/-}$ AEL mice after 8 weeks compared to chow and HFHC diets. Both HF only and HFHC diets had reduced IFNγ titres compared to chow diet while serum IL2 was reduced upon HFHC but not HF only diet feeding compared to chow diet. The HF only diet caused reduction in serum IL5 levels compared to that of HFHC diet for 8 weeks in male LDLr$^{-/-}$ AEL mice. Serum IgG1 was reduced upon high fat containing diet feeding while serum IgM titres were increased. In male LDLr$^{-/-}$ AEL mice, it appears that HF only diet is more inflammatory at the 8-week timepoint due to upregulation of CXCL1 and TNFα.

6.5.3 Impact of blocking IL6 on GC responses

Anti-IL6 treatment for 4 weeks had no impact on total and B cell numbers within the spleen and PALN but did result in increased relative and absolute numbers of GC cells in the spleen for both HFHC and HF only diets after 4 weeks in female LDLr$^{-/-}$ AEL mice. Treatment with anti-IL6 antibody increased the proportion and absolute number of EYFP labelled GC cells in the spleen, of both IgM+ and IgM- isotypes, in both HFHC and HF only diet-fed female LDLr$^{-/-}$ AEL mice after 4 weeks. There was no impact on overall GC responses in the PALN. However, the

EYFP GC and memory populations, mainly of IgM clonality, were expanded upon blocking anti-IL6 in the PALN of female LDLr$^{-/-}$ AEL mice fed HFHC diet for 4 weeks. In contrast, antagonism of IL6 reduced the EYFP cell population within the PPs, especially those of memory phenotype, upon HFHC diet feeding in female LDLr$^{-/-}$ AEL mice for 4 weeks. The duration of individual GCs was reduced upon anti-IL6 treatment in the PPs of female LDLr$^{-/-}$ AEL mice fed HFHC diet for 4 weeks while anti-IL6 treatment in HF only diet-fed female LDLr$^{-/-}$ AEL mice extended the duration of GCs within the spleen. From these results, blocking IL6 lifted a break on the total and EYFP labelled GC response in the spleen and PALN particularly within the HFHC diet-fed female LDLr$^{-/-}$ AEL mice. Meanwhile IL6 antagonism within the PPs suppressed EYFP cell populations.

Within the spleen, relative and absolute plasma cell output, particularly of IgM- clones, was reduced upon blockade of IL6 in HFHC diet-fed female LDLr$^{-/-}$ AEL mice after 4 weeks. Contrastingly, in the PPs anti-IL6 treatment enhanced the proportion of IgM+ PCs in both HF only and HFHC diet-fed female LDLr$^{-/-}$ AEL mice. IgM- PCs of the PPs were reduced upon anti-IL6 treatment in HF only diet-fed female LDLr$^{-/-}$ AEL mice for 4 weeks. Blocking IL6 resulted in a more active GC response within the spleen with reduced PC output while the opposite occurred in the PPs with reduced GC activity and enhanced PC output suggesting that selective inhibitory pressure on one stage of GC responses results in selective expansion on other stages.

After 8 weeks of diet, 4 weeks of anti-IL6 treatment increased total cholesterol, LDL, and triglyceride levels beyond that of isotype treatment in HF only diet-fed female LDLr$^{-/-}$ AEL mice. Anti-IL6 treatment had little impact on total cell numbers in the spleen and PALN yet it did reduce B cell numbers in the spleen of female LDLr$^{-/-}$ AEL mice fed the HFHC diet for 8 weeks. This suggests that dampening inflammation via IL6 can shrink the splenic B cell population. It is important to note that in this study, the chow diet-fed female LDLr$^{-/-}$ AEL mice had very low nearly undetectable levels in most parameters and therefore don't provide a particularly accurate comparison against the other diet types. The para-aortic GC response was unaffected by anti-IL6 treatment. IL6 blockade suppressed relative and absolute numbers of GC B cells in the spleen of female LDLr$^{-/-}$ AEL mice fed HFHC diet for 8 weeks as well as absolute GC cell numbers in female mice fed HF only diet for 8 weeks. Furthermore, there

was a reduction in the proportion and absolute numbers of EYFP GC cells upon anti-IL6 treatment in both spleen and LNs of 8-week HFHC and HF only diet-fed female LDLr$^{-/-}$ AEL mice. This reduction was less dramatic, mainly not significant, in HF only diet-fed female LDLr$^{-/-}$ AEL mice again suggesting that anti-IL6 has a greater impact in the presence of dietary cholesterol. This indicates that dampening inflammation has more impact on GC responses in the presence of dietary cholesterol highlighting its proinflammatory nature.

In male LDLr$^{-/-}$ AEL mice after 4 weeks of diet, anti-IL6 treatment did not affect cholesterol levels or splenic total and B cell numbers. Oddly, anti-IL6 treatment caused expansion of total and B cell numbers in the PALN of male mice fed chow diet. The GC population was unaffected in the spleen while HFD induced proliferation of para-aortic GC B cells compared to chow diet as seen previously. Meanwhile the number of EYFP labelled cells, both IgM+ and IgM- was diminished upon anti-IL6 treatment in LNs of chow diet-fed male LDLr$^{-/-}$ AEL mice. A similar effect was observed for the HFD group but did not reach significance. Anti-IL6 treatment also reduced the proportion of EYFP memory cells, particularly those of IgM- clonality, in the blood of chow and HFD-fed male LDLr$^{-/-}$ AEL mice. This suggests that while the total GC population was not affected by anti-IL6 treatment, the specific EYFP labelled population was dampened.

Within the PPs, anti-IL6 treatment reduced the GC population of chow diet-fed LDLr$^{-/-}$ AEL mice as well as the EYFP PC population. The total EYFP population was reduced upon anti-IL6 treatment in both chow and HFD-fed male LDLr$^{-/-}$ AEL mice. Both the EYFP GC and memory populations were specifically diminished upon anti-IL6 treatment in those male LDLr$^{-/-}$ AEL mice fed HFD. Finally, the EYFP class switch ratio was diminished in chow-fed male LDLr$^{-/-}$ AEL mice upon anti-IL6 treatment suggesting a skewing toward IgM- responses in treated mice. These results suggest that the magnitude of the GC response and its output is reduced by IL6 blockade.

6.5.4 Interplay between inflammation & hyperlipidaemia in atherosclerotic GC responses

My data shows that dietary cholesterol is critical for the induction of GC responses to atherosclerosis early in progression at 4 weeks in female LDLr$^{-/-}$ AEL mice and indeed these 2 variables are directly correlated. Furthermore pathways controlling B cell activation, antigen

binding and lipids are positively correlated with the development of atherosclerosis[318]. The PALNs are particularly sensitive to dietary cholesterol as they do not undergo hypertrophy without this component in the diet at the 4-week timepoint. Moreover, GC responses are more functional and longer lasting with higher levels of AID activity and produce greater output of PCs in the presence of dietary cholesterol. Furthermore, dietary cholesterol was more inflammatory through increased serum cytokine levels and hepatic inflammatory gene expression. However, by 8 weeks, dietary cholesterol has little impact on GC responses, only increasing total splenic B and GC B cell numbers, in females suggesting that once GCs are developed and the atherosclerotic inflammatory milieu has expanded, dietary cholesterol no longer plays such an important role.

The working assumption is that dietary cholesterol has the greatest inflammatory impact after 4 weeks at the earlier stages of atherosclerosis in female $LDLr^{-/-}$ AEL mice. At this time point, lipid levels are considerably elevated resulting in disrupted lipid homeostasis. An autoimmune B cell pathology, including exacerbated GC responses, ensues reacting to LDL-induced inflammation. I hypothesise that this pathology is not seen at the 8-week timepoint as dietary cholesterol has a more minor role thus the HF only diet has a similar effect to that of HFHC diet; in effect the HF only diet lipid levels have 'caught up' to that of the HFHC diet. Consequently, serum lipid levels and GC responses are high regardless of the presence of dietary cholesterol.

In male $LDLr^{-/-}$ AEL mice, contrasting results were discovered – HF only diet induced greater splenic GC responses, which resolved more quickly, and increased number of cells with AID activity at time of labelling after 4 and 8 weeks of diet. In the absence of dietary cholesterol, plasma cell production was increased across organ types studied suggesting a potential suppressive effect of dietary cholesterol on the PC pool resulting in greater memory cell output. Serum analysis showed that HF only diet induced greater markers of inflammation in males than did the HFHC diet suggesting differing roles for dietary cholesterol in male and female $LDLr^{-/-}$ AEL mice. This could be due in part to the fact that female mice have a greater capacity for cholesterol absorption and hepatocyte cholesterol uptake[294].

This work has uncovered a suppressive effect of HFD on GC responses within the PPs and from these studies, it would appear that dietary cholesterol plays a role in this suppression. Additionally blockade of IL6 induced suppression of PP GC responses. In all experiments within this chapter, mice were fasted for 18hrs prior to sacrifice to normalise cholesterol levels between animals. Recently, literature has shown that fasting can cause B cell emigration from the PPs to the BM via CXCL13 chemotaxis[319], additionally fasting induces GC B cell apoptosis resulting in reduced size of PPs[320]. This could mean that total and GC B cell numbers within PPs are not reflective of the situation prior to fasting and should be taken into account when looking at results. However, no increases were seen in B cell numbers within the BM.

Inflammation is a major driver of GC responses in female mice after 8 weeks of diet demonstrated by the fact that the anti-IL6 treatment blunted GC responses particularly when mice were fed HFHC diet. As the anti-IL6 treatment had the opposite effect of augmenting splenic GC responses including EYFP labelled populations at 4 weeks, this suggests that IL6 acts to suppress GC activity at earlier stages of atherosclerosis. Thus, anti-IL6 can dampen inflammation and does so mainly after 8 weeks especially in the context of high concentrations of dietary cholesterol.

6.5.5 Future work

The HF only diet is a useful tool for elucidating the specific role of dietary cholesterol within the GC response to atherosclerosis. As plasma LDL and levels of splenic GC population directly correlated in the HFHC diet-fed female mice at 4 weeks, it could be interesting to try a range of diets with increasing cholesterol content to determine whether a dose-dependent response exists. However, it does not recapitulate the human setting that the HFHC diet can with the myriad of conditions present concurrently including metabolic dysfunction.

Due to time limitations, only the impact of IL6 was investigated as a means of dampening inflammation to investigate its effect on the GC response. In fact, IL6 plays a key role in the GC response and therefore disentangling its role in suppressing inflammation and interfering with normal GC function is impossible to do properly. As the GC response is multifaceted and

involves the interplay of multiple different cell types, all research conducted into atherosclerotic cytokines found that they were involved in the GC response one way or the other. With more time, a more thorough literature review could be undertaken to determine whether there are any atherosclerotic cytokines which do not interfere with the GC response.

Clearly the microbiome has important functions and effects beyond the scope of this thesis, however it could be interesting to determine what impact dietary cholesterol and dietary fat have in a germ-free environment.

Further in-depth analysis of serum cytokine levels and hepatic inflammatory gene expression could be conducted to determine the timeline of these inflammatory changes. Additionally, with more time plaque analysis could be conducted to determine the impact of dietary cholesterol on plaques and whether high dietary fat content is sufficient to induce atherogenesis. This was not a priority in these experiments as I was focused on investigating the earliest induction of immune responses that occur in parallel with plaque formation.

More studies are required to determine with confidence the impact of cholesterol and inflammation on atherosclerosis throughout pathogenesis and sex specific differences. These investigations have shown that cholesterol levels can directly impact the GC population. The HF only diet used had 0.05% cholesterol while the HFHC diet had 0.15% cholesterol; future studies could look at increasing cholesterol content within the diet to determine if cholesterol had a dose-dependent effect on the magnitude of the GC response.

7 IgG2c and its receptor FcγRIV contribute to pathogenicity of GC in atherosclerosis

7.1 Abstract

To test the hypothesis that IgG2c and its receptor FcγRIV are involved in the pathogenesis of atherosclerosis, the effect of IgG2c *in vitro* was analysed. Myeloid-derived monocytes upregulated pro-inflammatory FcγRIV upon IFNγ treatment and resulted in high TNF production. IgG2c significantly enhanced TNF secretion by these FcγRIV-expressing cells which were CD11b+CD11c+. The data presented herein provide evidence that IgG2c has the potential to exacerbate inflammatory responses from plaque macrophages and dendritic cells. Using genetic deletion of FcγRIV in a bone marrow transfer setting, the proportions of neutrophils, GC B, B and T cells was altered in $LDLr^{-/-}$ mice. Overall, the results further suggest a pathogenic role for IgG2c in promoting an inflammatory profile for plaque cell types.

7.2 Introduction

IgG antibodies bind to FcγRs as a major pathway for effecting their functions[321]. IgG binding triggers tyrosine phosphorylation of ITAM by the SRC kinase family[322]. Phosphorylation leads to activation of PI3 kinase which generates PI3P thus creating docking sites for Bruton's tyrosine kinase (BTK) and phospholipase C (PLC)γ[322]. Activation of PLCγ causes increase in intracellular calcium and triggers downstream signalling – the RAS-RAF-MAPK pathway is of importance in cellular activation following Fcγ receptor stimulation[322].

FcγRs are immune cell surface receptors which can be distinguished by their function, activating receptors include FcγRI, III and IV in mice[323]. FcγRs bind immunoglobulins through the invariant homodimeric fragment created by the C-terminal halves of the gamma heavy chain[323]. FcγRs display very similar extracellular portions whilst the cytoplasmic portion determines specificity[324]. Activating FcγRs promote pro-inflammatory actions through immunoreceptor tyrosine-based activation motif-mediated signalling pathways[321]. The

activatory receptors are expressed on neutrophils, dendritic cells, monocytes and macrophages[321]. Inhibitory FcγRIIb is antagonistic to activating FcγRs via its intracellular immunoreceptor tyrosine-based inhibitory motif domains[321]. The overall effect of immunoglobulin-containing immune complex binding to Fcγ receptors depends on the ratio of signals from activating ITAM-containing FcγRs and inhibitory ITIM-containing FcγRIIb as well as the IgG valency and subtypes[324].

FcγRIIb is the sole inhibitory receptor[321] and is expressed on murine B cells and indeed in humans, B cells are the major cell type to express FcγRIIb[321]. Binding of both the BCR and FcγRIIb to IgG-bound immune complexes increases the threshold for activation more so than for soluble antigen alone thereby restraining B cell responses[321]. FcγRIIb has a pro-apoptotic role on B1 cells and plasma cells that is constantly offset through the action of survival factors like BAFF from the TNF family[321]. FcγRIIb is upregulated on FDCs and participates in IC binding once GCs are established[174]. Increased FcγRIIb on FDCs results in reduced rates of SHM mainly of the IgM isotype while absence of FcγRIIb on FDCs results in increased clonal diversity within GCs[174]. FcγRIIb is expressed on monocytes and can modulate the monocyte response to different IgG antibodies/complexes.

The Fcγ receptors have been implicated in atherosclerosis, indeed global knockout of the γ chain, cytoplasmic signalling portion, of activating FcγRs is atheroprotective with decreased atherosclerotic burden[30]. Global deficiency reduces lesion size in $Apoe^{-/-}$ females on a high cholesterol diet for 16 weeks which is accompanied by reduced macrophage and T cell numbers[325]. MCP1 and ICAM1 mRNA levels are diminished as are the number of NFκB positive cells[325]. The Fcγ receptor is the most critical for macrophages to be able to clear LDL-containing ICs[325]. In vitro, NFκB activity stimulated by ICs is reduced in $\gamma^{-/-}$ VSMCs[325]. Another study conducted transferred $\gamma^{-/-}Apoe^{-/-}$ BM into $Apoe^{-/-}$ donors showed atherosclerotic plaques were 2.5-fold smaller than those of $Apoe^{-/-}$[326]. These lesions had decreased lipid accumulation as well as monocyte/macrophage and T cell content[326]. Additionally, SMC and collagen content was elevated while necrosis was decreased[326]. IgG antibody titres to oxLDL were increased and NFκB activity of aortic cells was blunted[326]. This study demonstrated that FcγR expression on BM-derived cells promotes atherosclerotic plaque development and that

BM gene deficiency in the γ chain is enough to reduce lesion formation[326]. Thus FcγR deficiency is atheroprotective due to a more stable plaque phenotype characterised by blunted lipid accumulation, reduced macrophage and T cell accumulation, increased collagen and SMC content, diminished cytokine production and NFκB activation[325].

FcγRIIb has a potential important role in regulating B cell responses in disease setting as genetic mutations in the receptor have been linked with SLE[321]. FcγRIIb deficient mice develop an autoimmune phenotype characterised by an aggravated immune response and autoreactive GC clones[327]. Reduction in FcγRIIb levels increases BCR signalling and thus increases tolerance, autoreactive B cell anergy and deletion[328]. Meanwhile, increased expression of FcγRIIb dampens immune responses[325].

Numerous studies have investigated the impact of FcγRIIb on cardiovascular disease. Evidence for a protective role of FcγRIIb includes a study using Fcgr2b$^{-/-}$ bone marrow transfer into LDLr$^{-/-}$ mice in which atherosclerosis was exacerbated[321]. A global deficiency in the receptor is protective against the rise in blood pressure that is associated with HFD-induced obesity[329]. FcγRIIb$^{-/-}$ also had increased numbers of plasma cells[330]. When male Apoe$^{-/-}$ mice fed HFD had knock out of FcγRIIb$^{-/-}$, atherosclerosis was exacerbated independently of cholesterol levels[331]. An additional study confirmed this effect and showed evidence of increased lipid retention[332]. These mice develop a proinflammatory cytokine secretory phenotype, with increased levels of IL1β, IL6, MCP1 and TNFα[332]. Antibody titres to MDA-LDL and oxLDL as well as total IgG levels are also elevated[332]. Thus, deletion of FcγRIIb dysregulates the B cell population[332]. The results demonstrated that FcγRIIb plays a crucial role in dampening the B cell response to modified LDL in the context of hyperlipidaemia[332].

Using CD11c-Cre to specifically delete FcγRIIb on CD11c+ cells, after bone marrow transfer total lesion size in female mice was increased 60%[331]. In contrast, male mice had reduction in atherosclerotic plaque size by 44% associated with increased anti-oxLDL IgM[331]. Another contradictory study showed a 50% decrease in atherosclerotic plaque size in Apoe$^{-/-}$FcγRIIb$^{-/-}$ associated with reduced Th1 cytokine secretion by T cells and increased production of anti-

inflammatory cytokines, IL4 and IL10, by CD4 T cells[332]. Expression of FcγRIIb is found on long-lived BM PCs and without it, PCs are maintained in BM for excessive amount of time[330].

Our laboratory investigated the impact of FcγRIIb loss on B cells specifically to elucidate its role in atherosclerosis[321]. The data revealed FcγRIIb as a critical atherosclerosis regulator as male Apoe$^{-/-}$ mice with overexpression of FcγRIIb developed less atherosclerosis along with reduced magnitude of class-switched B cell responses as seen by decreased numbers of plasma cells, GC B cells and serum IgG levels[321]. In contrast, genetically reduced FcγRIIb expression on GC B cells reduced the threshold of activation thus leading to elevated GC responses and enhanced atherosclerosis[321].

Recently a study investigating the role of FcγRIIb on SMCs was conducted[333]. FcγRIIb prevents eNOS activation and endothelial cell NO production[333]. In FcγRIIb KO mice, AngII-induced hypertension, arterial wall thickening and aortic collagen deposition was reduced[333]. These results demonstrate that FcγRIIb participates in vascular remodelling and hypertension[333]. Through specifically deleting FcγRIIb in VSMCs, it was shown that these cells had reduced AngII-induced vascular contraction[333]. Mechanistically the authors showed that FcγRIIb is a novel angiotensin II receptor type 1 (AT1R) regulator which reduces AT1R internalisation within SMCs[333]. The interaction between IgG and FcγRIIb enhances AngII-induced vascular remodelling and hypertension by blocking AT1R internalisation[333].

Genomic mapping revealed that FcγRIV is located in the intergenic interval between RII and RIII and has a unique expression pattern suggesting a specialised function in activating myeloid cells[334]. FcγRIV recognises soluble IgG2b and IgG2c containing immune complexes[335] and binding stimulates production of cytokines, proteolytic enzymes and superoxide anion[328]. FcγRIV is highly expressed on murine Ly6C^{lo} monocytes within the aorta and mediates the pathogenic effects of IgG2c[321]. IgG2c binds to FcγRIV with 40-fold greater affinity than does IgG1[334] due to its greater conformational restriction[323]. Antibody-mediated blocking of FcγRIV binding limits IgG2c functions[336].

Although IgG2c has been implicated in atherosclerosis from the previous work mentioned, mechanistic studies have been conducted to investigate the mechanism by which IgG2c potentially has a proatherogenic role.

7.3 Aims

1. Investigate potential for IgG2c to directly affect atherosclerotic cell types through culture of bone marrow-derived myeloid cells in vitro

2. Determine the effect of FcγRIV on atherosclerosis through use of FcγRIV deficient mice upon the LDLr deficient background using bone marrow transfer

7.4 Results

7.4.1 IgG2c induces TNF in FcγRIV-expressing CD11c+CD11b+ cells

I hypothesise that IgG2c is pathogenic in atherosclerosis via its pro-inflammatory receptor FcγRIV. To begin to investigate potential effector mechanisms for IgG2c in the setting of atherosclerosis, I set out to develop assays to test the functional impact of IgG2c on myeloid cells. Previous experiments in the laboratory determined that CD45+CD11b+CD11c+ monocyte-derived macrophages/dendritic cells, within the murine atherosclerotic aorta, had high FcγRIV expression. To investigate the ability of IgG2c to directly impact atherosclerotic cell types, BM monocytes were differentiated with GM-CSF into CD11b+CD11c+MHCII+ dendritic cells (bone marrow-derived dendritic cells [BMDCs]) or using M-CSF to differentiate into macrophages (bone marrow-derived macrophages [BMDMs]). The cellular phenotype of these cells was confirmed by positive staining using flow cytometry for CD40, CD80 and CD86. FcγRIV expression on BMDCs was increased in response to the proatherosclerotic cytokine, IFNγ, more than TLR4 ligand, LPS, as determined by flow cytometry *(Figure 180A)* and qPCR *(Figure 180C)*. Flow cytometry also demonstrated that BMDMs displayed increased FcγRIV expression in response to IFNγ *(Figure 180B)*.

To examine the effect of immune complexes on moDC activation, two methods were used, and TNF secretion used as the read-out metric. Firstly, culture plates were precoated with either IgG1 or IgG2c and subsequently BMDCs and BMDMs were seeded in the presence of IFNγ. I conducted an IFNγ dose response assay to determine the effect of increasing IFNγ concentration on TNF production by BMDCs when incubated with IgG1 or IgG2c. On uncoated plates, IFNγ did not affect TNF production at any dose *(Figure 180D, blue line)*. In the absence of IFNγ, IgG1 coated plates induced a small amount of TNF and IgG2c coated plates resulted in significantly increased TNF production. IgG1-coated plates induced small amounts of TNF compared to uncoated plates, but TNF production did not vary with increasing doses of IFNγ *(Figure 180D, red line)*. Strikingly, IgG2c-coated plates resulted in significantly augmented TNF production in a dose-dependent manner with increasing IFNγ doses *(Figure 180D, green line)*. This demonstrates that IFNγ stimulates FcγRIV upregulation in a directly proportional manner and consequently indirectly increases IgG2c-induced TNF production in BMDCs. As such, IFNγ was used to prime FcγRIV expression on BMDCs and BMDMs and TNF used to quantify cellular activation.

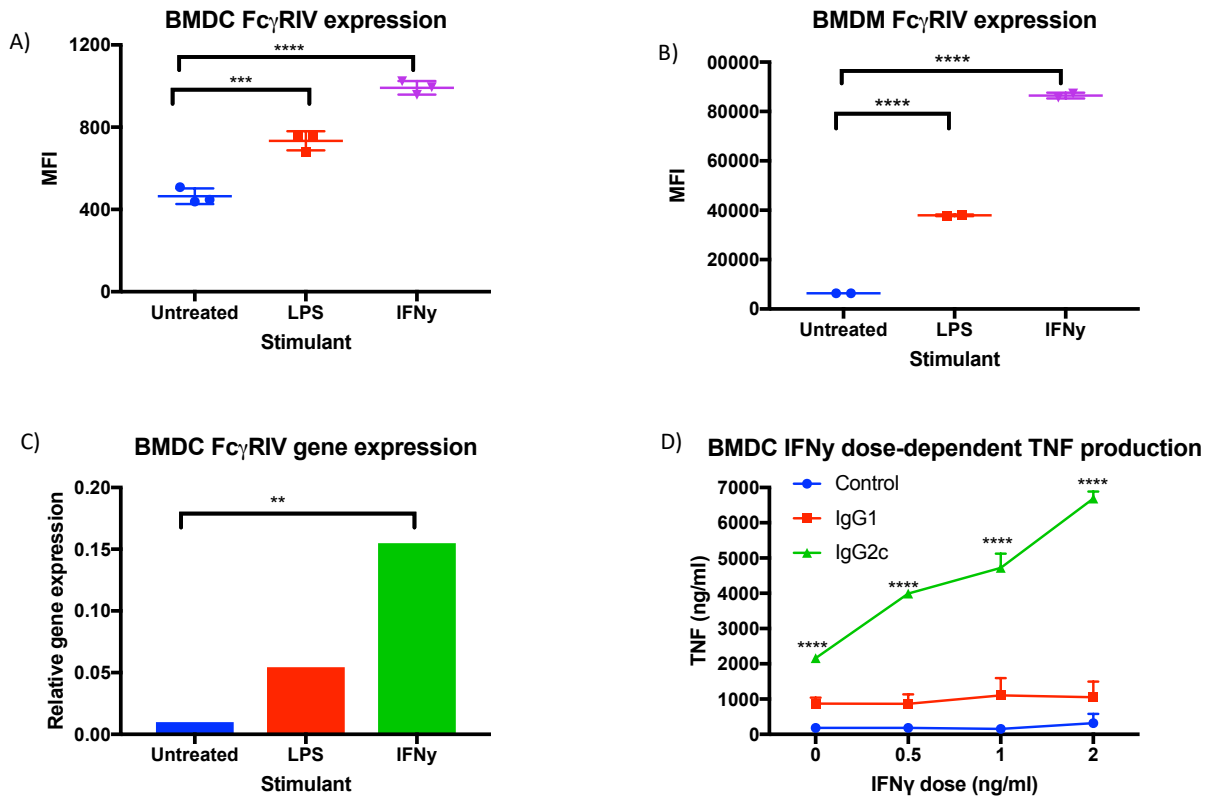

Figure 180. ***FcγRIV expression increased on BMDCs in response to IFNγ resulting in TNF production.*** *Bone marrow-derived monocytes were differentiated into **(A, C, D)** bone marrow-derived dendritic cells (BMDCs) using GM-CSF over a 10 day period and **(B)** bone-marrow derived macrophages (BMDMs) using M-CSF over a 7 day period. Cells were seeded at 2x10^6/ml in 96 well tissue culture plate and treated with either LPS (1μg/ml) or IFNγ (100μg/ml). After 24 hours, cells were harvested **(A, B)** for flow cytometry and stained with CD11c PE, MHCII eF450 and FcγRIV BV650 before running samples on the BD Fortessa. Cells were also harvested using Trizol **(C)**, RNA extracted, cDNA synthesised, and qPCR run using $2^{-\Delta\Delta CT}$ method. **(D)** IgG1 (10μg/ml) and IgG2c (10μg/ml) were incubated in 96 well tissue culture plates overnight. Supernatant was collected 48 hours later, and TNF production measured by ELISA. Statistics carried out using one-way ANOVA, * P < 0.05; ** P < 0.01; *** P < 0.001; **** P < 0.0001.*

IFNγ has important roles in atherosclerosis[337] and has been detected both in murine and human atherosclerotic plaques[338], expressed by Th1 cells and monocytes/macrophages[314]. T cell-released IFNγ primes macrophages and DCs[337] and enhances antigen presentation by inducing MHCII expression as well as production of cytokines and growth factors all of which can induce inflammatory cell migration[338]. Thus the cytokine increases monocyte and lymphocyte migration into the atherosclerotic plaque[339]. IFNγ induces plaque expansion by facilitating lipid uptake by macrophages and the formation of foam cells partly through preventing upregulation of LDL uptake receptors[339], LDLr, CD36 and scavenger receptor A (SR-A), along with receptors for reverse cholesterol transport[339] and partly through dampening of the anti-atherogenic macrophage sterol-responsive network (MSRN) network of proteins[340]. Further evidence for the atherogenic role played by IFNγ is shown by the finding that inhibition of macrophage IFNγ signalling was atheroprotective in LDLr$^{-/-}$ mice[340] and that

injection of exogenous IFNγ in Apoe$^{-/-}$ mice expanded atherosclerotic plaque size by 2-fold and augmented mmLDL uptake[341]. A bone marrow transfer experiment with IFNγ$^{-/-}$ bone marrow into LDLr$^{-/-}$ resulted in increased collagen production at the expense of cell number[338] and reduced atherosclerotic plaque size[338]. The same effect was observed in Apoe$^{-/-}$ males and females with IFNγ deficiency which also displayed reduced plaque lipid content[314].

After 48hrs incubation on pre-coated IgG1 or IgG2c culture plates, IFNγ-treated BMDCs cultured alone produced low levels of TNF *(Figure 181A)*. However, IgG2c-coated plates resulted in greater production of TNF from BMDCs and BMDMs than those plates coated with IgG1 suggesting a more inflammatory effect for IgG2c on these cells *(Figure 181)*. As a control, soluble IgG1 and IgG2c were supplemented into media with cells (in uncoated wells) and negligible TNF production was detected *(Figure 181)* implying that antibodies must be multivalent to have inflammatory properties.

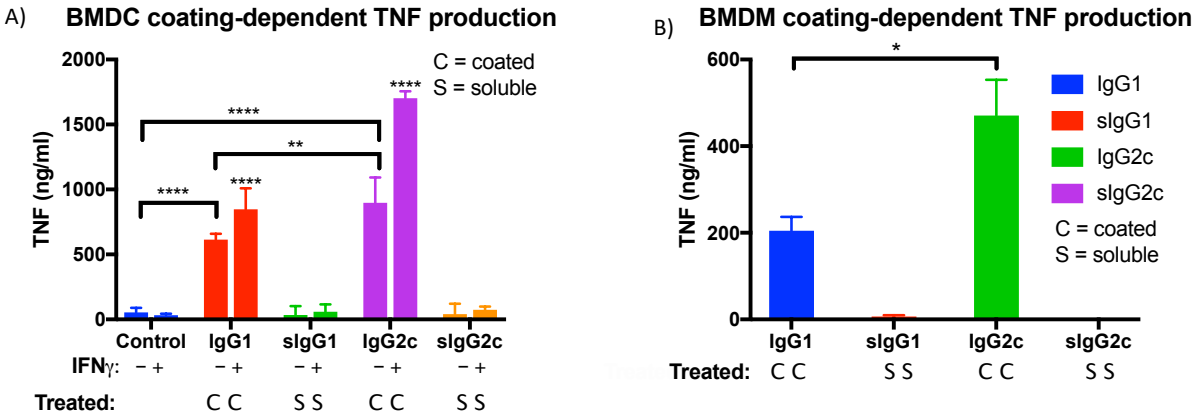

Figure 181. ***IgG2c coating results in TNF production from BMDCs and BMDMs.*** *Bone marrow-derived monocytes were differentiated into* ***(A)*** *bone marrow-derived dendritic cells (BMDCs) using GM-CSF over a 10 day period and* ***(B)*** *bone-marrow derived macrophages (BMDMs) using M-CSF over a 7 day period. IgG1 (10μg/ml) and IgG2c (10μg/ml) were incubated in 96 well tissue culture plates overnight. Cells were seeded at 2x10^6/ml in wells following antibody overnight incubation with either IFNγ treated (+) or control (-) GM-CSF media. Soluble IgG1 and IgG2c were added to media in the relevant wells. Supernatant was collected 48 hours later, and TNF production measured by ELISA. Statistics carried out using one-way ANOVA, * P < 0.05; ** P < 0.01; *** P < 0.001; **** P < 0.0001.*

The second approach involved the creation of antibody-coated particle mimics (in lieu of antibody-coated oxLDL or necrotic debris in plaque) using IgG1 or IgG2c-coated murine Ig-binding polystyrene beads. Beads, with or without coating, were incubated with IFNγ-pre-treated BMDCs *(Figure 182A)* or BMDMs *(Figure 182B)* and TNF production measured. Beads, alone or after IgG1 preincubation, produced little TNF when incubated with IFNγ-pre-treated

BMDMs while some TNF was produced from BMDCs beyond baseline TNF produced by IFNγ-treated BMDCs alone *(Figure 182A)*. In comparison, IgG2c-coated beads produced greater amounts of TNF while IgG1 coated beads failed to do so *(Figure 182)*.

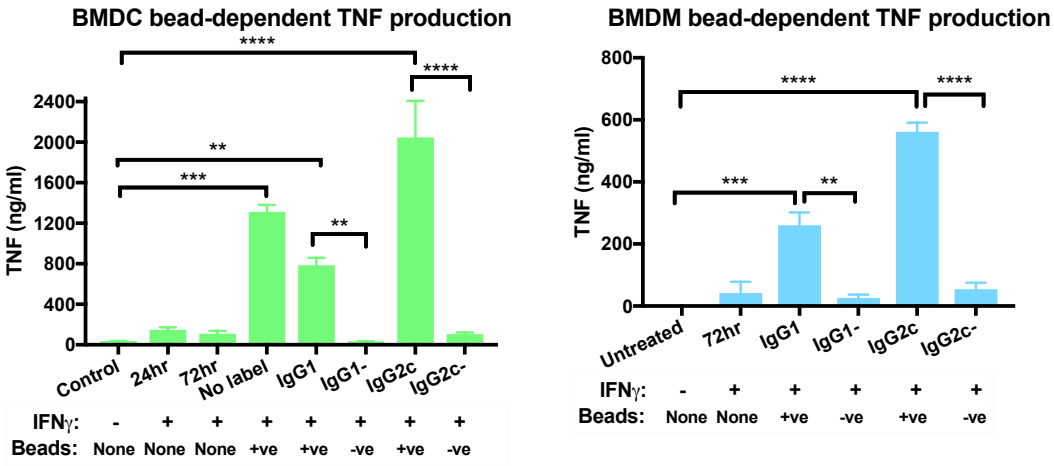

Figure 182. ***IgG2c beads result in TNF production from BMDCs and BMDMs.*** *Bone marrow-derived monocytes were differentiated into* ***(A)*** *bone marrow-derived dendritic cells (BMDCs) using GM-CSF over a 10- day period and* ***(B)*** *bone-marrow derived macrophages (BMDMs) using M-CSF over a 7-day period. Cells were plated in 96 well culture plates with either IFNγ media (+) or control (-) M-CSF media overnight. Polystyrene positive and negative beads were incubated with IgG1 (10μg/ml) and IgG2c (10μg/ml) for 1 hour. After removal of antibody mix, labelled and unlabelled (control) beads were resuspended in IFNγ M-CSF media and added to appropriate wells of 96 well culture plate. Supernatant was collected 48 hours later, and TNF production measured by ELISA. Statistics carried out using one-way ANOVA, * P < 0.05; ** P < 0.01; *** P < 0.001; **** P < 0.0001.*

Overall, these data support the hypothesis that IgG2c antibodies could be pathogenic by exacerbating inflammatory responses in plaque macrophages and/or dendritic cells.

7.4.2 Validation of FcγRIV$^{-/-}$ model

To investigate the role of IgG2c in the in vivo setting, mice lacking FcγRIV (CD16.2) were used[342] as FcγRIV is the main receptor through which IgG2c exerts its proinflammatory functions. FcγRIV is mainly expressed on monocytes, a key cell type in the pathogenesis in atherosclerosis. FcγRIV$^{-/-}$ bone marrow was used as donor in bone marrow transfer experiments into lethally irradiated LDLr$^{-/-}$ mice to investigate the role of FcγRIV in the atherosclerosis setting. After 4 weeks recovery, mice were started on HFD for 8 weeks and weighed weekly for health purposes. Upon sacrifice, blood, spleen, PALNs and BM were collected for analysis.

Body weights, cholesterol levels and antibody titres levels against IgG1, IgG2c, IgM and SAA were unaffected by loss of FcγRIV *(Figure 183)*.

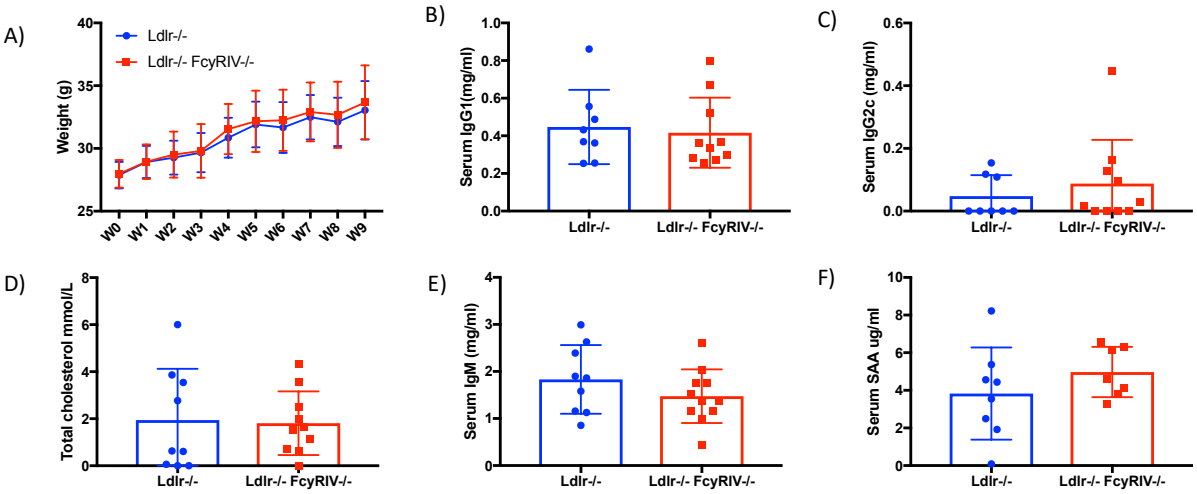

Figure 183. ***FcγRIV loss does not impact body weight, cholesterol, or antibody levels. (A)*** *LDLr$^{-/-}$ and LDLr$^{-/-}$FcγRIV$^{-/-}$ mice were weighed from before (W0) start of diet until week 9 (W9) and weight was measured in grams. Each point represents mean weight of group with standard deviation confidence intervals. Serum was analysed for antibody levels using ELISAs of* ***(B)*** *IgG1,* ***(C)*** *IgG2c,* ***(E)*** *IgM and* ***(F)*** *SAA and for* ***(D)*** *total cholesterol levels. Each dot represents 1 mouse, graphs show mean +/- SD.*

7.4.3 Fcγ receptor expression levels

To determine the impact of FcγRIV deletion, analysis of Fcγ receptor expression levels was conducted. FcγRI levels remained constant on neutrophils in the spleen *(Figure 184A)* and BM *(Figure 184B)* but were increased on blood neutrophils *(Figure 184C)* in LDLr$^{-/-}$FcγRIV$^{-/-}$. FcγRII/III levels didn't change on splenic neutrophils *(Figure 184D)* or blood borne neutrophils *(Figure 184F)* but were elevated in BM neutrophils *(Figure 184E)* in LDLr$^{-/-}$FcγRIV$^{-/-}$. As expected, FcγRIV levels were drastically reduced on neutrophils of the spleen, BM, and blood *(Figure 184G-I)* in LDLr$^{-/-}$FcγRIV$^{-/-}$.

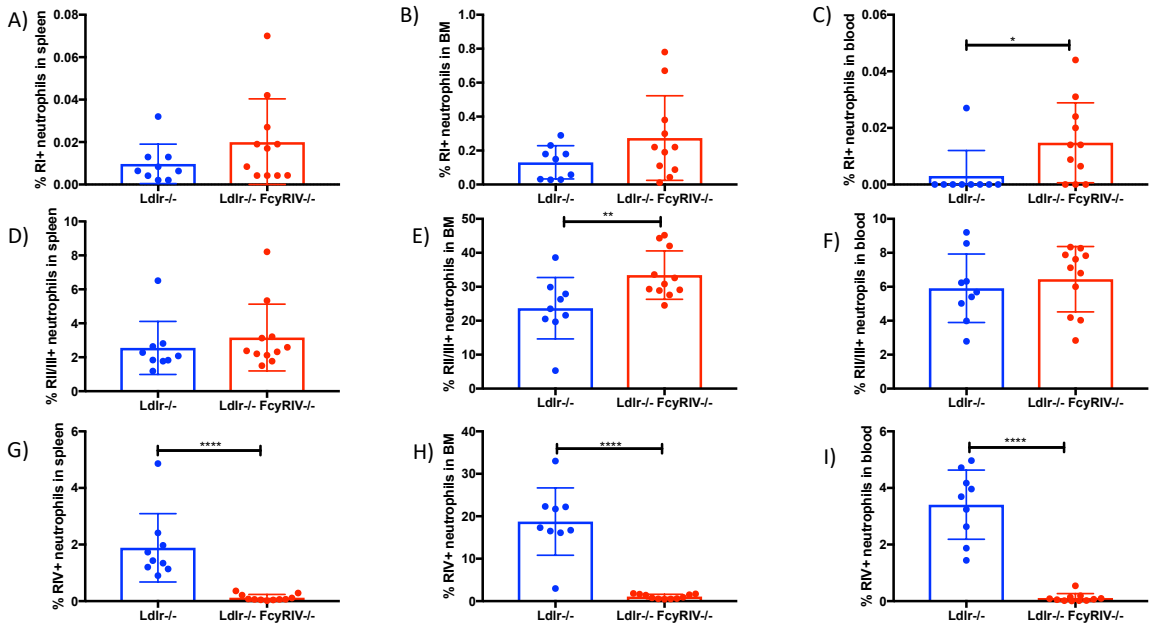

Figure 184. ***FcγR expression by neutrophils upon FcγRIV loss.*** *Percentage of neutrophils positive using flow cytometry for FcγRI in* ***(A)*** *spleen,* ***(B)*** *BM and* ***(C)*** *blood; FcγRII/III in* ***(D)*** *spleen,* ***(E)*** *BM and* ***(F)*** *blood and FcγRIV in* ***(G)*** *spleen,* ***(H)*** *BM and* ***(I)*** *blood. Each dot represents 1 mouse, graphs show mean +/- SD. Statistics carried out using Mann-Whitney test, * P < 0.05; ** P < 0.01; *** P < 0.001; **** P < 0.0001.*

FcγRI expression was not altered by FcγRIV deletion on monocytes in the spleen, BM, or blood *(Figure 185A-C)*. FcγRII/III expression was upregulated on splenic monocytes *(Figure 185D)* but not on BM or blood monocytes *(Figure 185E, F)* in LDLr$^{-/-}$FcγRIV$^{-/-}$. A dramatic reduction in FcγRIV on monocytes of the spleen, BM, and blood *(Figure 185G-I)* was confirmed.

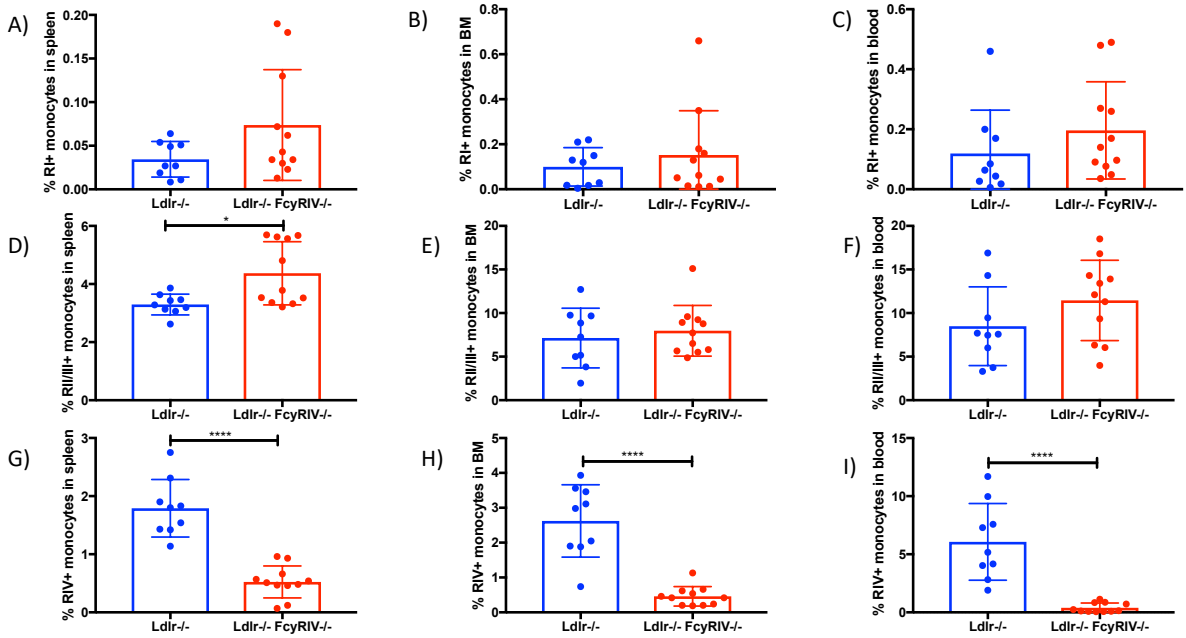

Figure 185. ***FcγR expression by monocytes upon FcγRIV loss.*** *Percentage of monocytes positive using flow cytometry for FcγRI in* ***(A)*** *spleen,* ***(B)*** *BM and* ***(C)*** *blood; FcγRII/III in* ***(D)*** *spleen,* ***(E)*** *BM and* ***(F)*** *blood and FcγRIV in* ***(G)*** *spleen,* ***(H)*** *BM and* ***(I)*** *blood. Each dot represents 1 mouse, graphs show mean +/- SD. Statistics carried out using Mann-Whitney test, * P < 0.05; ** P < 0.01; *** P < 0.001; **** P < 0.0001.*

FcγRI expression levels were not impacted by FcγRIV deletion in monocyte subsets within the spleen, BM, and blood *(Figure 186)*.

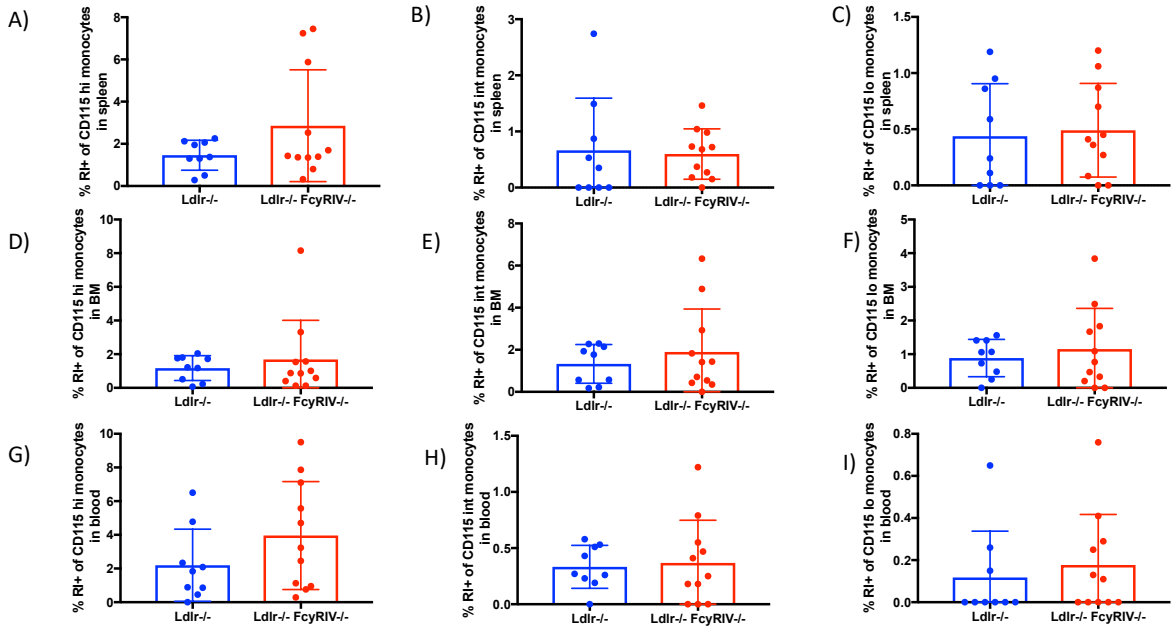

Figure 186. ***No impact of FcγRIV loss on FcγRI expression in monocyte subsets.*** *FcγRI expression (as % positive of total monocyte population) across monocyte subsets - CD115 hi monocytes are displayed* ***(A, D and G)****, CD115 int monocytes* ***(B, E and H)*** *and CD115 lo monocytes* ***(C, F, and I)****.* ***(A- C)*** *are within the spleen,* ***(D-F)*** *are within the BM and* ***(G-I)*** *are within the blood. Each dot represents 1 mouse, graphs show mean +/- SD.*

FcγRII/III was upregulated in all monocyte subsets of the spleen, BM and blood *(Figure 187A-D, F,H,I)* apart from CD115^{hi} monocytes of the blood *(Figure 187G)* and CD115^{int} monocytes of the BM *(Figure 187E)*.

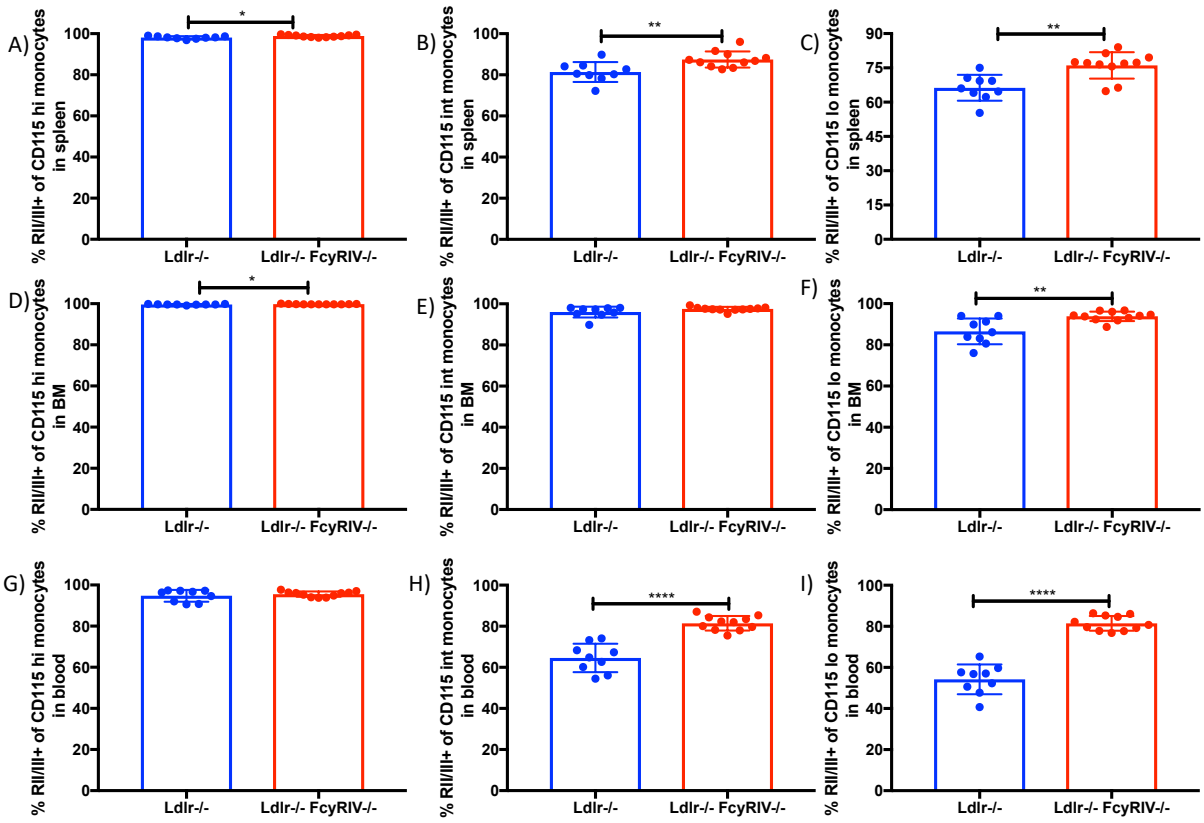

Figure 187. ***FcγRII/III expression upregulated upon FcγRIV loss in monocyte subsets.*** *FcγRII/III expression (as % positive of total monocyte population) across monocyte subsets - CD115 hi monocytes are displayed* ***(A, D and G)****, CD115 int monocytes* ***(B, E and H)*** *and CD115 lo monocytes* ***(C, F, and I)****.* ***(A- C)*** *are within the spleen,* ***(D-F)*** *are within the BM and* ***(G-I)*** *are within the blood. Each dot represents 1 mouse, graphs show mean +/- SD. Statistics carried out using Mann-Whitney test, * P < 0.05; ** P < 0.01; *** P < 0.001; **** P < 0.0001.*

Deletion of FcγRIV was confirmed by the severe reduction in its expression across all monocyte subsets in spleen, BM, and blood *(Figure 188)*.

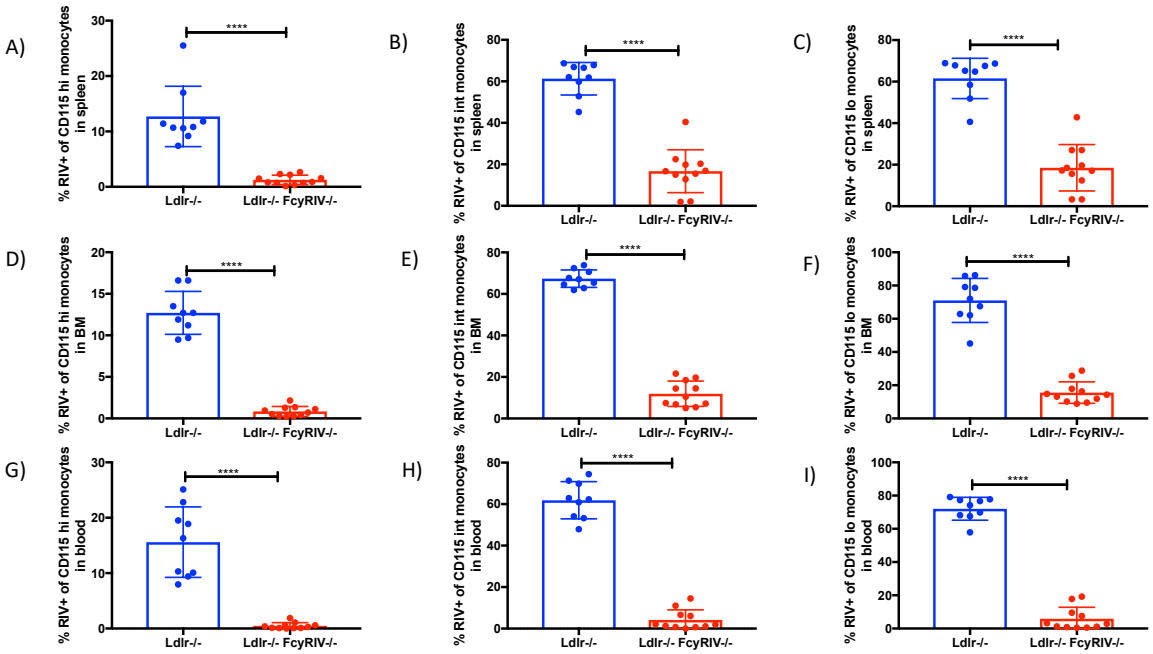

Figure 188. ***FcγRIV expression significantly reduced upon loss of FcγRIV in monocyte subsets.*** *FcγRV expression (as % positive of total monocyte population) across monocyte subsets - CD115 hi monocytes are displayed* ***(A, D and G)****, CD115 int monocytes* ***(B, E and H)*** *and CD115 lo monocytes* ***(C, F, and I)****.* ***(A- C)*** *are within the spleen,* ***(D-F)*** *are within the BM and* ***(G-I)*** *are within the blood. Each dot represents 1 mouse, graphs show mean +/- SD. Statistics carried out using Mann-Whitney test, * P < 0.05; ** P < 0.01; *** P < 0.001; **** P < 0.0001.*

7.4.4 Effect of FcγRIV deletion on specific cell populations

As this was the first experiment conducted with this particular mouse strain, a full characterisation of myeloid cell and T cell subsets was conducted. Within the spleen, follicular, marginal zone and transitional T2-marginal zone precursor B cells showed no differences between genotypes *(Figure 189A, B, D)*. However both T1 *(Figure 189C)* and immature $CD21^{lo}CD23^{-}$ B cells *(Figure 189E)* showed a decrease in the FcγRIV deficient mice compared to the LDLr deficient only mice.

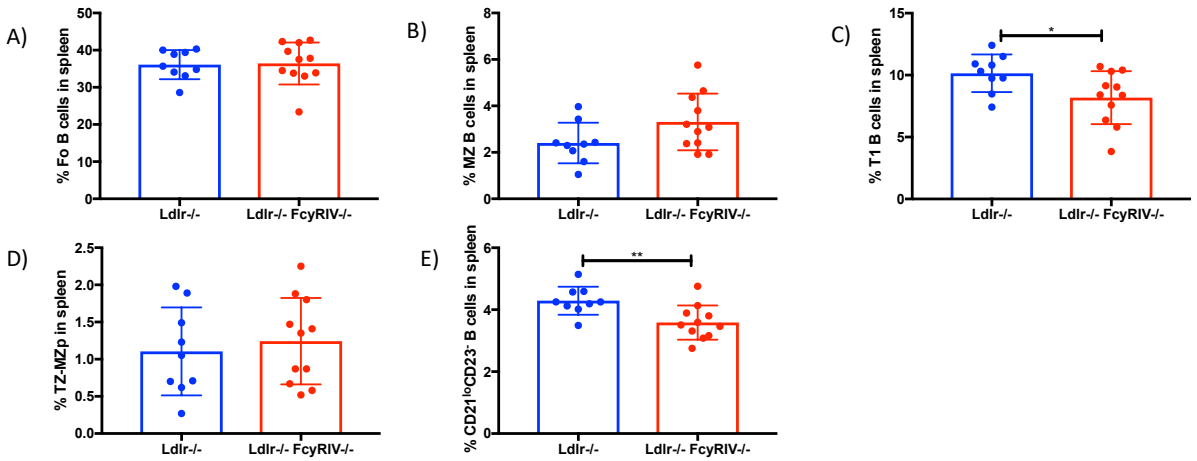

Figure 189. ***Impact of FcγRIV loss on splenic B cell subsets.*** *Proportion of B cell subsets of total spleen population as detected by flow cytometry;* ***(A)*** *follicular B cells,* ***(B)*** *MZ B cells,* ***(C)*** *T1 B cells,* ***(D)*** *TZ-MZp cells and* ***(E)*** *CD21^{lo}CD23^{-} B cells. Each dot represents 1 mouse, graphs show mean +/- SD. Statistics carried out using Mann-Whitney test, * P < 0.05; ** P < 0.01; *** P < 0.001; **** P < 0.0001.*

Full characterisation of splenic T cell subsets was conducted; CD4, CD8 and Treg T cells did not differ between the groups nor did naïve or central memory T cells *(Figure 190A-E)*. Both effector T cell populations *(Figure 190F)* and T follicular helper cells *(Figure 190G)* were reduced in LDLr$^{-/-}$FcγRIV$^{-/-}$ compared to control.

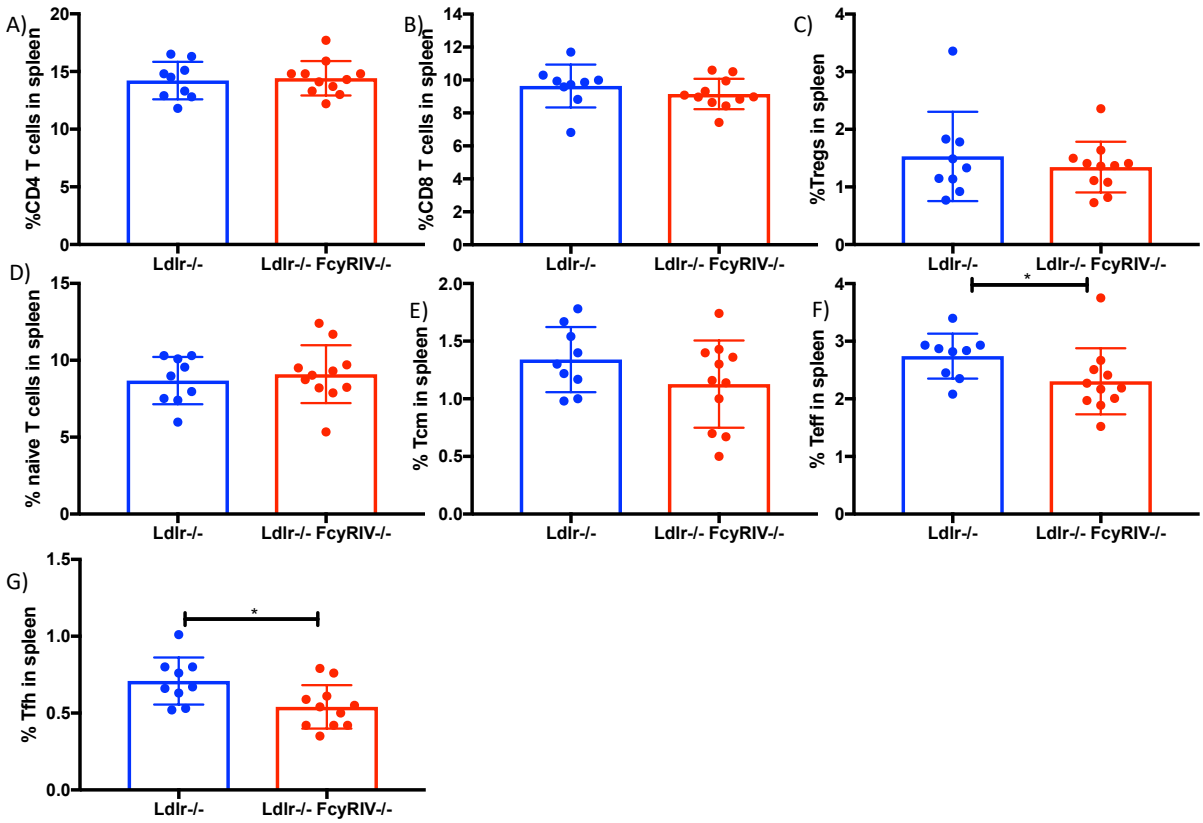

Figure 190. ***Impact of FcγRIV loss on splenic T cell subsets.*** *Proportion of T cell subsets of total spleen population as detected by flow cytometry;* ***(A)*** *CD4 T cells,* ***(B)*** *CD8 T cells,* ***(C)*** *Tregs,* ***(D)*** *naïve T cells,* ***(E)*** *central memory T cells,* ***(F)*** *effector T cells and* ***(G)*** *T follicular helper cells. Each dot represents 1 mouse, graphs show mean +/- SD. Statistics carried out using Mann-Whitney test, * P < 0.05; ** P < 0.01; *** P < 0.001; **** P < 0.0001.*

Cytokine secreting capacity was analysed for CD4 and CD8 T cells within the spleen. IFNγ secretion from CD4 and CD8 T cells *(Figure 191A, B)* was unaffected by the receptor deletion while IL10 and IL17 secretion from CD4 T cells *(Figure 191C, D)* was blunted.

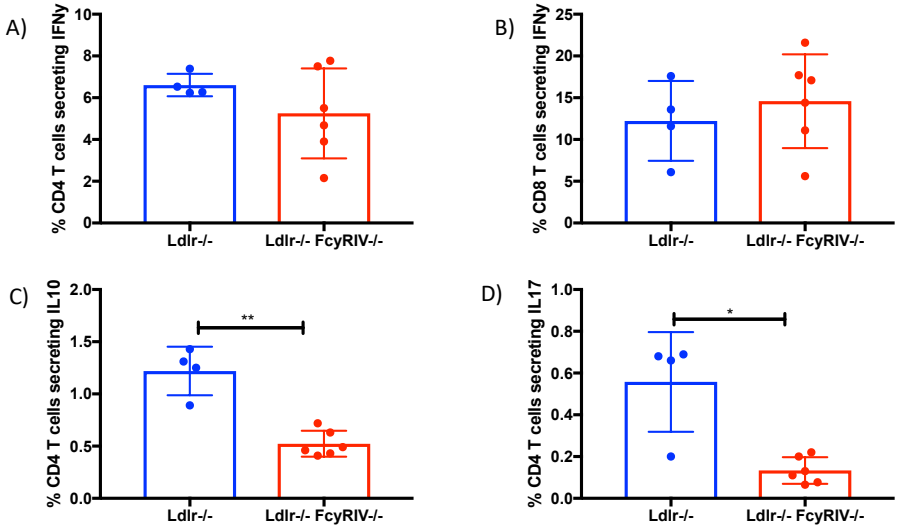

Figure 191. ***Impact of FcγRIV loss on T cell cytokine secretion capacity.*** *Proportion of total cells which are CD4+ secreting* ***(A)*** *IFNγ,* ***(C)*** *IL10 and* ***(D)*** *IL17. Proportion of total cells which are CD8+ secreting* ***(B)*** *IFNγ. Each dot represents 1 mouse, graphs show mean +/- SD. Statistics carried out using Mann-Whitney test, * P < 0.05; ** P < 0.01; *** P < 0.001; **** P < 0.0001.*

In the PALNs, no differences were observed between T cell subsets *(Figure 192)*.

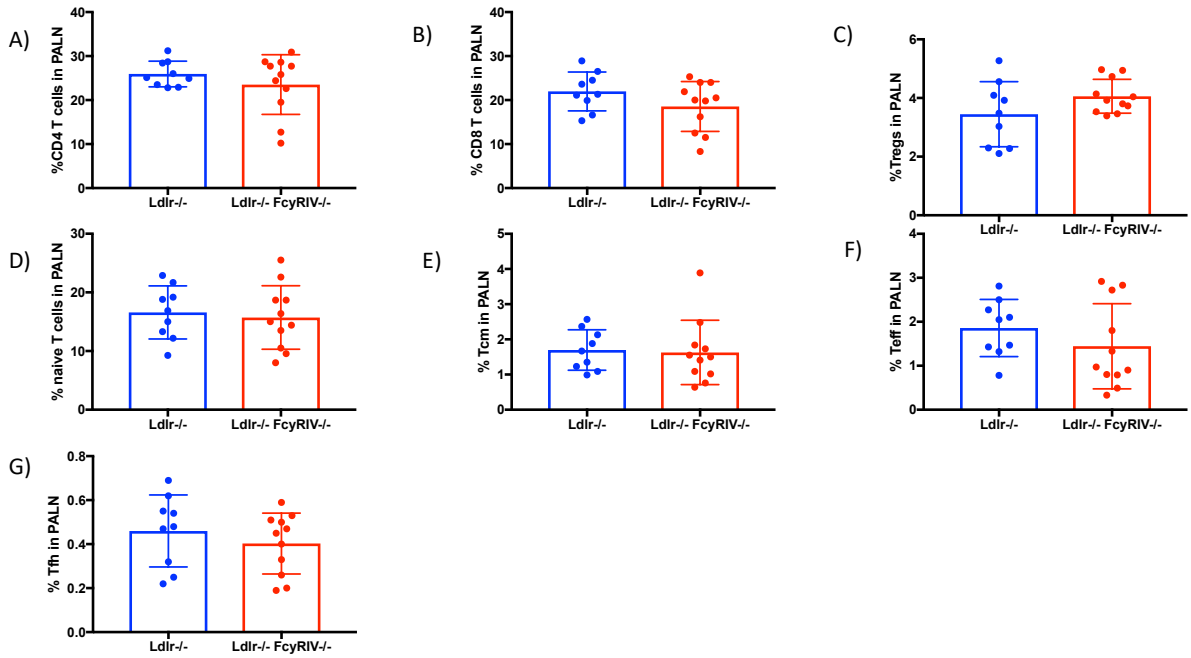

Figure 192. ***Impact of FcγRIV loss on T cell subsets within PALN.*** *Proportion of T cell subsets of total PALN population as detected by flow cytometry;* ***(A)*** *CD4 T cells,* ***(B)*** *CD8 T cells,* ***(C)*** *Tregs,* ***(D)*** *naïve T cells,* ***(E)*** *central memory T cells,* ***(F)*** *effector T cells and* ***(G)*** *T follicular helper cells. Each dot represents 1 mouse, graphs show mean +/- SD.*

The conventional dendritic cell (cDC) population was expanded *(Figure 193A)* in LDLr$^{-/-}$FcγRIV$^{-/-}$ within the spleen mainly due to an increase in the proportion of CD11b+ cDCs *(Figure 193C)* as CD8 cDCs were not impacted *(Figure 193C)*. Similar trends were observed for the PALNs *(Figure 193D-F)* although numbers were not high enough to reach statistical significance.

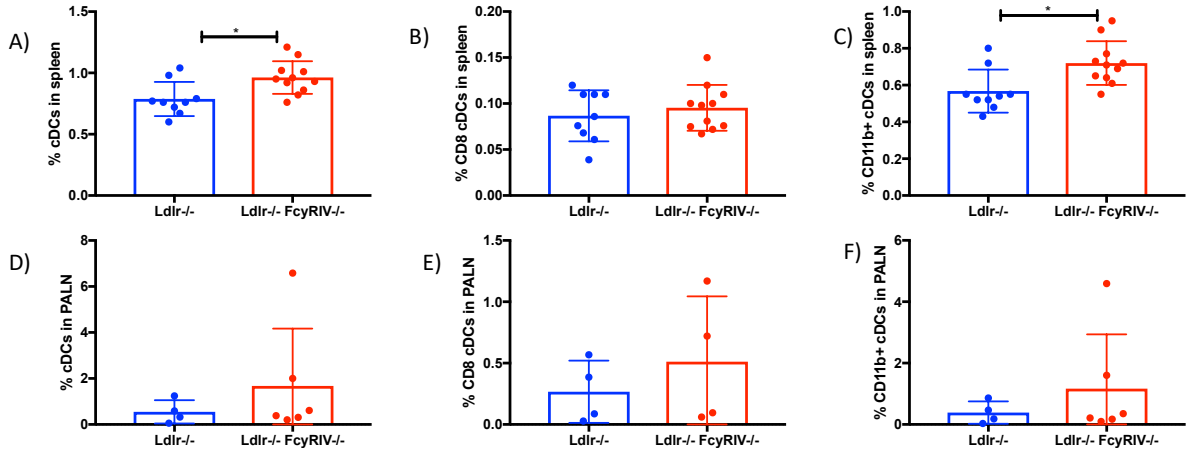

Figure 193. ***Impact of FcγRIV loss on cDCs in spleen and PALN.*** *Proportion of total cells in spleen which are* ***(A)*** *cDC,* ***(B)*** *CD8 cDCs and* ***(C)*** *CD11b+ cDCs. Proportion of total cells in PALN which are* ***(D)*** *cDC,* ***(E)*** *CD8 cDCs and* ***(F)*** *CD11b+ cDCs. Each dot represents 1 mouse, graphs show mean +/- SD. Statistics carried out using Mann-Whitney test, * P < 0.05; ** P < 0.01; *** P < 0.001; **** P < 0.0001.*

The splenic proportion of B cells, PBs and PCs were all unaffected *(Figure 194A, C, D)* by FcγRIV loss and isotype dynamics *(Figure 194E, F)* remained the same in the spleen as control. The GC population within the spleen was diminished *(Figure 194B)* in the absence of FcγRIV compared to control.

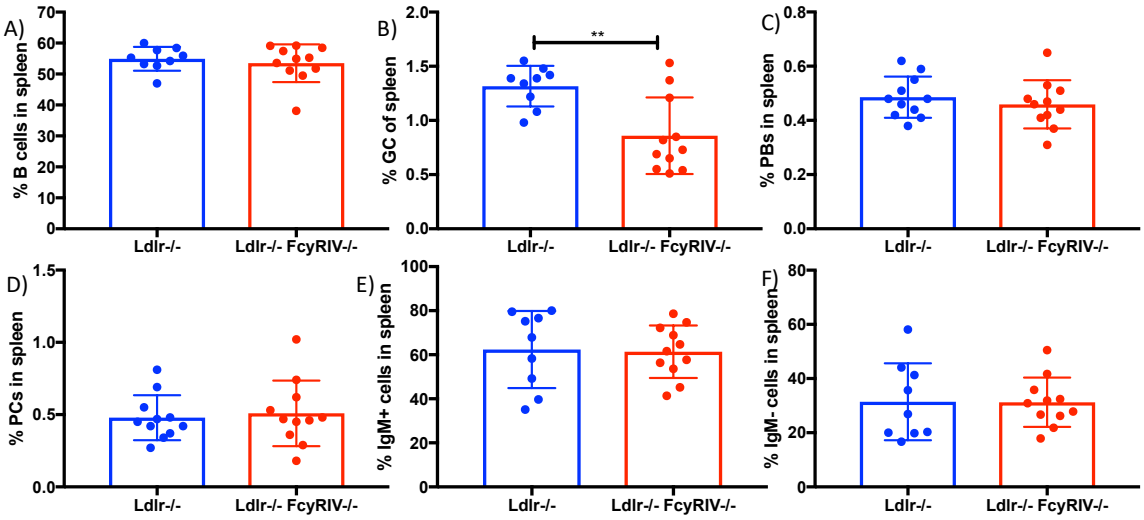

Figure 194. ***Impact of FcγRIV loss on GC associated cell types in spleen.*** *Proportion of total spleen cells which are* ***(A)*** *B cells,* ***(B)*** *GC B cells,* ***(C)*** *PBs,* ***(D)*** *PCs,* ***(E)*** *IgM+ and* ***(F)*** *IgM-. Each dot represents 1 mouse, graphs show mean +/- SD. Statistics carried out using Mann-Whitney test, * P < 0.05; ** P < 0.01; *** P < 0.001; **** P < 0.0001.*

Similar results were detected for the PALN although the GC population was also unaffected in the LDLr$^{-/-}$FcγRIV$^{-/-}$ *(Figure 195)*.

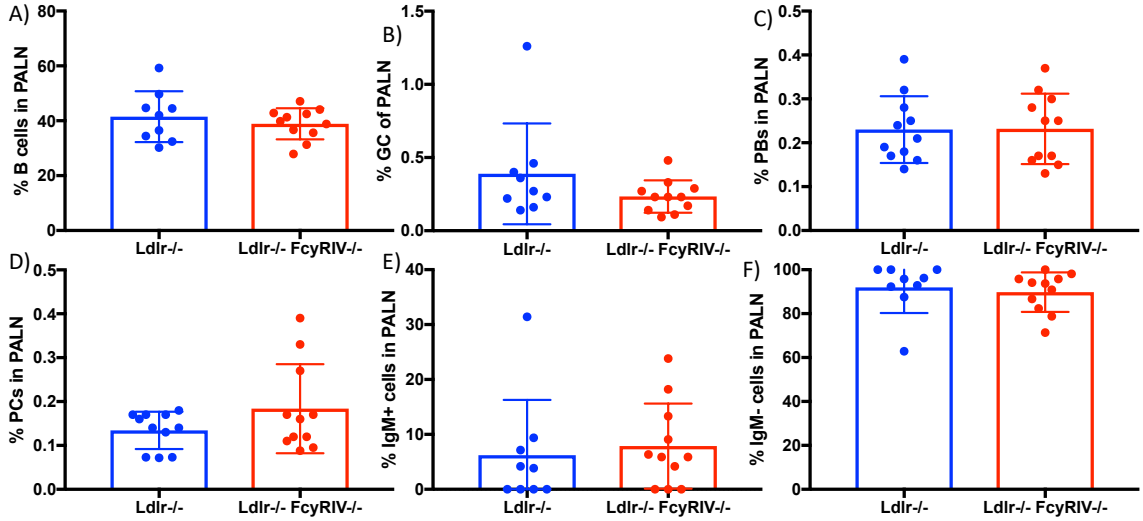

Figure 195. ***Impact of FcγRIV on GC-associated cell types in PALN.*** *Proportion of total PALN cells which are* ***(A)*** *B cells,* ***(B)*** *GC B cells,* ***(C)*** *PBs,* ***(D)*** *PCs,* ***(E)*** *IgM+ and* ***(F)*** *IgM-. Each dot represents 1 mouse, graphs show mean +/- SD.*

Monocyte populations were not impacted by deletion of FcγRIV in the spleen, BM, or blood *(Figure 196A-C)*. Neutrophils populations in the spleen or blood *(Figure 196D, F)* were not impacted by FcγRIV deletion but the neutrophil population in the BM was expanded *(Figure 196E)* in the FcγRIV$^{-/-}$ setting.

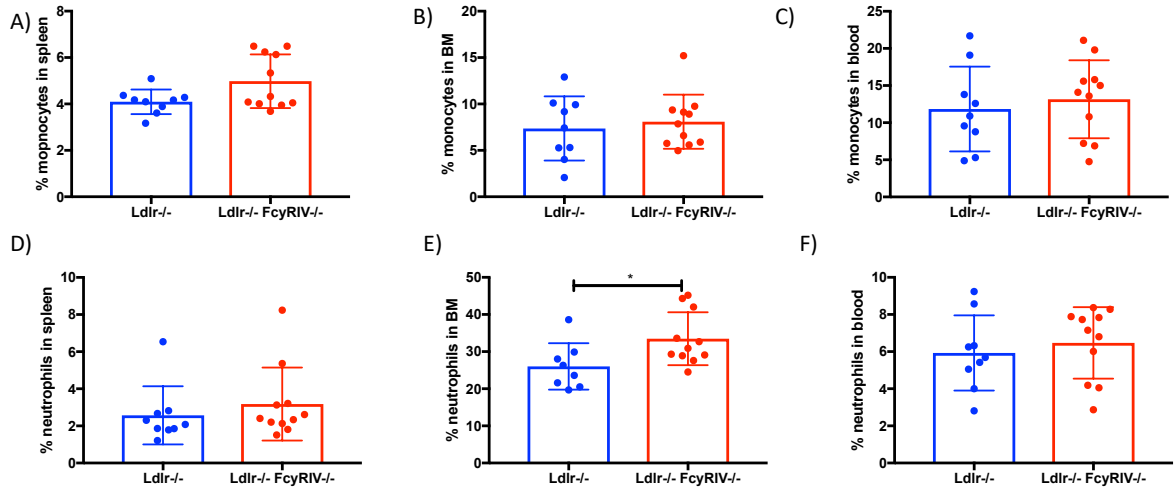

Figure 196. ***Impact of FcγRIV loss on monocytes and neutrophils.*** *Proportion of total cells which are monocytes in* ***(A)*** *spleen,* ***(B)*** *BM and* ***(C)*** *blood. Proportion of total cells which are neutrophils in* ***(D)*** *spleen,* ***(E)*** *BM and* ***(F)*** *blood. Each dot represents 1 mouse, graphs show mean +/- SD. Statistics carried out using Mann-Whitney test, * P < 0.05; ** P < 0.01; *** P < 0.001; **** P < 0.0001.*

All monocyte subsets, based on differential CD115 expression, remained constant *(Figure 197B-I)* apart from elevated CD115^{hi} monocytes within the spleen *(Figure 197A)* of LDLr$^{-/-}$ FcγRIV$^{-/-}$ mice. However, as can be seen half the LDLr$^{-/-}$FcγRIV$^{-/-}$ mice had similar proportion of CD115^{hi} monocytes to that of LDLr$^{-/-}$ demonstrating that the effect was not genotype wide.

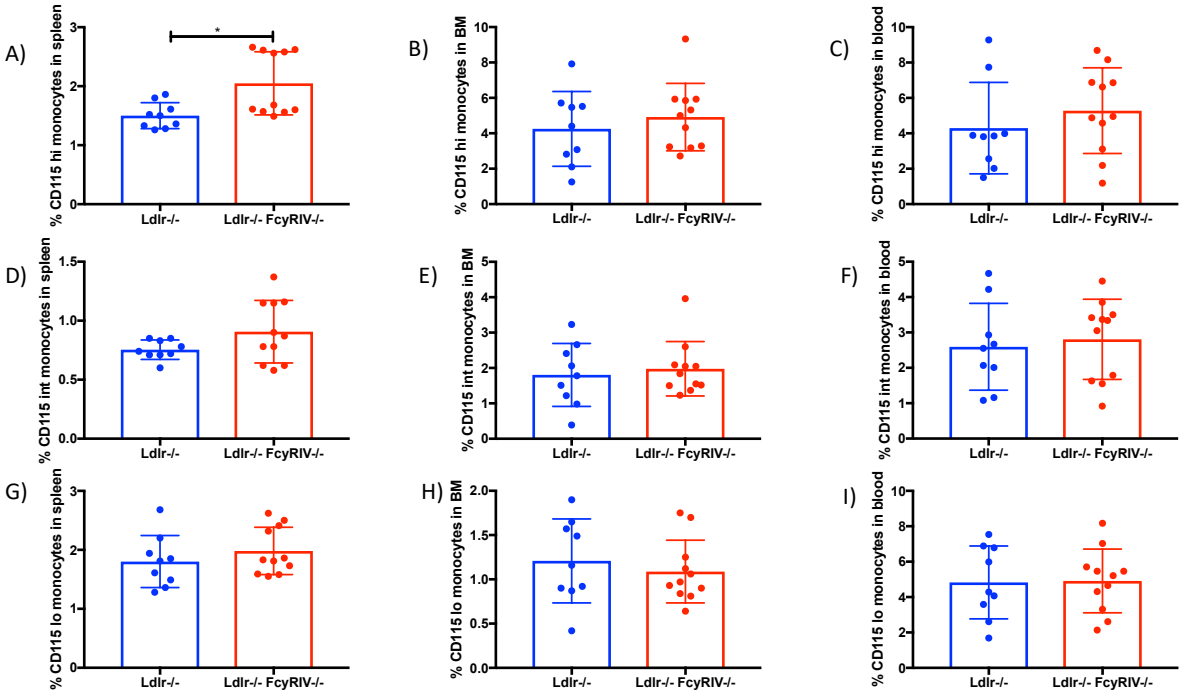

Figure 197. ***Impact of FcγRIV loss on monocyte subsets.*** *Proportion of total cells which comprise the CD115 hi subset in* ***(A)*** *spleen,* ***(B)*** *BM and* ***(C)*** *blood. Proportion of total cells which comprise the CD115 int subset in* ***(D)*** *spleen,* ***(E)*** *BM and* ***(F)*** *blood. Proportion of total cells which comprise the CD115 lo subset in* ***(G)*** *spleen,* ***(H)*** *BM and* ***(I)*** *blood. Each dot represents 1 mouse, graphs show mean +/- SD. Statistics carried out using Mann-Whitney test, * P < 0. 05; ** P < 0.01; *** P < 0.001; **** P <*

7.4.5 Loss of FcγRIV does not impact atherosclerosis plaque size

Deficiency of FcγRIV had little impact on atherosclerosis as LDLr$^{-/-}$WT and LDLr$^{-/-}$FcγRIV$^{-/-}$ mice had no difference in atherosclerosis *(Figure 198)*.

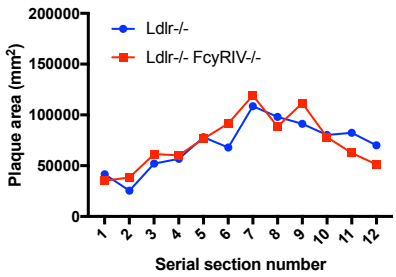

Figure 198. ***FcγRIV loss did not impact atherosclerotic plaque size.*** *Plaque area as quantified using ImageJ for 12 consecutive serial cryosections stained with Oil Red O to identify the plaque. Each dot represents the average of 10 mice.*

7.5 Discussion

This chapter has investigated the role that IgG2c could play in the progression of atherosclerosis through *in vitro* and *in vivo* studies showing that IgG2c increases the inflammatory output of FcγRIV-expressing myeloid intraplaque cells and that loss of FcγRIV alters certain cell populations implicated in atherosclerosis.

7.5.1 Impact of IgG2c on bone marrow-derived myeloid cells *in vitro*

The finding that BMDMs displayed increased FcγRIV expression in response to IFNγ replicated findings reported in Nimmerjahn et al[334]. BMDCs and BMDMs cultured on IgG2c pre-coated culture plates produced greater quantities of TNF compared to IgG1 pre-coated culture plates. Soluble IgG1 and IgG2c had little effect on cellular activation thus showing that antibodies must be multivalent for inflammatory effect. When IgG1 and IgG2c antibodies were coated on beads and incubated with BMDCs and BMDMs, TNF production was highest in the supernatant of cells subjected to IgG2c-coated beads. These results show that antibodies alone are not sufficient to elicit an inflammatory response from BMDCs and BMDMs but rather must be in an immunogenic complex. This *in vitro* data is corroborated by findings from Zhang et al which demonstrated that administration of IgE to media of WT BMDMs caused significant upregulation of TNFα mRNA levels along with inducible nitrogen oxide synthase (iNOS) and Mcp-1[236]. Furthermore, they demonstrated that when IFNγ was supplemented to WT BMDMs, IgE enhanced oxLDL uptake and foam cell generation[236]. Using human monocyte-derived macrophages, Saad et al showed that oxLDL immune complexes stimulate release of pro-inflammatory cytokines IL6, TNF and IL1β and this effect was augmented when cells were primed with IFNγ[343]. Rhoads et al showed that IgG-oxLDL immune complexes induce significant IL1β production from BMDCs and BMDMs and these immune complexes have increased inflammatory potency than either oxLDL or IgG antibodies individually[344]. Thus, these studies along with data from this chapter shows that antibody stimulation of bone marrow-derived myeloid cells drives inflammatory pro-atherogenic cytokine release which could go on to augment atherogenesis. For example, TNFα has been detected in human atherosclerotic lesions[314] and circulating TNFα acts as a biomarker,

associated with elevated risk of recurrent MI[314]. ApoE$^{-/-}$ mice with global TNFα loss had 50% decrease in atherosclerotic plaque size after WD-feeding for 10 weeks showcasing its atherogenic nature[314].

The finding that uncoated beads stimulated TNF production from BMDCs suggests that they are inherently immunogenic to the cells. As this presents a confounding variable it is a limitation of the study as not all inflammatory output from BMDCs or BMDMs can be attributed to the coating but will also be partly due to the inherent nature of the beads. To compensate for this, beads could be washed in PBS/3% FBS or results could be normalised to the TNF production from beads alone. An alternative approach would be to purify IgG1 and IgG2c antibodies from sera of atherosclerotic mice and treat BMDMs and BMDCs with these antibodies.

IgG2c has an especially potent FcR binding profile as the Fc portion of IgG2c has a much higher preference for binding to activating FcγRIV over inhibitory FcγRIIb[321]. LDLr$^{-/-}$ mice fed a HFD produced greater IgG2c autoantibody levels which led to SLE[251]. IgG2c antibodies have been characterised as more pathogenic than IgG1 antibodies as IgG2c antibodies can activate the complement pathway[345]. It is well-established that in macrophages and dendritic cells, binding FcγRIV induces proinflammatory cytokine production and T cell activation function[345]. In accordance with this study, atherosclerotic macrophages/dendritic cells express FcγRIV and the activatory: inhibitory ratio of inflammatory monocytes is increased in western diet compared with chow diet[321].

Pro-atherogenic cytokine IFNγ was found to upregulate FcγRIV on BMDCs and BMDMs by flow cytometry. The IFNγ-induced dose-dependent increase in TNF production by IgG2c-incubated BMDCs suggests that IFNγ stimulates FcγRIV upregulation in directly proportional manner and consequently indirectly increases IgG2c-induced TNF production. The data shows that IgG2c, both in an antibody immune complex form and in an antibody-coated particle form, has particularly potent inflammatory activity upon BMDCs and BMDMs. The results suggest that antibodies such as IgG2c which have originated from a GC reaction might have atherogenic

effects on plaque myeloid cells. Overall, IgG2c has been shown to induce inflammatory cytokine production in myeloid-derived cells *in vitro*.

7.5.2 Characterisation of the FcγRIV$^{-/-}$ mouse model

The in-depth characterisation of the FcγRIV mouse model on the LDLr background showed that weights, cholesterol, and antibody titres remained unchanged as did precursor, follicular and marginal zone B cells within the spleen. The FcγRIV$^{-/-}$ bone marrow transfer (BMT) study showed that when crossed to the LDLr$^{-/-}$ background, FcγRIV deficient mice had reduced T1 and immature CD21^{lo}CD23^{-} B cells. This suggests FcγRIV plays a role in B cell development given that loss of the receptor impacted development of some precursor B cell subsets. The splenic proportion of PCs and PBs along with IgM expression levels were not impacted by FcγRIV deletion. In contrast, the splenic proportion of GC cells was reduced in FcγRIV-LDLr deficient mice – this could be a knock-on effect of the impaired B cell development. In the PALN, similar results were seen however the GC population was not different between LDLr$^{-/-}$ and FcγRIV$^{-/-}$LDLr$^{-/-}$.

The splenic proportion of CD4, CD8, regulatory, naïve, and central memory T cells was unaffected by FcγRIV deletion. Within the PALNs, all T cell subsets remained constant. IFNγ secretion capacity from CD4 and CD8 T cells was unchanged upon FcγRIV deficiency. The proportion of effector and follicular helper T cells was decreased upon FcγRIV deletion, this could be linked with the smaller splenic GC population as the Tfh cell population works closely with GC B cells. CD4 T cell capacity to secrete IL10 and IL17 was blunted in the FcγRIV$^{-/-}$LDLr$^{-/-}$ mice. As IL10 is atheroprotective, the reduced concentrations could contribute to plaque formation.

The cDC population within the spleen was expanded upon FcγRIV deletion mainly due to CD11b+ cDCs. However, the cDC population was unaltered in the PALNs when FcγRIV was absent. As FcγRIV deletion impacts splenic cell populations more so than PALN cell populations, it suggests that FcγRIV plays a more significant role in global immune responses rather than specific localised immune responses which occur within the PALN. As FcγRIV only

has binding capacity for IgG2c, perhaps there are fewer IgG2c-mediated effects within the PALN.

Monocyte populations, including subsets, in the spleen, BM and blood were not impacted by FcγRIV deficiency. Only the splenic CD115^{hi} monocyte population was expanded in response to the FcγRIV deletion. FcγRI expression was not altered on monocytes or any monocyte subsets within the spleen, BM, or blood. FcγRIV was efficiently deleted from monocytes, across all subsets, and neutrophils within the spleen, BM, and blood. FcγRII/III expression was the same on BM and blood monocytes but raised in splenic monocytes. FcγRII/IIII was upregulated in CD115^{hi} monocytes within spleen, BM, and blood, CD115^{int} monocytes within spleen and blood, and CD115^{lo} monocytes within the BM and blood. Thus FcγRII/III is upregulated to compensate for the deficiency in FcγRIV; a fact which must be taken into consideration when drawing conclusions from this mouse model. This undesired effect makes it harder to disentangle the sole effect of FcγRIV from the impact that upregulation of FcγRII/III has. An alternative approach to overcome this issue could be to use blocking antibodies.

Neutrophils in the BM were expanded while splenic and blood neutrophil populations were steady upon FcγRIV deletion. FcγRI expression level remained the same on neutrophils in the spleen and BM but was elevated in blood neutrophils. FcγRII/III was constant on splenic and blood neutrophils but elevated on BM neutrophils. Nimmerjahn et al. also observed FcγRII/III upregulation on neutrophils upon FcγRIV deletion[342].

The human ortholog of murine FcγRIV is FcγRIIIA, based on protein sequence, genomic location, and functional studies, which interacts using its extracellular D1 and D2 domains to bind the 2 heavy chains of human IgG1[346]. FcγRIIIA is an integral membrane protein[346] and contains a signal transducing ITAM-containing γ chain in monocytes[322]. Recently, high-dimensional mass cytometry has identified a human monocyte subset with SLAN (unsialylated O-linked carbohydrate modification of P-selectin glycoprotein 1[347]) expression that express FcγRIIIA[347]. Our data with IFNγ treated mouse BMDC/BMDM is like that of human SLAN+ monocytes as these cells have high responsiveness to immune complexes and IgG1 induced

(murine IgG2c ortholog) TNF production. SLAN+ monocytes express CXCR6 and migrate toward CXCL16-expressing endothelial cells[347]. The CXCR6/CXCL16 interaction facilitates adhesion of monocytes to the atherosclerotic plaque endothelium[347]. Furthermore, this subset is expanded in cardiovascular disease patients and has been detected in atherosclerotic plaques[321]. Serum levels of monocyte FcγRIIIA are associated with atherosclerosis severity including risk factors such as the LDL: HDL ratio, ageing, diabetes, hypertension, and smoking[348]. Furthermore, levels of soluble FcγRIII are positively associated with the carotid maximum intima thickness[348]. Patients with a mutation in the FcγRIII receptor, V158 allele, have a 2-fold reduced risk of coronary stenosis[349].

These studies have suggested a pathogenic role for GC B cell IgG responses in atherosclerosis. The data support the idea that IgG2c potentially enhance inflammatory responses by plaque macrophages and/or dendritic cells.

7.5.3 Future work

7.5.3.1 In vitro work to study the impact of IgG2c

The degree of similarity between *in vitro* myeloid-derived cells and myeloid cells within the plaque is unknown and as such, a limitation of the *in vitro* studies. Future work will require further phenotypic characterisation of cell surface markers by flow cytometry of plaque and *in vitro* cells to compare the cell types to determine the relevance of cultured cells. SLAN+ monocytes could be cultured *in vitro,* and similar assays performed to enhance the translational aspect of this project within the human atherosclerotic setting. Indeed it has been reported that GM-CSF and IL4 treatment of SLAN+ monocytes leads to differentiated DCs while IL34 stimulates macrophage differentiation[350]. Studies have shown that stimulation of SLAN+ monocytes with LPS or CD40L results in high levels of TNFα[350].

7.5.3.2 FcγRIV$^{-/-}$ model

Due to issues with rederivation into a new animal unit, only 1 BMT study was conducted using the FcγRIV$^{-/-}$ mice. In the future a study should be undertaken to investigate the differences between the FcγRIV$^{-/-}$ genotype with and without the LDLr background. Additionally, the influence of diet, chow and HFD, and age should be analysed to determine the full impact of FcγRIV deletion. As FcγRIV is the main receptor for IgG2c to exert its pathogenic functions, IgG2c staining by immunofluorescence should be conducted on aortic root plaque sections to determine whether IgG2c levels within the plaque are reduced. Furthermore, aortic cells could be analysed by flow cytometry for IgG2c isotype staining. To further investigate the effect of FcγRIV on atherosclerosis, characterisation of intraplaque macrophage subtypes could be conducted to determine the balance between proinflammatory and anti-inflammatory cells. Although the GC and Tfh cell populations were reduced in the spleen, functional output of the GC response – i.e., PC, PB and antibody production, was unaffected. The other cell type produced from a GC response, the memory B cell, was not analysed within this study and should be to understand whether FcγRIV deletion impacts this population.

8 Concluding Remarks

The germinal centre B cell response is a critical component of the adaptive immune system responsible for the production of high affinity antibody-producing plasma cells and memory B cells. Together these cell types are capable of neutralising pathogens and retaining immunological memory in order to elicit a more efficient immune response upon future encounters with a specific pathogen. Under homeostatic conditions, this response is very beneficial protecting the organism from harm. However, under chronic inflammatory conditions self-antigens can be recognised as foreign resulting in pathological autoimmunity. Atherosclerotic cardiovascular disease is one such circumstance wherein the germinal centre response is activated in response to the immunogenic oxidised LDL epitope. Despite recent reports in the literature, the mechanism of the involvement of the germinal centre response in atherosclerosis is not fully elucidated thus highlighting a knowledge gap in the field. In this thesis, I sought to characterise and further understand the germinal centre B cell response to atherosclerosis.

Throughout this PhD, I have made use of a tamoxifen-inducible genetic lineage tracking mouse model system which centres around AID; the key enzyme involved in the processes of somatic hypermutation and isotype class-switching within the germinal centre B cell response. Upon tamoxifen administration, AID-expressing cells were permanently and irreversibly fluorescently labelled with EYFP. By crossing this genetic lineage tracing mouse model with the atherosclerosis-prone $Ldlr^{-/-}$ mouse model (AEL), I was able to track atherosclerosis-specific B cell clones over time during the progression of atherosclerosis. Validation confirmed that EYFP cells were only detectable after tamoxifen administration and that these cells were all derived from the germinal centre. Additionally, labelling efficiency was not impacted by the variables used throughout this thesis – genotype, time, and diet type.

To induce atherosclerosis in mice, a combination of genotype, diet and time is required. In order to distinguish the impacts of these 3 variables upon the germinal centre response, a full characterisation of germinal centre responses was carried out in WT and $Ldlr^{-/-}$ AEL mice fed

either chow diet or HFD for either 0, 4 or 8 weeks. The results demonstrated a time-dependent increase in germinal centre responses, as deduced from chow diet-fed WT mice. These responses were exacerbated by the presence of HFD, as shown in HFD-fed WT mice. Furthermore, WT mice fed a HFD demonstrated elevated serum cholesterol levels and the presence of class-switched germinal centre-derived clones. The absence of LDL receptors in the atherosclerosis-prone $LDLr^{-/-}$ model induced increases in serum cholesterol concentrations independently of HFD as observed in chow diet-fed $LDLr^{-/-}$ mice. In these mice, germinal centre responses were expanded, and a degree of class-switching was detected again highlighting a link between increased cholesterol levels and the pathogenicity of the germinal centre response. Combination of the $Ldlr^{-/-}$ genotype and HFD recapitulated atherosclerotic conditions resulting in augmented germinal centre responses and output likely contributing to hypertrophy of lymphoid organs and high degrees of isotype class-switching. Thus, this chapter identified a link between hyperlipidaemia and more pathogenic germinal centre responses.

By making full use of the tracking capabilities with the AEL mouse model, I was able to track EYFP germinal centre-derived clones over time and determine their dynamics in the context of atherosclerosis. Upon exposure to HFD, germinal centre reactions produced greater quantities of EYFP labelled memory and plasma cells compared to chow diet. Furthermore, these clones were more likely to have undergone isotype class-switching towards more pathogenic and potent antibody isotypes and tended to be longer-lived, persisting for longer durations. Thus, as a consequence of HFD feeding in atherosclerosis-prone $LDLr^{-/-}$ mice, germinal centre responses and outputs are longer-lived and exhibit a more pathogenic profile. Together, these features could augment the chronic inflammation associated with atherosclerosis.

As the HFD had resulted in elevated germinal centre responses, I sought to investigate the mechanism underlying this effect. To reduce inflammation induced by HFD, I used an anti-IL6 inhibitor which had no impact after 4 weeks but did result in diminished germinal centre responses after 8 weeks. This suggested that by 8 weeks of diet, systemic inflammation had reached a level pathogenic to the germinal centre (among other effects) resulting in exacerbation of germinal centre responses. To investigate the impact of high cholesterol

content of the HFD, I made use of a cholesterol uptake inhibitor drug and a cholesterol-free high fat-containing diet. Both interventions dampened germinal centre responses after 4 weeks of diet suggesting that dietary cholesterol plays a key role in driving pathogenic germinal centre responses.

Investigation into the role of IgG2c in atherosclerosis revealed that IgG2c augmented TNF secretion of FcγRIV-expressing myeloid-derived CD11b+CD11c+ monocytes. This suggests that germinal centre-derived IgG2c has the potential to exacerbate inflammatory responses from plaque myeloid-derived cells.

Combining all the findings, it is clear that there is a link between hyperlipidaemia and germinal centre responses. This thesis presents a model in which disrupted lipid homeostasis, which triggers atherosclerosis, is responsible for autoimmune adaptive B cell pathology resulting in augmented pathogenic germinal centres reacting to LDL-induced inflammation. Dietary cholesterol is inflammatory as evidenced by elevated cytokine concentrations and hepatic inflammatory gene expression levels. The data shows that dietary cholesterol is critical in fuelling germinal centre responses at the early stages of atherosclerosis progression at 4 weeks, presumably via reactions to oxidised LDL, while at later stages of 8 weeks, the inflammatory milieu associated with atherosclerosis drives pathogenic germinal centre responses. As lipid-lowering therapies are already a mainstay of therapy for cardiovascular disease patients, it would be of interest to analyse whether the therapy has a beneficial impact on the germinal centre response through dampening hyperlipidaemia.

The specificity of the germinal centre B cell response can be analysed through sequences of B cell receptors to identify rates of somatic hypermutation as well as clonal diversity. Evidence of reduced BCR repertoire diversity has already been identified in patients with acute MI and unstable angina compared to healthy patients[351]. Analysis of the V and J gene usage showed that acute coronary syndrome patients had skewing toward V3 segments[351]. Controls also had an increased proportion of productive BCR sequences compared to diseased patients[351]. Although initially an aim within my PhD, due to time constraints I was unable to undertake BCR sequencing and analysis. This should be conducted to determine any similarities in clonality to identify potential novel antigen targets.

To conclude, the data presented in this thesis has significantly contributed to our understanding of the germinal centre response during the course of atherosclerosis and the role that hyperlipidaemia plays in its pathology. Through elucidating the pathogenic impact that hyperlipidaemia can have on the germinal centre B cell response, this suggests that lipid-lowering therapy may have an additional benefit of reducing the pathogenicity of the germinal centre B cell response against atherosclerosis. Furthermore, this provides an opportunity to target B cell-related atherosclerosis-specific responses therapeutically.

Bibliography

1. Neely, H. R. & Flajnik, M. F. Emergence and Evolution of Secondary Lymphoid Organs. *Annu. Rev. Cell Dev. Biol.* **32**, 693–711 (2016).
2. Lewis, S. M., Williams, A. & Eisenbarth, S. C. Structure and function of the immune system in the spleen. *Sci. Immunol.* **4**, eaau6085 (2019).
3. Bronte, V. & Pittet, M. J. The Spleen in Local and Systemic Regulation of Immunity. *Immunity* **39**, 806–818 (2013).
4. Lucas, D. Structural organization of the bone marrow and its role in hematopoiesis. *Curr. Opin. Hematol.* **28**, 36–42 (2021).
5. Beck, T. C., Gomes, A. C., Cyster, J. G. & Pereira, J. P. CXCR4 and a cell-extrinsic mechanism control immature B lymphocyte egress from bone marrow. *J. Exp. Med.* **211**, 2567 (2014).
6. Benet, Z., Jing, Z. & Fooksman, D. R. Plasma cell dynamics in the bone marrow niche. *Cell Rep.* **34**, 108733 (2021).
7. Ise, W. & Kurosaki, T. Plasma cell generation during T-cell-dependent immune responses. *Int. Immunol.* **33**, 797–801 (2021).
8. Nutt, S. L., Hodgkin, P. D., Tarlinton, D. M. & Corcoran, L. M. The generation of antibody-secreting plasma cells. *Nat. Rev. Immunol.* **15**, 160–171 (2015).
9. Cornelis, R., Chang, H.-D. & Radbruch, A. Keeping up with the stress of antibody production: BAFF and APRIL maintain memory plasma cells. *Curr. Opin. Immunol.* **71**, 97–102 (2021).
10. Baumgarth, N. The Shaping of a B Cell Pool Maximally Responsive to Infections. *Annu. Rev. Immunol.* **39**, 103–129 (2021).
11. Yeo, K. P. *et al.* Efficient aortic lymphatic drainage is necessary for atherosclerosis regression induced by ezetimibe. *Sci. Adv.* **6**, eabc2697 (2020).
12. Tay, M. H. D. *et al.* Halted Lymphocyte Egress via Efferent Lymph Contributes to Lymph Node Hypertrophy During Hypercholesterolemia. *Front. Immunol.* **10**, 575 (2019).
13. Reboldi, A. & Cyster, J. G. Peyer's patches: organizing B-cell responses at the intestinal frontier. *Immunol. Rev.* **271**, 230–245 (2016).
14. Green, J. A. & Cyster, J. G. S1PR2 links germinal center confinement and growth regulation. *Immunol. Rev.* **247**, 36–51 (2012).
15. Poirot, J., Medvedovic, J., Trichot, C. & Soumelis, V. Compartmentalized multicellular crosstalk in lymph nodes coordinates the generation of potent cellular and humoral immune responses. *Eur. J. Immunol.* **51**, 3146–3160 (2021).
16. Phan, T. G., Gray, E. E. & Cyster, J. G. The microanatomy of B cell activation. *Curr. Opin. Immunol.* **21**, 258–265 (2009).
17. Ochiai, K. *et al.* Transcriptional Regulation of Germinal Center B and Plasma Cell Fates by Dynamical Control of IRF4. *Immunity* **38**, 918–929 (2013).
18. Phan, T. G., Green, J. A., Gray, E. E., Xu, Y. & Cyster, J. G. Immune complex relay by subcapsular sinus macrophages and noncognate B cells drives antibody affinity maturation. *Nat. Immunol.* **10**, 786–793 (2009).
19. Ishihara, S. *et al.* Rap1 Is Essential for B-Cell Locomotion, Germinal Center Formation and Normal B-1a Cell Population. *Front. Immunol.* **12**, 624419 (2021).
20. Lu, E. & Cyster, J. G. G-protein coupled receptors and ligands that organize humoral immune responses. *Immunol. Rev.* **289**, 158–172 (2019).
21. Schmidt, T. H., Bannard, O., Gray, E. E. & Cyster, J. G. CXCR4 promotes B cell egress from peyer's patches. *J. Exp. Med.* **210**, 1099 (2013).
22. Silva-Cayetano, A. & Linterman, M. A. Stromal cell control of conventional and ectopic germinal centre reactions. *Curr. Opin. Immunol.* **64**, 26–33 (2020).
23. Yi, T. *et al.* Oxysterol Gradient Generation by Lymphoid Stromal Cells Guides Activated B Cell Movement during Humoral Responses. *Immunity* **37**, 535–548 (2012).
24. Tangye, S. G. & Tarlinton, D. M. Memory B cells: Effectors of long-lived immune responses. *Eur. J. Immunol.* **39**, 2065–2075 (2009).
25. Moran, I. *et al.* Memory B cells are reactivated in subcapsular proliferative foci of lymph nodes. *Nat. Commun.* **9**, 3372 (2018).
26. Srikakulapu, P. *et al.* Artery tertiary lymphoid organs control multilayered territorialized atherosclerosis B-cell responses in Aged ApoE-/- mice. *Arterioscler. Thromb. Vasc. Biol.* **36**, 1174–1185 (2016).

27. Akhavanpoor, M. *et al.* Adventitial tertiary lymphoid organ classification in human atherosclerosis. *Cardiovasc. Pathol.* **32**, 8–14 (2018).
28. Roy, P., Ali, A. J., Kobiyama, K., Ghosheh, Y. & Ley, K. Opportunities for an atherosclerosis vaccine: From mice to humans. *Vaccine* **38**, 4495–4506 (2020).
29. Clement, M. *et al.* Control of the T Follicular Helper–Germinal Center B-Cell Axis by CD8+ Regulatory T Cells Limits Atherosclerosis and Tertiary Lymphoid Organ Development. *Circulation* **131**, 560–570 (2015).
30. Sage, A. P., Tsiantoulas, D., Binder, C. J. & Mallat, Z. The role of B cells in atherosclerosis. *Nat. Rev. Cardiol.* **16**, 180–196 (2019).
31. Fang, P. *et al.* Immune cell subset differentiation and tissue inflammation. *J. Hematol. Oncol.* **11**, 97 (2018).
32. Mårtensson, I.-L., Almqvist, N., Grimsholm, O. & Bernardi, A. I. The pre-B cell receptor checkpoint. *FEBS Lett.* **584**, 2572–2579 (2010).
33. Pieper, K., Grimbacher, B. & Eibel, H. B-cell biology and development. *J. Allergy Clin. Immunol.* **131**, 959–971 (2013).
34. Almqvist, N. & Mårtensson, I.-L. The Pre-B Cell Receptor; Selecting for or against Autoreactivity. *Scand. J. Immunol.* **76**, 256–262 (2012).
35. Zhang, M., Srivastava, G. & Lu, L. The pre-B cell receptor and its function during B cell development. *Cell. Mol. Immunol.* **1**, 89–94 (2004).
36. Nemazee, D. Mechanisms of central tolerance for B cells. *Nat. Rev. Immunol.* **17**, 281 (2017).
37. Chan, L. N., Aghania, E., Leveille, E. & Müschen, M. Metabolic determinants of B-cell selection. *Biochem. Soc. Trans.* **49**, 1467–1478 (2021).
38. Hardy, R. R. & Hayakawa, K. B Cell Development Pathways. *Annu. Rev. Immunol.* **19**, 595–621 (2001).
39. Melchers, F. Checkpoints that control B cell development. *J. Clin. Invest.* **125**, 2203 (2015).
40. Casellas, R. *et al.* Mutations, kataegis and translocations in B cells: understanding AID promiscuous activity. *Nat. Rev. Immunol.* **16**, 164–176 (2016).
41. Tsubata, T. B-cell tolerance and autoimmunity. *F1000Research* **6**, 391 (2017).
42. Clark, M. R., Mandal, M., Ochiai, K. & Singh, H. Orchestrating B cell lymphopoiesis through interplay of IL-7 receptor and pre-B cell receptor signalling. *Nat. Rev. Immunol.* **14**, 69 (2014).
43. Wang, L. D. & Clark, M. R. B-cell antigen-receptor signalling in lymphocyte development. *Immunology* **110**, 411 (2003).
44. Sandoval, H., Kodali, S. & Wang, J. Regulation of B cell fate, survival, and function by mitochondria and autophagy. *Mitochondrion* **41**, 58–65 (2018).
45. Calderón, L. *et al.* Pax5 regulates B cell immunity by promoting PI3K signaling via PTEN down-regulation. *Sci. Immunol.* **6**, abg5003 (2021).
46. Lee, J. *et al.* IFITM3 functions as a PIP3 scaffold to amplify PI3K signalling in B cells. *Nature* **588**, 491–497 (2020).
47. Yang, L. *et al.* CCL2 regulation of MST1-mTOR-STAT1 signaling axis controls BCR signaling and B-cell differentiation. *Cell Death Differ.* **28**, 2616–2633 (2021).
48. Wishnie, A. J., Chwat-Edelstein, T., Attaway, M. & Vuong, B. Q. BCR Affinity Influences T-B Interactions and B Cell Development in Secondary Lymphoid Organs. *Front. Immunol.* **12**, (2021).
49. Chan, T. D. *et al.* In vivo control of B-cell survival and antigen-specific B-cell responses. *Immunol. Rev.* **237**, 90–103 (2010).
50. He, C. *et al.* CD36 and LC3B initiated autophagy in B cells regulates the humoral immune response. *Autophagy* **17**, 3577–3591 (2021).
51. Zhang, S. *et al.* Conditional deletion of mTOR discloses its essential role in early B-cell development. *Mol. Carcinog.* **61**, 408–416 (2022).
52. Konforte, D., Simard, N. & Paige, C. J. IL-21: An Executor of B Cell Fate. *J. Immunol.* **182**, 1781–1787 (2009).
53. Kiss, M. G. *et al.* Complement factor H modulates splenic B cell development and limits autoantibody production. *Front. Immunol.* **1**, 1607 (2019).
54. Lee, S., Ko, Y. & Kim, T. J. Homeostasis and regulation of autoreactive B cells. *Cell. Mol. Immunol.* **17**, 561–569 (2020).
55. Fessler, M. B. Regulation of Adaptive Immunity in Health and Disease by Cholesterol Metabolism. *Curr. Allergy Asthma Rep.* **15**, 1–16 (2015).
56. Yam-Puc, J. C., Zhang, L., Zhang, Y. & Toellner, K.-M. Role of B-cell receptors for B-cell development and antigen-induced differentiation. *F1000Research* **7**, 429 (2018).
57. Yam-Puc, J. C. *et al.* Enhanced BCR signaling inflicts early plasmablast and germinal center B cell death.

iScience **24**, 102038 (2021).
58. Wakabayashi, C., Adachi, T., Wienands, J. & Tsubata, T. A Distinct Signaling Pathway Used by the IgG-Containing B Cell Antigen Receptor. *Science (80-.).* **298**, 2392–2395 (2002).
59. Meyer, S. J. *et al.* CD22 Controls Germinal Center B Cell Receptor Signaling, Which Influences Plasma Cell and Memory B Cell Output. *J. Immunol.* **207**, 1018–1032 (2021).
60. Huntington, N. D. *et al.* CD45 links the B cell receptor with cell survival and is required for the persistence of germinal centers. *Nat. Immunol.* **7**, 190–198 (2006).
61. Szodoray, P. *et al.* Integration of T helper and BCR signals governs enhanced plasma cell differentiation of memory B cells by regulation of CD45 phosphatase activity. *Cell Rep.* **36**, 109525 (2021).
62. Chou, M.-Y. *et al.* Oxidation-specific epitopes are dominant targets of innate natural antibodies in mice and humans. *J. Clin. Invest.* **119**, 1335–1349 (2009).
63. McKay, J. T. *et al.* PD-L2 regulates B-1 cell antibody production against phosphorylcholine through an IL-5–dependent mechanism. *J. Immunol.* **199**, 2020 (2017).
64. Gruber, S. *et al.* Sialic Acid-Binding Immunoglobulin-like Lectin G Promotes Atherosclerosis and Liver Inflammation by Suppressing the Protective Functions of B-1 Cells. *Cell Rep.* **14**, 2348–2361 (2016).
65. Tay, C. *et al.* B-cell-specific depletion of tumour necrosis factor alpha inhibits atherosclerosis development and plaque vulnerability to rupture by reducing cell death and inflammation. *Cardiovasc. Res.* **111**, 385–397 (2016).
66. Li, Y. *et al.* Glia maturation factor-γ is involved in S1P-induced marginal zone B-cell chemotaxis and optimal IgM production to type II T-independent antigen. *Int. Immunol.* **34**, 35–43 (2022).
67. Iwata, T. N., Ramírez-Komo, J. A., Park, H. & Iritani, B. M. Control of B lymphocyte development and functions by the mTOR signaling pathways. *Cytokine Growth Factor Rev.* **35**, 47–62 (2017).
68. You, Y. *et al.* Marginal Zone B Cells Regulate Antigen Capture by Marginal Zone Macrophages. *J. Immunol.* **186**, 2172–2181 (2011).
69. Pirgova, G., Chauveau, A., MacLean, A. J., Cyster, J. G. & Arnon, T. I. Marginal zone SIGN-R1 + macrophages are essential for the maturation of germinal center B cells in the spleen. *Proc. Natl. Acad. Sci.* **117**, 12295–12305 (2020).
70. Nus, M. *et al.* NR4A1 Deletion in Marginal Zone B Cells Exacerbates Atherosclerosis in Mice. *Arter. Thromb Vasc Biol* **40**, 2598–2604 (2020).
71. Srikakulapu, P. & McNamara, C. A. B Lymphocytes and Adipose Tissue Inflammation. *Arterioscler. Thromb. Vasc. Biol.* **40**, 1110–1122 (2020).
72. Pattarabanjird, T., Li, C. & McNamara, C. B Cells in Atherosclerosis. *JACC Basic to Transl. Sci.* **6**, 546–563 (2021).
73. Jellusova, J. Metabolic control of B cell immune responses. *Curr. Opin. Immunol.* **63**, 21–28 (2020).
74. Ripperger, T. J. & Bhattacharya, D. Transcriptional and Metabolic Control of Memory B Cells and Plasma Cells. *Annu. Rev. Immunol.* **39**, 345–368 (2021).
75. Choi, S.-C. & Morel, L. Immune metabolism regulation of the germinal center response. *Exp. Mol. Med.* **52**, 348–355 (2020).
76. Shlomchik, M. J., Luo, W. & Weisel, F. Linking signaling and selection in the germinal center. *Immunol. Rev.* **288**, 49–63 (2019).
77. Klein, U. *et al.* Transcriptional analysis of the B cell germinal center reaction. *Proc. Natl. Acad. Sci.* **100**, 2639–2644 (2003).
78. Okada, T. & Cyster, J. G. B cell migration and interactions in the early phase of antibody responses. *Curr. Opin. Immunol.* **18**, 278–285 (2006).
79. Kelly, L. M., Pereira, J. P., Yi, T., Xu, Y. & Cyster, J. G. EBI2 Guides Serial Movements of Activated B Cells and Ligand Activity Is Detectable in Lymphoid and Nonlymphoid Tissues. *J. Immunol.* **187**, 3026–3032 (2011).
80. Kara, E. E. *et al.* Atypical chemokine receptor 4 shapes activated B cell fate. *J. Exp. Med.* **215**, 801 (2018).
81. Pereira, J. P., Kelly, L. M., Xu, Y. & Cyster, J. G. EBI2 mediates B cell segregation between the outer and centre follicle. *Nature* **460**, 1122–1126 (2009).
82. Pae, J., Jacobsen, J. T. & Victora, G. D. Imaging the different timescales of germinal center selection. *Immunol. Rev.* **306**, 234–243 (2022).
83. De Silva, N. S., Klein, U., Silva, N. S. De & Klein, U. Dynamics of B cells in germinal centres. *Nat. Rev. Immunol. 2015 153* **15**, 137–148 (2015).
84. Kennedy, D. E. & Clark, M. R. Compartments and Connections Within the Germinal Center. *Front. Immunol.* **12**, (2021).
85. Laidlaw, B. J. & Cyster, J. G. Transcriptional regulation of memory B cell differentiation. *Nat. Rev.*

Immunol. **21**, 209–220 (2021).
86. Yi, T. & Cyster, J. G. EBI2-mediated bridging channel positioning supports splenic dendritic cell homeostasis and particulate antigen capture. *Elife* **2**, (2013).
87. Sun, S. & Liu, C. 7a25-dihydroxycholesterol-mediated activation of EBI2 in immune regulation and diseases. *Front. Pharmacol.* **06**, 00060 (2015).
88. JG, C. *et al. 25-Hydroxycholesterols in innate and adaptive immunity*. *Nature Reviews Immunology* vol. 14 731–743 (Nat Rev Immunol, 2014).
89. Zotos, D. *et al.* The concerted change in the distribution of cell cycle phases and zone composition in germinal centers is regulated by IL-21. *Nat. Commun.* **12**, 7160 (2021).
90. Pae, J. *et al.* Cyclin D3 drives inertial cell cycling in dark zone germinal center B cells. *J. Exp. Med.* **218**, e20201699 (2021).
91. Ghosh, D., Jiang, W., Mukhopadhyay, D. & Mellins, E. D. New insights into B cells as antigen presenting cells. *Curr. Opin. Immunol.* **70**, 129–137 (2021).
92. Victora, G. D. & Nussenzweig, M. C. Germinal Centers. *Annu. Rev. Immunol.* **40**, 413–442 (2022).
93. Liu, D. *et al.* BCL6 controls contact-dependent help delivery during follicular T-B cell interactions. *Immunity* **54**, 2245-2255.e4 (2021).
94. Luo, W. *et al.* The AKT kinase signaling network is rewired by PTEN to control proximal BCR signaling in germinal center B cells. *Nat. Immunol. 2019 206* **20**, 736–746 (2019).
95. Tangye, S. G. & Ma, C. S. Regulation of the germinal center and humoral immunity by interleukin-21. *J. Exp. Med.* **217**, e20191638 (2020).
96. Toboso-Navasa, A. *et al.* Restriction of memory B cell differentiation at the germinal center B cell positive selection stage. *J. Exp. Med.* **217**, e20191933 (2020).
97. Marsman, C., Jorritsma, T., ten Brinke, A. & van Ham, S. M. Flow Cytometric Methods for the Detection of Intracellular Signaling Proteins and Transcription Factors Reveal Heterogeneity in Differentiating Human B Cell Subsets. *Cells* **9**, 2633 (2020).
98. MM, D. *et al.* The CD40-TRAF6 axis is the key regulator of the CD40/CD40L system in neointima formation and arterial remodeling. *Blood* **111**, 4596–4604 (2008).
99. Bolduc, A. *et al.* Constitutive CD40L Expression on B Cells Prematurely Terminates Germinal Center Response and Leads to Augmented Plasma Cell Production in T Cell Areas. *J. Immunol.* **185**, 220–230 (2010).
100. Lee, M. S. J. *et al.* B cell–intrinsic TBK1 is essential for germinal center formation during infection and vaccination in mice. *J. Exp. Med.* **219**, e20211336 (2022).
101. Merino Tejero, E. *et al.* Multiscale Modeling of Germinal Center Recapitulates the Temporal Transition From Memory B Cells to Plasma Cells Differentiation as Regulated by Antigen Affinity-Based Tfh Cell Help. *Front. Immunol.* **11**, 620716 (2021).
102. Young, C. & Brink, R. The unique biology of germinal center B cells. *Immunity* **54**, 1652–1664 (2021).
103. Finkin, S., Hartweger, H., Oliveira, T. Y., Kara, E. E. & Nussenzweig, M. C. Protein Amounts of the MYC Transcription Factor Determine Germinal Center B Cell Division Capacity. *Immunity* **51**, 324-336.e5 (2019).
104. Zhong, M.-C. *et al.* SLAM family receptors control pro-survival effectors in germinal center B cells to promote humoral immunity. *J. Exp. Med.* **218**, e20200756 (2021).
105. Ni, X. *et al.* Death associated protein kinase 2 suppresses T-B interactions and GC formation. *Mol. Immunol.* **128**, 249–257 (2020).
106. Lau, A. W. & Brink, R. Selection in the germinal center. *Curr. Opin. Immunol.* **63**, 29–34 (2020).
107. Olson, W. J., Jakic, B. & Hermann-Kleiter, N. Regulation of the germinal center response by nuclear receptors and implications for autoimmune diseases. *FEBS J.* **287**, 2866–2890 (2020).
108. Tan, C. *et al.* NR4A nuclear receptors restrain B cell responses to antigen when second signals are absent or limiting. *Nat. Immunol. 2020 2110* **21**, 1267–1279 (2020).
109. Brooks, J. F. *et al.* Negative feedback by NUR77/Nr4a1 restrains B cell clonal dominance during early T-dependent immune responses. *Cell Rep.* **36**, 109645 (2021).
110. Liu, B. *et al.* Affinity-coupled CCL22 promotes positive selection in germinal centres. *Nature* **592**, 133–137 (2021).
111. Arulraj, T., Binder, S. C., Robert, P. A. & Meyer-Hermann, M. Germinal Centre Shutdown. *Front. Immunol.* **12**, 705240 (2021).
112. Pérez-García, A. *et al.* CTCF orchestrates the germinal centre transcriptional program and prevents premature plasma cell differentiation. *Nat. Commun.* **8**, 16067 (2017).
113. Li, Y. *et al.* EAF2 mediates germinal centre B-cell apoptosis to suppress excessive immune responses and

prevent autoimmunity. *Nat. Commun.* **7**, 10836 (2016).
114. Zhang, J., Kodali, S., Chen, M. & Wang, J. Maintenance of Germinal Center B Cells by Caspase-9 through Promotion of Apoptosis and Inhibition of Necroptosis. *J. Immunol.* **205**, 113–120 (2020).
115. Reimer, D. *et al.* B Cell Speed and B-FDC Contacts in Germinal Centers Determine Plasma Cell Output via Swiprosin-1/EFhd2. *Cell Rep.* **32**, 108030 (2020).
116. Kwak, K. *et al.* Intrinsic properties of human germinal center B cells set antigen affinity thresholds. *Sci. Immunol.* **3**, aau6598 (2018).
117. Nowosad, C. R., Spillane, K. M. & Tolar, P. Germinal center B cells recognize antigen through a specialized immune synapse architecture. *Nat. Immunol.* **17**, 870–877 (2016).
118. Li, Y., Bhanja, A., Upadhyaya, A., Zhao, X. & Song, W. WASp Is Crucial for the Unique Architecture of the Immunological Synapse in Germinal Center B-Cells. *Front. Cell Dev. Biol.* **9**, 646077 (2021).
119. Li, X. *et al.* Cbl and Cbl-b control the germinal center reaction by facilitating naive B cell antigen processing. *J. Exp. Med.* **217**, e20191537 (2020).
120. Li, X. *et al.* Cbl Ubiquitin Ligases Control B Cell Exit from the Germinal-Center Reaction. *Immunity* **48**, 530-541.e6 (2018).
121. Malinova, D. *et al.* Endophilin A2 regulates B-cell endocytosis and is required for germinal center and humoral responses. *EMBO Rep.* **22**, e51328 (2021).
122. Ersching, J. *et al.* Germinal Center Selection and Affinity Maturation Require Dynamic Regulation of mTORC1 Kinase. *Immunity* **46**, 1045-1058.e6 (2017).
123. Mayer, C. T. *et al.* The microanatomic segregation of selection by apoptosis in the germinal center. *Science (80-.).* **358**, eaao2602 (2017).
124. Shinnakasu, R. & Kurosaki, T. Regulation of memory B and plasma cell differentiation. *Curr. Opin. Immunol.* **45**, 126–131 (2017).
125. Pikor, N. B. *et al.* Remodeling of light and dark zone follicular dendritic cells governs germinal center responses. *Nat. Immunol.* **21**, 649–659 (2020).
126. Ramezani-Rad, P., Chen, C., Zhu, Z. & Rickert, R. C. Cyclin D3 Governs Clonal Expansion of Dark Zone Germinal Center B Cells. *CellReports* **33**, 108403 (2020).
127. Allen, C. D. C. *et al.* Germinal center dark and light zone organization is mediated by CXCR4 and CXCR5. *Nat. Immunol.* **5**, 943–952 (2004).
128. Inoue, T., Moran, I., Shinnakasu, R., Phan, T. G. & Kurosaki, T. Generation of memory B cells and their reactivation. *Immunol. Rev.* **283**, 138–149 (2018).
129. Luo, W. *et al.* B Cell Receptor and CD40 Signaling Are Rewired for Synergistic Induction of the c-Myc Transcription Factor in Germinal Center B Cells. *Immunity* **48**, 313-326.e5 (2018).
130. Li, L. *et al.* Regulation of humoral immune response by HIF-1α-dependent metabolic reprogramming of the germinal center reaction. *Cell. Immunol.* **367**, 104409 (2021).
131. Zhang, L. *et al.* PHF14 is required for germinal center B cell development. *Cell. Immunol.* **358**, 104221 (2020).
132. Davidzohn, N. *et al.* Syk degradation restrains plasma cell formation and promotes zonal transitions in germinal centers. *J. Exp. Med.* **217**, e20191043 (2020).
133. Stewart, I., Radtke, D., Phillips, B., McGowan, S. J. & Bannard, O. Germinal Center B Cells Replace Their Antigen Receptors in Dark Zones and Fail Light Zone Entry when Immunoglobulin Gene Mutations are Damaging. *Immunity* **49**, 477-489.e7 (2018).
134. Lee, J. *et al.* GSK3 Restrains Germinal Center B Cells to Form Plasma Cells. *J. Immunol.* **206**, 481–493 (2021).
135. Stebegg, M. *et al.* Regulation of the Germinal Center Response. *Front. Immunol.* **9**, 1–13 (2018).
136. Kennedy, D. E. *et al.* Novel specialized cell state and spatial compartments within the germinal center. *Nat. Immunol.* **21**, 660–670 (2020).
137. Mayer, C. T. *et al.* An apoptosis-dependent checkpoint for autoimmunity in memory B and plasma cells. *Proc. Natl. Acad. Sci.* **117**, 24957–24963 (2020).
138. Larijani, M. & Martin, A. The biochemistry of activation-induced deaminase and its physiological functions. *Semin. Immunol.* **24**, 255–263 (2012).
139. Dalloul, I. *et al.* UnAIDed Class Switching in Activated B-Cells Reveals Intrinsic Features of a Self-Cleaving IgH Locus. *Front. Immunol.* **12**, 737427 (2021).
140. Xu, Z., Zan, H., Pone, E. J., Mai, T. & Casali, P. Immunoglobulin class-switch DNA recombination: induction, targeting and beyond. *Nat. Rev. Immunol.* **12**, 517–531 (2012).
141. Siriwardena, S., Chen, K. & Bhagwat, A. S. The Functions and Malfunctions of AID/APOBEC Family Deaminases: the known knowns and the known unknowns. *Chem. Rev.* **116**, 12688 (2016).

142. Laffleur, B. *et al.* AID-induced remodeling of immunoglobulin genes and B cell fate. *Oncotarget* **5**, 1118–1131 (2014).
143. Stratigopoulou, M., van Dam, T. P. & Guikema, J. E. J. Base Excision Repair in the Immune System: Small DNA Lesions With Big Consequences. *Front. Immunol.* **11**, 1084 (2020).
144. Kothapalli, N. R. & Fugmann, S. D. Targeting of AID-mediated sequence diversification to immunoglobulin genes. *Curr. Opin. Immunol.* **23**, 184–189 (2011).
145. Zaheen, A. *et al.* AID constrains germinal center size by rendering B cells susceptible to apoptosis. *Blood* **114**, 547–554 (2009).
146. Català-Moll, F. *et al.* Activation-induced deaminase is critical for the establishment of DNA methylation patterns prior to the germinal center reaction. *Nucleic Acids Res.* **49**, 5057–5073 (2021).
147. Sundling, C. *et al.* Positive selection of IgG+ over IgM+ B cells in the germinal center reaction. *Immunity* **54**, 988-1001.e5 (2021).
148. Sun, L. *et al.* Transcription factor Ascl2 promotes germinal center B cell responses by directly regulating AID transcription. *Cell Rep.* **35**, 109188 (2021).
149. Roco, J. A. *et al.* Class-Switch Recombination Occurs Infrequently in Germinal Centers. *Immunity* **51**, 337-350.e7 (2019).
150. Dimenna, L. & Chaudhuri, J. Regulating infidelity: RNA-mediated recruitment of AID to DNA during class switch recombination HHS Public Access. *Eur J Immunol* **46**, 523–530 (2016).
151. Nicolas, L., Cols, M., Choi, J. E., Chaudhuri, J. & Vuong, B. Generating and repairing genetically programmed DNA breaks during immunoglobulin class switch recombination. *F1000Research* **7**, 458 (2018).
152. Häsler, J., Rada, C. & Neuberger, M. S. The cytoplasmic AID complex. *Semin. Immunol.* **24**, 273–280 (2012).
153. Wang, J. H. The role of activation-induced deaminase in antibody diversification and genomic instability. *Immunol. Res.* **55**, 287–297 (2013).
154. King, H. W. *et al.* Single-cell analysis of human B cell maturation predicts how antibody class switching shapes selection dynamics. *Sci. Immunol.* **6**, 6291 (2021).
155. Deenick, E. K., Hasbold, J. & Hodgkin, P. D. Decision criteria for resolving isotype switching conflicts by B cells. *Eur. J. Immunol.* **35**, 2949–2955 (2005).
156. Chang, X. *et al.* TLR7 Signaling Shapes and Maintains Antibody Diversity Upon Virus-Like Particle Immunization. *Front. Immunol.* **12**, 827256 (2022).
157. Moris, A., Murray, S. & Cardinaud, S. AID and APOBECs span the gap between innate and adaptive immunity. *Front. Microbiol.* **5**, (2014).
158. Zhang, Y., Fear, D. J., Willis-Owen, S. A. G., Cookson, W. O. & Moffatt, M. F. Global gene regulation during activation of immunoglobulin class switching in human B cells. *Sci. Rep.* **6**, 37988 (2016).
159. Stoler-Barak, L. *et al.* B cell dissemination patterns during the germinal center reaction revealed by whole-organ imaging. *J. Exp. Med.* **216**, 2515–2530 (2019).
160. Viant, C. *et al.* Antibody Affinity Shapes the Choice between Memory and Germinal Center B Cell Fates. *Cell* **183**, 1298-1311.e11 (2020).
161. Erwin, S., Childs, L. M. & Ciupe, S. M. Mathematical model of broadly reactive plasma cell production. *Sci. Rep.* **10**, 3935 (2020).
162. Bannard, O. & Cyster, J. G. Germinal centers: programmed for affinity maturation and antibody diversification. *Curr. Opin. Immunol.* **45**, 21–30 (2017).
163. Nakagawa, R. *et al.* Permissive selection followed by affinity-based proliferation of GC light zone B cells dictates cell fate and ensures clonal breadth. *Proc. Natl. Acad. Sci.* **118**, e2016425118 (2021).
164. Zhou, X., Zhu, X. & Zeng, H. Fatty acid metabolism in adaptive immunity. *FEBS J.* (2021) doi:10.1111/febs.16296.
165. Mesin, L. *et al.* Restricted Clonality and Limited Germinal Center Reentry Characterize Memory B Cell Reactivation by Boosting. *Cell* **180**, 92-106.e11 (2020).
166. Faro, J., von Haeften, B., Gardner, R. & Faro, E. A Sensitivity Analysis Comparison of Three Models for the Dynamics of Germinal Centers. *Front. Immunol.* **10**, 2038 (2019).
167. Sugimoto-Ishige, A. *et al.* Bim establishes the B-cell repertoire from early to late in the immune response. *Int. Immunol.* **33**, 79–90 (2021).
168. Kometani, K. *et al.* Repression of the Transcription Factor Bach2 Contributes to Predisposition of IgG1 Memory B Cells toward Plasma Cell Differentiation. *Immunity* **39**, 136–147 (2013).
169. Frölich, D. *et al.* Secondary Immunization Generates Clonally Related Antigen-Specific Plasma Cells and Memory B Cells. *J. Immunol.* **185**, 3103–3110 (2010).

170. Fallet, B. *et al.* Chronic Viral Infection Promotes Efficient Germinal Center B Cell Responses. *Cell Rep.* **30**, 1013-1026.e7 (2020).
171. Wang, X. *et al.* Follicular dendritic cells help establish follicle identity and promote B cell retention in germinal centers. *J. Exp. Med.* **208**, 2497–2510 (2011).
172. Wu, Y. *et al.* IL-6 produced by immune complex-activated follicular dendritic cells promotes germinal center reactions, IgG responses and somatic hypermutation. *Int. Immunol.* **21**, 745–756 (2009).
173. Arulraj, T., Binder, S. C. & Meyer-Hermann, M. Rate of Immune Complex Cycling in Follicular Dendritic Cells Determines the Extent of Protecting Antigen Integrity and Availability to Germinal Center B Cells. *J. Immunol.* **206**, 1436–1442 (2021).
174. van der Poel, C. E. *et al.* Follicular Dendritic Cells Modulate Germinal Center B Cell Diversity through FcγRIIB. *Cell Rep.* **29**, 2745-2755.e4 (2019).
175. Wang, X., Rodda, L. B., Bannard, O. & Cyster, J. G. Integrin-Mediated Interactions between B Cells and Follicular Dendritic Cells Influence Germinal Center B Cell Fitness. *J. Immunol.* **192**, 4601–4609 (2014).
176. Allen, C. D. C. & Cyster, J. G. Follicular dendritic cell networks of primary follicles and germinal centers: Phenotype and function. *Semin. Immunol.* **20**, 14–25 (2008).
177. Duan, L. *et al.* Follicular dendritic cells restrict interleukin-4 availability in germinal centers and foster memory B cell generation. *Immunity* **54**, 2256-2272.e6 (2021).
178. Avancena, P. *et al.* The magnitude of germinal center reactions is restricted by a fixed number of preexisting niches. *Proc. Natl. Acad. Sci. U. S. A.* **118**, (2021).
179. Weisel, F. J. *et al.* Germinal center B cells selectively oxidize fatty acids for energy while conducting minimal glycolysis. *Nat. Immunol.* **21**, 331–342 (2020).
180. Jellusova, J. *et al.* Gsk3 is a metabolic checkpoint regulator in B cells. *Nat. Immunol.* **18**, 303–312 (2017).
181. Cho, S. H. *et al.* Germinal centre hypoxia and regulation of antibody qualities by a hypoxia response system. *Nature* **537**, 234–238 (2016).
182. Abbott, R. K. *et al.* Germinal Center Hypoxia Potentiates Immunoglobulin Class Switch Recombination. *J. Immunol.* **197**, 4014–4020 (2016).
183. Chen, D. *et al.* Coupled analysis of transcriptome and BCR mutations reveals role of OXPHOS in affinity maturation. *Nat. Immunol.* **22**, 904–913 (2021).
184. Raybuck, A. L. *et al.* B Cell–Intrinsic mTORC1 Promotes Germinal Center–Defining Transcription Factor Gene Expression, Somatic Hypermutation, and Memory B Cell Generation in Humoral Immunity. *J. Immunol.* **200**, 2627–2639 (2018).
185. Sun, L., Yang, X., Yuan, Z. & Wang, H. Metabolic Reprogramming in Immune Response and Tissue Inflammation. *Arterioscler. Thromb. Vasc. Biol.* **40**, 1990–2001 (2020).
186. Haniuda, K., Fukao, S. & Kitamura, D. Metabolic Reprogramming Induces Germinal Center B Cell Differentiation through Bcl6 Locus Remodeling. *Cell Rep.* **33**, 108333 (2020).
187. Chevrier, S., Kratina, T., Emslie, D., Tarlinton, D. M. & Corcoran, L. M. IL4 and IL21 cooperate to induce the high Bcl6 protein level required for germinal center formation. *Immunol. Cell Biol.* **95**, 925–932 (2017).
188. Cook, S. L., Sievert, E. P. & Sciammas, R. B Cell–Intrinsic IRF4 Haploinsufficiency Impairs Affinity Maturation. *J. Immunol.* **207**, 2992–3003 (2021).
189. Wolf, D. *et al.* CD40L Deficiency Attenuates Diet-Induced Adipose Tissue Inflammation by Impairing Immune Cell Accumulation and Production of Pathogenic IgG-Antibodies. *PLoS One* **7**, e33026 (2012).
190. Daub, S., Lutgens, E., Münzel, T. & Daiber, A. CD40/CD40L and Related Signaling Pathways in Cardiovascular Health and Disease—The Pros and Cons for Cardioprotection. *Int. J. Mol. Sci.* **21**, 8533 (2020).
191. Karadimou, G. *et al.* Treatment with a Toll-like Receptor 7 ligand evokes protective immunity against atherosclerosis in hypercholesterolaemic mice. *J. Intern. Med.* **288**, 321–334 (2020).
192. Vijayashankar, D. P. & Vaidya, T. CD40 signaling-mediated delay in terminal differentiation of B cells enables alternate fate choices during early divisions. *Mol. Immunol.* **144**, 1–15 (2022).
193. Tay, C. *et al.* Follicular B Cells Promote Atherosclerosis via T Cell–Mediated Differentiation Into Plasma Cells and Secreting Pathogenic Immunoglobulin G. *Arterioscler. Thromb. Vasc. Biol.* **38**, e71–e84 (2018).
194. Kitamura, D. Mechanisms for the regulation of memory B-cell recall responses in mice. *Int. Immunol.* **33**, 791–796 (2021).
195. Inoue, T. *et al.* Exit from germinal center to become quiescent memory B cells depends on metabolic reprograming and provision of a survival signal. *J. Exp. Med.* **218**, e20200866 (2021).
196. Laidlaw, B. J., Duan, L., Xu, Y., Vazquez, S. E. & Cyster, J. G. The transcription factor Hhex cooperates with the corepressor Tle3 to promote memory B cell development. *Nat. Immunol.* **21**, 1082–1093 (2020).

197. Wang, Y. *et al.* Germinal-center development of memory B cells driven by IL-9 from follicular helper T cells. *Nat. Immunol.* **18**, 921–930 (2017).
198. Koike, T., Harada, K., Horiuchi, S. & Kitamura, D. The quantity of CD40 signaling determines the differentiation of B cells into functionally distinct memory cell subsets. *Elife* **8**, e44245 (2019).
199. Anderson, S. M., Tomayko, M. M., Ahuja, A., Haberman, A. M. & Shlomchik, M. J. New markers for murine memory B cells that define mutated and unmutated subsets. *J. Exp. Med.* **204**, 2103–2114 (2007).
200. Nakagawa, R. & Calado, D. P. Positive Selection in the Light Zone of Germinal Centers. *Front. Immunol.* **12**, 661678 (2021).
201. Viant, C. *et al.* Germinal center–dependent and –independent memory B cells produced throughout the immune response. *J. Exp. Med.* **218**, 20202489 (2021).
202. Tomayko, M. M. *et al.* Systematic Comparison of Gene Expression between Murine Memory and Naive B Cells Demonstrates That Memory B Cells Have Unique Signaling Capabilities. *J. Immunol.* **181**, 27–38 (2008).
203. Lau, A. W. Y. *et al.* BAFFR controls early memory B cell responses but is dispensable for germinal center function. *J. Exp. Med.* **218**, e20191167 (2021).
204. Akkaya, M., Kwak, K. & Pierce, S. K. B cell memory: building two walls of protection against pathogens. *Nat. Rev. Immunol.* **20**, 229–238 (2020).
205. Weisel, F. & Shlomchik, M. Memory B Cells of Mice and Humans. *Annu. Rev. Immunol.* **35**, 255–284 (2017).
206. Good-Jacobson, K. L. *et al.* PD-1 regulates germinal center B cell survival and the formation and affinity of long-lived plasma cells. *Nat. Immunol.* **11**, 535–542 (2010).
207. Johnson, J. L. *et al.* The Transcription Factor T-bet Resolves Memory B Cell Subsets with Distinct Tissue Distributions and Antibody Specificities in Mice and Humans. *Immunity* **52**, 842-855.e6 (2020).
208. Cancro, M. P. & Tomayko, M. M. Memory B cells and plasma cells: The differentiative continuum of humoral immunity. *Immunol. Rev.* **303**, 72–82 (2021).
209. Purtha, W. E., Tedder, T. F., Johnson, S., Bhattacharya, D. & Diamond, M. S. Memory B cells, but not long-lived plasma cells, possess antigen specificities for viral escape mutants. *J. Exp. Med.* **208**, 2599–2606 (2011).
210. Corinaldesi, C. *et al.* Tracking Immunoglobulin Repertoire and Transcriptomic Changes in Germinal Center B Cells by Single-Cell Analysis. *Front. Immunol.* **12**, 818758 (2022).
211. Vijay, G. K. M. & Singh, H. Cell fate dynamics and genomic programming of plasma cell precursors. *Immunol. Rev.* **303**, 62–71 (2021).
212. Ise, W. & Kurosaki, T. Plasma cell differentiation during the germinal center reaction. *Immunol. Rev.* **288**, 64–74 (2019).
213. Ise, W. *et al.* T Follicular Helper Cell-Germinal Center B Cell Interaction Strength Regulates Entry into Plasma Cell or Recycling Germinal Center Cell Fate. *Immunity* **48**, 702-715.e4 (2018).
214. Radtke, D. & Bannard, O. Expression of the Plasma Cell Transcriptional Regulator Blimp-1 by Dark Zone Germinal Center B Cells During Periods of Proliferation. *Front. Immunol.* **9**, 3106 (2019).
215. Santamaria, K. *et al.* Committed Human CD23-Negative Light-Zone Germinal Center B Cells Delineate Transcriptional Program Supporting Plasma Cell Differentiation. *Front. Immunol.* **12**, 744573 (2021).
216. Zhang, Y. *et al.* Plasma cell output from germinal centers is regulated by signals from Tfh and stromal cells. *J. Exp. Med.* **215**, 1227–1243 (2018).
217. Sze, M. *et al.* IRF4 Activity Is Required in Established Plasma Cells to Regulate Gene Transcription and Mitochondrial Homeostasis Article IRF4 Activity Is Required in Established Plasma Cells to Regulate Gene Transcription and Mitochondrial Homeostasis. *Cell Rep.* **29**, (2019).
218. Zhai, B. *et al.* Single-cell atlas of splenocytes reveals a critical role of a novel plasma cell–specific marker Hspa13 in antibody class-switching recombination and somatic hypermutation. *Mol. Immunol.* **141**, 79–86 (2022).
219. Gloury, R. *et al.* Dynamic changes in Id3 and E-protein activity orchestrate germinal center and plasma cell development. *J. Exp. Med.* **213**, 1095–1111 (2016).
220. Nguyen, D. C., Joyner, C. J., Sanz, I. & Lee, F. E.-H. Factors Affecting Early Antibody Secreting Cell Maturation Into Long-Lived Plasma Cells. *Front. Immunol.* **10**, 2138 (2019).
221. Willis, S. N. *et al.* Transcription Factor IRF4 Regulates Germinal Center Cell Formation through a B Cell–Intrinsic Mechanism. *J. Immunol.* **192**, 3200–3206 (2014).
222. Centa, M. *et al.* Germinal Center–Derived Antibodies Promote Atherosclerosis Plaque Size and Stability. *Circulation* **139**, 2466–2482 (2019).

223. Stone, S. L. *et al.* T-bet Transcription Factor Promotes Antibody-Secreting Cell Differentiation by Limiting the Inflammatory Effects of IFN-γ on B Cells. *Immunity* **50**, 1172-1187.e7 (2019).
224. Shaffer, A. L. *et al.* Blimp-1 Orchestrates Plasma Cell Differentiation by Extinguishing the Mature B Cell Gene Expression Program. *Immunity* **17**, 51–62 (2002).
225. Nadeau, S. & Martins, G. A. Conserved and Unique Functions of Blimp1 in Immune Cells. *Front. Immunol.* **12**, 805260 (2022).
226. Porsch, F., Mallat, Z. & Binder, C. J. Humoral immunity in atherosclerosis and myocardial infarction: from B cells to antibodies. *Cardiovasc. Res.* **117**, 2544–2562 (2021).
227. Corcoran, L. M. & Tarlinton, D. M. Regulation of germinal center responses, memory B cells and plasma cell formation—an update. *Curr. Opin. Immunol.* **39**, 59–67 (2016).
228. Wilmore, J. R. *et al.* IgA Plasma Cells Are Long-Lived Residents of Gut and Bone Marrow That Express Isotype- and Tissue-Specific Gene Expression Patterns. *Front. Immunol.* **12**, 791095 (2021).
229. Yang, J. *et al.* T-cell–derived extracellular vesicles regulate B-cell IgG production via pyruvate kinase muscle isozyme 2. *FASEB J.* **33**, 12780–12799 (2019).
230. Cao, Y. *et al.* Cytokines in the Immune Microenvironment Change the Glycosylation of IgG by Regulating Intracellular Glycosyltransferases. *Front. Immunol.* **12**, 724379 (2022).
231. Martin, S. W. & Goodnow, C. C. Burst-enhancing role of the IgG membrane tail as a molecular determinant of memory. *Nat. Immunol.* **3**, 182–188 (2002).
232. Kodama, T., Hasegawa, M., Sakamoto, Y., Haniuda, K. & Kitamura, D. Ubiquitination of IgG1 cytoplasmic tail modulates B-cell signalling and activation. *Int. Immunol.* **32**, 385–395 (2020).
233. Barr, T. A., Brown, S., Mastroeni, P. & Gray, D. B Cell Intrinsic MyD88 Signals Drive IFN-γ Production from T Cells and Control Switching to IgG2c. *J. Immunol.* **183**, 1005–1012 (2009).
234. Lee, M. S. J. *et al.* B cell-intrinsic MyD88 signaling controls IFN-γ-mediated early IgG2c class switching in mice in response to a particulate adjuvant. *Eur. J. Immunol.* **49**, 1433–1440 (2019).
235. Übelhart, R. *et al.* Responsiveness of B cells is regulated by the hinge region of IgD. *Nat. Immunol.* **16**, 534–543 (2015).
236. Zhang, X. *et al.* IgE Contributes to Atherosclerosis and Obesity by Affecting Macrophage Polarization, Macrophage Protein Network, and Foam Cell Formation. *Arterioscler. Thromb. Vasc. Biol.* **40**, 597–610 (2020).
237. Zhao, H. *et al.* Role of IgE-FcεR1 in Pathological Cardiac Remodeling and Dysfunction. *Circulation* **143**, 1014–1030 (2021).
238. Upadhye, A., Sturek, J. M. & McNamara, C. A. 2019 Russell Ross Memorial Lecture in Vascular Biology. *Arterioscler. Thromb. Vasc. Biol.* **40**, 309–322 (2020).
239. Khoo, L. H. B., Thiam, C. H., Soh, S. Y. & Angeli, V. Splenic extrafollicular reactions and BM plasma cells sustain IgM response associated with hypercholesterolemia. *Eur. J. Immunol.* **45**, 1300–1312 (2015).
240. Libby, P. The changing landscape of atherosclerosis. *Nat. 2021 5927855* **592**, 524–533 (2021).
241. Libby, P. Inflammation during the life cycle of the atherosclerotic plaque. *Cardiovasc. Res.* **117**, 2525–2536 (2021).
242. Que, X. *et al.* Oxidized phospholipids are proinflammatory and proatherogenic in hypercholesterolaemic mice. *Nature* **558**, 301–306 (2018).
243. Kim, K. *et al.* Transcriptome Analysis Reveals Nonfoamy Rather Than Foamy Plaque Macrophages Are Proinflammatory in Atherosclerotic Murine Models. *Circ. Res.* **123**, 1127–1142 (2018).
244. Li, Y. *et al.* Free Cholesterol-loaded Macrophages Are an Abundant Source of Tumor Necrosis Factor-α and Interleukin-6. *J. Biol. Chem.* **280**, 21763–21772 (2005).
245. Barrett, T. J. Macrophages in Atherosclerosis Regression. *Arterioscler. Thromb. Vasc. Biol.* **40**, 20–33 (2020).
246. Boyle, J. Macrophage Activation in Atherosclerosis: Pathogenesis and Pharmacology of Plaque Rupture. *Curr. Vasc. Pharmacol.* **3**, 63–68 (2005).
247. Tsiantoulas, D. *et al.* Circulating microparticles carry oxidation-specific epitopes and are recognized by natural IgM antibodies. *J. Lipid Res.* **56**, 440 (2015).
248. Bosmans, L. A., Bosch, L., Kusters, P. J. H., Lutgens, E. & Seijkens, T. T. P. The CD40-CD40L Dyad as Immunotherapeutic Target in Cardiovascular Disease. *J. Cardiovasc. Transl. Res.* **14**, 13 (2021).
249. Lutgens, E. *et al.* Deficient CD40-TRAF6 signaling in leukocytes prevents atherosclerosis by skewing the immune response toward an antiinflammatory profile. *J. Exp. Med.* **207**, 391–404 (2010).
250. Hutchinson, M. A. *et al.* Auto-Antibody Production During Experimental Atherosclerosis in ApoE-/- Mice. *Front. Immunol.* **12**, 2684 (2021).
251. Ryu, H. *et al.* Atherogenic dyslipidemia promotes autoimmune follicular helper T cell responses via IL-

27. *Nat. Immunol.* **19**, 583–593 (2018).
252. Chang, M. K. *et al.* Apoptotic cells with oxidation-specific epitopes are immunogenic and proinflammatory. *J. Exp. Med.* **200**, 1359–1370 (2004).
253. Richard, Y. *et al.* B Cell and CD4 T Cell Interactions Promote Development of Atherosclerosis. *Front. Immunol.* **10**, 1–15 (2020).
254. Caligiuri, G., Nicoletti, A., Poirierand, B. & Hansson, G. K. Protective immunity against atherosclerosis carried by B cells of hypercholesterolemic mice. *J. Clin. Invest.* **109**, 745–753 (2002).
255. Centa, M. *et al.* Acute Loss of Apolipoprotein E Triggers an Autoimmune Response That Accelerates Atherosclerosis. *Arterioscler. Thromb. Vasc. Biol.* **38**, e145–e158 (2018).
256. Lee, S., Bartlett, B. & Dwivedi, G. Adaptive Immune Responses in Human Atherosclerosis. *Int. J. Mol. Sci.* **21**, 9322 (2020).
257. Osma-Garcia, I. C. *et al.* The RNA-binding protein HuR is required for maintenance of the germinal centre response. *Nat. Commun.* **12**, 6556 (2021).
258. Inamine, A. *et al.* Two waves of memory B-cell generation in the primary immune response. *Int. Immunol.* **17**, 581–589 (2005).
259. Lorenzo, C. *et al.* ALDH4A1 is an atherosclerosis auto-antigen targeted by protective antibodies. *Nature* **589**, 287–292 (2021).
260. Binder, C. J. *et al.* IL-5 links adaptive and natural immunity specific for epitopes of oxidized LDL and protects from atherosclerosis. *J. Clin. Invest.* **114**, 427–437 (2004).
261. Tall, A. R. & Yvan-Charvet, L. Cholesterol, inflammation and innate immunity. *Nat. Rev. Immunol. 2015 152* **15**, 104–116 (2015).
262. Grasset, E. K. *et al.* Sterile inflammation in the spleen during atherosclerosis provides oxidation-specific epitopes that induce a protective B-cell response. *Proc. Natl. Acad. Sci.* **112**, E2030–E2038 (2015).
263. Lewis, M. J. *et al.* Immunoglobulin M Is Required for Protection Against Atherosclerosis in Low-Density Lipoprotein Receptor–Deficient Mice. *Circulation* **120**, 417–426 (2009).
264. Douna, H. *et al.* B- And T-lymphocyte attenuator stimulation protects against atherosclerosis by regulating follicular B cells. *Cardiovasc. Res.* **116**, 295–305 (2020).
265. Sun, X., Lyu, L., Zhong, X., Ni, Z. & Xu, Q. Application of genetic cell-lineage tracing technology to study cardiovascular diseases. *J. Mol. Cell. Cardiol.* **156**, 57–68 (2021).
266. Dogan, I. *et al.* Multiple layers of B cell memory with different effector functions. *Nat. Immunol. 2009 1012* **10**, 1292–1299 (2009).
267. Haniuda, K., Nojima, T. & Kitamura, D. In Vitro-Induced Germinal Center B Cell Culture System. in *Germinal Centers. Methods in Molecular Biology* (ed. Calado, D. P.) 125–133 (Humana Press, 2017). doi:10.1007/978-1-4939-7095-7_11.
268. Robinson, M. J. *et al.* BAFF, IL-4 and IL-21 separably program germinal center-like phenotype acquisition, BCL6 expression, proliferation and survival of CD40L-activated B cells in vitro. *Immunol. Cell Biol.* **97**, 826–839 (2019).
269. Streich, K. *et al.* Dietary lipids accumulate in macrophages and stromal cells and change the microarchitecture of mesenteric lymph nodes. *J. Adv. Res.* **24**, 291–300 (2020).
270. Le Gallou, S. *et al.* A splenic IgM memory subset with antibacterial specificities is sustained from persistent mucosal responses. *J. Exp. Med.* **215**, 2035–2053 (2018).
271. Trottier, M. D., Naaz, A., Li, Y. & Fraker, P. J. Enhancement of hematopoiesis and lymphopoiesis in diet-induced obese mice. *Proc. Natl. Acad. Sci.* **109**, 7622–7629 (2012).
272. Petta, I., Fraussen, J., Somers, V. & Kleinewietfeld, M. Interrelation of Diet, Gut Microbiome, and Autoantibody Production. *Front. Immunol.* **9**, (2018).
273. Chen, L., Ishigami, T., Doi, H., Arakawa, K. & Tamura, K. Gut microbiota and atherosclerosis: role of B cell for atherosclerosis focusing on the gut-immune-B2 cell axis. *J. Mol. Med.* **98**, 1235–1244 (2020).
274. Chen, L. *et al.* Commensal Microbe-specific Activation of B2 Cell Subsets Contributes to Atherosclerosis Development Independently of Lipid Metabolism. *EBioMedicine* **13**, 237–247 (2016).
275. Kiouptsi, K. *et al.* The Microbiota Promotes Arterial Thrombosis in Low-Density Lipoprotein Receptor-Deficient Mice. *MBio* **10**, e02298-19 (2019).
276. Garshick, M. S. *et al.* Reshaping of the gastrointestinal microbiome alters atherosclerotic plaque inflammation resolution in mice. *Sci. Rep.* **11**, 8966 (2021).
277. Barber, T. M. *et al.* Dietary Influences on the Microbiota–Gut–Brain Axis. *Int. J. Mol. Sci.* **22**, 3502 (2021).
278. Kasahara, K. *et al.* Commensal bacteria at the crossroad between cholesterol homeostasis and chronic inflammation in atherosclerosis. *J. Lipid Res.* **58**, 519 (2017).
279. Wang, Z. *et al.* Gut flora metabolism of phosphatidylcholine promotes cardiovascular disease. *Nature*

472, 57–63 (2011).
280. Brandsma, E. *et al.* A Proinflammatory Gut Microbiota Increases Systemic Inflammation and Accelerates Atherosclerosis. *Circ. Res.* **124**, 94 (2019).
281. Tsiantoulas, D., Sage, A. P., Mallat, Z. & Binder, C. J. Targeting B cells in atherosclerosis: Closing the gap from bench to bedside. *Arterioscler. Thromb. Vasc. Biol.* **35**, 296–302 (2015).
282. Ishibashi, S. *et al.* Hypercholesterolemia in low density lipoprotein receptor knockout mice and its reversal by adenovirus-mediated gene delivery. *J. Clin. Invest.* **92**, 883–893 (1993).
283. Weisel, F. J., Zuccarino-Catania, G. V., Chikina, M. & Shlomchik, M. J. A Temporal Switch in the Germinal Center Determines Differential Output of Memory B and Plasma Cells. *Immunity* **44**, 116 (2016).
284. Zhang, S. *et al.* Deep sequencing reveals the skewed B-cell receptor repertoire in plaques and the association between pathogens and atherosclerosis. *Cell. Immunol.* **360**, 104256 (2021).
285. Hartvigsen, K. *et al.* A Diet-Induced Hypercholesterolemic Murine Model to Study Atherogenesis Without Obesity and Metabolic Syndrome. *Arterioscler. Thromb. Vasc. Biol.* **27**, 878–885 (2007).
286. Cochain, C. & Zernecke, A. Macrophages and immune cells in atherosclerosis: recent advances and novel concepts. *Basic Res. Cardiol.* **110**, 34 (2015).
287. Slamanig, S. A. & Nolte, M. A. The Bone Marrow as Sanctuary for Plasma Cells and Memory T-Cells: Implications for Adaptive Immunity and Vaccinology. *Cells* **10**, 1508 (2021).
288. Amanna, I. J. & Slifka, M. K. Mechanisms that determine plasma cell lifespan and the duration of humoral immunity. *Immunol. Rev.* **236**, 125–138 (2010).
289. Echeverri Tirado, L. C. & Yassin, L. M. B cells interactions in lipid immune responses: implications in atherosclerotic disease. *Lipids Health Dis.* **16**, 30 (2017).
290. Angeli, V. *et al.* Dyslipidemia Associated with Atherosclerotic Disease Systemically Alters Dendritic Cell Mobilization. *Immunity* **21**, 561–574 (2004).
291. Wang, L. *et al.* The gut microbiota is associated with clinical response to statin treatment in patients with coronary artery disease. *Atherosclerosis* **325**, 16–23 (2021).
292. Milasan, A. *et al.* Apolipoprotein A-I Modulates Atherosclerosis Through Lymphatic Vessel-Dependent Mechanisms in Mice. *J. Am. Heart Assoc.* **6**, e006892 (2017).
293. Duc, D., Vigne, S. & Pot, C. Oxysterols in Autoimmunity. *Int. J. Mol. Sci.* **20**, 4522 (2019).
294. Andersen, C. Impact of Dietary Cholesterol on the Pathophysiology of Infectious and Autoimmune Disease. *Nutrients* **10**, 764 (2018).
295. van Loon, N. M. *et al.* Regulation of intestinal LDLR by the LXR-IDOL axis. *Atherosclerosis* **315**, 1–9 (2020).
296. Millatt, L. J., Bocher, V., Fruchart, J. C. & Staels, B. Liver X receptors and the control of cholesterol homeostasis: potential therapeutic targets for the treatment of atherosclerosis. *Biochim. Biophys. Acta - Mol. Cell Biol. Lipids* **1631**, 107–118 (2003).
297. Choi, C. & Finlay, D. K. Diverse Immunoregulatory Roles of Oxysterols—The Oxidized Cholesterol Metabolites. *Metabolites* **10**, 384 (2020).
298. Ito, A. *et al.* Cholesterol Accumulation in CD11c + Immune Cells Is a Causal and Targetable Factor in Autoimmune Disease. *Immunity* **45**, 1311–1326 (2016).
299. Bilotta, M. T., Petillo, S., Santoni, A. & Cippitelli, M. Liver X Receptors: Regulators of Cholesterol Metabolism, Inflammation, Autoimmunity, and Cancer. *Front. Immunol.* **11**, (2020).
300. Joyce, C. W. *et al.* ABCA1 Overexpression in the Liver of LDLr-KO Mice Leads to Accumulation of Pro-atherogenic Lipoproteins and Enhanced Atherosclerosis. *J. Biol. Chem.* **281**, 33053–33065 (2006).
301. Olkkonen, V. M. & Lehto, M. Oxysterols and oxysterol binding proteins: role in lipid metabolism and atherosclerosis. *Ann. Med.* **36**, 562–572 (2004).
302. Kennedy, D. J. *et al.* Dietary Cholesterol Plays a Role in CD36-Mediated Atherogenesis in LDLR Knockout Mice. *Arterioscler. Thromb. Vasc. Biol.* **29**, 1481 (2009).
303. Gan, L. T. *et al.* Hepatocyte free cholesterol lipotoxicity results from JNK1-mediated mitochondrial injury and is HMGB1 and TLR4-dependent. *J. Hepatol.* **61**, 1376–1384 (2014).
304. Subramanian, S. *et al.* Dietary cholesterol exacerbates hepatic steatosis and inflammation in obese LDL receptor-deficient mice. *J. Lipid Res.* **52**, 1626–1635 (2011).
305. Staprans, I., Pan, X.-M., Rapp, J. H. & Feingold, K. R. The role of dietary oxidized cholesterol and oxidized fatty acids in the development of atherosclerosis. *Mol. Nutr. Food Res.* **49**, 1075–1082 (2005).
306. Laplante, M.-A. *et al.* Distinct metabolic and vascular effects of dietary triglycerides and cholesterol in atherosclerotic and diabetic mouse models. *Am. J. Physiol. Metab.* **305**, E573–E584 (2013).
307. Ridker, P. M. & Rane, M. Interleukin-6 Signaling and Anti-Interleukin-6 Therapeutics in Cardiovascular Disease. *Circ. Res.* **128**, 1728–1746 (2021).
308. Hirano, T. IL-6 in inflammation, autoimmunity and cancer. *Int. Immunol.* **33**, 127–148 (2021).

309. Yan, Y., Wang, Y.-H. & Diamond, B. IL-6 contributes to an immune tolerance checkpoint in post germinal center B cells. *J. Autoimmun.* **38**, 1–9 (2012).
310. Ridker, P. M. *et al.* IL-6 inhibition with ziltivekimab in patients at high atherosclerotic risk (RESCUE): a double-blind, randomised, placebo-controlled, phase 2 trial. *Lancet* **397**, 2060–2069 (2021).
311. Alonso, R., Cuevas, A. & Mata, P. Lomitapide: a review of its clinical use, efficacy, and tolerability. *Core Evid.* **Volume 14**, 19–30 (2019).
312. Blom, D. J., Raal, F. J., Santos, R. D. & Marais, A. D. Lomitapide and Mipomersen—Inhibiting Microsomal Triglyceride Transfer Protein (MTP) and apoB100 Synthesis. *Curr. Atheroscler. Rep.* **21**, 48 (2019).
313. Hooper, A. J., Burnett, J. R. & Watts, G. F. Contemporary Aspects of the Biology and Therapeutic Regulation of the Microsomal Triglyceride Transfer Protein. *Circ. Res.* **116**, 193–205 (2015).
314. Kleemann, R., Zadelaar, S. & Kooistra, T. Cytokines and atherosclerosis: a comprehensive review of studies in mice. *Cardiovasc. Res.* **79**, 360–376 (2008).
315. Tyrrell, D. J. & Goldstein, D. R. Ageing and atherosclerosis: vascular intrinsic and extrinsic factors and potential role of IL-6. *Nat. Rev. Cardiol.* **18**, 58–68 (2021).
316. Boisvert, W. A. *et al.* Up-Regulated Expression of the CXCR2 Ligand KC/GRO-α in Atherosclerotic Lesions Plays a Central Role in Macrophage Accumulation and Lesion Progression. *Am. J. Pathol.* **168**, 1385–1395 (2006).
317. Wouters, K. *et al.* Dietary cholesterol, rather than liver steatosis, leads to hepatic inflammation in hyperlipidemic mouse models of nonalcoholic steatohepatitis. *Hepatology* **48**, 474–486 (2008).
318. Gwon, S.-Y., Lee, H. M., Rhee, K.-J. & Sung, H. J. Microarray and proteome array in an atherosclerosis mouse model for identification of biomarkers in whole blood. *Int. J. Med. Sci.* **16**, 882 (2019).
319. Okawa, T., Nagai, M. & Hase, K. Dietary Intervention Impacts Immune Cell Functions and Dynamics by Inducing Metabolic Rewiring. *Front. Immunol.* **11**, 623989 (2021).
320. Nagai, M. *et al.* Fasting-Refeeding Impacts Immune Cell Dynamics and Mucosal Immune Responses. *Cell* **178**, 1072-1087.e14 (2019).
321. Bagchi-Chakraborty, J. *et al.* B Cell Fcγ Receptor IIb Modulates Atherosclerosis in Male and Female Mice by Controlling Adaptive Germinal Center and Innate B-1-Cell Responses. *Arterioscler. Thromb. Vasc. Biol.* **39**, 1379–1389 (2019).
322. Laramée, A.-S. *et al.* Opposing Roles for the Related ETS-Family Transcription Factors Spi-B and Spi-C in Regulating B Cell Differentiation and Function. *Front. Immunol.* **11**, 1 (2020).
323. Falconer, D. J. & Barb, A. W. Mouse IgG2c Fc loop residues promote greater receptor-binding affinity than mouse IgG2b or human IgG1. *PLoS One* **13**, e0192123 (2018).
324. Vorsatz, C., Friedrich, N., Nimmerjahn, F. & Biburger, M. There Is Strength in Numbers: Quantitation of Fc Gamma Receptors on Murine Tissue-Resident Macrophages. *Int. J. Mol. Sci.* **22**, 12172 (2021).
325. Hernández-Vargas, P. *et al.* Fcγ Receptor Deficiency Confers Protection Against Atherosclerosis in Apolipoprotein E Knockout Mice. *Circ. Res.* **99**, 1188–1196 (2006).
326. Mallavia, B. *et al.* Gene Deficiency in Activating Fcγ Receptors Influences the Macrophage Phenotypic Balance and Reduces Atherosclerosis in Mice. *PLoS One* **8**, 66754 (2013).
327. Espéli, M. *et al.* FcγRIIb differentially regulates pre-immune and germinal center B cell tolerance in mouse and human. *Nat. Commun.* **10**, 1970 (2019).
328. Ratcliffe, N. R., Kennedy, S. M., Peter, M. & Morganelli. Immunocytochemical detection of Fcγ receptors in human atherosclerotic lesions. *Immunol. Lett.* **77**, 169–174 (2001).
329. Peng, J. *et al.* Supplementation With the Sialic Acid Precursor N-Acetyl-D-Mannosamine Breaks the Link Between Obesity and Hypertension. *Circulation* **140**, 2005–2018 (2019).
330. Xiang, Z. *et al.* FcγRIIb controls bone marrow plasma cell persistence and apoptosis. *Nat. Immunol. 2007 84* **8**, 419–429 (2007).
331. Marvin, J., Rhoads, J. P. & Major, A. S. FcγRIIb on CD11c+ cells modulates serum cholesterol and triglyceride levels and differentially affects atherosclerosis in male and female Ldlr−/− mice. *Atherosclerosis* **285**, 108–119 (2019).
332. Ng, H. P., Zhu, X., Harmon, E. Y., Lennartz, M. R. & Nagarajan, S. Reduced Atherosclerosis in apoE-inhibitory FcγRIIb–Deficient Mice Is Associated With Increased Anti-Inflammatory Responses by T Cells and Macrophages. *Arterioscler. Thromb. Vasc. Biol.* **35**, 1101–1112 (2015).
333. Song, X. *et al.* Blocking FcγRIIB in Smooth Muscle Cells Reduces Hypertension. *Circ. Res.* **129**, 308–325 (2021).
334. Nimmerjahn, F., Bruhns, P., Horiuchi, K. & Ravetch, J. V. FcγRIV: A Novel FcR with Distinct IgG Subclass Specificity. *Immunity* **23**, 41–51 (2005).
335. Syed, S. N. *et al.* Both FcγRIV and FcγRIII are essential receptors mediating type II and type III

autoimmune responses via FcRγ-LAT-dependent generation of C5a. *Eur. J. Immunol.* **39**, 3343–3356 (2009).
336. Nimmerjahn, F. & Ravetch, J. V. Divergent Immunoglobulin G Subclass Activity Through Selective Fc Receptor Binding. *Science (80-.).* **310**, 1510–1512 (2005).
337. Ley, K. Role of the adaptive immune system in atherosclerosis. *Biochem. Soc. Trans.* **48**, 2273 (2020).
338. Niwa, T. *et al.* Interferon-gamma Produced by Bone Marrow-derived Cells Attenuates Atherosclerotic Lesion Formation in LDLR-deficient Mice. *J. Atheroscler. Thromb.* **11**, 79–87 (2004).
339. Leon, M. L. A. & Zuckerman, S. H. Gamma interferon: a central mediator in atherosclerosis. *Inflamm. Res.* **54**, 395–411 (2005).
340. Reardon, C. A. *et al.* Obesity and Insulin Resistance Promote Atherosclerosis through an IFNγ-Regulated Macrophage Protein Network. *Cell Rep.* **23**, 3021–3030 (2018).
341. Koltsova, E. K. *et al.* Dynamic T cell–APC interactions sustain chronic inflammation in atherosclerosis. *J. Clin. Invest.* **122**, 3114–3126 (2012).
342. Nimmerjahn, F. *et al.* FcγRIV deletion reveals its central role for IgG2a and IgG2b activity in vivo. *Proc. Natl. Acad. Sci.* **107**, 19396–19401 (2010).
343. Saad, A. F., Virella, G., Chassereau, C., Boackle, R. J. & Lopes-Virella, M. F. OxLDL immune complexes activate complement and induce cytokine production by MonoMac 6 cells and human macrophages. *J. Lipid Res.* **47**, 1975–1983 (2006).
344. Rhoads, J. P. *et al.* Oxidized Low-Density Lipoprotein Immune Complex Priming of the Nlrp3 Inflammasome Involves TLR and FcγR Cooperation and Is Dependent on CARD9. *J. Immunol.* **198**, 2105–2114 (2017).
345. Mendez-Fernandez, Y. V *et al.* The inhibitory FcγRIIb modulates the inflammatory response and influences atherosclerosis in male apoE−/− mice. *Atherosclerosis* **214**, 73 (2011).
346. Masuda, M. *et al.* Soluble FcγRIIIaMϕ levels in plasma correlate with carotid maximum intima-media thickness (IMT) in subjects undergoing an annual medical checkup. *Mol. Med.* **14**, 436–442 (2008).
347. Hamers, A. A. J. *et al.* Human Monocyte Heterogeneity as Revealed by High-Dimensional Mass Cytometry. *Arterioscler. Thromb. Vasc. Biol.* **39**, 25–36 (2019).
348. Wang, X., Liu, X., Kishimoto, C. & Yuan, Z. The role of Fcγ receptors in atherosclerosis. *Exp. Biol. Med.* **237**, 609–616 (2012).
349. Gavasso, S. *et al.* Fcγ receptor IIIA polymorphism as a risk-factor for coronary artery disease. *Atherosclerosis* **180**, 277–282 (2005).
350. Ahmad, F. *et al. Current Concepts on 6-sulfo LacNAc Expressing Monocytes (slanMo)*. *Frontiers in Immunology* vol. 1 948 (2019).
351. Weng, R., Liu, S., Gu, X. & Zhong, Z. Characterization of the B cell receptor repertoire of patients with acute coronary syndrome. *Genes Genomics* **44**, 19–28 (2022).